

University of Alberta
Department of Civil &
Environmental Engineering



Structural Engineering Report

Shear Behaviour of Concrete Slabs and Beams Reinforced with High-Performance ASTM A1035 Steel

by

Admasu S. Desalegne

and

Adam S. Lubell

September, 2013

Shear Behaviour of Concrete Slabs and Beams Reinforced with High-Performance ASTM A1035 Steel

by

Admasu S. Desalegne
and
Adam S. Lubell

Structural Engineering Report

Department of Civil and Environmental Engineering
University of Alberta, Edmonton, Alberta

September 2013

ABSTRACT

High-performance steel bars manufactured to conform to ASTM A1035-11 have different metallurgy and microstructure than conventional reinforcing steel. These changes result in an effective yield strength significantly higher than conventional ASTM A615 steel while also being less susceptible to corrosion. Thus there is increasing interest in the use of ASTM A1035 steel to reduce life-cycle costs for new concrete structures. However, the lack of a well defined yield point for this material requires careful assessment of structural design models to ensure that they accurately account for influences from higher reinforcement strains.

This research focuses on the behaviour of shear-critical concrete members containing ASTM A1035 steel reinforcement. Laboratory tests were completed for six slab strips and ten beams with overall heights ranging from 300 mm to 1000 mm and shear span to depth ratios of 3.0 – 3.6. In the current study the term “*SLABS*” refer to concrete members longitudinally reinforced with ASTM A1035 steel without stirrups and “*BEAMS*” refer to members with stirrups containing combinations of ASTM A1035 or Grade 420 steel. The influence on shear and deflection behaviour from the reinforcement configurations and the nonlinear stress-strain response of the ASTM A1035 steel were of primary interest.

General analytical shear models were developed for members containing ASTM A1035 steel. Simplified design shear models were also developed where the

longitudinal ASTM A1035 reinforcement is proportioned on the basis of 690 MPa yield strength. All models were validated using the new experimental test results and data from the literature. The proposed shear models were also compared with existing analytical and numerical models. Improved capacity predictions were obtained from models that directly account for the influence of reinforcement strains and member depth.

It was observed that the service load deflections of beams were underestimated by existing code deflection models such as the *ACI ITG-6R-10* direct deflection model. Based on parametric studies, general deflection model and simplified deflection equations were developed for the beams containing ASTM A1035 steel reinforcement. The equations were validated against test results and were shown to be useful for deflection calculations in the design industry.

ACKNOWLEDGEMENTS

This report is based on the Doctor of Philosophy dissertation of the first author.

The authors thank MMFX Technologies Corporation and Lehigh Inland Cement for donations of the reinforcing steel and concrete used in the laboratory work reported in this document. Some fabrication assistance was also provided by Lafarge North America.

Financial support for this project was provided by the Natural Sciences and Engineering Research Council of Canada (NSERC), Armtec Infrastructure Limited, and by the University of Alberta.

The technical assistance of staff in the I.F. Morrison Structural Engineering Laboratory at the University of Alberta are acknowledged, including Sean Watt, Greg Miller, Michael Leitch, Sean Hudson and Rizaldy Mariano. Thanks are also extended to other graduate students that assisted in various stages of the laboratory work, especially Adel Shoaib and Laura Talboys.

TABLE OF CONTENTS

1. INTRODUCTION	1
1.1 Motivation	1
1.2 Research Significance	3
1.3 Organization	5
2. BACKGROUND AND LITERATURE REVIEW	9
2.1 General	9
2.2 Mechanics of Shear for Reinforced Concrete	12
2.2.1 General	12
2.2.2 Slender and Deep Members	13
2.2.3 Shear Behaviour of Slender Reinforced Concrete Members	14
2.2.4 Aggregate Interlock	16
2.3 The Modified Compression Field Theory (MCFT)	22
2.4 Shear Design Models	24
2.4.1 Analytical Models	25
2.4.1.1 <i>ACI 318-11</i>	25
2.4.1.2 <i>ACI ITG-6R-10</i>	27
2.4.1.3 <i>CSA A23.3.04</i> General Method	28
2.4.1.3.1 Background	28
2.4.1.3.2 Model Development	30
2.4.1.4 <i>Hoult et al.</i> Model	34
2.4.1.5 <i>Eurocode 2 (2004)</i>	37
2.4.2 Numerical Models	38
2.4.2.1 <i>VecTor2</i>	38
2.4.2.2 <i>Response 2000</i>	39
2.5 Concrete Slabs and Beams Reinforced with ASTM A1035 Steel	40
2.5.1 Previous Research on Flexural Behaviour	40
2.5.2 Previous Research on Shear Behaviour	44
2.6 Deflection of Reinforced Concrete Beams	52
2.6.1 General	52

2.6.2 Previous Research on Deflection of Concrete Beams	52
2.6.3 Numerical Models for Deflection of Concrete Beams.....	58
2.7 Summary	61
3. EXPERIMENTAL PROGRAM	64
3.1 General	64
3.2 Details of Slab Specimens	65
3.3 Details of Beam Specimens	68
3.3.1 Details of Specimens <i>RM1</i> & <i>RM2</i>	70
3.3.2 Details of Specimens <i>MR1</i> & <i>MM1</i>	72
3.3.3 Details of Specimens <i>MR2</i> & <i>MM2</i>	73
3.3.4 Details of Specimens <i>MR3</i> & <i>MM3</i>	75
3.3.5 Details of Specimens <i>MR4</i> & <i>MM4</i>	76
3.4 Materials	78
3.4.1 Reinforcing Steel	78
3.4.1.1 ASTM A1035 Reinforcing Steel	78
3.4.1.2 Grade 420 Reinforcing Steel	81
3.4.2 Concrete	82
3.5 Fabrication of Specimens	85
3.6 Instrumentation and Testing Procedures	86
3.6.1 General	86
3.6.2 Instrumentation	87
3.6.3 Data Acquisition System	91
3.6.4 Testing Procedures	92
4. TEST RESULTS AND DISCUSSION	93
4.1 General	93
4.2 Test Results	93
4.2.1 Slab Specimens	93
4.2.2 Beam Specimens	95
4.3 Discussion of Results	96
4.3.1 Slab Specimens	96
4.3.1.1 Load-Deflection Behaviour	96

4.3.1.2 Load-Stress Strain Behaviour	98
4.3.1.3 Failure Mode and Crack Pattern	100
4.3.1.4 Influence of Member Depth and Reinforcement Ratio ..	102
4.3.2 Beam Specimens	104
4.3.2.1 Load-Deflection Behaviour	104
4.3.2.2 Load-Longitudinal Steel Strain Behaviour	106
4.3.2.3 Load-Transverse Steel Strain Behaviour	111
4.3.2.4 Crack Pattern and Failure Mode	114
4.3.2.5 Influence of Stirrup Spacing and Reinforcement Ratio .	120
4.4 Summary	124
5. MODELING SHEAR CAPACITY OF ONE WAY-SLABS	125
5.1 General	125
5.2 Proposed Analytical Shear Design Models	126
5.2.1 Motivation	126
5.2.2 General Shear Model	126
5.2.2 Design Shear Model.....	128
5.3 Model Validation	131
5.3.1 Database of Tested Slab Specimens	131
5.3.2 Validation of the General Shear Model	132
5.3.3 Validation of the Design Shear Model	136
5.4 Comparison to Existing Shear Design Models	142
5.4.1 Code Model Predictions	142
5.4.2 Numerical Model Predictions	146
5.5 Summary	151
6. MODELING SHEAR CAPACITY OF BEAMS	153
6.1 Introduction	153
6.2 Development of Analytical Shear Design Models	154
6.2.1 General	154
6.2.2 General Shear Model	155
6.2.3 Design Shear Model	159
6.3 Model Validation	160

6.3.1 Database of Beam Specimens	160
6.3.2 Validation of the General Shear Model	163
6.3.3 Validation of the Design Shear Model	168
6.4 Comparison to Existing Shear Design Models	175
6.5 Influence of Design Parameters on Shear Capacity	181
6.6 Summary	187
7. DEFLECTION MODELS FOR BEAMS	189
7.1 General	189
7.2 Deficiency of Current Code Deflection Model	190
7.3 Database of Beam Specimens	194
7.4 Development of General Deflection Model	197
7.5 Model Validation	205
7.5.1 Validation of The General Beam Deflection Model	205
7.5.2 Development of General and Simplified Design Equations	208
7.5.3 Influence of Reinforcement Ratios on Deflection Equation	213
7.6 Comparison of Deflection Models for Concrete Beams	221
7.6.1 Overview of Deflection Models	221
7.6.1.1 <i>ACI ITG - 6R-10</i> Deflection Model	221
7.6.1.2 <i>VecTor 2</i>	223
7.6.1.3 <i>Response 2000</i>	224
7.7 Comparison of Model Beam Service Deflections	224
7.8 Influence of Design Parameters on Beam Deflection Models	232
7.9 Summary	244
8. CONCLUSIONS AND RECOMMENDATIONS	246
8.1 Summary	246
8.2 Conclusions	247
8.2.1 Shear Behaviour of Slab Specimens	247
8.2.2 Shear Behaviour of Beam Specimens	249
8.2.3 Deflection Behaviour of Beam Specimens	250
8.3 Recommendations for Future Work	252
REFERENCES	255

Appendix A LABORATORY TEST RESULTS	266
Appendix B SHEAR MODELS	302
Appendix C BEAM DEFLECTION MODEL.....	360

LIST OF TABLES

Table 2-1: Reinforcing Steel Design Stress Limits in Some Concrete Codes	12
Table 2-2: Details of Beams Tested by <i>Munikrishna et al.</i> (2008)	58
Table 3-1: Slab Specimen Details.	66
Table 3-2: Beam Specimen Details.	70
Table 3-3: Grade 420 and ASTM A1035 Grade 690 Reinforcement Steel Properties	80
Table 3-4: Compression Test Results at the Day of Test of Specimens	83
Table 4-1: Test Results for Slab Specimens	94
Table 4-2: Beam Specimen Details and Service Conditions	95
Table 4-3: Normalized Shear Stress at Failure for Slab Specimens	104
Table 4-4: Normalized Shear Stress at Failure for Beam Specimens	123
Table 5-1: Details of Slab Specimen from Prior Tests	132
Table 5-2: General Shear Model Predictions of Slabs in the Database	134
Table 5-3: Simplified Design Shear Model Predictions of Slabs	137
Table 5-4: Code Model Predictions of Slabs in the Database	144
Table 5-5: Numerical Model Predictions of Slab Specimens	149
Table 6-1 Details of Beam Specimens in the Database	162
Table 6-2: General Shear Model Predictions of All Beam Specimens.....	164
Table 6-3: Design Shear Model Predictions of All Beam Specimens	170
Table 6-4: Analytical and Numerical Model Predictions of All Beams ($f_{yt} = 550$ MPa).	178
Table 6-5: Analytical and Numerical Model Predictions of All Beams ($f_{yt} = 690$ MPa).	180
Table 7-1: Details of Beams with High Strength or ASTM A1035 Steel	195
Table 7-2: Details of Beams with Conventional Steel Reinforcement	196
Table 7-3: Prediction of General Deflection Model for Beams with A1035 Steel	206
Table 7-4: General Deflection Model Prediction for Beams with Conventional Steel	207

Table 7-5: Deflection Predictions with Variable Reinforcement Ratios	216
Table 7-6: Validation of Beam Deflection Equations (ASTM A1035 Steel) ...	220
Table 7-7: Deflection Prediction of Beams with High Strength or ASTM A1035 Steel.....	226
Table 7-8: Deflection Prediction of Beams with Conventional Steel	227

LIST OF FIGURES

Figure 1-1: Flow Chart Showing the Organizational Structure of the Report	8
Figure 2-1: Typical Stress-Strain Response for ASTM A1035 and ASTM A615 Steel from Coupon Testing	10
Figure 2-2: Classifying Shear Behaviour as Deep Members and Slender Members (Adapted from <i>Collins and Mitchell</i> , 1997)	14
Figure 2-3: Shear Resisting Mechanisms in Reinforced Concrete Slabs and Beams	15
Figure 2-3: Influence of member depth and aggregate size on shear stress at failure for tests carried out by <i>Shioya</i> 1989 (<i>Collins and Mitchell</i> , 1997)	19
Figure 2-4: The Influence of Longitudinal Reinforcement Ratio on Shear Stress at Failure (<i>Lubell et al.</i> 2009)	21
Figure 2-5: Maximum Concrete Compressive Stress as Function of Principal Tensile Strain (<i>ASCE-ACI445</i> 1999)	23
Figure 2-6: Equations of Modified Compression Field Theory (<i>Vecchio and Collins</i> 1986)	25
Figure 2-7: Basic Shear Resisting Mechanism Assumed in CSA A.23.3-04 code (adapted from <i>Bentz et al.</i> 2006)	28
Figure 2-8: Selection of Equation for θ (<i>Bentz</i> 2006)	34
Figure 2-9: Normalized Shear Stress versus Longitudinal Strain at Mid-Depth (<i>Hoult et al.</i> 2008)	36
Figure 2-10: Measured Tensile Properties of Reinforcing Steel (<i>Lepage et al.</i> 2011)	43
Figure 2-11: Load-Deflection Behaviour of Beams tested by <i>Hassan et al.</i> , 2008	46
Figure 2-12: Shear Load-Deflection Relationship, Set 1. (Adapted from <i>Sumpter et al.</i> , 2009)	49
Figure 2-13: Shear Load-Deflection Relationship, Group 1 beams. (Adapted from	

<i>Munikrishna et al.</i> , 2008)	50
Figure 2-14: Comparison of Deflection models (<i>Mohr et al.</i> 2010)	55
Figure 2-15: Typical Load–Deflection Response at Mid-Span of Beam <i>VS-A2</i> (<i>Navarro-Gregori et al.</i> 2013)	56
Figure 2-16: Test Results for Group 3 Beams (<i>Munikrishna et al.</i> 2008)	57
Figure 3-1: Details of Slab Specimens with $h = 305$ mm	67
Figure 3-2: Details of Beam Specimens with $h = 600$ mm	68
Figure 3-3: Details of Beam Specimens <i>RM1</i> [<i>RM2</i>]	71
Figure 3-4: Details of Beam Specimen <i>MR1</i> [<i>MM1</i>]	73
Figure 3-5: Details of Beam Specimen <i>MR2</i> [<i>MM1</i>]	74
Figure 3-6: Details of Beam Specimen <i>MR3</i> [<i>MM3</i>]	76
Figure 3-7: Details of Beam Specimen <i>MR4</i> [<i>MM4</i>]	77
Figure 3-8: Tension Coupon Test for Reinforcement Bars.....	78
Figure 3-9: Representative Tension Stress-Strain Response for Steel Coupons .	81
Figure 3-10 Typical Compression Test of Concrete Cylinder (Batch 4)	84
Figure 3-11 Typical Stress-Strain Curve of a Concrete Cylinder (Batch 4)	84
Figure 3-12 Steel Cages Prior to Casting of Specimens	85
Figure 3-13 Placing and Vibration of Concrete During Casting of Specimens ...	86
Figure 3-14 Typical Specimen Setup	87
Figure 3-15 Strain Gauge Layout for Slab Specimens	88
Figure 3-16 Strain Gauge Details for Beam Specimens	89
Figure 3-17: Test setup for beam specimen <i>MR1</i>	91
Figure 4-1: Load-Deflection Response at Mid-Span of Slab-Specimens	97
Figure 4-2: Load-Strain Response of Slab-Specimens	99
Figure 4-3: Crack Patterns of Slab Specimens at Failure Loads	101
Figure 4-4: Influence of Member Effective Depth and Longitudinal Reinforcement Ratio on Shear Stress at Failure	103
Figure 4-5: Load-deflection Response at Mid-Span of Beam-Specimens	107
Figure 4-6: Load-Longitudinal Steel Response of Beam-Specimens	111
Figure 4-7: Load-Transverse Steel Response of Beam-Specimens	114

Figure 4-8: Crack Patterns at Failure Loads for Beam Specimens with ASTM A1035 Longitudinal Reinforcement ($h = 1000$ mm)	116
Figure 4-9: Service Crack Patterns of Beam-Specimens with Conventional Longitudinal and ASTM A1035 Transverse Reinforcement. ($h = 600$ mm)	117
Figure 4-10: Service Crack Patterns of Beam-Specimens with ASTM A1035 Longitudinal and Conventional Transverse Reinforcement. ($h = 1000$ mm)	118
Figure 4-11: Service Crack Patterns of Beam-Specimens with ASTM A1035 Longitudinal and Transverse Reinforcement. ($h = 1000$ mm)	118
Figure 4-12: Influence on Normalized Shear Stress at Failure from (a) Stirrup Spacing (b) Equivalent Stirrup Ratio and (c) Longitudinal Reinforcement Ratio	123
Figure 5-1: Flowchart for the Proposed General Shear Model of Concrete Slabs	130
Figure 5-2: Validation of the General Shear Model for Size Effect and Strain Effect	135
Figure 5-3: Validation of the Design Shear Model for Size Effect and Strain Effect	138
Figure 5-4: Flexural and Shear capacity of members with different longitudinal reinforcement	141
Figure 5-5: Validation of the Analytical Shear Models for Size Effect	146
Figure 5-6: Typical <i>VecTor 2</i> (VT2) Slab Model	148
Figure 5-7: Typical <i>Response 2000</i> Slab Model	148
Figure 5-8: Validation of the Numerical Shear Models for Size Effect	150
Figure 6-1: Flowchart for The Proposed General Beam Shear Model	158
Figure 6-2: Influence of Longitudinal Reinforcement Ratio on General Shear Model... ..	167
Figure 6-3: Influence of Longitudinal Reinforcement Ratio on Design Shear Model.... ..	171

Figure 6-4: Influence of Longitudinal Reinforcement Ratio on Flexural and Shear Capacity of Beam Specimens	174
Figure 6-5: Influence of Longitudinal Reinforcement Ratio on Shear Prediction	182
Figure 6-6: Influence of Transverse Reinforcement Ratio on Shear Prediction..	184
Figure 6-7: Influence of Member Depth on Shear Prediction	185
Figure 6-8: Influence of Concrete Strength on Shear Prediction	186
Figure 7-1: Discrepancy Between Bernoulli Deflection and Measured Deflection	193
Figure 7-2: Considerations in The General Deflection Model	199
Figure 7-3: Calculated Bending Load-Deflection Response of Beam-MM4 at Different Load Levels	200
Figure 7-4: Flowchart Showing the Prediction of Relationship Between Shear Strain and Member Strain	201
Figure 7-5: Typical Longitudinal Member Strain and Shear Strain Relationship	202
Figure 7-6: Prediction of Total Deflection Using The General Deflection Model for Beam-MM4	204
Figure 7-7: Influence of Design Parameters on The General Deflection Model.	211
Figure 7-8: Correction Factors for Shear Deformation	212
Figure 7-9: Influence of Reinforcement Ratios on The General Deflection Equation	215
Figure 7-10: Validation of Proposed General and Simplified Deflection Equations	219
Figure 7-11: Load-Deflection Response of Representative Beams with Conventional Steel Reinforcement	228
Figure 7-12: Load-Deflection Response of Beams with ASTM A1035 Steel Tested in the Current Study	231
Figure 7-13: Influence of High Strength or ASTM A1035 Steel Transverse Reinforcement Ratio on Model Deflection Prediction	235

Figure 7-14: Influence of Conventional Steel Transverse Reinforcement Ratio on Model Deflection Prediction	236
Figure 7-15: Influence of High Strength or ASTM A1035 Steel Longitudinal Reinforcement Ratio on Model Deflection Prediction	237
Figure 7-16: Influence of Conventional Steel Longitudinal Reinforcement Ratio on Model Deflection Prediction	238
Figure 7-17: Influence of Member Depth on Model Deflection Prediction (High Strength or ASTM A1035 Steel Reinforced Beams)	240
Figure 7-18: Influence of Member Depth on Model Deflection Prediction (Conventionally Reinforced Beams)	241
Figure 7-19: Influence of Shear Span to Depth Ratio on Model Deflection Prediction (High Strength or ASTM A1035 Steel Reinforced Beams)	242
Figure 7-20: Influence of Shear Span to Depth Ratio on Model Deflection Prediction (Conventionally Reinforced Beams)	243

LIST OF NOTATIONS

$A, B \text{ \& } C$	Ramburg-Osgood parameters;
A_c, A_g	Gross area of concrete cross-section;
A_s, A_{sx}	Longitudinal reinforcement area;
A_v	Transverse reinforcement area;
$A_{v,min}$	Minimum area of shear reinforcement;
a	Shear span;
a/d	Shear-span to depth ratio;
a_g	Aggregate size;
b_w	Member width;
c_v	Maximum distance from the transverse reinforcement;
c_x	Maximum distance from the longitudinal reinforcement;
d	Effective depth of flexural tension reinforcement;
d_b, d_{bx}	Diameter of the longitudinal reinforcement;
d_{bv}	Diameter of the transverse reinforcement;
d_v	Effective shear depth ($= 0.9d$);
E_c	Secant stiffness of concrete;
E_s	Young's Modulus of steel reinforcement;
F_{lt}	Force capacity in the longitudinal reinforcement of a concrete member without axial load;
f_c'	Concrete compressive strength from cylinders;
f_{ck}	Characteristic compressive strength of concrete;
f_{cr}	Cracking stress in the concrete;
f_r	Modulus of rupture of concrete;
f_s	Stress in steel reinforcement;
f_{yL}	Yield strength of longitudinal reinforcement;
f_{yt}	Yield strength of transverse reinforcement;
f_u	Ultimate tensile strength of the bars;
f_v	Stress in the transverse reinforcement;
f_{vy}	Yield stress in the transverse reinforcement;

f_1	Principal tensile stress in the concrete;
f_2	Principal compressive stress in the concrete;
f_{2max}	Peak diagonal compressive stress;
h	Overall member height;
I_{cr}	Cracked, transformed moment of inertia;
I_e	Bischoff's effective moment of inertia;
I_{eb}	Branson's effective moment of inertia;
I_g	Gross moment of inertia;
K	Deflection coefficient based on static system;
k	Coefficient, for solving cracked section dimensions;
k_l	A coefficient that characterizes the bond properties of reinforcement bars ($k_l = 0.4$ for deformed bars);
L	Span length;
M, M_n	Nominal bending moment;
M_a	Maximum service moment;
M_{cr}	Cracking moment;
M_f	Factored bending moment;
n	Modular ratio;
P	Load carrying capacity for concrete members;
P_M	Load carrying capacity for flexure-critical concrete members;
P_S	Service load (load at 60% of the failure load);
P_V	Load carrying capacity for shear-critical concrete members;
S	The spacing between the transverse reinforcement;
s_{mx}	Crack spacing characteristics of the longitudinal reinforcement;
s_{mv}	Crack spacing characteristics of the transverse reinforcement;
$s_{m\theta}$	The spacing of inclined cracks;
S_r	Equivalent stirrup ratio;
s_x	The spacing between the longitudinal reinforcement;
S_{ze}	Effective crack spacing parameter;
T	Tensile force in the longitudinal steel;
V, V_n	Nominal shear force;

V_a	Vertical shear force component of the aggregate interlock;
V_c	The 'concrete contribution' to shear resistance;
$V_{C, ACI}$	Concrete contribution of members from the <i>ACI318-11</i> model;
$V_{C, ACIITG-6R-10}$	Concrete contribution of members from the <i>ACIITG-6R-10</i> model;
V_{CDB}	Concrete contribution of the design shear model for beams;
V_{CGB}	Concrete contribution of the general shear model for beams;
$V_{CDB, CSA}$	Concrete contribution of the <i>CSA A23.3-04</i> simplified shear model for beams;
$V_{C, CSA}$	Concrete contribution of concrete members from the <i>CSA A23.3-04</i> model;
$V_{C, EC2}$	Concrete contribution of concrete members from the <i>Eurocode2-04</i> model;
$V_{C,H}$	Shear force capacity from <i>Hoult et al.</i> model;
V_{cu}	Shear in the uncracked compression zone;
V_{DB}	Design shear model for beams containing ASTM A1035 steel;
V_{DS}	Design shear model for slabs containing ASTM A1035 steel;
V_d	Vertical shear force in the longitudinal steel due to dowel action;
V_f	Factored shear force;
V_{GB}	General shear model for beams containing ASTM A1035 steel;
V_{GS}	General shear model for slabs containing ASTM A1035 steel;
V_n	Nominal shear force at failure;
$V_{n, ACI}$	Nominal shear capacity of concrete members from the <i>ACI318-11</i> model;
$V_{n, CSA}$	Nominal shear capacity of concrete members from the <i>CSA A23.3-04</i> model;
$V_{n, EC2}$	Nominal shear capacity of concrete members from the <i>Eurocode2-04</i> model;
V_S	The steel contribution to shear resistance;
$V_{S, ACI}$	Steel contribution of concrete beams from the <i>ACI318-11</i> model;
$V_{S, CSA}$	Steel contribution of concrete members from the <i>CSA A23.3-04</i> model;

$V_{S, EC2}$	Steel contribution of concrete members from the <i>Eurocode2-04</i> model;
V_{SDB}	Steel contribution of the design shear model for beams;
$V_{SDB, CSA}$	Steel contribution of the <i>CSA A23.3-04</i> simplified shear model for beams;
V_{SGB}	Steel contribution of the general shear model for beams;
w	Concrete crack width;
y_t	Distance from centroid to flexural tension face;
α_1	Factor accounting for bond characteristics of the reinforcement; ($\alpha_1 = 1.0$ for deformed bars)
α_2	Factor accounting for the type of loading; ($\alpha_2 = 1.0$ for short-term monotonic loading)
β	A parameter representing the ability of a cracked concrete member to resist aggregate interlock stresses;
Δ_B	Bending deflection;
Δ_{GDE}	General design equation for deflection;
Δ_{GEN}	General analytical deflection model;
Δ_{ITG-6}	Bending deflection based on the <i>ACHITG-6R-10</i> model;
Δ_i	Instantaneous deflection;
Δ_{SDE}	Simplified design equation for deflection;
Δ_{st}	Shear deflection;
ΔT	Change in tensile force in the longitudinal steel;
Δ_{TEST}	Service deflection (deflection corresponding to service load P_S);
ε'_c	Compressive strain at peak compressive stress;
ε_s	Strain in steel reinforcement;
ε_t	Strain in the transverse reinforcement;
ε_x	Axial strain parameter for shear capacity;
ε_y	Yield strain of longitudinal reinforcement;
ε_1	Principal tensile strain in the concrete;
ε_2	Principal compressive strain in the concrete;
γ	Shear strain at a cross section;

γ_{cr}	Normalized cracking stress parameter;
v_a	Horizontal component of the aggregate interlock stress;
v_{ci}	Concrete shear stress on the crack surface;
v_n	Normalized shear stress at failure;
ν_1	Strength reduction factor for concrete cracked in shear;
ρ'	Longitudinal compression reinforcement ratio;
ρ_L, ρ_x	Longitudinal tension reinforcement ratio;
ρ_b, ρ_v	Transverse reinforcement ratio;
θ	The inclination of the crack from the longitudinal direction;

LIST OF ABBREVIATIONS

AHSS	Advanced High Strength Steel
CFT	Compression Field Theory
COV	Coefficient of variation
DIC	Digital Image Correlation
LVDT	Linear Variable Displacement Transducers
MCFT	Modified Compression Field Theory
NCHRP	National Cooperative Highway Research Program
RC	Reinforced Concrete
R2K	Response 2000
SLS	Serviceability Limit State
UHSS	Ultra High Strength Steel
ULS	Ultimate Limit State
VT2	VecTor2

1. INTRODUCTION

1.1 Motivation

The behaviour of reinforced concrete members with conventional steel reinforcement has been studied for decades. Methods for the design and analysis of these members are incorporated in standards (*ACI 318-11*, *CSA A23.3-04* and *Eurocode 2-04*) with models established based on theoretical and empirical considerations. However these design and analysis models need to be re-evaluated as new reinforcing materials are introduced into the concrete construction industry.

One of the major problems facing the engineering industry today is the corrosion of conventional steel reinforcement and the inherent structural weaknesses it causes on structural members. Congestion of reinforcement bars at beam-slab or beam-column joints is also another major problem that reduces the constructability of structures.

Steel bars manufactured to conform to the ASTM A1035-11 standard have different metallurgy and microstructure than conventional ASTM A615 (Grade 420 or 520 MPa) or ASTM A706 (420 MPa) reinforcing commonly used in most new construction in North America (*ASTM A1035-11* (2011)). ASTM A1035 steel has improved corrosion resistance (*Darwin et al. 2009* and *El-Hacha et al. 2002*) and can have breaking strengths up to three times that of the conventional Grade 420 reinforcing steel. ASTM A1035 reinforcing steel is commercially available as Grades 690 and 830 MPa (100 and 120 ksi). Thus in many applications, the higher strength of ASTM A1035 steel could allow for reductions in the required steel quantities compared to members reinforced with conventional steel.

High-performance ASTM A1035 steel exhibits a non-linear stress-strain response beyond the proportional limit. There is no well defined yield point or yield plateau in the stress-strain response of this material (*ACI ITG-6R-10*). Existing design code requirements for buildings or bridges (*e.g. ACI 318-11, CSA A23.3-04 and CSA S6-06*) restrict the maximum yield strength for design to values below the available strength of ASTM A1035 steel. As a result ASTM A1035 steel reinforcement has mainly been used by direct substitution for conventional steel at the same quantity, neglecting possible material savings from the available higher yield strength. To efficiently use the advantage of the available higher strength of ASTM A1035 steel, design and analysis models must be developed with due consideration to the actual material properties and stress-strain response of the material.

Prior research (*e.g. El-Hacha and Rizkalla 2002*) has established the material characteristics of ASTM A1035 steel. Sectional design models for flexure have been established based on simple analysis techniques that satisfy fundamental principles of equilibrium and compatibility (*Mast et al. 2008*). However, sectional shear models that consider the actual stress-strain behaviour of ASTM A1035 steel have not been previously developed. Furthermore, only limited prior research has examined the applicability of existing sectional shear design models for concrete members longitudinally reinforced with ASTM A1035 steel (*e.g. Hassan et al. 2008, Shahrooz. et al. (NCHRP 679, 2011)*). Only a limited range of design parameters known to influence shear behaviour were considered in this earlier work, such as transverse reinforcement ratio, member depth and shear-span to depth ratio. Few laboratory test results on concrete beams with limited range of design parameters indicate that ASTM A1035 steel can be efficiently used as shear reinforcement using existing design models (*Sumpter et al. 2009 and Munikrishna et al. 2011*).

The above conditions, coupled with the unique material characteristics of ASTM A1035 reinforcing steel, necessitates further study on the shear behaviour of

concrete members containing ASTM A1035 steel. Furthermore the applicability of current code shear models for the efficient design of concrete members containing ASTM A1035 steel longitudinal and transverse reinforcement needs to be validated with more test data considering a wider range of design parameters. Thus, it was determined that additional analytical, numerical and experimental studies were required to develop enhanced analysis and design models that could lead to more efficient use of ASTM A1035 steel.

The use of high strength steel, which results in lower longitudinal and transverse reinforcement ratios, can result in increased deflections and cracking for slender reinforced concrete beams with stirrups due to shear deformations. Such members usually exhibit greater deflection at service loads than predicted using the *ACI 318-11* deflection model which is based on the Navier-Bernoulli theory (*Bischoff et al.* 2005, *Ramsay et al.* 1979). Thus, the need for more accurate deflection calculation procedures that directly consider the shear deformations and the properties of ASTM A1035 steel is apparent.

The main objective of this research is to understand the shear behaviour of reinforced concrete members constructed with high performance ASTM A1035 steel. This includes development of general analytical and design-oriented models for predicting the shear and deflection response of reinforced concrete slabs and beams that are compatible with previously established flexural models. Recommendations for design code provisions that allow more efficient design of concrete members reinforced with high performance ASTM A1035 steel are proposed.

1.2 Research Significance

The use of high-performance ASTM A1035 steel in concrete members can lead to potential savings in the life-cycle costs of reinforced concrete structures. Compared to conventional reinforcing steel grades, the required steel quantity can

be reduced due to its higher strength and the overall member durability can be improved due to its enhanced corrosion resistance. This research presents the experimental investigation of sixteen large-scale shear-critical members reinforced with ASTM A1035 steel. New test data is presented for members with (i.e. beams) and without (i.e. slabs) shear reinforcement, including those showing non-linear response of the longitudinal steel prior to brittle shear failure. The test result, along with others from literature were used to develop and validate shear capacity and member deformation models.

It is known that the shear behaviour of slabs and beams is different. The presence of transverse reinforcement alters the straining and cracking pattern of beam specimens typically leading to more gradual and ductile behaviour compared to the brittle failure of shear-critical slab specimens. Thus the influence of the ASTM A1035 steel reinforcement on shear behaviour should be studied separately for the two member types and hence both slabs and beams were considered in this study.

The experimental program included testing to failure of six one-way slab strips longitudinally reinforced with ASTM A1035 steel and ten slender beams reinforced with either ASTM A1035 or conventional steel. Two of the ten beams were reinforced with conventional steel longitudinal reinforcement and ASTM A1035 steel transverse reinforcement. The remaining eight beams had longitudinal ASTM A1035 steel reinforcement and either conventional or ASTM A1035 steel transverse reinforcement. All specimens were designed as shear-critical and tested under three-point bending.

General shear capacity models were developed and validated for members with and without shear reinforcement. Simplified shear capacity models were also developed for use in designs completed with the simplified flexural model developed by *Mast et al.* (2008). These shear capacity models were developed

based on earlier design models derived from the Modified Compression Field Theory (MCFT) (*Vecchio and Collins, 1986*) with additional modifications to account for the actual stress-strain response of the ASTM A1035 steel. Existing analytical and numerical models were also used to predict the shear capacity of the specimens, including the code provisions of *ACI 318-11*, *CSA A23.3-04* and *Eurocode 2-04* and finite element programs *VecTor2* and *Response 2000*. Predicted load capacities using the various models were compared against measured values obtained from the laboratory tests. The quality of predictions of the proposed general and simplified shear models were assessed by comparing the test to model ratios to the other analytical and numerical models.

A new MCFT-based sectional analytical approach was developed to predict the load-deformation behaviour of reinforced concrete beams containing transverse reinforcement. The model uses a composition approach for both flexural and shear deformations that can be applicable to beams longitudinally and transversely reinforced with either conventional or ASTM A1035 steel. The model was validated using measured service load deflections from the new tests and other data from the literature. Deflection predictions using the direct deflection calculation from *ACI ITG-6* model were also compared with measured service deflections. The *Response 2000 (R2K)* and *VecTor2 (VT2)* numerical models, which both take into account shear deformations, were also considered. Based on parametric studies, simplified deflection equations were developed for the beam specimens containing ASTM A1035 steel reinforcement. The quality of predictions of the simplified deflection equations were assessed by comparing the test to model service deflection ratios to the other models.

1.3 Organization

This document comprises eight chapters discussing the research project on the shear and deflection behaviour of slender concrete members reinforced with high-

performance ASTM A1035 steel. Figure 1-1 shows the organizational structure with the main contents of this report.

The first chapter provides the motivation, objectives and research significance of the work accomplished in this research project.

Chapter 2 contains background information on previous research pertaining to the use of high-performance ASTM A1035 reinforcing steel in reinforced concrete one-way slabs and beams. A discussion on the flexural, shear and deflection behaviour is included. Existing analytical and numerical modeling approaches for concrete members containing ASTM A1035 steel reinforcement are also described.

The laboratory test program carried out during the project is presented in Chapter 3. The specimen configurations, instrumentation and test set up are described. The various material properties used in this research program are also provided in this chapter.

Chapter 4 discusses the experimental results using the data obtained during each test, which is presented using tables, graphs and figures. This information includes load-deflection and load-steel strain behaviour, failure mode and the crack patterns for each of the specimens. General trends about the influence of design parameters on member performance are discussed.

Modeling the shear capacity of slab specimens is presented in Chapter 5. Proposed general and simplified shear design models for concrete slabs with longitudinal ASTM A1035 steel reinforcement are developed. Comparisons between test results and model predictions of slab specimens are also presented. The influence of member depth and reinforcement ratio on shear capacity was studied for the new tests in the current study.

In Chapter 6, general and simplified shear design models for beams containing ASTM A1035 steel reinforcement are developed and validated. Comparisons between test results and analytical and numerical model predictions are also presented using the new and published test data. The influence on shear capacity from the main beam design parameters is investigated.

Chapter 7 presents the development of a general deflection model based on the Modified Compression Field Theory (MCFT). Comparisons of beam service deflections using models from the *ACI ITG-6R-10* provision and from two numerical models are included. The results of parametric studies conducted to develop and validate simplified deflection equations for calculation of service beam deflections are also presented.

Conclusions drawn from the analytical and experimental studies and recommendations for future research are presented in Chapter 8.

Appendix A contains a summary of significant test results for all specimens obtained from data acquisition and Digital Image Correlation (DIC) systems. The results of the sectional shear analytical models described in Chapter 2 are included in Appendix B. Appendix C describes the steps followed in the prediction of the load deflection response of beams containing ASTM A1035 steel using the general deflection model. It also shows the results of the load deflection relationships of the beam specimens from the general analytical deflection model.

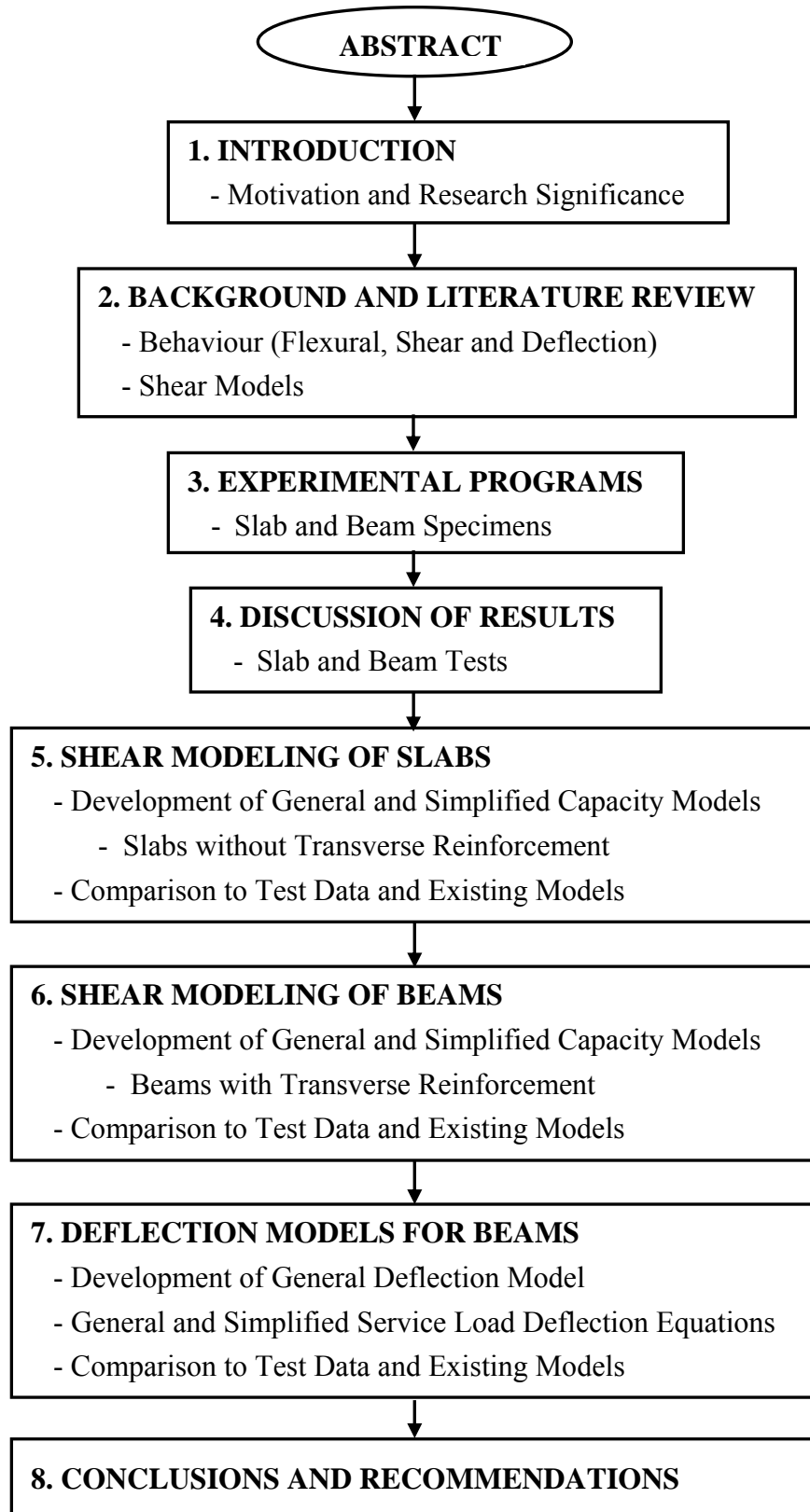


Figure 1-1: Flow Chart Showing the Organizational Structure of the Report

2. BACKGROUND AND LITERATURE REVIEW

This chapter presents the background information and literature review for previous research on the shear and deflection behaviour of slender reinforced concrete slabs and beams containing ASTM A1035 steel. Analytical modeling techniques from current codes of practice pertaining to flexure and shear design of steel-reinforced concrete members as well as service load deflections are described. Finally, numerical modeling of shear and deflection behaviour of concrete members using two finite element techniques is presented.

2.1 General

High performance ASTM A1035 steel reinforcement has increasingly been used in concrete members due to its higher yield strength and improved corrosion resistance in comparison with conventional reinforcing steel (*Darwin et al.* 2009 and *El-Hacha et al.* 2002). The higher yield strength of ASTM A1035 steel can be useful to reduce the quantity of reinforcement required, thereby reducing reinforcement congestion at beam-slab and beam-column joints, increasing the speed of construction and improving durability of structures. The improved corrosion resistance of ASTM A1035 steel compared to conventional reinforcing steels makes it well suited for use as reinforcement in concrete structures in aggressive environments including foundations, bridges, buildings and offshore structures (*ACI ITG-6R-10*).

Figure 2-1 depicts the typical stress-strain response for conventional Grade 420 steel and ASTM A1035 Grade 690 steel reinforcement bars obtained through coupon testing in this research program. The stress-strain response of ASTM A1035 steel and commonly used conventional steel (A615 Grade 420) are similar for values only up to the yield point of the conventional steel after which the responses are significantly different. (See Figure 2-1) The difference is mainly

due to the non linear stress-strain response of ASTM A1035 steel after the proportional limit of approximately 480 MPa, and the lack of a well defined yield point and corresponding yield plateau. The effective yield stress of ASTM A1035 Grade 690 MPa steel, estimated using the 0.2 % offset method, is typically close to 830 MPa or nearly twice that of the conventional steel. The corresponding yield strains in ASTM A1035 using the 0.2% offset method (0.006) are about three times the yield strains of conventional reinforcing steel (*ACI ITG-6R-10*). For the ASTM A1035 steel coupon tests completed and the average measured breaking strengths were 1050 MPa. The corresponding measured strain at failure of ASTM A1035 steel was 0.06 mm/mm as shown in Figure 2-1.

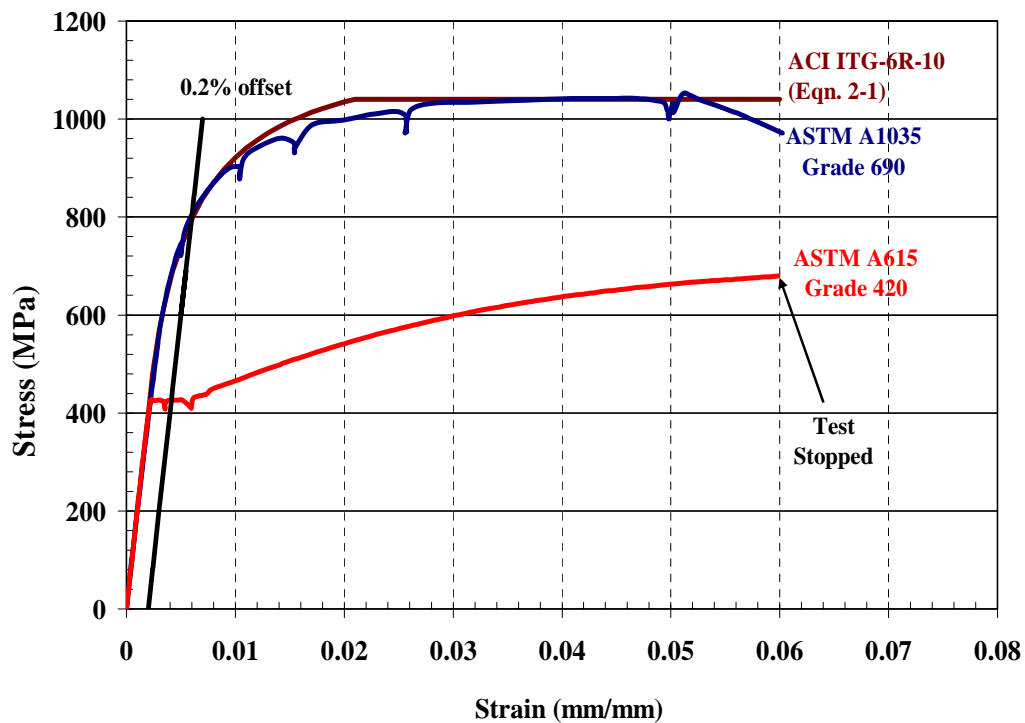


Figure 2-1: Typical Stress-Strain Response for ASTM A1035 and ASTM A615 Steel from Coupon Testing.

ACI ITG-6R-10 recommends a stress-strain relationship for design using ASTM A1035 Grade 690 steel that consists of linear, non linear and constant equations as given in equation 2-1.

$$f_s = \begin{cases} 200,000 \varepsilon_s & \text{for } \varepsilon_s \leq 0.0024 \\ 1170 - \frac{2.96}{\varepsilon_s + 0.0019} & \text{for } 0.0024 < \varepsilon_s \leq 0.02 \\ 1040 & \text{for } 0.02 < \varepsilon_s \leq 0.06 \end{cases} \quad (2-1)$$

Figure 2-1 compares the coupon test results of ASTM A1035 steel with equation 2-1. Equation 2-1 is in good agreement with the test results and is adopted for use in all analytical models in this study. Note that approximations to this stress-strain response are used in numerical models due to software limitations.

Current design code provisions typically limit the maximum permitted design stress for the reinforcement in reinforced concrete structures. (See Table 2-1) The code provisions are typically based on research completed on concrete members reinforced with conventional steel reinforcement. The strength limitations in Table 2-1 prevent the use of the full available strength of ASTM A1035 steel thereby neglecting the material saving benefits which could be obtained from the higher effective yield strength. Among the provisions is the *ACI ITG-6R-10* design guide for the use of ASTM A1035 Grade 690 steel bars for structural concrete, which was developed in parallel to, and incorporating preliminary results from, the research described in this study. *ACI ITG-6R-10* normally limits the maximum yield stress of ASTM A1035 steel bars at ULS to a value of 690 MPa unless more complex flexural analysis methods are used that directly consider the stress-strain response of the reinforcement, explained in *ACI ITG-6R-10* Appendix B. *ACI ITG-6R-10* does not provide explicit shear design methods if Appendix B is used for the flexural design, an area addressed by this study.

Table 2-1: Reinforcing Steel Design Stress Limits in Some Concrete Codes.

<i>Design Code</i>	<i>ULS</i>		<i>SLS</i>
	<i>Maximum Design Longitudinal Stress</i> f_{yL} (MPa)	<i>Maximum Design Transverse Stress</i> f_{yT} (MPa)	<i>Typical Maximum Longitudinal Stress</i> $0.67f_{yL}$ (MPa)
<i>ACI 318-11</i>	552	414	367
<i>ACI ITG-6R-10</i>	690*	550	460
<i>CSA A23.3-04</i>	500	500	333
<i>CSA S6-06</i>	525	525	350
<i>Eurocode 2-04</i>	600	600	400
<i>AASHTO LRFD - 07</i>	520	520	347

* This value can be exceeded using the *ACI ITG-6R-10* Appendix B method.

2.2 Mechanics of Shear for Reinforced Concrete

2.2.1 General

The axial and flexural behaviour of slender reinforced concrete members subjected to transverse loading is generally accepted to follow the well-known principles of Engineering Beam Theory - plane sections before bending remain plane after bending. This simple, general and accurate theory - the so-called Navier-Bernoulli theory - allows engineers to design structural members with confidence even when faced with new materials.

On the other hand, behaviour of reinforced concrete members in shear is a significantly more complex problem involving many variables. In contrast to the - general agreement that exists for flexural design methods for reinforced concrete members, the mechanisms of shear resistance and the corresponding design provisions have not reached international consensus. In some standards, (e.g. *ACI 318-11*) purely empirical methods are employed for shear design of slender concrete members. Other design standards (e.g. *CSA A23.3-04*) use methods that

are derived from mechanical models but include various simplifying assumptions. Among the shortcomings of the standards which are based on empirical or semi-empirical approaches are the lack of a clear model that can be extrapolated to cases not directly covered in the model development and the many equations and rules required for special cases. The unique material characteristics of ASTM A1035 reinforcing steel, which significantly differs from the conventional steel, necessitates further study on the shear and deflection behaviour of concrete members containing this material. Furthermore, for efficient use of ASTM A1035 steel reinforcement in concrete members, the applicability of current code shear models must be validated with more test data.

2.2.2 Slender and Deep Members

The shear span to depth ratio (a/d) of concrete members has a major impact on their shear capacity as shown in Figure 2-2. In most shear design models, the shear behaviour of steel reinforced concrete members show significant changes near a/d ratio of 2.5, which affects the shear transfer mechanism and failure modes (*Kani 1966, Wight and MacGregor 2009*). Reinforced concrete members having a/d ratio less than 2.5 transfer shear by direct struts from the load to the supports (i.e. arch action) and are commonly referred to as deep members. These members are typically analyzed by strut and tie models. Members having a/d greater than 2.5, which are termed as slender members, are characterized by smeared force transfer in cracked concrete and are treated by sectional models. Slender members transfer shear by a combination of stresses in the transverse reinforcement, if provided, ('steel contribution') and stresses in the uncracked and in the cracked concrete section ('concrete contribution'). The focus of the current research program is the shear and deflection behaviour of slender ($a/d > 2.5$) reinforced concrete members with ASTM A1035 steel.

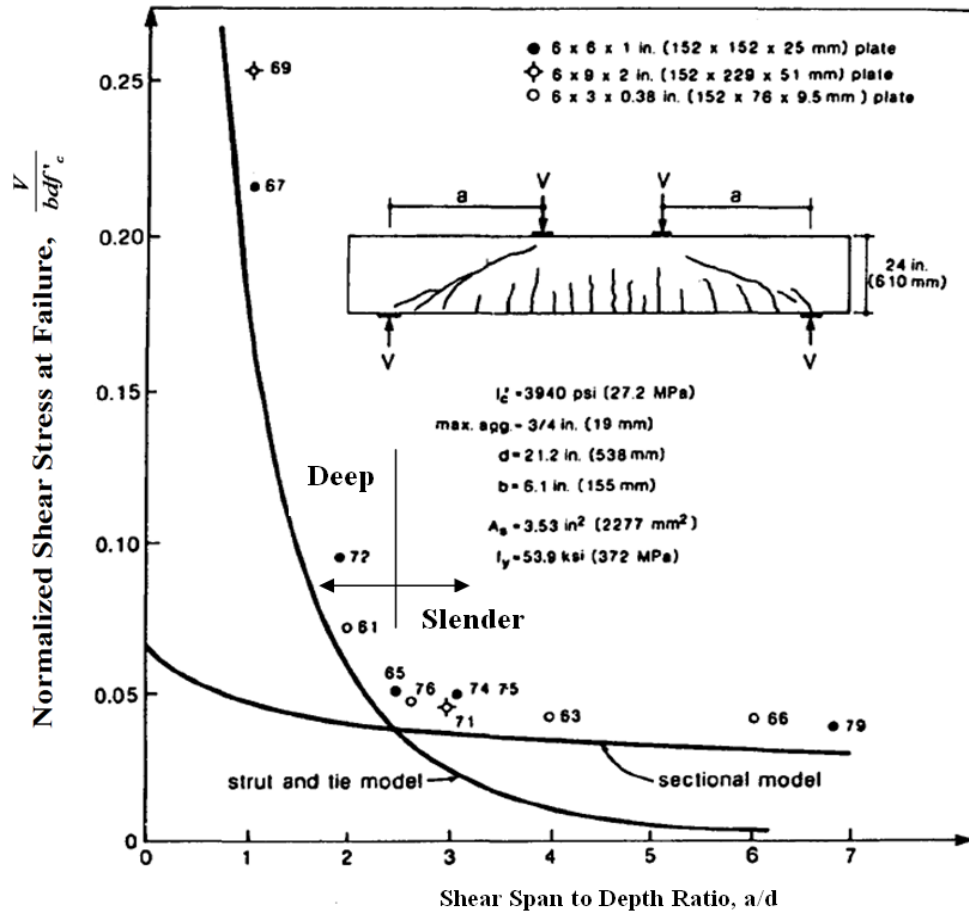


Figure 2-2: Classifying Shear Behaviour as Deep Members and Slender Members (Adapted from *Collins and Mitchell*, 1997).

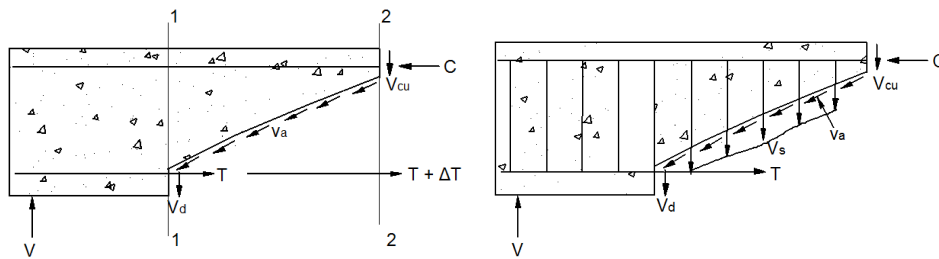
2.2.3 Shear Behaviour of Slender Reinforced Concrete Members

A slender reinforced concrete member subjected to shear will exhibit diagonal cracking by which the mechanisms that transfer shear forces across the diagonally cracked region is illustrated in the free-body diagrams in Figure 2-3. For members without transverse reinforcement (i.e. slabs) the vertical shear at the critical section is transferred by a combination of shear in the uncracked compression zone, V_{cu} , vertical force in the longitudinal steel due to dowel action, V_d , and the vertical component of the aggregate interlock, V_a , along the surface of the crack (*ASCE-ACI 426* (1973)). These three components are combined to form what is commonly referred to as 'the concrete contribution' to shear resistance, V_c . (See

Figure 2-3a). The relative proportions of the components of the concrete contribution acting at a concrete section have been the subject of research in the past. Factors which can affect the components of the concrete contribution and their relative proportions include: the depth of the compression zone, span-to-depth ratio, crack width, crack roughness, transverse and longitudinal reinforcement configurations, cover thickness, concrete strength, among others (*Fenwick and Paulay (1964, 1968), Taylor (1970), Kani et al. (1979)*)).

For members with transverse reinforcement (i.e. beams) the three components of the concrete contribution act in addition to the force transfer provided by the stirrups, V_s , which is commonly termed as ‘the steel contribution’ to shear resistance (Figure 2-3b). Note that in deriving the steel contribution, it is typically assumed that the stirrups are yielding at the time of failure.

A close examination of Figure 2-3a shows that the change in stress in the longitudinal steel reinforcement between sections 1-1 and 2-2 is balanced by the horizontal component of the aggregate interlock stresses along the crack. (i.e. the horizontal component of the aggregate interlock stress, v_a , is resisted by an increased tensile force ΔT in the longitudinal steel). This suggests that shear locally increases tensile stress in the longitudinal reinforcement ($T + \Delta T$) as shown in Figure 2-3a.



a) Member without stirrups

b) Member with stirrups

Figure 2-3: Shear Resisting Mechanisms in Reinforced Concrete Slabs and Beams.

2.2.4 Aggregate Interlock

Previous research on the shear response of concrete members without transverse reinforcement revealed that aggregate interlock has a significant role in shear behaviour (*Fenwick and Paulay* (1964, 1968), *Taylor* (1970), *Kani et al.* (1979), *Sherwood* (2008)). These researchers indicated that shear stresses had to be transferred across cracks by aggregate interlock action in order to maintain both vertical and longitudinal equilibrium of cracked sections.

Through direct measurements on cracked beams, *Fenwick and Paulay* (1968) concluded that 60% - 75% of the vertical shear is carried by aggregate interlock across the diagonal cracks. They also suggested that the dowel action carries not more than 20% of the vertical shear and the remaining portion is carried in the compression zone.

Taylor's work (*Taylor* 1970) supported the previous research by *Fenwick and Paulay* (1968) that shear force carried by concrete members is not just confined to the compression zone. He found that 33 - 50% of the vertical shear at the critical section was transferred by aggregate interlock action, 20 - 40% in the compression zone, and 15 - 25% by dowel action. He also suggested that near failure, force transfer by dowel action breaks down, with shear transferred to the aggregate interlock mechanism. Member failure was attributed to breakdown in aggregate interlock mechanism. *Taylor* identified that the aggregate interlock capacity and shear strength were influenced by the aggregate quality and the concrete strength in relation to the aggregate strength. *Taylor* concluded that the size effect in shear is attributed to reduced aggregate interlock capacity in large members due to lack of scaling of the aggregate size in relation to the member depth, which results in proportionally smoother cracks.

Kani et al. (1979) reported a major study investigating shear transfer mechanisms. A 48 in. deep beam without stirrups was loaded over several months and cycled

repeatedly. The results showed that 17 - 32% of the vertical shear at three adjacent cracks was transferred in the compression zone, with the remainder transferred by aggregate interlock and dowel action. The authors noted that 50 - 60 % of the vertical shear force may be transferred through aggregate interlock.

Sherwood (2008) performed an experimental program on thirty-seven large-scale members with a focus to improve understanding of the behaviour of large, lightly reinforced slabs subjected to shear. Through detailed measurements of flexural and shear stresses in the experimental specimens, *Sherwood* indicated that aggregate interlock is the primary mechanism of shear transfer in slender, lightly-reinforced members without stirrups. *Sherwood* (2008) also studied the so-called size effect in shear by varying two parameters within the test program: the effective depth, d , and the maximum aggregate size, a_g . A series of large, slender beams with an effective depth of 1400 mm with four different aggregate sizes, as well as a series of geometrically similar beams with an effective depth of 280 mm were tested. *Sherwood* found that the shear stress at failure of the large beams was uniformly less than the small beams.

Parameters Influencing Aggregate Interlock

The shear capacity of slender reinforced concrete members is influenced by many parameters including member depth, d , aggregate size, a_g , compressive strength of concrete, f'_c , and the longitudinal reinforcement ratio, ρ_L (*ASCE-ACI Committee 445* (1999)). For slender concrete members the shear span to depth ratio, a/d , has less influence on shear capacity as compared to non-slender members (as shown in Figure 2-2) and hence is ignored in many shear models. The influence of shear span to depth ratio can be accounted for by using a sectional shear model for slender members that considers the moment to shear ratio (M / V) at the critical section (*ASCE-ACI Committee 445* (1999)).

In simple terms, aggregate interlock capacity is the resistance of a cracked concrete member to transfer shear stresses along the crack, through interlocking of aggregates that provide resistance against slip (shear). The ability of a cracked concrete member to resist aggregate interlock stresses is directly related to the width of the crack and the crack roughness (*Walraven* 1981). As the cracks grow wider, the aggregate interlock resistance decreases and, thus, any condition that increases crack widths is associated with lower aggregate interlock and a decrease in the shear stress at failure.

Consider that a simple estimate of crack width can be obtained using the following equation (*Bentz et al.* 2006):

$$w = \varepsilon \cdot s \quad (2 - 2)$$

where ε is the average member strain and s is the crack spacing, both perpendicular to the crack.

If the crack spacing increases due to member size it can be expected that the shear stress at failure will decrease. This is called the size effect in shear and is an important consideration for members without transverse reinforcement. Similarly, if the average member strain increases due to, say, applied axial tension then the shear stress at failure will decrease. This is called the strain effect in shear and is another important part of the behaviour of members with and without stirrups. Experiments show that these are indeed the two most important aspects influencing shear stress at failure and should be included in any state of the art shear provisions.

Shioya (1989) conducted experimental tests on large scale beams to investigate the influence of member depth and aggregate size on shear strength. Lightly reinforced concrete members containing no transverse reinforcement with depths ranging from 100 mm to 3000 mm were tested under uniformly distributed loads.

As shown in Figure 2-4, *Shioya* found that the shear stress at failure decreased as the member size increased and as the aggregate size decreased. *Shioya* tests confirmed that size effect has significant influence on the shear capacity of concrete members without transverse reinforcement.

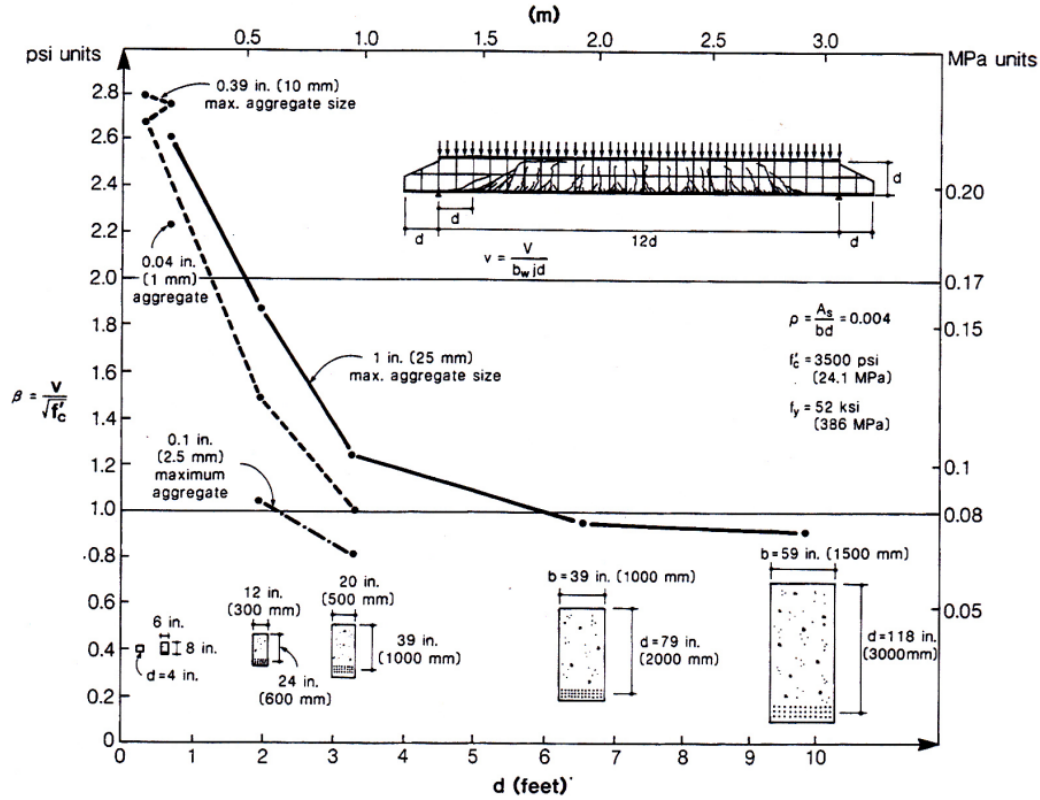


Figure 2-3: Influence of Member Depth and Aggregate Size on Shear Stress at Failure for Tests Carried out by *Shioya* 1989 (*Collins and Mitchell*, 1997).

Stanik (1998) performed a series of tests on shear critical specimens without transverse reinforcement in order to evaluate the influence of the amount, as well as the distribution, of the longitudinal reinforcement on the shear strength. The specimens tested had varying design parameters: depths ranging from 125 mm to 1000 mm, longitudinal reinforcement ratios ranging from 0.76% to 1.31% and concrete strengths, ranging from 37 MPa to 99 MPa. Some specimens contained distributed longitudinal reinforcement along the side faces. Other specimens contained the minimum transverse reinforcement ratio required by *CSA A23.3-94*

for beams. *Stanik* found that the size effect in shear is highly pronounced in lightly reinforced large members. Members containing the minimum amount of transverse reinforcement or side face distributed steel had higher strength than the companion specimens with only longitudinal reinforcing bars at the tension side. The performance of large members with side face distributed reinforcement was nearly the same as the shallow members containing only bottom longitudinal reinforcement. *Stanik* concluded that the size effect in shear is related to parameters reflecting the crack widths and crack spacing rather than the absolute depth of the member. Moreover, *Stanik* observed that very little increase in shear strength was obtained with the use of higher concrete strengths.

It is known that the longitudinal reinforcement configuration will influence the shear behaviour and failure modes of reinforced concrete members (*Rajagopalan and Ferguson 1968, Lubell et al. 2009, Hoult et al. 2008, Mohammed et al. 2009*). Higher reinforcement strains will correspond to higher member axial strains and wider cracks which reduce aggregate interlock capacity (*Walraven 1981*).

Lubell et al. (2009) studied the influence of the longitudinal reinforcement configuration on the one-way shear capacity for members of varying depth, reinforcement ratio, and reinforcement strain at the time of failure. Comparisons were made on the behaviour of geometrically similar members where the longitudinal reinforcement detailing was the main variable. Figure 2-4 shows that lower reinforcement ratios resulted in lower magnitudes of normalized shear stress at failure. Additional influence of member depth was also noted. It was found that shear design models that consider the stress or strain in the longitudinal reinforcement at the time of shear failure provided better correlation with test results compared to those models which incorporated the longitudinal reinforcement ratio parameter without direct consideration of the actual force demands on the reinforcement. The study concluded that the shear capacity of members without shear reinforcement is influenced by both the member depth, and the longitudinal reinforcement details. It was shown that considering these as

two independent actions was a reasonable simplification within one-way shear models.

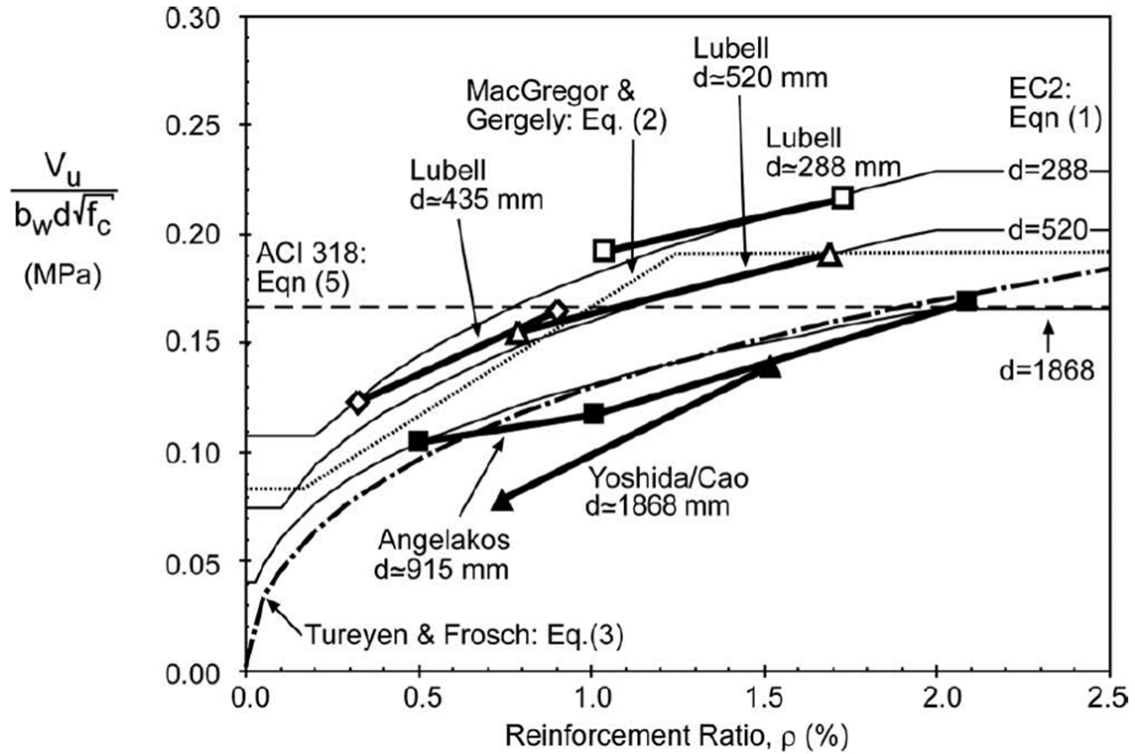


Figure 2-4: The Influence of Longitudinal Reinforcement Ratio on Normalized Shear Stress at Failure (*Lubell et al. 2009*).

An experimental investigation to clarify shear cracking behaviour of reinforced concrete beams with transverse reinforcement was carried out by *Mohamed et al. (2009)* through testing ten simply supported beam specimens with conventional steel. The effects of various influential parameters on the spacing between shear cracks and the relationship between shear crack width and stirrup strain at the cracks were investigated. The parameters considered in this study included the longitudinal reinforcement ratio and stirrup spacing (stirrup ratio). The investigation showed that shear crack widths proportionally increase with the strain of shear reinforcement and with the spacing between shear cracks, implying that the stirrup strain and diagonal crack spacing are main factors including shear

crack displacements. Greater diagonal crack spacings were found in larger beams resulting in wider shear cracks. The results also revealed that the reinforcement configuration including stirrup spacing (stirrup ratio) and the longitudinal reinforcement ratio play critical roles in controlling the diagonal crack spacing and widths. Larger stirrup spacing (or smaller stirrup ratio) resulted in greater shear crack widths at the same stirrup strain due to the increased effective concrete area over which the shear crack width is controlled by each stirrup. It was concluded that increasing the longitudinal reinforcement ratio can better control shear crack opening in the vicinity of longitudinal reinforcement. It was also inferred that larger amounts of longitudinal reinforcement can effectively restrict the widening of flexural cracks and their development into flexure-shear cracks.

2.3 The Modified Compression Field Theory (MCFT)

The early shear design procedures for reinforced concrete developed by *Ritter* (1899) and *Mörsch* (1920) assumed that cracked concrete in the web of a beam resisted shear stress only by diagonal compressive struts and that these struts were inclined at an angle of 45 degrees to the longitudinal axis of the member. Because this approach ignores any contributions of the tensile strength of the concrete, it can give very conservative estimates of shear strength, especially for members with small amounts of stirrups.

During the 1970s and 1980s, researchers focused attention on the fact that, in general, the angle of inclination of the diagonal compressive stresses is not 45 degrees. The development of the Compression Field Theory (CFT) by *Collins and Mitchell* (1978), was a significant step toward a more rational theory for shear. Unlike traditional models, the CFT uses the strain conditions in the web to determine the inclination θ of the diagonal compressive stresses. The angle θ can be considerably less than 45 degrees, which increases the predicted shear strength. Prestressing or axial compression can significantly lower the angle θ and thus

increases shear strength while axial tension increases θ and thus decreases shear strength.

Since the Compression Field Theory was developed by *Collins and Mitchell* (1978), a large amount of research on the stress-strain characteristics of diagonally cracked concrete has been conducted. Experimental studies have been conducted by many researchers typically on reinforced concrete elements subjected to uniform membrane stresses in special purpose testing machines. A summary of the results of many of these studies is given by *Vecchio and Collins* (1993).

The results of experimental studies provided strong evidence that the ability of diagonally cracked concrete to resist compression decreases as the amount of tensile straining increases as summarized by *ASCE-ACI 445* (1999). Figure 2-5 shows the relationship between the normalized maximum concrete compressive stress ($\frac{f_{2max}}{f'_c}$) against principal concrete tensile strain (ϵ_1).

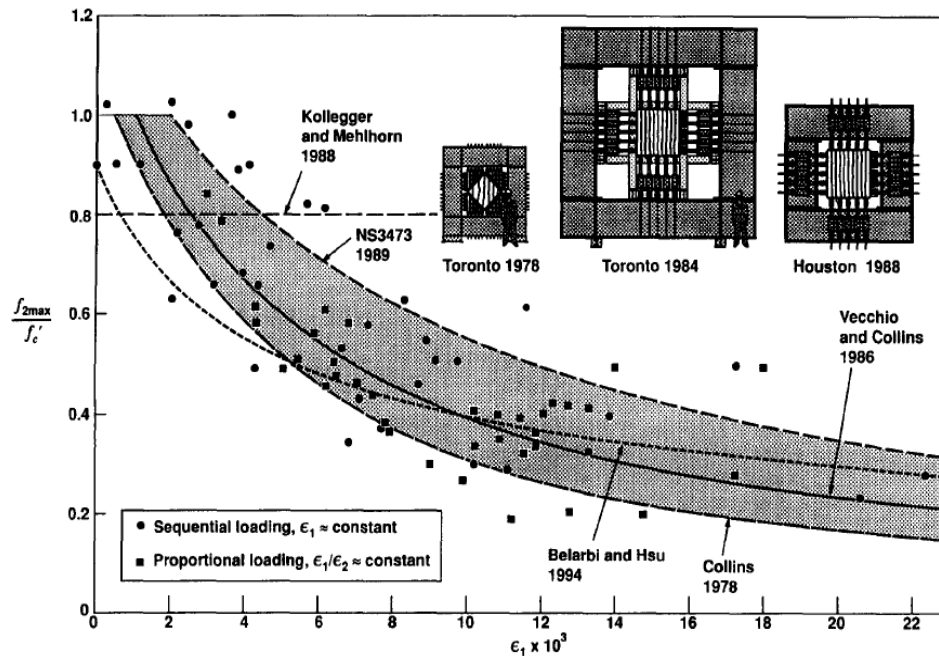


Figure 2-5: Maximum Concrete Compressive Stress as Function of Principal Tensile Strain (*ASCE-ACI 445*, 1999).

To study the relationship between the diagonal compressive stress and the diagonal compressive strain, *Vecchio and Collins* (1986) tested 30 reinforced concrete elements under biaxial stresses in an innovative testing machine. They found that the peak diagonal compressive stress (f_{2max}) is a function not only of the principal compressive strain but also of the coexisting principal tensile strain. They also found that even after extensive diagonal cracking, tensile stresses still existed in the concrete between the cracks. Combined with shear stresses on the crack faces, these tensile stresses increased the ability of the cracked concrete to resist shear. When the CFT relationships were modified to account for the average principal tensile stresses in the cracked concrete, the equilibrium, geometric, and constitutive relationships of the Modified Compression Field Theory (MCFT) were obtained (*Vecchio and Collins* 1986). The MCFT is an analytical model for predicting the response of reinforced concrete elements subject to in-plane normal and shear stresses, by considering the cracked concrete as an orthotropic material with smeared, rotating cracks. It is an accurate but relatively complex analysis method that is able to predict the full load deformation relationships of reinforced concrete panels involving the explicit solution of the equilibrium, constitutive and compatibility equations. Figure 2-6 gives the 15 equations used in the MCFT. Note that, in Figure 2-6, average strains refer to strains measured over base lengths at least equal to the crack spacing and stresses are calculated considering effects both at and between the cracks.

2.4 Shear Design Models

This section presents existing design models commonly used to predict the shear capacity of slender reinforced concrete members with and without transverse reinforcement. Three different analytical code models from current standards (*ACI 318-11*, *Eurocode 2-04* and *CSA A23.3-04*) and two numerical models (*VecTor2* and *Response 2000*) are considered in this study to predict the shear strength of reinforced concrete slabs and beams. The *ACI 318-11* and *Eurocode 2-04* models are based on empirical equations developed from experimental test

results while the *CSA A23.3-04*, *VecTor2* and *Response 2000* rely on solutions using simplifications to the Modified Compression Field Theory.

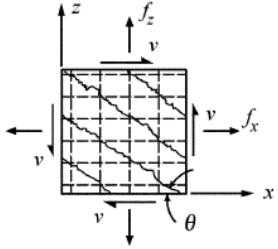
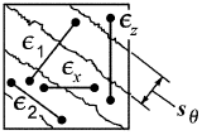
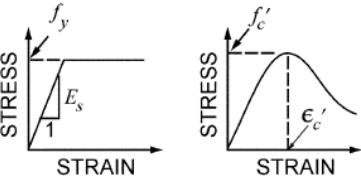
 <p>Equilibrium: Average Stresses:</p> $f_x = \rho_x f_{sx} + f_1 - v \cot \theta \quad (1)$ $f_z = \rho_z f_{sz} + f_1 - v \tan \theta \quad (2)$ $v = (f_1 + f_2) / (\tan \theta + \cot \theta) \quad (3)$ <p>Stresses at Cracks:</p> $f_{sxcr} = (f_x + v \cot \theta + v_{ci} \cot \theta) / \rho_x \quad (4)$ $f_{szcr} = (f_z + v \tan \theta - v_{ci} \tan \theta) / \rho_z \quad (5)$	 <p>Geometric Conditions: Average Strains:</p> $\tan^2 \theta = \frac{\epsilon_x + \epsilon_2}{\epsilon_z + \epsilon_2} \quad (6)$ $\epsilon_1 = \epsilon_x + \epsilon_z + \epsilon_2 \quad (7)$ $\gamma_{xz} = 2 (\epsilon_x + \epsilon_z) \cot \theta \quad (8)$ <p>Crack Widths:</p> $w = s_\theta \epsilon_1 \quad (9)$ $s_\theta = 1 / \left(\frac{\sin \theta}{s_x} + \frac{\cos \theta}{s_z} \right) \quad (10)$	 <p>Stress-Strain Relationships: Reinforcement:</p> $f_{sx} = E_s \epsilon_x \leq f_{yx} \quad (11)$ $f_{sz} = E_s \epsilon_z \leq f_{yz} \quad (12)$ <p>Concrete:</p> $f_2 = \frac{f'_c}{0.8 + 170 \epsilon_1} \left[2 \frac{\epsilon_2}{\epsilon'_c} - \left(\frac{\epsilon_2}{\epsilon'_c} \right)^2 \right] \quad (13)$ $f_1 = 0.33 \sqrt{f'_c} / \left(1 + \sqrt{500 \epsilon_1} \right) \text{ MPa} \quad (14)$ <p>Shear Stress on Crack:</p> $v_{ci} \leq \frac{0.18 \sqrt{f'_c}}{0.31 + \frac{24 w}{a_g + 16}} \text{ MPa, mm} \quad (15)$
--	---	--

Figure 2-6: Equations of Modified Compression Field Theory (*Vecchio and Collins 1986*).

2.4.1 Analytical Models

2.4.1.1 ACI 318-11

The *ACI 318-11* shear capacity model for slender reinforced concrete members uses empirical expressions developed from experimental test results. According to this model, the nominal shear capacity of a concrete member with transverse reinforcement can be determined using the equations:

$$V_{n, ACI} = V_{C, ACI} + V_{S, ACI} \quad (2 - 3)$$

$$V_{C, ACI} = 0.167\sqrt{f'_c}b_w d \quad (2 - 4)$$

$$V_{S, ACI} = \frac{A_v f_{yt} d}{S} \quad (2 - 5)$$

Equation 2-4, termed as the ‘concrete contribution’, is taken as the shear causing significant inclined cracking, and is determined from an average shear stress acting over a cross-section area of $b_w d$. In equation 2-4, it is assumed that there is no variation in the shear stress magnitude due to the design parameters of member depth, longitudinal reinforcement configuration or presence of stirrups. As discussed in Section 2.2.4 these parameters have significant influence on the shear stress at failure. Note that the nominal shear capacity of a concrete member without transverse reinforcement is given by equation 2-4.

For members with transverse reinforcement the nominal shear capacity in the *ACI 318-11* model (equation 2-3) is determined through a compositional approach of a ‘concrete contribution’ (equation 2-4) and a ‘steel contribution’ (equation 2-5). The ‘steel contribution’ term, V_s , is based on an assumed 45° truss model with fully yielding stirrups.

ACI 318-11 requires that, a minimum area of shear reinforcement not less than that given by equation 2-6 is required in order to restrain the growth of inclined cracking and to provide sufficient ductility and warning of failure for reinforced concrete beams.

$$A_{v, \min} = 0.0623\sqrt{f'_c} \frac{b_w S}{f_{yt}} \geq 0.345 \frac{b_w S}{f_{yt}} \quad (2 - 6)$$

The maximum values of the ‘concrete contribution’ and the ‘steel contribution’ are combined to give $V_{n, max}$ using the equivalent metric notation as:

$$V_{n, Max, ACI} = 0.96\sqrt{f'_c}b_w d \quad (2-7)$$

2.4.1.2 ACI ITG-6R-10

According to the *ACI ITG-6R-10* guidelines for reinforced concrete slabs and beams using *ASTM A1035/A1035M* bars as reinforcement, design for shear should follow Sections 11.1, 11.2, 11.4, and 11.5 of *ACI 318-11*, with a few exceptions. As discussed in Section 4.11 of *ACI ITG-6R-10* guide, research has demonstrated that for members without shear reinforcement, the shear stress at failure decreases as the member depth increases and as the reinforcement ratio decreases. For one-way slabs containing *ASTM A1035/A1035M* longitudinal bars, *Desalegne and Lubell* (2010) developed a simplified model for shear strength prediction using a simplification to the *Hoult et al.* (2008) model as part of the current research project. (See Section 2.4.1.4). The model was validated using laboratory test results of seven slab specimens containing ASTM A1035 longitudinal steel reinforcement. (Also see Section 5.2.3). The simplification to the *Hoult et al.* model assumed a longitudinal reinforcement strain of 0.0042, which corresponds to the stress of 690 MPa, and an aggregate size of $a_g = 0$. *ACI ITG-6R-10* uses this expression (equation 2-8) as a direct replacement for equation 2-4 in the *ACI 318-08* code for members without transverse reinforcement as given below.

$$V_{C, ACIITG-6R-10} = \left(\frac{154}{1000 + 2.1d} \right) \sqrt{f'_c} b_w d \quad (2-8)$$

ACI ITG-6R-10 guide recommends that all lightly reinforced beams should contain minimum shear reinforcement since unsafe predictions of shear capacity can result from the use of equation 2-4. This was demonstrated by laboratory tests of concrete slabs with longitudinal ASTM A1035/A1035M Grade 690 steel

(Hassan *et al.* 2008, Desalegne and Lubell 2010). According to the *ACI ITG-6R-10*, a design yield strength f_{yt} of 550 MPa for ASTM A1035/A1035M Grade 690 stirrups as shear reinforcement is appropriate if appearance and serviceability due to shear cracking is not a critical design consideration. Otherwise, f_{yt} used in design should be limited to 410 MPa to provide a control on diagonal crack width at service load levels.

2.4.1.3 CSA A23.3-04 General Method

2.4.1.3.1 Background

The *CSA A23.3-04* shear design provisions for concrete members are based on the Modified Compression Field Theory (MCFT). These provisions are based on the shear resisting mechanism shown in Figure 2-7, where the diagonal shear crack intersects the transverse and longitudinal reinforcements as well as the top flexural compression region. Flexural moments (M_f) and axial tension (N_f) are resisted by the force couple between the compressive force C and the tension in the reinforcement F_{lt} , here calculated at the diagonal crack. Other North American shear design provisions for concrete members, such as *AASHTO LRFD-07* and *CSA S6-06-CAN-CSA* are based on a similar assumed mechanism.

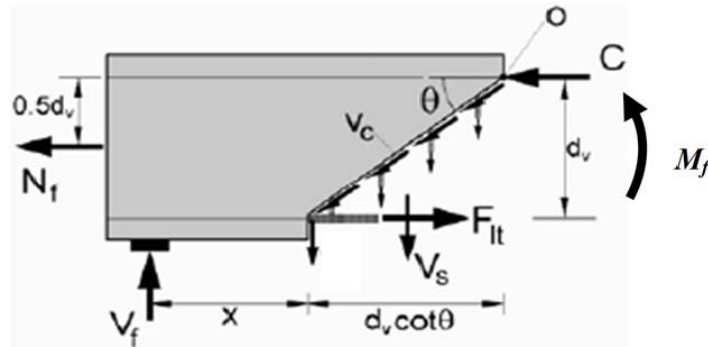


Figure 2-7: Basic Shear Resisting Mechanism Assumed in *CSA A.23.3-04* Code (adapted from Bentz *et al.* 2006).

For reinforced concrete members with transverse reinforcement the applied shear forces (V_f) are assumed to be resisted by two mechanisms: shear stress (v_c) on the crack surface (aggregate interlock) which was shown to be the primary method of shear resistance for members without stirrups by many researchers (see Section 2.2.4) and a steel contribution, V_s , provided by the stirrups that cross the diagonal crack. Note that the shear stress on the crack, v_c , has a vertical component that resists shear and a horizontal component that induces additional strain in the longitudinal reinforcement as described in Section 2.2.3. This suggests that shear force causes stress in the longitudinal reinforcement and this should be addressed in the design provisions. Hence it is necessary to ensure that the longitudinal reinforcement does not fail under the combined effect of applied shear and moment. The additional tensile stresses due to shear may result in yielding or anchorage failure of the longitudinal reinforcement before pure shear failure occurs. To ensure that this does not occur, the necessary force capacity in the longitudinal reinforcement of a concrete member without axial load is derived from Figure 2-7 by taking moments about point O and is given by the following equation.

$$F_{lt} = \frac{M_f}{d_v} + (V_f - 0.5V_s) \cot \theta \quad (2-9)$$

For analysis of concrete members for shear, if equation 2-9 is not satisfied, then the applied loads (M_f , V_f) can be proportionately reduced until it is satisfied, and these new values provide the estimate of the member strength. A member which is controlled by equation 2-9 is predicted to fail in a flexure-shear mode rather than simply in pure flexure or shear alone.

2.4.1.3.2 Model Development

The *CSA A23.3-04* shear design model was developed using simplifications to the Modified Compression Field Theory (*Bentz et al.* 2006). The model is based on the compositional approach of a 'concrete contribution' and a 'steel contribution' as:

$$V_{n, CSA} = V_{C, CSA} + V_{S, CSA} \quad (2-10)$$

For members without transverse reinforcement aggregate interlock is assumed as the only shear resisting mechanism. The *CSA A23.3-04* gives a simple equation (2-11) for the 'concrete contribution' of a member as:

$$V_{C, CSA} = \beta \sqrt{f_c'} b_w d_v \quad (2-11)$$

The 'steel contribution' term, V_S , is developed from a compatible rotating angle truss model as given below.

$$V_{S, CSA} = \frac{A_v f_y d_v \cot \theta}{S} \quad (2-12)$$

The ability of a cracked concrete member to resist aggregate interlock stresses is represented by the parameter β . The following simplified equation is developed for the value of β which defines the concrete contribution based on the MCFT relationships (*Bentz et al.* 2006). The parameter β accounts for the influence from the strain effect and the size effect on shear capacity of concrete members.

$$\beta = \left(\frac{0.4}{1 + 1500 \cdot \varepsilon_x} \right) \cdot \left(\frac{1300}{1000 + S_{ze}} \right) \quad (2-13)$$

The first term in equation 2-13 accounts for the strain effect whereby members with higher longitudinal member strains are weaker in shear. The term ε_x , represents the average longitudinal strain in the cross-section taken at the mid-depth. For reinforced concrete members subjected to bending and shear, without axial loads and where the flexural tension reinforcement is concentrated at the tension zone only, the strain at mid-depth of the member, ε_x , is reasonably approximated as one half of the strain in the flexural tension reinforcement (*Bentz et al.* 2006). The equation to determine ε_x can be developed from the free body diagram in Figure 2-7, assuming a 45° crack inclination, as:

$$\varepsilon_x = \frac{\frac{M_f}{d_v} + V_f}{2E_s A_s} \quad (2-14)$$

In the use of equation 2-14, the values of M_f and V_f are always taken as positive. The numerator of the equation represents the total axial force that must be resisted by the longitudinal tension reinforcement of a member. The denominator converts this force to a strain in the tension reinforcement by dividing by the area and stiffness of flexural reinforcement. The simplified form of equation 2-13 was developed through a formulation derived with the knowledge that the longitudinal member strain parameter ε_x will rarely exceed a value of about 0.001 for practical design cases using typical Grade 420 reinforcing steel (*Bentz et al.* 2006). Note also that the denominator of equation 2-14 assumes a linear stress-strain response for the reinforcement up to failure.

The second term in equation 2-13 accounts for the size effect whereby members with larger effective crack spacing (larger S_{ze}) are weaker in shear. The effective

crack spacing parameter, S_{ze} , is formulated to consider the influence on shear stress from member depth and aggregate size as:

$$S_{ze} = \frac{35S_z}{a_g + 15} \geq 0.85S_z \quad (2-15)$$

where d_v is the shear depth ($d_v = 0.9d$) parameter; a_g is the maximum aggregate size and S_z shall be taken as d_v or as the maximum distance between layers of distributed longitudinal reinforcement, whichever is less. For high strength concrete the aggregate tends to fracture and does not contribute to crack roughness. The model uses $a_g = 0$ for $f'_c > 70$ MPa. To avoid a discontinuity in strength predictions, the value of a_g is linearly reduced from the specified value at $f'_c = 60$ MPa to zero at $f'_c = 70$ MPa.

For members with transverse reinforcement the shear capacity is formulated as a compositional approach of ‘concrete contribution’, $V_{C,CSA}$, and ‘stirrup contribution’, $V_{S,CSA}$, terms as given in equations 2-11 and 2-12. However, since the stirrups will control the crack spacing for members with transverse reinforcement, parameter S_{ze} is taken as 300 mm whereby the size effect term cancels out.

Members with at least a minimum amount of transverse reinforcement bars, but below a maximum shear stress limit, are predicted to fail by yielding of the stirrups and eventual crushing of the concrete in the web rather than by breakdown of aggregate interlock. This implies that the shear capacity of reinforced concrete beams with stirrups can be governed by the capacity of the compression struts which in turn is affected by the magnitude of tensile strains, as shown in Figure 2-5. Thus it is important to understand the behaviour of compression struts and the angle of principal compression, θ , in cracked concrete

members, especially when members are reinforced with materials showing different stress-strain behaviour (such as ASTM A1035 steel) than the more common conventional steel.

As shown in equation 2-12 the angle of the fictitious crack, θ , is necessary to determine the steel contribution, $V_{s, CSA}$. The crack angle, θ , and longitudinal stirrup spacing S both influence the number of stirrup legs crossed by the crack. Figure 2-8 shows the limits on the allowable angle of principal compression, θ , based on the MCFT for members with conventional Grade 420 steel and heavily loaded in shear for different strains in the member at mid-depth (ϵ_x). As can be seen, the range of allowable angles to select from at this high shear loading is limited between lower and upper values corresponding to safe shear design. Members designed based on angles in the upper shaded region would be expected to fail in shear before yielding of the transverse steel making the use of equation (2-12) unconservative. Members designed based on angles from the lower shaded region would also be unconservative as the member is predicted to fail by crushing of the concrete in diagonal compression before achieving the design shear strength. Only within the unshaded region would a heavily loaded member be predicted to resist the applied shear force. Based on the MCFT analysis for members loaded in shear a simple linear equation that lies within the allowable range is developed by *Bentz et al.* (2006), and is given by:

$$\theta = 29^\circ + 7000 \cdot \epsilon_x \quad (2-16)$$

According to the *CSA A23.3-04* model the maximum nominal shear resistance of a concrete member is given as:

$$V_{n, Max, CSA} = 0.25 f'_c b_w d \quad (2-17)$$

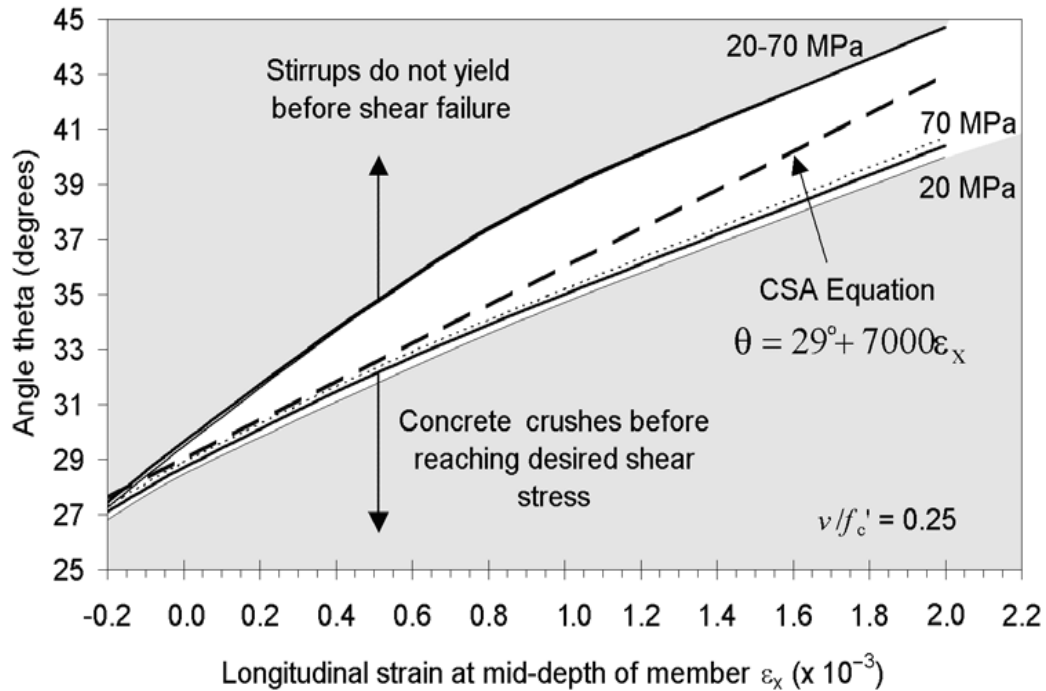


Figure 2-8: Selection of Equation for θ (Bentz 2006).

2.4.1.4 Hoult *et al.* Model

The ‘concrete contribution’ term in the *CSA A23.3-04* shear design model (equation 2-11) was developed to produce a simple equation assuming that in practice ϵ_x will not exceed a value of about 0.001. This corresponds to the yield strain of typical Grade 420 reinforcing steel (Bentz *et al.* 2006). However, when reinforcement consists of higher strength materials such as ASTM A1035 steel or internal fibre reinforced polymer bars, higher longitudinal strains can be expected.

Hoult *et al.* (2008) demonstrated that a modified version of the *CSA A23.3-04* shear model (termed as *Hoult et al. Model*) can be safely applied to members with internal fiber reinforced polymer (FRP) reinforcing bars. A so-called second-order equation that does not make prior assumption of the range of ϵ_x values can be used was proposed that offered improved prediction quality. For members with higher

strength reinforcing materials the *Hoult et al.* model, as a direct substitute for equation 2-11, is given as:

$$V_{C,H} = \left(\frac{0.3}{0.5 + (1000 \varepsilon_x + 0.15)^{0.7}} \right) \left(\frac{1300}{1000 + S_{ze}} \right) \sqrt{f'_c} b_w d_v \quad (2-18)$$

Note that all other equations in the *CSA A23.3-04* model (equations 2-14 to 2-16) are used to predict the shear capacity of concrete members using equation 2-18.

The use of lower stiffness reinforcement, such as FRP, which results in higher strains and crack widths at failure was considered in the shear prediction. The *Hoult et al.* shear model, which considers strain effect, were optimized for a wider range of strains associated with materials exhibiting larger strains before failure than the conventional steel.

The *Hoult* model was validated to provide better correlation with test results of concrete members with or without shear reinforcement and having large ε_x magnitudes up to 0.006 mm/mm compared to the *CSA A23.3-04* code model. A database of 146 shear failures of specimens reinforced with various FRP or steel bars was used for validation of the *Hoult et al.* model. For more accurate prediction of shear capacity of members having a wide range of high strength reinforcing materials equation 2-18 offers improved prediction quality, particularly for members reported to fail in shear at higher longitudinal strains as shown in Figure 2-9. The results indicated a strong correlation between the proposed expression for the strain effect and the shear capacity of both steel and FRP reinforced concrete beams. The findings of the *Hoult et al.* study also support the argument that aggregate interlock is the primary shear resisting mechanism for members without stirrups.

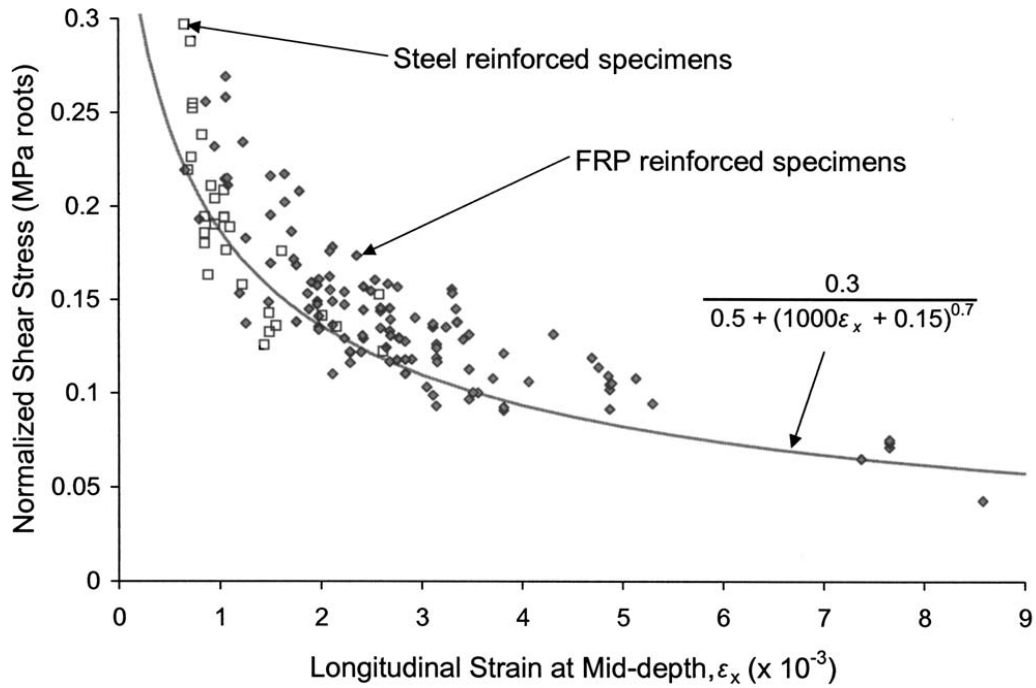


Figure 2-9: Normalized Shear Stress versus Longitudinal Strain at Mid-Depth (*Hoult et al. 2008*).

Bentz et al. (2010) tested eleven large scale reinforced concrete beams with GFRP longitudinal reinforcement including six beams that contained GFRP stirrups. Main test variables included the member depth, the member flexural reinforcement ratio, and the amount of shear reinforcement provided. The authors used the *Hoult et al. (2008)* shear model to predict the shear capacity of both types of specimens - with and without stirrups. Their analysis showed that FRP-reinforced concrete members show the same size-effects and strain effects on shear strength as steel-reinforced concrete. They also showed that the *Hoult et al. (2008)* shear equation provided excellent predictions of shear strength for all specimens. They concluded that the fundamental shear behaviour of FRP-reinforced beams is similar to that of steel-reinforced beams despite the brittle nature of the FRP reinforcement.

2.4.1.5 Eurocode 2 (2004)

In this model, the expression for shear capacity of concrete members without shear reinforcement was empirically derived and considers influences on the shear stress at failure from the longitudinal reinforcement ratio ρ_L and the effective depth d . The expression for the 'concrete contribution' to shear capacity is given as:

$$V_{C,EC2} \geq \begin{cases} 0.18 \left(1 + \sqrt{200/d} \right) (100 \rho_L \cdot f_{ck})^{1/3} b_w d \\ 0.035 \left(1 + \sqrt{200/d} \right)^{3/2} \sqrt{f_{ck}} b_w d \end{cases} \quad (2-19)$$

where:

$$\rho_L = \frac{A_{sL}}{b_w d} \leq 0.02 \quad (2-20)$$

The EC2 model for members with shear reinforcement (equation 2-21) is based only on the 'steel contribution' term, which is derived from a variable angle truss model. The truss angle θ between the diagonal concrete compression struts and the longitudinal axis is limited between 21.8° and 45° :

$$V_{S,EC2} \leq \begin{cases} \frac{A_{sw}}{S} Z f_{yw} d \cot \theta \\ \frac{\alpha_{cw} b_w Z v_1 f_{cd}}{\cot \theta + \tan \theta} \end{cases} \quad (2-21)$$

$$v_1 = 0.6 \left(1 - \frac{f_{ck}}{250} \right) \quad (2-22)$$

$$1 \leq \cot \theta \leq 2.5 \quad (2-23)$$

The applicable rules for design and detailing in *Eurocode 2-04* are valid for a specified yield strength range, $f_{yk} = 400$ to 600 MPa.

Because the *EC2* model relies directly on a truss analogy, it is necessary to also verify that the longitudinal reinforcement has sufficient capacity to carry the longitudinal forces due to the compression diagonals. Based on the beam configurations in this study, the longitudinal reinforcement verification is similar to the flexural analysis.

2.4.2 Numerical Models

Two numerical models were employed in this research work to understand the capability of currently available programs to predict the shear behaviour of concrete members reinforced with ASTM A1035 steel. Both models are based on the Modified Compression Field Theory (*Vecchio and Collins* 1986). The MCFT is an analytical model for predicting the response of reinforced concrete elements subject to in-plane normal and shear stresses, that models cracked concrete as an orthotropic material with smeared, rotating cracks. (See Section 2.3).

2.4.2.1 *VecTor2*

VecTor2 (*VT2*) (*Vecchio* 1990-2002) is a nonlinear finite element program based on the MCFT for the analysis of two-dimensional reinforced concrete membrane structures. This software has been developed at University of Toronto since 1990. Subsequent developments on *VT2* have incorporated disturbed stress field model and alternative constitutive models for a variety of second-order effects including compression softening, tension stiffening, tension softening, and tension splitting. For the numerical shear predictions of the specimens in the current study *VecTor2* (*FormWorks, VecTor2 & Augustus Bundle (Version 3.5)*) was used.

In using this program, each member is treated as a two-dimensional structure with constant thickness through a rectangular mesh of four-node rectangular elements. Longitudinal reinforcing steel is modeled as truss bars, by lumping all reinforcement at the same level together. The stirrups are modeled as smeared reinforcement components of a reinforced concrete material.

VT2 can predict the load-deformation response of a variety of reinforced concrete structures exhibiting well-distributed cracking when subjected to short-term static monotonic, cyclic and reverse cyclic loading. The program utilizes an incremental total load, iterative secant stiffness algorithm to produce an efficient and robust nonlinear solution.

2.4.2.2 Response 2000

Response 2000 (R2K) (Bentz, 2000) implements the MCFT relationships for analysis of cracked concrete using a layered sectional approach. It can calculate strengths and deformations for beams and columns subjected to combinations of axial load, moment and shear. The assumptions implicit in the program are that plane sections remain plane and that there is no transverse clamping stress across the depth of the beam. For sections of a beam or column a reasonable distance away from a support or point load, these are appropriate assumptions.

R2K performs sectional analyses using the stress-strain relationships for the cracked concrete and the stress-strain relationship for the steel reinforcement. *R2K* can perform two types of analysis for a reinforced concrete member: sectional analysis and member analysis. Sectional analysis predicts the sectional behaviour at any location along the member due to the combined effects of moment and shear while member response predicts the full member behaviour including deflections for a given span. Only specimens with point loading at mid span or uniformly distributed loading can be modeled using the full member

response option due to limitations in this program to handle members with non-symmetrical loading.

2.5 Concrete Slabs and Beams Reinforced with ASTM A1035 Steel

Limited prior research has examined the flexure, shear and deflection behaviour of concrete slabs and beams reinforced with ASTM A1035 steel. The main emphasis of these prior test programs were on the performance of members containing ASTM A1035 steel as a direct replacement for the same amount of conventional Grade 420 steel, with validation of the use of existing design code provisions developed for concrete members with conventional steel reinforcement.

2.5.1 Previous Research on Flexural Behaviour

Research on the use of ASTM A1035 steel as reinforcement for concrete members has been ongoing since 2002. The flexural behaviour of concrete members reinforced with ASTM A1035 reinforcing bars has been investigated experimentally by a number of researchers.

Ansley et al. (2003) conducted 4 beam tests to compare the behaviour of slender beams with stirrups reinforced with longitudinal ASTM A1035 Grade 690 MPa steel against geometrically similar beams with conventional Grade 420 MPa reinforcing steel. Companion test specimens consisted of two beams that varied by the reinforcement configuration. Specimens had the same cross-section properties with a width of 12 in. (305 mm) and a height of 18 in. (457 mm). *Ansley et al.* found that the difference in beam behaviour was due solely to the difference in the reinforcing material properties. The behaviour of the beams up to the yield point of the conventional Grade 420 MPa reinforcing steel was similar, regardless of the reinforcement strength. After that point, the load-deflection curve for the beam reinforced with ASTM A1035 steel maintained a non-linear

response until failure. However, for the beam with Grade 420 MPa steel, larger deflection was observed for the same load compared to similar beams containing ASTM A1035 steel. At failure, the beam reinforced with ASTM A1035 steel resisted more applied load than the beam reinforced with Grade 420 MPa steel.

Yotakhong et al. (2003) carried out an experimental program to study the flexural behaviour of rectangular concrete beams with conventional steel stirrups and longitudinally reinforced with ASTM A1035 or conventional steel. Four large-scale concrete beams with dimensions of 16 feet long (4880 mm), 12 inches (305 mm) wide, and 18 inches (457 mm) high were tested. Three beams were longitudinally reinforced with ASTM A1035 steel, and one beam was reinforced with conventional steel. All beams were reinforced identically with conventional steel for shear reinforcement and on the compression side. Three beams were tested under static loading conditions, while the remaining ASTM A1035 steel reinforced beam was tested under a slow cyclic loading condition. All beams reinforced with A1035 steel showed non-linear load-deflection behaviour after the initiation of the first crack and continued to behave in a similar manner up to failure. It was observed that all A1035 reinforced concrete beams experienced higher ultimate strength and a comparable amount of ductility in comparison to the control beam. The failure mode of all beams was classified as ductile flexural failure due to significant straining of the tension reinforcement preceding the crushing of the concrete at the top of the beams. The researchers concluded that flexural behaviour of the A1035 beams can be accurately predicted by using current available reinforced concrete flexural models. Design recommendations and guidelines were proposed based on the results from *Yotakhong's* investigation and additional parametric study.

Based on the prior published data, *Mast et al.* (2008) developed a methodology for the flexural strength design of concrete beams reinforced with Grade 100 ksi (690 MPa) steel bars that conform to the requirements of ASTM A1035-07. The design method is based on simple analysis techniques that satisfy fundamental

principles of equilibrium and compatibility. The model uses an idealized linearly elastic - perfectly plastic material model, with an initial elastic modulus of 29,000 ksi (200,000 MPa) and yield strength of 100 ksi (690 MPa) to represent the stress-strain behaviour of the longitudinal reinforcing steel. The *Mast et al.* flexural model incorporates the well known assumption that plane sections before bending remain plane after bending such that a linear distribution of axial strains is assumed over the cross-section height. The *ACI* rectangular stress block approach is used to determine the concrete stress for a given compression strain in the extreme fibre. Strain limits for tension-controlled sections and compression-controlled sections were proposed that are consistent with the approach of *ACI 318-02*. The proposed method was compared with experimental results previously reported by others. *Mast et al.* concluded that the simplified method and the proposed strain limit criteria can be used in the flexural design of members containing ASTM A1035 Grade 690 steel longitudinal reinforcement.

Lepage et al. (2011) conducted an experimental study by subjecting reinforced concrete beams and columns to a cyclic loading protocol, to explore the applicability of using Ultra High Strength Steel (UHSS) with f_y up to 120 ksi (830 MPa) as primary reinforcement. The mechanical behaviour of these members was compared to similar members reinforced with conventional Grade 420 steel. Figure 2-10 shows the representative stress-strain curves of both conventional (Grade 420) and UHSS steels used in the experimental program. Steel with yield strength in excess of 80 ksi commercially available in the U.S. is often referred to as Advanced High Strength Steel (AHSS) or Ultra High Strength Steel (UHSS) (ISSI, 2006; ASTM A1011, 2010).

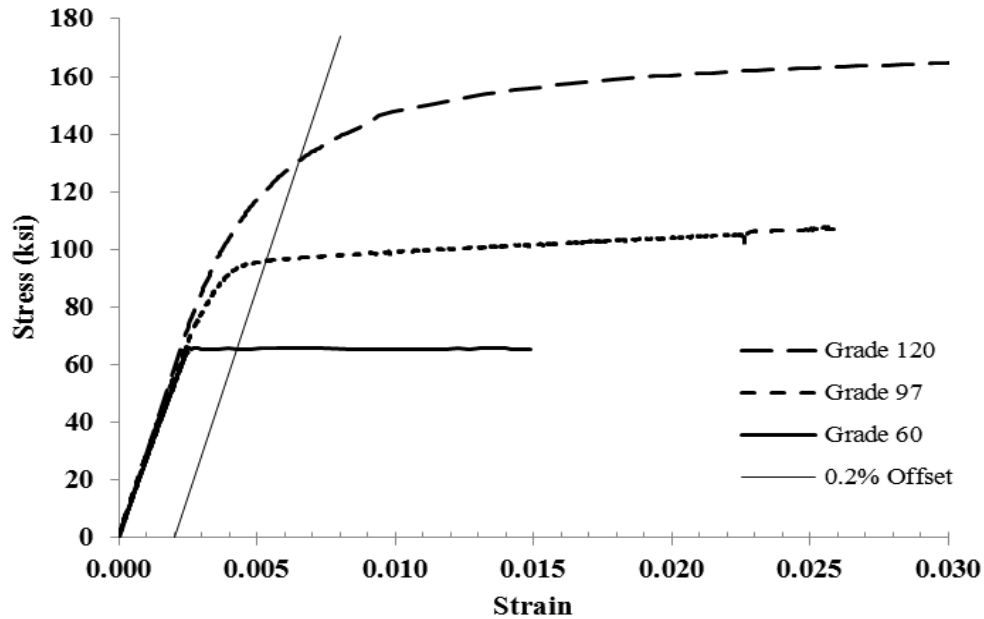


Figure 2-10: Measured Tensile Properties of Reinforcing Steel
(Lepage *et al.* 2011)

For this purpose a series of experiments was designed at Penn State University and Purdue University. The test variables include nominal yield strength of longitudinal reinforcement, (60, 97, and 120 ksi) and the applied axial force. Test data from this study showed that the use of UHSS is a viable option for earthquake-resistant construction. The test results suggested that beams or columns with Ultra High Strength Steel (UHSS) as longitudinal reinforcement had similar drift capacities to beams or columns reinforced with (approximately twice as much) conventional high strength steel. The tested beams tolerated drift ratios in excess of 10% without failure while the tested columns tolerated ultimate drift ratios of 5%. The specimens reinforced with UHSS required less steel than specimens reinforced with 60 ksi steel to reach the same moment capacity, resulting in less congestion. However, the reduction in the reinforcement ratio caused a reduction in stiffness beyond cracking, which reduced the energy dissipation as measured by the area of the hysteresis loops.

In parallel to the current study, a design guide for the use of ASTM A1035/A1035M Grade 100 (690) steel bars for structural concrete was published as *ACI ITG-6R-10* (2010). The document presented guidelines for design of reinforced concrete members, including beams, columns, slab systems, walls, footings, and mat foundations using ASTM A1035/A1035M steel as adaptations to *ACI 318-08*. Two sectional flexural analysis models are included in *ACI ITG-6R-10*: a simplified model adapted from *Mast et al.* (2008), and a general model presented in Appendix B of the *ACI ITG-6R-10* guide. Both sectional flexural models assume a linear distribution of axial strains over the cross-section height from the well known assumption that plane sections before bending remain plane after bending. For the simplified flexural model, an idealized elastic-plastic representation for the stress-strain response of ASTM A1035 steel is used with an equivalent assumed yield stress of 690 MPa. In the general model, the full non-linear stress-strain relationship for ASTM A1035 steel according to equation 2-1 is used. For both approaches, the maximum concrete strain at the extreme compression fibre of -0.003 is used to determine the maximum load. In the *ACI ITG-6R-10* guide, it is stated that the tension-controlled and compression-controlled strain limits and the corresponding strength reduction factor ϕ are adjusted compared to the values using the simplified *Mast et al.* model. This adjustment ensures satisfactory member behaviour by taking into account the actual non-linear stress-strain response of the ASTM A1035 steel.

2.5.2 Previous Research on Shear Behaviour

Only limited prior research has examined the applicability of existing sectional shear design models for concrete members longitudinally and/or transversely reinforced with ASTM A1035 steel.

Hassan et al. (2008) tested six large-scale concrete specimens reinforced with either conventional or high-strength steel at North Carolina State University. The specimens were constructed without web reinforcement to evaluate the nominal

shear strength provided by the concrete. The main test variables included the a/d ratio, concrete compressive strength, and the longitudinal steel reinforcement ratio. All specimens had identical cross-sectional dimensions of 460 mm x 915 mm and a total length of 4900 mm. Two specimens had shear span to depth ratios of 2.7. One beam of each group was reinforced with conventional Grade 420 MPa steel while the other beam was reinforced with ASTM A1035 steel bars. It was found that use of ASTM A1035 steel strongly influenced the shear behaviour of the concrete specimens without web reinforcement and hence ignoring the stress-strain characteristics of the material could result in unreliable predictions of the ultimate load-carrying capacity and mode of failure.

Specimen *M-2.7-32* reinforced with ASTM A1035 steel exhibited higher deflections than the companion specimen reinforced with Grade 420 MPa steel (*G-2.7-32*) at the same load level as shown in Figure 2-11. This behaviour was attributed to the smaller area of reinforcing steel in *M-2.7-32* used and the higher induced steel strain. However, despite the reduction in the longitudinal reinforcement ratio by 40%, the shear strength of the concrete specimen reinforced with ASTM A1035 steel was higher (16%) than that of the specimen reinforced with Grade 420 MPa steel. (See Figure 2-11).

Hassan et al. (2008) also evaluated the limitations of the *ACI 318-05* shear design provisions to recognize the influence of high-strength steel reinforcement on the shear strength of concrete specimens. It was concluded that the *ACI 318-05* simplified expression for the shear contribution of concrete is unconservative for large-size concrete specimens without web reinforcement and an alternate model is needed that can account for the size effect and the reinforcement characteristics.

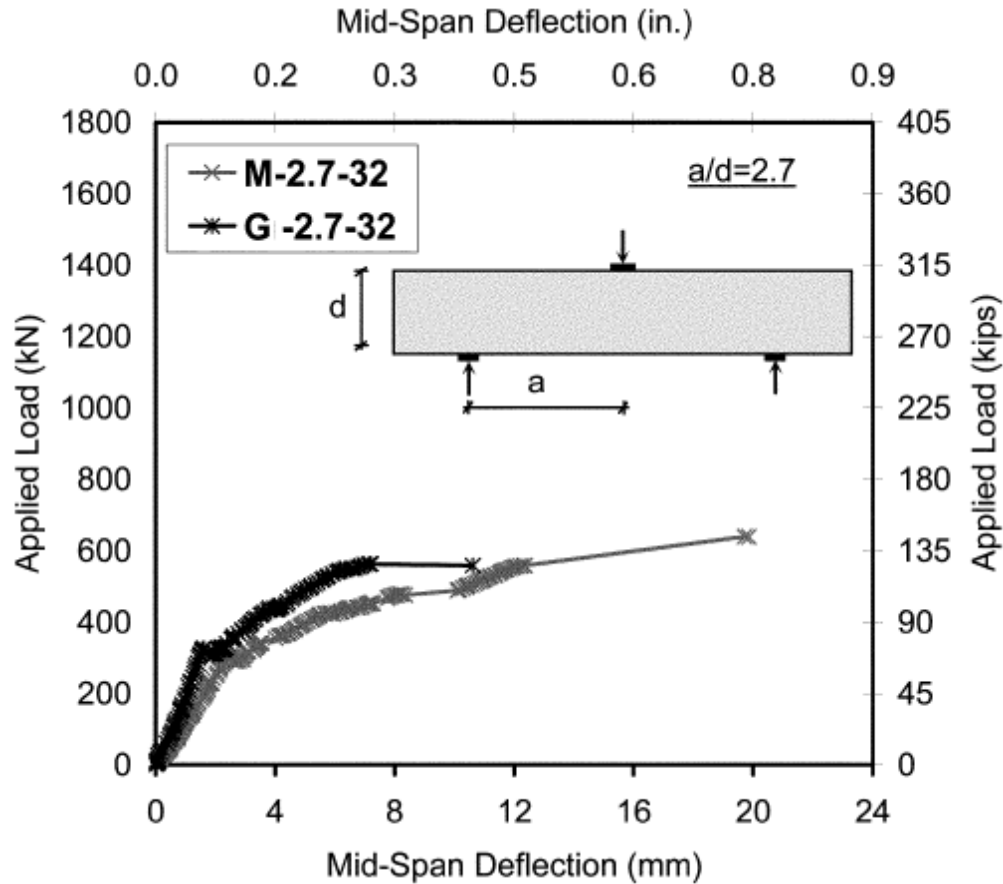


Figure 2-11: Load-Deflection Behaviour of Slender Beams tested by *Hassan et al.*, 2008.

Garay-Moran and Lubell (2008) investigated the behaviour of members longitudinally reinforced with ASTM A1035 steel having small shear span to depth ratios through laboratory tests of ten large-scale deep members under four-point bending. Constant cross-section dimensions of $b = 300$ mm and $h = 607$ mm were provided for all the specimens. However, different span lengths were utilized to obtain shear span to depth ratios (a/d) of 1.2, 1.8 and 2.4. The percentage of longitudinal main reinforcement varied from 0.52% to 2.29%. For all specimens, the center to center distance between the loading points was 500 mm. Six specimens were longitudinally reinforced with ASTM A1035 steel and contained conventional steel web reinforcement. Two specimens were longitudinally and vertically reinforced with conventional steel. The remaining

two specimens were longitudinally reinforced with ASTM A1035 steel but did not contain web reinforcement. The concrete compressive strength used in the specimens ranged from 23 MPa to 48 MPa. It was found that member capacity decreased as the shear-span-to-depth ratio increased, and as the longitudinal reinforcement ratio decreased. The inclusion of web reinforcement significantly increased the member strength and ductility. The study also demonstrated that it was possible to design members to efficiently exploit the high strength reinforcing steel when applying Strut-and-Tie modeling techniques according to *CSA A23.3-04*, *ACI 318-05* and *Eurocode 2-04* provisions.

The tests conducted at North Carolina State University by *Hassan et al.* (2008) and at the University of Alberta by *Garay-Moran and Lubell* (2008) typically had small shear span to depth ratios, $a/d < 2.5$. In these specimens the dominant shear response is believed to be by arch action and the appropriate analytical shear model is a strut-and-tie approach. On the other hand all the other tests had slender members where $a/d > 2.5$ and sectional shear and flexural models are applicable. (See Figure 2-2). The focus of this study is the shear and deflection behaviour of slender ($a/d > 2.5$) concrete members containing ASTM A1035 steel reinforcement.

Sumpter et al. (2009) carried out an experimental program to test nine reinforced concrete beams with different combinations of ASTM A1035 steel and conventional steel reinforcement. The beams were divided into three main categories according to the type of reinforcement. The shear reinforcement ratio varied (0.31 % - 0.61%) by changing the stirrup spacing. All beams had nominal cross-sectional dimensions of 12" x 16" (305 mm x 406 mm) with a total length of 16 feet (4877 mm), and were designed to have a nominal concrete compressive strength of 4000 psi (27.5 MPa). The total length was selected in order to have one test at each end of the specimen, and thus double the test data. In addition, all beams were provided with the same longitudinal reinforcement ratio to keep the effect of dowel action constant so that changes in the observed behaviour could be attributed to either the ASTM A1035 steel or to the stirrup spacing. Two layers of

three #9 bars were used in the bottom and one layer of three #9 bars was used in the top of the beams, with all stirrups of #3 bar size. The stirrup spacing was varied to reflect a minimum, intermediate, and maximum level of spacing as allowed by the ACI Code. The testing was performed using a single concentrated load positioned closer to one end of the beam to allow for two tests per beam.

Sumpter et al. (2009) indicated that direct replacement of conventional Grade 420 stirrups with ASTM A1035 stirrups increased the shear load capacity of members as shown in Figure 2-12 for beams in category 1. The ASTM A1035 shear reinforcement also enhanced the serviceability in terms of reducing crack spacing and crack widths. They observed that pairing ASTM A1035 steel longitudinal and transverse reinforcement shows an optimum design in terms of strength gain and reduction in crack width. They suggested that combining high performance steel with high strength concrete could lead to a better utilization of the materials. It also was concluded that *ACI 318-05*, *CSA A23.3-04*, and *AASHTO LRFD-04* design codes can conservatively be used for the design of concrete beams with ASTM A1035 steel longitudinal and transverse reinforcement up to a stirrup yield strength of 80 ksi (550 MPa).

Munikrishna et al. (2008) completed an experimental program comprised of eighteen tests using nine large-sized reinforced concrete beams subjected to static loading up to failure. All beams had total length of 22 ft. (6706 mm), and were designed using nominal concrete compressive strength of 4000 psi (27.5 MPa). All beams were classified into three groups based on their shear resistance. Specimens in each group were of similar geometry. The total length was chosen in order to test each beam twice, and thus double the amount of collected data. The shear span-to-depth ratio, a/d , of specimens was kept constant at $a/d = 3.0$ while the spacing of shear reinforcement was varied. Of the nine beams four of them were designed without shear reinforcement to estimate the nominal shear strength provided by concrete, V_c . Test specimens with stirrups were designed to induce stresses of 80 ksi and 100 ksi in the ASTM A1035 steel stirrups. Within each group, beams reinforced with stirrups were designed to achieve the same

ultimate nominal shear capacity. The transverse reinforcement ratios of the beams with stirrups varied between 0.07 % to 0.31%. In each group the beams reinforced with ASTM A1035 steel stirrups were compared with beams reinforced with conventional Grade 420 steel stirrups. The type of steel used and the amount of shear reinforcement were the main parameters considered in the experimental program.

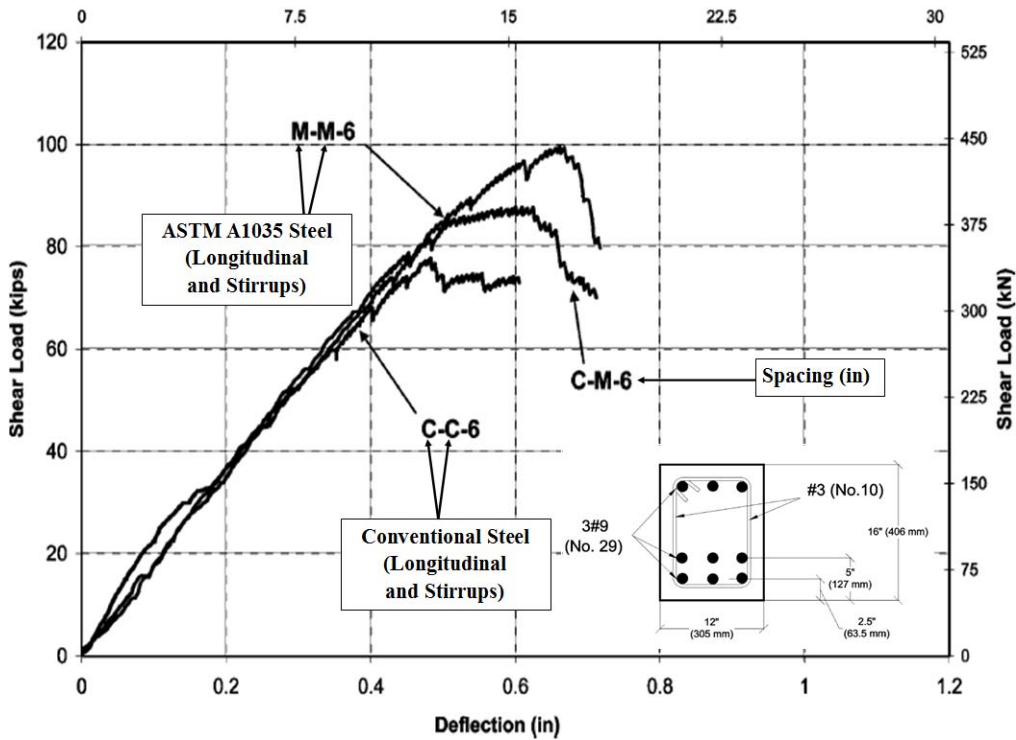


Figure 2-12: Shear Load-Deflection Relationship, Set 1. (Adapted from *Sumpter et al.*, 2009)

Results from the *Munikrishna et al.* (2008) tests showed that by utilizing the higher yield strength and consequently reducing both the longitudinal and transverse reinforcement ratio of ASTM A1035 steel, the beams can achieve almost similar load carrying capacity as the beams reinforced with conventional Grade 420 steel. (See Figure 2-13). In addition, their analytical study showed that the *ACI 318-05*, *CSA A23.3-04*, and *AASHTO LRFD-04* design codes can closely

predict the ultimate shear strength for beams reinforced with ASTM A1035 longitudinal and transverse steel having yield strength up to 100 ksi. The beams were also analyzed using *Response 2000* to predict the shear behaviour of beams reinforced with ASTM A1035 steel. Based on the results and findings of the experimental and analytical research, design recommendations were given for the use of ASTM A1035 steel as shear reinforcement in concrete beams.

Based on the results of tests of full-scale beams by *Munikrishna et al.* (2008) and *Sumpter et al.* (2009) the behaviour of beams containing stirrups reinforced with ASTM A1035/A1035M Grade 690 and designed with f_{yt} of 550 MPa were found to be similar to the behaviour of companion beams reinforced with conventional Grade 420 stirrups. At service load levels, inclined shear crack widths were larger, as expected, for beams reinforced with ASTM A1035/A1035M Grade 690 stirrups. However, in all cases, the crack widths were less than the commonly accepted limit of 0.016 in. (0.41 mm).

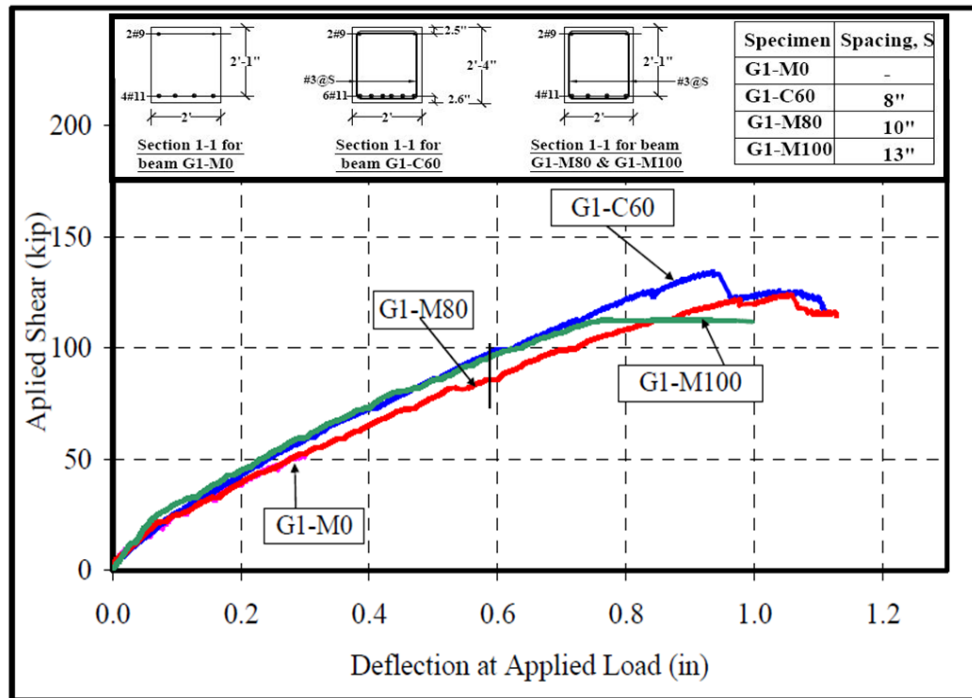


Figure 2-13: Shear Load-Deflection Relationship, Group 1 beams. (Adapted from *Munikrishna et al.*, 2008)

Shahrooz. et al. (NCHRP 679, 2011) evaluated the current *AASHTO LRFD Bridge Design Specifications* relevant to the use of high-strength reinforcing steel using an integrated experimental and analytical program. More emphasis was given on steel having no distinct yield plateau. Included in the experimental program were testing of five large-scale reinforced-concrete beams to evaluate the performance of high-strength A1035 steel as shear reinforcement in comparison to that of the commonly used A615 steel. All beams were 305 mm (12 in) wide by 610 mm (24 in) deep and were longitudinally reinforced with #8 ASTM A1035 steel reinforcement. Four beams contained both A1035 and A615 shear reinforcement in either half of the beam with nominal concrete strength of 70 MPa (10 ksi). One beam had ASTM A1035 stirrups and nominal concrete strength of 105 MPa (15 ksi). The transverse reinforcement ratios varied between 0.14 % and 0.39%. The value of f_y was taken as 690 MPa and 400 MPa for A1035 and A615 steel, respectively in all analysis reported. Shear capacities were computed according to the Sectional Design Model in the *AASHTO LRFD Specifications*. *Response 2000 (Bentz 2000)* was also used to predict the shear response of the specimens. It was reported that the load-deflection responses predicted by *Response 2000* were reasonably close to the experimental results. All of the specimens exceeded the predicted capacities based on *AASHTO LRFD*. The measured and computed capacities suggested there was adequate shear strength of members when ASTM A1035 stirrups were designed based on current *AASHTO* design equations with the stirrup yield strength taken as 690 MPa (100 ksi).

Crack patterns for the regions with A615 and A1035 stirrups were similar in terms of the load at which cracks formed and how they propagated. All beams exhibited good performance with little difference between the behaviour of spans reinforced with ASTM A1035 or A615 transverse steel.

2.6 Deflection of Reinforced Concrete Beams

2.6.1 General

Reinforced concrete members are expected to undergo large deformations before failure. The load-deformation response of slender members are normally predicted based on the common hypothesis that plane sections before bending remain plane after bending. Thus shear deformations are neglected in most conventional deflection calculation methods for slender concrete beams with transverse reinforcement.

Members without transverse reinforcement (slabs) are expected to fail shortly after the formation of diagonal cracking in a relatively brittle manner. Hence conventional deflection calculation procedures are usually sufficient for slabs without the consideration of shear deformations. On the other hand, slender reinforced concrete members containing transverse reinforcement usually exhibit greater deflection at service loads than predicted using design standards (*Bischoff et al.* 2005, *Ramsay et al.* 1979). The discrepancy between the actual and calculated deflections can be even more significant for the case of slender reinforced concrete beams with relatively small shear span to depth ratios where the shear deformation as a fraction of the total deformation is greater. With the introduction of higher strength reinforcing steel in recent years, such as ASTM A1035 steel, which can result in concrete members with lower reinforcement ratios, the need for more reliable and accurate deflection calculation procedures is apparent.

2.6.2 Previous Research on Deflection of Reinforced Concrete Beams

Prior studies have attempted to address the inaccuracies in design code approaches for the prediction of deflections of reinforced concrete members. The causes of discrepancy between predicted and measured member deflection values

can result from two main problems – inaccuracy in the formulation of the effective moment of inertia of a cracked concrete member and ignoring shear deformations.

Branson (1977) developed a deflection calculation method based on the concept of an effective moment of inertia for cracked concrete members. In a reinforced concrete member subject to transverse loading it is expected that flexural cracking occurs in the portion of the member with higher bending moments while the low moment regions remain uncracked. Branson estimated the transition from the uncracked flexural stiffness based on the gross section properties ($E_c I_g$) to a fully cracked stiffness ($E_c I_{cr}$) using the following expression.

$$I_{eb} = \left(\frac{M_{cr}}{M_a} \right)^3 \cdot I_g + \left[1 - \left(\frac{M_{cr}}{M_a} \right)^3 \right] \cdot I_{cr} \quad (2 - 24)$$

Bischoff (2005) developed an alternative formulation for effective moment of inertia I_e , (equation 2-25) which could be used in place of the formulation developed by *Branson* (equation 2-24). Bischoff's model recognizes that the effective stiffness is influenced by tension stiffening, which arises from tension carried by the concrete between the flexural cracks. The model uses a tension stiffening factor that decreases with increasing load, once the member has cracked in flexure. Estimates of member deflection using Bischoff's formulation for I_e are in better agreement with test results for slabs than using *Branson's* model. (*Bischoff* (2005a, 2005b), *Bischoff and Scanlon* 2007 and *Gilbert* 2007).

$$I_e = \frac{I_{cr}}{1 - \left(1 - \frac{I_{cr}}{I_g} \right) \left(\frac{M_{cr}}{M_a} \right)^2} \leq I_g \quad (2 - 25)$$

Mohr et al. (2010) proposed a finite element approach to predict the load-deflection response of slender concrete beams using a frame element model which combined the influences of shear, bending and axial force effects. The main hypothesis of the *Mohr et al.* model is that the full displacement field of any fibre element in the cross section can be approximated by the sum of the plane-section displacement field of the cross-section and an additional displacement field that enables the section to distort and warp (i.e. shear deformation). Three cases were considered for the cross-section deformation component, namely, the Navier-Bernoulli theory with no shear-distortion (0SD), the Timoshenko theory with linear shear-distortion (1SD) and the proposed frame element model with non linear shear-distortion (NLSD), as shown in Figure 2-14. The warping-distortion field is obtained by a function defined in the domain of the cross-section, and it is approximated by a finite series of predefined shape functions and their corresponding coefficients. Normal, shear and vertical stresses are taken into account in the finite element model. *Mohr et al.* compared a small database of test results from three experimental programs for analysis using the Navier-Bernoulli theory, the Timoshenko theory and the proposed frame element model with non-linear shear strain distribution. Different failure modes and shear span to depth ratios were analyzed through all cases studied. Good agreement was obtained between the experimental and the theoretical results provided by the frame element model. This showed its capability to reproduce displacements, stresses and strains in the concrete and in the reinforcements. According to *Mohr et al.* (2010), the frame element model had better agreement to the test results than the solutions based on the Navier-Bernoulli and the Timoshenko theories, highlighting the need to consider both bending and shear deformations.

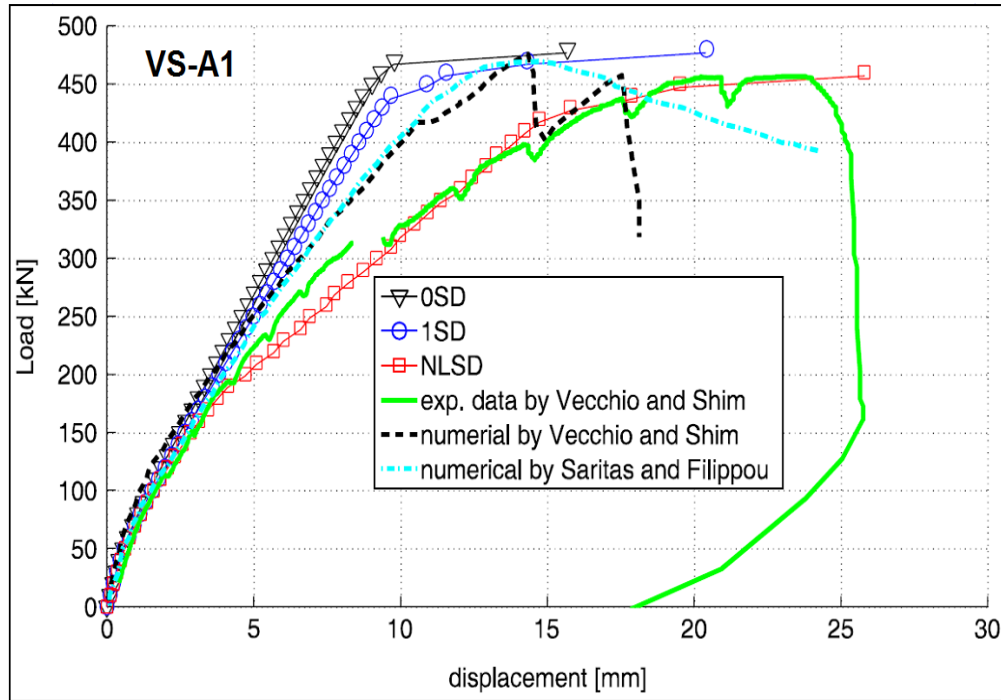


Figure 2-14: Comparison of Deflection Models (*Mohr et al. 2010*).

Navarro-Gregori et al. (2013) developed a model for the analysis of reinforced concrete beams under monotonic loading conditions, including axial, bending, and shear forces, in order to effectively capture the mechanisms of shear transfer. The proposed model (PR model) is based upon the Timoshenko Beam Theory. The constitutive material model for reinforced concrete follows the basic assumptions of the Modified Compression Field Theory (MCFT). The validity of the model was established by comparing predicted deflections with this model to the *Bresler–Scordelis (1968)* and *Vecchio–Shim (2004)* experimental tests. Despite the assumption of a simple shear strain profile, the proposed model gave reasonable predictions of the load–deflection response and the ultimate load capacity for the experimental tests but differed as the loading approached failure. (See Figure 2-15) The proposed model was shown to be suitable for analysis of shear critical reinforced concrete beams subjected to monotonic loading conditions. It was able to capture the effect of diagonal cracking and the subsequent sudden change of shear stiffness.

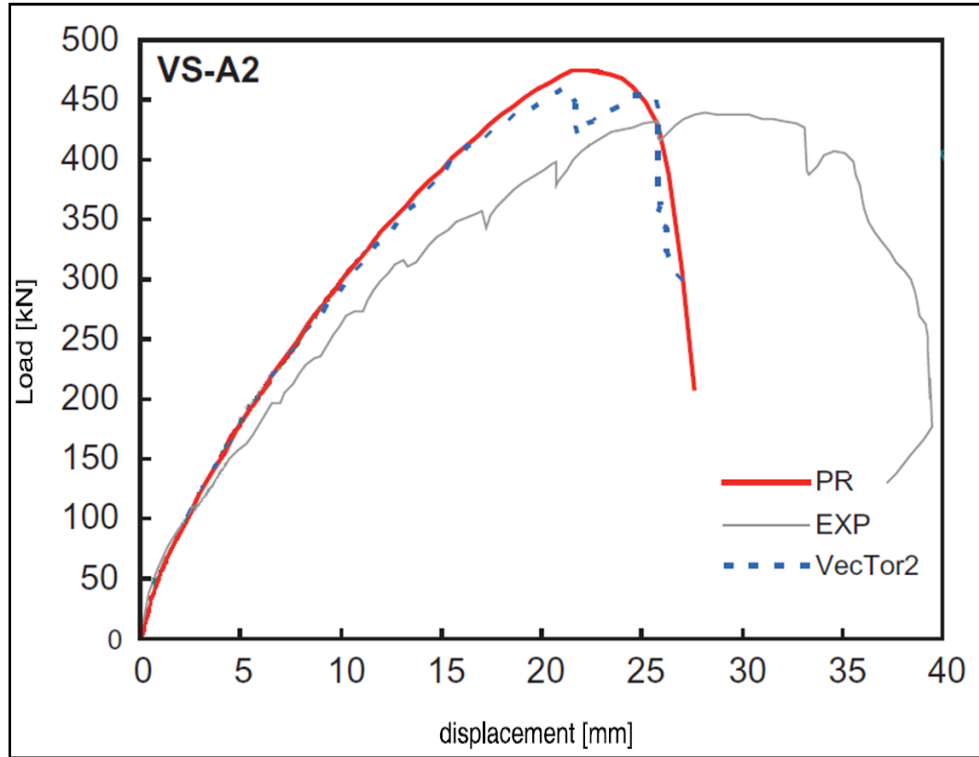


Figure 2-15: Typical Load–Deflection Response at Mid-span of (Beam *VS-A2* units kN, mm) (Navarro-Gregori *et al.* 2013).

The prior studies on deflection behaviour of concrete members discussed in earlier paragraphs dealt only with members containing conventional reinforcing steels. No independent study examining the deflection behaviour of concrete beams with ASTM A1035 steel reinforcement have been published. The shear tests by *Sumpter et al.* (2009) on beams containing ASTM A1035/A1035M Grade 690 stirrups showed a similar load-deflection behaviour to beams reinforced with deformed Grade 420 stirrups. (See Figure 2-12). Direct replacement of conventional Grade 420 stirrups with ASTM A1035 stirrups increased the shear load capacity of members and enhanced the serviceability in terms of distributing cracks and reducing crack width. Note that the higher strength of ASTM A1035 steel was not utilized in the stirrups of the beams tested by *Sumpter et al.* (2009). However, when the higher strength of ASTM A1035 steel was utilized by reducing the transverse reinforcement ratio for beams tested by *Munikrishna et al.*

(2008), the post cracking stiffness of beams with ASTM A1035 steel reinforcement was observed to be lower than that of the companion beams with conventional Grade 420 steel reinforcement. As a consequence service load deflection was higher. Moreover, the strain in the stirrups and the stress (and strain) in the longitudinal reinforcement at service load levels, for beams with ASTM A1035 steel, were significantly higher than the corresponding values for similar beams with conventional steel reinforcement, while the load carrying capacity was nearly the same. These behaviours can be distinctly observed for beams in *G3* series as shown in Figure 2-16. For instance, the service deflection (the deflection corresponding to 60% of ultimate load) of the beams containing ASTM A1035 steel in *G3* series were observed to be up to 33% higher than those of similar beams with conventional Grade 420 steel reinforcement. (See Figure 2-16 and Table 2-2). This behaviour can justify the need for more reliable and accurate deflection calculation method for concrete beams reinforced with ASTM A1035 steel reinforcement.

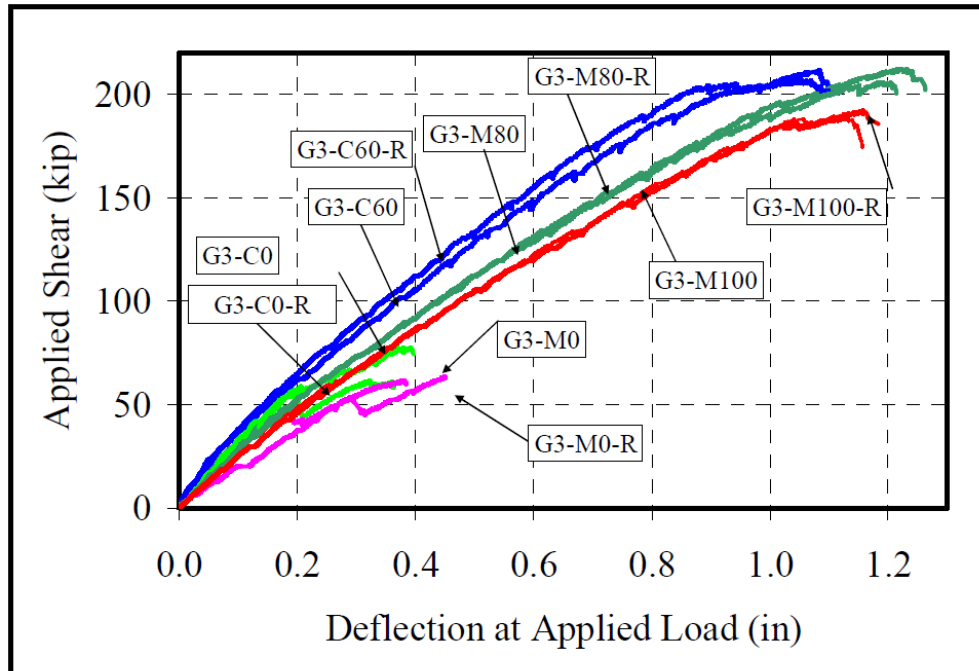


Figure 2-16: Shear Load-Deflection Response for Beams (Adapted from *Munikrishna et al.* 2008).

Table 2-2: Details of Beams Tested by *Munikrishna et al.* 2008.

Beam ID	b_w (mm)	d (mm)	a/d	Yield strength, f_y (MPa)		Reinforcement Ratio (%)		f_c' (MPa)
				Longitudinal	Transverse	ρ_L	ρ_t	
G1-C60	610	645	3.1	430	430	1.53	0.12	33
G1-M0	610	645	3.1	690	-	1.02	-	31
G1-M80	610	645	3.2	690	550	1.04	0.09	33
G1-M100	610	645	3.2	690	690	1.04	0.07	34
G2-M0	610	645	3.1	690	-	1.02	-	31
G2-M80	610	645	3.2	690	550	1.04	0.09	33
G2-M100	610	645	3.2	690	690	1.04	0.07	34
G3-C0	406	457	3.0	430	-	3.80	-	37
G3-C60	406	457	2.9	430	430	3.70	0.31	35
G3-M0	406	457	3.0	690	-	2.71	-	37
G3-M80	406	457	3.0	690	550	2.69	0.25	36
G3-M100	406	457	3.0	690	690	2.69	0.20	40
G3-C0-R	406	457	3.0	430	-	3.80	-	37
G3-C60-R	406	457	2.9	430	430	3.70	0.31	35
G3-M0-R	406	457	3.1	690	-	1.02	-	31
G3-M80-R	406	457	3.0	690	550	2.69	0.25	36
G3-M100-R	406	457	3.0	690	690	2.69	0.20	40

2.6.3 Numerical Models for Deflection of Reinforced Concrete Beams

Two existing numerical models were utilized to predict the deflection behaviour of reinforced concrete beams in this study. Both models are based on the Modified Compression Field Theory (MCFT), a model for predicting the response of cracked reinforced concrete elements subject to in-plane normal and shear stresses.

VecTor2 (VT2) (*Vecchio* 1990 - 2002) is a nonlinear finite element modeling tool for the analysis of two-dimensional reinforced concrete members. This program

can predict the load-deformation response of a variety of reinforced concrete structures. The theoretical bases of *VecTor2* are the Modified Compression Field Theory (*Vecchio and Collins 1986*) and the Disturbed Stress Field Model (*Vecchio et al. 2001*). *VecTor2* models cracked concrete as an orthotropic material with smeared, rotating cracks. Recent versions of *VecTor2* (*FormWorks, VecTor2 & Augustus Bundle (Ver. 3.5)*) have incorporated additional constitutive models over that of MCFT for a variety of second-order effects including compression softening, tension stiffening, tension softening, and tension splitting. *VecTor2* is based on finite element models for use in a fine mesh of low-powered elements which has advantages of computational efficiency and numerical stability. It is also well suited to reinforced concrete structures, which require a relatively fine mesh to model reinforcement detailing and local crack patterns. Depending on the member geometry, loading condition and reinforcement configuration the number of elements used in this program varies with the maximum limit for this program being 1000 elements. *VecTor2* reads ASCII text files for input and outputs binary and ASCII text files for analysis results. The software *Augustus* provides graphical post-processing capabilities for the analysis results of *VecTor2*. *Navarro-Gregori et al. (2013)* utilized *VecTor2* in their shear load-deflection response comparisons and concluded that *VecTor2* resulted in close response prediction to their model (PR model) for most of the specimens considered except some minor differences near ultimate load. (See Figure 2-15).

Response 2000 (R2K) (*Bentz, 2000*) is a non-linear sectional analysis program for the analysis of reinforced concrete elements subjected to shear based on the Modified Compression Field Theory. *Response 2000* uses a layered sectional program to implement the MCFT relationships for analysis of cracked reinforced concrete. It can calculate the strength and deformation for beams and slabs subjected to combinations of axial load, moment and shear. *Response 2000* is based on the assumptions, implicit in the program, that plane sections remain plane and that there is no transverse clamping stress across the depth of the beam which are generally regarded as appropriate for sections located a reasonable

distance away from load or reaction locations. Input parameters include member geometry, loading, and material properties including the stress-strain relationships for the reinforcement and for the concrete. The stress-strain response of concrete and conventional steel can be selected from different defined models built into the program. *R2K* can calculate the load-deflection response for a prismatic reinforced concrete member subjected to point loads or a uniformly distributed loading. To allow this it is necessary to calculate the full moment-shear interaction diagram and the stress / strain state for a series of cross sections. *R2K* divides the member under consideration into 20 short segments and for each segment the axial load, moment and shear force are determined from the applied loads. Then the curvature and shear strain corresponding to these load level is interpolated from the interaction diagram and is integrated with the moment-area method to calculate the load deflection relationship.

No publication suggests the explicit use of *Response 2000* for deflection modeling of reinforced concrete beams. Studies conducted by *Munikrishna et al. (2008)* and *Sumpter et al. (2009)* utilized the program *Response 2000* solely for predicting the shear strength of the specimens without further look on the full shear-deflection behaviour.

2.7 Summary

High performance ASTM A1035 Grade 690 steel has mechanical properties different from conventional Grade 420 reinforcing steel with an effective yield strength nearly twice as large. In addition ASTM A1035 steel is more corrosion resistant than the conventional Grade 420 steel. Thus, there is increasing interest in the use of ASTM A1035 steel to reduce maintenance and construction costs of new reinforced concrete structures. However, due to the lack of a distinct yield point for ASTM A1035 steel and the restrictions in the existing design code requirements on the maximum yield strength for design, the efficient use of this material has not been achieved in new construction.

Literature has shown that both a size effect and a strain effect in shear exist and are significant. There is no general agreement as to how or whether to account for these effects explicitly in current design standards such as the *ACI 318* code. There is also evidence that aggregate interlock is the dominant mechanism of shear transfer in slender concrete members without stirrups and one of the components of shear resistance in members with transverse reinforcement. (*Fenwick and Paulay* (1964, 1968), *Taylor* (1970), *Kani et al.* (1979), *Sherwood* (2008)). Studies have shown that the shear crack width proportionally increases with the average member strain (related to strain in the reinforcement) and with the spacing between shear cracks implying that the reinforcement strain and diagonal crack spacing are main factors on shear behaviour of concrete members. (*Bentz et al.* 2006). There is clearly a need for further investigation of the strain effect in shear behaviour, with particular emphasis on the non-linear stress-strain response of ASTM A1035 steel.

The shear strength of reinforced concrete slabs and beams is influenced by several parameters reflecting the loading, member geometry and reinforcement configuration. Previous studies showed that the shear stress at failure decreases as the reinforcement ratio decreases and that the shear capacity relationships that

consider longitudinal reinforcement strains have better correlation with test data than models based on other parameters. (*Lubell et al. 2009*) It is also noted that different sectional shear capacity code models do not consider the influence of reinforcement configuration equally. Since the use of higher yield strength ASTM A1035 steel for concrete members will result in lower reinforcement ratios, validating the shear behaviour for the higher corresponding reinforcement strains is evident. The applicability of existing shear design models for concrete members constructed with ASTM A1035 steel longitudinal and transverse reinforcement needs to be validated. Modifications to these models to account for the non-linear stress-strain response of the reinforcement should be considered. Moreover, development of more accurate general analytical shear design models for concrete members reinforced with ASTM A1035 steel reinforcement is required for the efficient use of this innovative material.

The use of ASTM A1035 steel with higher yield strength which results in lower reinforcement ratios, increases the possibility of serviceability deflection and cracking problems. This warrants a review and possible modification of current code provisions for member deflection. Prior studies have shown that the calculated deflection based on code models is in general much less than the actual deflections. (*Branson (1977), Bischoff (2005), Tang and Lubell (2008)*). One reason for the possible under-estimation of the deflection models may be caused by ignoring the shear deformations. This may be even more significant for the case of slender reinforced concrete beams containing ASTM A1035 steel with relatively lower shear span to depth ratios where the shear deformation as a fraction of the total deformation is greater. When using the nonlinear stress-strain curve of ASTM A1035 steel reinforcement in design, the tensile stress in the reinforcement under service loads may exceed the proportional limit. The impact of this higher tensile stress on member deflection and crack control should be considered. Thus, it is important to evaluate and develop a deflection model that takes into account the relationships between the shear deformations and other design parameters.

The experimental tests and analytical studies conducted in this research and described in the following chapters have been designed to address the above issues. The ultimate goal of the current study is to improve the generality, accuracy and safety of shear design models and the efficient utilization of high performance ASTM A1035 steel reinforcement for slender reinforced concrete beams and slabs. Moreover evaluation and modification of current deflection models for reinforced concrete beams is a key goal.

3. EXPERIMENTAL PROGRAM

3.1 General

An experimental program was conducted at the I.F. Morrison Structural Engineering Laboratory at the University of Alberta to study the behaviour of concrete members reinforced with ASTM A1035 steel. The main objective of this experimental program was to investigate the influence of higher reinforcement strains on the shear and deflection behaviour of one-way concrete slabs and beams. Test specimens used in this study were reinforced with different combinations of ASTM A1035 and A615 steel as longitudinal and/or transverse reinforcement. The influence of the longitudinal reinforcement ratio and the transverse reinforcement type on the load-deflection response and the shear strength of members were given emphasis by testing specimens with a large range of reinforcement configurations. The influence of member size on shear strength of members without stirrups was also considered by using a range of slab depths. Note that these main test parameters were selected as they can affect the so called “size effect” and “strain effect” on shear in reinforced concrete by influencing the aggregate interlock of cracked concrete members.

A total of sixteen shear critical specimens were constructed and tested in the laboratory. Six specimens referred to as “*SLABS*” were longitudinally reinforced with ASTM A1035 steel but did not contain stirrups. The remaining ten specimens, referred to as “*BEAMS*”, contained either ASTM A1035 or Grade 420 stirrups and were longitudinally reinforced with either ASTM A1035 or Grade 420 steel. All specimens were tested under three-point bending. Test specimens were designed using an assumed yield strength of 830 MPa for the ASTM A1035 steel (i.e. the effective yield strength based on the 0.2% offset method) and with an average measured value of about 440 MPa for the conventional Grade 420 reinforcement. All specimens were designed according to the general requirements of the three shear design code models considered in this study: *CSA A23.3-04*, *ACI 318-11* and *Eurocode 2-04*. The current test data are believed to

complement and widen the range of parameters considered in the limited existing test data available in the literature for shear behaviour of concrete members reinforced with ASTM A1035 steel. (*Hassan et al. (2008), Garay-Moran and Lubell (2008), Sumpter et al. (2009), Munikrishna et al. (2008), Shahrooz et al. (NCHRP 679, (2011)).*

3.2 Details of Slab Specimens

Six slab strips were constructed in the laboratory and tested to failure under three-point bending. All specimens contained ASTM A1035 longitudinal reinforcement and no transverse reinforcement. The main test parameters included the longitudinal reinforcement ratio ρ_L , concrete compression strength f'_c and the overall depth, h . Details of all slab specimens are summarized in Table 3-1 and in Figures 3-1 and 3-2.

Specimens were constructed to two different overall heights h of 305 mm and 600 mm, having total lengths of 2675 and 4845 mm, respectively. Span lengths L of 1925 mm and 4095 mm were utilized to achieve nearly constant shear-span to depth ratio (average a/d of about 3.57) for the specimens. This value of a/d (in the range of 2.5 – 4.0) was selected to study slender members showing significant shear behaviour as more slender members are typically governed by flexural strength (*Wight and MacGregor 2009*). The width of all specimens was $b_w = 305$ mm. Previous research showed that the one-way shear stress at failure is unaffected by member width when relatively uniform loading and geometry conditions occur across the member width (e.g. *Lubell 2006, Sherwood et al. 2006*). Thus, the specimens would be representative of the performance of wider one-way slabs in practice.

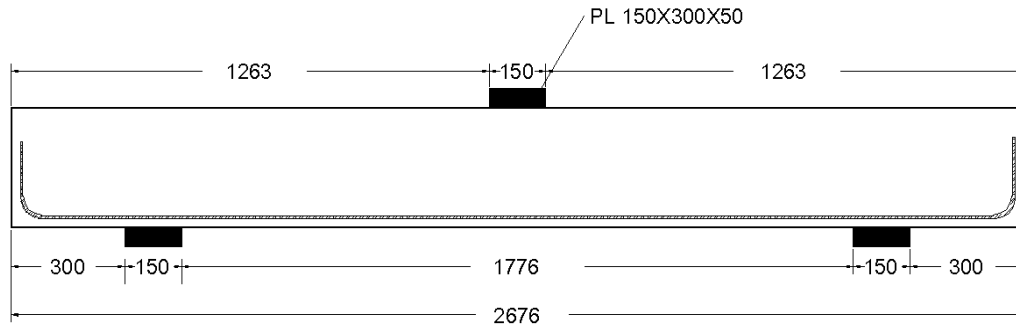
Specimens had longitudinal reinforcement ratios of $\rho_L = 0.45 \%$ or 0.23% . Reinforcement ratios were selected to achieve a range of reinforcement stresses (or strains) at time of failure. Moreover the range of reinforcement ratios used are

within the minimum and maximum limits specified in the design codes summarized in Chapter 2. The longitudinal reinforcement was placed in a single layer with clear cover to the specimen soffit of 20 mm, consistent with typical slab construction practices. The longitudinal reinforcing bars were hooked upward beyond the support locations to enhance the anchorage conditions. There were two companion specimens for each configuration, where specimens were from different batches of ready-mix concrete.

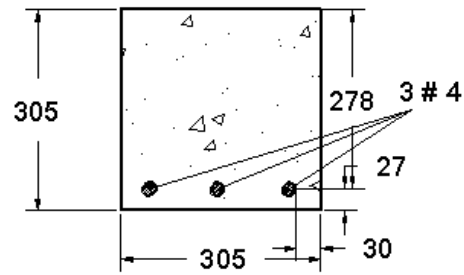
Table 3-1: Slab Specimen Details.

<i>Specimen</i>	<i>b_w</i> (mm)	<i>d</i> (mm)	<i>h</i> (mm)	<i>a /d</i>	<i>Longitudinal Reinforcement (ASTM A1035)</i>	<i>ρ_L</i> (%)	<i>f_{yL}*</i> (MPa)	<i>f_c'</i> (MPa)
<i>S-1</i>	305	278	305	3.55	3 # 4	0.46	825	53
<i>S-2</i>	305	278	305	3.55	3 # 4	0.46	825	59
<i>S-3</i>	305	569	600	3.60	2 # 7	0.45	830	49
<i>S-4</i>	305	569	600	3.60	2 # 7	0.45	830	57
<i>S-5</i>	305	573	600	3.57	3 # 4	0.23	825	53
<i>S-6</i>	305	573	600	3.57	3 # 4	0.23	825	57

* Equivalent yield strength based on the 0.2 % offset method.



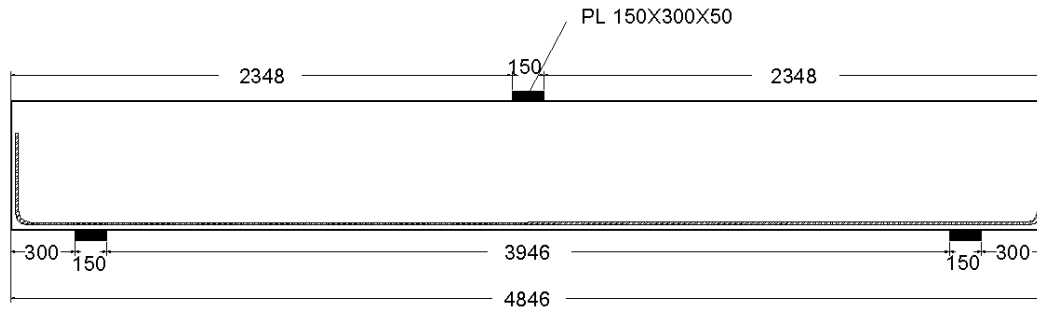
(a)



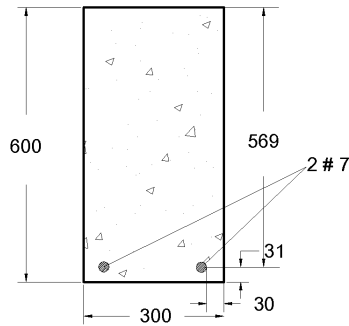
(b) *S-1* and *S-2*

All dimensions shown in this Figure are in mm.

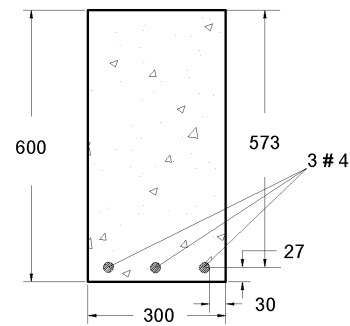
Figure 3-1: Details of Slab Specimens *h* with 305 mm (a) Elevation (b) Cross section.



(a)



(b) S-3 and S-4



(c) S-5 and S-6

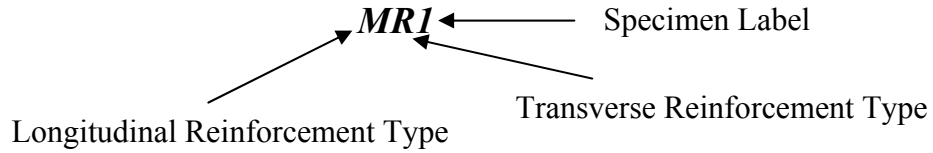
All dimensions shown in this Figure are in mm.

Figure 3-2: Details of Slab Specimens h with 600 mm (a) Elevation (b) and (c) Cross sections.

3.3 Details of Beam Specimens

Ten large scale beam specimens were constructed in the I.F. Morrison Structural Engineering Laboratory and tested to failure. All beams were designed according to the general requirements of three current design codes, namely, *CSA A23.3-04*, *ACI 318-11* and *Eurocode 2-04*. Specimens contained longitudinal reinforcement and transverse reinforcement with different combinations of ASTM A1035 Grade 690 steel and conventional Grade 420 steel. The main test parameters included the type of steel used in the longitudinal and transverse reinforcement and the corresponding reinforcement ratios.

The nomenclature used for the beam specimens is described as follows.



where;

M - is high-performance ASTM A1035 reinforcing steel.

R - is conventional Grade 420 steel.

For each specimen ID the first letter represents the type of longitudinal reinforcement, the second letter designates the type of transverse reinforcement, and the number is the specimen label.

The shear span to depth ratio (a/d) was selected to study slender members showing significant shear behaviour (*Wight and MacGregor 2009*). Reinforcement ratios were selected to achieve a range of reinforcement stresses (or strains) at time of failure. The range of reinforcement ratios and the spacing of stirrups used are within the minimum and maximum limits specified in the design codes summarized in Chapter 2. There were two companion specimens for each configuration using ASTM A1035 longitudinal reinforcement, where specimens were made to have different type of steel in the transverse reinforcement. Two specimens with Grade 420 longitudinal steel reinforcement differed by the spacing of ASTM A1035 stirrups.

In all cases the longitudinal reinforcing bars were hooked upward beyond the support locations to enhance the anchorage of the longitudinal bars. The target compressive strength of the concrete for all beam specimens was 50 MPa. Details of the beam specimens are summarized in Table 3-2 and described in Sections 3.3.1 through 3.3.5.

Table 3-2: Beam Specimen Details.

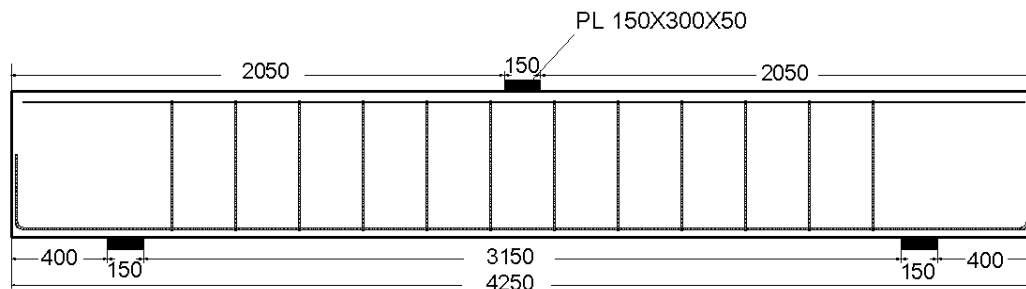
<i>Specimen</i>	<i>h</i> (mm)	<i>d</i> (mm)	<i>a/d</i>	<i>Longitudinal</i> <i>Reinforcement</i>	<i>Transverse</i> <i>Reinforcement</i>	f_{yL}^* (MPa)	f_{yt}^* (MPa)	f_c' (MPa)
<i>RM1</i>	600	523	3.2	8 – 25M	# 3 @ 320 mm	408	550	41
<i>RM2</i>	600	523	3.2	8 – 25M	# 3 @ 265 mm	408	550	45
<i>MR1</i>	1000	935	3.0	4 # 7	10M @ 440 mm	690	426	49
<i>MR2</i>	1000	935	3.0	3 # 9	10M @ 440 mm	690	426	50
<i>MR3</i>	1000	885	3.0	11 # 7	10M @ 440 mm	690	426	48
<i>MR4</i>	1000	885	3.0	11 # 7	10M @ 220 mm	690	426	50
<i>MM1</i>	1000	935	3.0	4 # 7	# 3 @ 440 mm	690	550	50
<i>MM2</i>	1000	935	3.0	3 # 9	# 3 @ 440 mm	690	550	52
<i>MM3</i>	1000	885	3.0	11 # 7	# 3 @ 440 mm	690	550	48
<i>MM4</i>	1000	885	3.0	11 # 7	# 3 @ 220 mm	690	550	48

* Yield strength for ASTM A1035 steel based on *ACI ITG-6R-10*. Average measured yield strength for conventional Grade 420 steel.

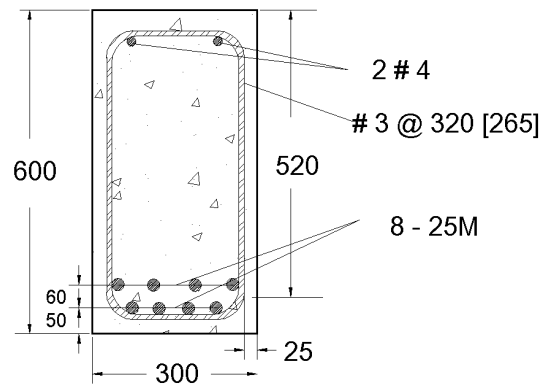
3.3.1 Details of Specimens *RM1* & *RM2*

Specimens *RM1* & *RM2* each had a rectangular cross section of 300 x 600 mm. Span lengths of 3300 mm were utilized to achieve a constant shear-span to depth ratio of 3.2 for both specimens. The longitudinal tensile reinforcement consisted of 8-25M conventional Grade 420 bars in two layers giving $\rho_L = 2.55\%$. The transverse reinforcement ratios were 0.15% and 0.18% for *RM1* and *RM2*, respectively. The transverse reinforcement consisted of ASTM A1035 Grade 690 steel bars. The corresponding equivalent stirrup ratios ($A_v f_{yt} / b_w s$) were 0.83 MPa and 0.99 MPa, respectively based on a yield strength f_{yt} of 550 MPa. The stirrup bars were size #3, with center to center spacing of either 320 mm or 265 mm (i.e. $0.7d_v$ or $0.5d$) for specimens *RM1* and *RM2*, respectively where $d_v = 0.9d$. The spacing of the transverse reinforcement for *RM1* & *RM2* were selected in accordance with the maximum permitted spacing specified in *CSA A23.3-04* and

ACI 318-11 design standards, respectively. Dimensions and reinforcement details of specimens *RM1* & *RM2* are shown in Figure 3-3.



(a)



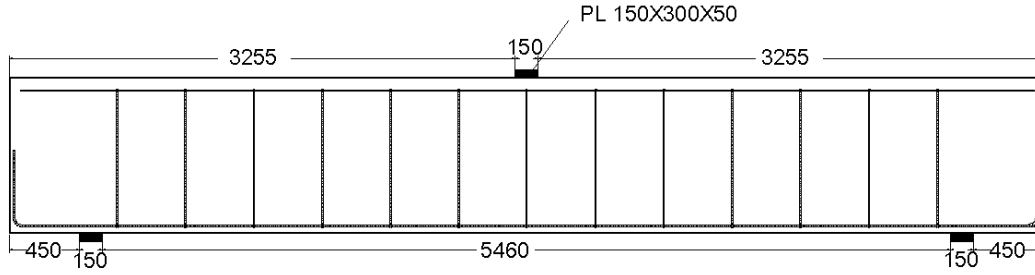
(b)

All dimensions shown in the Figures are in mm.

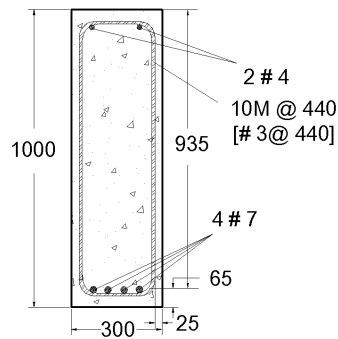
Figure 3-3: Details of Beam Specimens *RM1* [*RM2*] (a) Elevation (b) Cross section.

3.3.2 Details of Specimens *MR1* & *MM1*

Specimens *MR1* & *MM1* each had a rectangular cross section of 300 x 1000 mm. The longitudinal tensile reinforcement consisted of 4 # 7 ASTM A1035 Grade 690 steel in single layer with the corresponding steel reinforcement ratio of $\rho_L = 0.55\%$. The transverse reinforcement consisted of 10M conventional Grade 420 bars for beam *MR1* and # 3 ASTM A1035 Grade 690 bars for beam *MM1*. In both specimens the center to center spacing of the transverse reinforcement was 440 mm. The spacing of the transverse reinforcement were selected in accordance with the maximum permitted spacing specified in the *ACI 318-11* design code ($0.5d$). The transverse reinforcement ratios were $\rho_t = 0.15\%$ and $\rho_t = 0.11\%$ for *MR1* and *MM1*, respectively. The corresponding equivalent stirrup ratios (A_{vf}/b_wS) were 0.64 MPa and 0.61 MPa, respectively. The total length of each specimen was 6660 mm with center to center span between supports of 5610 mm and a shear span to depth ratio of 3.0. Dimensions and reinforcement details of specimens *MR1* & *MM1* are shown in Figure 3-4.



(a)



(b)

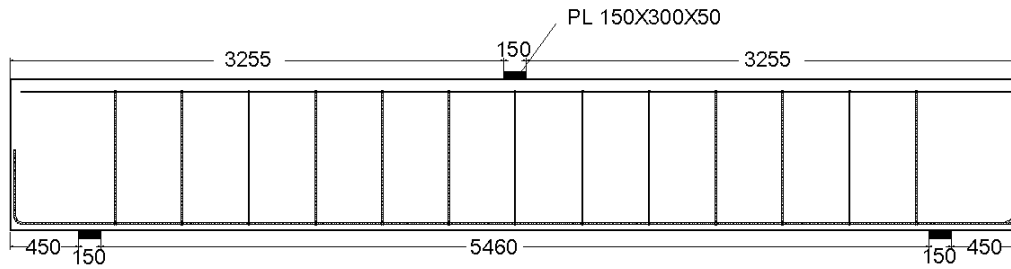
All dimensions shown in the Figures are in mm.

Figure 3-4: Details of Beam Specimen *MR1* [MMI] (a) Elevation (b) Cross section.

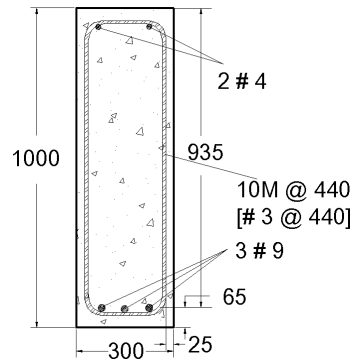
3.3.3 Details of Specimens *MR2* & *MM2*

Specimens *MR2* & *MM2* each had a rectangular cross section of 300 x 1000 mm. The longitudinal tensile reinforcement consisted of 3 # 9 ASTM A1035 Grade 690 steel in single layer with the corresponding steel reinforcement ratio of $\rho_L = 0.69\%$. The transverse reinforcement consisted of 10M conventional Grade 420 bars for beam *MR2* and # 3 ASTM A1035 Grade 690 bars for beam *MM2*. In both specimens the center to center spacing of the transverse reinforcement was 440 mm. The spacing of the transverse reinforcement were selected in accordance with the maximum permitted spacing specified in the *ACI 318-11* design code.

The transverse reinforcement ratios were $\rho_t = 0.15\%$ and $\rho_t = 0.11\%$ for *MR2* and *MM2*, respectively. The corresponding equivalent stirrup ratios ($A_{vf}/b_w S$) were 0.64 MPa and 0.61 MPa, respectively. The total length of each specimen was 6660 mm with center to center span between supports of 5610 mm and a shear span to depth ratio of 3.0. Dimensions and reinforcement details of specimens *MR2* & *MM2* are shown in Figure 3-5.



(a)



(b)

All dimensions shown in the Figures are in mm.

Figure 3-5: Details of Beam Specimen *MR2* [*MMI*] (a) Elevation (b) Cross section.

3.3.4 Details of Specimens *MR3* & *MM3*

Specimens *MR3* & *MM3* each had a rectangular cross section of 300 x 1000 mm. The longitudinal tensile reinforcement consisted of 11 # 7 ASTM A1035 Grade 690 steel in three layers with the corresponding steel reinforcement ratio of $\rho_L = 1.60\%$. The transverse reinforcement consisted of 10M conventional Grade 420 bars for beam *MR3* and # 3 ASTM A1035 Grade 690 bars for beam *MM3*. In both specimens the center to center spacing of the transverse reinforcement was 440 mm. The spacing of the transverse reinforcement were selected in accordance with the maximum permitted spacing specified in the *ACI 318-11* design code. The transverse reinforcement ratios were $\rho_t = 0.15\%$ and $\rho_t = 0.11\%$ for *MR3* and *MM3*, respectively. The corresponding equivalent stirrup ratios ($A_v f_y / b_w S$) were 0.64 MPa and 0.61 MPa, respectively. The total length of each specimen was 6360 mm with center to center span between supports of 5310 mm and a shear span to depth ratio of 3.0. Dimensions and reinforcement details of specimens *MR3* & *MM3* are shown in Figure 3-6.

Technical drawing of a channel section. The drawing shows a cross-section of a channel with a total width of 5160 mm. The channel has a depth of 150 mm. The material is specified as PL 150X300X50. The drawing includes dimensions for the flanges (3105 mm) and the web (150 mm). The channel is shown with a U-shaped profile and a central web.

77

3.4 Materials

3.4.1 Reinforcing Steel

Two different types of reinforcing steel were used, high performance ASTM A1035 Grade 690 steel and conventional Grade 420 steel. Tension coupon tests were completed for three randomly selected bars from each bar size and steel type to determine the stress-strain behaviour of the material according to ASTM A370-07. The tension coupon samples were 500 mm long and were tested until failure in an MTS 1000 machine under a displacement controlled protocol, as shown in Figure 3-8. For each test an extensometer having 50 mm gauge length was utilized to measure the load-elongation response of the coupon to peak load. The extensometer was removed prior to failure. The average yield strength f_y and modulus of elasticity E_s were obtained from the resulting stress-strain curves.

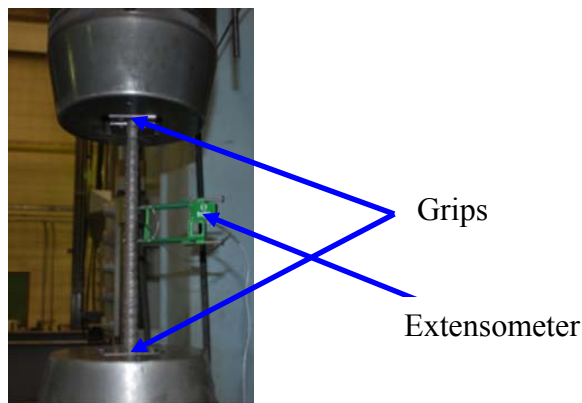


Figure 3-8: Tension Coupon Test for Reinforcement Bars.

3.4.1.1 ASTM A1035 Reinforcing Steel

All specimens in this research program contained a commercially available micro-composite multi-structural formable steel (MMFX2) conforming to ASTM A1035-11 as longitudinal and/or transverse reinforcement. Reinforcing bars were produced to US customary sizes of #3, #7 and #9. Tension coupon tests were

completed and for each coupon a linear stress-strain response was observed up to a stress level of approximately 480 MPa, beyond which the axial stiffness reduced at an increasing rate. There was no well defined yield point or yield plateau. An effective yield stress (f_y) and corresponding yielding strain (ϵ_y) were estimated using the 0.2 % offset method (ASTM A370-07). The ultimate tensile strengths of the bars (f_u) were also determined from the tests. Typical stress-strain results from coupon tests using extensometer readings are summarized in Table 3-3 and Figure 3-9.

The *ACI ITG-6R-10* stress-strain relationship for ASTM A1035 Grade 690 steel in metric notation is given as:

$$f_s = \begin{cases} 200,000 \epsilon_s & \text{for } \epsilon_s \leq 0.0024 \\ 1170 - \frac{2.96}{\epsilon_s + 0.0019} & \text{for } 0.0024 < \epsilon_s \leq 0.02 \\ 1040 & \text{for } 0.02 < \epsilon_s \leq 0.06 \end{cases} \quad (3-1)$$

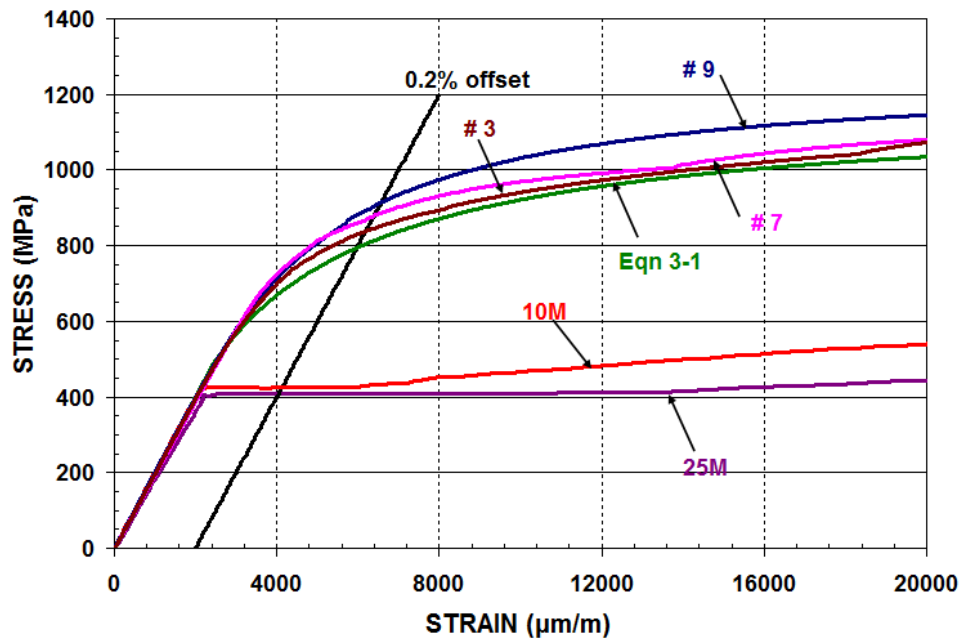
Figure 3-9 compares the coupon test results of the Grade 690 steel rebars (#3, #7 and #9) with equation 3-1. Equation 3-1 gives the lower bound stress for a given strain of ASTM A1035 steel. This makes equation 3-1 to slightly overestimate the strain in the steel at higher stress levels. However, in general equation 3-1 is in good agreement with the test results and was adopted for use in the analytical and numerical models in this study.

Table 3-3: Conventional Grade 420 and ASTM A1035 Grade 690 Reinforcement Steel Average Properties.

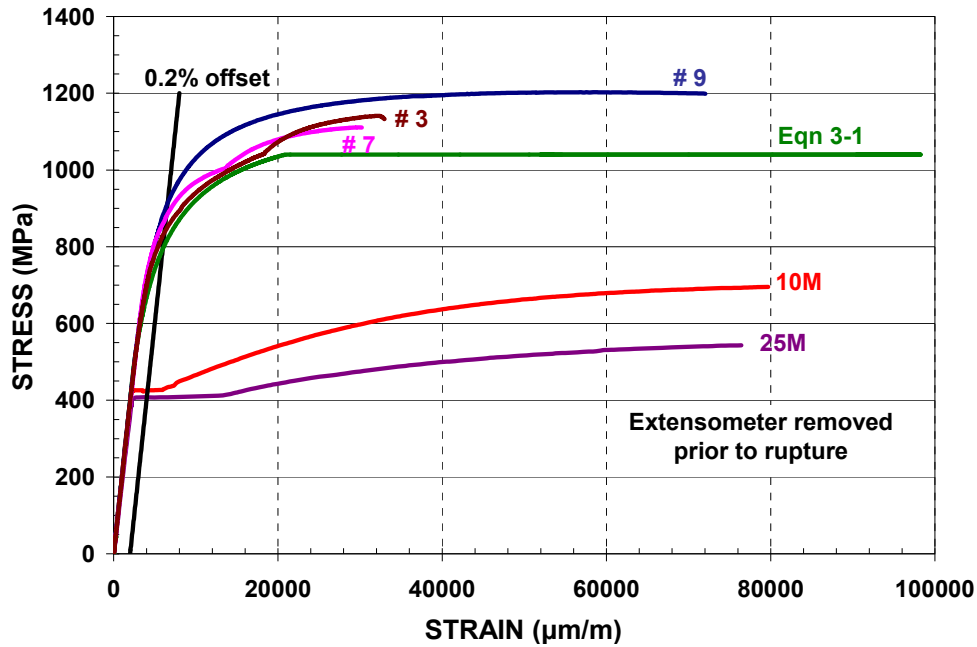
<i>Bar</i>	<i>Steel Type</i>	<i>Area (mm²)</i>	<i>E_s (MPa)</i>	<i>f_y[*] (MPa)</i>	<i>ε_y[*] (mm/mm)</i>	<i>f_y^{**} (MPa)</i>	<i>ε_y^{**} (mm/mm)</i>	<i>f_u (MPa)</i>
10M	Grade 420	100	194300	426	0.0025	-	-	630
25M	Grade 420	500	183800	408	0.0022	-	-	545
#3	Grade 690	71	198000	830	0.0061	790	0.0060	1140
#4	Grade 690	129	196700	825	0.0060	790	0.0060	1051
#7	Grade 690	387	197800	830	0.0061	790	0.0060	1110
#9	Grade 690	645	200300	920	0.0067	790	0.0060	1200

* Effective yield strength and yield strain for ASTM A1035 Grade 690 steel (0.2 % offset method) and measured yield strength/strain for conventional Grade 420 steel.

** Yield strength and yield strain for ASTM A1035 Grade 690 steel (equation 3-1).



(a)



(b)

Figure 3-9: Representative Tension Stress-Strain Response for conventional Grade 420 and ASTM A1035 Coupons (a) Enlarged Initial Response, (b) Full Response up to Failure.

3.4.1.2 Grade 420 Reinforcing Steel

Grade 420W deformed reinforcing steel bars in the Canadian standard size designations of 10M and 25M were used for transverse reinforcement of beam series *MR* and for longitudinal reinforcement of beam series *RM*, respectively. Tension coupon tests were completed to determine the stress-strain behaviour as shown in Figure 3-8. Linear stress-strain responses were observed up to a stress level of approximately 400 MPa at which point a defined yield plateau was formed followed by strain hardening portion before rupture. (See Figure 3-9). Using extensometer readings, average stress-strain results from three randomly selected specimens are summarized in Table 3-3.

3.4.2 Concrete

All concrete was supplied by a local ready-mix company and had a maximum aggregate size of 10 mm. The concrete mix design was varied based on the specimen type to achieve different target concrete strengths. Specimens were moist cured under wet burlap and plastic sheeting for 7 days, and then removed from the formwork and stored in the ambient laboratory conditions until the day of testing.

Standard 100 x 200 mm cylinders were produced for each casting and cured under the same conditions as the specimens. Compression cylinder tests were conducted according to ASTM C39 / C39M-05 on the 28th day after casting as well as on the day of test of each specimen. A 2600 kN capacity MTS universal testing machine was used to perform the compression tests on the cylinders as shown in Figure 3-10. Most of the cylinders were tested to determine their breaking strengths. Three cylinders were capped with sulfur prior to testing and instrumented using a collar with three linear variable displacement transducers (LVDTs) at 120° separation to measure the average vertical deformation at mid-height. The LVDTs, with initial gauge length of 100 mm, were connected to a data acquisition system along with the MTS output. A displacement controlled loading rate of 0.2 mm/min was used for each test, allowing capture of the full load-displacement relationship in compression including the post-peak response (see Figure 3-11). The average measured concrete strengths of three cylinders on the day of test of each specimen are summarized in Table 3-4.

Table 3-4 Compression Test Results and age of Samples at the Day of Test of Specimens.

<i>Specimen</i>	<i>Batch Label</i>	<i>Average f_c' (MPa)</i>	<i>Age (days)</i>
<i>S-1</i>	A	53	92
<i>S-3</i>	A	49	75
<i>S-5</i>	A	53	92
<i>S-2</i>	B	59	92
<i>S-4</i>	B	57	51
<i>S-6</i>	B	57	51
<i>RM1</i>	1	41	35
<i>RM2</i>	1	45	60
<i>MM1</i>	2	50	49
<i>MR1</i>	2	49	56
<i>MM2</i>	3	52	48
<i>MR2</i>	3	50	51
<i>MM3</i>	4	48	45
<i>MR3</i>	4	48	43
<i>MM4</i>	5	48	52
<i>MR4</i>	5	50	56

The preliminary design of slab specimens (Section 3.2) was completed on the basis of normal density concrete with nominal target compressive strengths of 35 MPa (Batch A) and 70 MPa (Batch B). Specimens *S-1*, *S-3* and *S-5* were from Batch A, while *S-2*, *S-4*, and *S-6* were from Batch B (See Section 3.2). However, as shown in Table 3-4 the test results showed that the concrete strength from Batch A and Batch B were similar, thereby giving near duplicate test specimens.

For the beam specimens described in Section 3.3, preliminary design of the specimens was completed on the basis of normal density concrete with a nominal compressive strength of 50 MPa. Five batches of concrete were ordered to cast two beam specimens at a time. Table 3-4 shows the batch label, specimen designations and the corresponding compressive strength on the day of test. The

test results showed that the compressive strength from all batches of concrete for the beam specimens was close to the target strength.

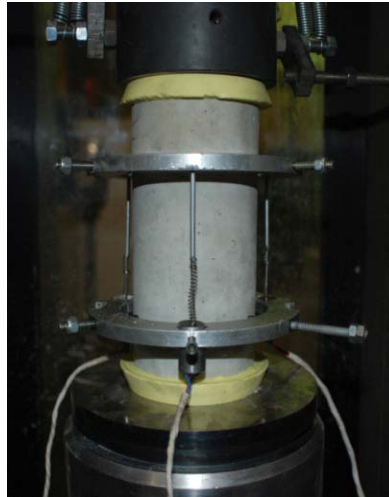


Figure 3-10 Typical Compression Test of Concrete Cylinder (Batch 4).

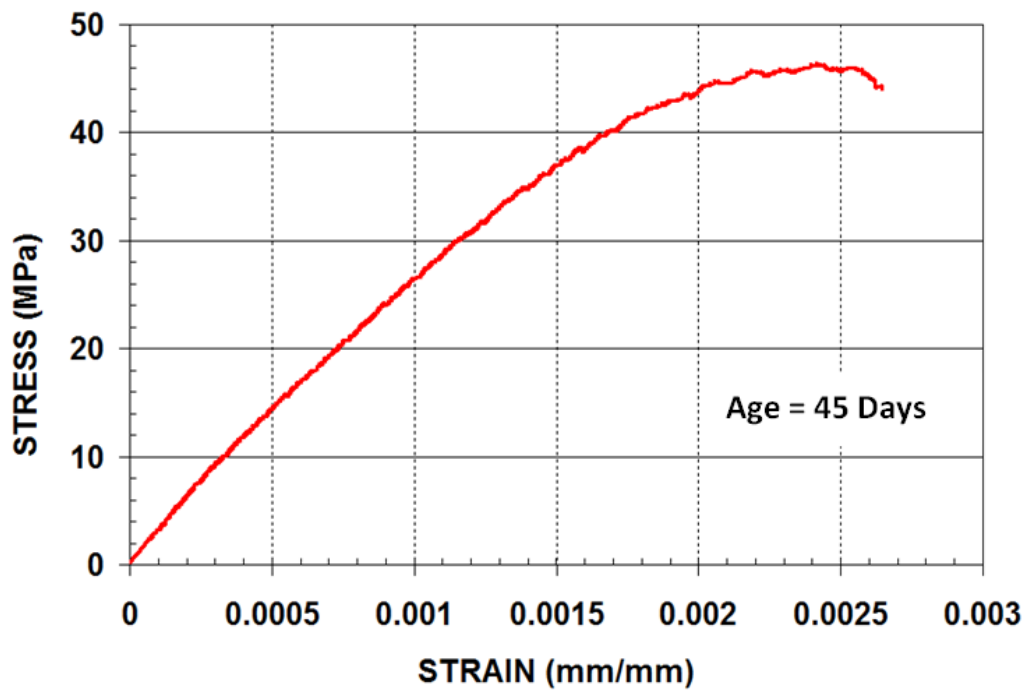


Figure 3-11 Typical Stress-Strain Curve of a Concrete Cylinder (Batch 4).

3.5 Fabrication of Specimens

All specimens were built in the I. F. Morrison Structural Engineering Laboratory at the University of Alberta. Existing wooden formwork was used for the large size specimens ($h = 600$ mm and $h = 1000$ mm). Steel formwork was used for slab specimens with height $h = 305$ mm. The formwork was leveled, oiled and all dimensions were checked prior to each casting. The construction process of each specimen started with the instrumentation of the reinforcing bars using electrical resistance strain gauges. The steel cages were assembled and carefully placed in the formwork using the overhead crane in the laboratory (See Figure 3-12). Lifting hooks using steel rebars were placed outside of the test region as shown in Figure 3-12 for handling during instrumentation and testing. Figure 3-13 shows the placing and vibration of the concrete during the casting process.

Seven separate castings were scheduled to build six slab strips and ten beam specimens. The specimens were moist cured under wet burlap and plastic for one week, removed from the formwork and stored in the ambient laboratory environment until testing. Cylinder samples were also cast simultaneously with the beams for each casting and were cured under the same conditions, as described in Section 3.4.2.



a) Slab Specimens

b) Beam Specimens

Figure 3-12 Steel Cages Prior to Casting of Specimens.



a) Slab Specimens



b) Beam Specimens

Figure 3-13 Placing and Vibration of the Concrete During Casting of Specimens.

3.6 Instrumentation and Testing Procedures

3.6.1 General

All slab and beam specimens were simply supported at each end and loaded at mid-span using a single concentrated load applied from an MTS 6000 testing frame. A typical specimen setup prior to test is shown in Figure 3-14. Steel plates 150 mm wide and 50 mm thick were used across the full specimen width as bearing plates at the load and support points. A thin layer of high strength plaster between the concrete and the bearing plates was used to ensure uniform contact. As depicted in Figure 3-14 the support bearing plates were placed on knife edge supports which were situated above roller assemblies to allow free in plane rotation and longitudinal translation of specimens during the test. The supporting system was placed on a stiffened steel beam which in turn was supported on the laboratory strong floor.

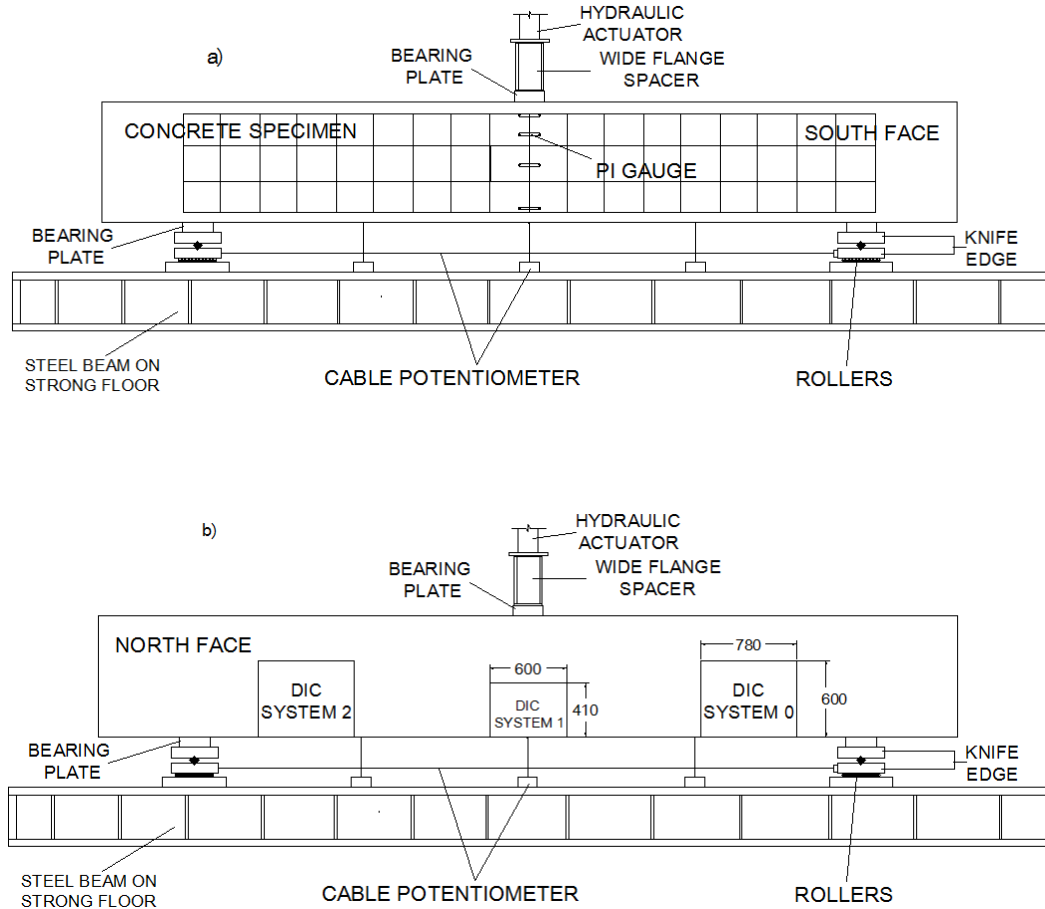


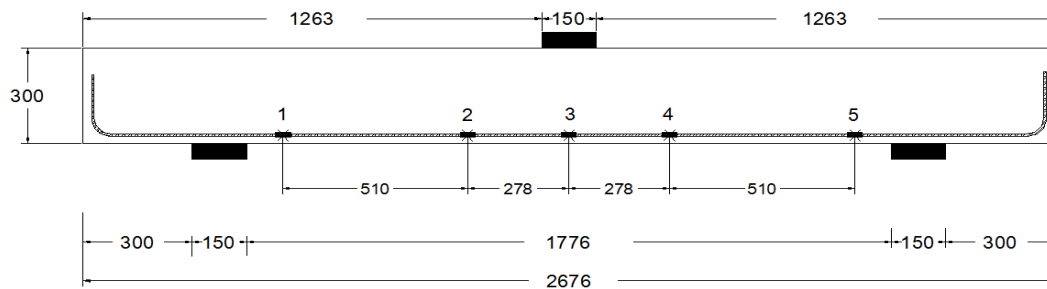
Figure 3-14 Typical Specimen Setup a) South Face b) North Face.

3.6.2 Instrumentation

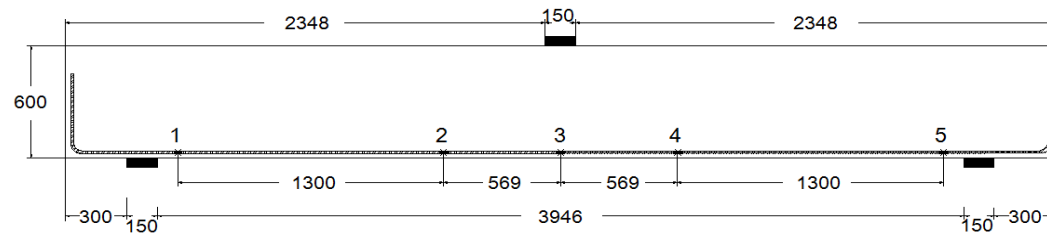
In order to quantify the shear and deflection behaviour, instrumentation was used in important zones of the specimens. Strains in the reinforcement, member deformations and the crack development were important parameters measured during the experimental program. For this purpose, strain gauges, linear variable displacement transducers (LVDTs), PI gauges and crack width comparator gauges were used. The relative longitudinal movement of the supports was measured using a cable transducer affixed to the interior faces of the support points. A deformation measurement system based on the digital image correlation technique

(Correlated Solutions Inc., 2009) was also used for the beam specimens. Details of the instrumentation used are shown in Figure 3-14.

Electrical resistance strain gauges were mounted on the longitudinal tension reinforcement to measure the strain at locations of interest: at mid-span, at the critical shear locations taken at ‘d’ away from mid-span on each side, and close to each support. The behaviour of the transverse reinforcement was also studied using strain gauges mounted at mid height of selected stirrups in the shear span zone for the beam specimens. The strain gauges used in this project were 120 Ω gauges. All strain gauges were placed on the reinforcing bars prior to building the steel cages. The quantity of strain gauges for slab specimens was eight with two strain gauges near the mid-span locations (2, 3 & 4) and one strain gauge near support locations (1 & 5). Beam specimens contained between 14 and 24 strain gauges on multiple layers of reinforcement. Details of strain gauge locations for specimens are shown in Figures 3-15 and 3-16.

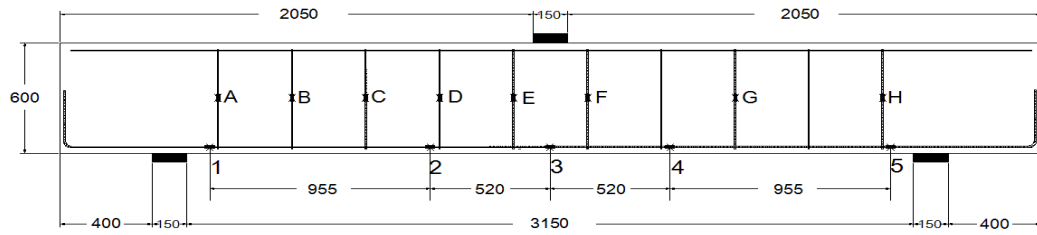


a) Specimen with $h = 300$ mm (S-1 & S-2)

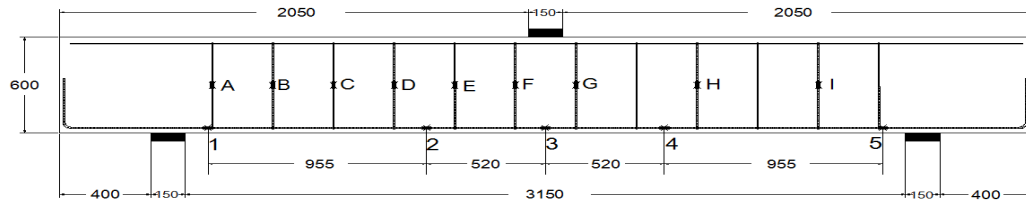


b) Specimen with $h = 600$ mm (S-3, S-4, S-5 & S-6)

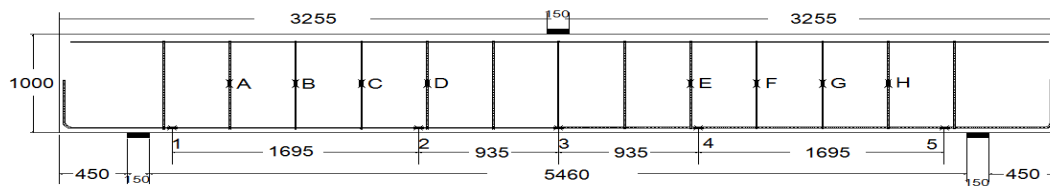
Figure 3-15 Strain Gauge Layout for Slab Specimens.



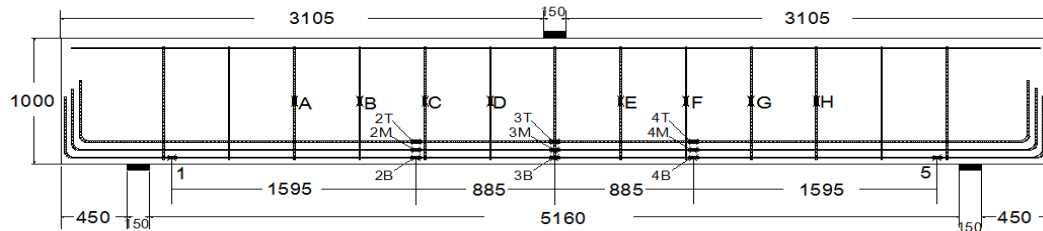
a) Beam Specimen *RM1*



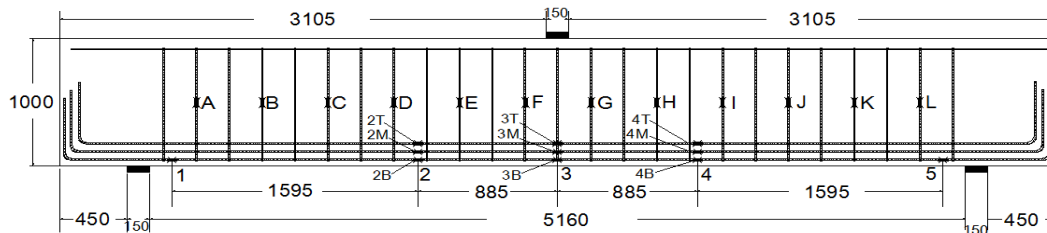
b) Beam Specimen *RM2*



c) Beam Specimens *MR1*, *MR2*, *MM1* & *MM2*



d) Beam Specimens *MR3* & *MM3*



e) Beam Specimens *MR4* & *MM4*

Figure 3-16 Strain Gauge Details for Beam Specimens.

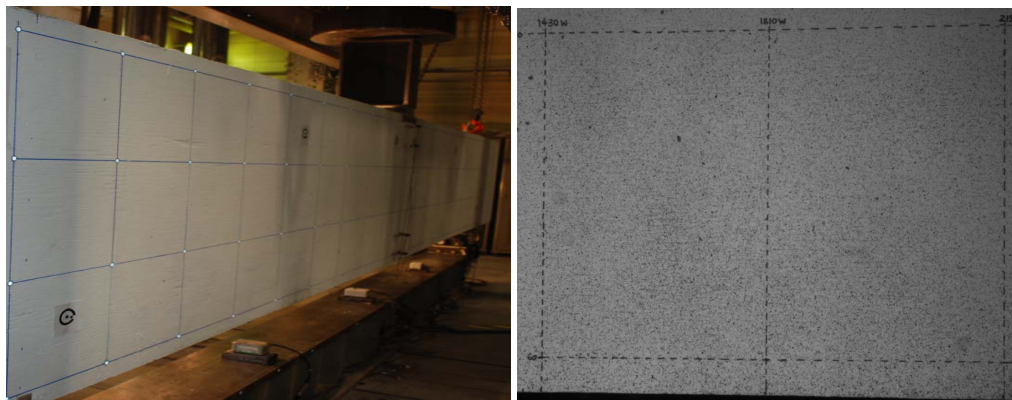
Four PI gauges with initial gauge lengths of 100 mm were used to measure axial concrete surface deformations of the beam specimens at different elevations at mid-span. Two PI gauges were used to measure deformations in the compression zone - one close to the compression face (50 mm from the top extreme fibre) and the other at the predicted level of the neutral axis depth at failure. The remaining two PI gauges were placed in the tension zone - one at mid-height and the other at the level of the bottom layer of tension reinforcement.

Two LVDTs and three cable potentiometers were used to measure the vertical deflections at selected locations. The LVDTs were used to measure the support settlements while the cable potentiometers were used to measure the deflections of mid-span and quarter-span points. All reported deflections were adjusted for the measured support displacements.

For the purpose of photogrammetric studies square grids were drawn on the south face of each specimen. (See Figure 3-14a). At every grid intersection, small round reflective targets were placed. Larger coded targets were positioned at arbitrary locations along the length of the specimens as shown in Figure 3-17a. A series of photographs were taken along the length of the specimens before testing began, and subsequently at each load stage using a fixed focal length camera. The reflection of the targets along with the position of the identifying circles allows for a software analysis of the images, to determine the specimen deflection and cracking throughout the test. Due to time constraints, the photogrammetry data was not analysed as part of the current study and left for future research.

A non-contact deformation measurement system based on the digital image correlation technique was used for beam specimens (*Correlated Solutions Inc.*, 2009). This system was employed to record and measure the surface deformation on the north face of the beam specimens. (See Figure 3-14b). This system included three pairs of digital cameras with 12.5 mm or 35 mm focal length lenses

to capture images using software *Vic Snap 2009* at a rate of 10 seconds per image pair during each test. Based on the camera lens sizes, their distance from the specimen, and their angular separation ($15^\circ \sim 45^\circ$), each pair of cameras imaged an area of interest on the specimen surface. (See Figure 3-14b). Accordingly the specimen surface was speckled with black dots of different sizes as shown in Figure 3-17b. By using the post processing software (*Vic 3D 2009*) the images were analysed to extract member deformations including the mid-span deflection and crack widths at the different applied load levels.



a) Photogrammetry

b) Speckle for DIC

Figure 3-17: Test setup for beam specimen *MRI*

3.6.3 Data Acquisition System

A data acquisition system which monitored up to 37 channels was used to continuously store the readings from all instrumentation all the way up to failure during each test. Prior to testing all instrumentation readings were zeroed to offset any residual measurements. A typical data sample rate every 10 seconds was used for each test which is similar to the image capture time interval for the DIC system. (See Section 3.6.2). The same load channel was connected to both the testing machine and the DIC system. The load-deflection measurements obtained

from the DIC system and those from the data acquisition were compared and found to be in good agreement. (See Appendix A.2.2).

3.6.4 Testing Procedures

All specimens reported in this study were tested under concentrated loading at mid-span using an MTS 6000 universal testing machine. A displacement-controlled loading protocol was used at a rate of 0.20 to 0.40 mm/minute. The specimens were subjected to 5 to 10 loading stages prior to failure depending on their capacity. At each load stage, the deflection was held while the cracks were marked, measured with comparator gauges and photographed. Image capturing by the DIC system was also paused at each load stage. After all photographs were taken, the loading process resumed until the next load stage was reached and the same procedure was followed. Load, deflection, and strain gauge data were recorded continuously all the way up to failure. The duration of each test was 3 to 4 hours, depending on the reinforcement configuration of the specimen and the number of load stages.

4. TEST RESULTS AND DISCUSSION

4.1 General

In this chapter the results obtained from the laboratory tests for each specimen described in chapter 3 are presented. A summary of the ultimate shear capacity and mode of failure and other significant test results for each slab and beam specimen is presented in Section 4.2. A discussion on the behaviour of the specimens during the tests is provided in Section 4.3.

All slab and beam specimens were subjected to displacement controlled loading until failure in order to study the post peak behaviour. Failure was herein defined as significant drop in the applied load (by at least 20% of the peak load). The reported peak loads P_{max} in this chapter are based on the applied load from the MTS machine. The self-weight of the specimens and the weights of the loading plate and the wide flange spacer were not included. The total weight of the loading apparatus was calculated as 1.10 kN. The vertical deflections reported are based on the LVDT measurements at mid-span and have been corrected for support settlement. For some specimens, failure was identified when the measured load had dropped by about 20% from the peak load. In most cases, failure was observed as a sudden, large drop in load carrying capacity, along with a large increase in mid-span deflection.

4.2 Test Results

4.2.1 Slab Specimens

A summary of the ultimate shear capacity and failure mode of the slab specimens as well as the most important test results is presented in Table 4-1. Four specimens failed in shear and two specimens failed in flexure-shear mode.

Load-deflection response, load-reinforcement strain and crack patterns were monitored for each of the six slab specimens during the tests. Each specimen was studied based on the information obtained from manual measurements, photographs taken during test and the readings of the data acquisition systems. Load-deflection and load-strain graphs and crack development patterns are presented and discussed in Section 4.3.1.

The peak load, mid-span deflections at failure load along with the equivalent service load and the corresponding crack widths for the slab specimens are reported in Table 4-1. The equivalent service load levels are approximated as 60 % of the peak machine load.

The deflection and crack width of slab specimens at the equivalent service load are examined in Section 4.3. The influence of member depth and longitudinal reinforcement ratio on the shear strength of ASTM A1035 steel reinforced slab specimens is also investigated in more detail in Section 4.3.1.

Table 4-1: Test Results for Slab Specimens.

<i>Specimen</i>	<i>Smaller Specimens</i>		<i>Larger Specimens</i>			
	<i>S-1</i>	<i>S-2</i>	<i>S-3</i>	<i>S-4</i>	<i>S-5</i>	<i>S-6</i>
<i>Width, b_w (mm)</i>	305	305	300	300	300	300
<i>Effective Depth, d (mm)</i>	278	278	569	569	573	573
<i>Reinforcement Ratio, ρ (%)</i>	0.46	0.46	0.45	0.45	0.23	0.23
<i>Concrete Strength, f_c' (MPa)</i>	53	59	49	57	53	57
<i>Peak Machine Load, P_{max} (kN)</i>	153	149	245	223	182	144
<i>Mid-Span Deflection @ P_{max} (mm)</i>	8.7	8.1	15.3	14.5	21.9	15.6
<i>Mid-Span Reinforcement Strain @ P_{max} (mm/mm)</i>	0.0039	0.0032	0.0028	0.0028	0.0056	0.0047
<i>Equivalent Service Load, P_s (kN)*</i>	92	89	147	134	109	86
<i>Mid-Span Deflection at P_s (mm)</i>	4.1	4.1	7.8	6.4	8.9	5.9
<i>Maximum Diagonal Crack width, @ P_s (mm)</i>	0.33	0.40	0.40	0.33	0.50	0.60
<i>Mid-Span Reinforcement Strain @ P_s (mm/mm)</i>	0.0021	0.0017	0.0016	0.0016	0.0023	0.0023
<i>Failure Mode</i>	Shear	Shear	Shear	Shear	Flexure-Shear	Flexure-Shear

* P_s is the equivalent service load taken at 60 % of peak machine load.

4.2.2 Beam Specimens

The maximum shear load, mid-span deflection and failure mode of the beam specimens as well as other important test details is presented in Table 4-2. Of the ten beam specimens tested five specimens failed in shear, three specimens in flexure-shear and two specimens failed in flexural compression mode.

Table 4-2: Beam Specimen Details and Service Conditions.

<i>Specimen</i>	<i>RM1</i>	<i>RM2</i>	<i>MR1</i>	<i>MR2</i>	<i>MR3</i>	<i>MR4</i>	<i>MM1</i>	<i>MM2</i>	<i>MM3</i>	<i>MM4</i>
<i>Longitudinal Reinforcement Grade</i>	420	420	690	690	690	690	690	690	690	690
<i>Transverse Reinforcement Grade</i>	690	690	420	420	420	420	690	690	690	690
<i>Longitudinal Reinforcement Ratio (%)</i>	2.55	2.55	0.55	0.69	1.60	1.60	0.55	0.69	1.60	1.60
<i>Transverse Reinforcement Ratio (%)</i>	0.15	0.18	0.11	0.11	0.11	0.22	0.11	0.11	0.11	0.22
<i>Compressive Strength, f_c' (MPa)</i>	41	45	50	49	52	50	48	48	48	50
<i>Peak Machine Load, P_{max} (kN)</i>	840	956	915	875	1109	1510	933	957	1409	1822
<i>Mid-Span Deflection at P_{max} (mm)</i>	13.8	12.1	42.2	31.3	21.6	30.7	48.4	37.0	29.0	38.2
<i>Equivalent Service Load, P_s (kN)*</i>	530	645	540	490	720	990	560	640	900	1150
<i>Mid-Span Deflection at P_s (mm)</i>	6.1	5.5	16.9	14.7	8.9	13.1	19.2	16.2	12.8	16.0
<i>Mid-Span Longitudinal Steel Strain @ P_s (mm/mm)</i>	0.0012	0.0015	0.0027	0.0019	0.0020	0.0021	0.0028	0.0031	0.0020	0.0023
<i>Maximum Transverse Steel Strain @ P_s (mm/mm)</i>	0.0015	0.0030	0.0008	0.0012	0.0010	0.0018	0.0050	0.0047	0.0019	0.0033
<i>Maximum Diagonal Crack width @ P_s (mm)</i>	1.00	0.80	0.80	0.60	0.60	0.60	1.25	1.00	1.00	1.00
<i>Failure Mode **</i>	FC	FC	ST	ST	ST	ST	FS	FS	SC	FS

* P_s is the equivalent service load taken at 60 % of peak machine load.

* FC-Flexural Compression, ST-Shear Tension, SC-Shear Compression, FS-Flexure-Shear.

For each of the ten beam specimens tested load-deflection response, load-strain for longitudinal and transverse reinforcements and crack patterns were monitored during the test. Each specimen was studied based on the information obtained from manual measurements, photographs taken during test and the readings of the

data acquisition system. The peak load, mid-span deflections at failure along with the equivalent service load and the corresponding crack widths for the slab specimens are reported in Table 4-2. The equivalent service load levels are approximated as 60 % of the peak machine load.

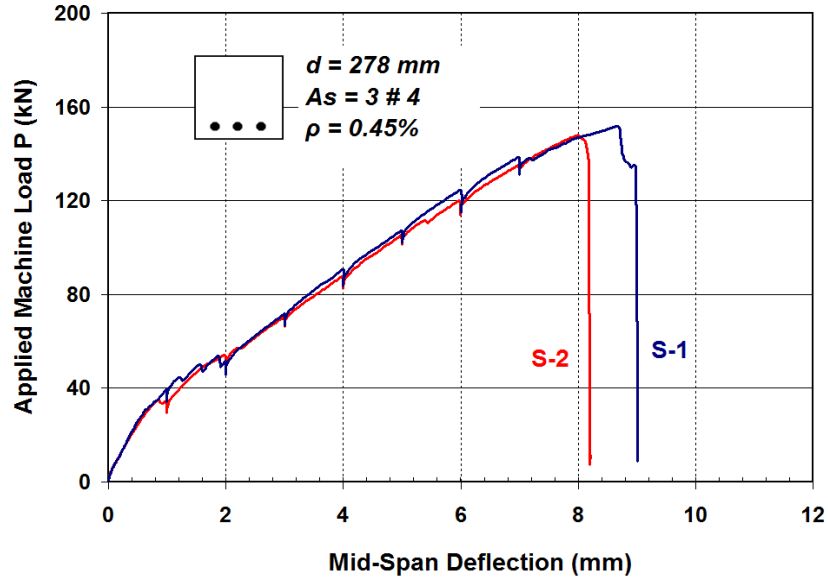
4.3 Discussion of Results

4.3.1 Slab Specimens

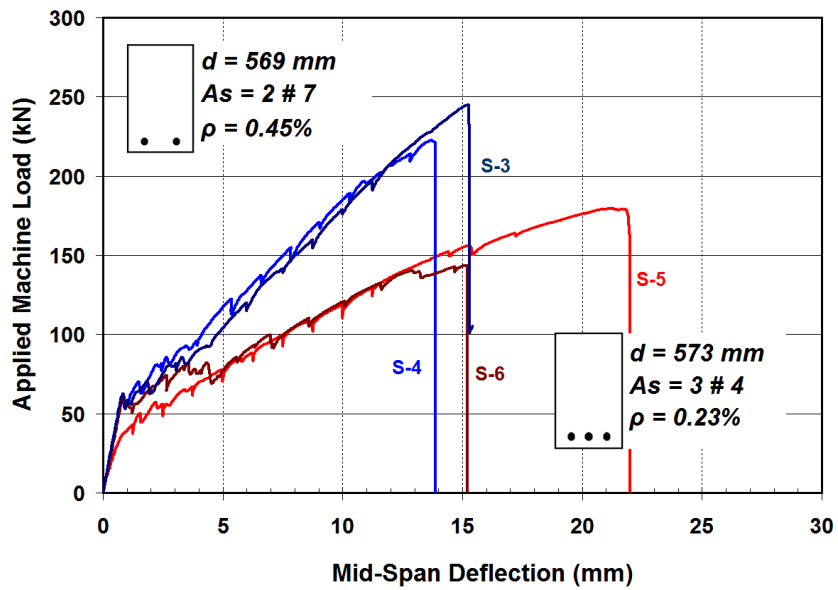
4.3.1.1 Load-Deflection Behaviour

The load-deflection behaviour of each slab specimen is shown in Figure 4-1, grouped by similar specimen depths. As shown in Figure 4-1, linear behaviour is observed up to the initiation of flexural cracking for each specimen. Then, near linear behaviour with reduced slope is observed for specimens *S-1*, *S-2*, *S-3* and *S-4* up to failure at the formation of significant diagonal cracking. At failure, a sudden and significant drop in load was recorded in each test. *S-6* exhibited nearly linear response up to a machine load of approximately $P = 140 \text{ kN}$ and then started to show a plateau in the load-deflection relationship due to non-linear response of the reinforcement. See Section 4.3.1.2. After some additional deformation, a significant diagonal crack formed leading to a shear failure, with sudden and significant drop in the recorded load. The difference in behaviour of *S-6* compared to *S-4* is attributed to the lower reinforcement ratio which resulted in much higher reinforcement strains at similar load levels. *S-5* was similar in dimensions and reinforcement configuration to *S-6* and behaved in a similar manner up to $P = 140 \text{ kN}$ after which about 26 % more load could be resisted prior to failure. Although *S-6* was expected to have a higher shear strength based on its slightly higher concrete strength, the actual result was the opposite. This could be attributed to the inherent variability in the shear strength of concrete members without shear reinforcement. However, the maximum load for *S-5* was only 75 % of the load of comparable specimen *S-3*, with the difference attributed

to the higher reinforcement ratio in *S-3*. Note that the final failure mode of *S-5* was a sudden and significant loss in load upon formation of diagonal cracking.



a) $h = 305$ mm

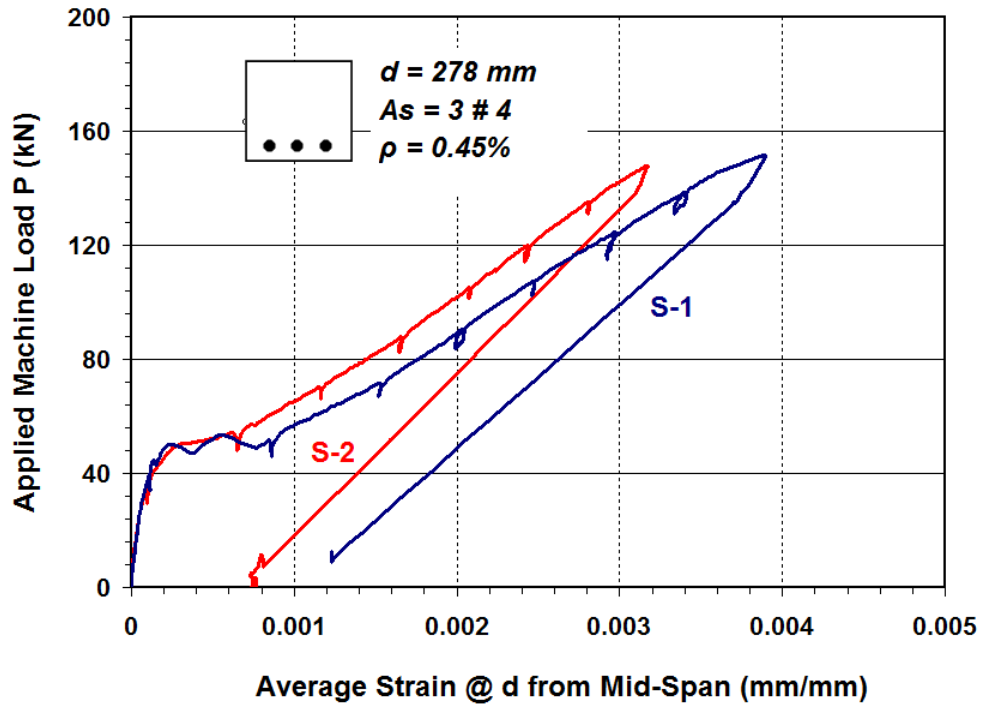


b) $h = 600$ mm

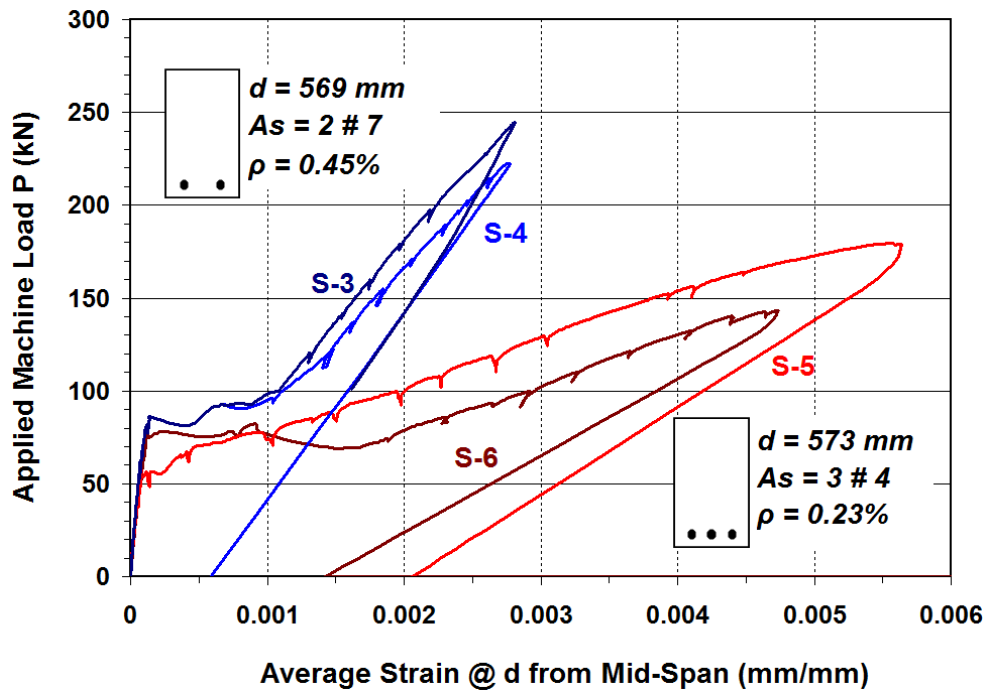
Figure 4-1: Load-Deflection Response at Mid-Span of Slab-Specimens.

4.3.1.2 Load-Steel Strain Behaviour

The measured load-steel strain relationships for all specimens are shown in Figure 4-2. Steel strains are from strain gauges located at the assumed analytical critical section for shear, taken in this study at a distance d from mid-span. For each specimen, linear behaviour was observed up to flexural cracking followed by some plateau. After cracking, linear behaviour with reduced slope was observed up to failure for specimens with higher reinforcement ratios (*S-1*, *S-2*, *S-3* and *S-4*). At the time of failure, the strain levels at the critical section for *S-1*, *S-2*, *S-3* and *S-4* were below a strain of 0.004 mm/mm but higher than the proportional limit strain of 0.0024 mm/mm. More pronounced non-linear behaviour was observed of specimens *S-5* and *S-6* with strain values of approximately 0.0056 mm/mm. Specimens *S-1*, *S-2*, *S-3* and *S-4* were classified to undergo shear failure before ‘yielding’ of the reinforcement, but after some non-linear response of the reinforcement occurred. For specimens *S-5* and *S-6* significant non-linear behaviour of steel occurred before the observed shear failure. However, for all specimens the strain levels at the critical section are lower than the tension controlled strain limit of 0.0066 mm/mm as per the *ACI ITG-6R-10* simplified flexural design provisions.



a) $h = 305 \text{ mm}$

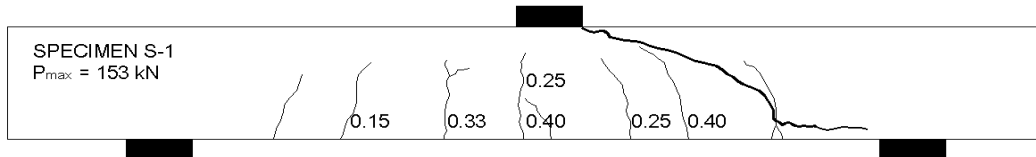


b) $h = 600 \text{ mm}$

Figure 4-2: Load-Strain Response of Slab-Specimens.

4.3.1.3 Failure Mode and Crack Pattern

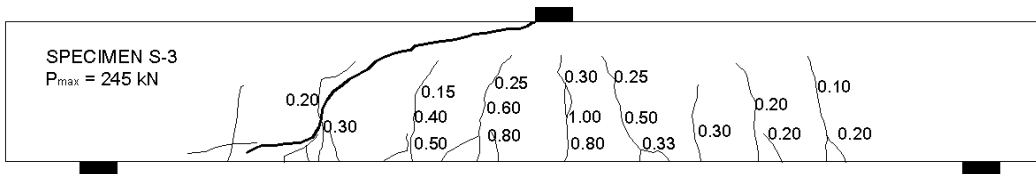
Crack development during each test was examined from manual measurements of crack widths at each load stage using a crack width comparator gauge. For each of the six specimens, flexural cracks were first detected under the applied load near mid-span. With further increases of load, new flexural cracks formed in the shear spans and curved towards the loading plate. In each specimen, failure occurred when a new or existing crack rapidly extended upwards to the loading plate followed by a companion crack forming along the longitudinal reinforcement. Crack patterns of each specimen after failure depict a curved shape of cracks, intercepting the longitudinal reinforcement a considerable distance from the support plates, as shown in Figure 4-3. The observed crack patterns confirmed that the shear failure of each specimen was of a sectional-type mode rather than through direct strut action. Assuming the service load to be 60 % of the ultimate machine load, the maximum service load crack width for each specimen was interpolated from measurements and summarized in Table 4-1. The maximum service crack widths were less than 0.4 mm for the specimens with higher reinforcement ratio (*S-1*, *S-2*, *S-3* and *S-4*) which is below the suggested maximum crack width of 0.41 mm according to *ACI 318-11*. For specimens *S-5* and *S-6* the service crack widths were higher than the *ACI 318-11* maximum permitted crack width. This is attributed to the lower reinforcement ratios compared to specimens *S-1* to *S-4*, which increased the average longitudinal member strain and hence the crack width as discussed in Section 2.2.4. (See Equation 2-2).



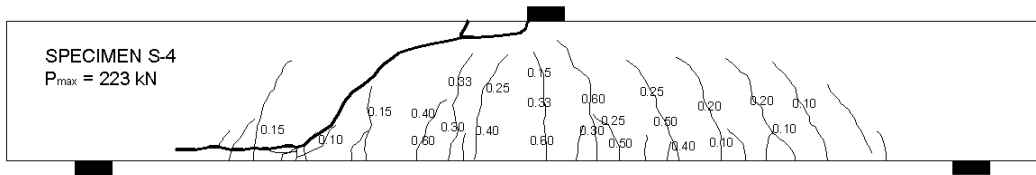
a) Specimen S-1.



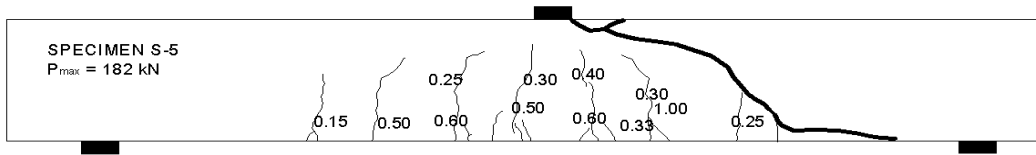
b) Specimen S-2.



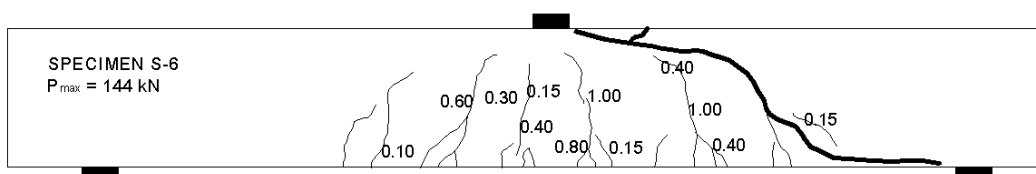
c) Specimen S-3.



d) Specimen S-4.



e) Specimen S-5.



f) Specimen S-6.

Figure 4-3: Crack Patterns of Slab Specimens at Failure Loads.

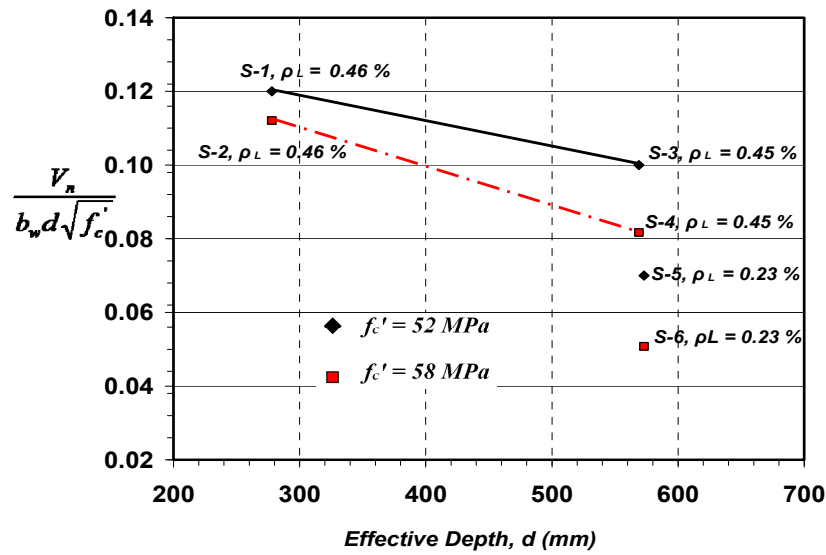
4.3.1.4 Influence of Member Depth and Longitudinal Reinforcement Ratio

In this section the normalized shear stress at failure is defined as the ratio of nominal average shear stress at failure ($V_n/b_w d$) normalized by the square root of concrete compressive strength, f'_c . The nominal failure shear force V_n was calculated as the shear force at failure at the critical section (at a distance d from mid-span) adjusted for the weight of the loading apparatus and self weight of specimen, as shown from Table 4-3.

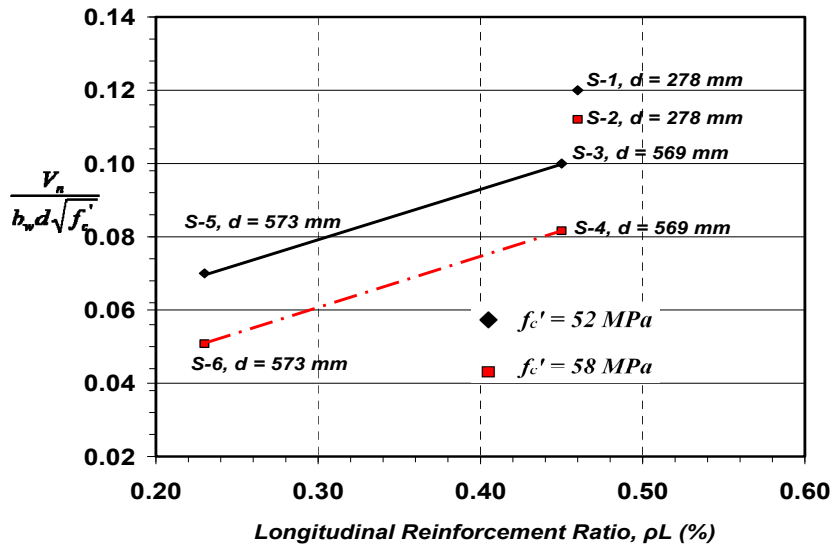
$$v_n = \frac{V_n}{b_w d \sqrt{f'_c}} \quad (4-1)$$

The relationships between normalized shear stress at failure (equation 4-1) versus effective depth, d , and longitudinal reinforcement ratio, ρ_L , for the slab specimens tested in the current study are plotted in Figures 4-4 a and b, respectively. The plots are made for two groups - each set containing three specimens having nearly similar compressive strength of concrete. Table 4-3 shows the comparison between the results. It is observed that the normalized shear stress at failure decreases by 19 % and 26 % as the depth increases from $d = 278$ mm for $S-1$ and $S-2$ to $d = 569$ mm for specimens $S-3$ and $S-4$, with similar longitudinal reinforcement ratios. (See Figure 4-4 a and Table 4-3). Furthermore, comparing $S-3$ with $S-5$ and $S-4$ with $S-6$ from Figure 4-4 b and Table 4-3, having similar effective depths, a decrease in longitudinal reinforcement ratio from 0.45 % to 0.23 % resulted in a 30 % and 37 % decrease in normalized shear stress for specimens $S-5$ and $S-6$, respectively. The observed relationships between normalized shear stress at failure (shear capacity) and member depth or reinforcement ratio for members longitudinally reinforced with ASTM A1035 steel reinforcement show that both the ‘size effect’ and ‘strain effect’ discussed in Section 2.2.4 have significant influence on the shear stress at failure. Note that this behaviour is similar to prior research conducted on members with

conventional longitudinal steel reinforcement and without stirrups (e.g. *Kani* (1967), *Collins and Kuchma* (1999), *Sherwood* (2008), *Lubell et al.* (2009)). These parameters (d and ρ_L) should be considered in the development of shear models for concrete members containing ASTM A1035 steel longitudinal reinforcement.



(a)



(b)

Figure 4-4: Influence on Normalized Shear Stress at Failure from (a) Member Effective Depth and (b) Longitudinal Reinforcement Ratio.

Table 4-3: Normalized Shear Stress at Failure for Slab Specimens.

<i>SLAB ID</i>	ρ_L (%)	<i>d</i> (mm)	f_c' (MPa)	V_n (kN)	$\frac{V_n}{b_w d \sqrt{f_c'}}$ (MPa)	% change in $V_n / (\sqrt{f_c'} b_w d)$ due to ρ_L	% change in $V_n / (\sqrt{f_c'} b_w d)$ due to <i>d</i>
<i>S-1</i>	0.46	278	53	75	0.12	-	-
<i>S-2</i>	0.46	278	59	73	0.11	-	-
<i>S-3</i>	0.45	569	49	118	0.10	-	-19
<i>S-4</i>	0.45	569	57	107	0.08	-	-26
<i>S-5</i>	0.23	573	53	86	0.07	-30	-
<i>S-6</i>	0.23	573	57	67	0.05	-37	-

4.3.2 Beam Specimens

4.3.2.1 Load-Deflection Behaviour

The load-deflection behaviour of the ten beam specimens are shown in Figure 4-5 grouped by the type of steel used as longitudinal and transverse reinforcement. Linear behaviour is observed up to the initiation of flexural cracks for each specimen as shown in Figure 4-5. In general non-linear behaviour was observed after cracking until the peak load. The discussion is based on comparisons between companion specimens.

At failure, beam specimens *RM1* and *RM2*, containing conventional Grade 420 longitudinal reinforcement and ASTM A1035 stirrups, exhibited non-linear response as shown in Figure 4-5a. *RM1* failed in a relatively brittle manner with rapid loss of load carrying capacity as the deflection increased beyond the peak load condition. *RM2* exhibited a large plateau in the load-deflection response indicating a more controlled flexural type failure which can be attributed to yielding of the longitudinal reinforcement and better confinement to the flexural compression zone. (Also see Sections 4.3.2.2 and 4.3.2.4). Moreover the load carrying capacity of *RM2* was 14% higher than the companion specimen *RM1* due to the 20% higher transverse reinforcement ratio in *RM2*. But this capacity

increase was limited in part by the flexural capacity. It is also noted that the post cracking stiffness of *RM2* was increased compared to *RM1* by providing a greater transverse reinforcement ratio for the same other design parameters.

Figures 4-5b and 4-5c depict the load-deflection response of the eight beam specimens with ASTM A1035 longitudinal reinforcement. Four specimens in the MM series contained ASTM A1035 transverse reinforcement while the remaining beams in the MR series were reinforced with conventional stirrups. As observed from Figures 4-5b and 4-5c, for each case a sudden and significant drop in load carrying capacity occurred at the peak load. It is observed from Figure 4-5 that the companion beams (compare *MR3* to *MR4*, *MM3* to *MM4*) behaved in a similar manner up to failure. In general increasing the longitudinal or transverse reinforcement ratio increased the maximum load at failure. Increasing the longitudinal reinforcement ratio is observed to increase the stiffness of the load-deflection response after cracking of specimens. This can be attributed to the increase in the bending stiffness of the transformed cross section (EI_{TRANS}) for specimens with higher longitudinal reinforcement ratios.

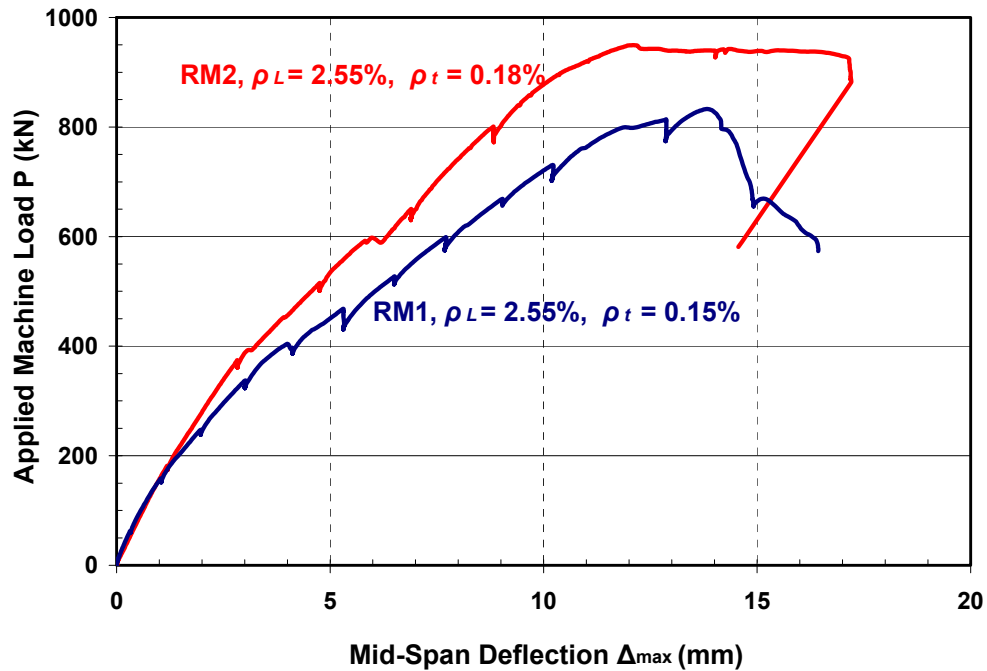
The influence of the transverse reinforcement type on the shear strength of companion beams was significant only at higher longitudinal reinforcement ratios. By using ASTM A1035 stirrups, up to 27% higher capacity was achieved for beams with $\rho_L = 1.6\%$ (*MM3* and *MR3*, *MM4* and *MR4*) while the increase in capacity was less than 10% for beams with lower longitudinal reinforcement ratios. (Compare *MM1* to *MR1*, *MM2* to *MR2*). It is also observed that reducing the spacing of transverse reinforcement by one half (thereby doubling the transverse reinforcement ratio, ρ_t) increased member capacity by 36% and 29% for beams *MR4* and *MM4*, compared to companion beams *MR3* and *MM3*, respectively.

The influence of stirrup ratio on shear capacity can also be observed in Figure 4-5. Increasing the transverse reinforcement ratio ρ_t increased the stiffness of the load-

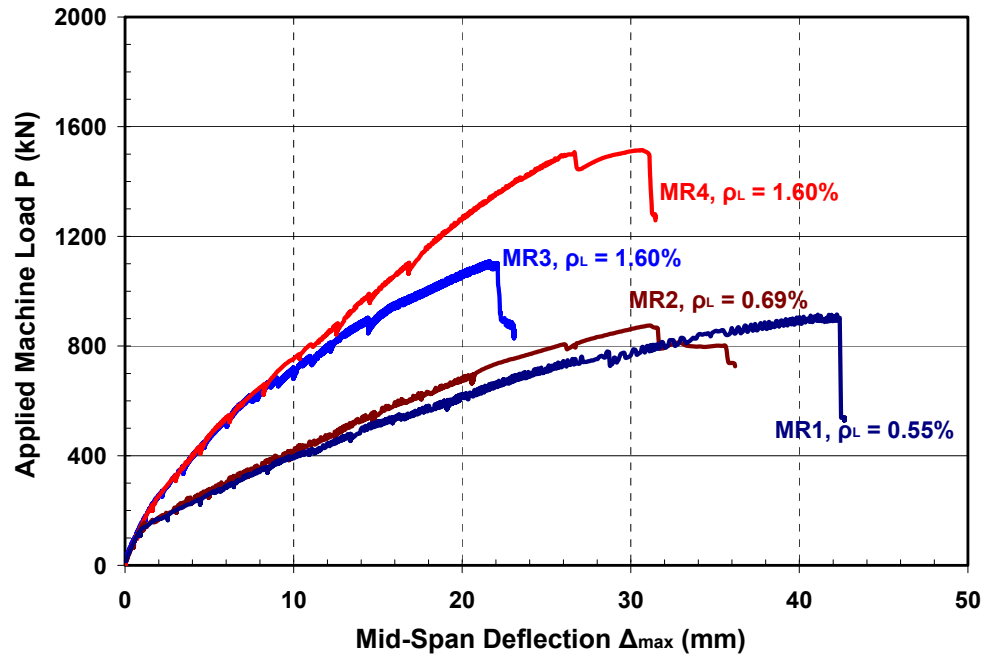
deflection response after cracking of specimens. (Compare *MM3* to *MM4*, *MR3* to *MR4*). The influence was more pronounced as the loading increased. This is attributed to the improved control of diagonal cracking for specimens with higher transverse reinforcement ratio and the increased confining effect on the concrete in specimens with closely spaced stirrups.

4.3.2.2 Load-Longitudinal Steel Strain Behaviour

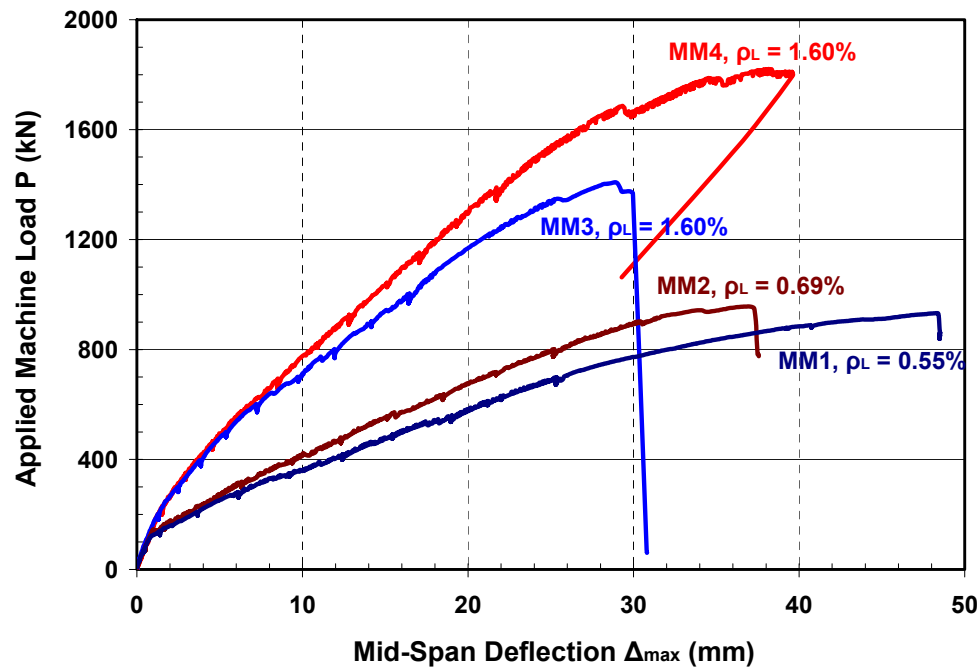
Figure 4-6 depicts the load-longitudinal steel strain behaviour of the ten beam specimens. Similar to the load-deflection response, linear behaviour is observed up to flexural cracking. After cracking, a linear response with lower slope was mostly observed, except for some beams which exhibited a non-linear response near the failure load. The discussion is based on the comparison between companion specimens that were geometrically similar but with different transverse reinforcement ratios or stirrup types.



a) Conventional Longitudinal and ASTM A1035 Transverse Reinforcement.
($h = 600$ mm)



b) ASTM A1035 Longitudinal and Conventional Transverse Reinforcement.
($h = 1000$ mm)



c) ASTM A1035 Longitudinal and A1035 Transverse Reinforcement.
($h = 1000$ mm)

Figure 4-5: Load-Deflection Response at Mid-Span of Beam Specimens.

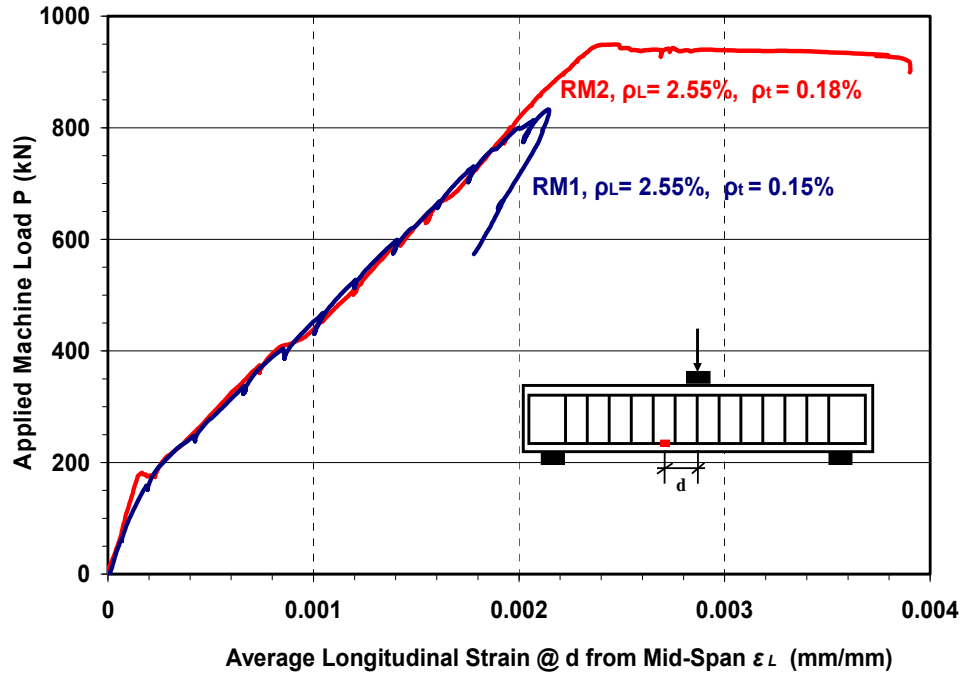
For *RM1* and *RM2* which contained conventional longitudinal reinforcement and ASTM A1035 stirrups, nearly linear response of the average longitudinal steel strain with load was observed after cracking until the peak load was reached. (See Figure 4-6a). The average longitudinal steel strain was calculated on the failing side of each specimen from the strain gauges mounted on the rebars at the critical sections. After the peak load was recorded a sudden drop in the member capacity was observed for beam *RM1* while a large plateau in maximum load was formed for beam *RM2* before failure. The discrepancy is due to the higher shear reinforcement ratio in beam *RM2* which precluded shear failure before significant yielding of the flexural reinforcement after which a plateau was formed as shown in Figure 4-6a. The yield strain for the longitudinal reinforcement was 0.0022. (See Table 3-3).

Figures 4-6b and 4-6c show the response of load-longitudinal reinforcement strain for the eight beam specimens with ASTM A1035 longitudinal reinforcement. Four beams in the *MM* series contained ASTM A1035 transverse reinforcement and the remaining four beams in the *MR* series were reinforced with conventional stirrups. The average longitudinal steel strain was calculated on the failing side of each specimen from the strain gauges mounted on the rebars at the critical sections. As observed from Figures 4-6b and 4-6c for *MM3*, *MR2* and *MR3*, a sudden drop in load occurred at failure without significant non-linear response of the longitudinal reinforcement. For the other beams (*MM1*, *MM2*, *MR1*, *MM4* and *MR4*), significant non-linear response of the longitudinal reinforcement was observed before failure. For *MM1* and *MR1*, this behaviour resulted from the lower longitudinal reinforcement ratios which caused the steel strain to exceed the proportional limit and respond in the non-linear stress-strain range of ASTM A1035 steel before the peak load was reached. For *MM4*, the higher transverse reinforcement ratio increased the shear carrying capacity and making the member flexure-critical where the significant non-linear response of ASTM A1035 steel was observed.

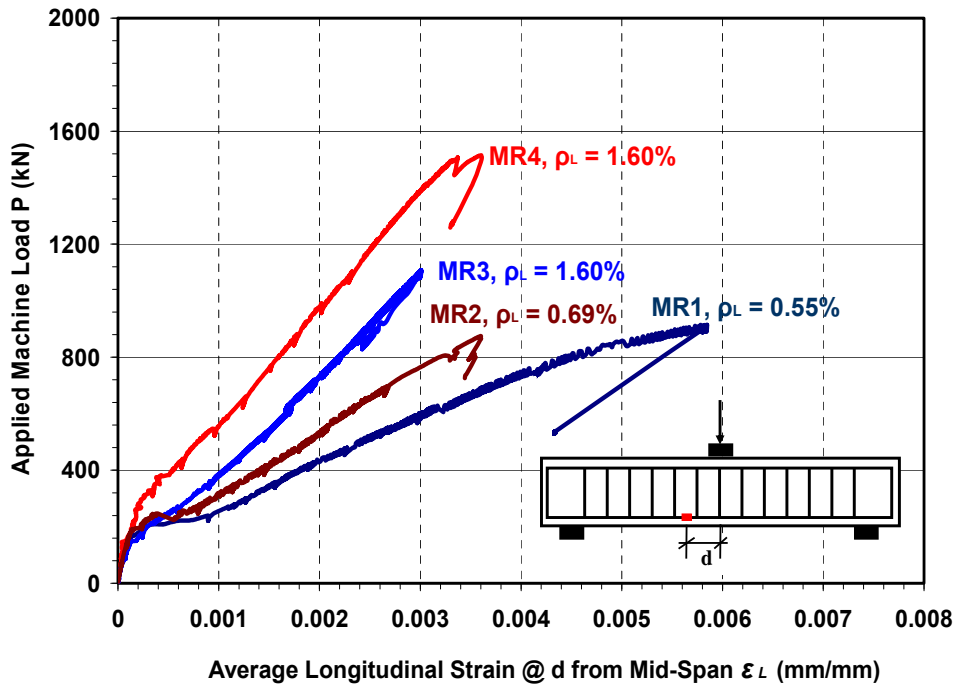
It was also observed from Figures 4-6b and 4-6c that the companion beams (*MR1* & *MM1*, *MR2* & *MM2*, *MR3* & *MM3* and *MR4* & *MM4*) showed similar response of the longitudinal reinforcement strain up to failure. The difference in the recorded longitudinal steel strains at failure is attributed to the different steel type in the transverse reinforcement which allowed higher shear capacities in the *MM* series.

Figures 4-6b and 4-6c illustrate that, in general, increasing the longitudinal reinforcement ratio reduced the longitudinal steel strain at the critical section at failure. This behaviour is more pronounced for beams containing conventional transverse reinforcement (*MR* series).

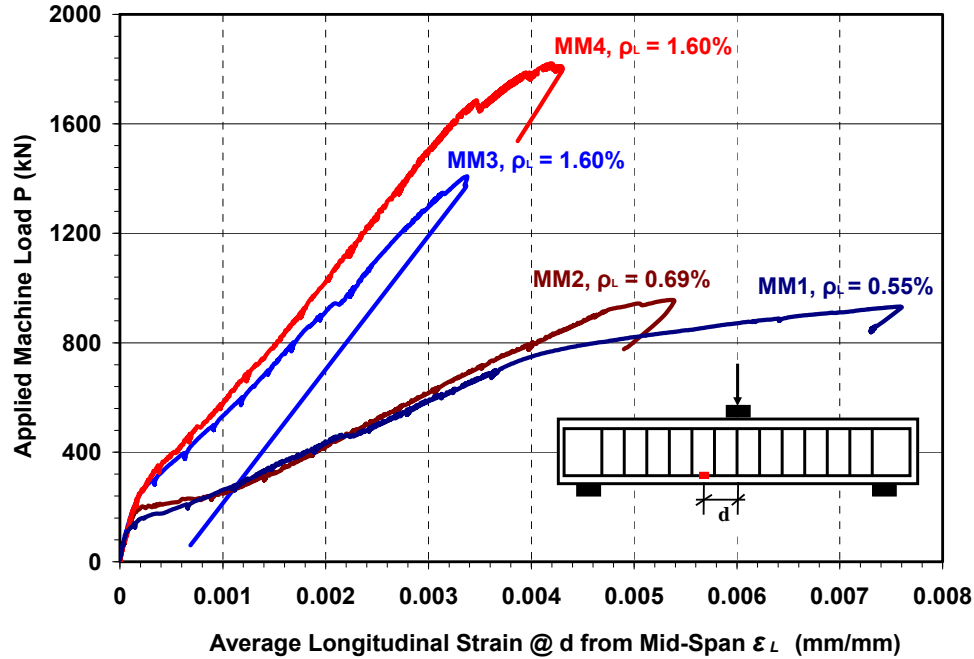
The influence of reinforcement ratios on the longitudinal reinforcement strains was also studied by comparing the service strains of companion beams from Figures 4-6b and 4-6c. For beams with conventional stirrups (*MR* series), the longitudinal reinforcement ratio had a greater influence on the corresponding service strain compared to beams in the *MM* series. Increasing the longitudinal reinforcement ratio by 25 % (*MR1* to *MR2*) resulted in a reduction in the longitudinal steel strain by 30 % at the corresponding service loads. See Table 4-2. On the other hand, for beams with ASTM A1035 stirrups (*MM* series), the longitudinal reinforcement ratio has minimal influence on the equivalent service steel strain. Increasing the longitudinal reinforcement ratio by 25 % (*MM1* to *MM2*) resulted in a reduction in the longitudinal steel service strain by only 6 % as shown in Table 4-2.



a) Conventional Longitudinal and ASTM A1035 Transverse Reinforcement.
($h = 600$ mm)



b) ASTM A1035 Longitudinal and Conventional Transverse Reinforcement.
($h = 1000$ mm)



c) ASTM A1035 Longitudinal and Transverse Reinforcement. ($h = 1000$ mm)

Figure 4-6: Load-Longitudinal Steel Response of Beam Specimens.

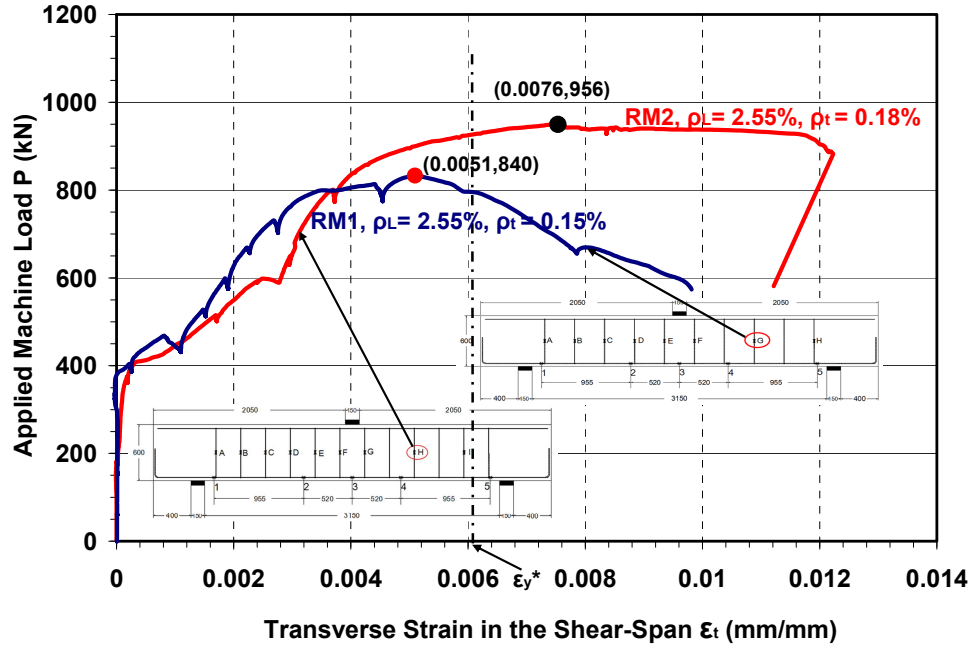
4.3.2.3 Load-Transverse Steel Strain Behaviour

The load versus transverse steel behaviour of the beam specimens are shown in Figure 4-7, grouped by beams of similar configuration. The ‘yield’ strain (ϵ_y^*) of stirrup reinforcement for each steel type, given in Table 3-3, was also marked in Figure 4-7. As shown in Figure 4-7 the stirrups are engaged at an applied load of approximately 250 kN for beams with $h = 600$ mm (*RM* series) and 400 kN for beams with $h = 1000$ mm (*MR* and *MM* series). After this load, nearly linear response with lower slope was observed for all specimens. The discussion of test results is based on the comparison between similar specimens.

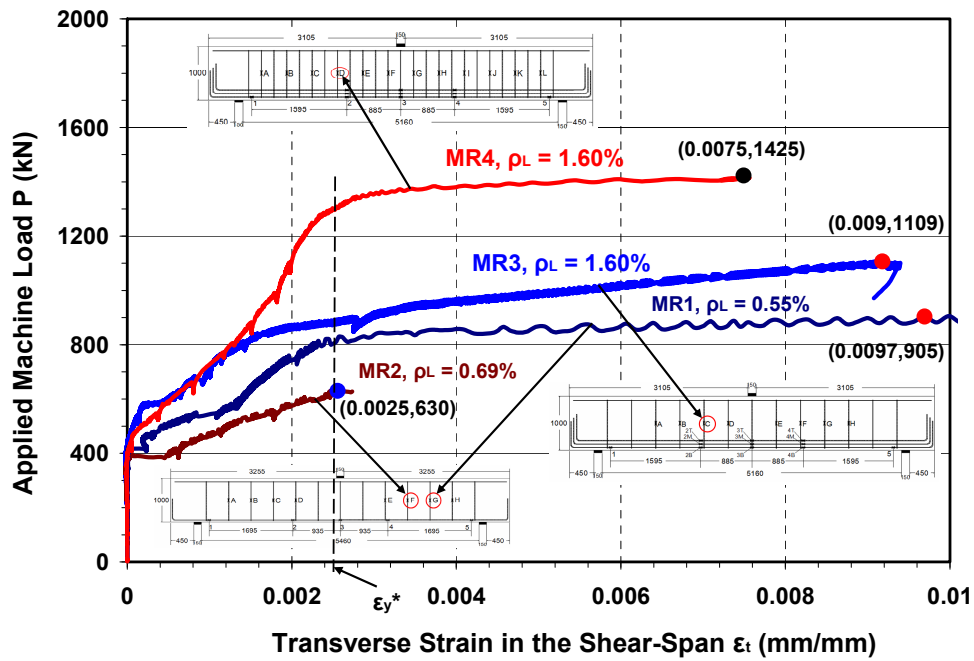
For *RM1* and *RM2* containing conventional longitudinal reinforcement the strain in the ASTM A1035 stirrups behaved linearly after cracking up to a load of about

800 kN followed by non-linear response. (See Figure 4-7a). The peak load of *RM1* was reached before the measured strains in the stirrups reached the effective yield strain. For *RM2*, failure occurred after ‘yielding’ of the stirrups with a large plateau in the load-strain response formed before the load dropped. The higher stirrup ratio in *RM2* increased the failure load and altered the load-strain response compared to the companion specimen *RM1*.

Figure 4-7b shows the load versus transverse reinforcement strain response of the four beam specimens with ASTM A1035 longitudinal and conventional stirrups reinforcement (*MR* series). The load-transverse reinforcement response for the remaining beam specimens (*MM* series), with ASTM A1035 longitudinal and transverse reinforcement is shown in Figure 4-7c. Beams with conventional stirrups (*MR* series) showed significant non-linear stress-strain response (yielding) of the stirrups before failure as observed from Figure 4-7b. Yielding of the stirrups occur at a steel strain value of 0.0025 with defined plateau for the *MR* series beams. On the other hand beams with ASTM A1035 transverse reinforcement (*MM* series) behaved in nearly linear load-strain response of the stirrups. The non linear load-strain response of the ASTM A1035 stirrups observed in the strain ranges 0.006 – 0.009 and failure occurred without the formation of plateau in the load-stirrup strain response.



a) Conventional Longitudinal and ASTM A1035 Transverse Reinforcement.
($h = 600$ mm)



b) ASTM A1035 Longitudinal and Conventional Transverse Reinforcement.
($h = 1000$ mm)

failure indicate that the conventional stirrups yielded before failure for beams in the *MR* series with eventual shear tension failures, as shown in Table 4-2.

The equivalent service load was assumed in this study as 60 % of the peak machine load. The maximum service load crack widths for each beam were obtained from crack width measurements at the nearest load stage and are summarized in Table 4-2. Service crack width patterns for the beam specimens are depicted in Figures 4-9, 4-10 and 4-11.

Crack widths were examined to determine the influence of using high performance ASTM A1035 steel on important serviceability criteria for concrete beams. Current North American design codes for reinforced concrete buildings neither limit the size of shear cracks nor provide a definitive guideline for the maximum permitted flexural crack width. However, the commentary of *ACI 318-05* provides a value of 0.016" (0.41 mm) for the maximum flexural crack in concrete members with Grade 420 steel reinforcement. Therefore, in this research it is assumed that an acceptable crack width at the service load level is equal to or less than 0.41 mm. As shown in Table 4-2 all ten beams reinforced with ASTM A1035 steel in this study had measured crack widths at the equivalent service load that exceeded 0.41 mm. As expected, increasing the transverse reinforcement ratios reduced the measured crack widths. For beams reinforced with ASTM A1035 stirrups the measured crack widths are even higher, as shown in Figure 4-11. This behaviour was also observed from the tests completed by *Munikrishna et al.* (2008) as described in Section 2.5.2.

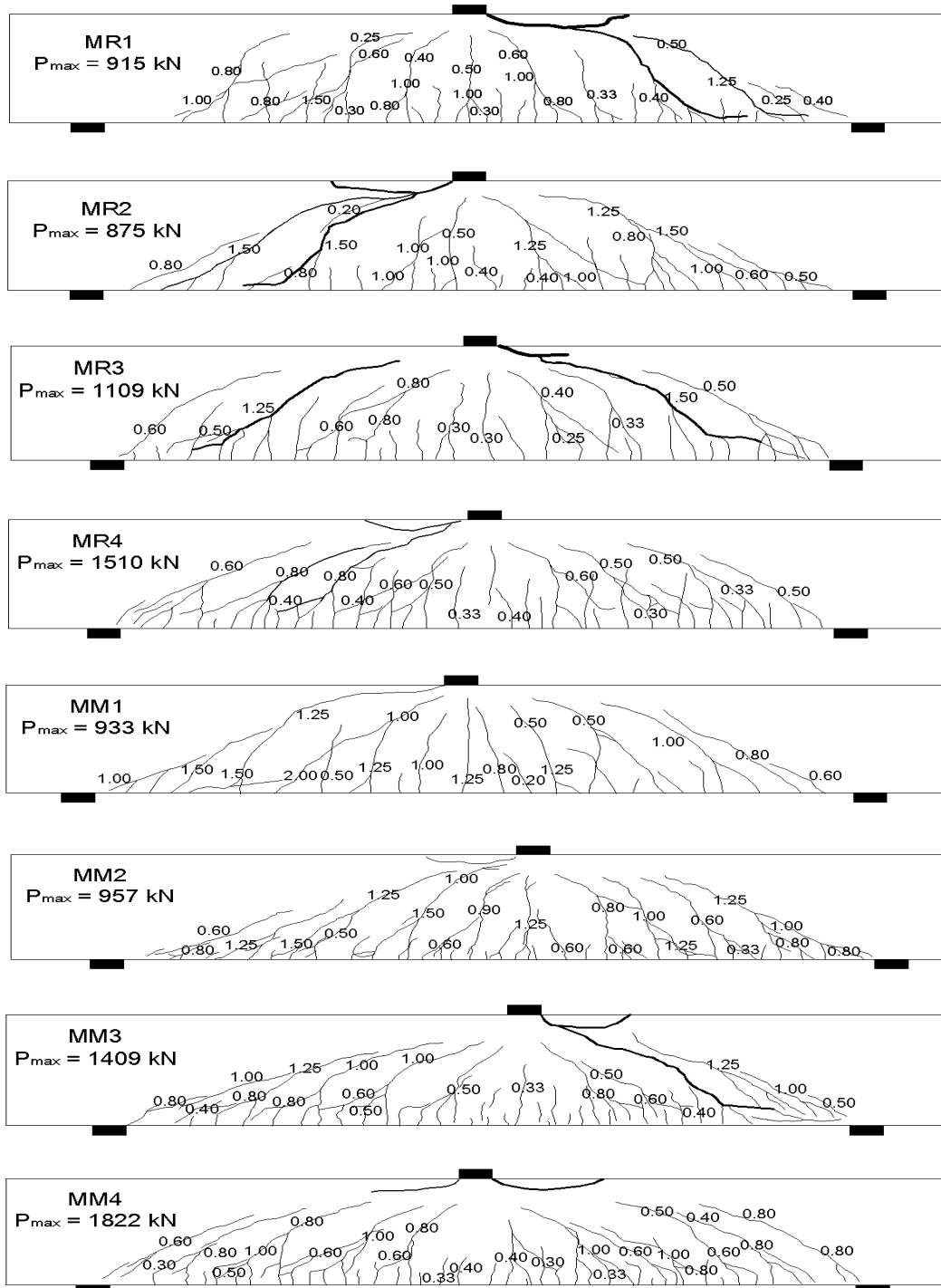


Figure 4-8 Crack Patterns at Failure Loads for Beam Specimens with ASTM A1035 Longitudinal Reinforcement. ($h = 1000$ mm).

The results of beam tests completed by *Munikrishna et al.* (2008) concluded that at service load levels the crack widths were less than the commonly accepted limit of 0.016 in. (0.41 mm). However the beams tested by *Munikrishna et al.* had different configurations compared to the specimens considered in the current study. *Munikrishna et al.* used higher longitudinal reinforcement ratios and the aspect ratio (member depth to width ratio) of their specimens varied between 1.17 to 1.38. In the current study more practical beam dimensions were considered ($h/b_w = 2 - 3.33$) and lower longitudinal reinforcement ratios were used. Thus beams containing ASTM A1035 steel transverse reinforcement can result in excessive service crack widths and may not satisfy the design requirements of *ACI 318-11* code. Further studies need to be conducted to evaluate the influence of beam design parameters to assess the minimum transverse reinforcement ratios and the corresponding limiting crack width for beams containing ASTM A1035 stirrups.

a) Spacing of Stirrups $S = 320 \text{ mm}$

b) Spacing of Stirrups $S = 265 \text{ mm}$

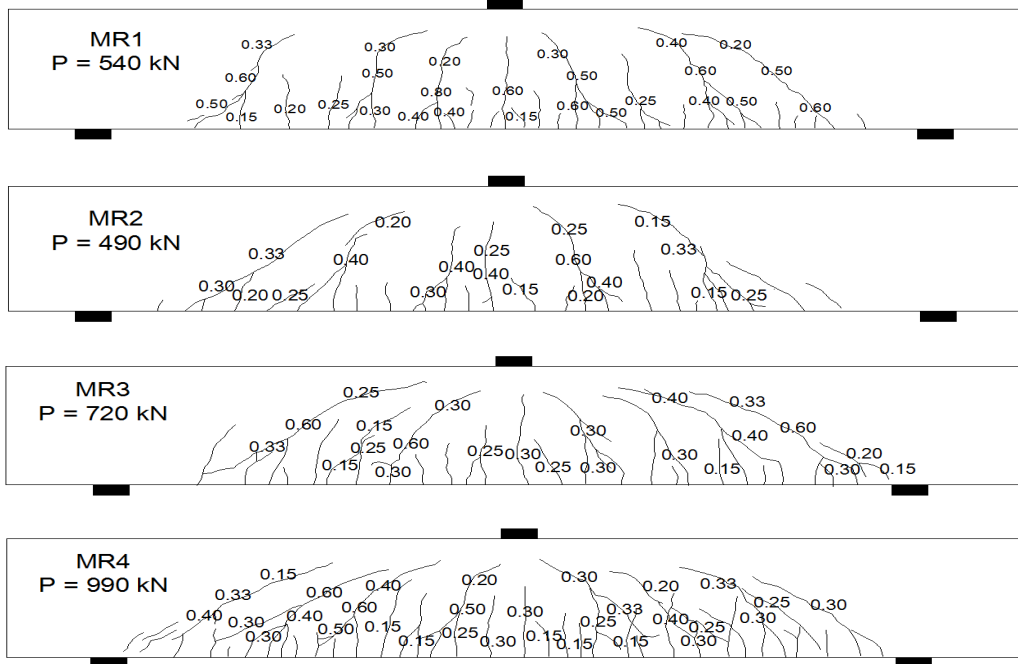


Figure 4-10: Service Crack Patterns of Beam Specimens with ASTM A1035 Longitudinal and Conventional Transverse Reinforcement. ($h = 1000 \text{ mm}$).

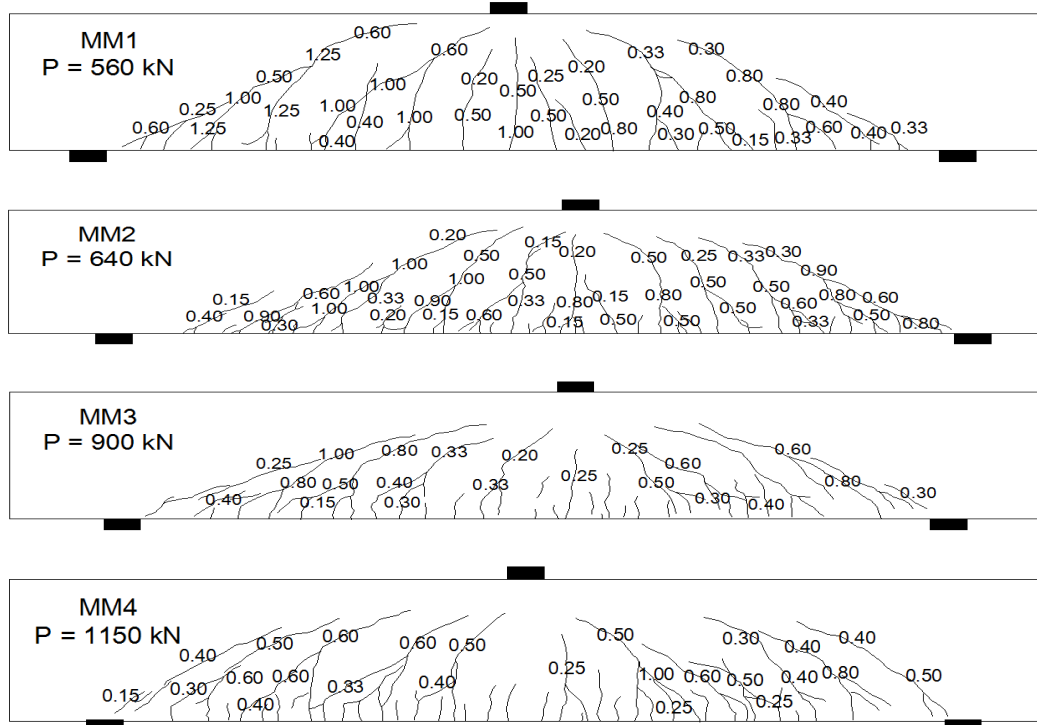


Figure 4-11: Service Crack Patterns of Beam Specimens with ASTM A1035 Longitudinal and Transverse Reinforcement. ($h = 1000 \text{ mm}$).

The mode of failure was observed during the experimental testing of each specimen. Shear failure was the typical observed mode of failure for the specimens with ASTM A1035 steel longitudinal reinforcement and conventional transverse reinforcement (*MR* series), regardless of the longitudinal reinforcement ratio, as shown in Table 4-2.

Failure of the two beams with conventional longitudinal and ASTM A1035 transverse reinforcement (*RM1* & *RM2*) was due to the crushing of concrete in flexural compression. Both beams were over-reinforced with longitudinal as well as transverse rebars, so that flexural compression failure occurred before yielding of reinforcement bars.

Beams with ASTM A1035 longitudinal and conventional transverse reinforcement (*MR* series) failed in shear-tension mode. Due to the lower tensile strength of the transverse reinforcement, yielding of the stirrups occurred before the strain in the longitudinal reinforcement reached the effective yield strain. This caused significant non-linear load-deflection response which eventually led to shear-tension failure before the strain in the longitudinal reinforcement reached the effective yield strain.

Failure of beams with ASTM A1035 longitudinal and transverse reinforcement (*MM* series) was typically due to the flexure-shear mode. Compared with beams in the *MR* series, the higher tensile strength of the transverse reinforcement in *MM* series beams resulted in significant non-linear response of the longitudinal reinforcement before the measured strain in the stirrups reached the effective yield strain. This led to flexure-shear failure in beams *MM1*, *MM2* & *MM4*. In the case of beam *MM3* shear-compression failure was the observed mode of failure due to the higher longitudinal reinforcement ratio compared with the geometrically similar beams *MM1* & *MM2*.

4.3.2.5 Influence of Stirrup Spacing and Reinforcement Ratios

The influence of the main parameters affecting the shear stress at failure of beams is studied using Figure 4-12 and Table 4-4. Figures 4-12a, b and c show the relationship between the normalized shear stress at failure $[V_n / (\sqrt{f'_c} b_w d)]$ against stirrup spacing, S , the equivalent stirrup ratio, $[A_v f_{yt} / (b_w S)]$, and the longitudinal reinforcement ratio, ρ_L , respectively.

The normalized shear stress at failure v_n is defined as the ratio of nominal average shear stress at failure ($V_n / b_w d$) normalized by the square root of concrete compressive strength, f'_c . The nominal failure shear force V_n was calculated as the peak load at the critical section adjusted for the weight of the loading apparatus and self weight of specimen, as shown from Table 4-4.

$$v_n = \frac{V_n}{b_w d \sqrt{f'_c}} \quad (4-2)$$

The equivalent stirrup ratio S_r , defined as the product of the transverse reinforcement ratio ($\rho_t = A_v / b_w S$) multiplied by the yield strength of stirrups f_{yt} and is given by equation 4-3:

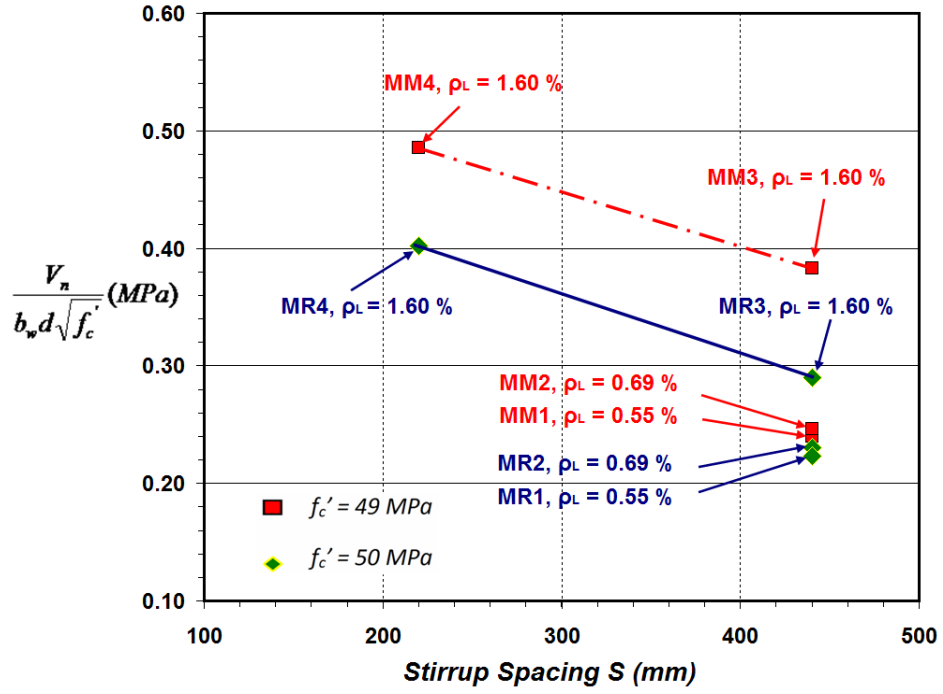
$$S_r = \frac{A_v f_{yt}}{b_w S} \quad (4-3)$$

From Figure 4-12a it is observed that the normalized shear stress at failure decreases as the stirrup spacing increases, regardless of the type of steel used in the stirrups. As the spacing of stirrups was doubled the shear stress at failure decreased by 39 % and 27 % for beams with conventional (*MR* series) and ASTM A1035 (*MM* series) stirrups, respectively. This is attributed in part to the wider

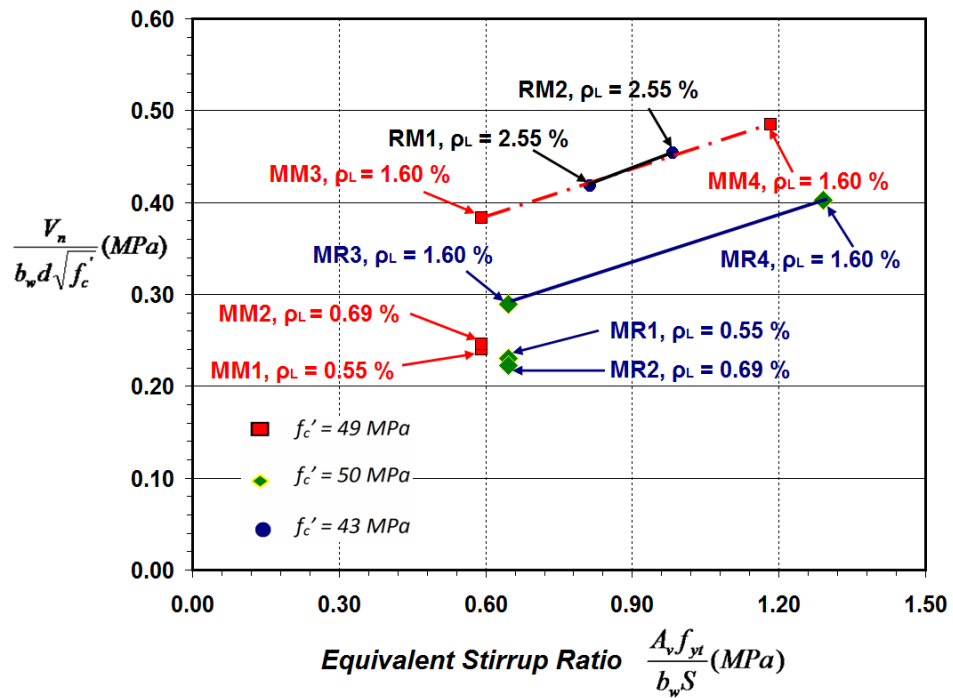
crack widths due to having less shear reinforcement area resulting in lower aggregate interlock action and hence lower shear stresses at failure.

The influence of the equivalent stirrup ratio $[A_v f_{yt} / (b_w S)]$ on the normalized shear stress at failure of reinforced concrete beams was also studied as illustrated in Figure 4-12b. Increasing the equivalent stirrup ratio increased the shear stress at failure. This is due to the reduced crack widths resulting in higher aggregate interlock and thereby improving the shear resistance. Note that the influence of steel type in the stirrup is included in the equivalent stirrup ratio $[A_v f_{yt} / (b_w S)]$. It was also observed that the failure shear stress of the beams with grade 690 stirrups (*MM* series) are higher than that of geometrically similar beams with stirrups yielding at $f_{yt} = 426$ MPa (*MR* series).

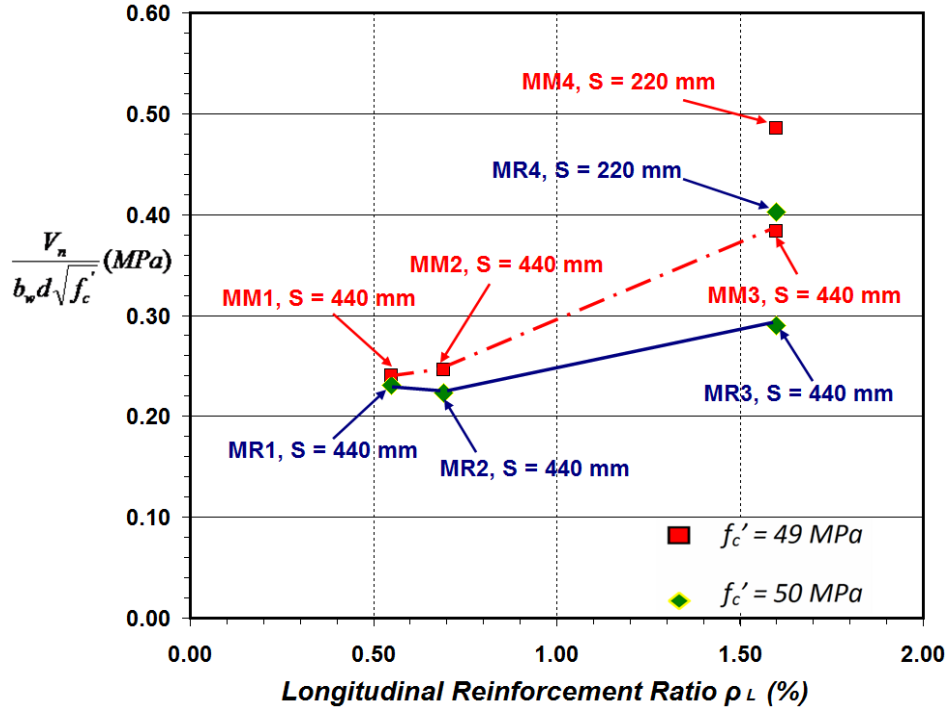
Figure 4-12c shows the influence of the longitudinal tensile reinforcement on the failure shear stress of beam specimens. In general, it is observed that lower longitudinal reinforcement ratios resulted in lower shear stress at failure. This behaviour is similar to the one observed for the slab specimens. (See Section 4.3.1.4). Table 4-4 shows that the normalized shear stress at failure increased by 30 % as the longitudinal reinforcement ratio, ρ_L , increased from 0.69 % to 1.60 %, for beams *MR2* & *MR3*. For beams *MM2* & *MM3* the normalized shear stress at failure increased by 56 % for the same increment in the longitudinal reinforcement ratio.



(a) Influence of Stirrup Spacing



(b) Influence of Equivalent Stirrup Ratio



(c) Influence of Longitudinal Reinforcement Ratio.

Figure 4-12: Influence on Normalized Shear Stress at Failure from (a) Stirrup Spacing (b) Equivalent Stirrup Ratio and (c) Longitudinal Reinforcement Ratio.

Table 4-4: Normalized Shear Stress at Failure for Beam Specimens.

BEAM ID	ρ_L (%)	ρ_t (%)	V_n (kN)	S (mm)	$\frac{A_v f_{yt}}{b_w S}$ (MPa)	$\frac{V_n}{b_w d \sqrt{f'_c}}$ (MPa)	% change in ρ_L	% change in ρ_t
RM1	2.55	0.15	420	320	0.81	0.42	-	-
RM2	2.55	0.18	478	265	0.98	0.45	-	9
MR1	0.55	0.11	458	440	0.65	0.23	-	-
MR2	0.69	0.11	438	440	0.65	0.22	-3	-
MR3	1.60	0.11	555	440	0.65	0.29	30	-
MR4	1.60	0.22	755	220	1.29	0.40	-	39
MM1	0.55	0.15	467	440	0.59	0.24	-	-
MM2	0.69	0.15	479	440	0.59	0.25	3	-
MM3	1.60	0.15	705	440	0.59	0.38	56	-
MM4	1.60	0.30	911	220	1.18	0.48	-	27

4.4 Summary

From the analysis and discussion of the experimental tests conducted on both slab and beam specimens, it was observed that some design parameters have significant influence on the shear strength of concrete members.

For slab specimens the relationships between shear stress at failure against member depth and longitudinal reinforcement ratio showed that both the size effect and strain effect have significantly influenced the shear stress at failure. The normalized shear stress at failure decreased as the member depth increased and as the longitudinal reinforcement ratio decreased.

For beam specimens plots of shear stress at failure against stirrup spacing, equivalent stirrup ratio and longitudinal reinforcement ratios were used to show that the shear stress at failure (shear capacity) is significantly influenced by the size effect and strain effect parameters. The normalized shear stress at failure decreased as the stirrup spacing increased, the equivalent stirrup ratio decreased and as the longitudinal reinforcement ratio decreased.

Some North American shear design models for concrete members with conventional Grade 420 steel reinforcement (*CSA A.23.3-04* and *AASHTO LRFD - 07*) were formulated using shear models that account the size effect and strain effect parameters. The analysis results indicated that both the size effect and strain effect parameters need to be considered in the development of shear models for concrete slabs and beams containing ASTM A1035 steel longitudinal reinforcement.

5. MODELING SHEAR CAPACITY OF ONE WAY-SLABS

5.1 General

The shear behaviour of reinforced concrete members depends on many parameters including member depth and longitudinal member strain. The influence of member depth is more significant for slabs without transverse reinforcement (See Section 2.2.4). This behavior was observed for the concrete members without stirrups considered in the current study as discussed in Section 4.3.1.4.

The influence of main design parameters on shear behaviour is well accounted for in the concrete shear models for use with conventional reinforcement that are based on the Modified Compression Field Theory (MCFT). (See Section 2.3). The longitudinal member strain is mainly dependent on the quantity and stress-strain behavior of the longitudinal reinforcement and the loading condition. Currently available design code models for shear either do not account for the influence of longitudinal member strain (e.g. *ACI 318-11* and *Eurocode2-04*) or are developed to account the influence of member strains based on conventional Grade 400 steel reinforcement (e.g. *CSA A23.3-04* and *AASHTO LRFD – 07*). These design code models were developed for concrete members with conventional steel reinforcement. However, similar shear models have not been fully assessed for members containing ASTM A1035 steel reinforcement.

In this chapter general and simplified analytical shear design models were developed for slabs longitudinally reinforced with ASTM A1035 steel and without transverse reinforcement. The models are validated against test results from the current study and those available from literature. The quality of predictions using the proposed models are also compared with predictions using the analytical and numerical shear models described in Section 2.4.

5.2 Proposed Analytical Shear Design Models

5.2.1 Motivation

Concrete slabs containing ASTM A1035 steel longitudinal reinforcement are expected to behave differently at higher strains compared to similar members with conventional Grade 420 steel reinforcement. This is mainly due to the difference in the stress-strain behaviour between the two reinforcing materials. The expected higher member strains for lightly reinforced slabs containing ASTM A1035 steel can result in wider diagonal crack widths. Based on the work of *Walraven (1981)* and *Vecchio and Collins (1986)*, the wider crack widths will reduce the aggregate interlock and lead to lower shear stress at failure. It is, therefore, necessary to develop and validate shear design models that directly incorporate the reinforcement stress-strain response which can account for the expected higher member strain, ϵ_x , for slabs containing ASTM A1035 steel longitudinal reinforcement.

5.2.2 General Shear Model

The general shear model for slabs without stirrups containing ASTM A1035 steel longitudinal reinforcement takes the same form as the *Hoult et al.* model. (See Section 2.4.1.4). *Hoult et al.* (2008) provided a so-called second order version of the expression for V_C adapted from the *CSA A23.3-04* shear capacity model. This model can be used for a wider range of ϵ_x values (up to 0.006 mm/mm) and was validated to be more accurate than other currently available code models for reinforced concrete members containing internal Fiber Reinforced Polymer (FRP) reinforcing bars where higher member strains are expected near failure. The *Hoult et al.* model was chosen as a basis for a new generalized shear model for concrete slabs without stirrups since higher member strains are also expected for concrete members containing longitudinal ASTM A1035 steel.

The equation for the general shear model for slabs with ASTM A1035 steel longitudinal reinforcement, V_{GS} , is given as:

$$V_{GS} = \left(\frac{0.3}{0.5 + (1000 \varepsilon_x + 0.15)^{0.7}} \right) \left(\frac{1300}{1000 + S_{ze}} \right) \sqrt{f'_c} b_w d_v \quad (5-1)$$

where the shear depth, $d_v = 0.9d$, and parameter S_{ze} is:

$$S_{ze} = \frac{35 S_z}{a_g + 15} \geq 0.85 S_z \quad (5-2)$$

The parameter ε_x represents the strain at mid-depth of the member under consideration.

The MCFT based shear models described in Section 2.4 (*CSA A23.3-04* and *Hoult et al., 2008*) assume a linear stress-strain response for the reinforcement up to failure, through the parameter ε_x . (See equation 2-13). This assumption was developed and validated for members with conventional Grade 420 steel longitudinal reinforcement where the stress-strain behaviour can typically be modeled by a bilinear elastic-plastic relationship. However, for members with high-performance ASTM A1035 steel longitudinal reinforcement this assumption can underestimate the value of ε_x . The ASTM A1035 steel begins to exhibit non-linear stress-strain response at a stress of about 480 MPa whereas the flexural design would typically use a higher value (*ACI ITG-6R-10*). Therefore, it is necessary to develop a new expression for ε_x which can directly account for the non-linear response of the ASTM A1035 reinforcement at higher strains.

Equation 5-3 was developed to directly estimate the longitudinal reinforcement stress from the combined flexure and shear effects at the cross section considered for members designed according to MCFT based shear models.

$$f_s = \frac{\frac{M}{d_v} + V}{A_s} \quad (5-3)$$

With the reinforcement stress from equation 5-3 and a representative stress-strain model for ASTM A1035 steel (equation 3-1), the corresponding reinforcement strain ε_s can be

determined. Finally, using a similar simplifying assumption as the *CSA A23.3-04* shear model development (*Bentz et al., 2006*), the axial strain parameter at mid-height ε_x is approximated as $\frac{1}{2}$ the reinforcement strain magnitude.

Note that equation 5-1 is a function of ε_x which is related to the loads effects at the cross section considered (M and V) through f_s . (See equation 5-3). As these load effects are unknown in the initial stage, determining the shear capacity involves iterative steps as summarized using the flow chart shown in Figure 5-1. For concrete slab under concentrated load, critical section is normally taken as the distance d_v from the loading point.

5.2.3 Design Shear Model

The simplified flexural design model proposed by *Mast et al. (2008)* and adopted by *ACI ITG-6R-10* for concrete members with ASTM A1035 steel longitudinal reinforcement specifies an elastic-plastic stress-strain model for reinforcement having a “design” yield strength of $f_y = 690$ MPa. This value is smaller than the effective yield strength (830 MPa) determined by the 0.2 % offset method. Consistent with the *Mast* flexural model, a simplified shear model is proposed based on the general shear model (equation 5-1).

In recognition of the influence of axial strain on member shear capacity, the longitudinal reinforcement strain due to applied forces (M & V) at the critical section should be determined. In the current study the proposed design shear model is based on a yield strength of 690 MPa for the ASTM A1035 steel. Thus the strain parameter ε_x at mid-depth can be determined as 0.00213 for $f_s = 690$ MPa using the stress strain relation for ASTM A1035 steel as in step 4 of Figure 5-1. Since the concrete components are rarely known at the time of member design, the maximum aggregate size, a_g , can be taken as zero which provides a lower bound estimate of shear capacity. Using $S_z = d_v$ in equation 5-2, and the above assumptions the following simplified design shear equation is obtained from equation 5-1:

$$V_{DS} = \left(\frac{171}{1000 + 2.3d_v} \right) \sqrt{f'_c} b_w d_v \quad (5-4)$$

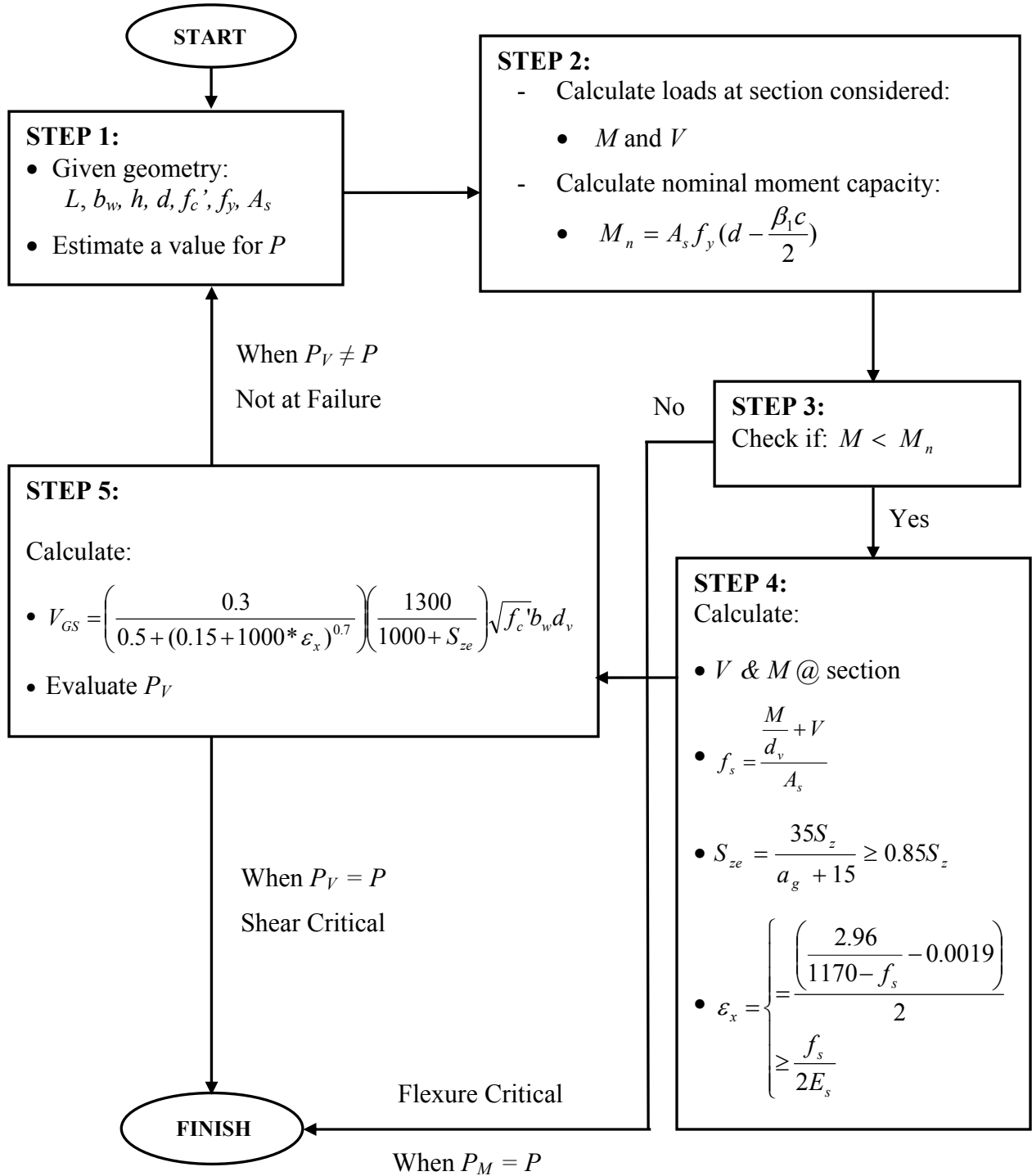


Figure 5-1: Flowchart for the Proposed General Shear Model of Concrete Slabs.

5.3 Model Validation

5.3.1 Database of Tested Slab Specimens

A database of slabs containing ASTM A1035 steel longitudinal reinforcement was assembled for use in validation of the general and simplified design shear models developed in Section 5.2. In addition to the six new slab test data described in chapter 4, slab specimens from prior tests were used for validation of the shear capacity models. The database of shear critical members included all known specimens which satisfied the following criteria:

- Longitudinal reinforcement with ASTM A1035 steel and no transverse reinforcement.
- Rectangular cross sections with shear span-to-depth ratio, $a/d \geq 2.5$.

In addition, the available specimens had the following range of design parameters:

- Overall member depth, h , between *305 mm and 915 mm*.
- Longitudinal reinforcement ratio, ρ_L , ranging from 0.23% to 2.71%.

In the database, the range of overall member depth values ($305 \text{ mm} \leq h \leq 915 \text{ mm}$) reflects the typical size of concrete members without stirrups in buildings, including slabs and footings. The shear-span to effective depth, a/d , was selected to represent slender concrete members showing a typical sectional shear behavior. As discussed in Section (2.2.2), this limiting value of $a/d \geq 2.5$ was used for slender members, as $a/d = 2.5$ is assumed to be a transition point between the beam action and arch action. Note also that the available specimens from prior tests in the database had concrete compressive strengths in the lower strength range ($30 \text{ MPa} \leq f'_c \leq 40 \text{ MPa}$) while members tested in the current study had concrete strengths in the range of $50 \text{ MPa} \leq f'_c \leq 60 \text{ MPa}$.

Table 5-1 shows the shear test results of all slab specimens in the database from new tests and prior tests conducted at North Carolina State University in two independent research programs. The database consists of ten slab specimens with parameters representing the

typical ranges in the design practice. All members were reinforced with Grade 690 ASTM A1035 steel longitudinal reinforcement without stirrups and tested under a concentrated load using three point bending. The effective member depth, d , ranged from 278 mm to 850 mm.

Table 5-1: Details of Slab Specimen from Prior Tests.

<i>Researcher</i>	<i>Slab Specimen</i>	b_w (mm)	d (mm)	$(a/d)_1$	$(a/d)_2$	ρ_L (%)	f_{yL}^* (MPa)	f_c' (MPa)	V_{TEST} (kN)
<i>New Tests</i>	<i>S-1</i>	305	278	3.55	3.55	0.46	690	53	77
<i>New Tests</i>	<i>S-2</i>	305	278	3.55	3.55	0.46	690	59	75
<i>New Tests</i>	<i>S-3</i>	300	569	3.60	3.60	0.45	690	49	123
<i>New Tests</i>	<i>S-4</i>	300	569	3.60	3.60	0.45	690	57	112
<i>New Tests</i>	<i>S-5</i>	300	573	3.57	3.57	0.23	690	53	91
<i>New Tests</i>	<i>S-6</i>	300	573	3.57	3.57	0.23	690	57	72
<i>Hassan et al. (2008)</i>	<i>M-2.7-32</i>	460	850	2.75	2.75	0.44	690	32	319
<i>Munikrishna et al. (2011)</i>	<i>G1-M0</i>	610	645	3.11	6.10	1.02	690	31	229
<i>Munikrishna et al. (2011)</i>	<i>G2-M0</i>	610	645	3.11	3.35	1.02	690	31	336
<i>Munikrishna et al. (2011)</i>	<i>G3-M0</i>	406	457	3.00	7.17	2.71	690	37	282

* Yield Stress for ASTM A1035 Steel as Recommended by *ACI ITG-6R-10(2010)*.

5.3.2 Validation of the General Shear Model

The proposed general shear model for concrete slabs developed in Section 5.2.2 was validated for the tests completed in the current and prior research works. The maximum measured shear load obtained from each test was compared to the prediction using the general shear model.

Table 5-2 shows the ratios of the measured to predicted shear strength for the ten concrete slabs in the overall database. The average test to predicted ratios of the specimens, the standard deviations, and coefficients of variation were calculated. It is observed that the general shear model (equation 5-1) was in good agreement with the test

data. The average test to predicted load of 1.03 and coefficient of variation of 0.18 were obtained.

Of the ten slab specimens considered, capacity predictions are poorer for three specimens (*G1-M0*, *S-4* & *S-6*). Specimen *G1-M0* had similar geometry with specimen *G2-M0* except that *G1-M0* was asymmetrically loaded and had a larger span length for which the shear span to depth ratio on either side of the loading point differed by a multiple of about 2. The shear span to depth ratios of the specimens on each side of the loading point is given in Table 5-1. The lower measured capacity for this specimen (compared to the companion specimen *G2-M0* with nearly symmetrical loading) can be attributed to the asymmetrical loading.

On the other hand the poorer results for specimens *S-4* & *S-6* can be attributed to the higher concrete strength where the average f_c' was 57 MPa. This strength value is near the 60 MPa limit where *Bentz et al.* (2006) and others have suggested to reduce a_g in equation 5-2 to account for aggregate fracture. Detailed assessment could be made on this limit in the future as more test data becomes available for slabs with high-strength concrete and longitudinally reinforced with ASTM A1035 steel.

Table 5-2: General Shear Model Predictions of Slabs in the Database.

<i>Author</i>	<i>Slab ID</i>	<i>P_{TEST} (kN)</i>	<i>P_{GS} (kN)</i>	<i>P_{TEST}/P_{GS}</i>
<i>New Test</i>	<i>S-1</i>	153	142	1.08
<i>New Test</i>	<i>S-2</i>	149	146	1.02
<i>New Test</i>	<i>S-3</i>	245	242	1.01
<i>New Test</i>	<i>S-4</i>	223	252	0.88
<i>New Test</i>	<i>S-5</i>	182	169	1.08
<i>New Test</i>	<i>S-6</i>	144	171	0.84
<i>Hassan et al. (2008)</i>	<i>M-2.7-32</i>	638	517	1.23
<i>Munikrishna et al. (2011)</i>	<i>G1-M0</i>	346	466	0.74
<i>Munikrishna et al. (2011)</i>	<i>G2-M0</i>	648	595	1.09
<i>Munikrishna et al. (2011)</i>	<i>G3-M0</i>	400	292	1.37
<i>P_{TEST}/P_{Model} (Average)</i>				1.03
<i>STDV</i>				0.18
<i>COV</i>				0.18

Once the general shear model for concrete slabs with ASTM A1035 longitudinal steel reinforcement was validated for the entire available slab tests it is important to evaluate the model based on the influence of main variables affecting the strain effect and the size effect parameters. Figure 5-2a shows the relationships between the ratios of the measured to predicted shear strength using the general model (equation 5-1) and member depth for the entire database. It is observed that the general shear model was in a reasonably consistent agreement with respect to member depth for all the test data. In general the observed behaviour for the specimens showed that the proposed general shear model captured the influence of member depth and hence the so-called size effect on shear prediction is adequately considered.

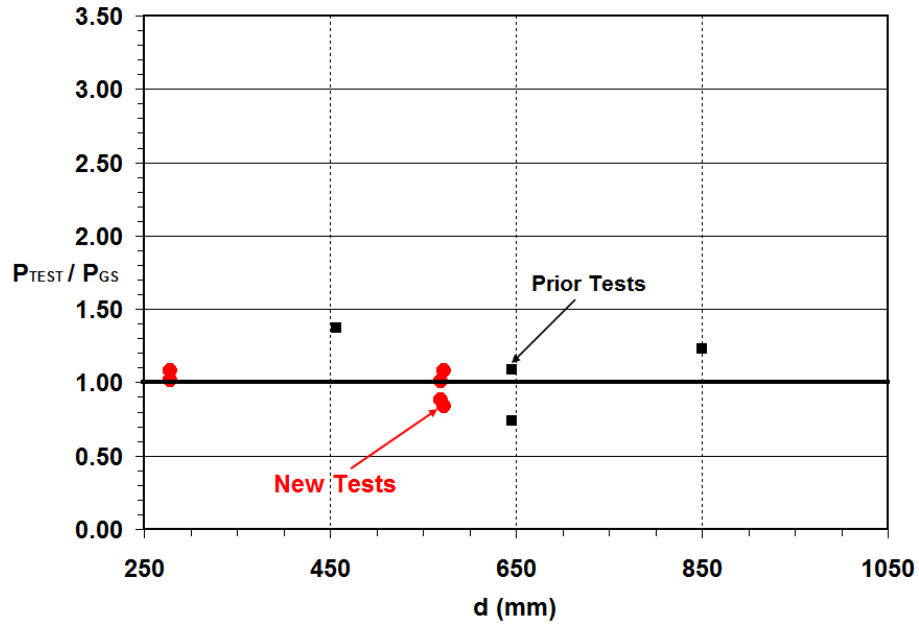
Figure 5-2b shows the relationships between the test to model ratios and calculated longitudinal member strain for all the available tested slabs. Once again, the general shear model was in a consistent agreement with respect to longitudinal member strain for all the test data. It can be concluded that the proposed general shear model adequately captured the so-called strain effect on shear capacity prediction.

5.3.3 Validation of the Design Shear Model

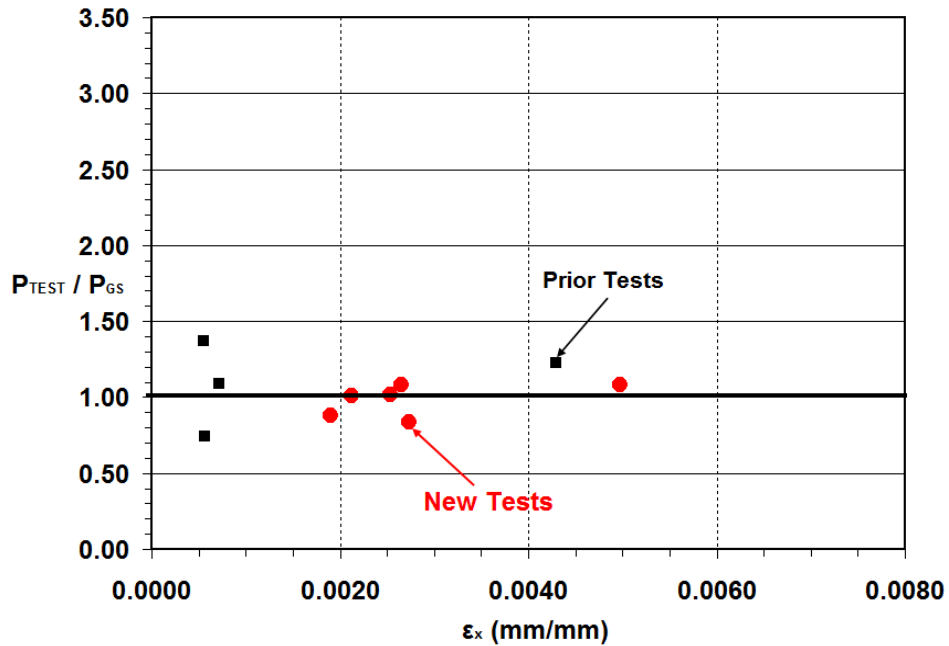
The simplified design shear model developed in section 5.2.3 for concrete slabs containing ASTM A1035 longitudinal steel reinforcement was validated for all the available slab tests in the database. As part of the validation the same parameters considered in Section 5.3 (d and ε_x) were used to study their influence on the shear capacity prediction of slabs with ASTM A1035 steel.

Table 5-3 shows that, except for one specimen (*S-6*), the design model results in conservative predictions with $P_{TEST}/P_{DS} > 1.0$. The average test to predicted load ratio of 1.67 and coefficient of variation of 0.46 were obtained. Compared with the general model, the design model showed significantly higher test to prediction ratios and coefficient of variation. This can be clearly shown by comparing the test to predicted load

ratios of the general model (Table 5-2) with the design model (Table 5-3) upon which the design model was based.



a) Influence of member depth.



b) Influence of average member strain.

Figure 5-2: Validation of the General Shear Model for Size Effect and Strain Effect.

The conservative assumptions used in developing the design model, such as neglecting the aggregate interlock component ($a_g = 0$) can result in lower strength predictions especially for members with larger size aggregates.

Predictions using the design model are more conservative (with $P_{TEST}/P_{DS} > 2.0$) for three slab specimens (*M-2.7-32*, *G2-M0*, *G3-M0*). Both *G2-M0* and *G3-M0* failed at ϵ_x values that are much lower than the value assumed in developing the design model. Note also that *M-2.7-32* had lower shear span to depth ratio ($a/d = 2.75$) which is close to limiting value of 2.5, a transition point between the beam action and arch action. It is expected that arch action might have been developed and result in a higher capacity than the prediction by the sectional model for specimen *M-2.7-32*, as was already observed in Table 5-2. Note also that specimen *M-2.7-32* had highest effective depth $d = 850$ mm and maximum aggregate size $a_g = 20$ mm which would both amplify the error from the assumption in the simplified model where $a_g = 0$.

The other reason could be due to neglecting the compression reinforcement provided for all the four prior tested specimens shown in Table 5-1. Note that the design shear model is developed for singly reinforced concrete members and doesn't account for the additional member capacity from the compression reinforcement.

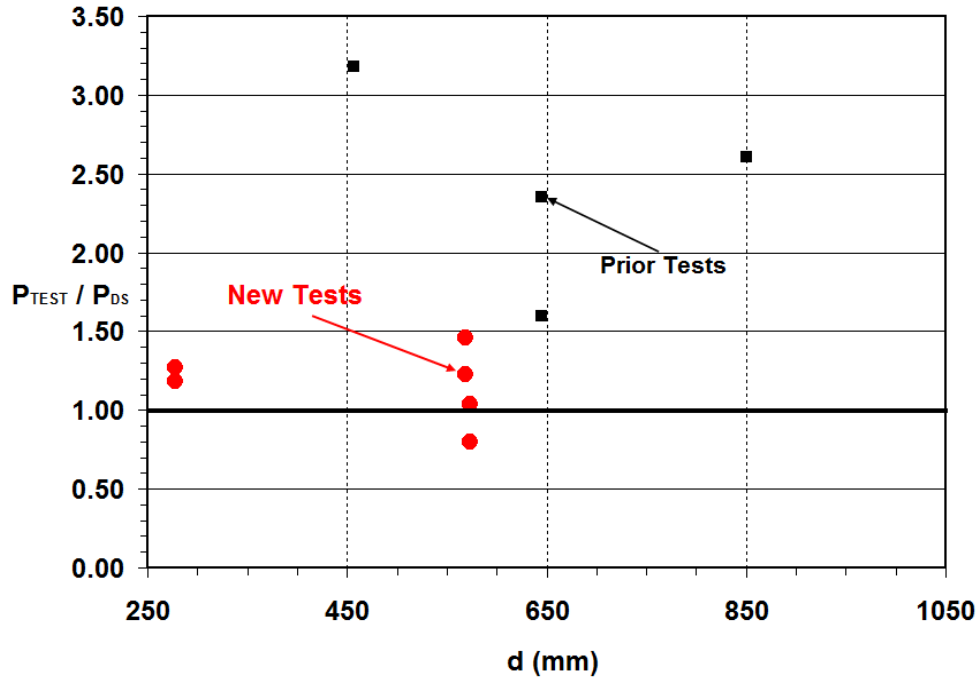
On the other hand the six specimens tested in the current study had ϵ_x values close to the assumption used in deriving the simplified model and had no compression reinforcement. The predictions using the design shear model were more accurate ($P_{TEST}/P_{DS} = 1.16$ & $COV = 0.20$) in comparison to the four specimens from prior tests.

Table 5-3: Simplified Design Shear Model Predictions of Slabs in the Database.

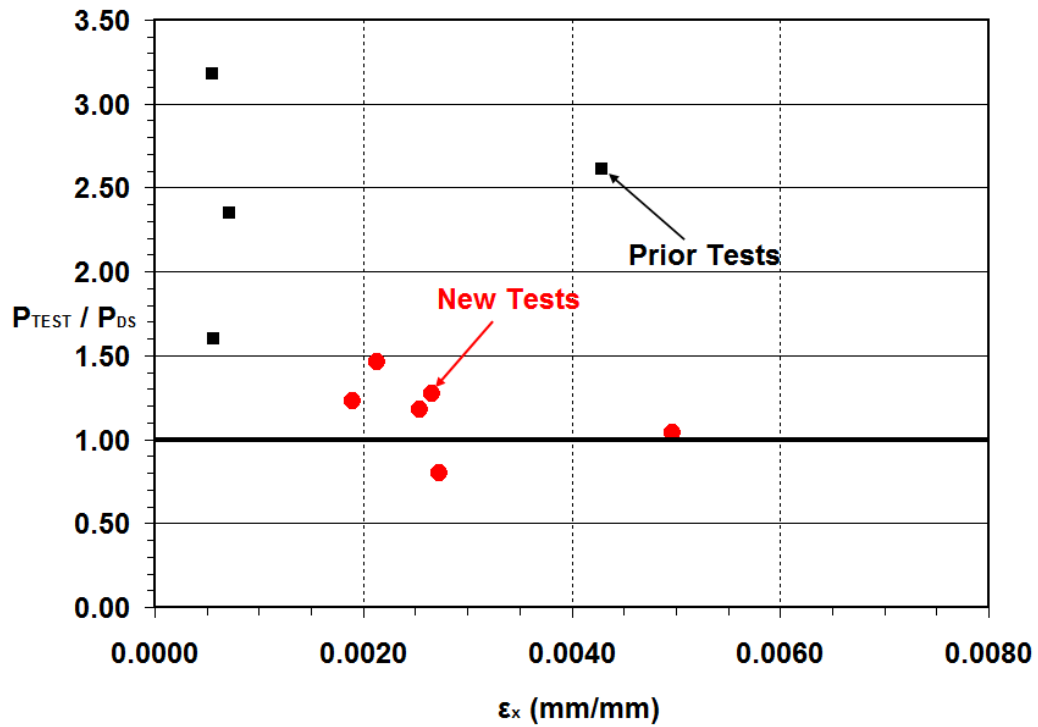
<i>Author</i>	<i>Slab ID</i>	<i>P_{TEST} (kN)</i>	<i>P_{DS} (kN)</i>	<i>P_{TEST}/P_{DS}</i>
<i>New Test</i>	<i>S-1</i>	153	120	1.27
<i>New Test</i>	<i>S-2</i>	149	127	1.18
<i>New Test</i>	<i>S-3</i>	245	168	1.46
<i>New Test</i>	<i>S-4</i>	223	181	1.23
<i>New Test</i>	<i>S-5</i>	182	175	1.04
<i>New Test</i>	<i>S-6</i>	144	181	0.80
<i>Hassan et al. (2008)</i>	<i>M-2.7-32</i>	638	245	2.61
<i>Munikrishna et al. (2011)</i>	<i>G1-M0</i>	346	216	1.60
<i>Munikrishna et al. (2011)</i>	<i>G2-M0</i>	648	276	2.35
<i>Munikrishna et al. (2011)</i>	<i>G3-M0</i>	400	126	3.18
<i>P_{TEST}/P_{Model} (Average)</i>				1.67
<i>STDV</i>				0.78
<i>COV</i>				0.46

Figure 5-3a shows the relationships between the ratios of the measured to predicted shear capacity using the design model (equation 5-4) and member depth for the available ten slender concrete slabs. Although the data cloud has wide scatter due to the conservative shear capacity predictions, it can be concluded that the design shear model was able to capture the influence of the so-called size effect on shear capacity as similar trend is observed for most of the specimens having wide range of member depths.

Figure 5-3b shows the relationships between the test to design model ratios and the average longitudinal member strain ϵ_x for all the available tested slabs. Again, the design shear model was in a consistent agreement with respect to member strain for the test data, although the conservative shear predictions resulted in a wide scatter of the data cloud. From the Figure it can be seen that the simplified design shear model adequately captured the so-called strain effect on shear capacity prediction.



a) Influence of member depth.



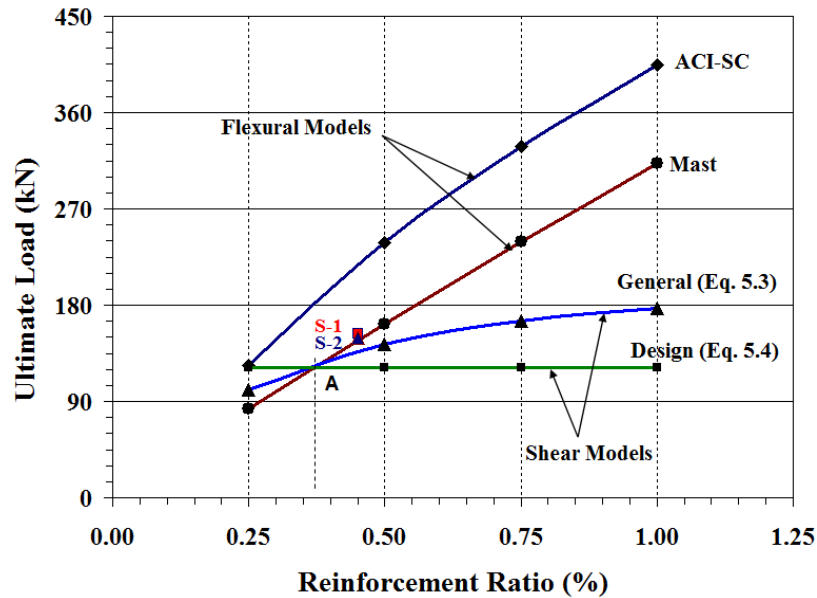
b) Influence of average member strain.

Figure 5-3: Validation of the Design Shear Model for Size Effect and Strain Effect.

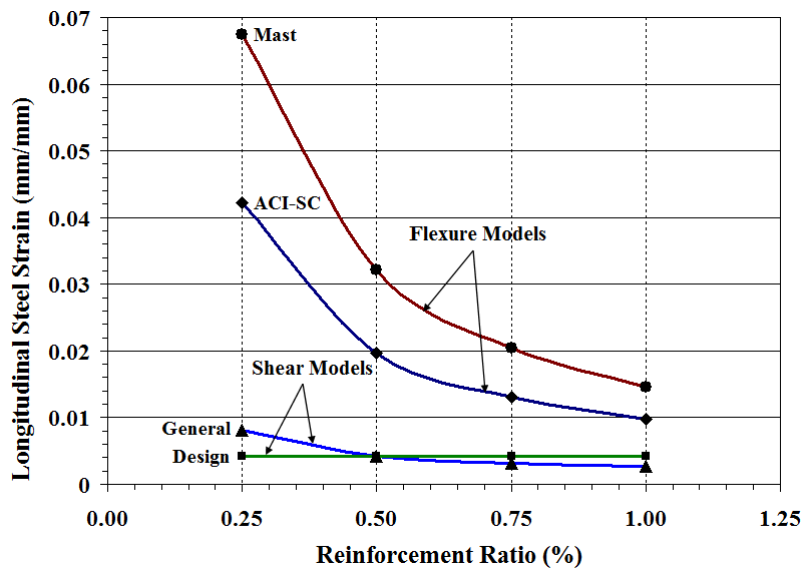
Equation 5-4 was used to predict the shear capacities, test to predicted load ratios and coefficients of variations for the six new slab specimens tested in the current study. The average test to proposed load of 1.16 and coefficient of variation of 0.20 was obtained. Compared with results using the general model the higher variation is due to the lower reinforcement ratios in specimens *S-5* and *S-6* which leads to large reinforcement stresses and strains considerably exceeding the simplifying assumption of $f_y = 690$ MPa ($\epsilon_s = 0.00427$) in the model. Hence equation 5-4 should not be used for *S-5* and *S-6* in this study since they show significant non-linear behaviour before failure and had reinforcement stresses and strains considerably larger than the simplifying assumption used in the model. (See Figure 4-2). For the other four specimens (*S-1* to *S-4*) in Table 5-2, the proposed design shear model shows consistent prediction and better agreement with test results and gives an average test to model ratio of 1.29 and COV of 0.08.

Since equation 5-4 is developed for an assumed reinforcement strain condition ($\epsilon_s = 0.00427$) corresponding to a 'yield' strength of $f_y = 690$ MPa, it is necessary to validate that this condition results in safe predictions of flexural or shear capacity for slabs with ASTM A1035 steel reinforcement when used alongside the simplified flexural design model. The capacity of concrete members reinforced with ASTM A1035 steel and without stirrups having reinforcement ratios from $\rho_L = 0.25\%$ to 1.0% , a/d from 2.7 to 4.9 and d from 150 to 600 mm were evaluated. Members are assumed to be loaded under 3-point bending. Figure 5-4 illustrates the results for $d = 300$ mm and $a/d = 3.5$, which are representative of other cases studied. In Figure 5-4a, the flexural capacity according to the *Mast et al.* simplified model and the *strain compatibility (SC)* flexural model of *ACI ITG-6R-10* Appendix B are shown. As expected, the flexural capacity increases with increasing reinforcement ratio, and the strain compatibility model predicts higher flexural capacity than the *Mast et al.* model. This is due to consideration of the pseudo strain hardening of the steel beyond the 690 MPa design yield strength assumed by the *Mast et al.* model. The proposed general shear model (equation 5-1) gives increasing shear capacity as reinforcement ratio increases, but the slope of this relationship is flatter than for the flexural strength increase with reinforcement ratio. By comparing the general model and strain compatibility model, all member configurations represented in Figure 5-

4 are expected to be shear critical. For all values of reinforcement ratio greater than about 0.37% (Point A on Figure 5-4a), the proposed design shear model, equation 5-4, predicts a conservative capacity below that of the general model.



(a) Member capacity



(b) Longitudinal steel strain

Figure 5-4: Flexural and Shear capacity of members with different longitudinal reinforcement.

However, when $\rho_L < 0.37\%$, the capacity by the general shear model is less than the design shear model capacity. The reason for this estimation can be observed in Figure 5-4b, where the reinforcement strain at the failure condition is plotted for each capacity model condition shown in Figure 5-4a. In the $\rho_L < 0.37\%$ range, it is observed that the longitudinal reinforcement strain will exceed the value 0.00427 mm/mm corresponding to a stress of 690 MPa. However, the Mast flexural model would govern the design capacity in this range, thereby mitigating concerns that the proposed design shear model can overestimate the actual shear strength. For other design parameters studied, such as member depth, the divergence between the flexure and shear curves and the ρ_L corresponding to point *A* may change, but the similar result of compatible simplified flexure (i.e. *Mast*) and design shear (i.e. equation 5-4) models continue to result in safe limiting design conditions.

5.4 Comparison to Existing Shear Design Models

The influence on sectional shear behavior of the design parameters including reinforcement ratios and the member depth is considered in different manners in current shear design codes. The main differences are briefly described here.

The *CSA A23.3-04* shear provisions which are based on the Modified Compression Field Theory (MCFT) directly consider a decrease in shear strength as the member depth increases, represented as “size effect”. Furthermore, the model considers a decrease in shear capacity due to increased strains in the longitudinal reinforcement which represents the “strain effect”.

The *ACI 318-11* does not consider the influences of member depth or strain in the longitudinal reinforcement, in the prediction of shear capacity of concrete members without stirrups. Instead, similar empirical shear capacity model applies to all cases regardless of member depth or reinforcement strain magnitude.

Eurocode 2, on the other hand, does not directly consider the “size effect” or the “strain effect”, in the prediction of shear capacity, although the parameters d & ρ_L are considered in the model.

Note that every code model uses different resistance factors to the concrete and the steel contribution of shear capacity prediction of reinforced concrete members. In this study, nominal shear capacities are considered for all models with resistance factors taken as 1.0.

5.4.1 Code Model Predictions

The maximum measured shear loads obtained from tests were compared to the predictions using the *ACI 318-11* Code, the Canadian Standards Association (*CSA A.23.3.04*) Code and *Eurocode 2 - 2004 (EC2)*. The various equations used to calculate the code predictions can be found in Section 2.4. It should be noted that shear analysis for all codes is based on using a yield strength of 690 MPa (100 ksi) for the ASTM A1035 Grade 690 longitudinal steel reinforcement.

Table 5-4 presents the test to predicted load ratios of the three code models for all specimens in the database, including the six new slab test results from this study. It is observed that the *CSA A23.3-04* shear model, with the proposed modifications for higher strains (See equation 5-3), is in good agreement with the test data. The average test to prediction ratio is 1.15 and coefficient of variation of 0.16. Lower capacity prediction ratios were obtained for two specimens (*S-4* & *G1-M0*). This is due the lower reinforcement ratio in S4 and the highly eccentric loading in G1-M0 resulting in significant non-linear stress-strain response in the ASTM A1035 steel and leading to possible premature flexure-shear failure. Table 5-4 also shows that both the *ACI 318* and *EC2* shear models, resulted in unsafe predictions of shear capacity with average test-to-prediction ratio of 0.72 and 0.89 with coefficients of variation of 0.45 and 0.22, respectively. For the *ACI 318-11* code, it is observed that the prediction quality decreases significantly as the depth increases (e.g., compare *S-3* to *S-1* and *S-4* to *S-2*). While

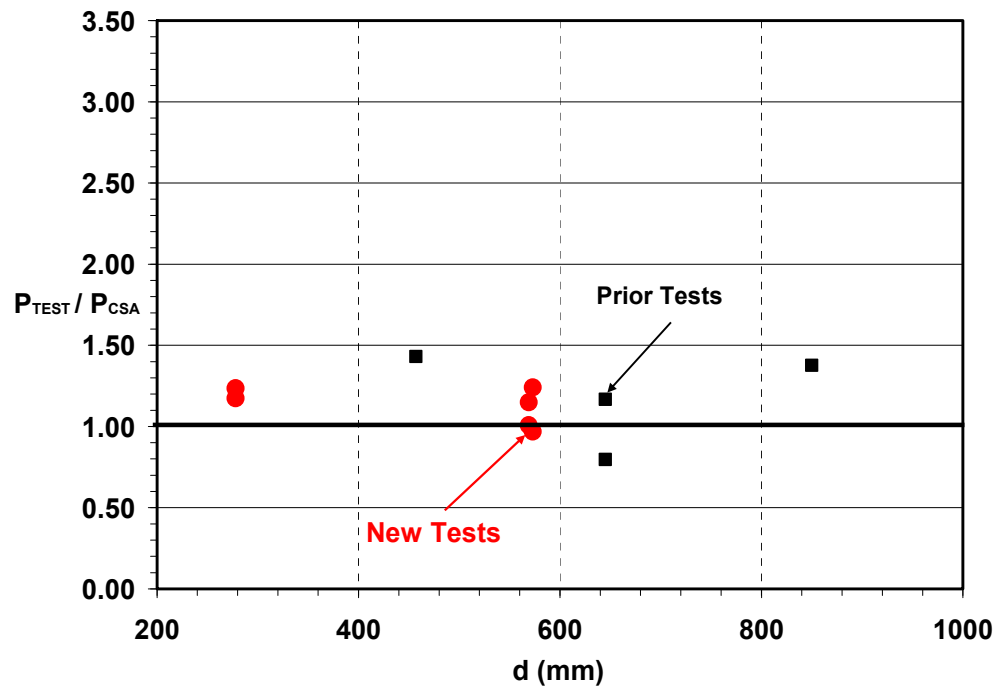
equation 2-16 for *EC2* includes parameters to consider member depth, the relationship appears inadequate when comparing the prediction quality of *S-3* to *S-1* and *S-4* to *S-2*. Furthermore, the prediction quality of *ACI 318* and *EC2* is worse for *S5* and *S6* since the non-linear reinforcement response is not adequately considered in both models. The test results indicate that the *CSA* model is capable to conservatively predict the shear capacity while the *ACI 318* and *EC2* shear models are viewed as inadequate for slabs longitudinally reinforced with ASTM A1035 steel.

Table 5-4: Code Model Predictions of Slabs in the Database.

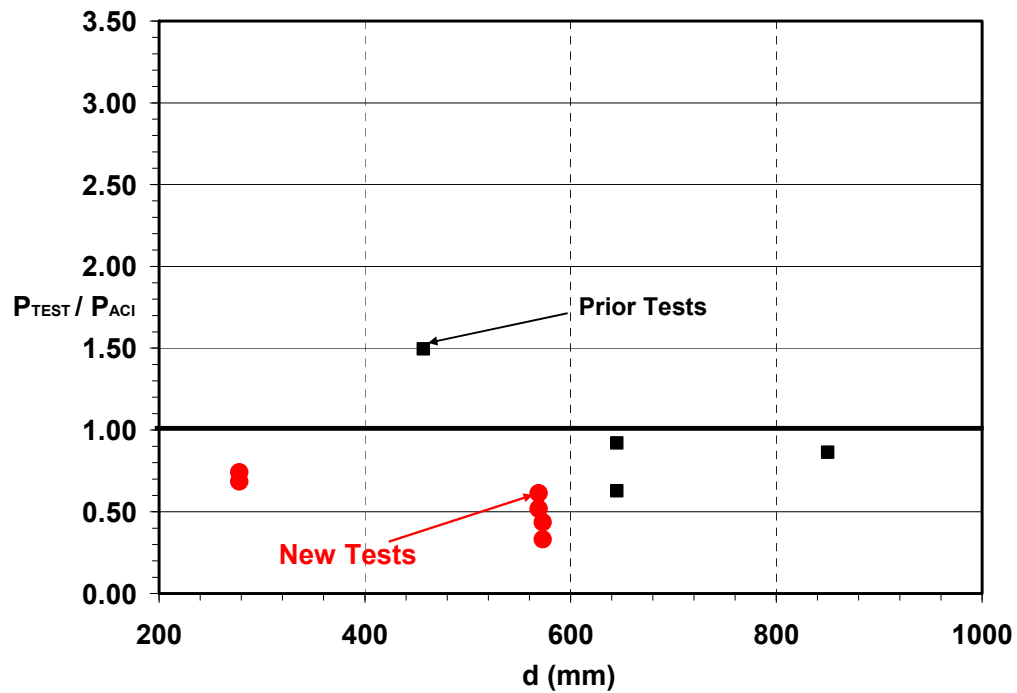
<i>Slab ID</i>	$P_{TEST} (kN)$	$P_{CSA} (kN)$	P_{TEST} / P_{CSA}	$P_{ACI} (kN)$	P_{TEST} / P_{ACI}	$P_{EC2} (kN)$	P_{TEST} / P_{EC2}
<i>S-1</i>	153	124	1.24	206	0.74	163	0.94
<i>S-2</i>	149	127	1.17	218	0.68	169	0.88
<i>S-3</i>	245	213	1.15	399	0.61	275	0.89
<i>S-4</i>	223	221	1.01	430	0.52	289	0.77
<i>S-5</i>	182	147	1.24	418	0.44	225	0.81
<i>S-6</i>	144	149	0.97	433	0.33	230	0.62
<i>M-2.7-32</i>	638	463	1.37	739	0.86	503	1.27
<i>G1-M0</i>	346	434	0.80	551	0.63	526	0.66
<i>G2-M0</i>	648	555	1.17	704	0.92	672	0.96
<i>G3-M0</i>	400	279	1.43	267	1.50	366	1.09
$P_{TEST} / P_{MODEL} (Average)$			1.15		0.72		0.89
STDV			0.19		0.33		0.19
COV			0.16		0.45		0.22

Figure 5-5 shows the relationships between test to predicted shear capacity ratios and member depth based on the analytical code models for all the specimens in the database. From Figure 5-5 it is observed that the *CSA A23.3-04* shear code model showed consistent agreement with respect to member depth for all the test data compared with the *ACI 318-11* and *EC2* shear models. It can be observed that the *CSA A23.3-04* design shear model adequately captured the size effect on shear capacity prediction. On the other

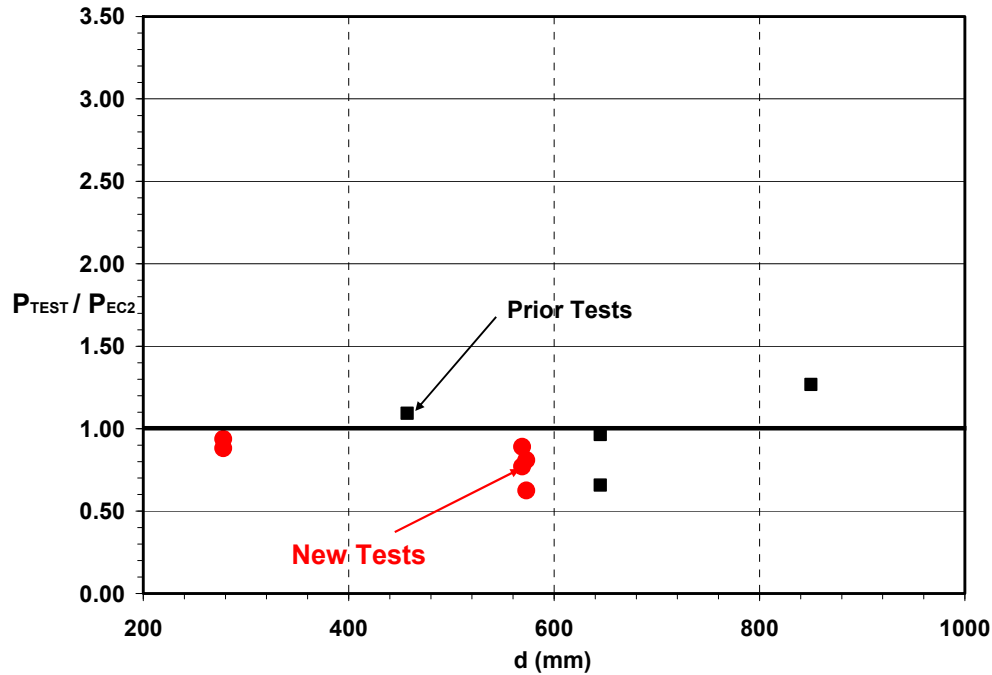
hand the *ACI 318-11* and *EC2* shear models showed inadequate consideration for size effect resulting in poor prediction quality with a wide scatter in the data cloud.



a) Influence of Member Depth for *CSA A23.3-04* Shear Code Model.



b) Influence of Member Depth for *ACI 318-11* Shear Code Model.



c) Influence of Member Depth for *EC2* Shear Code Model.

Figure 5-5: Validation of the Analytical Shear Models for Size Effect.

5.4.2 Numerical Model Predictions

Two numerical models, *VecTor2* (*VT2*) and *Response 2000* (*R2K*) described in Section 2.4.2, were employed to predict the shear capacity of the slab specimens studied in this project. The maximum loads obtained from each test were compared to the predictions using the numerical models. The procedures used to model the members can be found in Section 2.4.2. Figures 5-6 and 5-7 show typical beam models using the *VT2* and *R2K* programs.

The analysis for *VecTor2* (*VT2*) model is based on using an idealized bi-linear elastic-plastic stress-strain relationship with a yield strength of 690 MPa for the ASTM A1035 steel longitudinal reinforcement (*ACI ITG-6R-10*). For *Response 2000* (*R2K*) the non-linear stress-strain response of the ASTM A1035 longitudinal steel was simulated as

unstressed prestressing steel using a modified Ramburg-Osgoode (R-O) relationship (*Collins and Mitchell, 1997*). The R-O approximation for the stress-strain response of ASTM A1035 longitudinal steel (adapted from *Collins and Mitchell, 1997*) is given by the following equation.

$$f_s = \begin{cases} 200,000 \varepsilon_s \left\{ A + \frac{1-A}{[1 + (B\varepsilon_s)^C]^{\frac{1}{C}}} \right\} \\ 1040 \end{cases} \quad (5-5)$$

The R-O parameters in equation 5-5 were solved as $A = 0.006$, $B = 200$ & $C = 2.2$ from the *ACI ITG-6R-10* stress-strain response model for ASTM A1035 steel (equation 3-1) using a technique described in *Collins and Mitchell, 1997*).

The ratios of measured-to-predicted shear strength of concrete slabs from prior tests and new tests completed in this study are given in Table 5-5. The average, standard deviations, and coefficients of variation of the test-to-predicted ratios were determined using statistical analysis.

From Table 5-5 it is observed that both the *VT2* and *R2K* numerical shear models are in good agreement with the test data. The average test-to-prediction ratios of the ten slab specimens using the *VT2* model is 1.08 with coefficient of variation of 0.20. The corresponding values for the *R2K* model are 1.12 and 0.17, respectively. The results indicate that both the *VT2* and *R2K* models can predict the failure shear load of slabs with ASTM A1035 steel longitudinal reinforcement with reasonable accuracy.

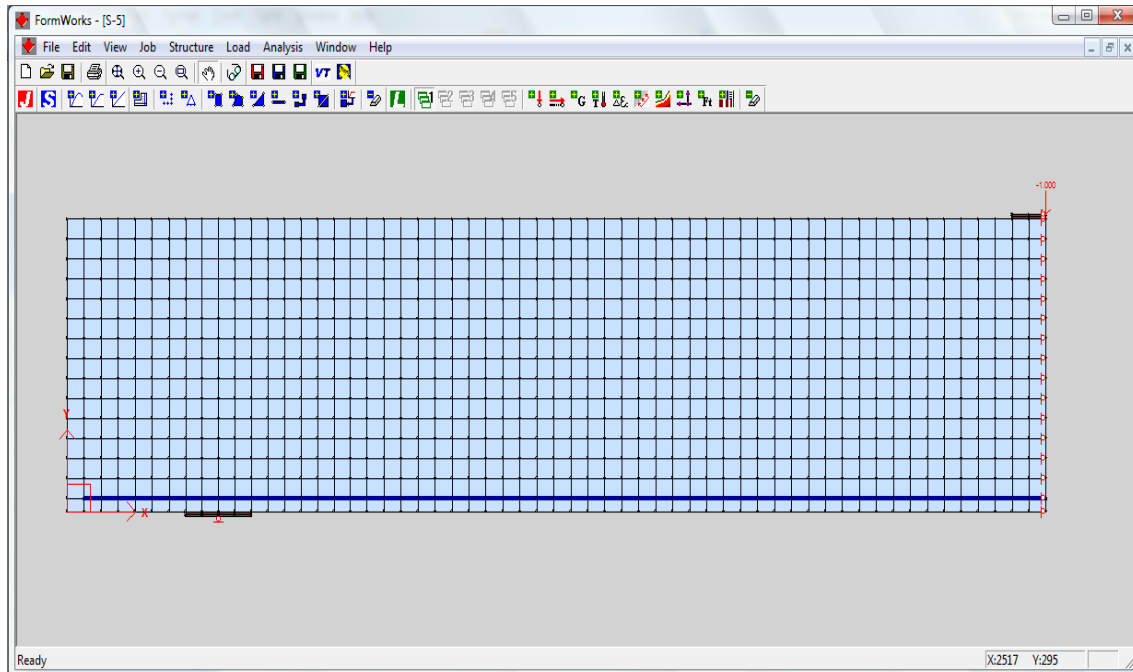


Figure 5-6: Typical mesh for *VecTor 2 (VT2)* Slab Model.

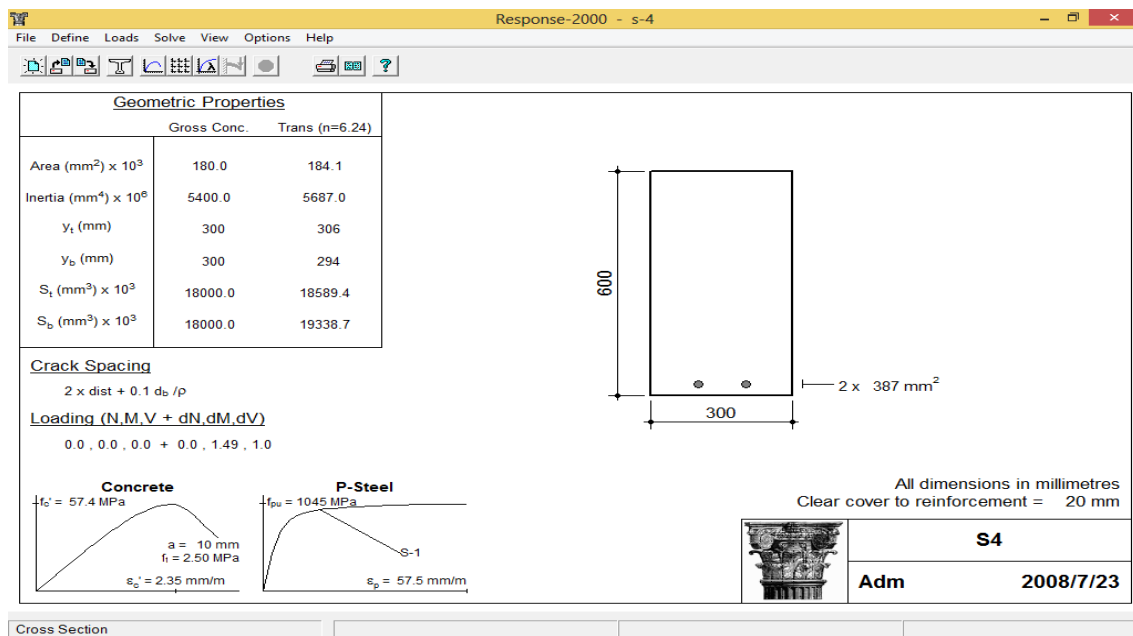


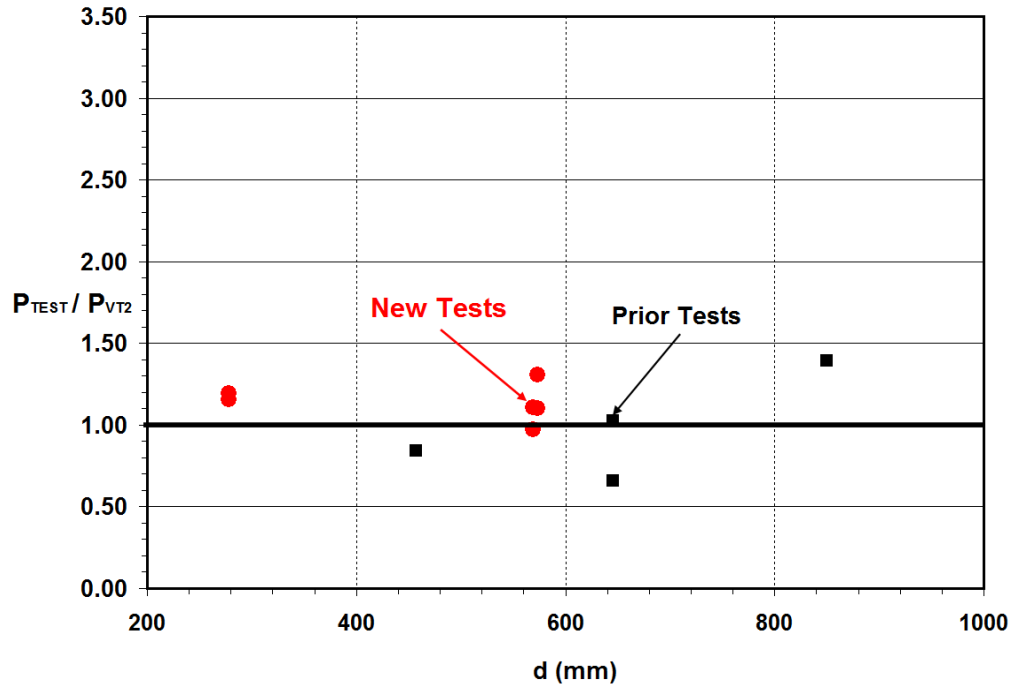
Figure 5-7: Typical *Response 2000* Slab Model.

Table 5-5: Numerical Model Predictions of Slab Specimens.

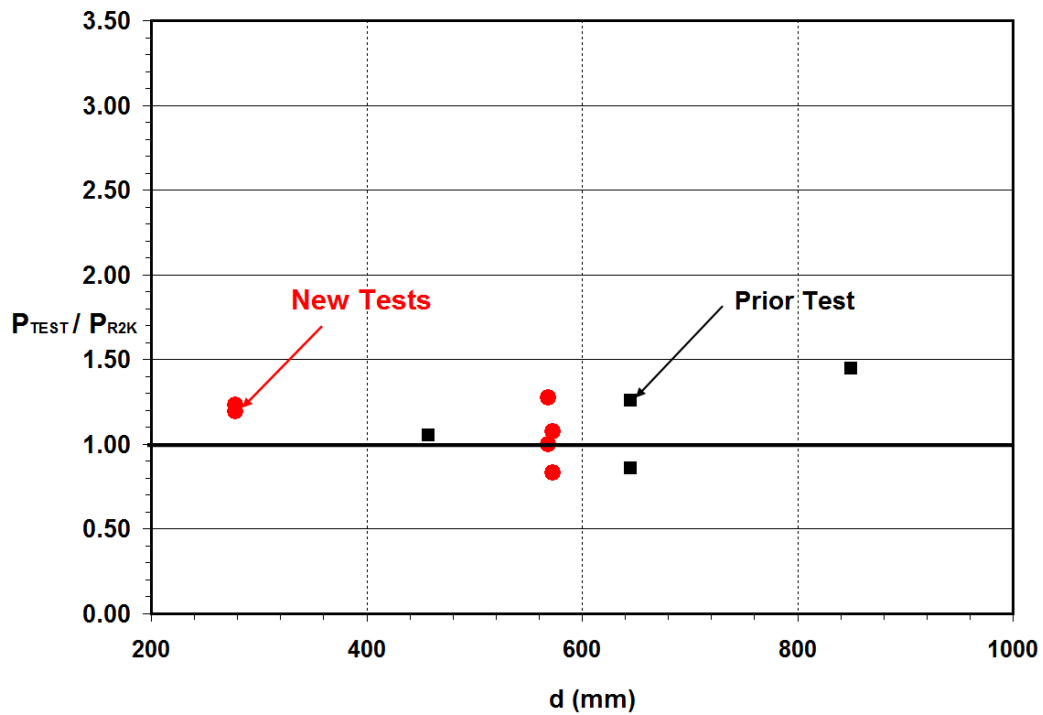
<i>Slab ID</i>	<i>P_{TEST} (kN)</i>	<i>P_{VT2} (kN)</i>	<i>P_{TEST} / P_{VT2}</i>	<i>P_{R2K} (kN)</i>	<i>P_{TEST} / P_{R2K}</i>
<i>S-1</i>	153	128	1.20	128	1.20
<i>S-2</i>	149	129	1.16	121	1.23
<i>S-3</i>	245	221	1.11	192	1.28
<i>S-4</i>	223	230	0.97	223	1.00
<i>S-5</i>	182	137	1.32	169	1.08
<i>S-6</i>	144	131	1.10	173	0.83
<i>M-2.7-32</i>	638	458	1.39	440	1.45
<i>G1-M0</i>	346	527	0.66	403*	0.86
<i>G2-M0</i>	648	632	1.03	515*	1.26
<i>G3-M0</i>	400	474	0.84	379*	1.06
<i>P_{TEST} / P_{MODEL} (Average)</i>			1.08		1.12
<i>STDV</i>			0.22		0.19
<i>COV</i>			0.20		0.17

*Results based on Sectional Response.

The relationships between test to predicted shear capacity ratios and member depth for all the specimens in the database using the two numerical models (*VT2* and *R2K*) are shown in Figure 5-8. From Figure 5-8 it is observed that the both models showed consistent agreement with respect to member depth for all the test data. This is attributed to the models being based up on the MCFT which adequately considers the size effect for concrete members without transverse reinforcement. It can be concluded that *VT2* and *R2K* adequately captured the size effect on shear capacity prediction.



a) Influence of Member Depth for $VT2$ Shear Model.



b) Influence of Member Depth for $R2K$ Shear Model.

Figure 5-8: Validation of the Numerical Shear Models for Size Effect.

5.5 Summary

In this chapter analytical general and simplified design shear models were developed and validated for slender concrete members with ASTM A1035 Grade 690 steel longitudinal reinforcement and without transverse reinforcement. The shear capacity of slab specimens tested in the current study and those from the literature were predicted using these shear models. For the purpose of comparison predictions were also completed using three design code models from current standards (*CSA A23.3-04*, *ACI 318-11*, *Eurocode 2-04*) and two numerical models (*VT2* and *R2K*). Based on the comparison the adequacy of the code provisions and the numerical models for the design and analysis of slabs with ASTM A1035 steel were evaluated.

The proposed general model developed in this study is based on the *Hoult et al.* model that takes into account the strain effect and size effect in shear. It was observed that the general model adequately account for the influences from higher member depths (size effect) and higher longitudinal member strains (strain effect) on shear capacity. Similar trends were observed for all the specimens in the database having a wide range of member depths and reinforcement ratios. Using the ten available slab tests in the database, the general shear model gave average test to predicted load ratio of 1.03 and coefficient of variation of 0.18. It can be concluded that the general shear model can be used for the design and analysis of slender concrete members with ASTM A1035 Grade 690 steel longitudinal reinforcement without stirrups. On the other hand, the design model which is derived from the general model after simplifying assumptions can be used as a quick and simplified model to predict a lower bound estimate for the shear load carried by slender slabs with ASTM A1035 longitudinal steel reinforcement in combination with the *Mast et al.* flexural design model.

Predictions obtained from the MCFT based *CSA A23.3-04* code shear model were more accurate than the other code models considered. The predicted loads were closer to the measured loads resulting in lower variation and average test to model ratio closer to one. The accurate results from the MCFT based *CSA A23.3-04* model show that the model can account for the influences from higher member depths and higher longitudinal member

strains. Thus, the *CSA A23.3-04* model can be used to predict the shear capacity of concrete slabs reinforced with ASTM A1035 longitudinal steel.

The predicted capacities obtained by *ACI 318-11* and *Eurocode -04* were significantly higher than the measured capacities resulting in average test to model ratios less than one with higher variation in the results. This can be attributed to the inadequacy of the models to appropriately account for the influences from higher member depths (size effect) and higher longitudinal member strains (strain effect) both of which can reduce shear resistance of concrete slabs.

The numerical models (*VT2* and *R2K*) which are also based on the MCFT, result in better prediction than the *ACI 318-11* and *Eurocode 2* shear models. The results show that both models can reasonably account for the influences from the strain effect and size effect in shear. Hence that the numerical models (*VT2* and *R2K*) can be used to predict the shear capacity of concrete slabs containing ASTM A1035 steel with reasonable accuracy.

Of the four MCFT based shear models, the best results were obtained using the proposed analytical general model. This model accurately considered the influences from member depth and longitudinal member strain represented by the size effect and strain effect parameters in shear, respectively. The numerical models (*VT2* and *R2K*) can also be used to predict the shear capacity of concrete slabs containing ASTM A1035 steel with reasonable accuracy. Moreover the simplified design shear model can also be used for preliminary calculations of shear capacity of slabs with ASTM A1035 steel longitudinal reinforcement.

6. MODELING SHEAR CAPACITY OF BEAMS

6.1 Introduction

The shear behaviour of reinforced concrete beams depends on many parameters including member depth and configuration of longitudinal and transverse reinforcement. The influence of member depth is not significant for members with transverse reinforcement (beams). This is due to the negligible influence from size effect for members with at least minimum stirrups (*Bentz et al. 2006*). On the other hand, the influence from reinforcement configuration is significant for both members with and without transverse reinforcement. (See Section 2.2.4). The longitudinal member strain is mainly dependent on the quantity and stress-strain behavior of the longitudinal reinforcement. Most shear design code models either do not account for the influence of longitudinal member strain (e.g. *ACI 318-11* and *Eurocode2-04*) or are developed to account for the influence of member strains based on conventional Grade 400 steel reinforcement (e.g. *CSA A23.3-04* and *AASHTO LRFD – 07*). Moreover, the stress-strain response of transverse reinforcement, which can also influence the shear strength of a concrete beam, is not given due consideration in most shear models.

In this chapter general and simplified analytical shear design models for beams containing ASTM A1035 steel longitudinal and transverse reinforcement were developed. These models were validated against test results from the current study and those available from literature. The quality of shear capacity predictions using the proposed models are also compared with predictions using the analytical and numerical models described in Sections 2.4.

Since ASTM A1035 steel exhibits non-linear stress-strain response beyond the proportional limit, there is no well defined yield point or yield plateau for this material. (See Equation 3-1). For the purpose of comparison two nominal yield strengths of stirrup reinforcement f_{yt} were used for beams containing Grade 690 ASTM A1035 steel transverse reinforcement. First, the yield strength of ASTM A1035 steel was limited to

the maximum value of $f_{yt550} = 550$ MPa as recommended in *ACI ITG-6R-10*. A higher stirrup yield strength was also considered in the shear models by using $f_{yt690} = 690$ MPa which is the same value as the *ACI ITG-6R-10* yield assumption in the simplified flexural model (Section 2.5.1). For beams containing ASTM A1035 steel longitudinal reinforcement, a yield strength of $f_{yL} = 690$ MPa was used as per the *ACI ITG-6R-10* simplified flexural model. This value is used for evaluation of all shear models considered in the current study except the proposed general shear model and the *CSA A23.3-04* shear models. These two models are strain based models that directly consider the member longitudinal strain (i.e. longitudinal steel strain) and hence the full stress-strain response of ASTM A1035 longitudinal steel was used with the modification described Section 5.2.2.

6.2 Development of Analytical Shear Design Models

6.2.1 General

Concrete beams containing longitudinal reinforcement from ASTM A1035 steel are expected to behave differently at higher strains compared to members with conventional Grade 420 steel longitudinal reinforcement. This is mainly due to the difference in the stress-strain behaviour between ASTM A1035 and Grade 420 steels. The expected higher longitudinal member strain for lightly reinforced beams containing ASTM A1035 longitudinal steel can result in wider diagonal crack widths. According to *Bentz et al. 2006* the wider crack widths will reduce the aggregate interlock and lead to lower shear stresses at failure. By extension, higher transverse reinforcement strains would also correspond to wider diagonal cracks. It is, therefore, necessary to develop and validate beam shear design models that directly incorporate the reinforcement stress-strain response.

6.2.2 General Shear Model

A new general shear model for beams with ASTM A1035 steel longitudinal reinforcement and containing transverse reinforcement was developed in this study. The new model adopts a similar format to the *CSA A23.3-04* general method for shear, based

on the compositional approach of a ‘concrete contribution’ and a ‘steel contribution’.
(Bentz *et al.* 2006)

The ‘concrete contribution’ term in the general model, V_{CGB} , is based on the V_{CH} term in the Hoult *et al.* (2008) model which was previously shown to provide better correlation with reinforced concrete members having large ε_x magnitudes near failure than the CSA A23.3-04 V_C term. (See Section 2.4.1).

The ‘steel contribution’ term in the general model, V_{SGB} , takes the same form as the CSA A23.3-04 V_S term (Section 2.4.1), regardless of the type of reinforcement in the stirrups. Thus the general shear model for members with ASTM A1035 steel longitudinal reinforcement is given as:

$$V_{GB} = V_{CGB} + V_{SGB} \quad (6-1)$$

$$V_{CGB} = \beta \sqrt{f'_c} b_w d_v \quad (6-2)$$

$$\beta = \left(\frac{0.3}{0.5 + (1000 \varepsilon_x + 0.15)^{0.7}} \right) \left(\frac{1300}{1000 + S_{ze}} \right) \quad (6-3)$$

$$V_{SGB} = \frac{A_v f_{yt} d_v \cot \theta}{S} \quad (6-4)$$

$$\theta = 29 + 7000 \varepsilon_x \quad (6-5)$$

A similar modeling approach was described by Bentz *et al.* (2010) for members with FRP longitudinal reinforcement that contained GFRP stirrups. However, note that the stress-strain response of FRP is very different than the reinforcement materials in the current study.

The influence of the non-linear stress-strain response of the ASTM A1035 steel in the longitudinal reinforcement at higher strain magnitudes was taken into consideration as described in Section 5.2.2.1. The longitudinal reinforcement stress can be directly

determined from the combined flexure and shear effects at the cross section considered as given by equation 5-3.

$$f_s = \frac{\frac{M}{d_v} + V}{A_s} \quad (5 - 3)$$

Then the corresponding reinforcement strain, ε_s , can be determined from the representative stress-strain model for ASTM A1035 steel (equation 3-1) and the axial strain parameter at mid-height, ε_x , is approximated as $\frac{1}{2}$ the reinforcement strain, ε_s , magnitude.

The effective crack spacing parameter in equation 6-3, S_{ze} , is taken as 300 mm since for members with at least minimum quantity of stirrups at reasonable maximum spacing, the crack spacing will be controlled and hence the size effect will have negligible influence on shear capacity of beams. (*Bentz et al. 2006*).

Figure 2-8 in Section 2.4.1.3.2 shows the limits on allowable angle of principal compression, θ , based on the MCFT for members heavily loaded in shear and for different strains in the member at mid-depth (ε_x). As can be seen, the range of allowable angles to select from at high shear loading is limited between lower and upper limits corresponding to safe shear design. Since concrete beams with stirrups containing ASTM A1035 steel reinforcement are expected to behave in a similar way, the same linear equation for θ (i.e. equation 6-5) developed by *Bentz et al. (2006)* can be used in the general shear model.

In equation 6-4 two nominal yield strengths of stirrup reinforcement f_{yt} were used for predicting the steel contribution V_{SGB} of shear capacity of beams with ASTM A1035 stirrups. These values are the limiting yield strength of ASTM A1035 steel transverse reinforcement $f_{yt550} = 550$ MPa as per the *ACI ITG-6R-10* and a higher stirrup yield strength value of $f_{yt690} = 690$ MPa.

The shear capacity prediction of reinforced concrete beams with ASTM A1035 steel longitudinal reinforcement and containing stirrups involves an iterative calculation procedure summarized in the flow chart shown in Figure 6-1.

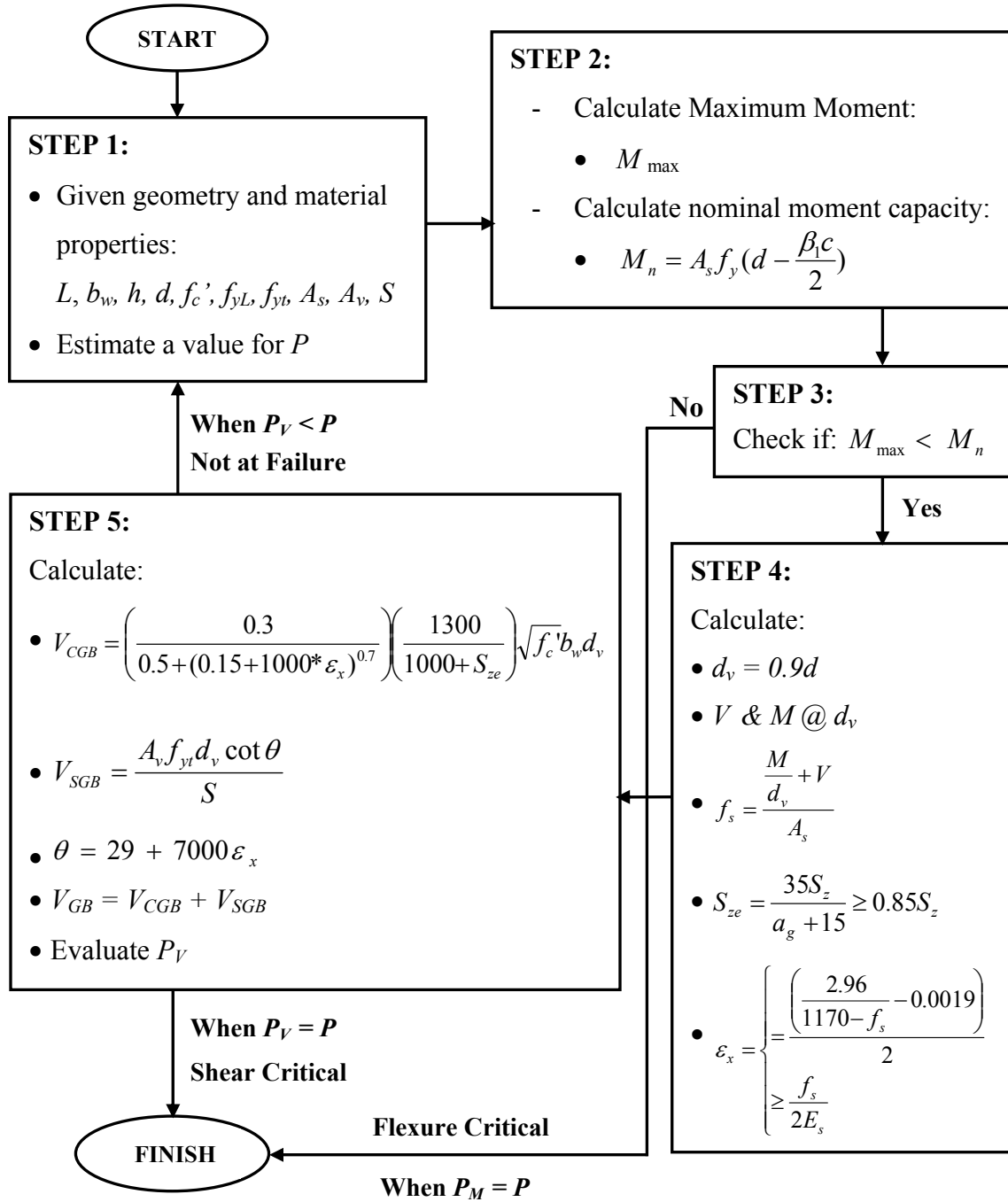


Figure 6-1: Flowchart for the Proposed General Beam Shear Model.

6.2.3 Design Shear Model

The simplified flexural design model proposed by *Mast et al. (2008)* and adopted by *ACI ITG-6R-10* for concrete members with ASTM A1035 steel longitudinal reinforcement specifies an elastic-plastic stress-strain model for reinforcement having a “design” yield strength of $f_{yL} = 690$ MPa for longitudinal reinforcement. This value is smaller than the typical effective yield strength (830 MPa) as determined by the 0.2 % offset method.

Consistent with the Mast simplified flexural model, a simplified design shear model is developed based on the general shear model (Section 6.2.2), for reinforced concrete beams with ASTM A1035 steel longitudinal reinforcement. The design shear model is based on the yield strength of $f_{yL} = 690$ MPa, for the ASTM A1035 steel reinforcement. This value corresponds to a reinforcement strain of $\varepsilon_s = 0.00427$ using the representative stress-strain model (equation 3-1). The strain parameter ε_x at mid-depth for shear is assumed as 80 % of $\varepsilon_s/2$ and is $\varepsilon_x = 0.0017$ following the procedure in Section 5.2.2. This value of ε_x is directly used in equations 6-3 and 6-5 to obtain the values of $\beta = 0.147$ and $\theta = 40.9$ degrees, respectively. Thus, the design shear model for beams reinforced with ASTM A1035 steel longitudinal reinforcement becomes:

$$V_{DB} = V_{CDB} + V_{SDB} \quad (6 - 6)$$

$$V_{SDB} = \frac{1.15 A_v f_{yt} d_v}{S} \quad (6 - 8)$$

$$V_{CDB} = 0.147 \sqrt{f'_c} b_w d_v \quad (6 - 7)$$

Note that in equation 6-8 a value of $f_{yt} = 400$ MPa was used for beams with conventional stirrups. For beams with ASTM A1035 stirrups two values of f_{yt} (*i.e.* $f_{yt550} = 550$ MPa and $f_{yt690} = 690$ MPa) were used as described in Section 6.1.

Note that the *CSA A23.3-04* standard (Section 11.3.6.3) specifies that for members with conventional Grade 400 steel longitudinal reinforcement, $f'_c \leq 60$ MPa and containing at least minimum stirrups, a simplified shear model can be used to predict shear capacity with values of $\beta = 0.18$ and $\theta = 35^\circ$. Hence for reinforced concrete beams with Grade 400 conventional longitudinal steel reinforcement, the design shear model takes the same form as the *CSA A23.3-04* standard.

$$V_{CDB,CSA} = 0.18\sqrt{f'_c}b_wd_v \quad (6-9)$$

$$V_{SDB,CSA} = \frac{1.43A_{vyl}f_yd_v}{S} \quad (6-10)$$

6.3 Model Validation

6.3.1 Database of Beam Specimens

A database of concrete beams containing ASTM A1035 steel reinforcement was assembled for use in validation of the general and simplified shear design models developed in the current study. In addition to the new test data for ten beams reported in Chapter 4, shear critical beams from prior tests conducted in four independent research programs were used for validation of the proposed shear models in Sections 6.2.2 and 6.2.3. Table 6-1 lists the details of the beam specimens in the database. This database included all known shear critical beam specimens which satisfied the following criteria:

- Rectangular cross section with overall depth, h , between *300 mm* and *1000 mm*.
- Shear span-to-depth ratio, a/d , between *2.62* - *3.29*.
- Longitudinal and/or transverse reinforcement with ASTM A1035 steel.
- Longitudinal reinforcement ratio, ρ_L , ranging from 1.02% to 6.92%.
- Transverse reinforcement ratio, ρ_t , ranging from 0.07% to 3.02%.
- Concrete compressive strength, f'_c , ranging from 30 to 116 MPa.

· No prestressing or axial forces applied.

Table 6-1 Details of Beam Specimens in the Database.

<i>Researcher</i>	<i>Beam ID</i>	<i>b_w</i> (mm)	<i>d</i> (mm)	<i>a/d</i>	<i>ρ_L</i> (%)	<i>ρ_t</i> (%)	<i>f_{yL}*</i> (MPa)	<i>f_{yt}*</i> (MPa)	<i>f_c'</i> (MPa)
New Test	RM1	300	523	3.15	2.55	0.15	408	690	41
New Test	RM2	300	523	3.15	2.55	0.18	408	690	45
New Test	MR1	300	935	3.00	0.55	0.11	690	426	49
New Test	MR2	300	935	3.00	0.69	0.11	690	426	50
New Test	MR3	300	885	3.00	1.60	0.11	690	426	48
New Test	MR4	300	885	3.00	1.60	0.22	690	426	50
New Test	MM1	300	935	3.00	0.55	0.15	690	690	50
New Test	MM2	300	935	3.00	0.69	0.15	690	690	52
New Test	MM3	300	885	3.00	1.60	0.15	690	690	48
New Test	MM4	300	885	3.00	1.60	0.30	690	690	48
Sumpter et al. (2009)	C-M-6	305	311	2.62	4.08	0.31	427	690	30
Sumpter et al. (2009)	C-M-4	305	311	3.08	4.08	0.46	427	690	31
Sumpter et al. (2009)	C-M-3	305	311	3.08	4.08	0.61	427	690	33
Sumpter et al. (2009)	M-M-6	305	311	2.62	4.08	0.31	690	690	32
Sumpter et al. (2009)	M-M-4	305	311	3.08	4.08	0.46	690	690	32
Sumpter et al. (2009)	M-M-3	305	311	3.08	4.08	0.61	690	690	33
Munikrishna et al. (2011)	G1-M80	610	645	3.11	1.02	0.09	690	550	33
Munikrishna et al. (2011)	G1-M100	610	645	3.11	1.02	0.07	690	690	34
Munikrishna et al. (2011)	G2-M80	610	645	3.11	1.02	0.09	690	550	33
Munikrishna et al. (2011)	G2-M100	610	645	3.11	1.02	0.07	690	690	34
Munikrishna et al. (2011)	G3-M80	406	457	3.00	2.71	0.25	690	550	36
Munikrishna et al. (2011)	G3-M100	406	457	3.00	2.71	0.20	690	690	40
Lee et al. (2010)	F40-1	200	252	3.00	2.52	0.59	690	510	37
Lee et al. (2010)	F40-3	200	252	3.00	2.52	1.02	690	510	37
Lee et al. (2010)	F40-5	200	252	3.00	3.78	1.43	690	510	37
Lee et al. (2010)	F60-1	200	252	3.00	2.55	0.51	690	508	63
Lee et al. (2010)	F60-2	200	252	3.00	2.55	1.06	690	508	63
Lee et al. (2010)	F60-3	200	252	3.00	3.82	1.41	690	508	63
Lee et al. (2010)	F60-4	200	252	3.00	5.54	1.95	690	508	63
Lee et al. (2010)	F80-1	200	252	3.00	2.55	0.98	690	508	85
Lee et al. (2010)	F80-2	200	252	3.00	3.82	1.49	690	508	85
Lee et al. (2010)	F80-3	200	252	3.00	5.10	2.01	690	508	85
Lee et al. (2010)	F80-4	200	252	3.00	5.54	2.53	690	508	85
Lee et al. (2010)	F80-5	200	252	3.00	6.92	3.02	690	508	85
NCHRP 679 (2011)	SR1 (A)	305	525	3.19	1.91	0.35	690	414	84
NCHRP 679 (2011)	SR1 (B)	305	525	3.19	1.91	0.22	690	690	84
NCHRP 679 (2011)	SR2 (A)	305	530	3.16	1.57	0.26	690	414	89
NCHRP 679 (2011)	SR2 (B)	305	530	3.16	1.57	0.14	690	690	89
NCHRP 679 (2011)	SR3 (A)	305	495	3.08	1.69	0.26	690	414	90
NCHRP 679 (2011)	SR3 (B)	305	495	3.08	1.69	0.14	690	690	90
NCHRP 679 (2011)	SR4 (A)	305	501	3.04	1.67	0.39	690	414	90
NCHRP 679 (2011)	SR4 (B)	305	501	3.04	1.67	0.19	690	690	90
NCHRP 679 (2011)	SR5	305	510	3.29	1.96	0.22	690	690	116

* 690 MPa is reported here for ASTM A1035 Grade 690 steel which does not have a well defined yield point.

The range of overall member depth values ($300\text{ mm} \leq h \leq 1000\text{ mm}$) and the concrete compressive strength ($30\text{ MPa} \leq f'_c \leq 116\text{ MPa}$) reflect the typical values for buildings in the industry practice. The shear-span to effective depth ratio a/d was selected to consider slender concrete beams showing a typical sectional shear behavior. As discussed in Section 2.2.2, $a/d = 2.5$ is assumed to be a transition point between shear critical members dominated by beam action or arch action. All beams in the database, except five specimens in the *RM* and *C-M* series, were longitudinally reinforced with ASTM A1035 Grade 690 steel. The five beam specimens in the *RM* and *C-M* series were longitudinally reinforced with conventional Grade 400 steel. The transverse reinforcement consisted either of conventional or ASTM A1035 steel. Four beams (*SR1-SR4*) reported in *NCHRP 679(2011)* contained both types of steel in the stirrups provided in either half of the span and are labelled as (A) and (B).

6.3.2 Validation of the General Shear Model

The general shear model developed in section 6.2.2 for beams with ASTM A1035 steel reinforcement was validated using the test data from 43 test results in Table 6-1. The maximum measured shear load obtained from each test was compared to the prediction using the general shear model. Statistical analysis was performed to determine the average, standard deviation, and coefficient of variation of the measured to predicted capacity ratios. The standard deviation indicates the scatter of data relative to the mean. The coefficient of variation is a statistical measure of the dispersion of data points about the mean and is helpful for comparing data sets with different means. For accurate models it is desirable to have the standard deviation and coefficient of variation as low as possible.

Table 6-2 shows the ratio of the measured to predicted shear capacity of forty three in the database for the proposed general shear model using two yield strength values of stirrups described in Section 6.1. Limiting the stirrup yield strength to a maximum value of f_{yt550}

= 550 MPa (as recommended by *ACI ITG-6R-10*) resulted in average measured to predicted capacity ratio of all beams to 1.18 with a coefficient of variation of 0.15.

Table 6-2: General Shear Model Predictions of All Beam Specimens.

<i>Researcher</i>	<i>Beam ID</i>	P_{TEST} (kN)	P_{GB} (kN) ($f_{yt} = 550$ MPa)	P_{TEST}/P_{GB} ($f_{yt} = 550$ MPa)	P_{GB} (kN) ($f_{yt} = 690$ MPa)	P_{TEST}/P_{GB} ($f_{yt} = 690$ MPa)
<i>New Test</i>	<i>RM1</i>	840	688	1.22	760	1.11
<i>New Test</i>	<i>RM2</i>	956	798	1.20	887	1.08
<i>New Test</i>	<i>MR1</i>	915	713	1.28	713	1.28
<i>New Test</i>	<i>MR2</i>	875	809	1.08	809	1.08
<i>New Test</i>	<i>MR3</i>	1109	1047	1.06	1047	1.06
<i>New Test</i>	<i>MR4</i>	1510	1354	1.12	1354	1.12
<i>New Test</i>	<i>MM1</i>	933	699	1.33	728	1.28
<i>New Test</i>	<i>MM2</i>	957	795	1.20	833	1.15
<i>New Test</i>	<i>MM3</i>	1409	1010	1.40	1083	1.30
<i>New Test</i>	<i>MM4</i>	1822	1288	1.41	1409	1.29
<i>Sumpter et al. (2009)</i>	<i>C-M-6</i>	512	440	1.16	501	1.02
<i>Sumpter et al. (2009)</i>	<i>C-M-4</i>	607	602	1.01	692	0.88
<i>Sumpter et al. (2009)</i>	<i>C-M-3</i>	660	722	0.91	876	0.75
<i>Sumpter et al. (2009)</i>	<i>M-M-6</i>	569	450	1.26	515	1.10
<i>Sumpter et al. (2009)</i>	<i>M-M-4</i>	669	618	1.08	709	0.94
<i>Sumpter et al. (2009)</i>	<i>M-M-3</i>	711	739	0.96	850	0.84
<i>Munikrishna et al.</i>	<i>G1-M80</i>	832	877	0.95	877	0.95
<i>Munikrishna et al.</i>	<i>G1-M100</i>	824	828	0.99	878	0.94
<i>Munikrishna et al.</i>	<i>G2-M80</i>	1162	1121	1.04	1121	1.04
<i>Munikrishna et al.</i>	<i>G2-M100</i>	1173	1059	1.11	1123	1.04
<i>Munikrishna et al.</i>	<i>G3-M80</i>	1338	1030	1.30	1030	1.30
<i>Munikrishna et al.</i>	<i>G3-M100</i>	1192	913	1.31	1033	1.15
<i>Lee et al. (2010)</i>	<i>F40-1</i>	433	428	1.01	428	1.01
<i>Lee et al. (2010)</i>	<i>F40-3</i>	524	562	0.93	562	0.93
<i>Lee et al. (2010)</i>	<i>F40-5</i>	690	786	0.88	786	0.88
<i>Lee et al. (2010)</i>	<i>F60-1</i>	484	415	1.17	415	1.17
<i>Lee et al. (2010)</i>	<i>F60-2</i>	709	573	1.24	573	1.24
<i>Lee et al. (2010)</i>	<i>F60-3</i>	874	796	1.10	796	1.10
<i>Lee et al. (2010)</i>	<i>F60-4</i>	983	1106	0.89	1106	0.89
<i>Lee et al. (2010)</i>	<i>F80-1</i>	717	562	1.27	562	1.27
<i>Lee et al. (2010)</i>	<i>F80-2</i>	1061	824	1.29	824	1.29
<i>Lee et al. (2010)</i>	<i>F80-3</i>	1200	1086	1.10	1086	1.10
<i>Lee et al. (2010)</i>	<i>F80-4</i>	1267	1128	1.12	1128	1.12
<i>Lee et al. (2010)</i>	<i>F80-5</i>	1519	1521	1.00	1521	1.00
<i>NCHRP 679 (2011)</i>	<i>SR1 (A)</i>	1179	953	1.24	953	1.24
<i>NCHRP 679 (2011)</i>	<i>SR1 (B)</i>	1179	889	1.33	961	1.23
<i>NCHRP 679 (2011)</i>	<i>SR2 (A)</i>	1015	819	1.24	819	1.24
<i>NCHRP 679 (2011)</i>	<i>SR2 (B)</i>	1015	753	1.35	799	1.27
<i>NCHRP 679 (2011)</i>	<i>SR3 (A)</i>	538	397	1.36	397	1.36
<i>NCHRP 679 (2011)</i>	<i>SR3 (B)</i>	538	363	1.48	387	1.39
<i>NCHRP 679 (2011)</i>	<i>SR4 (A)</i>	654	461	1.42	461	1.42
<i>NCHRP 679 (2011)</i>	<i>SR4 (B)</i>	654	402	1.63	432	1.51
<i>NCHRP 679 (2011)</i>	<i>SR5</i>	1335	884	1.51	944	1.41
		P_{TEST}/P_{MODEL} (All)		1.18		1.13

	<i>STDV</i>	0.18		0.18
	<i>COV</i>	0.15		0.16

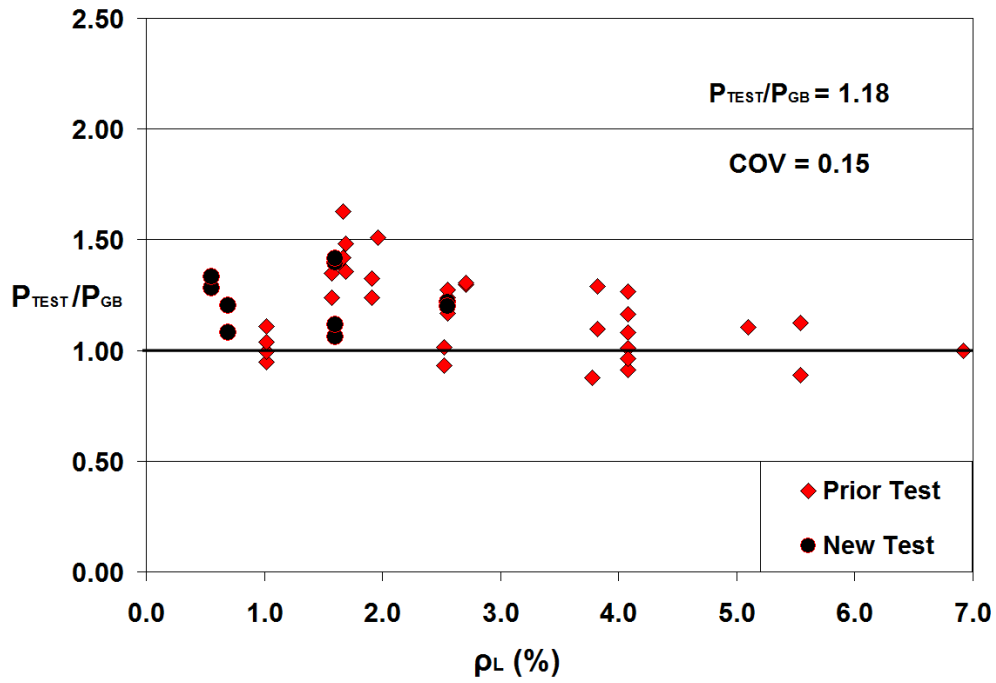
Statistical data were also compared for the specimens in the database, grouped by the combinations of steel used in the longitudinal and transverse reinforcement. Of all specimens in the data base the twenty beams which contained ASTM A1035 Grade 690 longitudinal reinforcement and conventional Grade 400 stirrups, gave average test to predicted capacity ratio of 1.14 and coefficient of variation of 0.13. For the five beams with conventional longitudinal reinforcement and ASTM A1035 stirrups, the average test to predicted capacity ratio and coefficient of variation were 1.10 and 0.12, respectively. The remaining eighteen beams that were entirely reinforced with ASTM A1035 steel had an average test to prediction capacity ratio of 1.26 with coefficient of variation of 0.16. The results obtained for the ten new beams tested in the current study indicated an average load to prediction ratio of 1.23 and coefficient of variation of 0.10.

Table 6-2 also shows the statistical data for predictions using a higher yield strength value of $f_{yt690} = 690$ MPa for beams containing ASTM A1035 stirrups. In general the use of a higher yield strength of stirrups in the calculations improved the statistical results. The average measured to predicted capacity ratio of all beams was 1.13 with a coefficient of variation of 0.16. The results obtained for the new beams showed an average load to prediction ratio of 1.17 and a coefficient of variation of 0.09. This indicated that use of a higher yield strength of stirrups in the calculations (similar to the yield strength of the longitudinal reinforcement, $f_{yL} = f_{yt} = 690$ MPa) for beams containing ASTM A1035 stirrups can result in better prediction quality. However it is important to recognize that as P_{GB} increases as a higher f_{yt} is used (See Table 6-2), the equivalent service load will also increase and it may become more difficult to satisfy serviceability requirements.

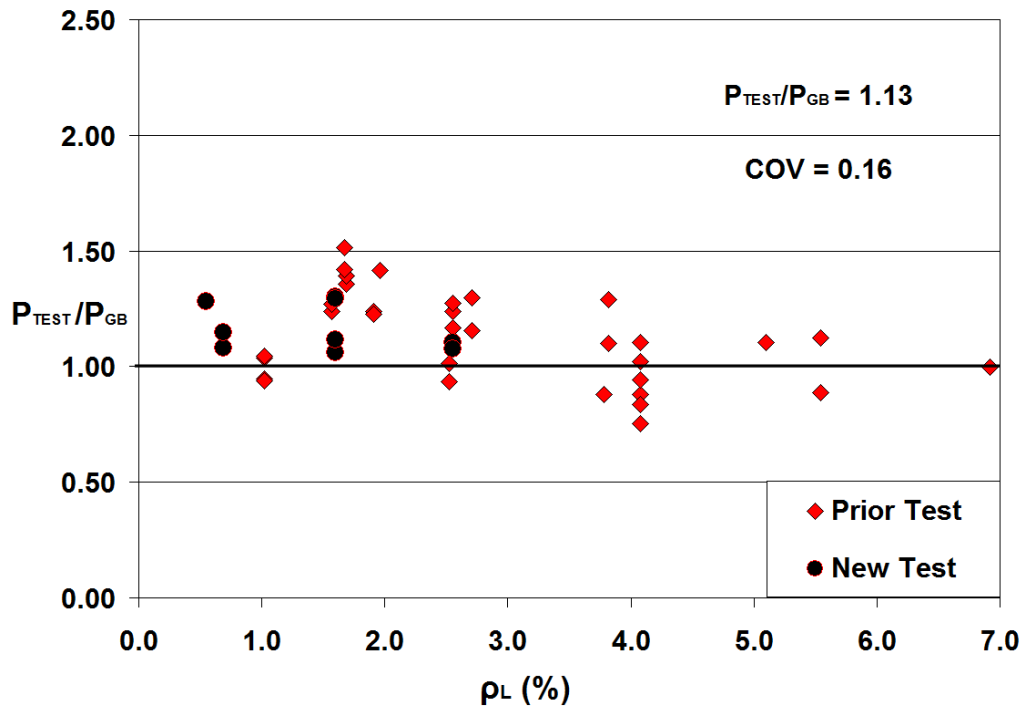
The general shear model is observed to be consistently a safe model for beams containing either longitudinal or transverse ASTM A1035 steel reinforcement. Of the forty three tests considered for model validation only nine beams from prior tests based on $f_{yt690} = 690$ MPa (seven beams based on $f_{yt550} = 550$ MPa) were poorly predicted with test load to prediction ratio less than one but no tests had measured to predicted ratios less than 0.75.

These beams were observed as specimens having higher longitudinal reinforcement ratios (typically $\rho_L = 1.02\%$ to 5.54%) as shown in Table 6-1. The higher predicted shear capacity can be attributed to the higher longitudinal reinforcement ratio.

Figure 6-2(a) depicts the relationship between test to prediction capacity ratio and longitudinal reinforcement ratio for all beams in the database based on $f_{yt} = 550$ MPa. The relationship indicates that the proposed general model is in good agreement with the test results for a wide range of longitudinal reinforcement ratios considered. A similar relationship is observed for the case with $f_{yt} = 690$ MPa as shown in Figure 6-2(b). In general, slightly conservative predictions observed for specimens with lower longitudinal reinforcement ratios and slightly unconservative predictions are observed for specimens with higher longitudinal reinforcement ratios. It can be concluded that the proposed general model can be safely applicable for beams in the industry practice with a wide range of longitudinal reinforcement ratios if appropriate load and resistance factors are used within a limit states based design approach.



(a) $f_{yt550} = 550$ MPa



(b) $f_{yt690} = 690$ MPa

Figure 6-2: Influence of Longitudinal Reinforcement Ratio on the General Shear Model.

6.3.3 Validation of Design Shear Model

Table 6-3 lists the ratios of the measured load to predicted shear capacity based on the proposed design shear model for all beam test results in the database. The average test to predicted capacity ratio, the standard deviation, and coefficient of variation were calculated for all specimens in the database. The average measured to predicted load ratio for all beams in the database was 1.25 with a coefficient of variation of 0.22. The higher variation in the load ratios for the design shear model compared to the general shear model in Section 6.3.2 is due to the wide range of longitudinal reinforcement ratios used in the beam specimens ($\rho_L = 0.55\%$ to 6.92%). This can result in member strains ϵ_x that are significantly different from the value assumed in developing the design model ($f_s = f_{yL} = 690$ MPa, $\epsilon_x = 0.0017$). Note that longitudinal reinforcement ratio is one of the main factors influencing the ‘strain effect’ in shear which depends on the longitudinal reinforcement strain at failure. For ease of comparison specimens in the database were grouped by the type of steel used in the longitudinal and transverse reinforcement. The results obtained for the new beam tests in the current study were an average load to prediction ratio of 1.26 and coefficient of variation of 0.20. The twenty beams in the database with ASTM A1035 Grade 690 longitudinal reinforcement and conventional Grade 400 stirrups had an average load ratio of 1.11 and coefficient of variation of 0.19. For the five beams with conventional longitudinal reinforcement and ASTM A1035 stirrups, the average load ratio and coefficient of variation were 1.14 and 0.18, respectively. The remaining eighteen beams that are entirely reinforced with ASTM A1035 steel had an average test to prediction capacity ratio of 1.43 with coefficient of variation of 0.18.

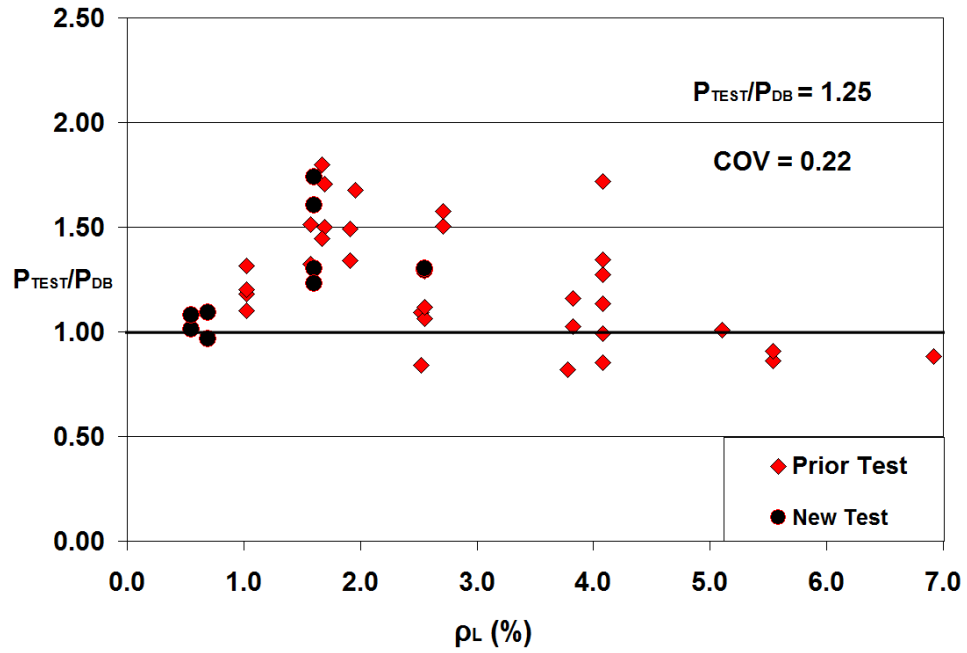
Table 6-3 also shows the statistical data for calculations using a higher yield strength value of $f_{y690} = 690$ MPa for beams containing ASTM A1035 stirrups. In general the use of higher yield strength of stirrups improved the statistical results. The average measured to predicted capacity ratio of all beams was 1.17 with a coefficient of variation of 0.20. The results obtained for the new beams showed an average load to prediction ratio of 1.18 and a coefficient of variation of 0.17. This indicated that use of a higher yield strength of stirrups in the calculations (similar to the yield strength of the longitudinal

reinforcement, $f_{yL} = f_{yt} = 690$ MPa) for beams containing ASTM A1035 stirrups can result in better prediction quality. However it is important to recognize that as P_{DB} increases as a higher f_{yt} is used (See Table 6-3), the equivalent service load will also increase and it may become more difficult to satisfy serviceability requirements if a higher f_{yt} is used.

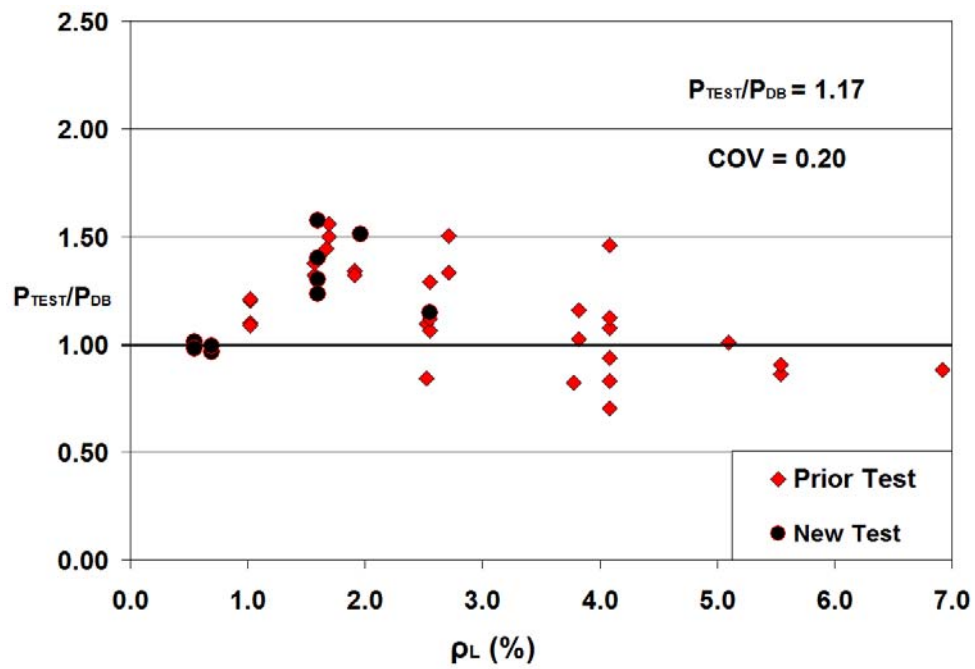
The statistical results indicate that the proposed design shear model is slightly unconservative for beams with lower longitudinal reinforcement ratios and slightly conservative for beams with higher longitudinal reinforcement ratios, compared to the general design model as shown in Figure 6-3(a). Similar trends were observed for both f_{yt} values considered as shown in Figure 6-3(b). The general shear model in Section 6.3.2, which can directly account for the variation of reinforcement stresses and strains due to variable reinforcement ratios, results in more uniform and consistent prediction compared to the results of the simplified design shear model. However, for beams with practical reinforcement configurations the design shear model can be used as a simplified method in the design industry for quick and easy preliminary calculations.

Table 6-3: Design Shear Model Predictions of All Beam Specimens.

<i>Researcher</i>	<i>Beam ID</i>	P_{TEST} (kN)	P_{DB} (kN) ($f_{yt} = 550$ MPa)	P_{TEST}/P_{DB} ($f_{yt} = 550$ MPa)	P_{DB} (kN) ($f_{yt} = 690$ MPa)	P_{TEST}/P_{DB} ($f_{yt} = 690$ MPa)
<i>New Test</i>	<i>RM1</i>	840	650	1.29	732	1.15
<i>New Test</i>	<i>RM2</i>	956	733	1.30	833	1.15
<i>New Test</i>	<i>MR1</i>	915	905	1.01	905	1.01
<i>New Test</i>	<i>MR2</i>	875	907	0.96	907	0.96
<i>New Test</i>	<i>MR3</i>	1109	852	1.30	852	1.30
<i>New Test</i>	<i>MR4</i>	1510	1225	1.23	1225	1.23
<i>New Test</i>	<i>MM1</i>	933	863	1.08	951	0.98
<i>New Test</i>	<i>MM2</i>	957	876	1.09	964	0.99
<i>New Test</i>	<i>MM3</i>	1409	811	1.74	894	1.58
<i>New Test</i>	<i>MM4</i>	1822	1136	1.60	1302	1.40
<i>Sumpter et al. (2009)</i>	<i>C-M-6</i>	512	402	1.27	475	1.08
<i>Sumpter et al. (2009)</i>	<i>C-M-4</i>	607	611	0.99	733	0.83
<i>Sumpter et al. (2009)</i>	<i>C-M-3</i>	660	776	0.85	938	0.70
<i>Sumpter et al. (2009)</i>	<i>M-M-6</i>	569	331	1.72	390	1.46
<i>Sumpter et al. (2009)</i>	<i>M-M-4</i>	669	497	1.35	595	1.12
<i>Sumpter et al. (2009)</i>	<i>M-M-3</i>	711	627	1.13	758	0.94
<i>Munikrishna et al.</i>	<i>G1-M80</i>	832	757	1.10	757	1.10
<i>Munikrishna et al.</i>	<i>G1-M100</i>	824	697	1.18	758	1.09
<i>Munikrishna et al.</i>	<i>G2-M80</i>	1162	967	1.20	967	1.20
<i>Munikrishna et al.</i>	<i>G2-M100</i>	1173	891	1.32	969	1.21
<i>Munikrishna et al.</i>	<i>G3-M80</i>	1338	890	1.50	890	1.50
<i>Munikrishna et al.</i>	<i>G3-M100</i>	1192	757	1.57	893	1.33
<i>Lee et al. (2010)</i>	<i>F40-1</i>	433	396	1.09	396	1.09
<i>Lee et al. (2010)</i>	<i>F40-3</i>	524	624	0.84	624	0.84
<i>Lee et al. (2010)</i>	<i>F40-5</i>	690	841	0.82	841	0.82
<i>Lee et al. (2010)</i>	<i>F60-1</i>	484	376	1.29	376	1.29
<i>Lee et al. (2010)</i>	<i>F60-2</i>	709	667	1.06	667	1.06
<i>Lee et al. (2010)</i>	<i>F60-3</i>	874	854	1.02	854	1.02
<i>Lee et al. (2010)</i>	<i>F60-4</i>	983	1140	0.86	1140	0.86
<i>Lee et al. (2010)</i>	<i>F80-1</i>	717	641	1.12	641	1.12
<i>Lee et al. (2010)</i>	<i>F80-2</i>	1061	915	1.16	915	1.16
<i>Lee et al. (2010)</i>	<i>F80-3</i>	1200	1190	1.01	1190	1.01
<i>Lee et al. (2010)</i>	<i>F80-4</i>	1267	1398	0.91	1398	0.91
<i>Lee et al. (2010)</i>	<i>F80-5</i>	1519	1723	0.88	1723	0.88
<i>NCHRP 679 (2011)</i>	<i>SR1 (A)</i>	1179	880	1.34	880	1.34
<i>NCHRP 679 (2011)</i>	<i>SR1 (B)</i>	1179	791	1.49	891	1.32
<i>NCHRP 679 (2011)</i>	<i>SR2 (A)</i>	1015	767	1.32	767	1.32
<i>NCHRP 679 (2011)</i>	<i>SR2 (B)</i>	1015	671	1.51	737	1.38
<i>NCHRP 679 (2011)</i>	<i>SR3 (A)</i>	538	359	1.50	359	1.50
<i>NCHRP 679 (2011)</i>	<i>SR3 (B)</i>	538	315	1.71	345	1.56
<i>NCHRP 679 (2011)</i>	<i>SR4 (A)</i>	654	453	1.44	453	1.44
<i>NCHRP 679 (2011)</i>	<i>SR4 (B)</i>	654	364	1.80	407	1.61
<i>NCHRP 679 (2011)</i>	<i>SR5</i>	1335	796	1.68	883	1.51
		P_{TEST}/P_{MODEL} (All)		1.25		1.17
		STDV		0.27		0.24
		COV		0.22		0.20



(a) $f_{yt550} = 550$ MPa



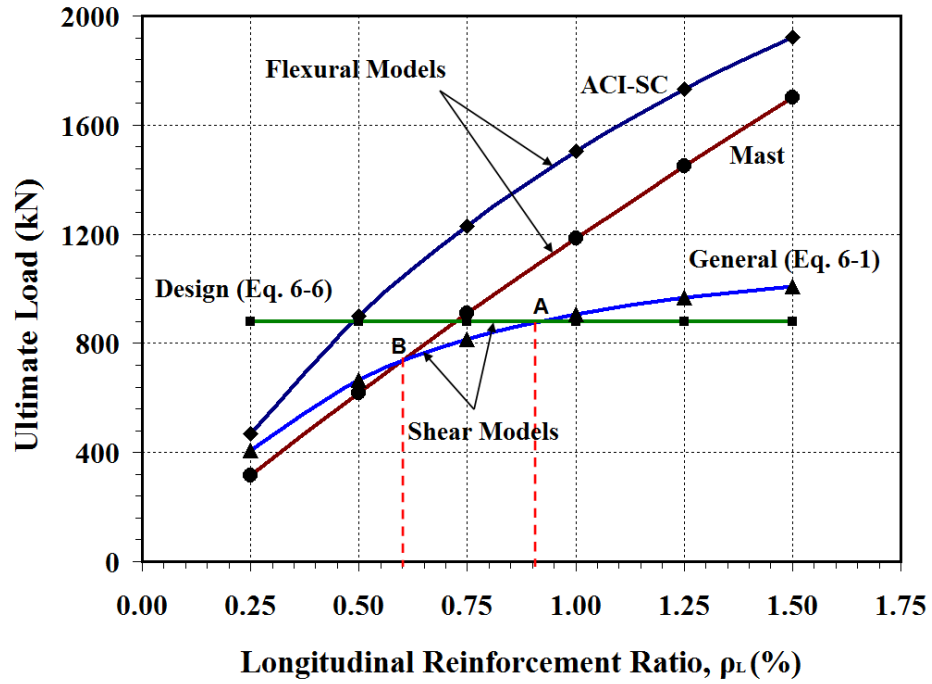
(b) $f_{yt690} = 690$ MPa

Figure 6-3: Influence of Longitudinal Reinforcement Ratio on the Design Shear Model.

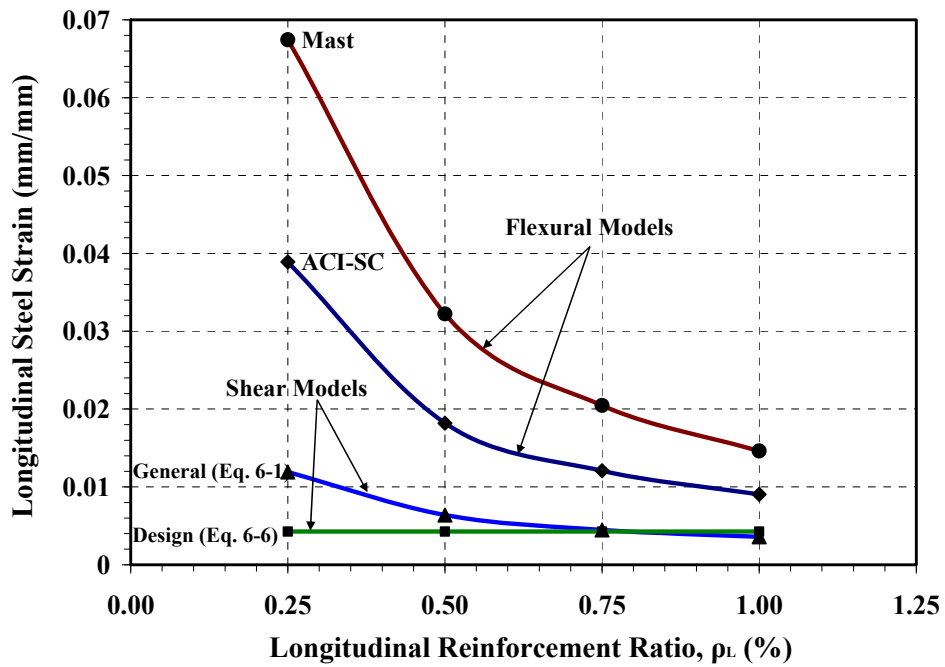
The design shear model developed in Section 6.2.3 assumed a reinforcement strain condition $\varepsilon_s = 0.00427$ corresponding to a 'yield' strength of $f_{yL} = 690$ MPa for the longitudinal ASTM A1035 Grade 690 steel reinforcement. Thus, it is necessary to validate that this condition results in safe predictions of flexural or shear capacity for beams with stirrups containing ASTM A1035 steel longitudinal reinforcement. The capacity of concrete beams reinforced with ASTM A1035 steel longitudinal and transverse reinforcement were evaluated through a parametric study. The longitudinal reinforcement ratios were varied from $\rho_L = 0.25\%$ to 1.0% with increment of 0.25% and a constant transverse reinforcement ratio of $\rho_t = 0.11\%$ was used to represent typical specimens considered in the current study. Members were assumed to be loaded under 3-point bending. Figure 6-4 illustrates the results for $d = 1000$ mm, $f'_c = 50$ MPa, $f_{yt} = 550$ MPa and $a/d = 3.0$, which are representative of shear critical beams considered in the current study. In Figure 6-4a, the flexural capacity according to the *Mast et al.* simplified model and the *strain compatibility (SC)* flexural model from *ACI ITG-6R-10* Appendix B are shown. As expected, the flexural capacity increases with increasing reinforcement ratio, and the strain compatibility model predicts higher flexural capacity than the *Mast et al.* model. This is due to consideration of the pseudo strain hardening of the steel beyond the 690 MPa design yield strength assumed by the *Mast et al.* model. The proposed general shear model (Section 6.2.2) gives increasing shear capacity as the longitudinal reinforcement ratio increases, but the slope of this relationship is flatter than for the flexural strength increase with reinforcement ratio.

By comparing the general shear model and *strain compatibility* flexural model, all member configurations represented in Figure 6-4 are expected to be shear critical. For all values of reinforcement ratio greater than about 0.90% (Point *A* on Figure 6-4a), the proposed design shear model in Section 6.2.3 predicts a conservative capacity below that of the general model. However, when $\rho_L < 0.90\%$, the capacity by the general model is less than the design shear model capacity. The reason for this can be observed in Figure 6-4b, where the reinforcement strain at the failure condition is plotted for each capacity model condition shown in Figure 6-4a. In the $\rho_L < 0.90\%$ range, it is observed that for the general model the longitudinal reinforcement strain will exceed the value 0.00427

mm/mm corresponding to a stress of 690 MPa. The *Mast et al.* flexural model would govern the design capacity in the $\rho_L < 0.60\%$ range, which mitigates concerns that the proposed design shear model can overestimate the actual shear strength. In the intermediate range between points A and B on Figure 6-4a where $0.60\% < \rho_L < 0.90\%$, the discrepancy between the shear capacities of the general and design models is less than 13 %. For other design parameters, such as member depth and transverse reinforcement ratio, the divergence between the flexure and shear curves and the ρ_L corresponding to points A and B may change, but the similar result of compatible simplified flexure (i.e. *Mast et al.*) and design shear models continue to result in general safe limiting design conditions with a region where some discrepancy occurs (between A and B). This potential discrepancy should be considered when establishing resistance factors for use in a limit states design approach, but such evaluation is beyond the scope of the current study.



(a) Member Capacity



(b) Longitudinal Steel Strain

Figure 6-4: Influence of Longitudinal Reinforcement Ratio on Flexural and Shear Capacity of Beam Specimens.

6.4 Comparison to Existing Shear Design Models

In order to evaluate the applicability of existing shear models for shear capacity prediction of concrete beams reinforced with ASTM A1035 steel, some of the analytical and numerical models described in Section 2.4 were considered. Three design code models (*CSA A23.3-04* with modifications to the non-linear stress-strain response, *ACI ITG-6R* and *Eurocode2-2004*) and the two numerical models (*VecTor 2* and *Response 2000*) were used for comparison.

Table 6-4 shows the ratio of the measured-to-predicted shear capacity of all beam specimens in the database described in Section 6.3.1 based on $f_{yt} = 550$ MPa for beams containing ASTM A1035 stirrups. The average test to predicted load ratios for the three analytical shear design models (*CSA A23.3-04*, *ACI ITG-6R* and *Eurocode2-2004*) were calculated as 1.24, 1.30 and 1.48, respectively. The corresponding coefficients of variation were 0.16, 0.19 and 0.33. The results obtained for the ten new beam tests conducted in the current study showed average load to prediction ratios of 1.31, 1.19 and 1.43 with coefficients of variation of 0.10, 0.22 and 0.21 for the *CSA A23.3-04*, *ACI ITG-6R* and *Eurocode2-2004*, respectively. In order to study the influence of reinforcement type on shear capacity prediction, specimens in the database were grouped by the combination of steel used in the longitudinal and transverse reinforcement. The first group, consisting of twenty beams with ASTM A1035 longitudinal reinforcement and conventional stirrups, had average load ratios of 1.19, 1.27 and 1.32 with coefficients of variation of 0.15, 0.21 and 0.34 for the *CSA A23.3-04*, *ACI ITG-6R* and *Eurocode2-2004* models, respectively. The second group, containing five beams with conventional longitudinal reinforcement and ASTM A1035 stirrups had the average load ratios of 1.13, 1.36 and 1.67 and coefficients of variation of 0.14, 0.14 and 0.41, for the *CSA A23.3-04*, *ACI ITG-6R* and *Eurocode2-2004* models, respectively. The remaining eighteen beams in the third set are entirely reinforced with ASTM A1035 steel and had average test load to prediction ratios of 1.33, 1.32 and 1.60 with coefficients of variation of 0.15, 0.19 and 0.27, for the *CSA*, *ACI* and *EC2* models, respectively.

Based on the above it can be seen that the *CSA A23.3-04* code model results in better predictions to the actual shear capacities with less scatter than the *ACI ITG-6R* and *Eurocode2-2004* code models. This can be attributed to the direct consideration, with modifications to account for the non linear stress and strain response of the steel, of strain effect and size effect parameters in the MCFT based *CSA A23.3-04* shear model. The results indicate that the *CSA A23.3-04* model can be used to safely predict the shear strength of concrete beams with ASTM A1035 steel reinforcement. However, the proposed shear models developed in Section 6.2 demonstrated better results compared to all analytical code models as shown in Tables 6-2 and 6-3. The proposed general and design shear models resulted in an average test load to prediction ratios of 1.18 and 1.25 with coefficients of variation of 0.15 and 0.22, respectively. This is attributed to the adequate consideration of the expected larger member strain magnitudes for beams with ASTM A1035 longitudinal reinforcement in the model development. On the other hand, the *ACI ITG-6R* and *Eurocode2-2004* code models which do not adequately account for the size effect and strain effect in shear can result in inconsistent shear capacity prediction accuracy resulting in poorer overall prediction quality.

For beams with ASTM A1035 steel longitudinal reinforcement the analysis using *VecTor2 (VT2)* model was based on using an idealized bi-linear elastic-plastic stress-strain relationship with a yield strength of 690 MPa (*ACI ITG-6R-10*). For *Response 2000 (R2K)* the non-linear stress-strain response of the ASTM A1035 longitudinal steel was simulated as unstressed prestressing steel using a modified Ramburg-Osgoode (R-O) relationship (*Collins and Mitchell, 1997*). The R-O approximation for the stress-strain response of ASTM A1035 longitudinal steel is the same equation used in modeling the slab specimens (equation 5-5) and repeated here for convenience.

$$f_s = \begin{cases} 200,000 \varepsilon_s \left\{ A + \frac{1-A}{[1 + (B\varepsilon_s)^C]^{\frac{1}{C}}} \right\} \\ 1040 \end{cases} \quad (6-11)$$

where parameters were solved as $A = 0.006$, $B = 200$ & $C = 2.2$.

Table 6-4 also lists the statistical results based on the numerical models for all beams in the database. The calculated test to predicted average load ratios were 1.25 and 1.19 with coefficients of variation of 0.18 and 0.18, for *VT2* and *R2K*, respectively. Looking at the set of beams with similar reinforcement types, the twenty beams in the database which contain ASTM A1035 longitudinal reinforcement and conventional stirrups, had average load ratios of 1.25 and 1.13 with coefficients of variation of 0.19 and 0.17 for the *VT2* and *R2K* models, respectively. For the five beams with conventional longitudinal reinforcement and ASTM A1035 stirrups, the average load ratios were 1.04 and 1.16 and coefficients of variation of 0.13 and 0.14, for *VT2* and *R2K* models, respectively. The remaining eighteen beams in the database, that are entirely reinforced with ASTM A1035 steel gave average test load to prediction ratios of 1.32 and 1.27 with coefficients of variation of 0.14 and 0.18, for *VT2* and *R2K* models, respectively. The ten new beam specimens tested in the current study had results with average load to prediction ratios of 1.27 and 1.27 and coefficients of variation of 0.17 and 0.17 for *VT2* and *R2K* models, respectively.

Table 6-4: Analytical and Numerical Model Predictions of All Beams ($f_{yt} = 550$ MPa).

<i>Beam ID</i>	<i>P_{TEST} (kN)</i>	<i>P_{TEST}/P_{CSA}</i>	<i>P_{TEST}/P_{ACI}</i>	<i>P_{TEST}/P_{EC2}</i>	<i>P_{TEST}/P_{VT2}</i>	<i>P_{TEST}/P_{R2K}</i>
<i>RM1</i>	840	1.29	1.43	1.25	1.14	1.31
<i>RM2</i>	956	1.25	1.46	1.12	1.23	1.31
<i>MR1</i>	915	1.39	0.90	1.77	1.31	1.12
<i>MR2</i>	875	1.17	0.86	1.41	1.03	1.03
<i>MR3</i>	1109	1.13	1.16	1.42	1.05	1.32
<i>MR4</i>	1510	1.17	1.14	1.13	1.03	1.00
<i>MM1</i>	933	1.45	0.95	1.58	1.43	1.26
<i>MM2</i>	957	1.31	0.96	1.36	1.39	1.26
<i>MM3</i>	1409	1.49	1.53	2.03	1.69	1.76
<i>MM4</i>	1822	1.50	1.48	1.21	1.44	1.38
<i>C-M-6</i>	512	1.16	1.57	1.17	0.93	1.19*
<i>C-M-4</i>	607	1.01	1.25	2.27	0.95	1.00*
<i>C-M-3</i>	660	0.91	1.08	2.54	0.98	0.99*
<i>M-M-6</i>	569	1.30	1.71	1.01	1.00	1.24*
<i>M-M-4</i>	669	1.11	1.37	1.18	1.04	1.05*
<i>M-M-3</i>	711	0.98	1.17	1.26	0.96	0.96*
<i>G1-M80</i>	832	1.02	0.97	1.28	1.15	0.94*
<i>G1-M100</i>	824	1.08	1.03	1.33	1.21	1.07*
<i>G2-M80</i>	1162	1.12	1.06	1.67	1.28	1.02*
<i>G2-M100</i>	1173	1.20	1.15	1.75	1.43	1.20*
<i>G3-M80</i>	1338	1.34	1.46	1.49	1.22	1.22*
<i>G3-M100</i>	1192	1.35	1.50	1.37	1.21	1.18*
<i>F40-1</i>	433	1.04	1.07	0.73	0.92	0.89
<i>F40-3</i>	524	0.97	1.02	0.88	1.06	0.86
<i>F40-5</i>	690	0.89	1.35	1.16	1.04	0.99
<i>F60-1</i>	484	1.21	1.23	1.97	1.09	0.86
<i>F60-2</i>	709	1.26	1.06	0.80	1.41	1.02
<i>F60-3</i>	874	1.12	1.31	0.99	1.17	1.15
<i>F60-4</i>	983	0.90	1.47	1.11	1.57	1.23
<i>F80-1</i>	717	1.31	1.10	0.68	1.35	1.00
<i>F80-2</i>	1061	1.31	1.37	1.01	1.43	1.32
<i>F80-3</i>	1200	1.12	1.55	1.14	1.20	1.35
<i>F80-4</i>	1267	1.14	1.78	1.27	1.20	1.39
<i>F80-5</i>	1519	1.01	1.97	1.45	1.78	1.56
<i>SR1 (A)</i>	1179	1.31	1.24	2.17	1.44	1.20
<i>SR1 (B)</i>	1179	1.41	1.36	2.21	1.44	1.37
<i>SR2 (A)</i>	1015	1.33	1.20	2.25	1.54	1.30
<i>SR2 (B)</i>	1015	1.46	1.34	2.32	1.54	1.65
<i>SR3 (A)</i>	538	1.45	1.35	1.45	1.00	1.13
<i>SR3 (B)</i>	538	1.60	1.52	1.56	1.32	1.42
<i>SR4 (A)</i>	654	1.50	1.34	1.60	1.27	0.95
<i>SR4 (B)</i>	654	1.61	1.62	1.66	1.33	1.37
<i>SR5</i>	1335	1.62	1.51	2.59	1.71	1.47
<i>P_{TEST}/P_{MODEL} (All)</i>		1.24	1.30	1.44	1.25	1.19
<i>STDV</i>		0.20	0.25	0.48	0.23	0.21
<i>COV</i>		0.16	0.19	0.33	0.18	0.18

* Results Based on Sectional Response.

Based on the above statistical results it can be seen that the numerical models (*VT2* and *R2K*) can give better prediction of shear capacity of reinforced concrete beams with ASTM A1035 steel with much better accuracy than the *ACI ITG-6R* or *Eurocode2-2004* design code models. On the other hand, the numerical models resulted in prediction quality results similar to the CSA code model. These three models (*CSA A23.3-04*, *VT2* and *R2K*) are all based on the MCFT and take into account the strain effect and size effect in shear. The results suggest that the numerical models can be slightly conservative for beams with conventional steel longitudinal reinforcement and ASTM A1035 stirrups. In general, *VT2* and *R2K* shear models can be used to predict the shear capacity of beams with ASTM A1035 steel reinforcement. However, the proposed general shear model developed in Section 6.2 demonstrated slightly better results compared to the numerical models as shown in Table 6-2 when $f_{yt} = 550$ MPa. This is due to the adequate consideration of the higher member strain magnitudes for beams containing ASTM A1035 longitudinal reinforcement in the proposed general shear model.

Shear predictions were also calculated using the analytical and numerical models for beams ASTM A1035 stirrups based on a higher yield strength ($f_{yt} = 690$ MPa) as given in Table 6-5. In general the use of higher yield strength of ASTM A1035 stirrups in the capacity calculations improved the statistical results for both the analytical and numerical models considered. This indicated that use of a higher yield strength of stirrups in the calculations for beams containing ASTM A1035 stirrups can result in better prediction quality. However it is important to recognize that as the predicted load increases as a higher f_{yt} is used (See Table 6-5), the equivalent service load will also increase and it may become more difficult to satisfy serviceability requirements.

Table 6-5: Analytical and Numerical Model Predictions of All Beams ($f_{yt} = 690$ MPa).

<i>Beam ID</i>	P_{TEST} (kN)	P_{TEST}/P_{CSA}	P_{TEST}/P_{ACI}	P_{TEST}/P_{EC2}	P_{TEST}/P_{VT2}	P_{TEST}/P_{R2K}
<i>RM1</i>	840	1.16	1.29	1.17	1.04	1.31
<i>RM2</i>	956	1.12	1.30	1.28	1.13	1.31
<i>MR1</i>	915	1.39	0.90	1.77	1.31	1.12
<i>MR2</i>	875	1.17	0.86	1.41	1.03	1.03
<i>MR3</i>	1109	1.13	1.16	1.42	1.05	1.32
<i>MR4</i>	1510	1.17	1.14	1.13	1.03	1.00
<i>MM1</i>	933	1.38	0.88	1.78	1.34	1.14
<i>MM2</i>	957	1.24	0.89	1.51	1.31	1.13
<i>MM3</i>	1409	1.38	1.41	1.61	1.33	1.54
<i>MM4</i>	1822	1.36	1.31	1.34	1.30	1.20
<i>C-M-6</i>	512	1.21	1.34	0.81	0.89	1.19*
<i>C-M-4</i>	607	1.12	1.05	0.80	0.88	1.00*
<i>C-M-3</i>	660	1.07	0.98	0.85	0.94	0.99*
<i>M-M-6</i>	569	1.33	1.47	0.91	0.95	1.11*
<i>M-M-4</i>	669	1.23	1.16	0.86	0.97	0.94*
<i>M-M-3</i>	711	1.09	1.06	0.91	0.88	0.85*
<i>G1-M80</i>	832	1.19	0.89	1.79	1.15	0.82*
<i>G1-M100</i>	824	1.18	0.96	1.78	1.21	0.94*
<i>G2-M80</i>	1162	1.30	0.98	1.37	1.28	0.89*
<i>G2-M100</i>	1173	1.32	1.07	1.43	1.43	1.05*
<i>G3-M80</i>	1338	1.53	1.23	2.12	1.22	1.20*
<i>G3-M100</i>	1192	1.37	1.29	1.89	1.09	1.05*
<i>F40-1</i>	433	1.04	1.07	0.73	0.92	0.89
<i>F40-3</i>	524	0.97	1.02	0.88	1.06	0.86
<i>F40-5</i>	690	0.89	1.35	1.16	1.04	0.99
<i>F60-1</i>	484	1.21	1.23	1.97	1.09	0.86
<i>F60-2</i>	709	1.24	1.06	0.80	1.41	1.02
<i>F60-3</i>	874	1.12	1.31	0.99	1.17	1.15
<i>F60-4</i>	983	0.98	1.47	1.11	1.57	1.23
<i>F80-1</i>	717	1.31	1.10	0.68	1.35	1.00
<i>F80-2</i>	1061	1.31	1.37	1.01	1.43	1.32
<i>F80-3</i>	1200	1.15	1.55	1.14	1.20	1.35
<i>F80-4</i>	1267	1.03	1.78	1.27	1.20	1.39
<i>F80-5</i>	1519	1.00	1.97	1.45	1.78	1.56
<i>SR1 (A)</i>	1179	1.31	1.24	2.17	1.20	1.20
<i>SR1 (B)</i>	1179	1.30	1.22	2.16	1.20	1.22
<i>SR2 (A)</i>	1015	1.33	1.20	2.25	1.40	1.30
<i>SR2 (B)</i>	1015	1.36	1.24	2.26	1.40	1.40
<i>SR3 (A)</i>	538	1.45	1.35	1.45	1.00	1.13
<i>SR3 (B)</i>	538	1.49	1.40	1.48	1.17	1.23
<i>SR4 (A)</i>	654	1.50	1.34	1.60	1.17	0.95
<i>SR4 (B)</i>	654	1.61	1.47	1.66	1.16	1.18
<i>SR5</i>	1335	1.51	1.37	2.54	1.32	1.25
P_{TEST}/P_{MODEL} (All)		1.19	1.23	1.41	1.19	1.13
STDV		0.20	0.24	0.48	0.20	0.19
COV		0.17	0.19	0.34	0.17	0.16

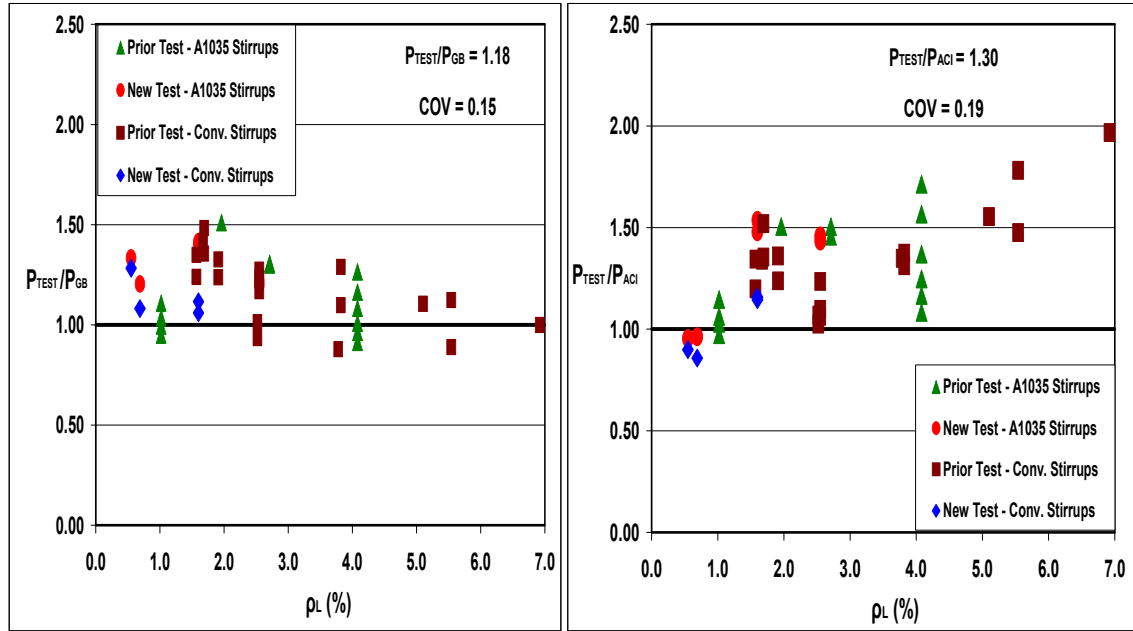
* Results Based on Sectional Response.

6.5 Influence of Design Parameters on Shear Capacity

Section 2.2.4 identified that the shear strength of reinforced concrete members is influenced by several design parameters including longitudinal and transverse reinforcement ratios, ρ_L & ρ_t , compressive strength of concrete, f'_c , and member depth, d . These were also confirmed as important variables from the new test data reported in Sections 3.2 and 3.3. In order to determine the effectiveness of shear capacity models to account for the influences of these parameters, the test-to-model capacity prediction ratios were plotted against these parameters in Figures 6-5 to 6-8. For this purpose all beams in the database were considered based on the proposed general shear model (i.e. Section 6.2.2), the *ACI ITG-6R* code shear model and the MCFT based numerical shear models (i.e. *VT2* and *R2K*). These models were chosen to be representative of all the analytical and numerical shear capacity models considered in the current study. The parametric studies were based on $f_{yt} = 550$ MPa for the yield strength of ASTM A1035 stirrups as per *ACI ITG-6R-10*. Similar trends occur regardless of the type and yield strength of the transverse reinforcement.

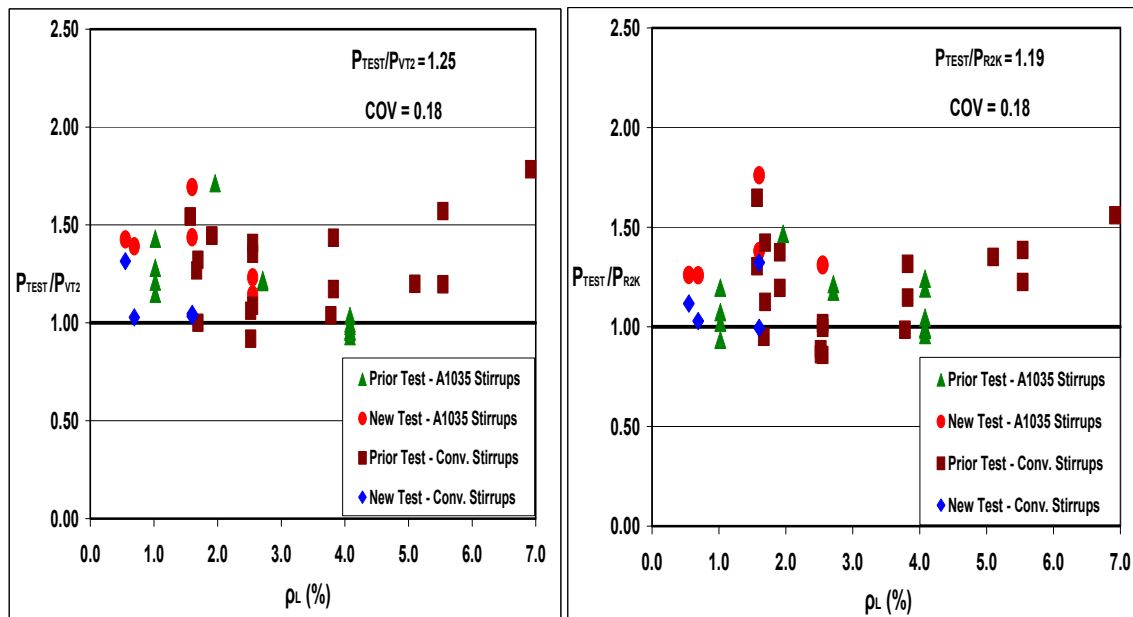
Figure 6-5 depicts the influence from the longitudinal reinforcement ratio on the shear capacity prediction of beams containing ASTM A1035 steel. It is observed in Figure 6-5b that as the longitudinal reinforcement ratio increases the discrepancy between the actual and predicted shear capacity is significantly higher for the *ACI ITG-6R* model than the other models. The MCFT based shear models predicted the shear capacity of beams with more consistent results for all ranges of reinforcement ratios. On the other hand the *ACI ITG-6R* model underestimated the failure load for members with higher longitudinal reinforcement ratios and generally showed lower prediction quality with a wide scatter in the data cloud. This can be attributed to that the *ACI ITG-6R* shear model does not account for the influence on shear capacity from higher member strains which in turn depends on the reinforcement ratio. Compared to the *ACI ITG-6R* code model, the numerical models (*VT2* and *R2K*) showed better shear prediction quality for a wide range of longitudinal reinforcement ratios considered. Of the three MCFT based shear models, the proposed general shear model exhibited the best results with more consistent and uniform shear strength prediction quality. It can be seen in Figure 6-5a that the influence

of member strain resulting from longitudinal reinforcement ratios on beam shear capacity prediction has been accounted for by the general shear model.



a) General shear model

b) ACI ITG-6R shear model



c) VecTor2 shear model

d) Response 2000 shear model

Figure 6-5: Influence of Longitudinal Reinforcement Ratio on Shear Prediction.

Plots of test to model ratios against transverse reinforcement ratios for all beams in the database are shown in Figure 6-6. For the *ACI ITG-6R* code shear model a wide scatter in the data cloud of the test-to-model shear predictions were observed. As shown in Figure 6-6b the *ACI ITG-6R* model is inconsistent in the quality of the predictions and does not account for the influence from transverse reinforcement ratios. The MCFT based numerical shear models (*VT2* and *R2K*) predicted the shear capacity of beams with better results for all ranges of transverse reinforcement (ρ_t) ratios compared to the *ACI ITG-6R* model. (See Figures 6-6c & d). As shown in Figures 6-6a, the proposed general shear model exhibited more consistent and uniform shear capacity prediction quality compared to the other shear models. The general shear model is observed to be slightly conservative for beams with lower transverse reinforcement ratios. However, it is observed that the influence of transverse reinforcement ratios on the scatter is relatively constant for all ρ_t values considered and for all shear reinforcement grades. Hence it can be concluded that the general shear model can be used for shear capacity prediction of slender concrete beams regardless of the type and amount of transverse reinforcement.

Figure 6-7 shows the relationships between the measured to predicted shear load ratios and member depths of all beams in the database. It is observed that member depth has no significant influence on shear strength prediction for all models. This trend confirms that it is justified to omit the size effect in shear for MCFT-based models by using $S_{ze} = 300 \text{ mm}$ in the proposed general and design shear models. Note that the presence of at least minimum stirrups controls the diagonal crack widths in concrete members thereby limiting the potential size effects in shear as described in *Bentz and Collins (2006)*.

The influence of concrete strength, f'_c , on the prediction quality of the models was also studied using plots shown in Figure 6-8 for all beams in the database. Similar to the behaviour observed for the other parameters the *ACI ITG-6R* shear model showed a wide scatter in prediction quality compared to the MCFT based models. The proposed general shear model showed more consistent and uniform trend in the prediction quality for the wide range of concrete strengths considered. This showed that the general shear model can be safely applicable to the wide range of concrete strengths in the industry practice.

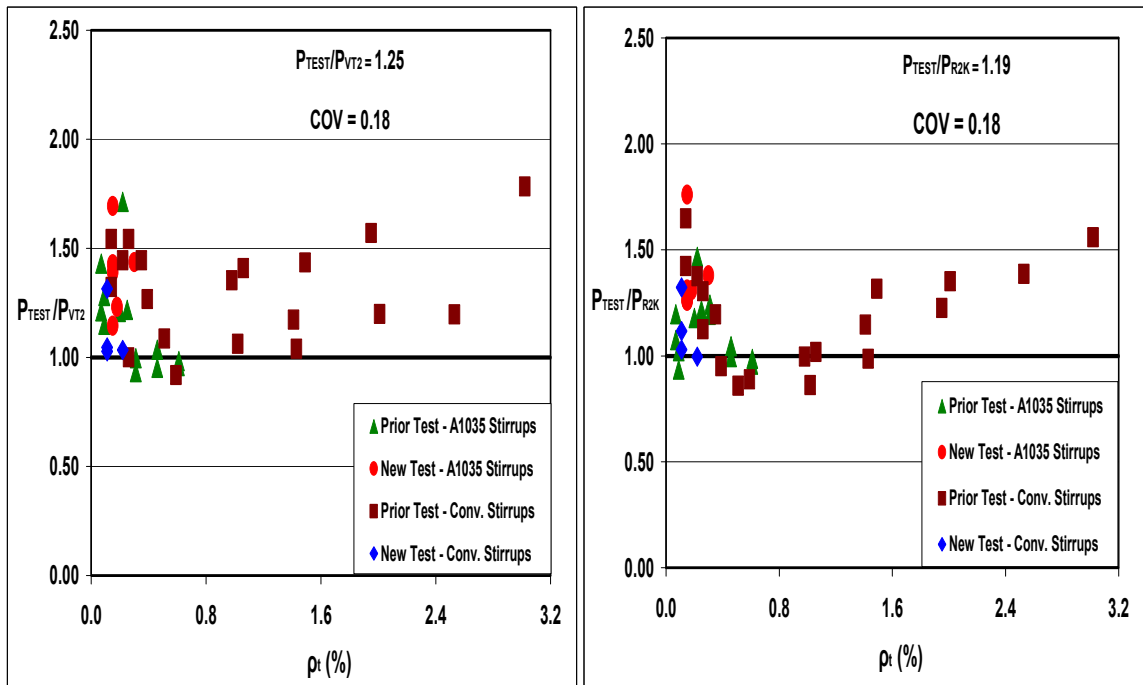
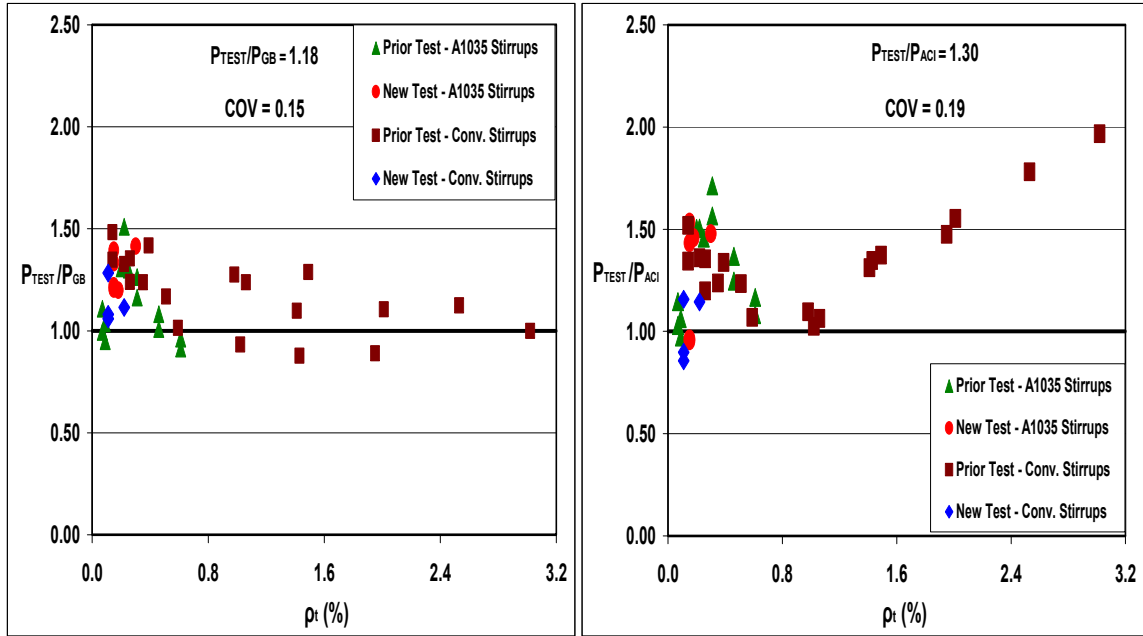


Figure 6-6: Influence of Transverse Reinforcement Ratio on Shear Prediction.

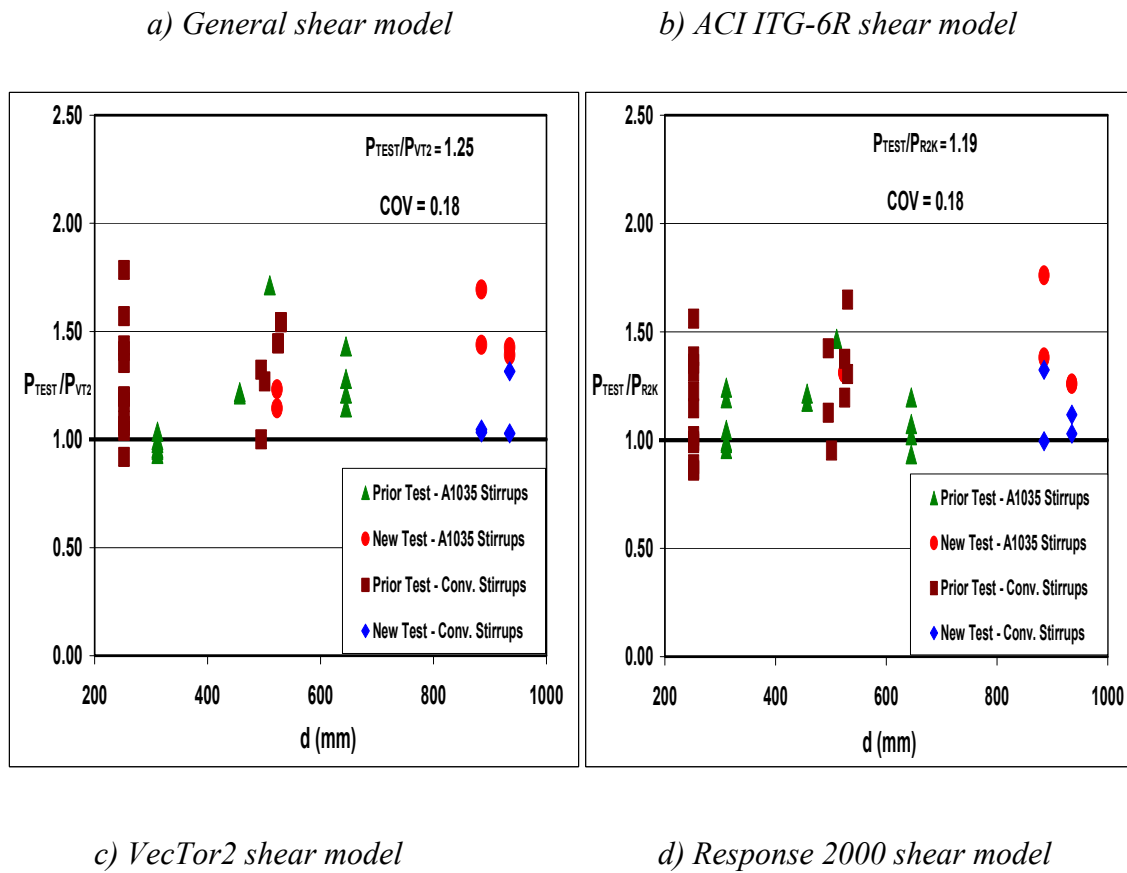
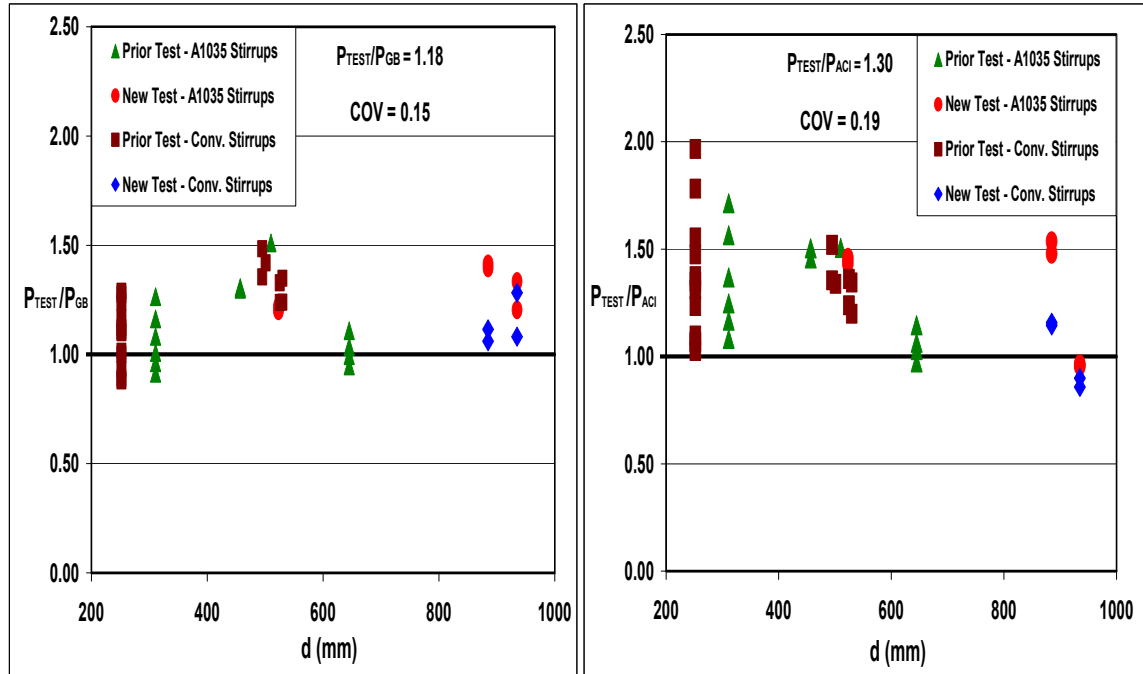
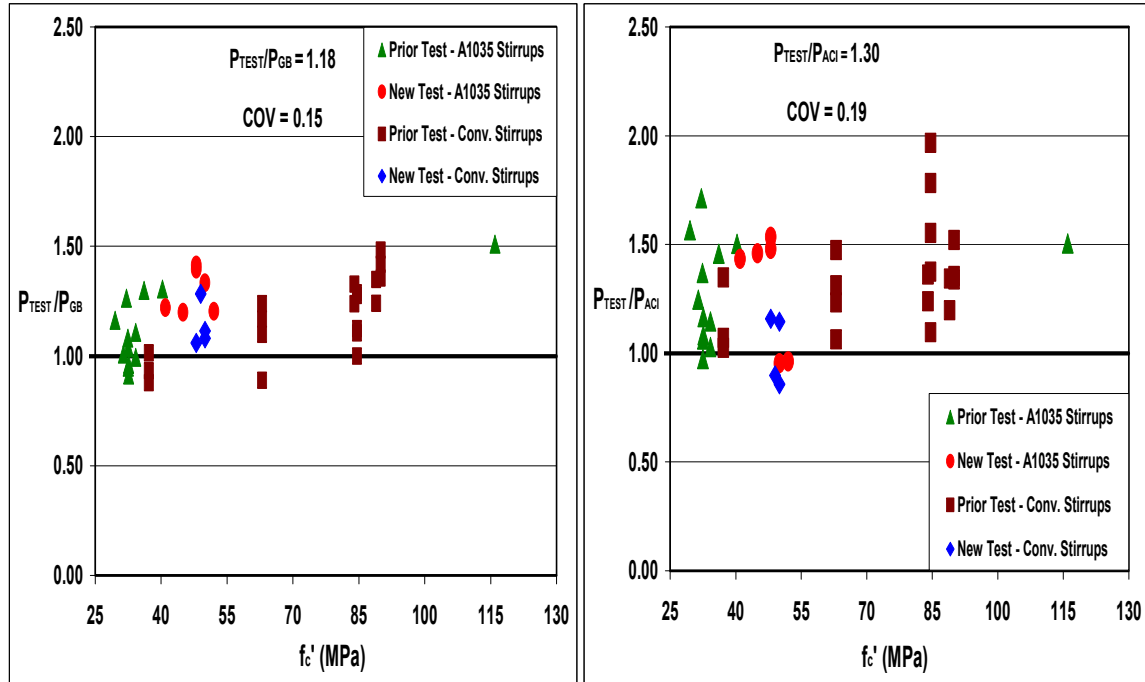
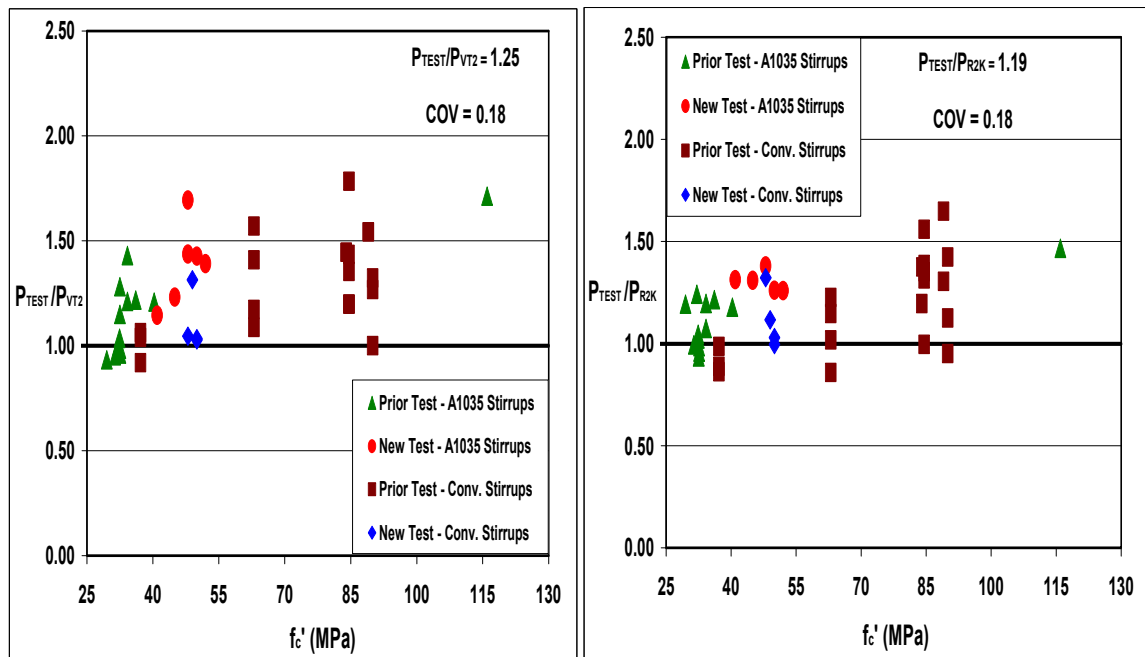


Figure 6-7: Influence of Member Depth on Shear Prediction.



a) General shear model

b) ACI ITG-6R shear model



c) VecTor2 shear model

d) Response 2000 shear model

Figure 6-8: Influence of Concrete Strength on Shear Prediction.

6.6 Summary

In this chapter modeling of the shear capacities of slender reinforced concrete beams reinforced with ASTM A1035 Grade 690 steel tested in the current study and in prior studies was considered. Analytical general and simplified design shear models were developed for use in combination with the *Mast et al.* flexural model included in *ACI ITG-6R-10*. The proposed models were validated for the design and analysis of members containing ASTM A1035 Grade 690 steel as longitudinal and/or transverse reinforcement. Three code models from current standards - *CSA A23.3-04*, *ACI ITG-6R*, *Eurocode 2-04* - and two numerical models (*VT2* and *R2K*) were also evaluated.

A database of forty three tests of beam specimens containing ASTM A1035 steel with transverse reinforcement ($f_{yt} = 550 \text{ MPa}$) were used for model validation. Using all specimens in the database, the predicted capacities obtained from the *ACI ITG-6R* and *Eurocode 2-04* were in poor agreement with test results. Moreover results using these code models showed higher variation compared to that of the MCFT based models. This is due to the inadequacy of the *ACI ITG-6R* and *Eurocode 2-04* models to appropriately account for the strain effect resulting from the higher longitudinal member strains of concrete beams with ASTM A1035 steel longitudinal reinforcement. More accurate predictions of shear capacity were obtained from the MCFT based *CSA A23.3-04* shear code model and the two numerical models considered (*VT2* and *R2K*) compared to the *ACI ITG-6R* and *Eurocode 2-04* shear code models. The more accurate results from the MCFT based models (*CSA A23.3-04*, *VT2* and *R2K*) show that they can adequately account for the influences from higher longitudinal member strains. However, the proposed general shear model developed in Section 6.2 demonstrated the best results compared to all the models considered. This is due to the adequate consideration of larger member strain magnitudes for beams containing ASTM A1035 longitudinal reinforcement. The shear capacity predictions of all the models considered were also shown to be improved by using a higher yield strength of stirrups ($f_{yt} = 690 \text{ MPa}$) in the calculations for beams containing ASTM A1035 steel transverse reinforcement.

The influence on shear capacity prediction quality from the main beam design parameters, namely the longitudinal and transverse reinforcement ratios (ρ_L & ρ_t), member depth (d) and concrete strength (f_c') were studied using plots of test-to-prediction ratios of all beams in the database. The models considered for this purpose were selected to represent models based on empirical approaches (*ACI ITG-6R*) and MCFT based analytical (proposed general) and numerical models (*VT2* & *R2K*). The study showed that as the parameters ρ_L , ρ_t , d and f_c' increased the discrepancy between the measured and predicted shear capacity is significantly higher for the *ACI ITG-6R* model than the MCFT based models. The MCFT based shear models predicted the shear capacity of beams with more consistent results for all ranges of ρ_L , ρ_t , d and f_c' while the *ACI 318-11* shear model showed a wide scatter in prediction quality. The proposed general shear model exhibited the best results with more consistent and uniform shear capacity prediction for all ranges of the parameters considered. Compared to the other shear models, better prediction quality is observed for the proposed general model for beams with ASTM A1035 steel reinforcement. It can be concluded that the proposed general shear model can be used for predicting the shear strength of concrete beams with ASTM A1035 steel reinforcement with reasonable accuracy for practical beam geometry and reinforcement configuration. Moreover the simplified design shear model can also be used for easy preliminary calculations of shear critical concrete beams with ASTM A1035 steel reinforcement.

7. DEFLECTION MODELS FOR BEAMS

7.1 General

Design of reinforced concrete members involves satisfying both the ultimate limit state (*ULS*) and serviceability limit state (*SLS*) requirements. The reinforcement quantity and configuration is typically selected by considering the loading demand is normally governed by the *ULS* conditions. On the other hand, the overall member size is typically governed by *SLS* criteria in addition to satisfying the *ULS* strength requirements. For a one-way reinforced concrete member to be serviceable for its intended use the deflections must not be excessive.

Deflections of reinforced concrete members depend on many factors including member geometry, the degree of cracking, the mechanical properties of the reinforcement and the support and loading conditions (*ACI 435, 2003*). The increased use of high performance reinforcing materials, such as ASTM A1035 steel, which results in low longitudinal reinforcement ratios, can alter the deflection and cracking behaviour of slender concrete beams. It is, therefore, important to have accurate methods to predict the service deflection of reinforced concrete members which take into account these factors.

Most currently available design codes for concrete structures provide a direct computation method for deflection control of slender reinforced concrete beams. This method is based on the Navier-Bernoulli theory which assumes the service deflection of concrete beams is entirely caused by so-called flexural deformations. In general, so-called shear deformations are presumed to be minimal in most design code models.

In this chapter general analytical and simplified deflection models that consider both flexural and shear deformations are developed. The models are validated using a database of fifty two beam specimens containing either conventional steel or ASTM A1035 steel reinforcement. The general model is developed based on various assumptions and modifications on the Modified Compression Field Theory (MCFT) and simplifications on member response along the span. The general deflection model is validated using

available data from current study and prior beam tests. A simplified deflection model is also developed based on the study of the different parameters influencing service deflection according to the general model. Comparisons of prediction quality for deflections at the equivalent service load condition are also made using models from current deflection provisions in *ACI ITG-6R-10* and from numerical methods, *VecTor2* (VT2) and *Response 2000* (R2K).

The scope of this study is limited to longitudinally and transversely reinforced slender concrete beams that are expected to undergo large shear deformations before failure. Emphasis was placed on development of models for service load deflection for slender concrete beams longitudinally reinforced with ASTM A1035 steel. Deflection predictions were also made for beams with traditional reinforcement configurations containing conventional steel. Since members without transverse reinforcement (slabs) are expected to fail shortly after the formation of diagonal cracking in a relatively brittle manner the conventional deflection calculation procedures are believed to be sufficient for these members without the need to directly consider shear deformations (*Desalegne and Lubell, 2012*).

7.2 Deficiency of Current Code Deflection Model

Prior studies have attempted to address the inaccuracies in design code approaches for the prediction of deflections of reinforced concrete members, as discussed in Section 2.6. (*Bischoff 2005, Tang and Lubell, 2008*). Design code models, including *ACI 318-11*, typically rely on the Navier-Bernoulli theory which considers flexural deformations but ignores shear deformations. *Bischoff (2005)* developed an expression for the effective moment of inertia I_e which accounts for the tension stiffening influence on the effective stiffness for use in the Navier-Bernoulli deflection calculations. Estimates of slab deflection using Bischoff's formulation for I_e are in better agreement with test results for slabs compared to the formulation originally developed by Branson (1977). (See Section 2.6.2.) Note that *ACI ITG-6R-10* recommends the use of Bischoff's formulation for I_e for slender concrete members with and without stirrups and containing ASTM A1035 longitudinal bars. In this study the *ACI ITG-6R-10* deflection model (*ITG-6*) with

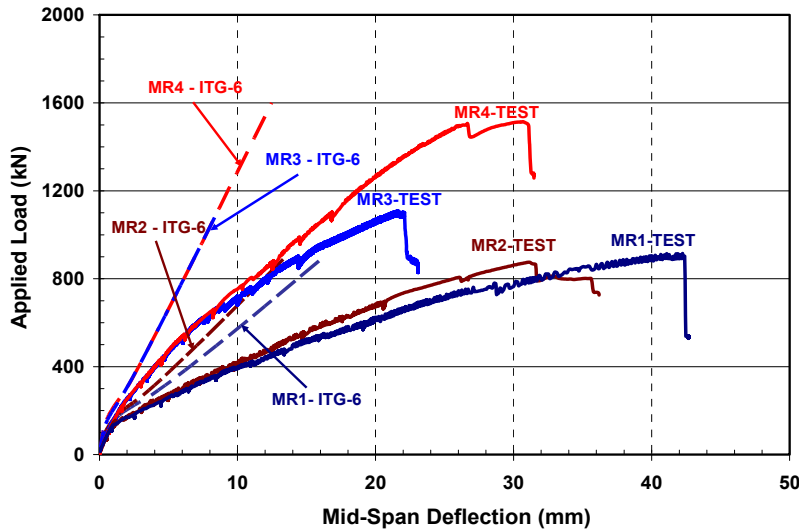
Bischoff's effective moment of inertia of cracked concrete section, I_e , is used for computation of Bernoulli deflections.

Previously an analytical study was conducted to compare the maximum span-depth ratios for one-way slabs from the *ACI 318-08* implicit deflection provisions with corresponding ratios determined from direct deflection calculations. Emphasis was placed on deflection control at the serviceability limit state (*SLS*) for concrete slabs longitudinally reinforced with ASTM A1035 steel where the nominal steel stress at the ultimate limit state (*ULS*) ranged from 414 to 828 MPa. The results of this analytical study were published in *Desalegne and Lubell* (2012). Since concrete slabs without stirrups are expected to fail in a relatively brittle manner if diagonal cracks form, minimal or no shear deformations would occur and these members are therefore beyond the scope of the current study on deflections.

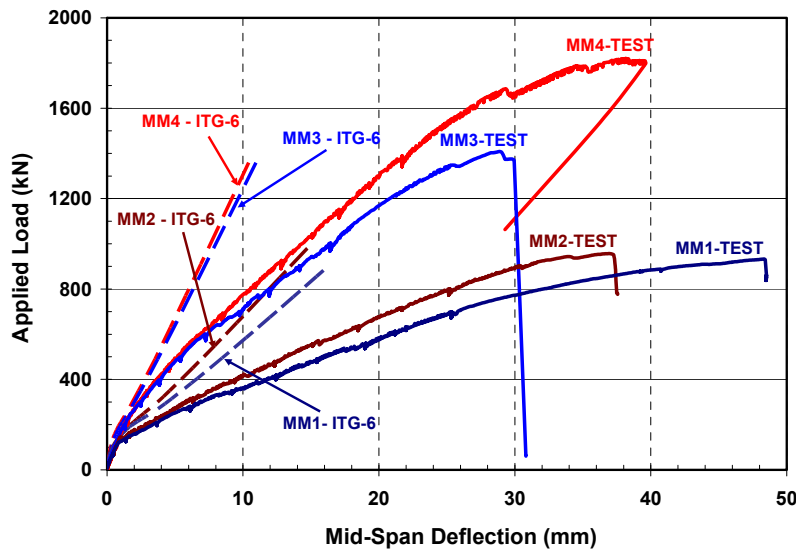
For slender concrete beams with stirrups, many cases have been reported in which the measured deflections are higher than the predicted deflections. One reason for the possible under-estimation of the deflection models may be from their neglecting of the shear deformations. Since these members may exhibit excessive deflections compared to the design code predictions, actual performance may not comply with the corresponding code deflection control requirements at the *SLS* condition. This may be more significant for the case of slender reinforced concrete beams with relatively small shear span to depth ratios ($a/d = 2.8$ to 4.0) where the shear deformation as a fraction of the total deformation is greater. Moreover, with the introduction of higher strength reinforcing steel in recent years, which results in concrete members to have lower longitudinal and/or transverse reinforcement ratios, the need for more reliable and accurate deflection calculation procedure is essential. Thus, it is important to study deflection modeling approaches that consider the relationships between the shear deformations and other design parameters.

Figure 7-1 shows the measured load-deflection response of eight concrete beams with ASTM A1035 longitudinal reinforcement tested in the current study in comparison to the *ACI ITG-6* deflection model which is merely based on flexural deformations. It can be

seen in Figure 7-1 that the *ITG-6* deflection model significantly underestimates the measured deflection response regardless of the type of steel in the transverse reinforcement. The discrepancy is even higher for beams with lower longitudinal reinforcement ratios (*MR1*, *MR2*, *MM1* & *MM2*). Hence it is important to develop and validate service deflection models that satisfy serviceability requirements for beams with ASTM A1035 steel reinforcement.



a) Beams with Conventional Grade 400 Stirrups



b) Beams with ASTM A1035 Grade 690 Stirrups

Figure 7-1: Discrepancy between Bernoulli Deflection Model and Measured Deflection.

7.3 Database of Beam Specimens

A database of beams with transverse reinforcement was assembled for use in validation of deflection models developed in the current study and for comparison between deflection models considered. In addition to the ten new test data for beams reported in Chapter 4, forty seven beam specimens were assembled from seven independent research programs conducted at different laboratories [*Mohr et al. (2010)*; *Sumpter et al. (2009)*; *Munikrishna et al (2011)*; *Lee and Hwang (2010)*; *Vecchio et al. (2004)*; *Bresler et al. (1963)*; *Leonhardt and Walther (1961)*]. The database included beam specimens which satisfied the following criteria:

- Rectangular cross section with overall depth, h , between 300 mm and 1000 mm.
- Shear span-to-depth ratio, a/d , between 2.8 - 4.0.
- Longitudinal and transverse reinforcement with either conventional or ASTM A1035 steel.
- Longitudinal reinforcement ratio, ρ_L , ranging from 0.55% to 6.92%.
- Transverse reinforcement ratio, ρ_t , ranging from 0.07% to 3.02%.
- Concrete compressive strength, f_c' , ranging from 27 to 85 MPa.

Most of the beams in the database listed in Tables 7-1 and 7-2 are the same beams used in the shear capacity model validation described in Section 6.3. The range of the various parameters reflects the typical values for buildings in the industry practice. Of the total of fifty seven specimens, thirty five beams shown in Table 7-1 contained high strength or ASTM A1035 steel reinforcement. Table 7-2 shows the remaining twenty two beams entirely reinforced with conventional steel.

Table 7-1: Details of Beams with High Strength or ASTM A1035 Steel Reinforcement.

Author	Beam ID	Longitudinal f_{yL} * (MPa)	Transverse f_{yt} * (MPa)	Reinforcement Ratio (%)		f_c ' (MPa)	a/d	h (mm)
				ρ_L	ρ_t			
New Test	RM1	430	830	2.55	0.15	41	3.2	600
New Test	RM2	430	830	2.55	0.18	45	3.2	600
New Test	MR1	830	430	0.55	0.11	49	3.0	1000
New Test	MR2	830	430	0.69	0.11	50	3.0	1000
New Test	MR3	830	430	1.60	0.11	48	3.0	1000
New Test	MR4	830	430	1.60	0.22	50	3.0	1000
New Test	MM1	830	830	0.55	0.11	50	3.0	1000
New Test	MM2	830	830	0.69	0.11	52	3.0	1000
New Test	MM3	830	830	1.60	0.11	48	3.0	1000
New Test	MM4	830	830	1.60	0.22	48	3.0	1000
Sumpter et al. (2009)	C-M-6	427	830	4.08	0.31	30	2.8	406
Sumpter et al. (2009)	C-M-4	427	830	4.08	0.46	31	3.3	406
Sumpter et al. (2009)	C-M-3	427	830	4.08	0.61	33	3.3	406
Sumpter et al. (2009)	M-M-6	830	830	4.08	0.31	32	2.8	406
Sumpter et al. (2009)	M-M-4	830	830	4.08	0.46	32	3.3	406
Sumpter et al. (2009)	M-M-3	830	830	4.08	0.61	33	3.3	406
Munikrishna et al. (2011)	G1-M80	830	550	1.04	0.09	33	3.2	711
Munikrishna et al. (2011)	G1-M100	830	830	1.04	0.07	34	3.2	711
Munikrishna et al. (2011)	G2-M80	830	550	1.04	0.09	33	3.2	711
Munikrishna et al. (2011)	G2-M100	830	830	1.04	0.07	34	3.2	711
Munikrishna et al. (2011)	G3-M80	830	550	2.69	0.25	36	3.0	559
Munikrishna et al. (2011)	G3-M100	830	830	2.69	0.20	40	3.0	559
Lee et al. (2010)	F40-1	1068	510	2.55	0.59	37	3.0	300
Lee et al. (2010)	F40-3	1068	510	2.55	1.02	37	3.0	300
Lee et al. (2010)	F40-5	1068	510	3.82	1.43	37	3.0	300
Lee et al. (2010)	F60-1	1068	508	2.55	0.51	63	3.0	300
Lee et al. (2010)	F60-2	1068	508	2.55	1.06	63	3.0	300
Lee et al. (2010)	F60-3	1068	508	3.82	1.41	63	3.0	300
Lee et al. (2010)	F60-4	1068	508	5.54	1.95	63	3.3	300
Lee et al. (2010)	F60-5	1068	508	5.54	2.53	63	3.3	300
Lee et al. (2010)	F80-1	1068	508	2.55	0.98	85	3.0	300
Lee et al. (2010)	F80-2	1068	508	3.82	1.49	85	3.0	300
Lee et al. (2010)	F80-3	1068	508	5.10	2.01	85	3.0	300
Lee et al. (2010)	F80-4	1068	508	5.54	2.53	85	3.3	300
Lee et al. (2010)	F80-5	1068	508	6.92	3.02	85	3.3	300

Note:- * Yield strength with well-defined yield point is the value reported for prior tested beams or 830 MPa for ASTM A1035 steel based on the 0.2% offset method.

Table 7-2: Details of Beams with Conventional Steel Reinforcement.

Author	Beam ID	Longitudinal f_{yL} * (MPa)	Transverse f_{yt} * (MPa)	Reinforcement Ratio (%)		f_c' (MPa)	a/d	h (mm)
				ρ_L	ρ_t			
Sumpter et al. (2009)	C-C-6	427	427	4.08	0.31	27	2.8	406
Sumpter et al. (2009)	C-C-4	427	427	4.08	0.46	27	3.3	406
Sumpter et al. (2009)	C-C-3	427	427	4.08	0.31	27	3.3	406
Munikrishna et al. (2011)	G1-C60	430	430	1.53	0.12	33	3.1	711
Munikrishna et al. (2011)	G2-C60	430	430	1.53	0.12	33	3.1	711
Munikrishna et al. (2011)	G3-C60	430	430	3.70	0.31	35	2.9	559
Lee et al. (2010)	F20-1	525	508	1.44	0.20	27	3.0	450
Lee et al. (2010)	F20-2	525	508	2.40	0.40	27	3.0	450
Lee et al. (2010)	F20-3	525	508	3.35	0.60	27	3.0	450
Lee et al. (2010)	F20-4	525	508	3.83	0.80	27	3.0	450
Lee et al. (2010)	F20-5	525	508	4.79	1.03	27	3.0	450
Mohr et al. (2010)	ET-1	420	320	1.40	0.17	29	3.5	350
Mohr et al. (2010)	H50-2	500	530	2.28	0.11	50	3.1	400
Mohr et al. (2010)	H50-3	500	540	2.29	0.24	50	3.1	400
Vecchio et al. (2004)	VS-A1	445	600	1.73	0.10	23	4.0	552
Vecchio et al. (2004)	VS-B1	445	600	2.30	0.15	23	4.0	552
Vecchio et al. (2004)	VS-C1	436	600	2.01	0.20	23	4.0	552
Bresler et al. (1963)	BS-A1	552	325	1.80	0.10	24	3.9	561
Bresler et al. (1963)	BS-B1	552	325	2.40	0.15	25	4.0	556
Bresler et al. (1963)	BS-C1	552	325	1.79	0.20	30	3.9	559
Leonhardt et al.(1962)	E4	530	516	2.40	0.59	37	2.8	320
Leonhardt et al.(1962)	E5-1	530	567	2.40	0.59	37	2.8	320

Note:- * Yield strength with well-defined yield point is the value reported for prior tested beams.

7.4 Development of General Deflection Model

The use of high-performance ASTM A1035 steel in concrete members can lead to potential savings in the longitudinal and transverse reinforcement ratios due to the available higher yield strength. Reinforced concrete beams containing high-strength or ASTM A1035 steel are expected to behave differently at higher imposed strain levels compared to members with conventional Grade 400 steel reinforcement. This is mainly due to the difference in the stress-strain behaviour between the two materials. Moreover, beams containing high strength or ASTM A1035 steel are expected to undergo more extensive cracking, including diagonal cracking, at high imposed shear stresses. This may also result in higher deflections. It is, therefore, necessary to develop and validate deflection models that consider the expected higher member strain for lightly reinforced members containing high-strength or ASTM A1035 steel.

The deflection of slender reinforced concrete beams results from two main components - the bending deformations and the shear deformations. Based in part on the Modified Compression Field Theory (MCFT) a new deflection model that accounts for both bending deformations and shear deformations was developed for beams containing conventional and/or ASTM A1035 steel reinforcement. (See Figure 7-2) The model considers the variations in curvatures and strains along the member length. The entire model is implemented in an Excel spreadsheet using the approach described below.

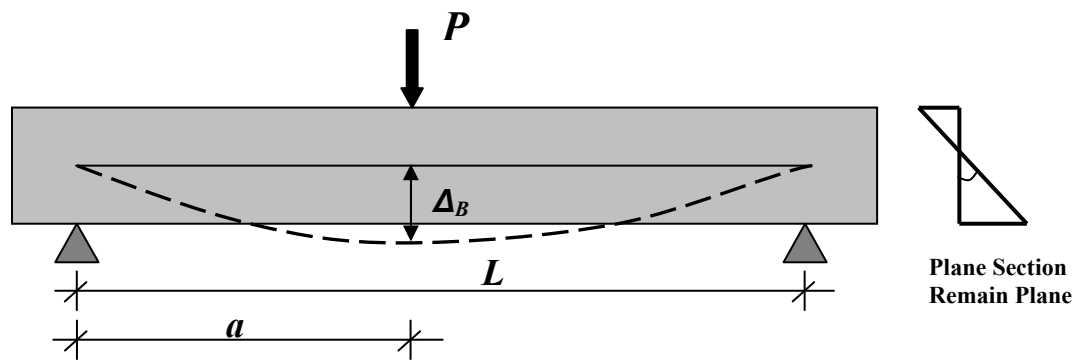
Bending deformations are based on the Navier-Bernoulli theory with the same format as the *ACI 318-11* deflection model. The bending deflection model (termed as ITG-6 deflection model) is based on Bischoff's effective moment of inertia I_e (Bischoff, 2005) as recommended in *ACI ITG-6R-10*. The curvatures are integrated along the member length for cracked concrete beams using the effective moment of inertia, I_e , formulated by Bischoff. (See equations 7-1 and 7-2). Using the Navier-Bernoulli theory, bending deformations can be formulated for any loading and support conditions. Figure 7-2a shows an idealized simple slender beam which is normally assumed to satisfy the

engineering beam theory - plane section before loading remain plane after loading. The mid-height deflected shape of a beam with a concentrated load is shown by the dotted line. For the case of simply supported reinforced concrete beam subjected to a concentrated load the bending deflection Δ_B at any location, a , from the left support is given by equation 7-1. Similar equations for other loading cases are available elsewhere (e.g. Hibbeler, 2012).

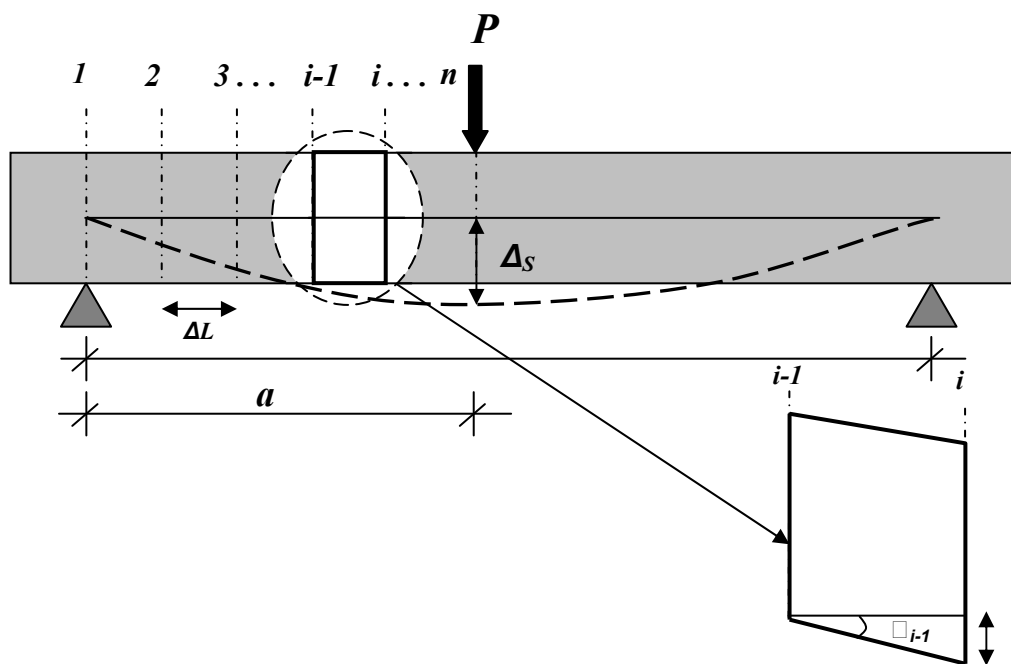
Figure 7-3 shows predicted bending deflection response Δ_B at different load levels for one of the beams tested in the current study (MM4) using equation 7-1.

$$\Delta_B = \frac{Pa^2(L-a)^2}{3E_c I_e L} \quad (7-1)$$

$$I_e = \frac{I_{cr}}{1 - \left(1 - \frac{I_{cr}}{I_g}\right) \left(\frac{M_{cr}}{M_a}\right)^2} \leq I_g \quad (7-2)$$



a) Bending Deformation



b) Shear Deformation

Figure 7-2: Considerations in The General Deflection Model.

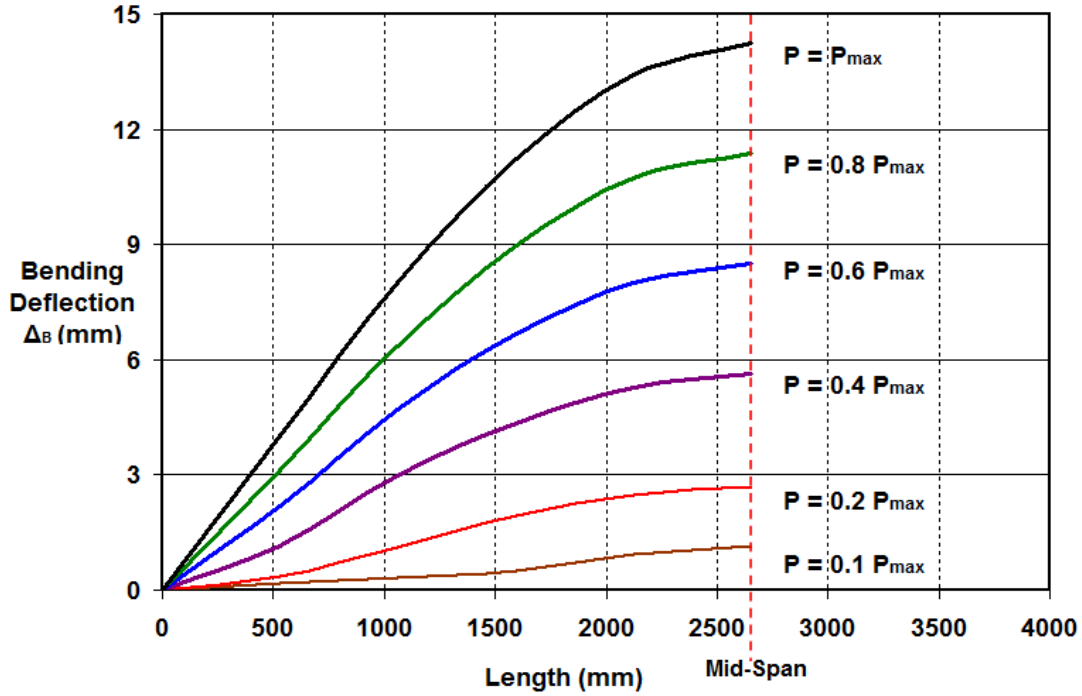


Figure 7-3: Calculated Bending Load-Deflection Response of Beam-MM4 at Different Load Levels.

The shear deflection component Δ_{st} is solved by using simplifications to the MCFT relationships to consider the variation in shear strains that occur at different cross-sections along the member. The required calculations follow the methods described in *Collins and Mitchell (1997)* and are demonstrated using the flow chart shown in Figure 7-4. A detailed explanation of the calculations is given in Appendix C. For given input parameters including the cross-section geometry and the reinforcement configuration, the MCFT relationships in Figure 7-4 are iteratively solved using an Excel spreadsheet for different loading conditions. From these results, a relationship can be extracted between the shear strain at a cross-section, γ , and the corresponding average longitudinal strain ϵ_x for the loading conditions considered. Figure 7-5 shows a typical relationship between the longitudinal member strain, ϵ_x , and shear strain, γ , for one of the beam specimens tested in the current study (MM4). It is observed that γ increases at an increasing rate as ϵ_x increases. To simplify further analysis with this result, a 3rd order polynomial was fit to the γ versus ϵ_x relationship. (See Figure 7-5).

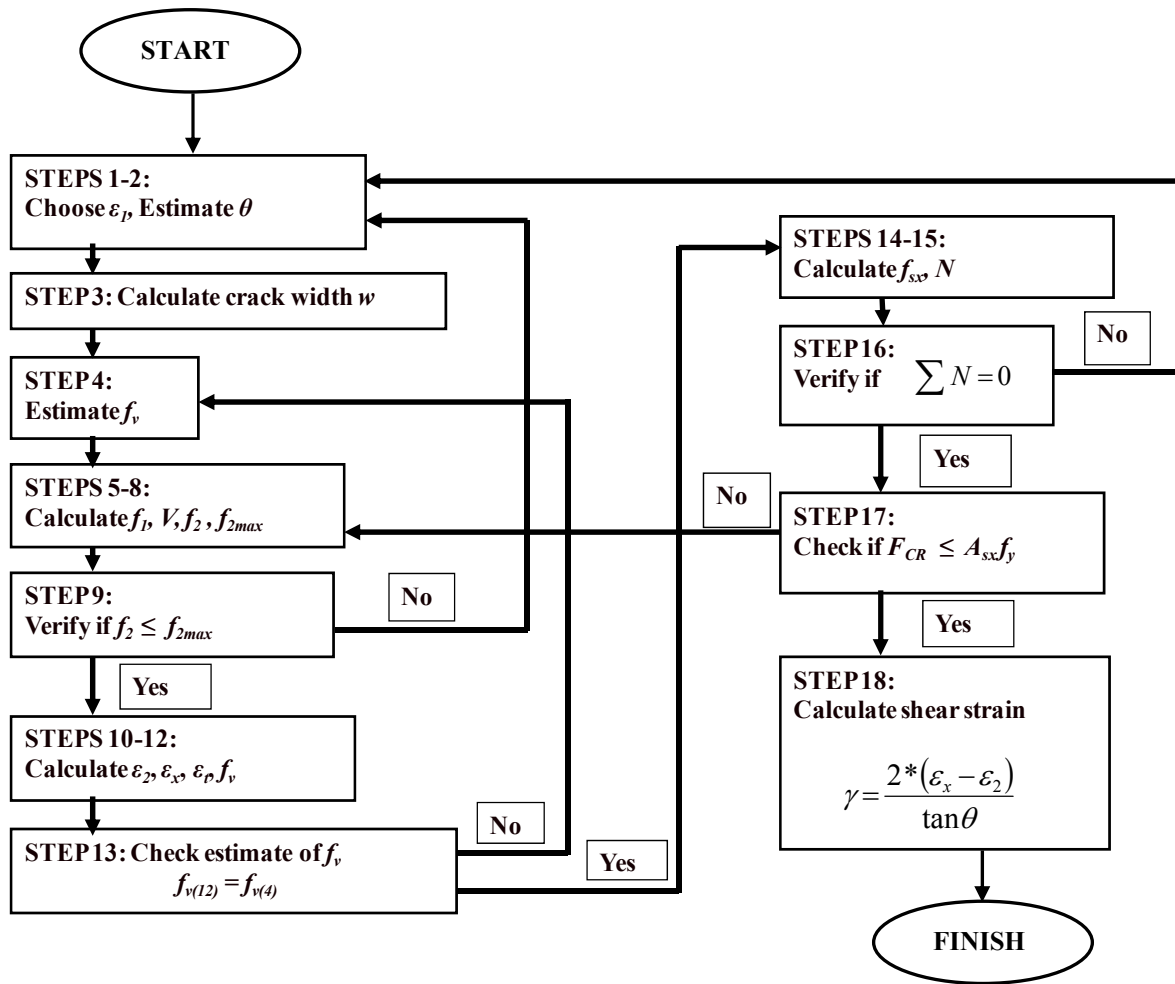


Figure 7-4: Flowchart Showing the Prediction of Relationship Between Shear Strain and Member Strain.

Popovics, 1970 proposed an expression for the modulus of elasticity E_c of normal-weight concrete ($E_c = 4730\sqrt{f'_c}$), as described in *Collins and Mitchell* (1997). However *Carrasquillo et al.*, 1981 concluded that the expression by *Popovics* overestimates the stiffness of concretes with $f'_c > 41 \text{ MPa}$ and developed an alternative expression ($E_c = 3320\sqrt{f'_c + 6900}$). Hence in the calculation of shear deformations using the simplified MCFT relationships, the expressions given by *Popovics*, 1970 and *Carrasquillo et al.*, 1981 are combined to estimate the modulus of elasticity E_c of normal-weight concrete as given below.

$$E_c = \begin{cases} 4730 \sqrt{f'_c} & \text{for } f'_c \leq 41 \text{ MPa} \\ 3320 \sqrt{f'_c} + 6900 & \text{for } f'_c > 41 \text{ MPa} \end{cases} \quad (7-3)$$

The relationship between ε_x and γ developed for each beam specimen can be used to calculate the values of γ along the length of the beam at a given load level. For a given load level j , the longitudinal reinforcement steel stress at a cross-section i is estimated using the relationship described in Section 5.2.2.1 (equation 5-3):

$$f_{s,ij} = \frac{\frac{M_{ij}}{d_v} + V_{ij}}{A_s} \quad (7-4)$$

where M_{ij} and V_{ij} are the bending moment and shear force at section i , respectively, for the load level j being considered. The corresponding strain in the reinforcement $\varepsilon_{s,ij}$ can be determined from the stress-strain relationship of the steel material (see equation 3-1) with the maximum stress limited by the yield strength f_{yL} reported for each beam test as given in Tables 7-1 and 7-2. Finally, the average longitudinal strain at a cross-section $\varepsilon_{x,ij}$ can be approximated as one-half of the steel strain value as described in Section 5.2.2.1.

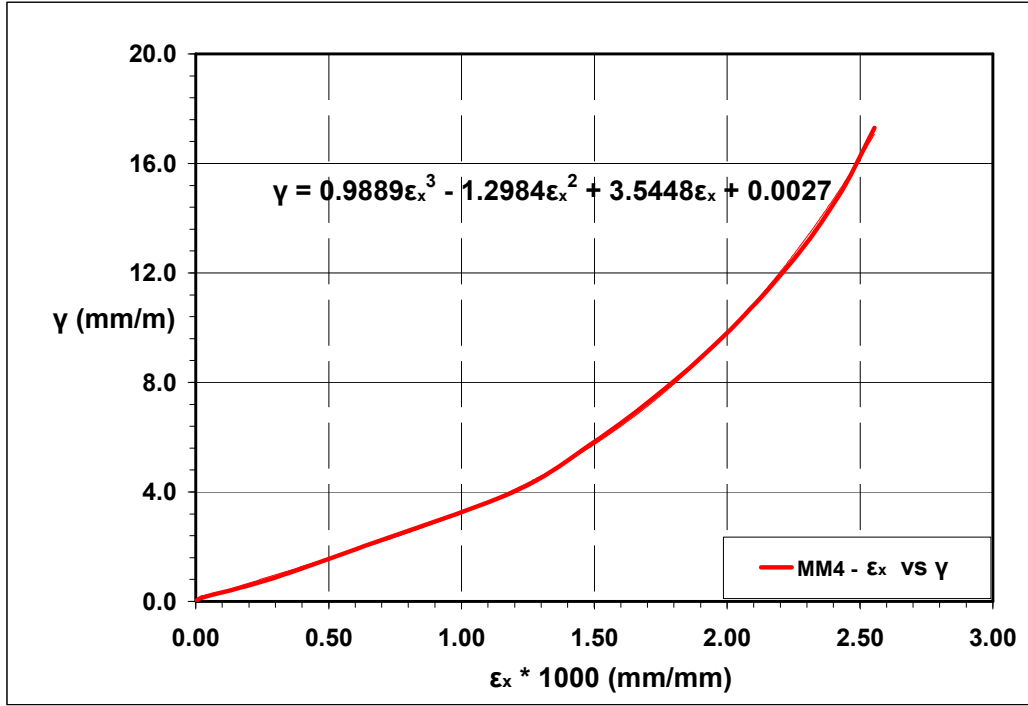


Figure 7-5: Typical longitudinal member strain and shear strain relationship (Beam-MM4).

The incremental shear deflection Δ_{si} between two adjacent sections $i-1$ and i is approximated as the shear strain at section $i-1$ multiplied by the longitudinal distance between the two sections. Thus, for a simply supported beam with concentrated load, the total shear deflection under the load at a particular load level j , Δ_{stj} , is the sum of the shear deflections of each segment between the support and the load. Sensitivity analysis on the maximum length of sections ΔL between $\Delta L \leq d_v$ and $\Delta L \leq 0.25 d_v$ showed that the equivalent service load deflections at $P_s = 0.6 P_{max}$ did not differ by more than 7% for MM4 (See Figure 7-6b). The maximum difference was similar for the other new tests in this study. Hence in the general model sections with maximum length of $\Delta L \leq 0.5 d_v$ along the length are considered to approximate the actual curve of the deflected shape, where $d_v = 0.9d$. Parameter n is used to represent the number of sections between the support and the load as shown in Figure 7-2.

$$\Delta_{si} = \gamma_{i-1} \cdot \Delta L \quad (7-5)$$

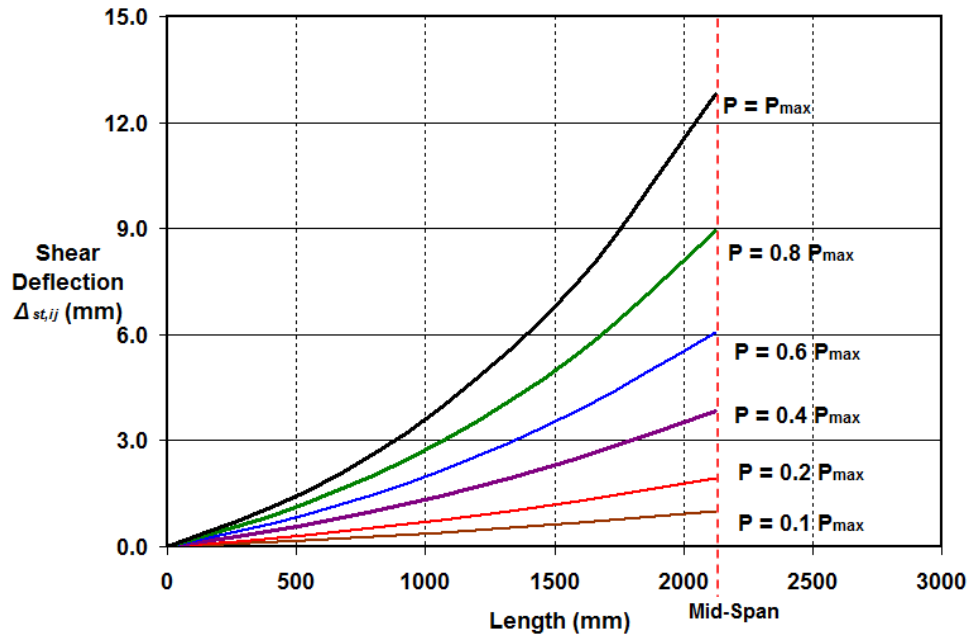
$$\Delta_{stj} = \sum_{i=1}^n \Delta_{si} = \sum_{i=1}^n \gamma_{i-1} \cdot \Delta L \quad (7-6)$$

$$\Delta L = \frac{a}{n-1} \leq \frac{d_v}{2} \quad (7-7)$$

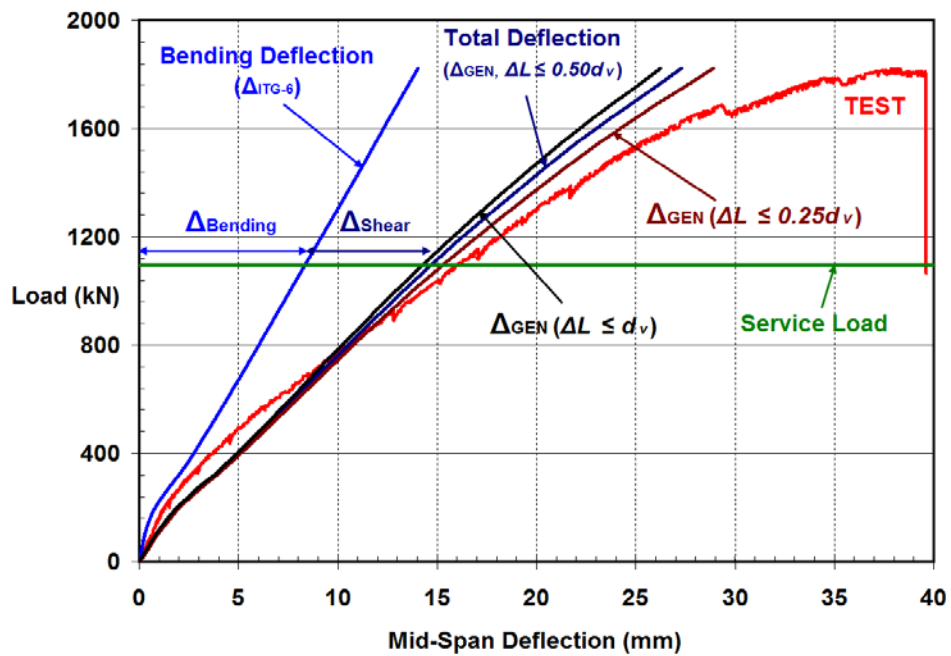
Thus, the total deflection using the general analytical method, Δ_{GEN} , uses a compositional approach of the bending deflection and the shear deflection and is given:

$$\Delta_{GEN} = \Delta_B + \Delta_{st} \quad (7-8)$$

Figure 7-6a shows typical shear deflection plots at different load levels for beam MM4. As shown in the figure the shear deflection at mid-span of beam MM4 at a particular load is significant compared with the bending deflection (*ITG-6*) shown in Figure 7-3. Figure 7-6b shows the comparison between the bending deflection from *ITG-6* deflection model and the total deflection from the general deflection model for the load-deflection response of beam MM4. From Figures 7-6 and 7-7 it is clearly observed that consideration of the shear deformations through equation 7-6 results in more accurate estimates of the equivalent service load deflection of beams with ASTM A1035 steel reinforcement.



a) Shear deflection along span for different load levels.



b) Comparison between Bending Deflection (*ITG-6*) and measured deflection.

Figure 7-6: Prediction of Total Deflection Using The General Deflection Model for Beam-MM4.

7.5 Model Validation

7.5.1 Validation of The General Beam Deflection Model

The database of fifty seven tests containing ASTM A1035 or conventional reinforcement (Tables 7-1 and 7-2) were used to validate the general beam deflection model developed in this study. Tables 7-3 and 7-4 compare the service deflection of beam specimens, grouped by the type of reinforcement used, with the corresponding predictions for the proposed general deflection model described in Section 7.4. Material properties were as reported by the researchers for each specimen in the database. For the purpose of comparison, the equivalent service deflection of each beam was assumed to be the deflection corresponding to 60 % of the ultimate load reported for the particular test. For each beam specimen, the service load P_s , the corresponding measured service deflection Δ_{TEST} , the predicted service deflection Δ_{GEN} , and test to model deflection ratio are provided in Tables 7-3 and 7-4.

The average test to model service deflection ratios and coefficients of variation (COV) were calculated as 1.04 and 0.14 for beams in group one (beams containing high strength or ASTM A1035 reinforcement) and 0.97 and 0.20 for beams in group one (beams entirely reinforced with conventional steel), respectively. Two beams in group one and three beams in group two gave low predictions of service deflection resulting in higher test to model ratios beyond the common tolerance in deflection calculations for reinforced concrete beams ($\pm 30\%$) (Ramsay *et al.* 1979). However, in general, the analytical general deflection model resulted in good prediction of measured service deflections especially for beams containing high strength or ASTM A1035 steel as shown in Tables 7-3 and 7-4.

Table 7-3: Prediction of General Deflection Model for Beams with ASTM A1035 Steel.

<i>Beam ID</i>	$P_S = 0.6 P_{max} \text{ (kN)}$	$\Delta_{TEST} @ P_S \text{ (mm)}$	$\Delta_{GEN} \text{ (mm)}$	$\Delta_{TEST}/\Delta_{GEN}$
<i>RM1</i>	504	6.11	6.33	0.97
<i>RM2</i>	574	5.53	7.26	0.76
<i>MR1</i>	549	16.91	20.38	0.83
<i>MR2</i>	525	14.67	15.76	0.93
<i>MR3</i>	665	8.93	10.44	0.86
<i>MR4</i>	906	13.10	13.40	0.98
<i>MM1</i>	560	19.24	20.02	0.96
<i>MM2</i>	574	16.16	17.03	0.95
<i>MM3</i>	845	12.83	13.29	0.97
<i>MM4</i>	1093	15.95	15.44	1.03
<i>C-M-6</i>	231	7.11	6.10	1.17
<i>C-M-4</i>	249	7.87	7.37	1.07
<i>C-M-3</i>	263	8.38	8.64	0.97
<i>M-M-6</i>	245	7.11	6.60	1.08
<i>M-M-4</i>	249	7.87	7.62	1.03
<i>M-M-3</i>	289	9.40	9.14	1.03
<i>G1-M80</i>	320	11.18	11.94	0.94
<i>G1-100</i>	294	9.14	11.18	0.82
<i>G2-M80</i>	360	8.89	9.91	0.90
<i>G2-100</i>	369	8.89	10.16	0.88
<i>G3-M80</i>	561	14.22	16.00	0.89
<i>G3-100</i>	494	14.22	13.72	1.04
<i>F40-1</i>	270	4.90	4.05	1.21
<i>F40-3</i>	300	5.75	4.10	1.40
<i>F40-5</i>	390	4.85	4.16	1.17
<i>F60-1</i>	288	4.32	3.82	1.13
<i>F60-2</i>	420	6.40	5.46	1.17
<i>F60-3</i>	528	6.73	5.07	1.33
<i>F60-4</i>	594	5.94	5.38	1.10
<i>F60-5</i>	600	6.00	5.34	1.12
<i>F80-1</i>	435	6.03	5.54	1.09
<i>F80-2</i>	630	7.42	5.95	1.25
<i>F80-3</i>	660	5.60	4.89	1.15
<i>F80-4</i>	750	6.90	6.40	1.08
<i>F80-5</i>	900	7.50	6.56	1.14
			<i>AVERAGE</i>	1.04
			<i>STDV</i>	0.14
			<i>COV</i>	0.14

Table 7-4: General Deflection Model Prediction for Beams with Conventional Steel.

<i>Beam ID</i>	$P_s = 0.6 P_{max} (kN)$	$\Delta_{TEST} @ P_s (mm)$	$\Delta_{GEN} (mm)$	$\Delta_{TEST}/\Delta_{GEN}$
<i>C-C-6</i>	227	7.87	6.10	1.29
<i>C-C-4</i>	209	6.86	6.60	1.04
<i>C-C-3</i>	263	8.89	8.89	1.00
<i>G1-C60</i>	347	11.18	9.40	1.19
<i>G2-C60</i>	414	7.62	8.38	0.91
<i>G3-C60</i>	587	13.46	13.21	1.02
<i>F20-1</i>	246	3.16	3.21	0.98
<i>F20-2</i>	510	6.60	5.20	1.27
<i>F20-3</i>	738	7.00	6.61	1.06
<i>F20-4</i>	798	7.50	6.10	1.23
<i>F20-5</i>	960	8.54	7.14	1.20
<i>ET-1</i>	150	6.20	8.01	0.77
<i>H50-2</i>	107	2.99	4.02	0.74
<i>H50-3</i>	144	5.20	5.16	1.01
<i>VS-A1</i>	270	7.92	8.70	0.91
<i>VS-B1</i>	255	7.75	8.84	0.88
<i>VS-C1</i>	165	7.20	8.22	0.88
<i>BS-A1</i>	276	4.92	8.13	0.61
<i>BS-B1</i>	255	5.13	7.90	0.65
<i>BS-C1</i>	186	6.80	9.88	0.69
<i>E4</i>	235	5.47	5.70	0.96
<i>E5-1</i>	240	5.99	5.84	1.03
AVERAGE				0.97
STDV				0.20
COV				0.20

7.5.2 Development of General and Simplified Design Equations

The analytical MCFT based deflection model developed in Section 7.4 involves many lengthy iterations of the various MCFT relationships shown in Figure 7-4 to determine the shear deflection component for a given beam configuration. This can be very tedious and impractical for estimating the beam service deflection in the design industry. Therefore it is desired to have simplified equations which can easily be used in day to day calculation of service deflection of beams with transverse reinforcement. Since the focus of the current study is on the deflection behaviour of beams containing ASTM A1035 steel, the simplified equations are developed only for the thirty five specimens in Table 7-2. However, similar procedures can be followed to come up with simplified equations for beams reinforced with conventional reinforcement.

The general design equation for deflection (Δ_{GDE}) was developed based on the basic deflection equations given in equation 7-8 as the superposition of the bending deformation and shear deformation. As the bending deformation is based on the *ACI ITG-6R-10* recommendation using Bischoff's effective moment of inertia I_e , equation 7-8 can be rewritten as:

$$\Delta_{GDE} = \Delta_{ITG-6} \cdot \left(1 + \frac{\Delta_{st}}{\Delta_{ITG-6}}\right) \quad (7-9)$$

The second term in the parenthesis in equation 7-9 can be envisaged as the correction factor for shear deformation to be added to the bending deformation to calculate the total service deflection of concrete beams. Hence the proposed simplified equation for service deflection of beams with shear reinforcement can be reduced to the determination of the correction factor for shear deformations.

As identified in Section 2.2.4, the most important parameters influencing the shear behaviour and hence the shear deformations of beams are the longitudinal and transverse reinforcement ratios (ρ_t & ρ_L) and member depth, h . Note that for the thirty five slender

beam specimens containing ASTM A1035 steel reinforcement ρ_t, ρ_L and h are the most variable parameters with wide range of values as shown in Table 7-2.

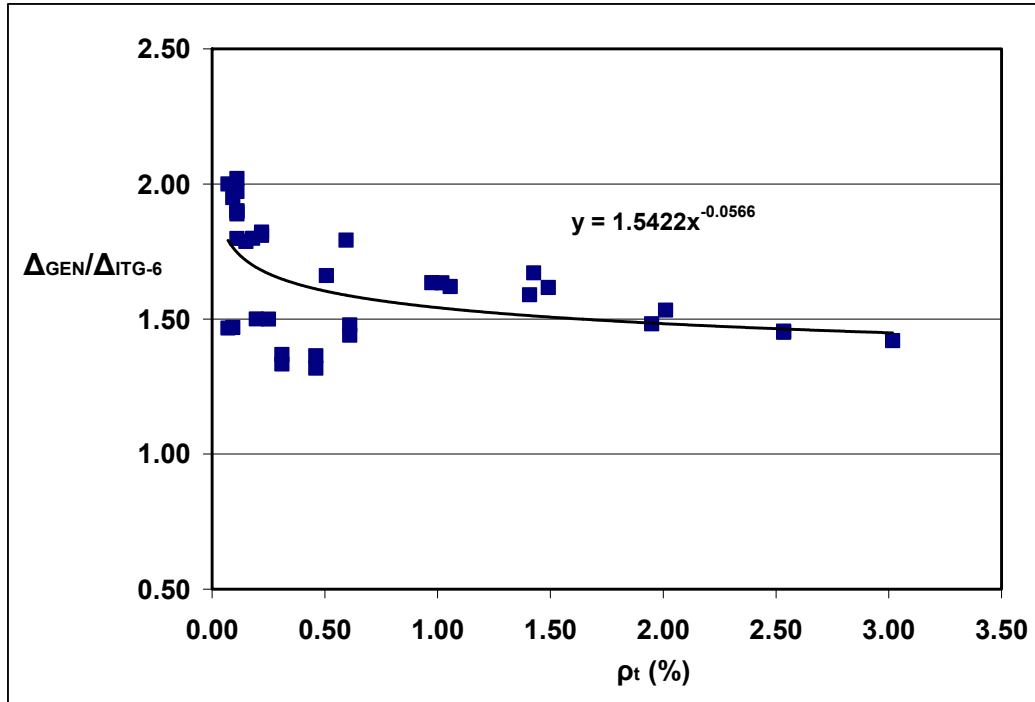
Figures 7-7 a, b and c show the relationships between the service deflection ratios of the general model to the *ITG-6* model $\left(\frac{\Delta_{GEN}}{\Delta_{ITG-6}} \right)$ and the selected parameters for the beam

specimens in Table 7-2. In order to determine the influence of a single parameter, trend lines of the data cloud were calculated from the relationship between $\left(\frac{\Delta_{GEN}}{\Delta_{ITG-6}} \right)$ and each

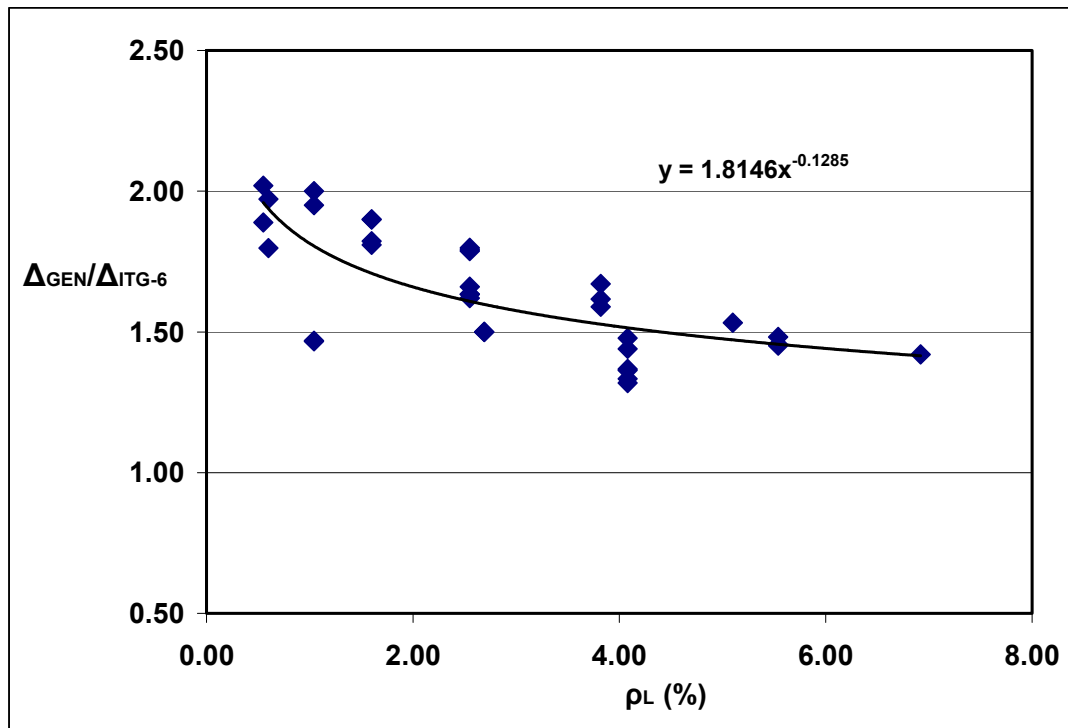
parameter. These relationships are used to determine the normalized deflection ratio $\left(\frac{\Delta_{GEN}}{\Delta_{ITG-6}} \right)$ normalized by two of the three parameters) corresponding to each parameter.

For instance, the normalized deflection ratio for ρ_t was determined as the ratio of $\left(\frac{\Delta_{GEN}}{\Delta_{ITG-6}} \right)$ to the product of the relationships in Figures 7-7 b and c. Therefore, the

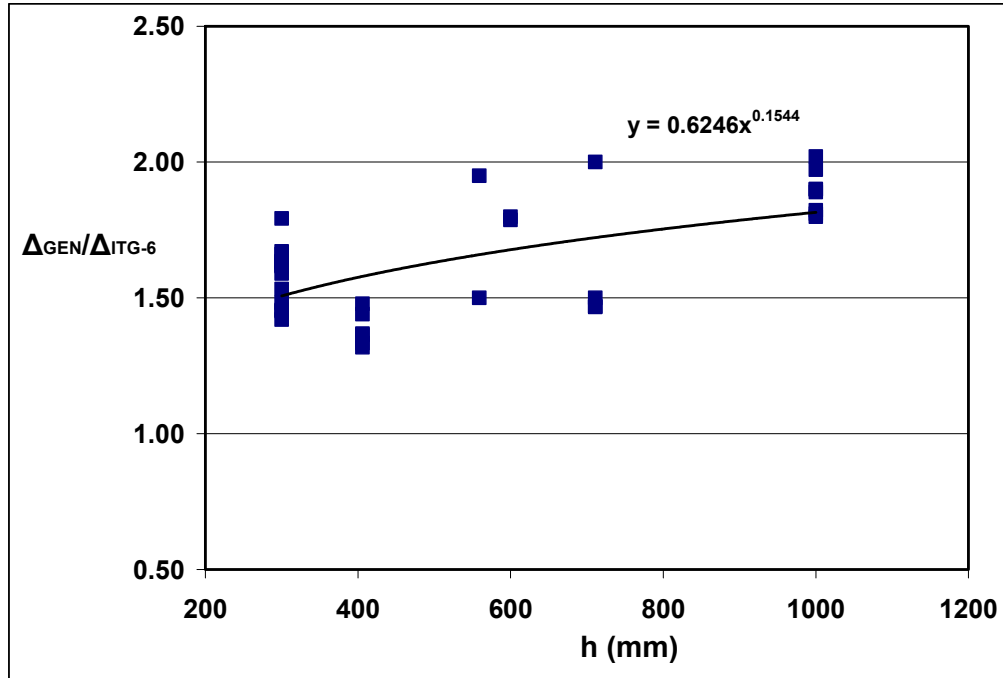
correction factors for shear deformations of the selected parameters (ρ_t, ρ_L and h) were determined from Figures 7-8 a, b, and c as $0.03\rho_t^{0.37}$, $0.01\rho_L^{0.50}$ and $\frac{1.29}{h^{0.12}}$, respectively.



a) Transverse Reinforcement Ratio

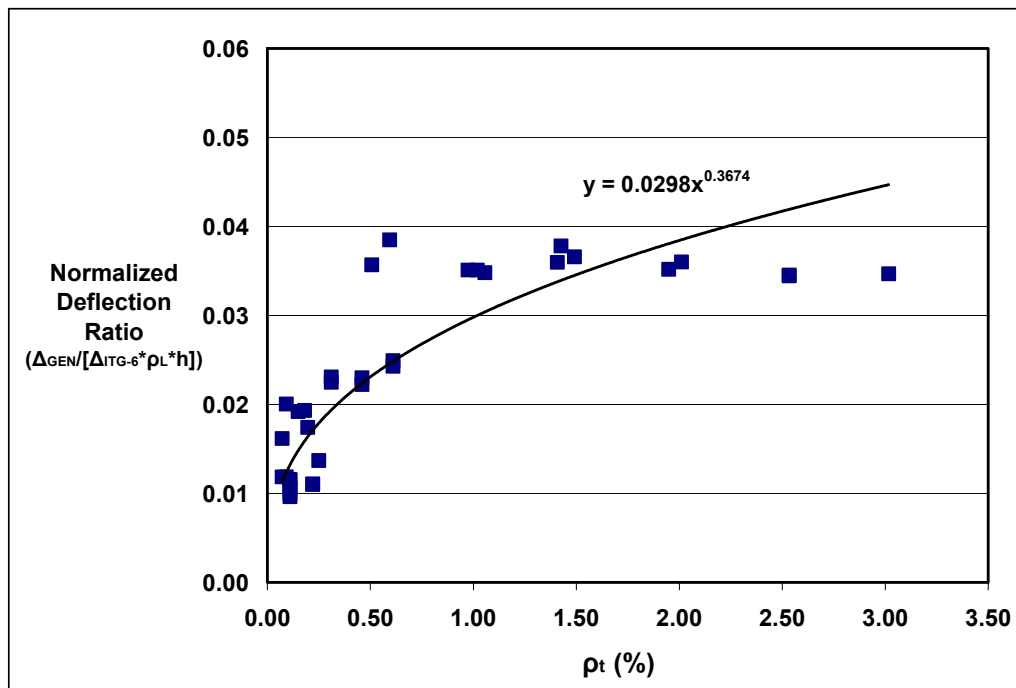


b) Longitudinal Reinforcement Ratio

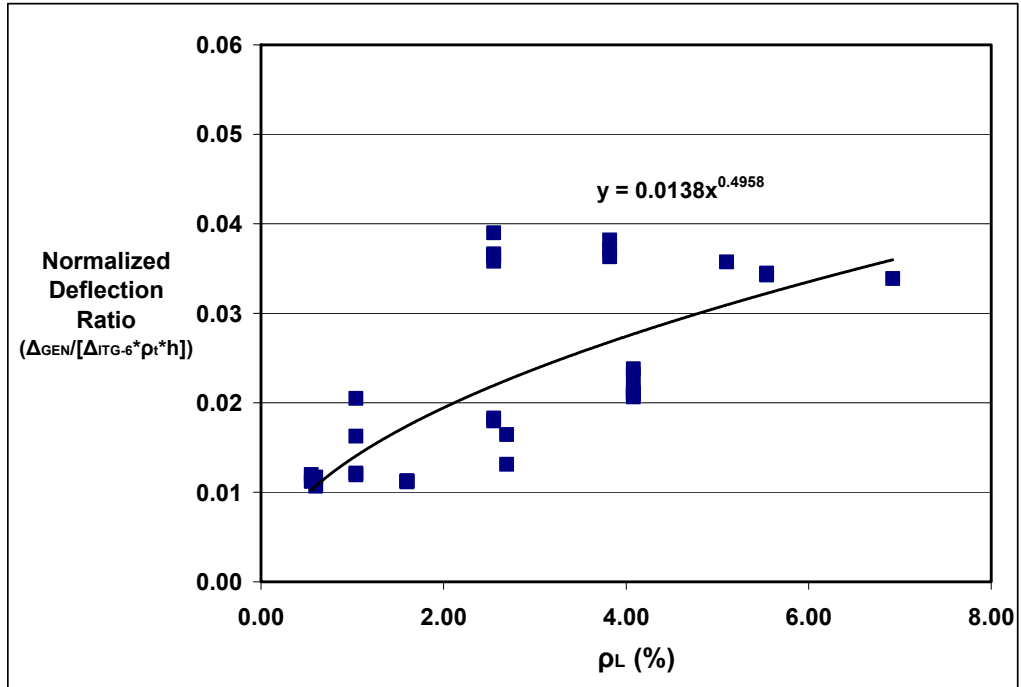


c) Overall Member Depth

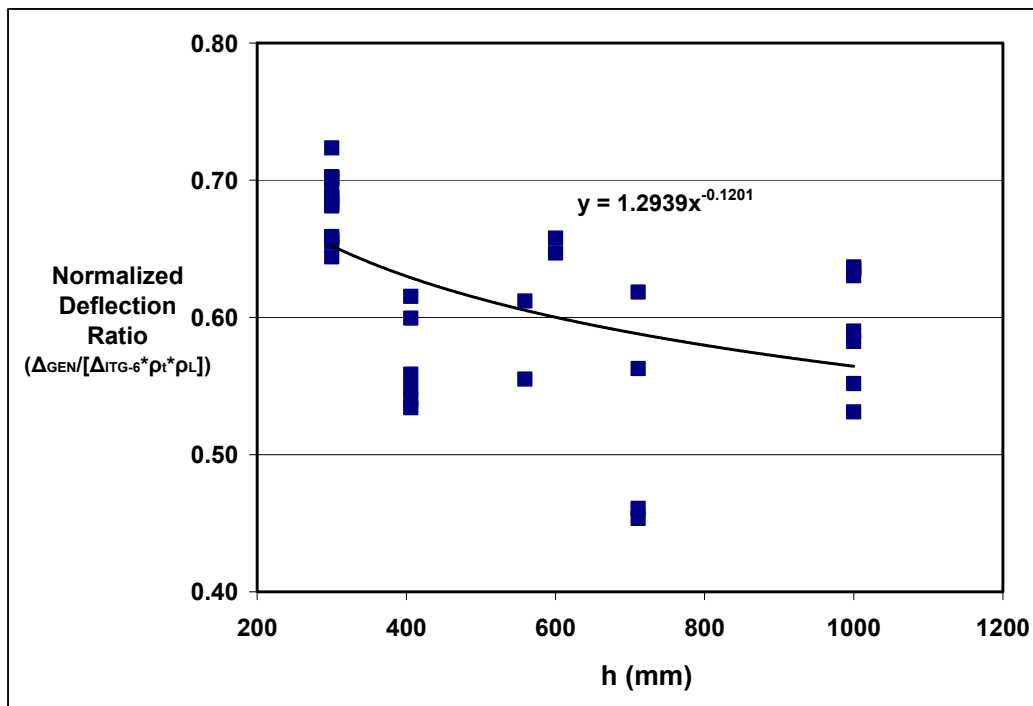
Figure 7-7: Influence of Design Parameters on the General Deflection Model.



a) Correction Factor from Transverse Reinforcement Ratio.



b) Correction Factor from Longitudinal Reinforcement Ratio



c) Correction Factor from Overall Member Depth

Figure 7-8: Correction Factors for Shear Deformation.

Hence, for slender concrete beams with ASTM A1035 steel, the analytical deflection model (equation 7-8) can be formulated as:

$$\Delta_{GDE} = \Delta_{ITG-6} \cdot (1 + 0.03\rho_t^{0.37} + 0.01\rho_L^{0.50} + \frac{1.29}{h^{0.12}}) \quad (7-10)$$

where ρ_t and ρ_L are the transverse and longitudinal reinforcement ratios, respectively, in % and h is the overall member depth in mm.

Note that equation 7-10 predicts the service deflection corresponding to approximately 60% of the failure load for beams containing ASTM A1035 steel. However as the failure load or failure mode is not determined within equation 7-10, use of the general model from Section 7-4 may be appropriate for detailed analysis.

7.5.3 Influence of Reinforcement Ratios on The Simplified Deflection Equation

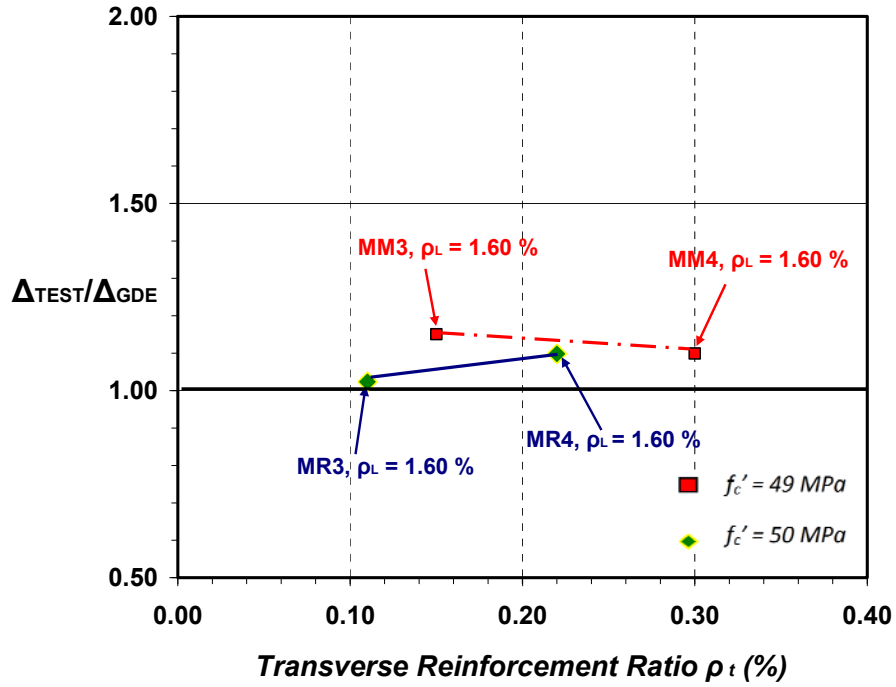
Equation 7-10 shows that the service deflection of beams with ASTM A1035 steel is directly related to the transverse and longitudinal reinforcement ratios ρ_t and ρ_L . Increases in ρ_t and ρ_L typically also increase the member strength. Thus, for a certain beam geometry as ρ_t or ρ_L increases the service deflection from equation 7-10 is expected to increase along with the expected higher load assuming that the change in ρ_L would not affect the beam flexural stiffness significantly. It is therefore important to evaluate whether the service deflection predictions are overestimated or underestimated as the reinforcement ratio ρ_t or ρ_L is varied for a given beam geometry. For this purpose the eight beams with ASTM A1035 steel longitudinal reinforcement tested in the current study were used.

Figure 7-9a shows the relationship between the transverse reinforcement ratio ρ_t and the test to predicted service deflection $\Delta_{TEST}/\Delta_{GDE}$ ratio using equation 7-10. The beams used for this Figure (*MR3*, *MR4*, *MM3* & *MM4*) had similar geometry and longitudinal

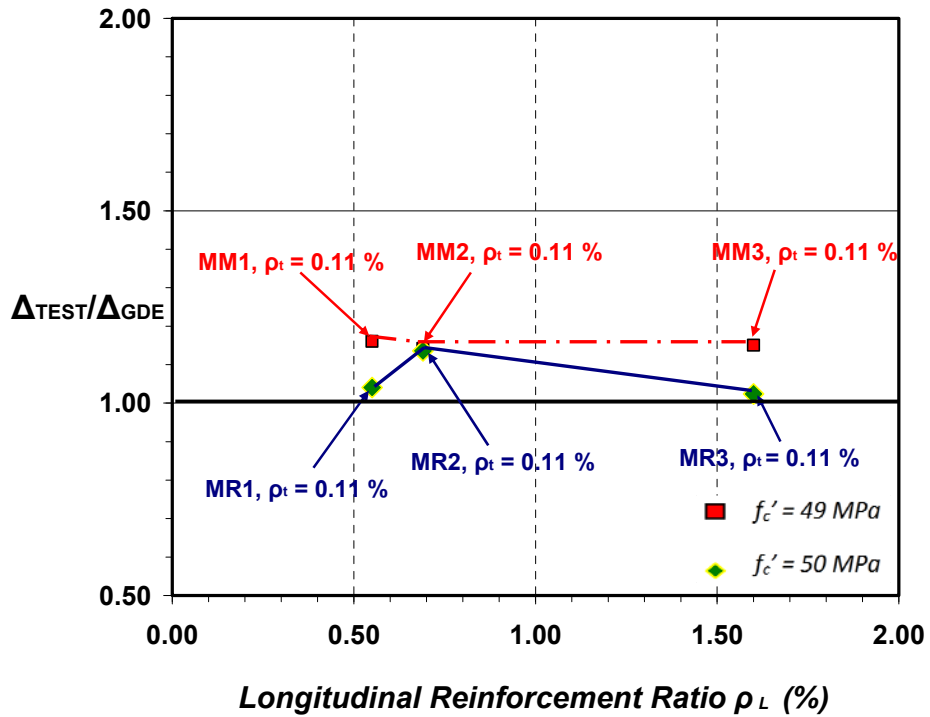
reinforcement configurations, but different type of steel and transverse reinforcement ratios in the stirrups. It is observed that the test to predicted service deflection ratio changed slightly as the transverse reinforcement ratio increases. Table 7-5 shows that as the transverse reinforcement ratio was doubled the service deflection ratio increased by 7 % and -4 % for beams with conventional (*MR3* & *MR4*) and ASTM A1035 (*MM3* & *MM4*) stirrups, respectively.

Figure 7-9b shows the influence of the longitudinal reinforcement ratio ρ_L on the service deflection ratio $\Delta_{TEST}/\Delta_{GDE}$ of beam specimens with ASTM A1035 longitudinal steel grouped by the type of steel in the stirrups. The beams used for this Figure had similar geometry and transverse reinforcement configuration, but different longitudinal reinforcement ratios. In general, it is observed that increasing the longitudinal reinforcement ratio resulted in lower test to predicted service deflection ratios. As the longitudinal reinforcement ratio was increased by 25 % and 191 % for beams with conventional stirrups (*MR1* to *MR2* and *MR1* to *MR3*) the test to predicted service deflection ratio increased by 9 % and -2 %, respectively. The corresponding changes in the test to predicted service deflection ratio for beams with ASTM A1035 steel stirrups (*MM1* to *MM2* and *MM1* to *MM3*) were -2 % and -1 %, respectively, as shown in Table 7-5.

Based on the above evaluation and discussion it is seen that the proposed general design equation for deflection (equation 7-10) can predict the service deflection of beams with ASTM A1035 steel reinforcement with reasonable accuracy. The maximum variation in the prediction of service deflection with respect to longitudinal reinforcement ratio was only 9%. This shows that the general deflection equation (equation 7-10) can be applicable for the wide range of practical reinforcement ratios of beams with conventional or ASTM A1035 steel stirrups. This is attributed to the general model being based on the MCFT which captures the most influencing parameters in the shear behaviour of cracked concrete members that can be extended to beams containing ASTM A1035 steel; the general design model was empirically derived from this general model.



(a) Influence of Transverse Reinforcement Ratio.



(b) Influence of Longitudinal Reinforcement Ratio.

Figure 7-9: Influence of Reinforcement Ratios on The General Deflection Equation.

Table 7-5: Deflection Predictions with Variable Reinforcement Ratios.

BEAM ID ($h = 1000$ mm)	ρ_t (%)	ρ_L (%)	Δ_{TEST} (mm)	Δ_{GDE} (mm) (Eqn. 7-8)	$\Delta_{TEST}/\Delta_{GDE}$	% change in ρ_t	% change in ρ_L
<i>MR1</i>	0.11	0.55	16.91	16.25	1.04	-	-
<i>MR2</i>	0.11	0.69	14.67	12.91	1.14	-	9
<i>MR3</i>	0.11	1.60	8.93	8.72	1.02	-	-2
<i>MR4</i>	0.22	1.60	13.1	11.93	1.10	7	-
<i>MM1</i>	0.15	0.55	19.24	16.57	1.16	-	-
<i>MM2</i>	0.15	0.69	16.16	14.13	1.14	-	-2
<i>MM3</i>	0.15	1.60	12.83	11.14	1.15	-	-1
<i>MM4</i>	0.30	1.60	15.95	14.50	1.10	-4	-

Figure 7-10a compares the measured service deflections against the corresponding predicted values from the ITG-6 model and from the general deflection equation (7-10), for the thirty five beam specimens with high strength or ASTM A1035 steel listed in Table 7-2. As can be seen from the Figure, equation 7-10 predicted the service deflections more accurately than the *ITG-6* model. The data points for the thirty five beams, including the ten new tests completed in the current study (highlighted) are closer to the measured values using the general deflection equation (7-10).

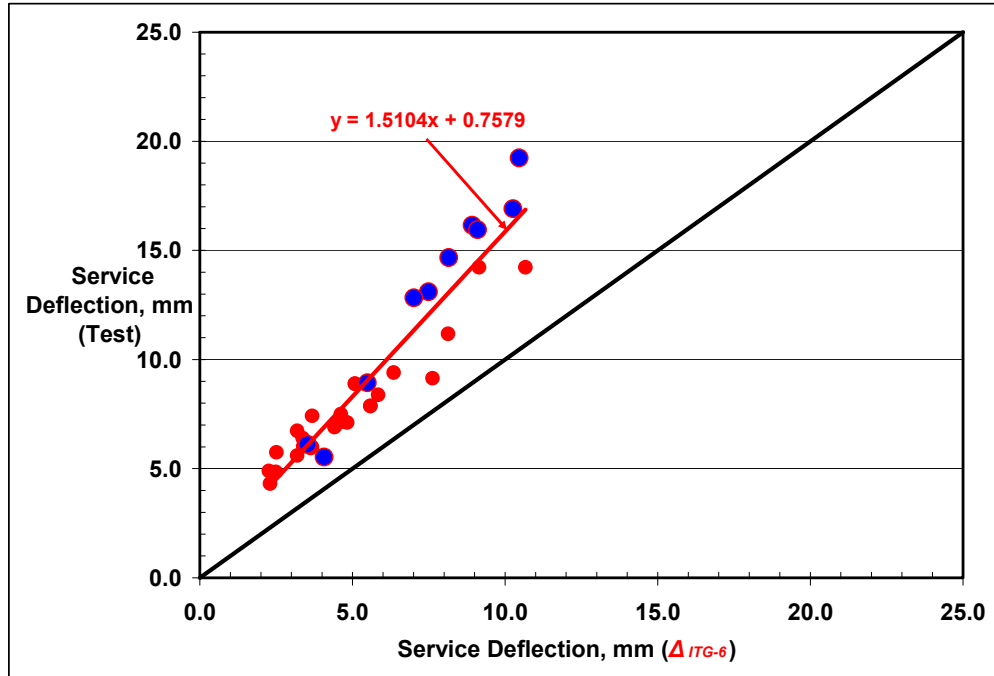
Equation 7-10 can be further simplified for quick evaluation of service deflections of beams with ASTM A1035 steel. Comparing the linear trend lines of the general design equation and the *ITG-6* model in Figure 7-10, the service deflection can be approximated from the ratio of the trend line slopes. Therefore the service deflection equation is estimated at $\left(\frac{1.5104}{0.9637}\right)$ times that of the deflection computed using the *ITG-6* model.

Hence the proposed simplified design equation for deflection is given as:

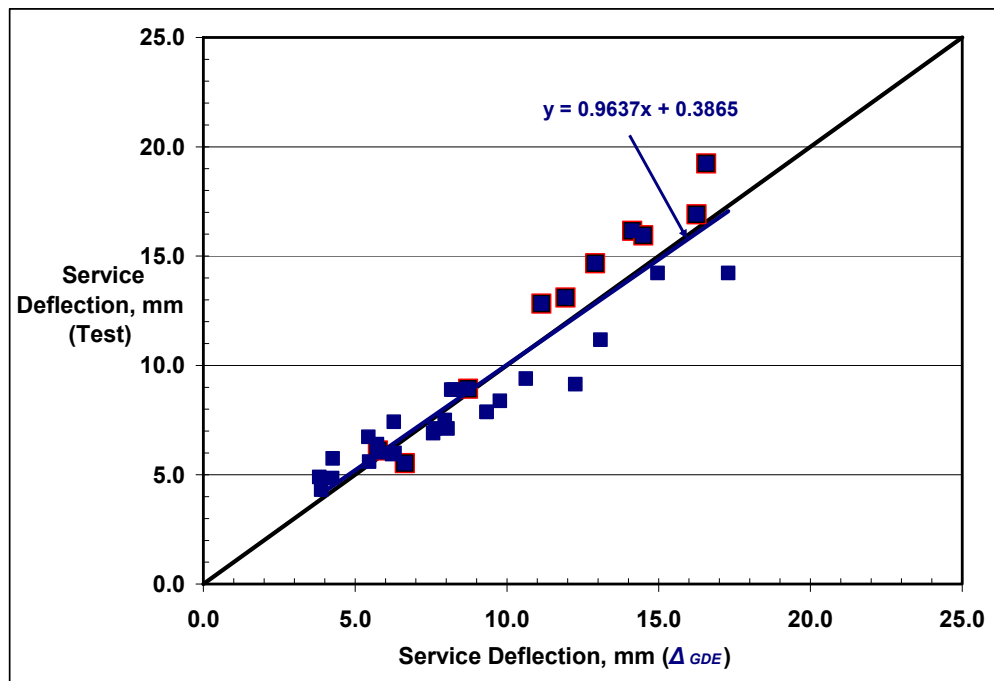
$$\Delta_{SDE} = 1.60 \cdot \Delta_{ITG-6} \quad (7-11)$$

Figure 7-10c shows the comparison between the measured service deflections against the corresponding predicted values using the simplified deflection design equation (7-11), for the beams in Table 7-2. Similar to the general deflection design equation (7-9), the simplified deflection equation (7-11) results in deflection predictions that agree reasonably well with the test results.

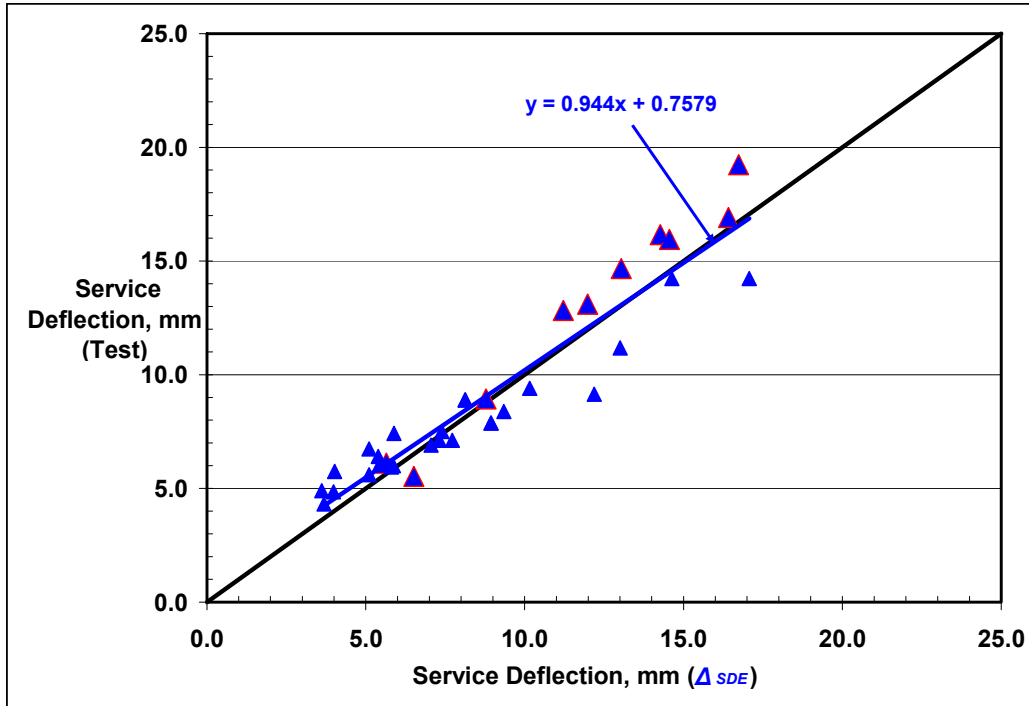
Table 7-6 compares the measured service deflections of the beam specimens (Δ_{TEST}) containing ASTM A1035 steel, with the corresponding predictions from the general deflection design equation and simplified deflection design equation (7-10 & 7-11). The general deflection design equation (7-10) results in slightly better prediction quality compared to the simplified deflection design equation (7-11). The average test to model service deflection ratios were 1.02 and 1.06 and coefficients of variation (COVs) of 0.14 and 0.15, respectively. These values are close to the results obtained using the rigorous analytical MCFT based deflection model (average ratio = 1.04 and COV = 0.14) described in Section 7.4 and shown in Table 7-4. This suggests that the simplified deflection design equation (7-11) can be used to predict the service deflection of beams with ASTM A1035 steel thereby avoiding the tedious calculations in the analytical approach. Furthermore, the proposed simplified deflection design equation (7-11) can be used for a quick calculation of the service deflection of beams with ASTM A1035 steel reinforcement.



a) ITG-6 Service Deflection



b) General Service Deflection



c) Simplified Service Deflection

Figure 7-10: Validation of Proposed General and Simplified Deflection Equations.

Table 7-6: Validation of Proposed Beam Deflection Equations (ASTM A1035 Steel).

<i>Beam ID</i>	$P_S = 0.6 P_{max}$ (kN)	Δ_{TEST} (mm)	Δ_{GDE} (mm)	$\Delta_{TEST}/$ Δ_{GDE}	Δ_{SDE} (mm)	$\Delta_{TEST}/$ Δ_{SDE}
<i>RM1</i>	504	6.11	5.75	1.06	5.65	1.08
<i>RM2</i>	574	5.53	6.64	0.83	6.51	0.85
<i>MR1</i>	549	16.91	16.25	1.04	16.42	1.03
<i>MR2</i>	525	14.67	12.91	1.14	13.04	1.13
<i>MR3</i>	665	8.93	8.72	1.02	8.78	1.02
<i>MR4</i>	906	13.10	11.93	1.10	11.98	1.09
<i>MM1</i>	560	19.24	16.57	1.16	16.74	1.15
<i>MM2</i>	574	16.16	14.13	1.14	14.27	1.13
<i>MM3</i>	845	12.83	11.14	1.15	11.22	1.14
<i>MM4</i>	1093	15.95	14.50	1.10	14.56	1.10
<i>C-M-6</i>	231	7.11	7.62	0.93	7.37	0.97
<i>C-M-4</i>	249	7.87	9.40	0.84	8.89	0.88
<i>C-M-3</i>	263	8.38	9.65	0.86	9.40	0.90
<i>M-M-6</i>	245	7.11	8.13	0.88	7.62	0.92
<i>M-M-4</i>	249	7.87	9.40	0.84	8.89	0.88
<i>M-M-3</i>	289	9.40	10.67	0.88	10.16	0.93
<i>G1-M80</i>	320	11.18	12.95	0.85	12.95	0.86
<i>G1-100</i>	294	9.14	12.19	0.75	12.19	0.75
<i>G2-M80</i>	360	8.89	8.38	1.08	8.13	1.09
<i>G2-100</i>	369	8.89	8.13	1.09	8.13	1.09
<i>G3-M80</i>	561	14.22	17.27	0.82	17.02	0.83
<i>G3-100</i>	494	14.22	14.99	0.95	14.73	0.97
<i>F40-1</i>	270	4.90	3.82	1.28	3.62	1.36
<i>F40-3</i>	300	5.75	4.26	1.35	4.02	1.43
<i>F40-5</i>	390	4.85	4.24	1.14	3.98	1.22
<i>F60-1</i>	288	4.32	3.89	1.11	3.68	1.17
<i>F60-2</i>	420	6.40	5.72	1.12	5.39	1.19
<i>F60-3</i>	528	6.73	5.44	1.24	5.10	1.32
<i>F60-4</i>	594	5.94	6.22	0.96	5.81	1.02
<i>F60-5</i>	600	6.00	6.30	0.95	5.87	1.02
<i>F80-1</i>	435	6.03	5.75	1.05	5.42	1.11
<i>F80-2</i>	630	7.42	6.27	1.18	5.89	1.26
<i>F80-3</i>	660	5.60	5.46	1.03	5.10	1.10
<i>F80-4</i>	750	6.90	7.57	0.91	7.06	0.98
<i>F80-5</i>	900	7.50	7.96	0.94	7.39	1.01
AVERAGE				1.02		1.06
STDV				0.14		0.15
COV				0.14		0.15

7.6 Comparison of Deflection Models for Concrete Beams

In this section some of the currently available deflection models from code standards and numerical methods were used for comparison of service deflection predictions. The *ITG-6* model and two numerical models from *Vector 2* and *Response 2000* were used for the comparisons.

7.6.1 Overview of Deflection Models

7.6.1.1 ACI ITG - 6 Deflection Model

The *ACI ITG-6* deflection model, which is based on the *ACI 318-08* code model, provides a direct computation method for deflection control of slender reinforced concrete beams using an effective moment of inertia I_e . Based on the *ITG-6* deflection model the instantaneous deflection of a concrete member subjected to a concentrated load at mid-span can be computed with the well-known relationship:

$$\Delta_i = \frac{PL^3}{48E_c I_e} \quad (7-12)$$

Note that equation 7-12 does not take into account shear deformations. (See Figure 7-2a)

In deflection calculation of reinforced concrete members evaluation of an appropriate modulus of elasticity E_c and moment of inertia I_e for the concrete cross-section is required. The modulus of elasticity E_c of normal-weight concrete was determined from the expressions given by *Popovics*, 1970 and *Carrasquillo et al.*, 1981. (See equation 7-3). *Bischoff* (2005) developed an expression for I_e which accounts for the tension stiffening influence from the longitudinal reinforcement on the effective stiffness. Estimates of member deflection using *Bischoff's* formulation for I_e are in better agreement with test results for lightly reinforced members than those using the I_e formulation originally developed by Branson as described in Section 2.6.2.

For beams using ASTM A1035 longitudinal bars, which may result in lightly reinforced members, *ACI ITG-6R-10* recommends the use of Bischoff's model (equation 7-13). Hence, the Bischoff I_e model given by equation 7-13 was used in the current study for deflection calculations.

$$I_e = \frac{I_{cr}}{1 - \left(1 - \frac{I_{cr}}{I_g}\right) \left(\frac{M_{cr}}{M_a}\right)^2} \leq I_g \quad (7-13)$$

In equation 7-12, M_a is the maximum characteristic moment under the load considered; M_{cr} is the cracking moment; I_g is the moment of inertia of the gross section about the centroidal axis, neglecting the reinforcement and I_{cr} is the cracked moment of inertia of a singly reinforced section, given by equation 7-14.

$$I_{cr} = \frac{1}{3} b_w \cdot (kd)^3 + n \cdot A_s \cdot (d - kd)^2 \quad (7-14)$$

$$k = \sqrt{2n\rho + (n\rho)^2} - n\rho \quad (7-15)$$

Note that equation 7-13 is mainly developed for evaluation of member deflection for singly reinforced sections, such as slabs. In the case of beams, which are usually doubly reinforced, it can be important to account for the influence of the compression reinforcement in the evaluation of I_e . Hence, in the current study the modified effective moment of inertia, I_{el} is used for beams with compression reinforcement.

$$I_{el} = I_e + (n-1) \cdot A_s' \cdot (kd - d_2)^2 \quad (7-16)$$

where A_s' is the area of longitudinal compression reinforcement and d_2 is the distance from the extreme concrete fiber in compression to the centroid of the compression reinforcement.

According to ACI 318-08 on which the ITG-6 deflection model was based, the cracking moment for normal weight concrete, M_{cr} , is related to the modulus of rupture $f_r = 0.623\sqrt{f_c}$ MPa and the gross section properties through the expression:

$$M_{cr} = \frac{\gamma_{cr} f_r I_g}{y_t} \quad (7-17)$$

Parameter γ_{cr} was introduced as a coefficient that accounts for the reduction of the cracking moment due to restrained shrinkage and taken as 0.67 as per the recommendation of Bischoff and Scanlon (2007).

7.6.1.2 *VecTor 2*

VecTor2 (VT2) is a nonlinear finite element program based on the Modified Compression Field Theory (MCFT) for the two-dimensional analysis of planar reinforced concrete structures. As described in Section 2.3, the MCFT is an analytical model for predicting the response of reinforced concrete elements subject to in-plane normal and shear stresses, by considering the cracked concrete as an orthotropic material with smeared, rotating cracks. Program VT2 utilizes an incremental total load, iterative secant stiffness algorithm to produce an efficient and robust nonlinear solution. *VecTor2* can be used to predict the load-deformation response of a variety of reinforced concrete structures exhibiting well-distributed cracking when subjected to short-term static monotonic, cyclic and reverse cyclic loading.

In the current study, each member modeled with VT2 was treated as a two-dimensional structure with constant thickness through a rectangular mesh of four-node rectangular elements. Default values of concrete material model (*Popovics*) were utilized in VT2 analysis. Reinforcing steel was modeled as truss bar by lumping all reinforcement at the same level together. Depending on the member geometry, loading conditions and reinforcement configuration, between 630 and 980 elements were used to model the member, within the 1000 element limit for the program version used.

7.6.1.3 Response 2000

The program *Response 2000 (R2K)* uses a layered sectional approach to implement the MCFT relationships for analysis of cracked reinforced concrete members. (See section 2.4) *R2K* can calculate the load-deformation response for beams subjected to combinations of axial load, moment and shear. The assumptions implicit in the program are that plane sections remain plane and that there is no transverse clamping stress across the depth of the beam which are generally regarded as appropriate for sections located a reasonable distance away from load or reaction locations. Input parameters include member geometry, loading, and material properties including the stress-strain relationships for the reinforcement and for the concrete. The stress-strain response of concrete and conventional steel can be selected from different defined models built into the program. For the load-deflection analysis of specimens using *R2K* default values of concrete material model (*Popovics*) were utilized. Only specimens with concentrated loading at mid-span were modeled using this program due to limitations in the program for handling members with non-symmetrical loading.

7.7 Comparison of Model Beam Service Deflections

Tables 7-5 and 7-6 compare the service deflections of beam specimens, grouped by the type of reinforcement used, with the corresponding predictions for the three deflection models described in Section 7.6. For the purpose of comparison, the equivalent service deflection of each beam was determined as the deflection corresponding to the service load which is taken as 60 % of the failure load reported for the particular test. The service deflection from the test Δ_{TEST} , from model predictions and the test-to-model deflection ratios are provided in the Tables for each beam specimen considered.

The *ITG-6* deflection model is observed to be in poor agreement with the test results of beams for each category as shown in Tables 7-5 and 7-6. For beams in group one containing high strength or ASTM A1035 steel reinforcement shown in Table 7-5 the average test-to-model service deflection ratio was 1.69 with a coefficient of variation

(COV) of 0.15. The corresponding values for beams in group 2 that are entirely reinforced with conventional steel reinforcement were 1.53 and 0.25, respectively.

The numerical models *VT2* & *R2K* both of which consider shear deformation as an integral part of their solution approaches generally predicted stiffer responses compared to the test results. However, the predicted service deflection was in better agreement with the test results compared to the *ITG-6* deflection model. The average test-to-model service deflection ratios for beams in group one were 1.48 and 1.35 with COVs of 0.10 and 0.13 for *VT2* and *R2K*, respectively. The corresponding values for beams in group two were 1.43 and 1.38 with COVs of 0.23 and 0.36, respectively.

Figure 7-11 shows the load-deflection response for representative beams reinforced with conventional steel only. Similar plots are shown in Figure 7-12 for the ten new beams with ASTM A1035 steel reinforcement. The load-deflection responses were plotted using the analytical and numerical models (Section 7.6) including the general analytical model developed in Section 7.2) and compared with test results of the beam specimens reported in published articles. Figures 7-11 and 7-12 show the load-deflection responses from each model considered for comparison and the measured responses from test results.

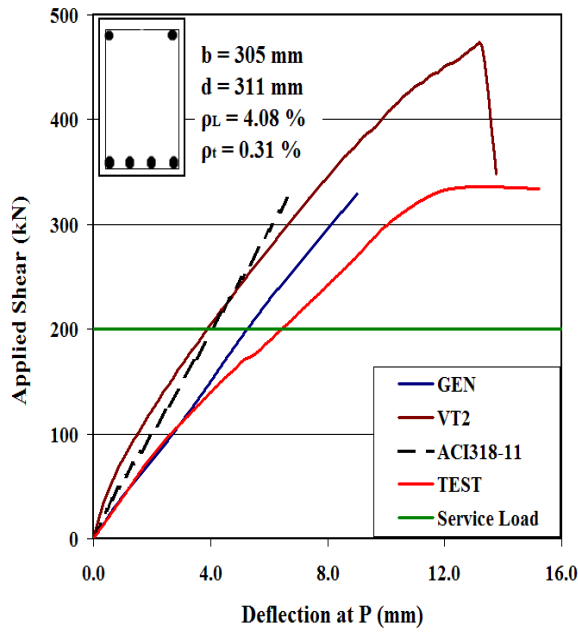
Table 7-7: Deflection Prediction of Beams with High Strength or ASTM A1035 Steel.

<i>Beam ID</i>	Δ_{TEST} (mm)	Δ_{ITG-6} (mm)	$\Delta_{TEST}/$ Δ_{ITG-6}	Δ_{VT2} (mm)	$\Delta_{TEST}/$ Δ_{VT2}	Δ_{R2K} (mm)	$\Delta_{TEST}/$ Δ_{R2K}
<i>RM1</i>	6.11	3.53	1.71	3.85	1.59	4.52	1.35
<i>RM2</i>	5.53	4.07	1.36	4.44	1.25	5.27	1.05
<i>MR1</i>	16.91	10.26	1.77	12.44	1.36	13.29	1.27
<i>MR2</i>	14.67	8.15	1.95	8.03	1.83	9.73	1.51
<i>MR3</i>	8.93	5.49	1.78	5.68	1.57	6.86	1.30
<i>MR4</i>	13.10	7.49	1.88	8.54	1.53	10.14	1.29
<i>MM1</i>	19.24	10.46	1.98	12.48	1.54	14.20	1.35
<i>MM2</i>	16.16	8.92	1.94	9.26	1.75	11.51	1.40
<i>MM3</i>	12.83	7.01	1.91	8.53	1.50	10.50	1.22
<i>MM4</i>	15.95	9.10	1.91	11.55	1.38	13.73	1.16
<i>C-M-6</i>	7.11	4.57	1.56	4.57	1.56	-	-
<i>C-M-4</i>	7.87	5.59	1.41	5.84	1.35	-	-
<i>C-M-3</i>	8.38	5.84	1.43	6.10	1.38	-	-
<i>M-M-6</i>	7.11	4.83	1.47	4.57	1.56	-	-
<i>M-M-4</i>	7.87	5.59	1.41	5.84	1.35	-	-
<i>M-M-3</i>	9.40	6.35	1.48	6.86	1.37	-	-
<i>G1-M80</i>	11.18	8.13	1.38	7.37	1.52	-	-
<i>G1-M100</i>	9.14	7.62	1.20	6.10	1.50	-	-
<i>G2-M80</i>	8.89	5.08	1.75	5.33	1.67	-	-
<i>G2-M100</i>	8.89	5.08	1.75	5.33	1.67	-	-
<i>G3-M80</i>	14.22	10.67	1.33	11.68	1.22	-	-
<i>G3-M100</i>	14.22	9.14	1.56	9.91	1.44	-	-
<i>F40-1</i>	4.90	2.26	2.17	3.04	1.61	3.00	1.63
<i>F40-3</i>	5.75	2.51	2.29	3.30	1.74	3.30	1.74
<i>F40-5</i>	4.85	2.49	1.95	3.42	1.42	3.35	1.45
<i>F60-1</i>	4.32	2.30	1.88	2.91	1.48	3.15	1.37
<i>F60-2</i>	6.40	3.37	1.90	4.44	1.44	4.72	1.36
<i>F60-3</i>	6.73	3.19	2.11	4.32	1.56	4.50	1.50
<i>F60-4</i>	5.94	3.63	1.64	4.71	1.26	4.71	1.26
<i>F60-5</i>	6.00	3.67	1.63	4.68	1.28	4.66	1.29
<i>F80-1</i>	6.03	3.39	1.78	4.33	1.39	3.60	1.68
<i>F80-2</i>	7.42	3.68	2.02	4.98	1.49	5.31	1.40
<i>F80-3</i>	5.60	3.19	1.76	4.18	1.34	4.49	1.25
<i>F80-4</i>	6.90	4.41	1.56	4.53	1.52	6.02	1.15
<i>F80-5</i>	7.50	4.62	1.62	5.86	1.28	6.52	1.15
	AVERAGE		1.69		1.48		1.35
	STDV		0.25		0.15		0.17
	COV		0.15		0.10		0.13

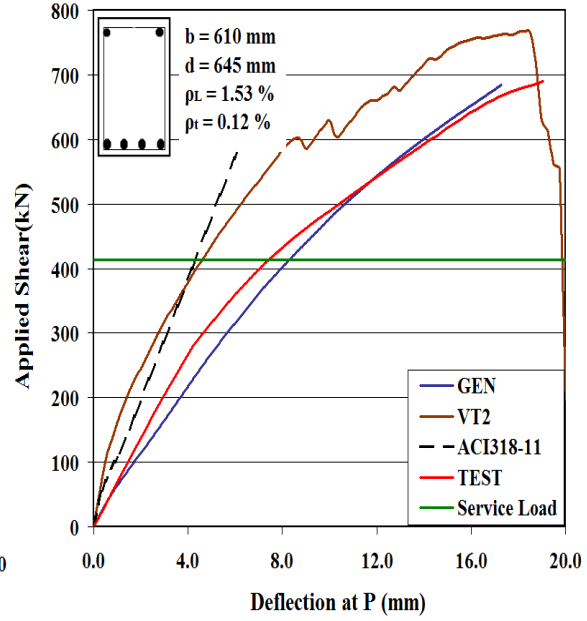
Table 7-8: Deflection Prediction of Beams with Conventional Steel.

<i>Beam ID</i>	Δ_{TEST} (mm)	Δ_{ITG-6} (mm)	$\Delta_{TEST}/$ Δ_{ITG-6}	Δ_{VT2} (mm)	$\Delta_{TEST}/$ Δ_{VT2}	Δ_{R2K} (mm)	$\Delta_{TEST}/$ Δ_{R2K}
<i>C-C-6</i>	7.87	4.57	1.72	4.57	1.72	-	-
<i>C-C-4</i>	6.86	4.57	1.50	4.57	1.50	-	-
<i>C-C-3</i>	8.89	5.84	1.52	6.10	1.46	-	-
<i>G1-C60</i>	11.18	6.60	1.69	5.84	1.91	-	-
<i>G2-C60</i>	7.62	4.32	1.76	4.57	1.67	-	-
<i>G3-C60</i>	13.46	8.64	1.56	9.91	1.36	-	-
<i>F20-1</i>	3.16	1.82	1.74	1.67	1.95	1.29	2.45
<i>F20-2</i>	6.60	3.01	2.19	3.35	1.94	3.05	2.16
<i>F20-3</i>	7.00	3.65	1.92	4.44	1.75	3.95	1.77
<i>F20-4</i>	7.50	3.61	2.08	4.49	1.64	4.52	1.66
<i>F20-5</i>	8.54	4.02	2.12	5.02	1.62	5.16	1.65
<i>ET-1</i>	6.20	5.88	1.05	4.66	1.33	3.51	1.77
<i>H50-2</i>	2.99	2.07	1.44	2.24	1.33	2.63	1.14
<i>H50-3</i>	5.20	2.85	1.82	3.40	1.53	3.95	1.32
<i>VS-A1</i>	7.92	5.68	1.39	5.82	1.36	6.21	1.28
<i>VS-B1</i>	7.75	5.95	1.30	6.46	1.20	6.64	1.17
<i>VS-C1</i>	7.20	6.16	1.17	6.74	1.07	7.61	0.95
<i>BS-A1</i>	4.92	5.28	0.93	5.68	0.87	6.49	0.76
<i>BS-B1</i>	5.13	5.53	0.93	6.18	0.83	6.54	0.78
<i>BS-C1</i>	6.8	6.99	0.97	7.63	0.89	8.07	0.84
<i>E4</i>	5.47	4.07	1.34	4.20	1.30	4.68	1.17
<i>E5-1</i>	5.99	4.15	1.44	4.31	1.39	4.80	1.25
	<i>AVERAGE</i>		1.53		1.43		1.38
	<i>STDV</i>		0.38		0.33		0.49
	<i>COV</i>		0.25		0.23		0.36

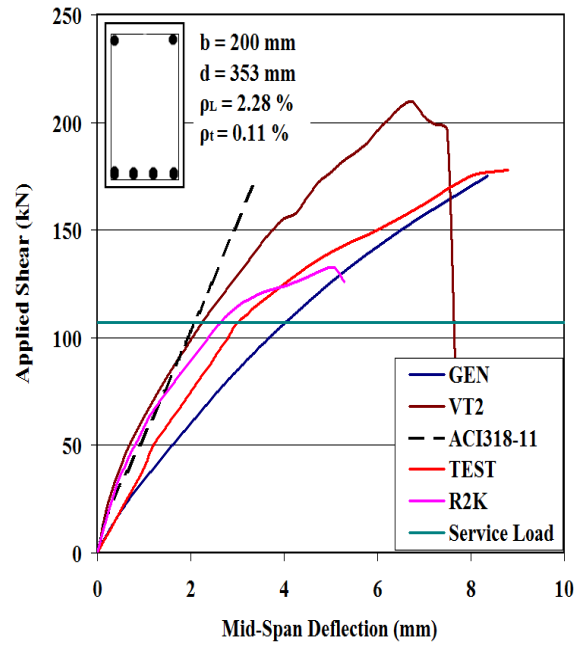
Note: For each specimen the service deflection Δ_{TEST} is the deflection corresponding to service load P_s at 60 % of the failure load.



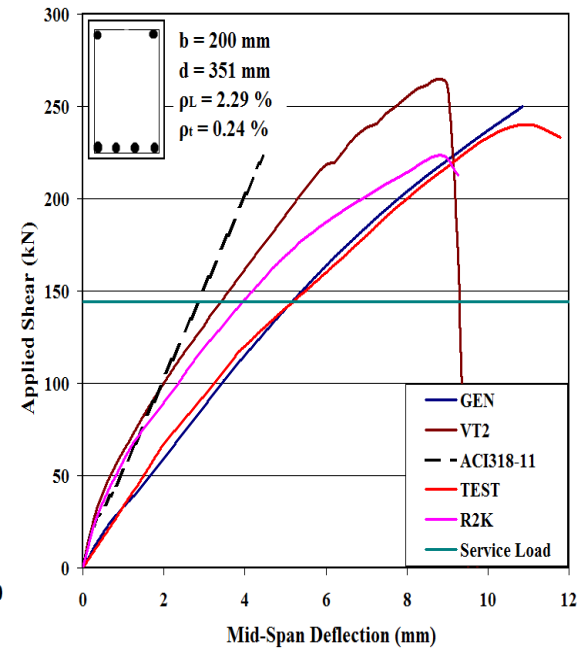
a) Beam - C-C-6



b) Beam - G2-C60

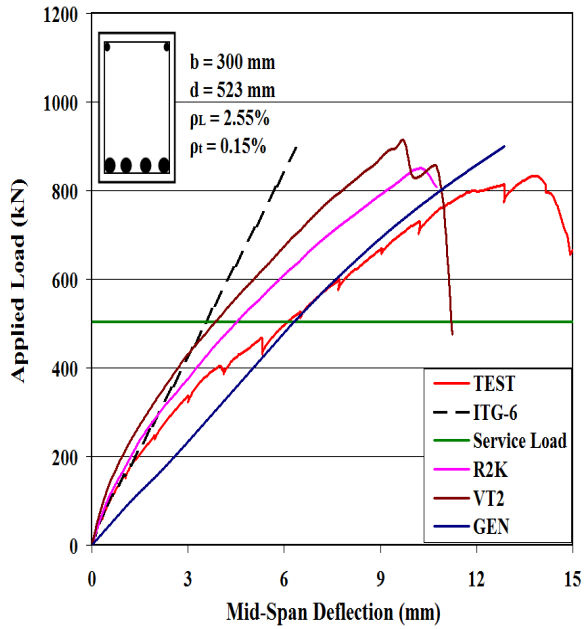


c) Beam - H50-2

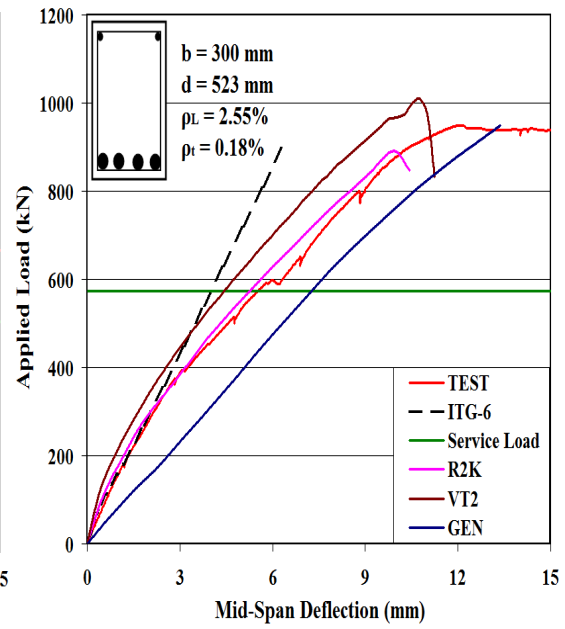


d) Beam - H50-3

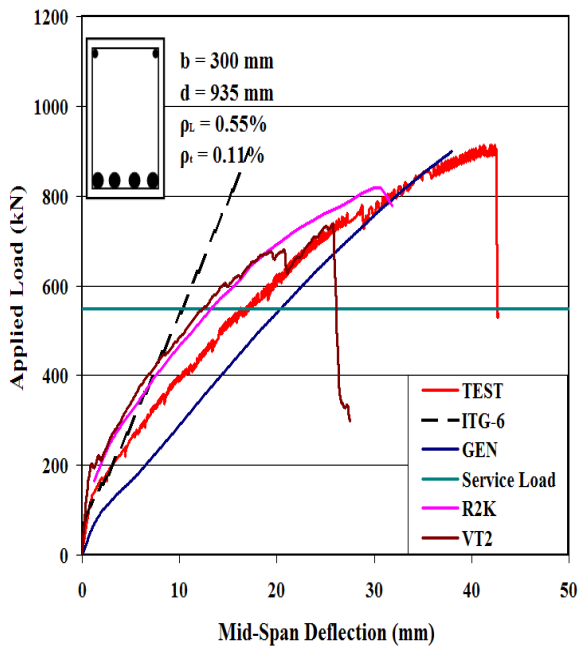
Figure 7-11: Load-Deflection Response of Representative Beams with Conventional Steel Reinforcement.



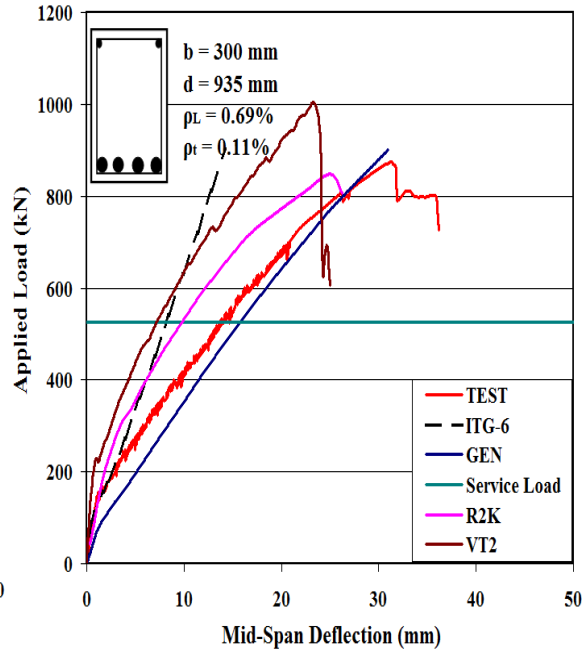
a) Beam - RM1



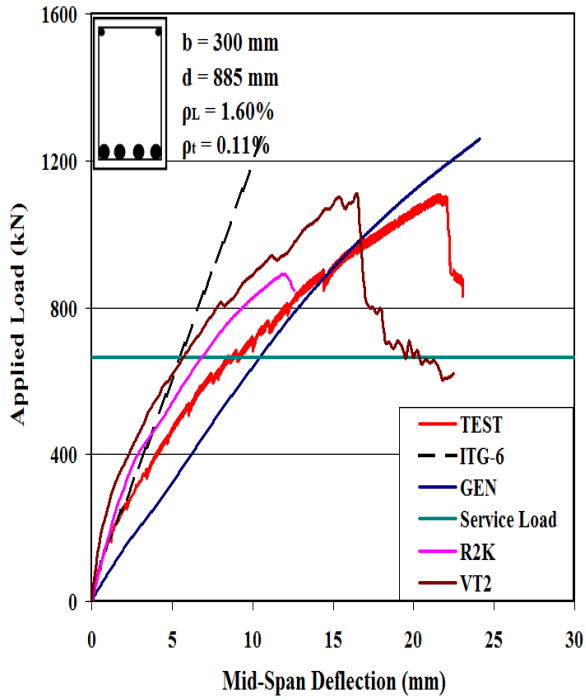
b) Beam - RM2



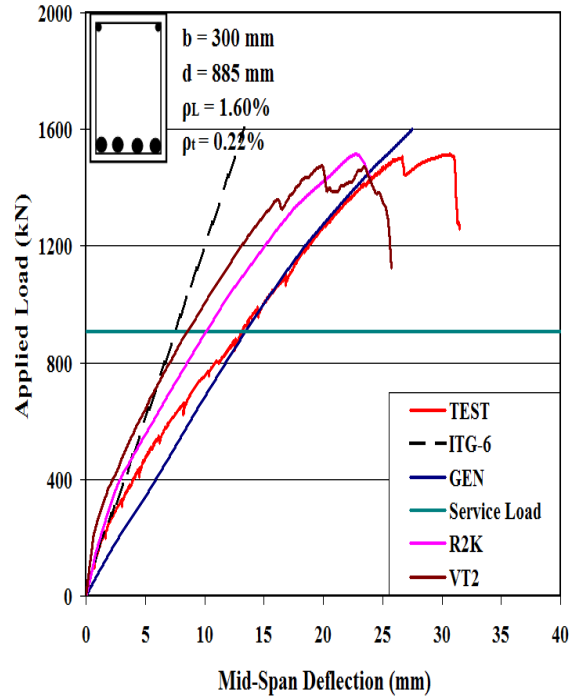
c) Beam - MR1



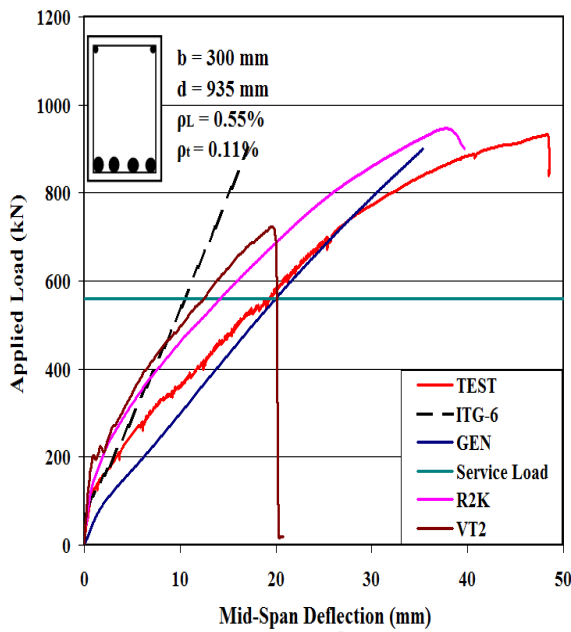
d) Beam - MR2



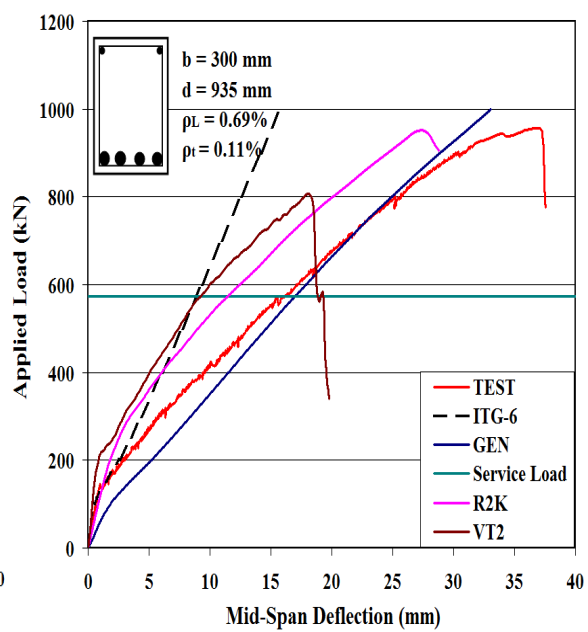
e) Beam - MR3



f) Beam - MR4



g) Beam - MM1



h) Beam - MM2

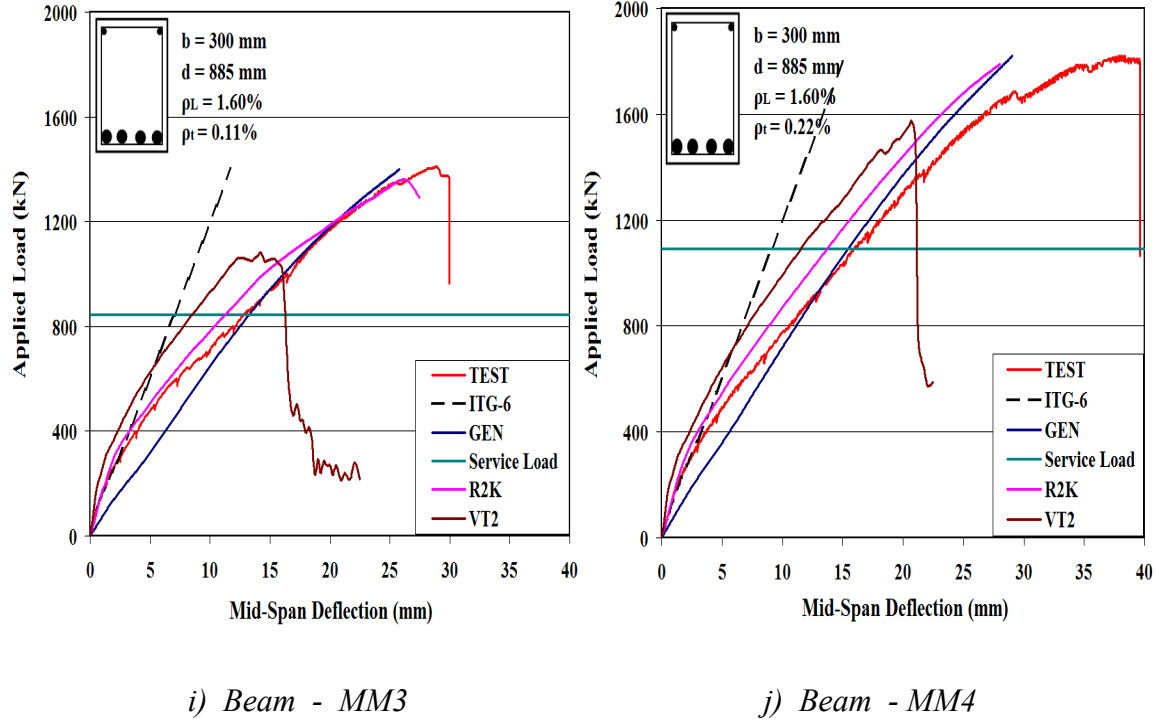


Figure 7-12: Load-Deflection Response of Beams with ASTM A1035 Steel Tested in The Current Study.

The comparison of beam deflection response between the models considered showed that the *ITG-6* model resulted in poor prediction of beam deflections of all beams. The observed load deflection response (Figure 7-11 & 7-12) and the prediction of service deflections (Tables 7-5 & 7-6) suggest that the *ITG-6* model consistently underestimates beam deflections. This is due to the *ITG-6* model which neglects shear deformations that can significantly increase member deflections, especially for lightly reinforced beams containing high strength or ASTM A1035 steel. The numerical models generally predicted stiffer load-deflection response compared to measured response but the results were better than the *ITG-6* model. This is due to some consideration of shear deformations in the MCFT based *VT2* and *R2K* models.

Of all the models considered, the general model developed in Section 7-4 predicted the deflection response of all beams in better agreement with the measured response as shown in Figure 7-11 & 7-12. This is clearly due to the consideration of shear

deformation in addition to the bending deformation as part of the beam deflection calculation. This justified that the general deflection model can be used in prediction of load-deflection response for concrete beams with transverse reinforcement, regardless of the type of steel used in the transverse and longitudinal reinforcement.

7.8 Influence of Design Parameters on Beam Deflection Models

The most important parameters influencing the shear behaviour of beams with transverse reinforcement were identified as the reinforcement configurations: (See Sections 2.2.4, 6.5, 7.5.2 & 7.5.3). It is therefore reasonable to assume that shear deformations are more highly influenced by the reinforcement ratios, than the other parameters for slender concrete beams with shear reinforcement. Hence the transverse reinforcement ratio, ρ_t , and the longitudinal reinforcement ratio, ρ_L , were considered as the most influential parameters to be studied. In addition the influence of overall member depth, h , and the shear span to depth ratio, a/d are also considered to justify previous assumptions on the shear deformations (due to size effect) and range considered for shear span to depth ratios.

For the parametric study all beams in the database grouped by steel reinforcement type were considered based on the general deflection model (Section 7.4), the *ITG-6* model and the numerical models (*VT2* and *R2K*). These models were chosen to be representative of all the analytical and numerical deflection models considered in the current study on deflection of slender concrete beams. The test-to-model deflection prediction ratios for the selected models were plotted against transverse reinforcement ratios as shown in Figure 7-13 for beams containing high strength or ASTM A1035 steel. Figure 7-14 shows similar plots for beams entirely reinforced with conventional steel. A similar analysis was performed in Section 7.5.3 to study the influence of transverse and longitudinal reinforcement ratios on the simplified deflection equation (equation 7-10).

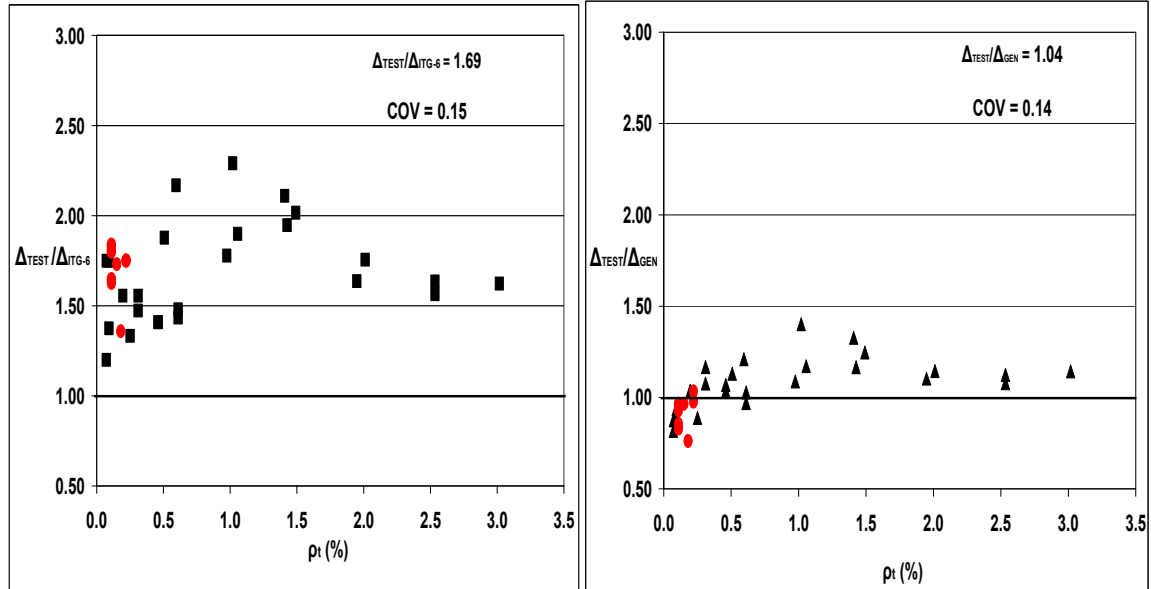
The discrepancy between the measured and calculated deflection is significantly larger at higher transverse reinforcement ratios for the *ITG-6* model than the other models

considered. This behaviour is more pronounced for beams reinforced with conventional steel. (See Figure 7-14). It is observed that the *ITG-6* deflection model can underestimate the service deflection of beams with higher transverse reinforcement ratios. This may be attributed to the expected higher shear deformations that result from more extensive diagonal cracking in beams with higher transverse reinforcement ratios. For beams containing high strength or ASTM A1035 steel the discrepancy between the measured and calculated service deflection becomes smaller when the transverse reinforcement ratio is higher than about 1.5 % for all the models considered for comparison as shown in Figure 7-13. This can be due to the tendency of beams to become flexure critical at higher transverse reinforcement ratios and thereby altering the relationship between ρ_t and P_{max} , making the shear deformations similar at $0.6P_{max}$.

Similarly, when the longitudinal reinforcement ratio becomes lower the discrepancy between the measured and predicted service deflection is in general larger for the *ITG-6* model than the other models for beams with high strength or ASTM A1035 steel. This shows that the *ITG-6* deflection model will underestimate the service deflection of beams with lower longitudinal reinforcement ratios. (See Figure 7-15a) This may be attributed to the expected higher shear deformations that result from higher longitudinal member strains in beams with lower longitudinal reinforcement ratios. When the longitudinal reinforcement ratio for beams containing high strength or ASTM A1035 steel exceeds a certain amount (say 3 %), the discrepancy between the actual and calculated deflection for all models becomes smaller, as shown in Figure 7-15. This can be attributed to the tendency of beam capacities controlled by compression failure at higher longitudinal reinforcement ratios, which can reduce the amount of shear deformation at $0.6P_{max}$.

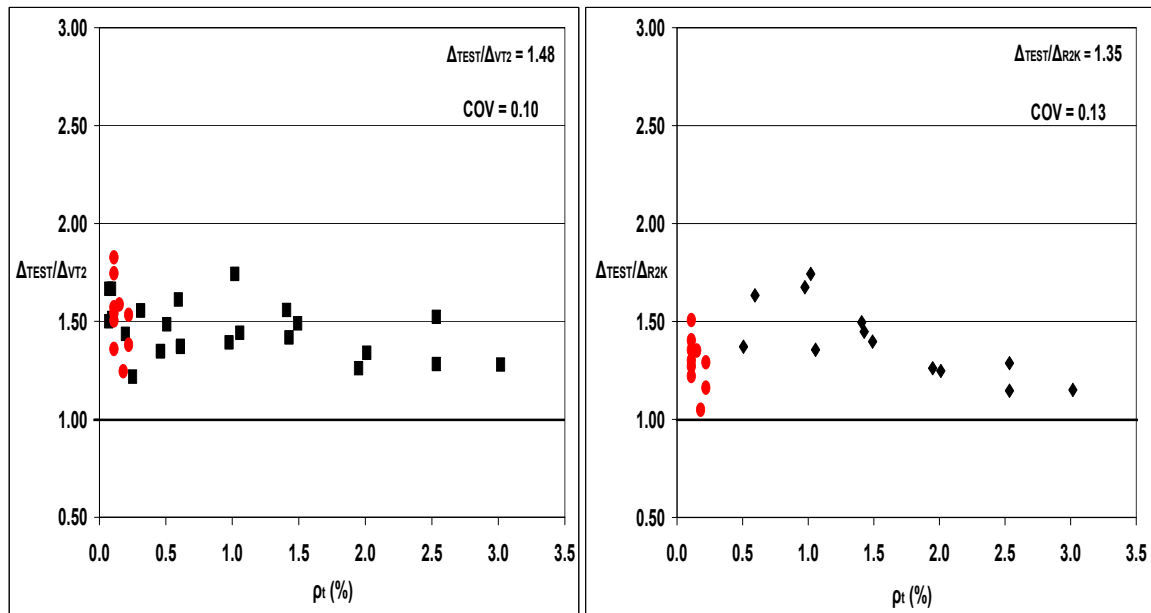
Based on the above analysis the *ITG-6* deflection model is inconsistent in the quality of predictions for the two common design parameters of transverse and longitudinal reinforcement ratios. On the other hand deflection ratios computed using the MCFT-based general models were more consistent in prediction quality with less scatter in the data cloud. The quality of deflection predictions using the numerical models (*VT2* and *R2K*) were better than that of the *ITG-6* deflection model. However, of all the models

predictions using the general model were more accurate and consistent for the wide range of longitudinal and transverse reinforcement ratios considered.



a) *ITG-6 deflection model*

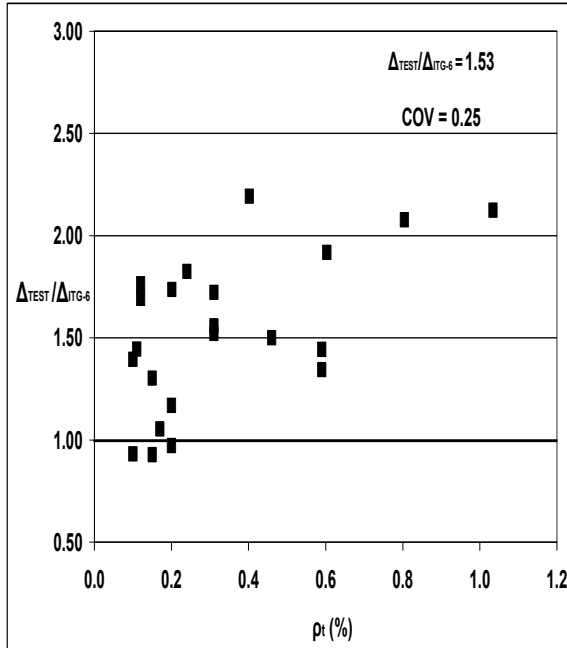
b) *General deflection model*



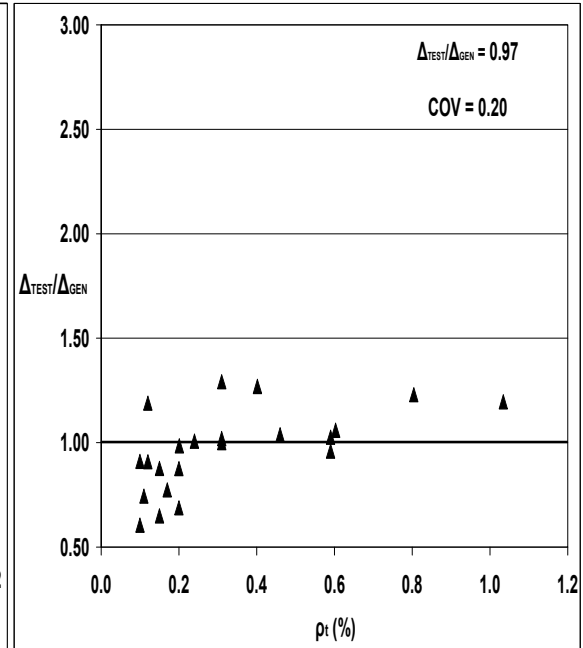
c) *VecTor2*

d) *Response 2000*

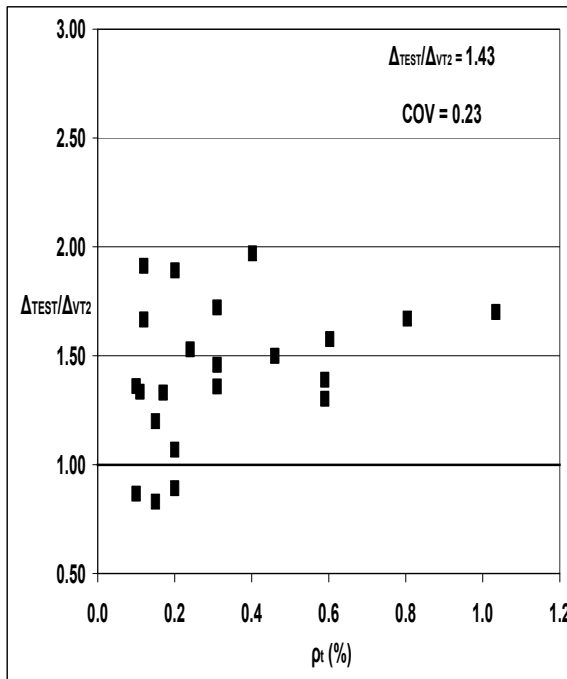
Figure 7-13: Influence of High Strength or ASTM A1035 Steel Transverse Reinforcement Ratio on Model Deflection Prediction.



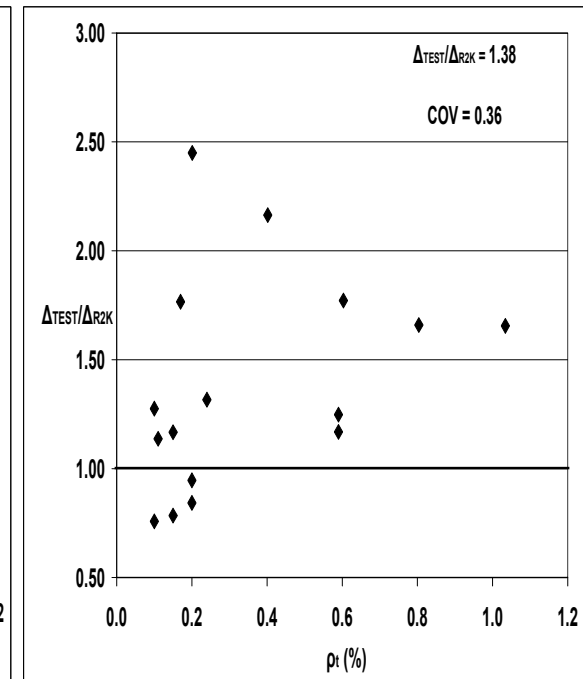
a) *ITG-6 deflection model*



b) *General deflection model*

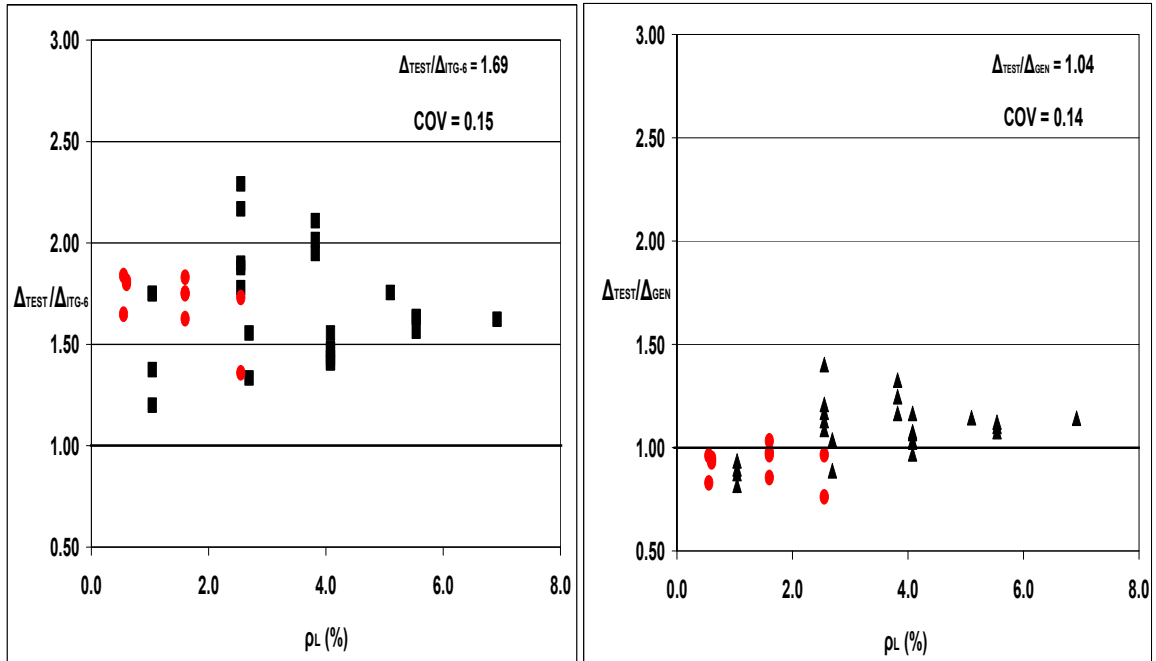


c) *VecTor2*



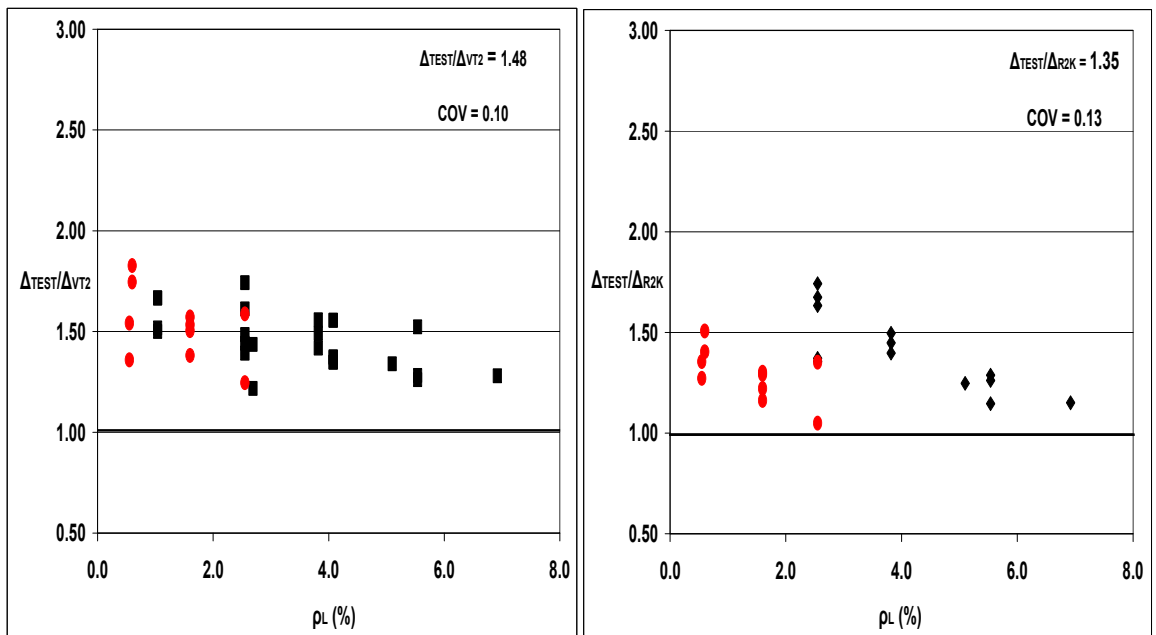
d) *Response 2000*

Figure 7-14: Influence of Conventional Steel Transverse Reinforcement Ratio on Model Deflection Prediction.



a) *ITG-6 deflection model*

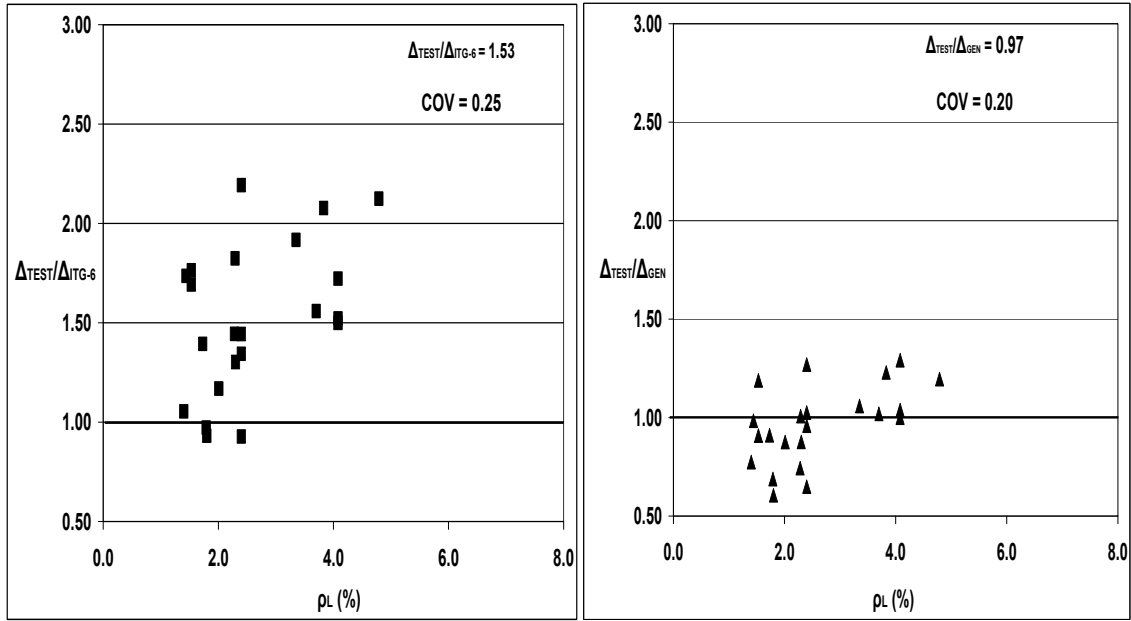
b) *General deflection model*



c) *VecTor2*

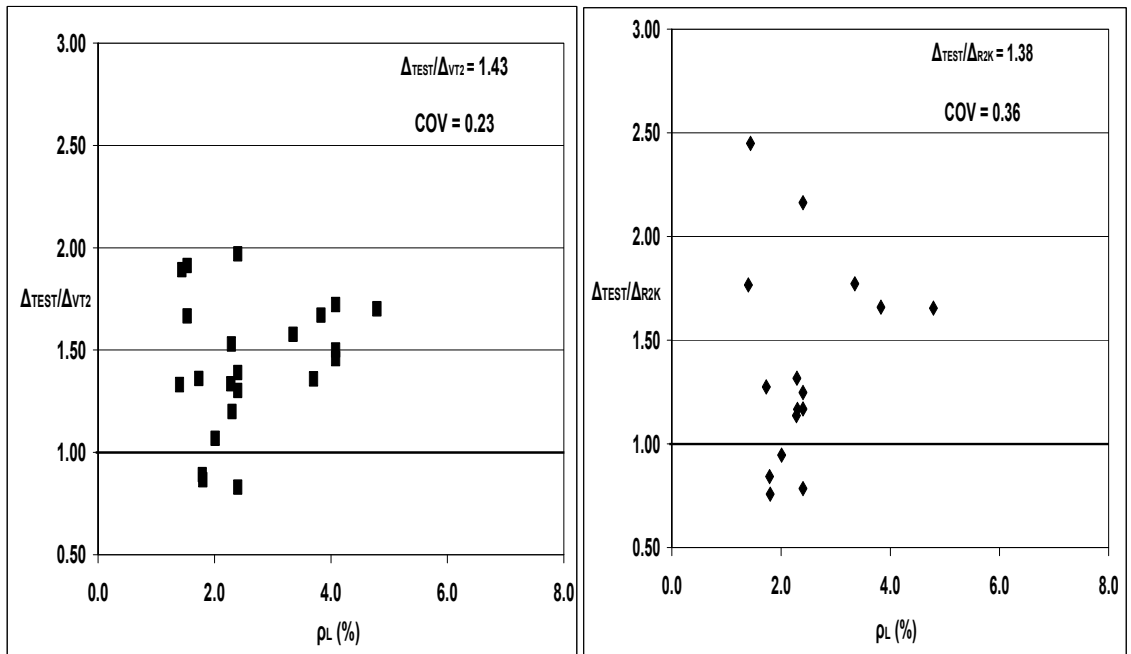
d) *Response 2000*

Figure 7-15: Influence of High Strength or ASTM A1035 Steel Longitudinal Reinforcement Ratio on Model Deflection Prediction.



a) *ITG-6 deflection model*

b) *General deflection model*



c) *VecTor2*

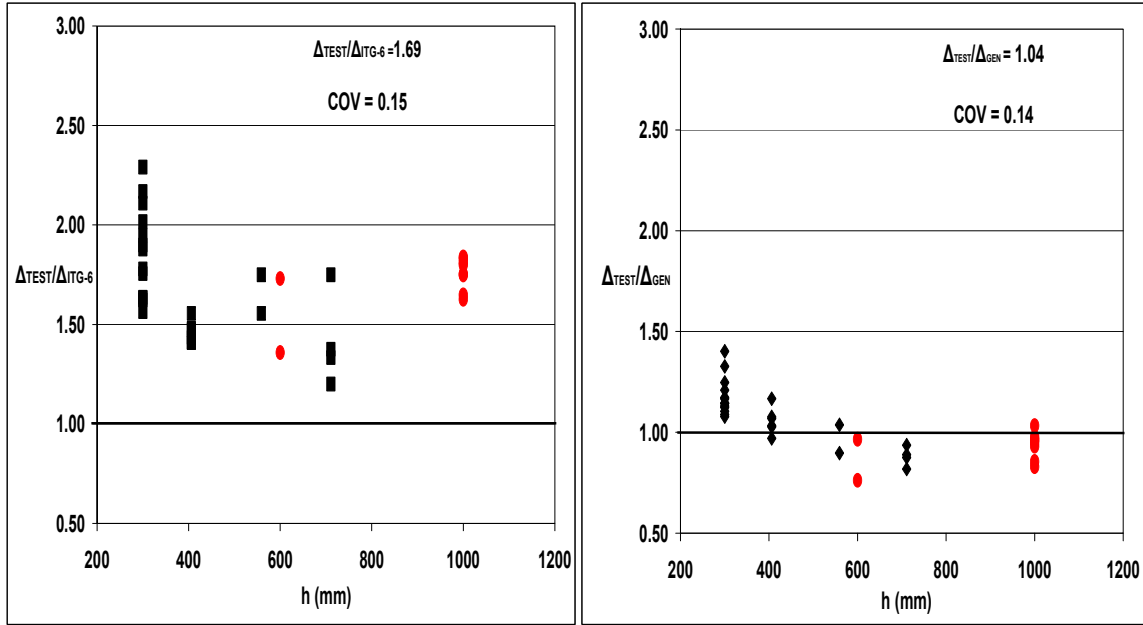
d) *Response 2000*

Figure 7-16: Influence of Conventional Steel Longitudinal Reinforcement Ratio on Model Deflection Prediction.

The influence of member depth is studied using the selected deflection models for all beams in the database grouped by the type of steel reinforcement. As shown in Figures 7-17 and 7-18 member depth has no significant influence on the test to model deflection ratios of all models considered in both beam groups. It can be attributed to the presence of stirrups which control the crack spacing and restrict crack widths of concrete beams thereby reducing the shear deformations (*Bentz and Collins, 2006*).

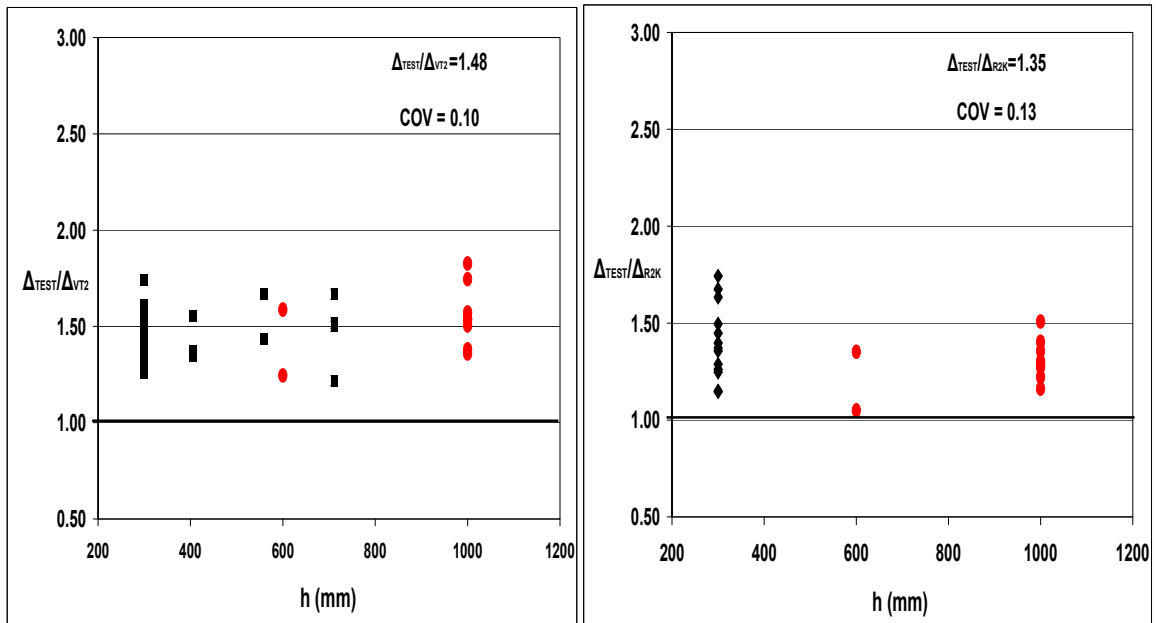
The influence of shear-span to depth ratio (a/d) is also studied using Figures 7-19 and 7-20 for beams in groups one and two, respectively. For beams in group one containing high strength or ASTM A1035 steel a/d has no significant influence on deflection ratios for all models as shown in Figures 7-19. This is due to the beams in this group being more shear critical with a/d values between 2.8 - 3.3. For beams in group two that are entirely reinforced with conventional steel the test to model ratios become lower when a/d is increased. For shear span to depth ratios in the range $3.5 < a/d < 4.0$ the deflection ratios become closer to 1.0 for all the models considered. This is due to the reduced influence on the predictions from the shear deflection relative to the total deflection.

The *ITG-6* deflection model predictions are observed to be lower (i.e. giving high test to prediction ratios) for beams with lower a/d . This justified that the *ITG-6* deflection model which is based only on bending deformations can underestimate the service deflections of shear critical beams. On the other hand deflection predictions computed using the proposed general model were observed to be relatively more accurate for shear critical beams with $a/d < 4.0$. Predictions using the general model tend to be more conservative for a/d values near 4.0. This shows that the proposed general model can overestimate shear deformations for flexure critical beams, as shown from Figure 7-20 b. In the future an expanded dataset for beams with $a/d > 3.0$ can help to establish the limits on the use of the general deflection model.



a) *ITG-6 deflection model*

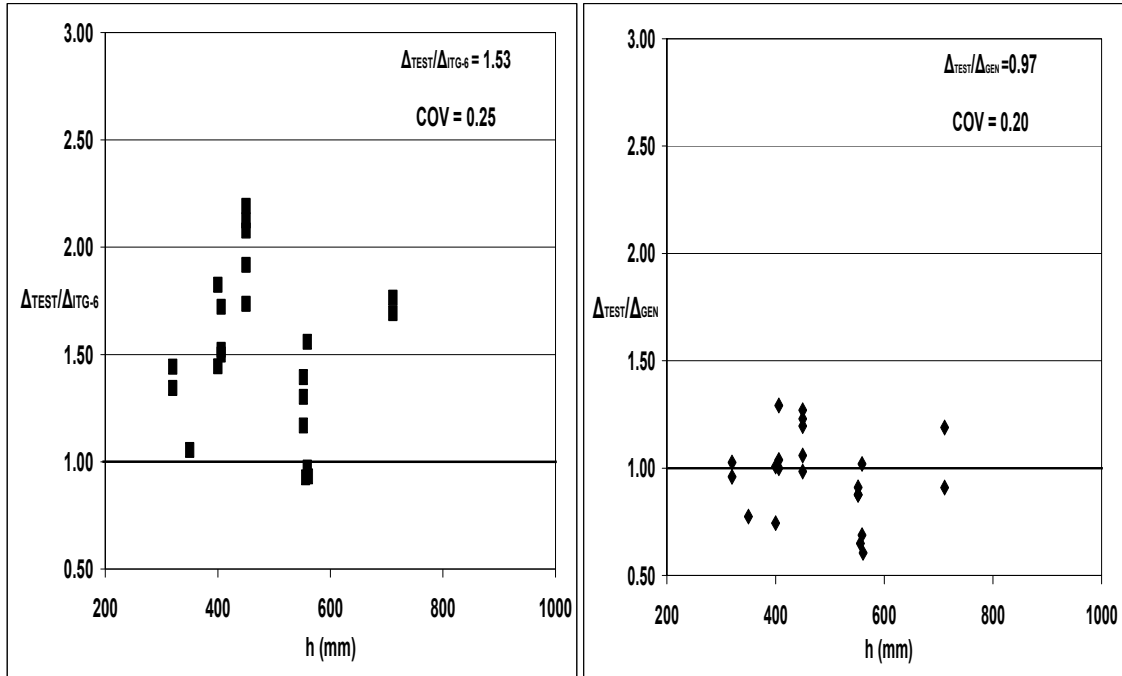
b) *General deflection model*



c) *VecTor2*

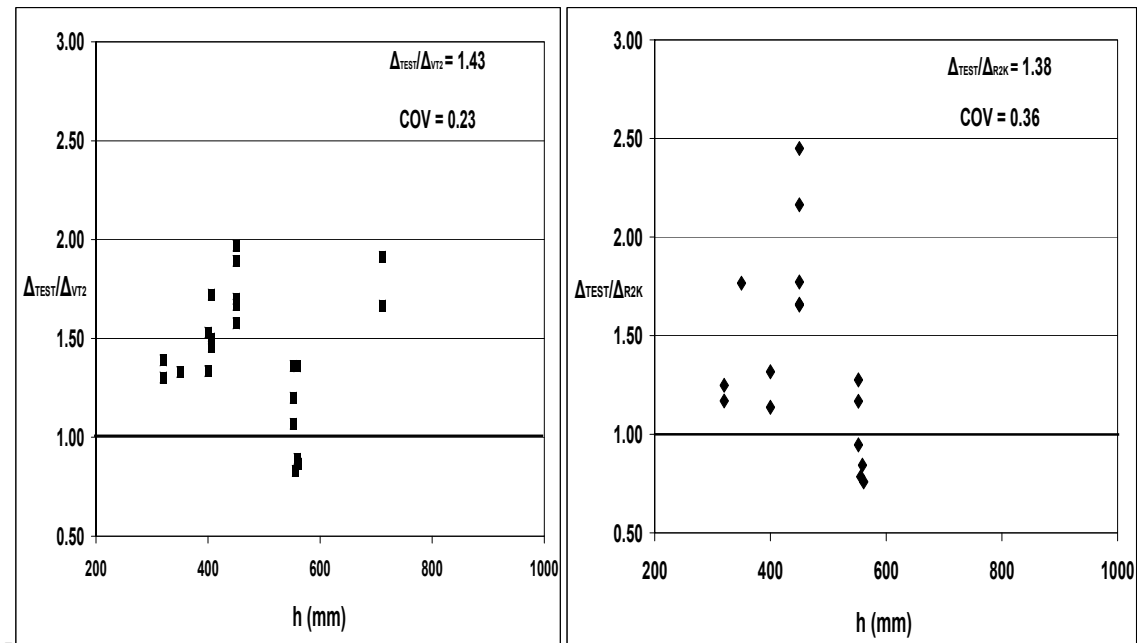
d) *Response 2000*

Figure 7-17: Influence of Member Depth on Model Deflection Prediction (High Strength or ASTM A1035 Steel Reinforced Beams).



a) *ITG-6 deflection model*

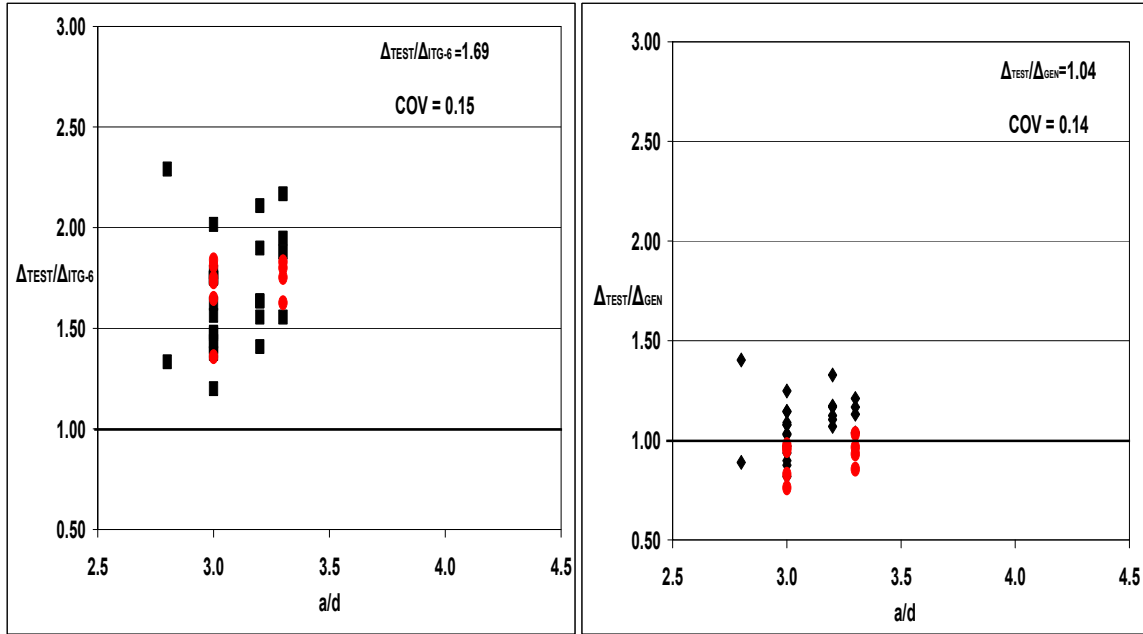
b) *Proposed general deflection model*



c) *VecTor2*

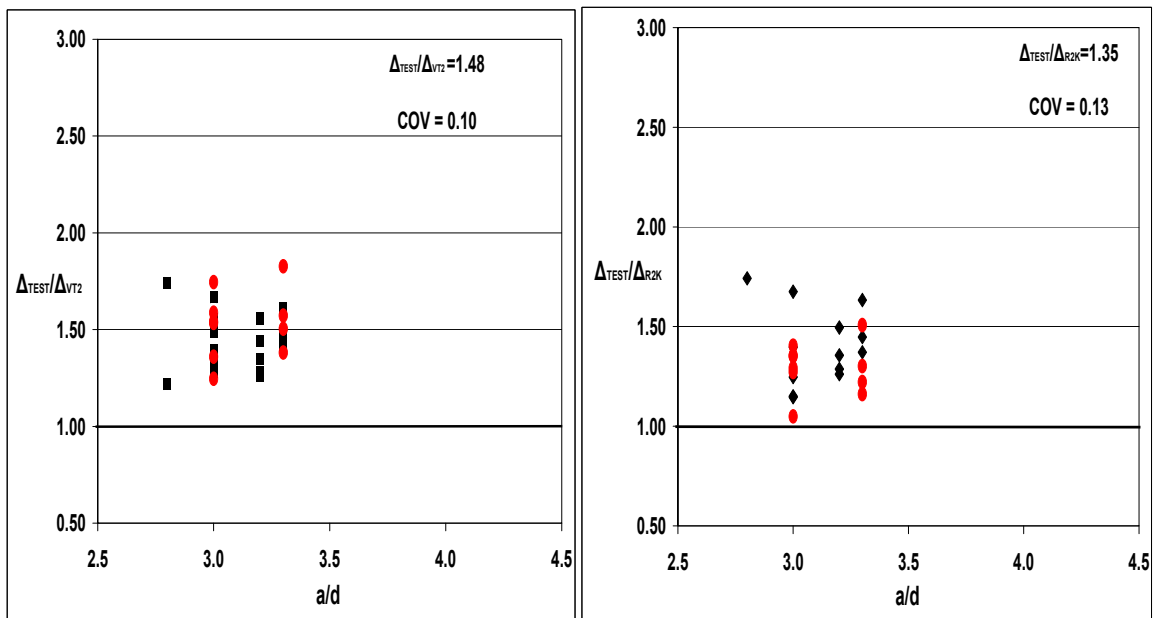
d) *Response 2000*

Figure 7-18: Influence of Member Depth on Model Deflection Prediction (Conventionally Reinforced Beams).



a) *ITG-6 deflection model*

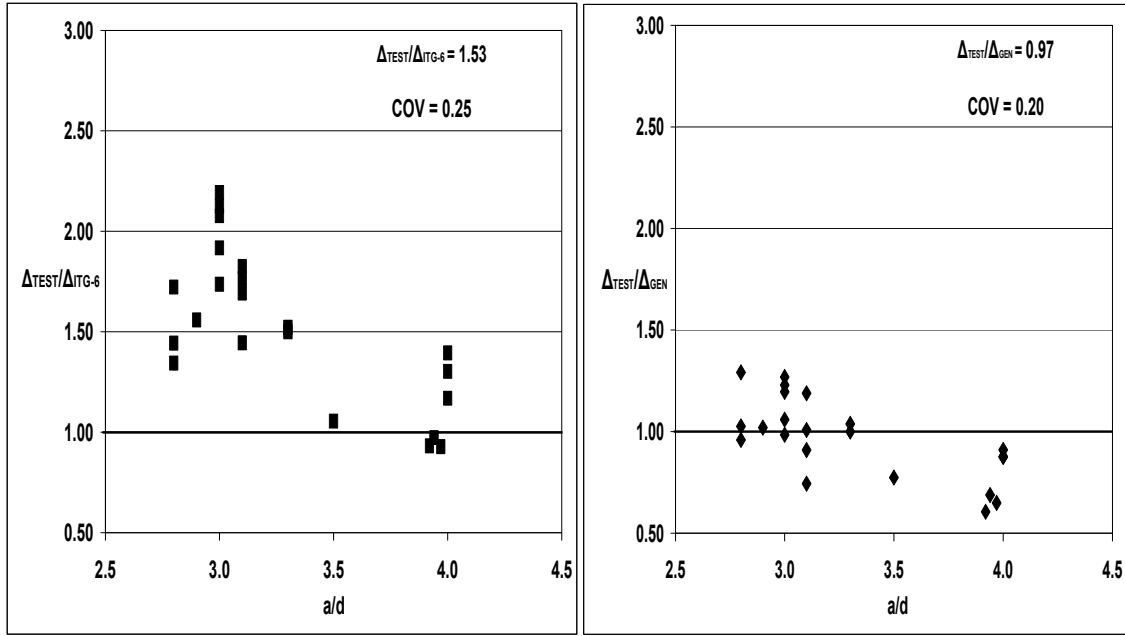
b) *General deflection model*



c) *VecTor2*

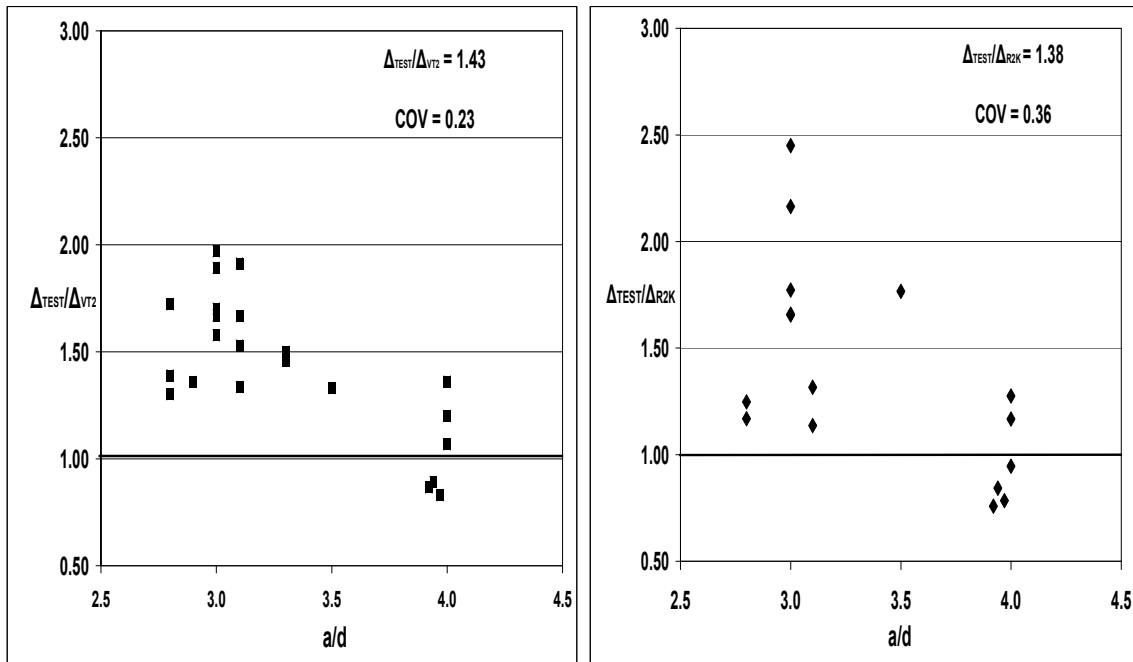
d) *Response 2000*

Figure 7-19: Influence of Shear Span to Depth Ratio on Model Deflection Prediction (High Strength or ASTM A1035 Steel Reinforced Beams).



a) *ITG-6 deflection model*

b) *General deflection model*



c) *VecTor2*

d) *Response 2000*

Figure 7-20: Influence of Shear Span to Depth Ratio on Model Deflection Prediction (Conventionally Reinforced Beams).

7.9 Summary

Using various simplifications and assumptions on the Modified Compression Field Theory (MCFT), rigorous analytical general deflection model was developed by considering both the bending and shear deformations of slender concrete beams with transverse reinforcement. The analytical model was validated using a database of fifty seven beam specimens including the ten new beam tests conducted in the current study, grouped by the type of reinforcement used. The *ITG-6* deflection model and two numerical models (*VT2* and *R2K*) were used to predict the load-deformation response and to evaluate the service deflections of the beam specimens and compare with test results. The comparison of the service deflections of beams in the database were presented for beams in each group. Practical general and simplified deflection equations were developed and proposed for service beam deflection calculations in the design industry.

The *ACI ITG-6* deflection model which neglects shear deformations, predicted the service deflections of beams poorly compared to the other models. This can be attributed to the inadequacy of the models to account for the expected higher shear deformations in shear critical beam specimens. The discrepancy is higher for beams with ASTM A1035 steel reinforcement where higher longitudinal member strains are expected, which can induce - shear deformations. More accurate results were obtained from the proposed general and simplified deflection equations for beams containing high strength or ASTM A1035 steel. This is due to the consideration of shear deformations in prediction of load-deformation response of concrete beams with stirrups. The numerical models (*VT2* and *R2K*), also based on the MCFT, generally show better prediction quality than the *ITG-6* deflection model. Of all the deflection models considered, the general model predicted the deflection response of all beams in better agreement with the measured response due to the consideration of shear deformation in addition to the bending deformation. The general deflection model demonstrated that it can be used in prediction of load-deflection response and service deflection calculation for concrete beams with transverse reinforcement, regardless of the type of steel used in the transverse and longitudinal reinforcement.

The influence the main design parameters (ρ_b , ρ_L , h and a/d) on service deflections were studied from plots of the test-to-predicted service deflection ratios of all beams in the database. The *ITG-6* deflection model and three MCFT based models (the proposed general model, *VT2* and *R2K*) were used for the parametric study. In general the study showed that as both ρ_b , ρ_L and a/d increased the discrepancy between the measured and predicted deflection is reduced for all the deflection models considered. On the other hand the overall member depth, h , had no significant influence on the test to measured deflection ratios. The parametric study showed that the proposed general deflection model exhibited the best results with more consistent and uniform service deflection predictions for the wide range of the parameters considered.

8.0 CONCLUSIONS AND RECOMMENDATIONS

8.1 Summary

This chapter summarizes the research findings of the analytical and experimental programs completed in this study at the University of Alberta. The research undertaken investigated the shear behaviour of concrete slabs and beams containing high performance ASTM A1035 Grade 690 steel reinforcement. ASTM A1035 steel is characterized by a significantly higher strength with enhanced corrosion resistance when compared to conventional Grade 420 steel. Considering the non-linear stress-strain response of ASTM A1035 steel reinforcement in appropriate analysis and design models can lead to significant savings by reducing the material requirements.

In the experimental program, a total of sixteen tests were conducted on large scale rectangular slender concrete members, consisting of six slabs and ten beams. All six slab specimens and eight beam specimens were reinforced with ASTM A1035 longitudinal reinforcement. Two beams contained conventional Grade 420 longitudinal steel reinforcement. The beams were reinforced for shear with either conventional or ASTM A1035 steel. All specimens were tested to failure using a single concentrated load positioned at mid-span, in order to study the shear behaviour. The deflection behaviour of beams with stirrups containing ASTM A1035 steel was also studied using a database of specimens from the current and prior tests. The research focused on development and validation of general analytical and simplified models to predict the shear capacity of concrete slabs and beams reinforced with ASTM A1035 steel. General analytical and simplified deflection models were also developed and validated for prediction of load-deflection response and service deflection of reinforced concrete beams with ASTM A1035 steel reinforcement.

The experimental results conducted in this research program and other published data from prior studies were compared with the analytical predictions from current available shear models. Three code shear models from *CSA A23.3-04*, *ACI 318-11* and *Eurocode 2-04* as well as two numerical models (*VT2* and *R2K*) were used for the comparison.

Comparison of service beam deflections was also made using the *ACI ITG-6* deflection model and the numerical models (*VT2* and *R2K*). Based on the comparison the adequacy of the code provisions and the numerical models for prediction of shear capacity and service deflection of concrete members with ASTM A1035 steel were evaluated.

Based on the experimental and analytical investigations performed on the shear and deflection behaviour concrete members with ASTM A1035 steel several conclusions and recommendations for future work are suggested.

8.2 Conclusions

The following conclusions were made based on the findings and observations from the experimental program and analytical investigations carried out on reinforced concrete slabs and beams tested in the current study and others reported in the literature.

8.2.1 Shear Behaviour of Slab Specimens

- Of the six slab specimens tested in the current study, four specimens with higher reinforcement ratios failed in shear mode with reinforcement strains below that corresponding to the *ACI ITG-6R-10* stress limit of 690 MPa for the ASTM A1035 steel reinforcement. Two specimens with lower reinforcement ratios failed in flexure-shear mode (i.e. shear failure after significant non-linear response of the ASTM A1035 steel). For all specimens the strain levels at the critical section were lower than the tension controlled strain limit of 0.0066 as per *ACI ITG-6R-10*.
- The maximum service crack width was less than 0.4 mm for the slab specimens with higher reinforcement ratios ($\rho_L = 0.45\%$) which is below the suggested maximum crack width of 0.41 mm according to *ACI 318-11*.

- The relationships between shear stress at failure against member depth and longitudinal reinforcement ratios were studied. It was observed that increasing member depth and/or reducing the ASTM A1035 longitudinal reinforcement ratio of slabs decrease the shear stress at failure.
- Based on the *Hoult et al.* (2008) shear capacity model and using a new method to account for the non-linear stress-strain response of ASTM A1035 steel at higher strains, general analytical and simplified design shear models were developed. The simplified design model is intended for use in combination with the *Mast et al.* flexural design model for slabs longitudinally reinforced with ASTM A1035 steel. The models were validated using a database of ten slab specimens from current and prior studies.
- The proposed general and design shear models adequately capture the strain effect and size effect in the shear capacity prediction of all slabs in the database with wide range of reinforcement ratios and member depths.
- The *CSA A23.3-04* shear model can accurately predict the shear capacity of slab specimens, after application of the proposed method to account for the non-linear response of the ASTM A1035 steel reinforcement at the time of failure. The numerical models (*VT2* and *R2K*) can also predict the shear capacity of concrete slabs provided the non-linear response of the ASTM A1035 steel is considered in the analysis.
- The *ACI 318-11* and *Eurocode2-04* expressions for shear capacity of concrete members without web reinforcement resulted in unsafe predictions of shear capacity. The average test to predicted failure loads were 0.72 and 0.89, with coefficients of variation of 45% and 22 %, respectively. Both models do not adequately account for the influences of member depth or reinforcement strains on shear capacity.

- Compared to the other models the *ACI 318-11* shear model significantly underestimates the shear stress at failure for slabs without stirrups. Larger discrepancy was observed as the member thickness increases.
- Of all the shear models considered the best results were obtained using the proposed general shear model which captured the influence of main design parameters with average test-to-model ratios of 1.03 and coefficient of variation of 18%.

8.2.2 Shear Behaviour of Beam Specimens

- From the ten beam specimens tested in the current study, seven specimens failed in shear mode with longitudinal reinforcement strains below that corresponding to the *ACI ITG-6R-10* typical stress limit of 690 MPa for ASTM A1035 steel longitudinal reinforcement. Three specimens failed in flexure-shear mode with observed significant non-linear response of the ASTM A1035 steel longitudinal reinforcement.
- The relationships between shear stress at failure against stirrup spacing, equivalent stirrup ratio and longitudinal reinforcement ratios were studied. The results showed that both the transverse and longitudinal reinforcement configurations significantly influence the shear stress at failure for beams with stirrups containing ASTM A1035 steel.
- General analytical and simplified design shear models for beams containing ASTM A1035 steel were developed and validated using a database of beam specimens from the current and prior tests. The proposed general and design shear models adequately captured the influences from the wide range of transverse and longitudinal reinforcement ratios in the shear capacity prediction of all beams in the database.
- The *ACI ITG-6* and *Eurocode 2-04* shear models showed poor agreement with test results having higher variation compared to the other models. These models may result in too conservative or unconservative shear prediction of reinforced concrete

beams with ASTM A1035 steel. These models do not appropriately account for the influence of higher longitudinal member strain at the time of failure. The discrepancy between the measured and predicted shear is significantly higher than the other models considered resulting in a wide scatter in the data cloud for the *ACI ITG-6* model with increasing reinforcement ratios (ρ_L and ρ_t) and concrete strength, f_c' .

- *CSA A23.3-04* shear model could be used to predict the shear capacity of concrete beams with ASTM A1035 steel reinforcement, after application of a proposed method to account for the non-linear longitudinal reinforcement response at the time of failure. The model demonstrated good agreement with the test results of members with longitudinal ASTM A1035 Grade 690 steel reinforcement for all practical ranges of reinforcement ratio.
- The numerical models (*VT2* and *R2K*) showed better shear prediction quality compared to *ACI ITG-6* and *Eurocode 2-04* shear capacity models for a wide range of longitudinal reinforcement ratios considered. These models can be used to predict shear capacity as they can adequately account for the influences from higher longitudinal member strains near failure loads.
- The shear capacity predictions of all the models considered were shown to be improved by using a higher yield strength of stirrups in calculations ($f_{yt} = 690 \text{ MPa}$) compared to the maximum value recommended in *ACI ITG-6R-10* ($f_{yt} = 550 \text{ MPa}$) for beams containing ASTM A1035 steel transverse reinforcement.
- The best results were obtained using the proposed general shear model which accurately considers the non-linear stress-strain response of the longitudinal ASTM A1035 steel along with $f_{yt} = 690 \text{ MPa}$. Of all the shear models considered the general model exhibited the best results with more consistent shear capacity prediction for all ranges of ρ_L , ρ_t and f_c' considered.

8.2.3 Deflection of Beam Specimens

- Based in part on various simplifications to the Modified Compression Field Theory (MCFT), a rigorous general analytical deflection model was developed that considers both the bending and shear deformations of slender concrete beams with transverse reinforcement. The general deflection model was validated using a database of fifty seven beam specimens from the current study and prior tests.
- Based on parametric studies, general and simplified deflection design equations were developed to predict service deflections for beam specimens containing ASTM A1035 steel reinforcement. The equations were validated against the test results and are shown to be more accurate than the code equations and the numerical models for practical deflection calculations in the design industry.
- The *ACI ITG-6* model and two numerical models (*VT2* and *R2K*) were used to predict the load-deflection response and the service deflections of beams tested in the current study and other published articles.
- The *ACI ITG-6* deflection model was in poor agreement with the test results and may result in poor conformance with SLS requirements of reinforced concrete beams with stirrups. The average test to model service deflection ratio and COV at the equivalent service load were 1.69 and 0.15 for beams containing ASTM A1035 steel and 1.53 and 0.25, respectively, for conventionally reinforced beams.
- The numerical models *VT2* & *R2K* generally predicted stiffer responses than the test results. However, the predicted service deflections were in better agreement with the test results than the *ACI ITG-6* model.
- The influence of the main design parameters (ρ_b , ρ_L , h and a/d) on service deflections were studied using plots of the test-to-predicted service deflection ratios of all beams in the database. The study showed that, in general, as ρ_b , ρ_L or a/d increased the

discrepancy between the measured and predicted deflection was reduced while the overall member depth, h , had no significant influence on the test to predicted deflection ratios.

- Of all the deflection models considered the general analytical deflection model demonstrated the best overall agreement with the test results. The average test to model service deflection ratio at the equivalent service load was 1.04 with a COV of 0.14 for the proposed general analytical deflection equation.

8.3 Recommendations for Future Work

Based on the evaluation of the analytical and experimental test results, there are some issues which are not dealt with in the scope of the current study. Additional studies need to be conducted in order to address these issues. The following recommendations are suggested for future work on the use of ASTM A1035 steel reinforcement in concrete structures:

- In the current study, three slab specimens had higher concrete strength near to the 60 MPa upper limit indicated for the applicable range of the existing *CSA A23.3-04* shear model. For higher concrete compressive strength f'_c , the *CSA A23.3-04* model introduces an adjustment by the aggregate size a_g term. Equation 5-1 predicted the failure load poorly for specimens with higher f'_c compared to those specimens with lower concrete strength. The 60 MPa limit for maximum compressive strength of concrete in the model before an adjustment to a_g should be assessed in the future using additional laboratory tests conducted on the shear behaviour of slabs and beams constructed with ASTM A1035 steel in combination with high-strength concrete.
- The general and simplified design shear models for beams developed in this study were based on yield strengths of $f_{yL} = 690$ MPa and $f_{yt} = 550$ MPa or 690 MPa for the longitudinal and transverse reinforcements, respectively, using a database of beam tests from the current and prior studies. These values are based on the *ACI ITG-6R-10*

guide to make the shear models compatible with the *Mast et. al* simplified flexural model. However, higher effective yield strengths of up to 830 MPa (based on the 0.2% offset method) should be considered for the ASTM A1035 steel as more research is conducted on the behaviour of members containing ASTM A1035 steel reinforcement. These proposed shear models can be further modified and refined when more test data are available to support a modeling approach which uses higher f_{yL} and f_{yt} values.

- In the current study the longitudinal spacing requirements of conventional and ASTM A1035 stirrups for the beam specimens considered were based on the values recommended in the *CSA A23.3-04* and *ACI 318-11* codes. These values are proposed for beams with conventional steel longitudinal and transverse reinforcement. It is recommended to study the spacing requirements of stirrups for beams containing conventional or ASTM A1035 steel longitudinal reinforcement.
- The current study examined that the crack width of beams containing ASTM A1035 steel at serviceability limit state exceeded the limiting value recommended for conventionally reinforced beams. A detailed study on the cracking behaviour of beams with ASTM A1035 steel at serviceability limit state is recommended.
- The scope of the current study was mainly focused on the shear and deflection behaviour of reinforced concrete rectangular members in the building design practice. In the future extensive laboratory tests can be conducted for T and I-sections to study the use of ASTM A1035 steel as longitudinal and shear reinforcement and to explore extended applications including prestressed bridge girders and columns.
- All specimens in this research program were experimentally tested and analytically modelled under a single concentrated load at mid-span using the available test setup in the laboratory. Other loading setups that are more practical to the construction industry, such as UDL and four point loadings, need to be considered to extend the applicability of the current research output.

- Due to the shortage of time and the limited scope of this study, the DIC system was used only to compare the DIC determined load-deflection response of beams specimens with results measured using more traditional instrumentation such as LVDT's. In the future, the data collected by the DIC system can be used to study the crack widths, concrete strains and other deformation characteristics of concrete beams and slabs containing ASTM A1035 steel.
- Due to the limited number of test data assembled for slender beam specimens with conventional steel reinforcement, simplified deflection equations were not developed and validated for these type of beams. However, when more test data are available in the future, similar procedures can be followed to come up with simplified equations as for beams with ASTM A1035 steel.
- More research work is recommended to develop a simplified deflection equations containing the main influencing parameters, such as shear strain, to obtain a generalized deflection equation that is valid for practical ranges of common design parameters.
- The proposed deflection models in the current study were based on a database of shear critical beams. More study is recommended in the future to examine deflection behaviour of flexure critical beams containing ASTM A1035 steel.

References

AASHTO LRFD (2004), “Bridge Design Specifications and Commentary,” third edition, American Association of State and Highway Transportation Officials, Washington, D.C., 1450 pp.

AASHTO LRFD (2007), “Bridge Design Specifications and Commentary,” third edition, American Association of State and Highway Transportation Officials, Washington, DC, 2007, 1463 pp.

ACI-ASCE Committee 426 (1973), “The Shear Strength of Reinforced Concrete Members,” *ACI Journal Proceedings*, 70(7), 471-473.

ACI-ASCE Committee 445 (1999), “Recent Approaches to Shear Design of Structural Concrete,” *Journal of Structural Engineering*, 124(12), 1375-1417.

ACI Committee 318 (2005), “Building Code Requirements for Reinforced Concrete (ACI 318-05) and Commentary ACI 318 R-05,” American Concrete Institute, Detroit, 430 pp.

ACI Committee 318 (2008), “Building Code Requirements for Structural Concrete and Commentary,” American Concrete Institute, Farmington Hills, MI, 465 pp.

ACI Committee 318 (2011), “Building Code Requirements for Structural Concrete and Commentary,” American Concrete Institute, Farmington Hills, MI, 503 pp.

ACI Committee 435 (2003), “Control of Deflection in Concrete Structures (ACI 435R-95),” American Concrete Institute, Farmington Hills, MI., 89 pp.

Ansley, M.H. (2002), “Investigation into the Structural Performance of MMFX Reinforcing,” (www.mmfxsteel.com/technical_resources/Default.asp)

ASTM C39/C39M (2005), “Standard Test Method for Compressive Strength of Cylindrical Concrete Specimens”, ASTM International, West Conshohocken, PA, 7 pp.

ASTM A1035 (2007), “Standard Specification for Deformed and Plain, Low-Carbon, Chromium, Steel Bars for Concrete Reinforcement,” ASTM International, West Conshohocken, PA, 5 pp.

ASTM A1035/ ASTM A1035-11 (2011), “Standard Specification for Deformed and Plain, Low Carbon, Chromium, Steel Bars for Concrete Reinforcement,” ASTM International, West Conshohocken, PA.

ASTM A615-06 (2006), “Standard Specification for Deformed and Plain Carbon-Steel Bars for Concrete Reinforcement,” ASTM International, West Conshohocken, PA, 6 pp.

ASTM A706-08, (2008), “Standard Specification for Low-Alloy Steel Deformed and Plain Bars for Concrete Reinforcement,” ASTM International, West Conshohocken, PA, 6 pp.

ASTM A370-07, “Standard Test Methods and Definitions for Mechanical Testing of Steel Products”, ASTM International, West Conshohocken, PA, 2007, p.47.

Bentz, E.C., Vecchio, F. J., and Collins, M. P. (2006), “The Simplified MCFT for Calculating the Shear Strength of Reinforced Concrete Elements,” *ACI Structural Journal*, 103(4), 614-624.

Bentz, E.C., and Collins, M. P., (2006), “Development of the 2004 CSA A23.3 Shear Provisions for Reinforced Concrete,” *Canadian Journal of Civil Engineering*, V. 33, No. 5, pp. 521-534.

Bentz, E.C., (2006), “Summary of Development and Use of CSA 2004 Shear Design Provisions,” *Advances in Engineering Structures, Mechanics & Construction*, 67–80.

Bentz, E.C. (2000), "Response 2000," accessed Mar. 25, 2009.(<http://www.ecf.utoronto.ca/~bentz/r2k.htm>)

Bentz, E.C., Massam L., and Collins M.P. (2000), "Shear Strength of Concrete Members with FRP Reinforcement," *Journal of Composites for Construction, ASCE*, 10.1061/(ASCE) CC.1943-5614.0000108, No. 2, pp. 637-646.

Bischoff, P.H. (2005), "A Rational Proposal for Predicting Beam Deflection," In Proceedings of the 33rd Annual Conference of the Canadian Society for Civil Engineering, Toronto, Ontario, Canada, 2005a, June, GC-299-1/10.

Bischoff, P.H., and Scanlon, A. (2009), "Span-Depth Ratios for One-Way Members Based on ACI 318 Deflection Limits," *ACI Structural Journal*, V. 106, No. 5, pp.617-626.

Bischoff, P.H. (2005), "Re-evaluation of Deflection Prediction for Concrete Beams Reinforced with Steel and Fiber Reinforced Polymer Bars," *Journal of Structural Engineering*, ASCE, 131(5):, pp 752-767.

Bischoff, P.H., and Scanlon, A., (2007), "Effective Moment of Inertia for Calculating Deflections of Concrete Members Containing Steel Reinforcement and Fiber-Reinforced Polymer Reinforcement," *ACI Structural Journal*, 104(1): pp. 68-75.

Branson, D.E. (1977), "Deformation of Concrete Structures," McGraw Hill, Toronto, ON, 546 pp.

Bresler B, Scordelis A.C. (1963), "Shear Strength of Reinforced Concrete Beams," *Journal of American Concrete Institute*; 60(1), pp. 51–72.

Carrasquillo, R.L., Nilson A.H., and Slate, F.O., (1981), "Properties of High Strength Concrete Subject to Short Term Loads," *ACI Journal*, Vol. 78, No. 3, pp. 171-178.

CEN, Eurocode 2 (EN1992-1-1) (2004), "Design of Concrete Structures - Part 1-1: General Rules and Rules for Buildings," *European Committee for Standardization*, Brussels, 225 pp.

Collins, M.P., and Kuchma, D. (1999), "How Safe are Our Large, Lightly Reinforced Concrete Beams, Slabs, and Footings?" *ACI Structural Journal*, 96(4), pp. 482-490.

Collins, M.P., and Mitchell, D., (1978), "Towards a Rational Theory for RC Members in Shear," *Proceedings*, ASCE, V. 104, ST4, Apr. 1987, pp. 396-408.

Collins, M.P., and Mitchell, D., (1997), "Prestressed Concrete Structures", Response Publications, Toronto, ON, Canada, 766 pp.

Collins, M.P., and Kuchma, D. (1999), "How Safe Are Our Large, Lightly-Reinforced Concrete Beams, Slabs and Footings?" *ACI Structural Journal*, 96(4), pp. 482-490.

Correlated Solutions Inc. (2009). Vic-Snap 2009 and Vic-3D 2009 [computer software]. Available from <http://www.correlatedsolutions.com/support>.

Correlated Solutions Inc. (2010). Vic-3D 2010 Testing Guide. Retrieved from <http://www.correlatedsolutions.com/support>.

CSA Committee A23.3 (2004), "Design of Concrete Structures," *Canadian Standards Association*, Mississauga, ON, 214 pp.

CSA S6-06 (2006), "Canadian Highway Bridge Design Code," *Canadian Standard Association*, Rexdale, ON, 733 pp.

Darwin, D., Browning, J., O'Reilly, M., Xing, L., and Ji, J., (2009), "Critical Chloride Threshold of Galvanized Reinforcing Bars," *ACI Materials Journal*, V. 106, No. 2, March , pp. 176-183.

Darwin, D., Browning, J., Nguyen, T. V., and Locke, C. Jr. (2002), "Mechanical and Corrosion Properties of a High-Strength, High Chromium Reinforcing Steel for Concrete," Report No. SD2001-05-F, South Dakota Department of Transportation, 142 pp.

Desalegne, A.S. and Lubell, A.S. (2010), "Shear Behaviour of Concrete Slabs Longitudinally Reinforced with High-Performance Steel," *ACI Structural Journal*, V. 107, No. 2, pp. 228-236.

Desalegne, A.S. and Lubell, A.S. (2012), "Deflection Control of Concrete Slabs Longitudinally Reinforced with ASTM A1035/A1035M-07 Steel," *ACI Structural Journal*, V. 109, No. 6, pp. 867-877.

El-Hacha, R.; and Rizkalla, S. (2002), "Fundamental Material Properties of MMFX Steel Bars", NCSU-CFL Report 02-04, Raleigh, NC, 60 pp.

Fenwick, R.C., and Paulay, T. (1968), "Mechanisms of Shear Resistance of Concrete Beams," *Journal of the Structural Division*, ASCE, V. 94, No. ST10, pp. 2235-2350.

Garay-Moran, J.D.; and Lubell, A.S. (2009), "Behaviour of Deep Beams Containing High-Strength Longitudinal Reinforcement," submitted to *ACI Structural Journal*.

Gilbert, I., (2007), "Tension Stiffening in Lightly Reinforced Concrete Slabs", *Journal of Structural Engineering*, ASCE, **133**(6): pp. 899-903.

Hassan, T.K.; Seliem, H.M.; Dwairi, H.; Rizkalla, S.H.; and Zia, P. (2008), "Shear Behaviour of Concrete Beams Reinforced with High-Strength Steel," *ACI Structural Journal*, V. 105, No. 2, pp. 173-179.

Hibbeler, R.C. (2012), "Structural Analysis", 8th edition, Pearson Prentice Hall, New Jersey, USA, 695 pp.

Hoult, N.A.; Sherwood, E. G.; Bentz, E. C.; and Collins, M. P., (2008), "Does the Use of FRP Reinforcement Change the One-Way Shear Behaviour of Reinforced Concrete Slabs?" *Journal of Composites for Construction*, ASCE, V. 12, No. 2, pp. 125-133.

Kani, G. N. J., (1966), "Basic Facts Concerning Shear Failure," *ACI Journal Proceedings*, 63(6), pp. 675-692.

Kani, G. N. J., (1967), "How Safe Are Our Large Concrete Beams?," *ACI Journal Proceedings*, 64(3), pp. 128-141.

Kani, M. W., Huggins, M. W., and Wittkopp, R. R., (1979), "Kani on Shear in Reinforced Concrete", *University of Toronto Press*, 225 pp.

Lee J.Y.; and Hwang H.B. (2010), "Maximum Shear Reinforcement of Reinforced Concrete Beams," *ACI Structural Journal*, V. 107, No. 5, pp.580-588.

Leonhardt F.; and Walther R., "The Stuttgart Shear Tests, Contributions to the Treatment of the Problems of Shear in Reinforced Concrete Construction – A Translation of the Articles that Appeared in 'Beton-und Stahlbetonbau'," *Cement and Concrete Association*, 52 Grosvenor Gardens London SW1, V. 56 , No. 12, 1961, V. 57, Nos. 2, 3, 6, 7 and 8, 1962, Number 111, 134 pp.

Lubell, A., Sherwood, T., Bentz, E. C., and Collins, M. P. (2004), "Safe Shear Design of Large, Wide Beams," *Concrete International*, 26(1), 66-78.

Lubell, A.S. (2006), "Shear in Wide Reinforced Concrete Members," *Ph.D. Dissertation*, Civil Engineering, University of Toronto, Toronto, Ontario, May 455 pp.

Lubell, A. S.; Bentz, E. C.; and Collins, M. P., (2009), "Influence of Longitudinal Reinforcement on One-Way Shear in Slabs and Wide Beams," *Journal of Structural Engineering*, ASCE, V. 135, No. 1, pp. 78-87.

Lepage, A.; Tavallali, H.; Pujol, S.; and Rutenberg, J. (2008), "Towards Earthquake-Resistant Concrete Structures with Ultra High-Strength Steel Reinforcement," *Proceedings of the 14th World Conference on Earthquake Engineering*, Beijing, China, Oct. 12-17, 8 pp.

Mast, R.F.; Dawood, M.; Sami H.; Rizkalla, S.H.; and Zia, P., (2008), "Flexural Strength Design of Concrete Beams Reinforced with High-Strength Steel Bars," *ACI Structural Journal*, V. 104, No. 4, pp. 570-577.

Mohamed Z., Tamon U., Zhimin W., and Liang M., (2009), "Experimental Investigation on Shear Cracking Behaviour in Reinforced Concrete Beams with Shear Reinforcement," *Journal of Advanced Concrete Technology, Japan Concrete Institute*, Vol. 7, No. 1, pp.79-96.

Mohr S.; Bairán J.M.; and Marí A. R., (2010), "A Frame Element Model for the Analysis of Reinforced Concrete Structures Under Shear and Bending," *Engineering Structures*, doi: 10.1016/j.engstruct.2010.09.005.

Mörsch, E. (1920), "Der Eisenbetonbau-Seine Theorie und Anwendung (Reinforced Concrete Construction - Theory and Application)", 5th Ed., Wittwer, Stuttgart, Vol. 1, Part 1.

Munikrishna A., Hosny A., Rizkalla S., and Zia P., (2011), "Behaviour of Concrete Beams Reinforced with ASTM A1035 Grade 100 Stirrups under Shear," *ACI Structural Journal*, 108 (1), pp.34-41.

Navarro-Gregori J.; Miguel P.F.; Fernandez M.A.; and Marti-Vergas J.R, (2013), "A Theoretical Model for Including the Effect of Monotonic Shear Loading in the Analysis of Reinforced Concrete Beams," *Engineering Structures*, 52, pp.257-272.

Popovics S., (1970),"A Review of Stress-Strain Relationships for Concrete," *ACI Structural Journal*, Vol. 67, No. 3, (2), pp. 243-248.

Rajagopalan, K.S., and Ferguson, P.M. (1968), "Exploratory Shear Tests Emphasizing Percentage of Longitudinal Reinforcement", *Journal of the American Concrete Institute*, **65**(8): 634–638.

Ramsay, R.; Mirza, S. A.; and MacGregor, J. G. (1979), "Monte Carlo Study of Short Time Deflections of Reinforced Concrete Beams," *ACI JOURNAL, Proceedings V. 76*, No. 8, pp. 897-918.

Ritter, W. (1899), "Die Bauweise Hennebique (Construction Techniques of Hennebique)," *Schweizerische Bauzeitung*, Zürich, Vol. 33, No. 7, pp. 59-61.

Seliem, H. M. A. (2003), "Behavior of Concrete Bridges Reinforced with High-Performance Steel Reinforcing Bars, doctoral dissertation, North Carolina State University, Raleigh, NC, 287 pp.

(www.lib.ncsu.edu/theses/available/etd-05042007-174633/unrestricted/etd.pdf)

Shahrooz, B.M.; Miller, R.A.; Harries, K.A.; Russell, H.G. (2011),"Design of Concrete Structures Using High-Strength Steel Reinforcement," Transportation Research Board of the National Academies, Washington, D.C., Report 679 MI., 72 pp.

Sherwood, E.G. (2008), "One-Way Shear Behaviour of Large, Lightly-Reinforced Concrete Beams and Slabs," *Ph.D. Dissertation*, Civil Engineering, University of Toronto, Toronto, Ontario, 332 pp.

Sherwood, E. G., Bentz, E. C., and Collins, M. P. (2007), "Effect of Aggregate Size on Beam-Shear Strength of Thick Slabs," *ACI Structural Journal*, 104 (2), pp. 180-190.

Sherwood, E. G.; Lubell, A. S.; Bentz, E. C.; and Collins, M. P. (2006), "One-Way Shear Strength of Thick Slabs and Wide Beams," *ACI Structural Journal*, V. 103, No. 6, Nov.-Dec. 2006, pp. 794-802.

Shioya, T., Iguro, M., Nojiri, Y., Akiyama, H., and Okada, T. (1989), "Shear Strength of Large Reinforced Concrete Beams," *Fracture Mechanics: Application to Concrete*, ACI SP-118, *American Concrete Institute*, pp. 259-279.

Stanik, B.A. (1998), "The Influence of Concrete Strength, Distribution of Longitudinal Reinforcement, Amount of Transverse Reinforcement and Member Size on Shear Strength of Reinforced Concrete Members," *Master's Thesis*, Civil Engineering, University of Toronto, Toronto, Ontario, 711 pp.

Sumpter, M.S.; Rizkalla, S.H.; and Zia, P. (2009), "Behaviour of high-Performance Steel as Shear Reinforcement for Concrete Beams," *ACI Structural Journal*, 106 (2), pp. 171-177.

Tang, J., and Lubell, A.S. (2008), "Influence of Longitudinal Reinforcement Strength on One-Way Slab deflection," *Canadian Journal of Civil Engineering*, doi: 10.1139/L08-050, pp. 1076-1087.

Taylor, H.P.J. (1970), "Investigation of Forces Carried across Cracks in Reinforced Concrete Beams by Interlock of Aggregates," TRA 42.447, Cement and Concrete Association, London, 22 pp.

Vecchio, F. J. and Collins, M. P. (1986), "The Modified Compression-Field Theory for Reinforced Concrete Elements Subjected to Shear," *ACI Journal Proceedings*, 83(2), 219-231.

Vecchio, F. J. and Collins, M. P. (1993), "Compression Response of Cracked Reinforced Concrete," *Journal of Structural Engineering*, ASCE, 119(12), 3590-3610.

Vecchio, F.J., Lai, D., Shim, W., and Ng, J. (2001), "Disturbed Stress Field Model for Reinforced Concrete: Validation," *ASCE Journal of Structural Engineering*, **127**(4): 350–358.

Vecchio F.J., Shim W. (2004), "Experimental and Analytical Re-examination of Classic Concrete Beam Tests", *Journal of Structural Engineering*;130(3):460–9.

Vecchio, F.J., (1990), "VecTor 2," accessed Mar. 25, 2009. (<http://www.civ.utoronto.ca/vector>)

Walraven, J. C. (1981), "Fundamental Analysis of Aggregate Interlock," *ASCE Journal of Structural Engineering*, 107(11), 2245-2270.

Wight, J.K. and MacGregor, J.G. (2009), "Reinforced Concrete: Mechanics and Design (5th edition), Pearson Prentice Hall, Upper Saddle River, New Jersey.

Yotakhong, P. (2003), "Flexural Performance of MMFX Reinforcing Rebars in Concrete Structures," master's thesis, North Carolina State University, Raleigh, NC, 162pp.

Zia, P.; Lubell, A.S.; Ghosh, S.K.; Lepage, A.; Luttrell, K.A.; Mast. R.F.; Paulson, C.; Russell, H.G.; and Sanders, J.C. (2010), "Design Guide for the Use of ASTM A1035/A1035M Grade 100 (690) Steel Bars for Structural Concrete," *American Concrete Institute*, Farmington Hills, MI., 94 pp.

APPENDIX A: LABORATORY TEST RESULTS

A.1 Slab Specimens

A.1.1 Material Tests



Figure A-1: Typical Compression Test of Concrete Cylinder.

Table A-1: Compression Test Results at the Day of Test of Slab Specimens.

<i>Cylinder ID</i>	<i>Slab Specimens</i>					
	<i>S-1</i>	<i>S-2</i>	<i>S-3</i>	<i>S-4</i>	<i>S-5</i>	<i>S-6</i>
<i>1</i>	54	57	50	57	54	57
<i>2</i>	52	59	51	54	52	54
<i>3</i>	53	60	47	59	53	59
<i>Average f'_c (MPa)</i>	53	59	49	57	53	57
<i>COV</i>	0.019	0.026	0.042	0.044	0.019	0.044
<i>Age (days)</i>	92	92	75	51	92	51



Figure A-2: Typical Tension Coupon Test of ASTM A1035 Steel Rebars.

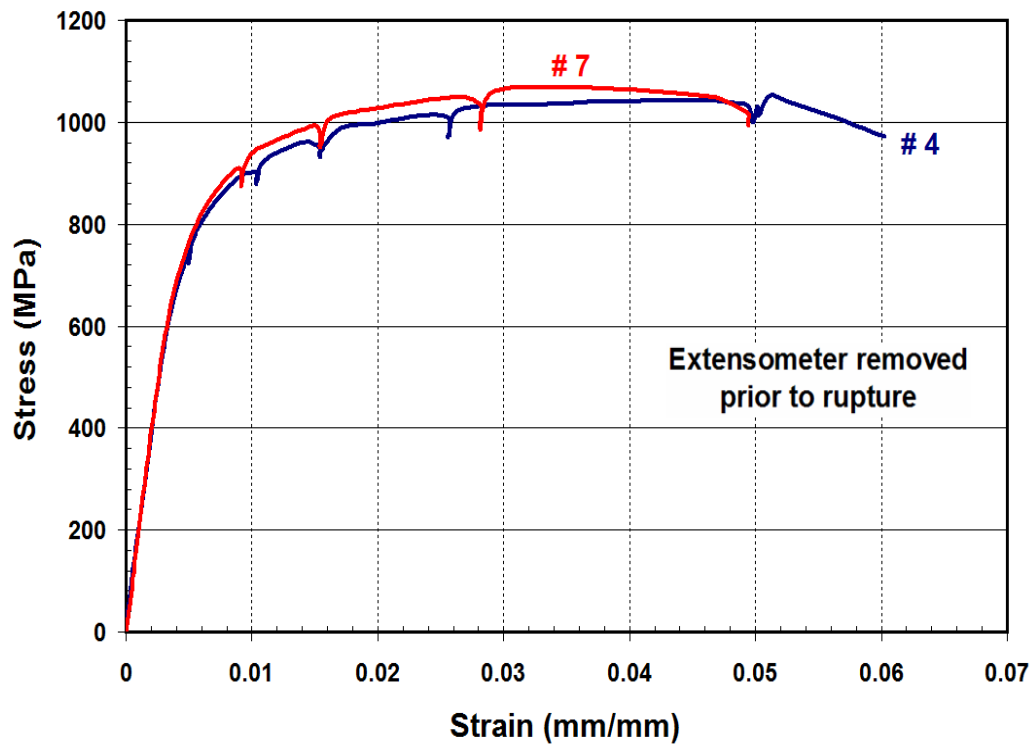
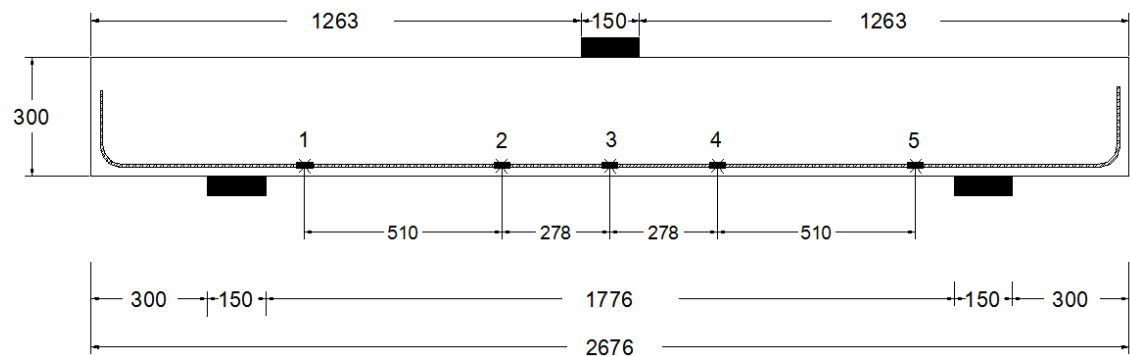


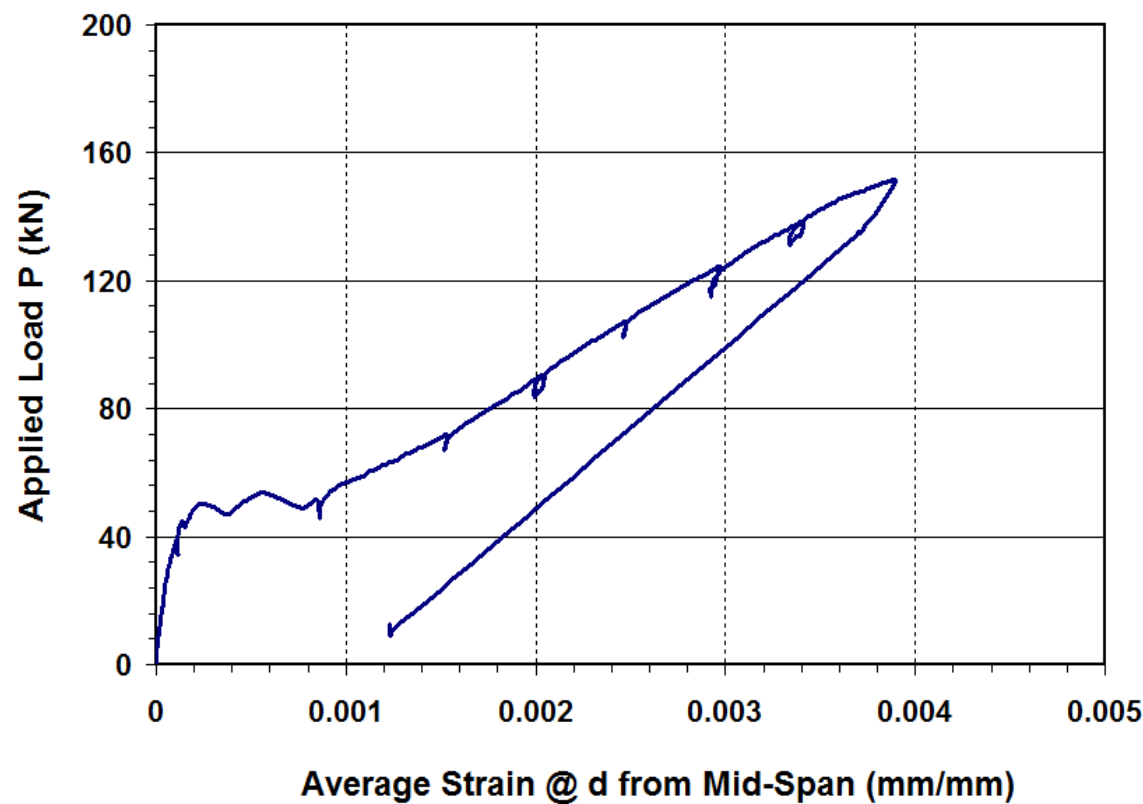
Figure A-3: Average Tension Stress-Strain Response for ASTM A1035 Coupons.

A.1.2 Structural Tests

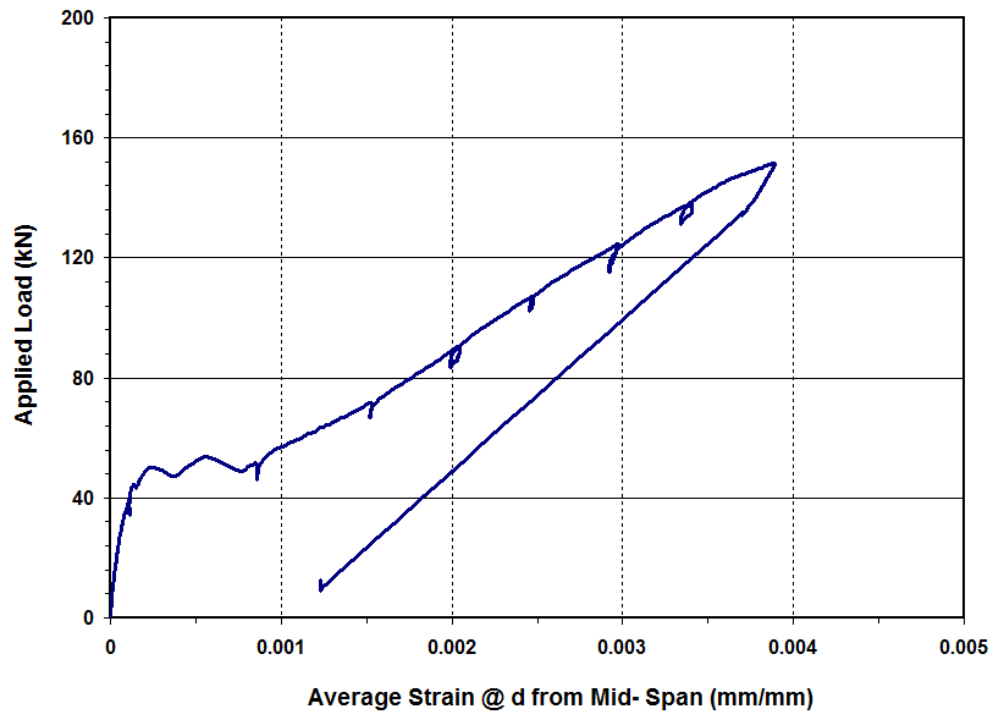
Specimen S-1



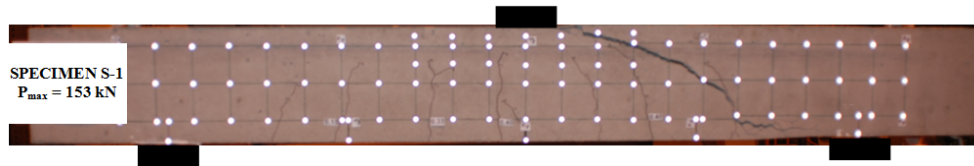
a) Elevation



b) Load - Mid-Span Deflection Response



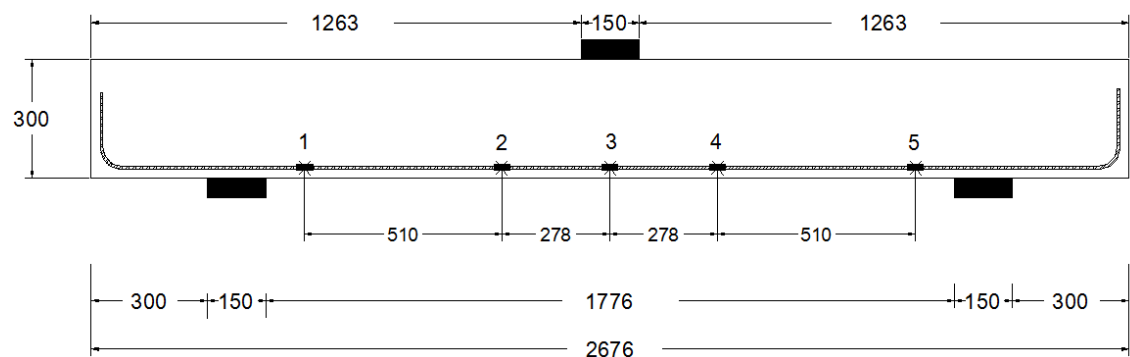
c) Typical Load - Average Steel Strain Response (@ d from mid-span)



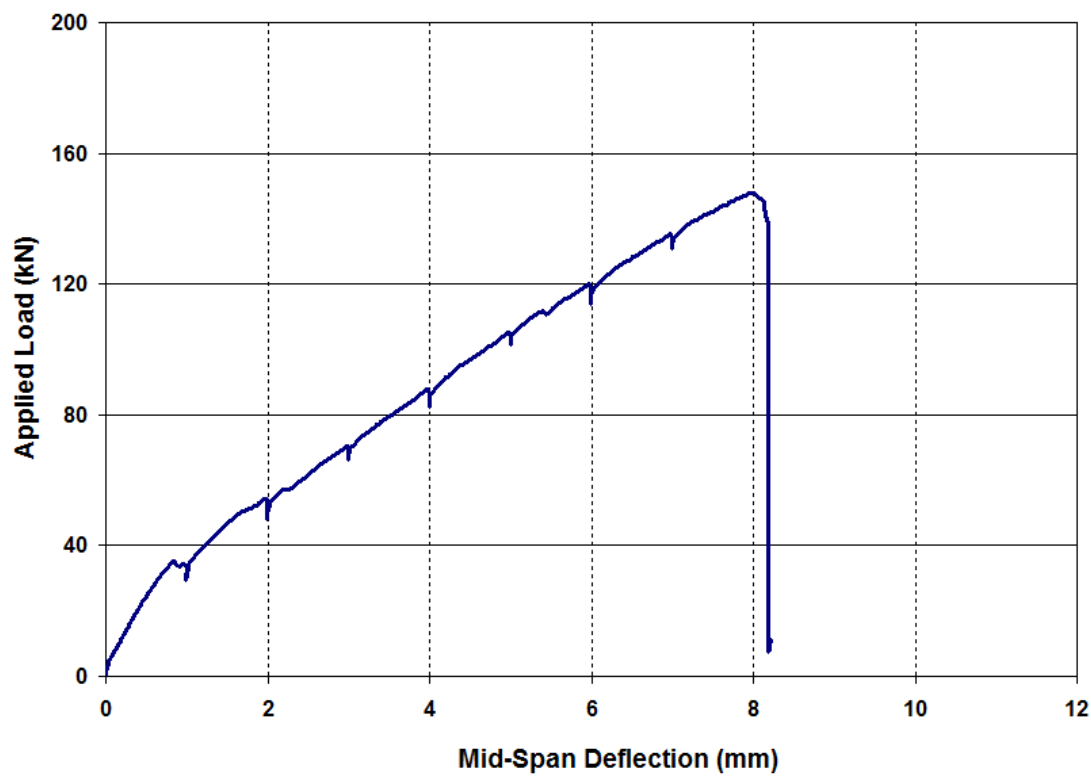
d) Crack Patterns After Failure

Figure A-4: Test Results of Specimen S-1.

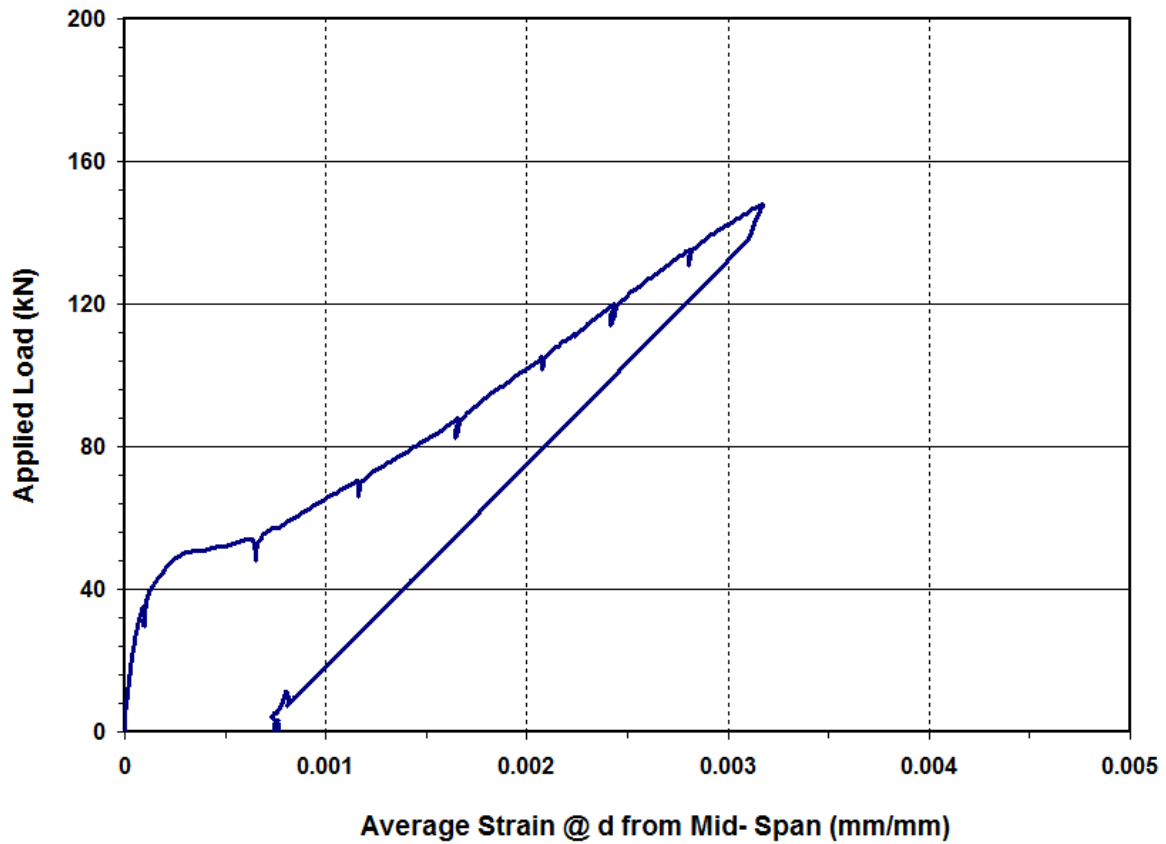
Specimen S-2



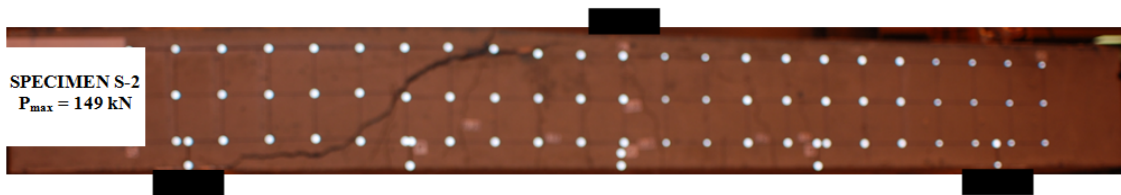
a) Elevation



b) Load Versus Mid-Span Deflection Response



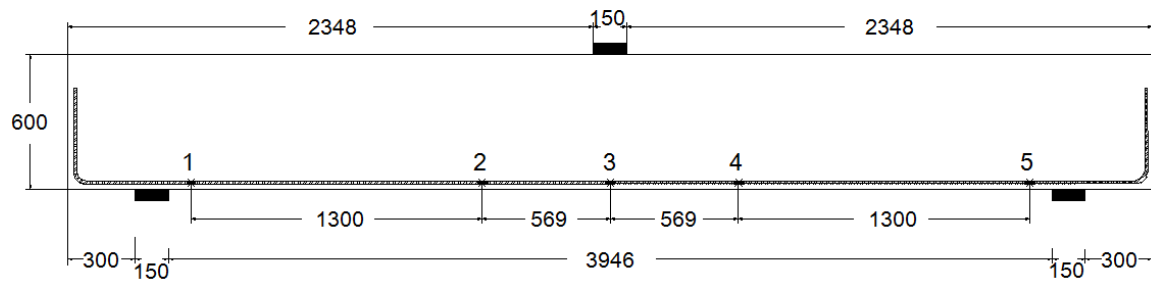
c) Typical Load - Average Longitudinal Steel Strain Response (@ d from mid-span)



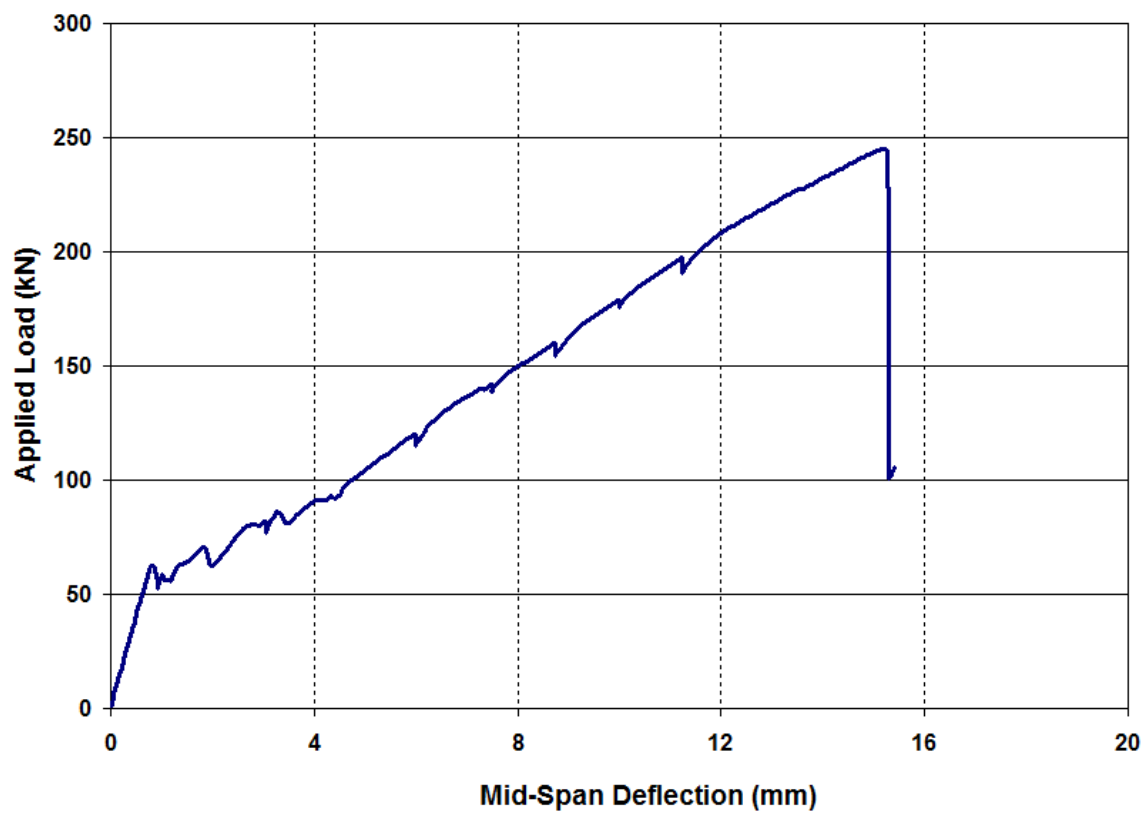
d) Crack Patterns After Failure

Figure A-5: Test Results of Specimen S-2.

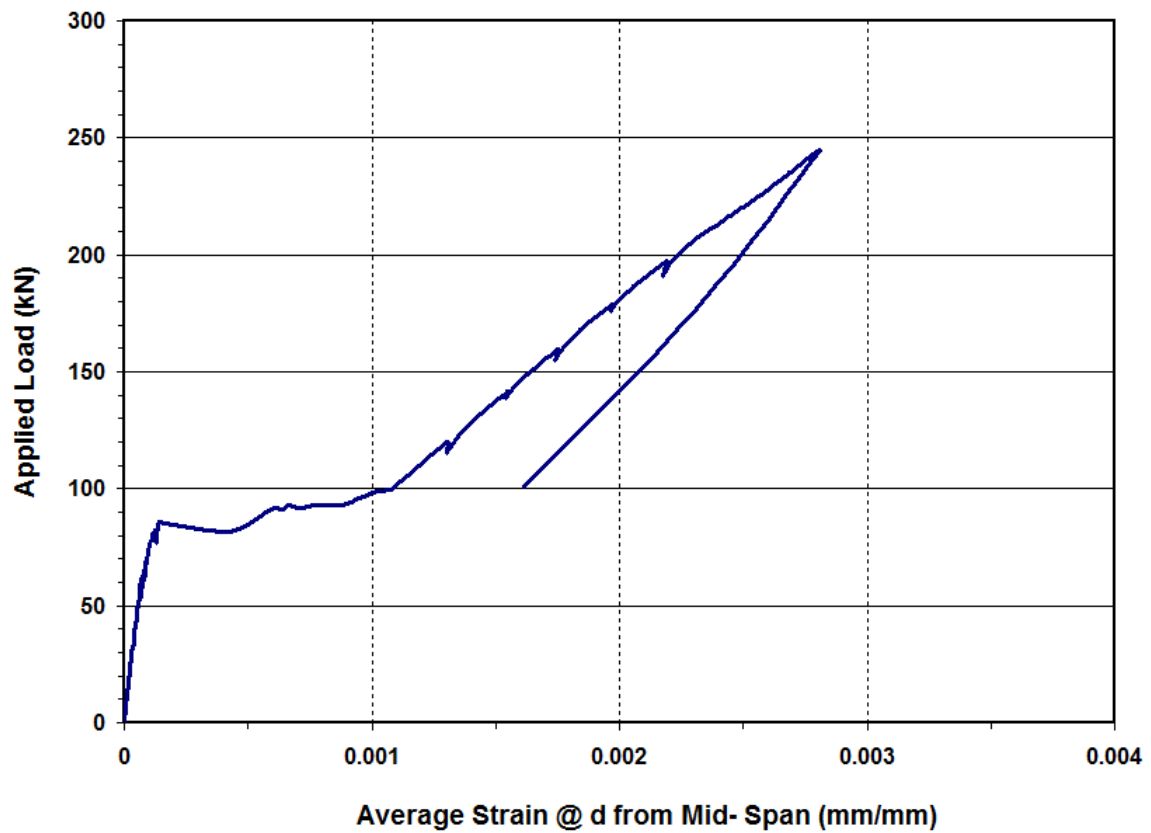
Specimen S-3



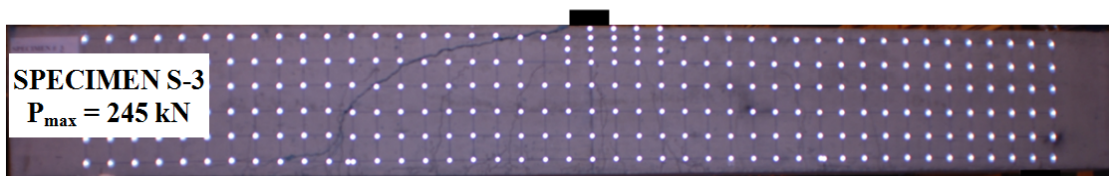
a) Elevation



b) Load - Mid-Span Deflection Response



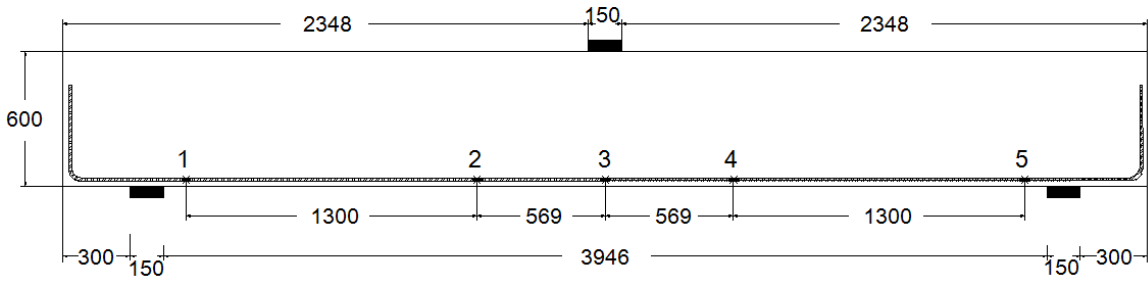
c) Typical Load - Average Longitudinal Steel Strain Response (@ d from mid-span)



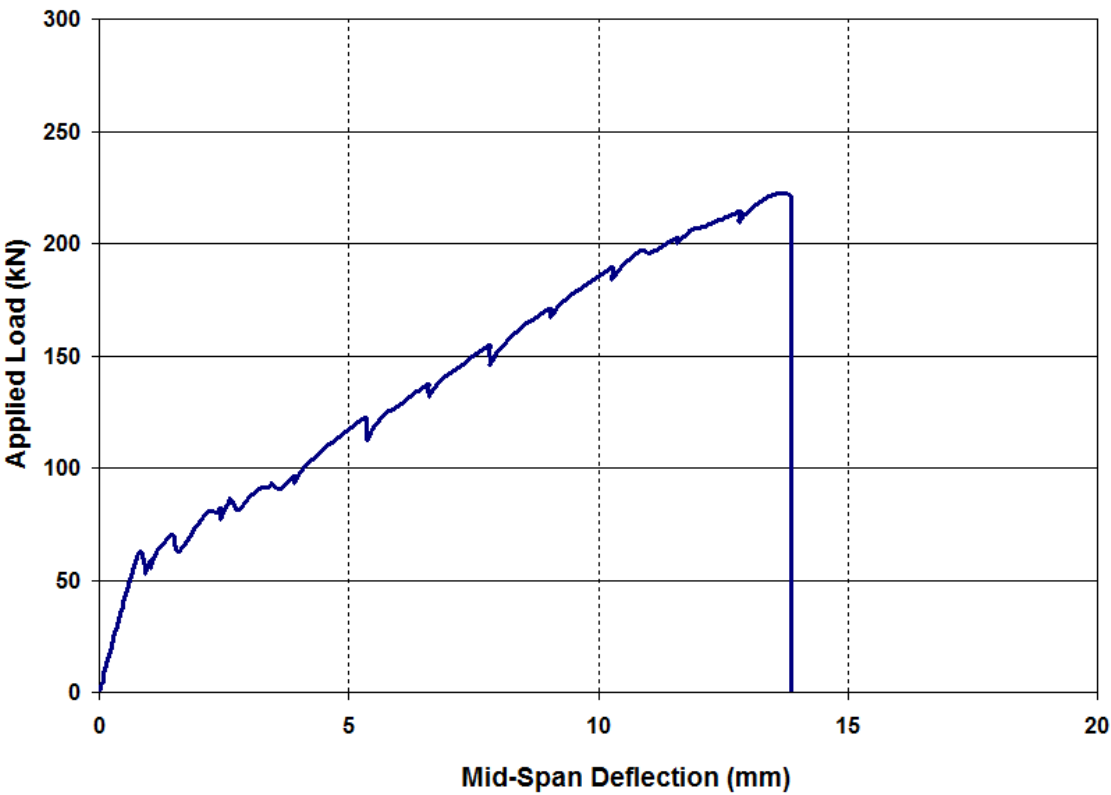
d) Crack Patterns After Failure

Figure A-6: Test Results of Specimen S-3.

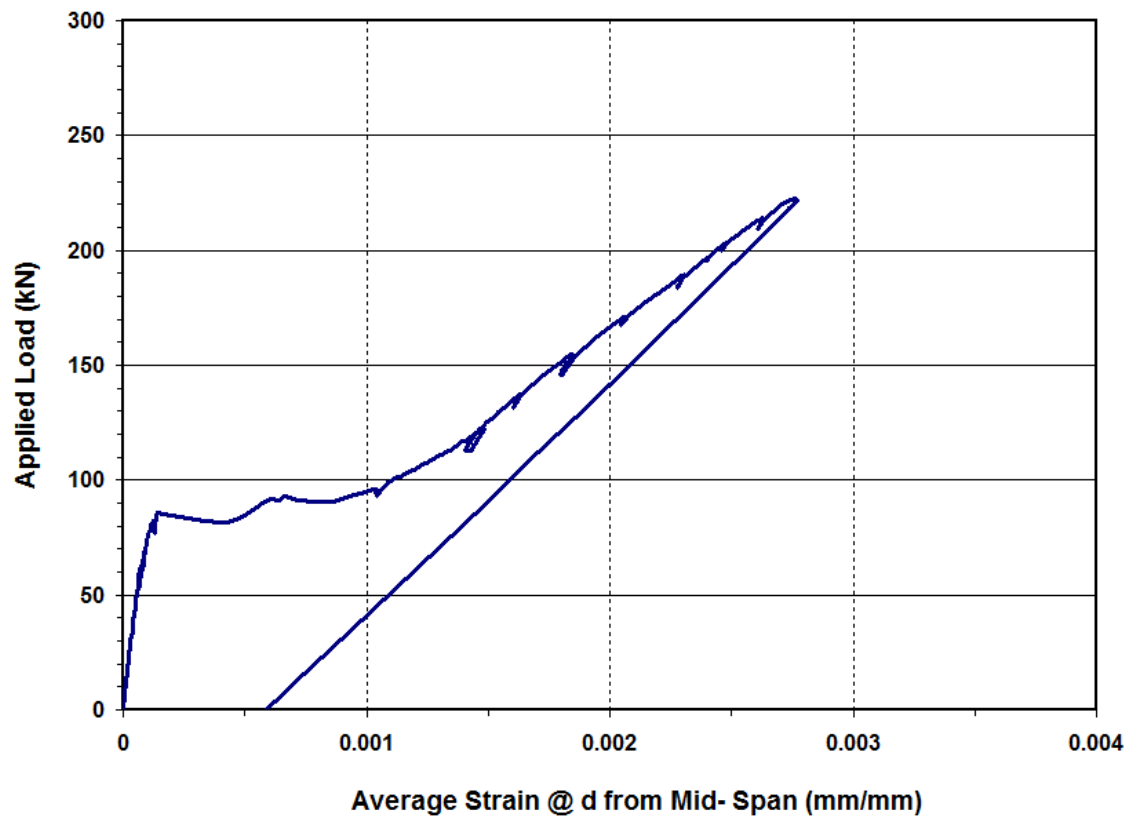
Specimen S-4



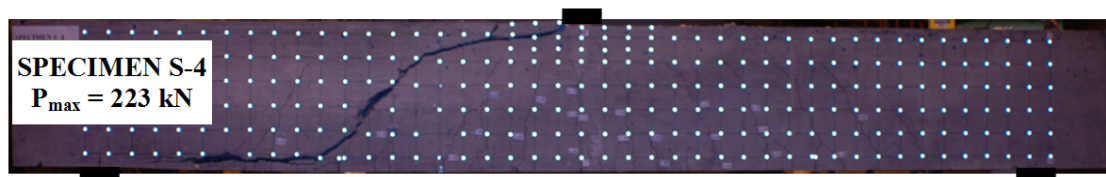
a) Elevation



b) Load - Mid-Span Deflection Response



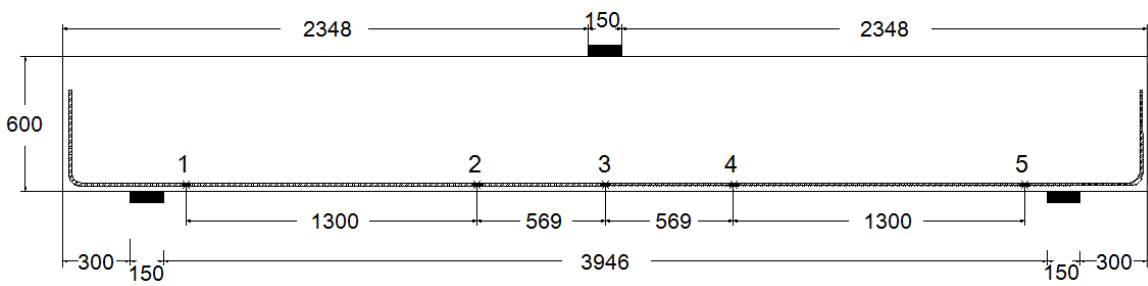
c) Typical Load - Average Longitudinal Steel Strain Response (@ d from mid-span)



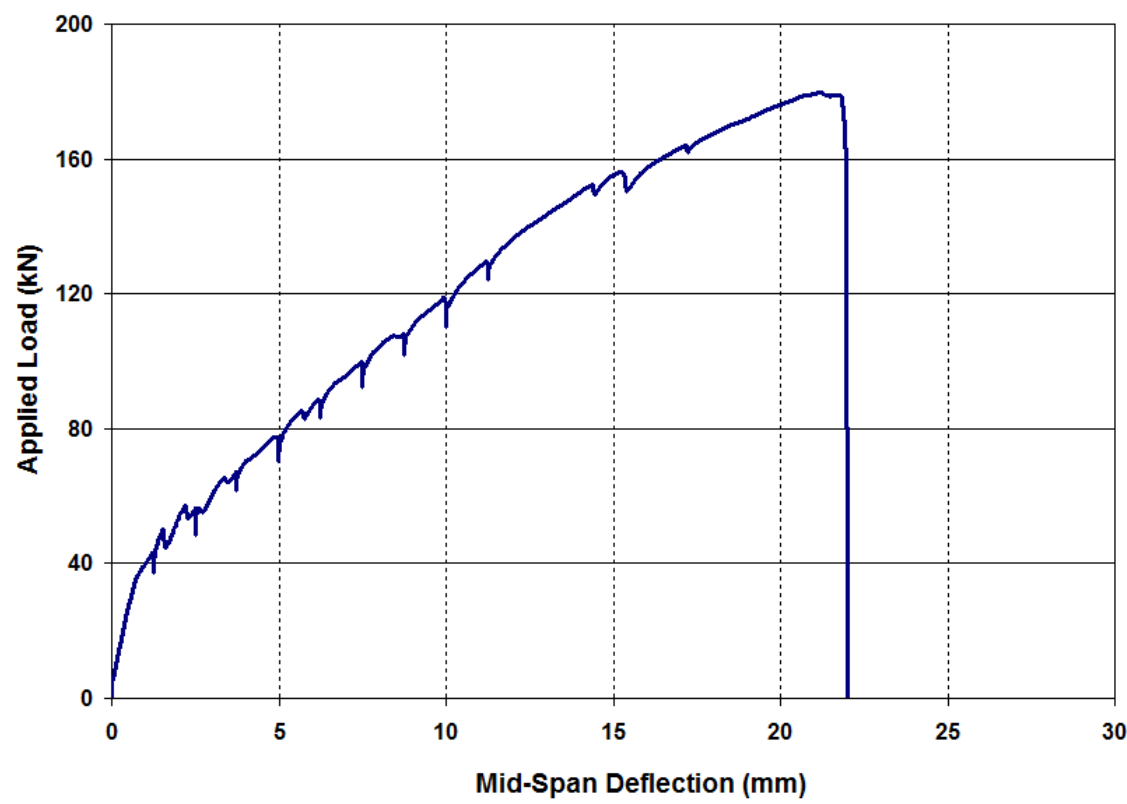
d) Crack Patterns After Failure

Figure A-7: Test Results of Specimen S-4.

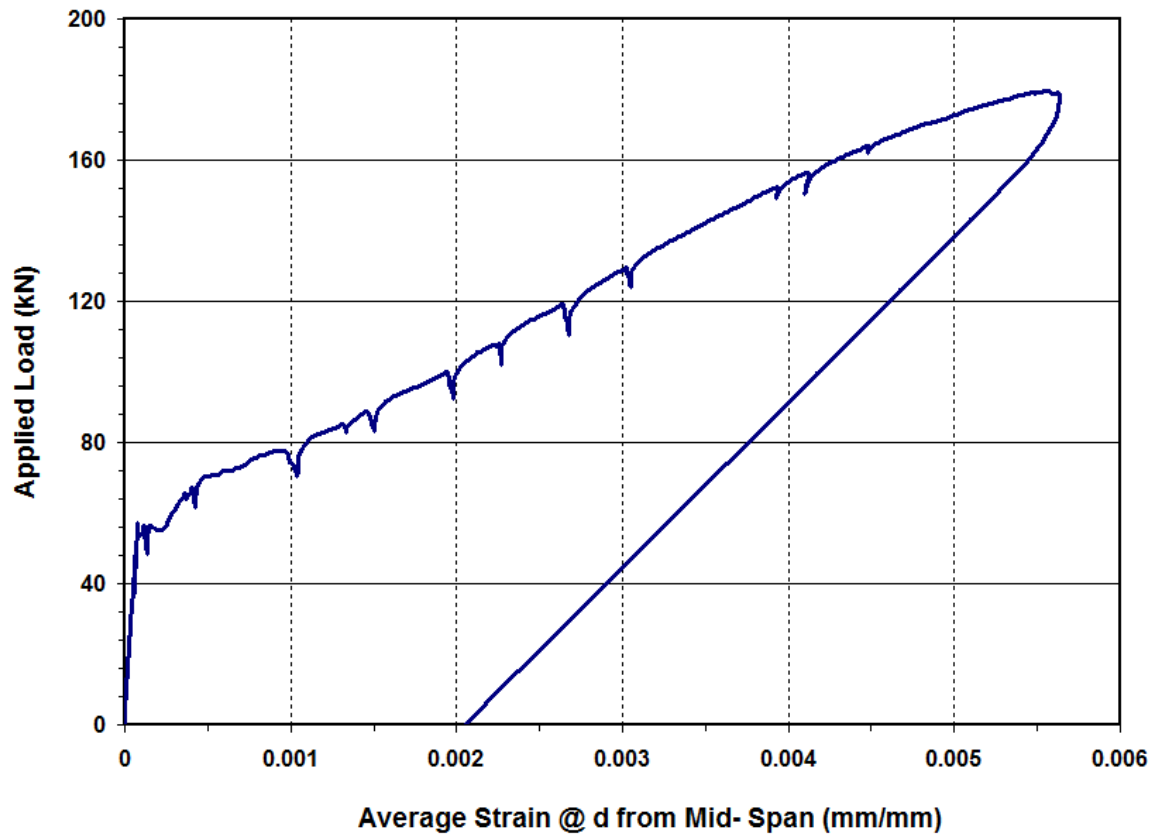
Specimen S-5



a) Elevation



b) Load - Mid-Span Deflection Response



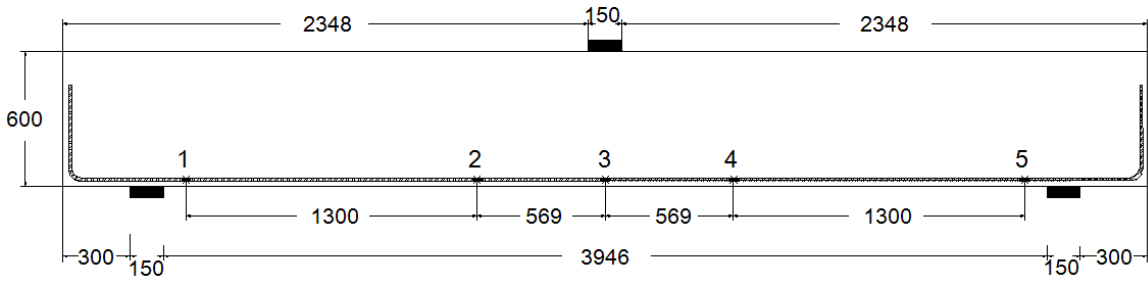
c) Typical Load - Average Longitudinal Steel Strain Response (@ d from mid-span)



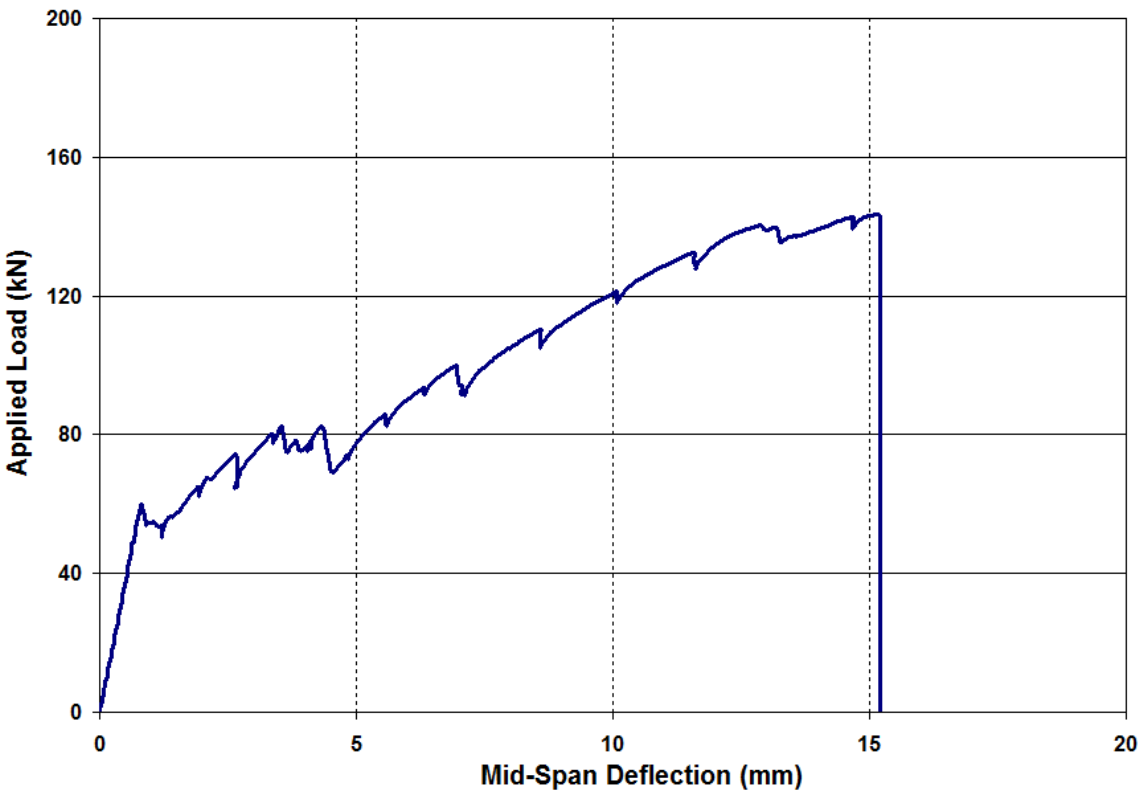
d) Crack Patterns After Failure

Figure A-8: Test Results of Specimen S-5.

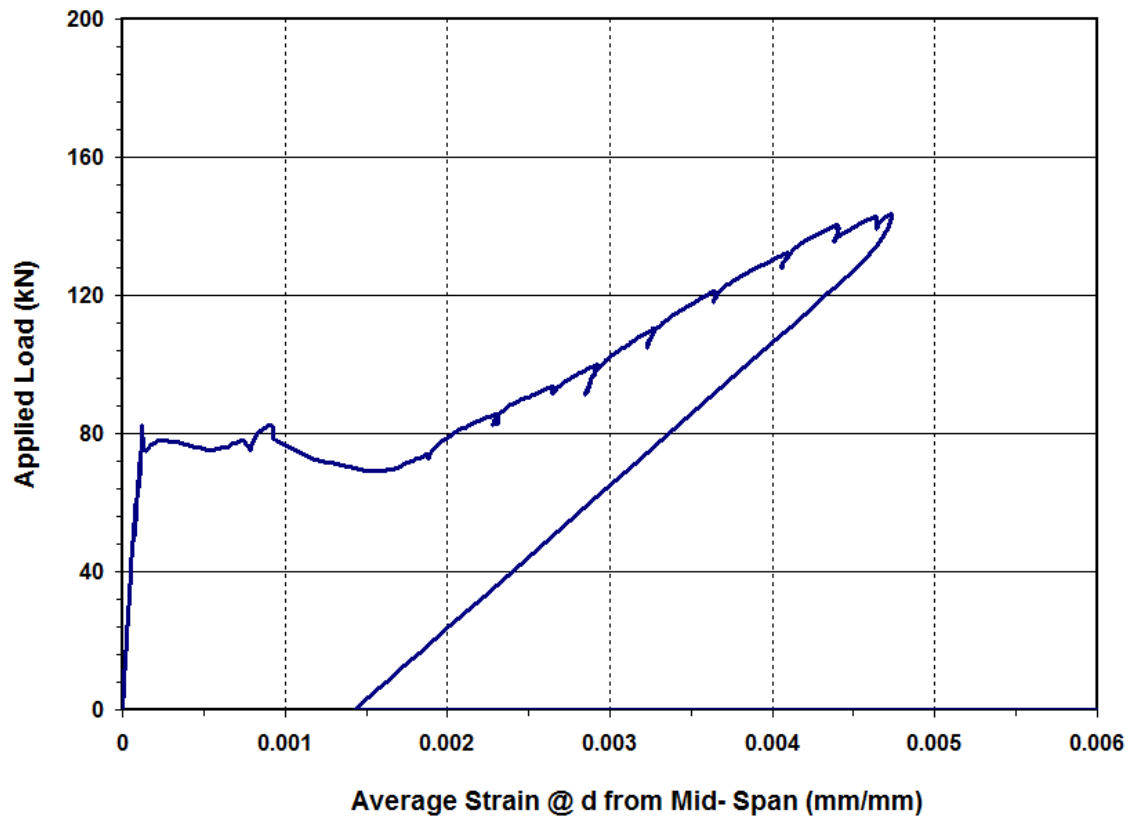
Specimen S-6



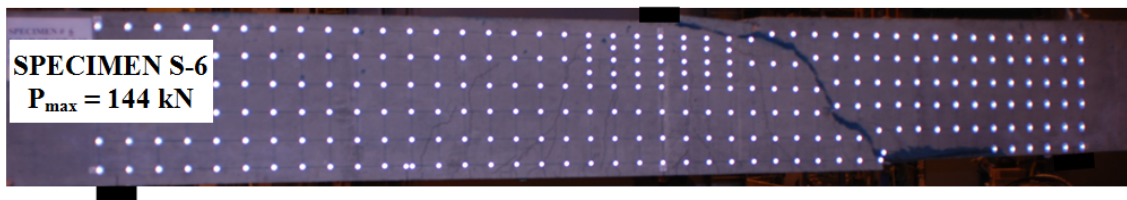
a) Elevation



b) Load - Mid-Span Deflection Response



c) Typical Load - Average Longitudinal Steel Strain Response (@ d from mid-span)



d) Crack Patterns After Failure

Figure A-9: Test Results of Specimen S-6.

A.2 Beam Specimens

A.2.1 Material Tests



Figure A-10: Typical Compression Test of Concrete Cylinder.

Table A-2: Compression Test Results at the Day of Test of Slab Specimens.

<i>Cylinders</i>	<i>Beam Specimens</i>									
	<i>RM1</i>	<i>RM2</i>	<i>MM1</i>	<i>MM2</i>	<i>MM3</i>	<i>MM4</i>	<i>MR1</i>	<i>MR2</i>	<i>MR3</i>	<i>MR4</i>
<i>1</i>	40	45	50	51	47	47	52	47	47	48
<i>2</i>	41	44	48	51	48	49	51	51	48	51
<i>3</i>	43	46	51	54	49	48	45	50	49	51
<i>Average f_c' (MPa)</i>	41	45	50	52	48	48	49	50	48	50
<i>COV</i>	0.037	0.022	0.031	0.033	0.021	0.021	0.077	0.042	0.021	0.035
<i>Age (days)</i>	35	60	49	48	45	52	56	51	43	56



Figure A-11: Typical Tension Coupon Test of Steel Rebars.

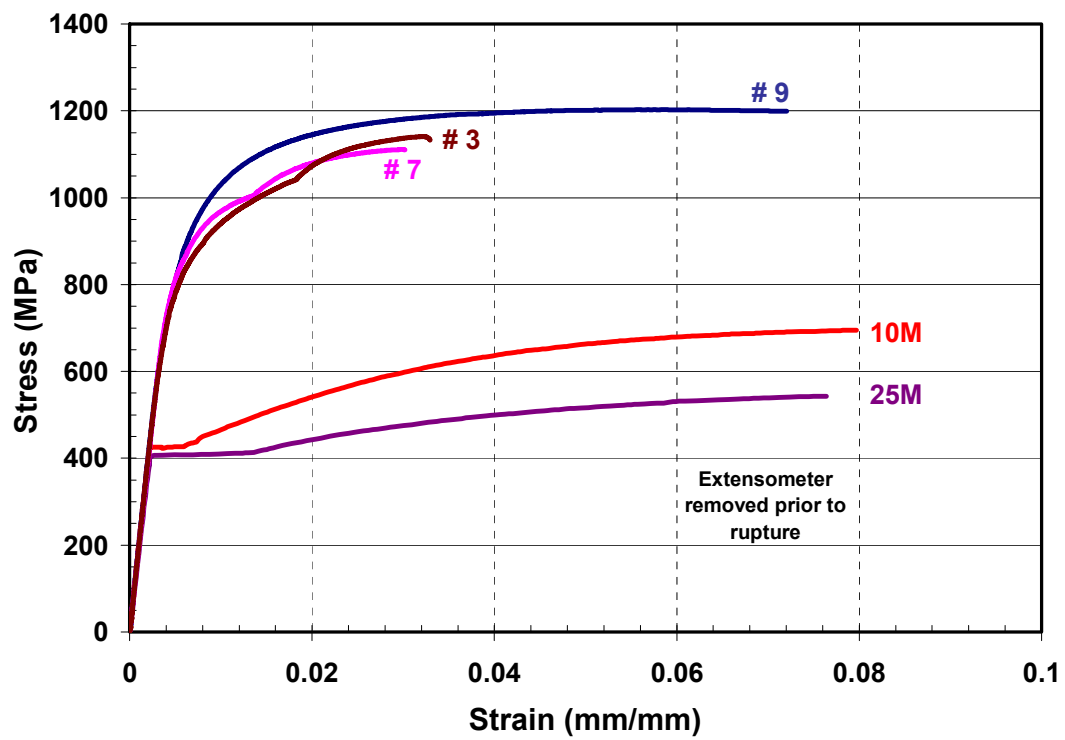
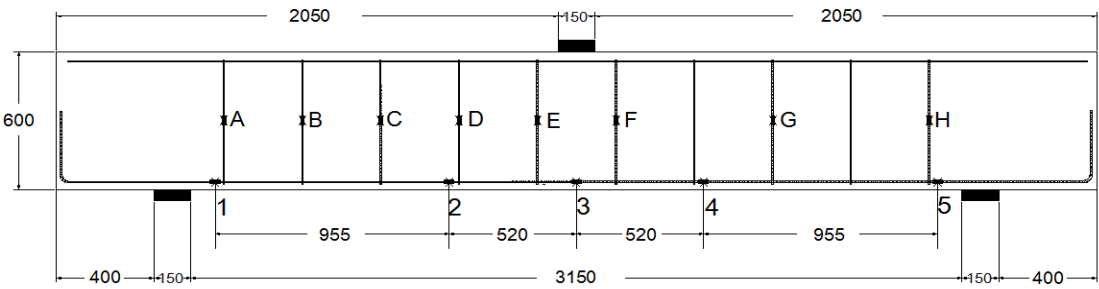


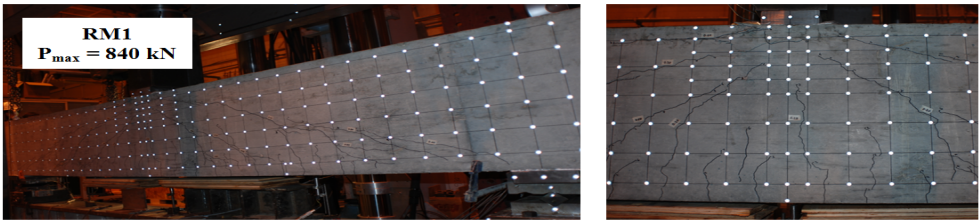
Figure A-12: Average Tension Stress-Strain Response for ASTM A1035 and Conventional Steel Coupons.

A.2.2 Structural Tests

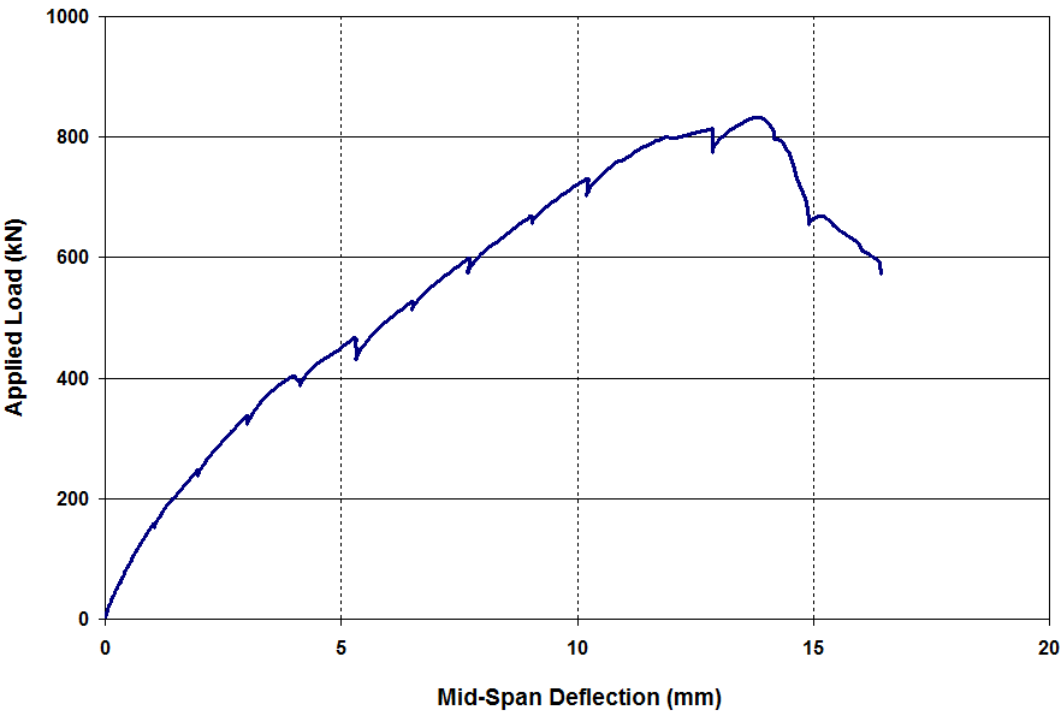
Specimen RM1



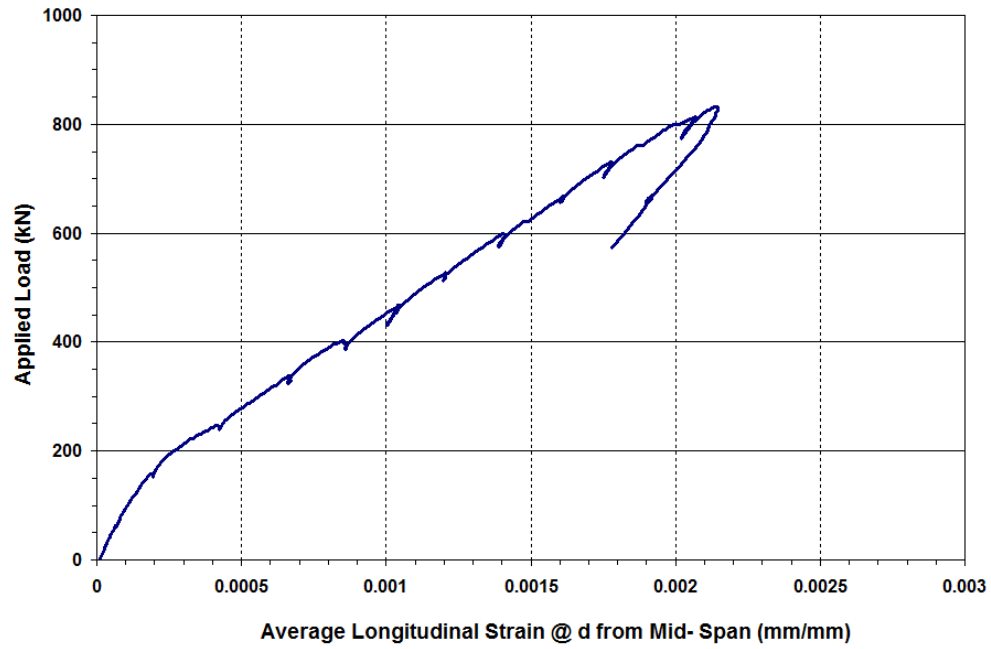
a) Elevation



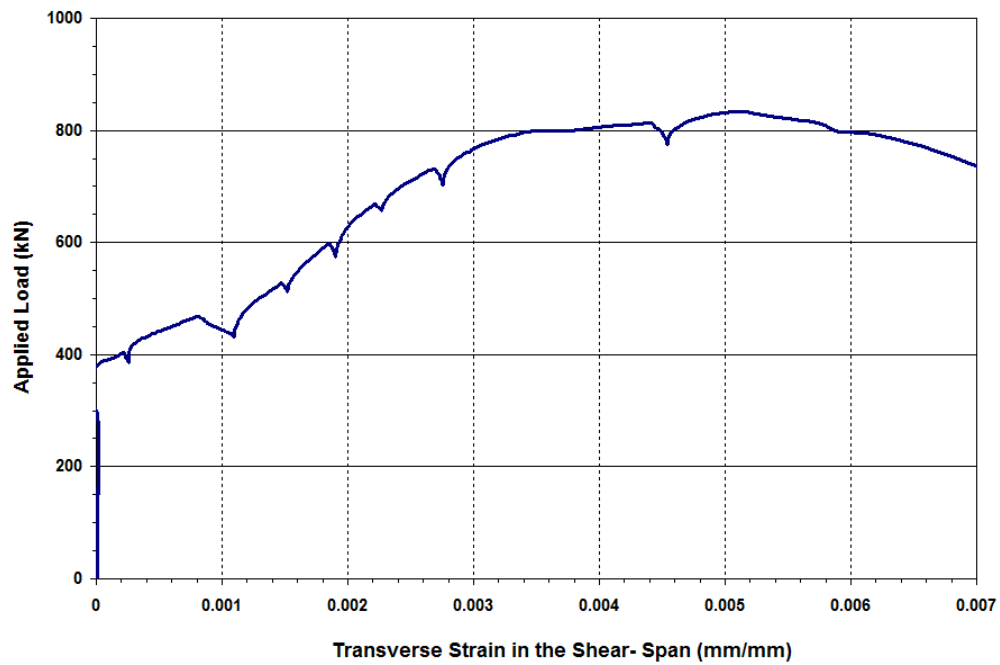
b) Crack Patterns After Failure



c) Load - Mid-Span Deflection Response



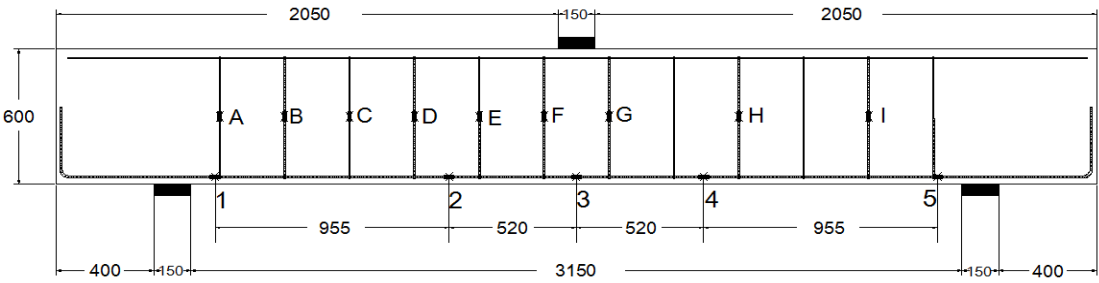
d) Typical Load - Average Longitudinal Steel Strain Response (@ d from mid-span)



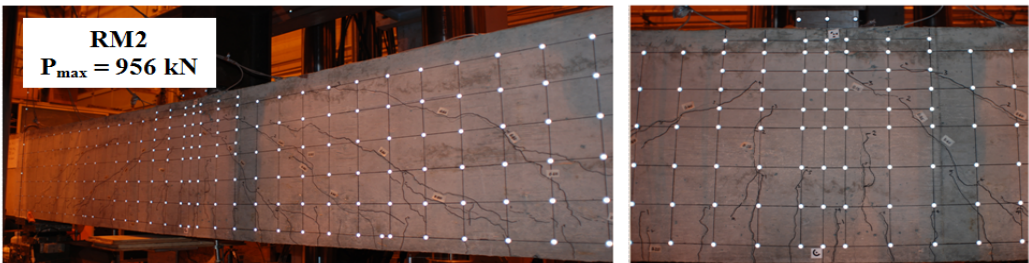
e) Maximum Load - Transverse Steel Strain Response

Figure A-13: Test Results of Specimen RM1.

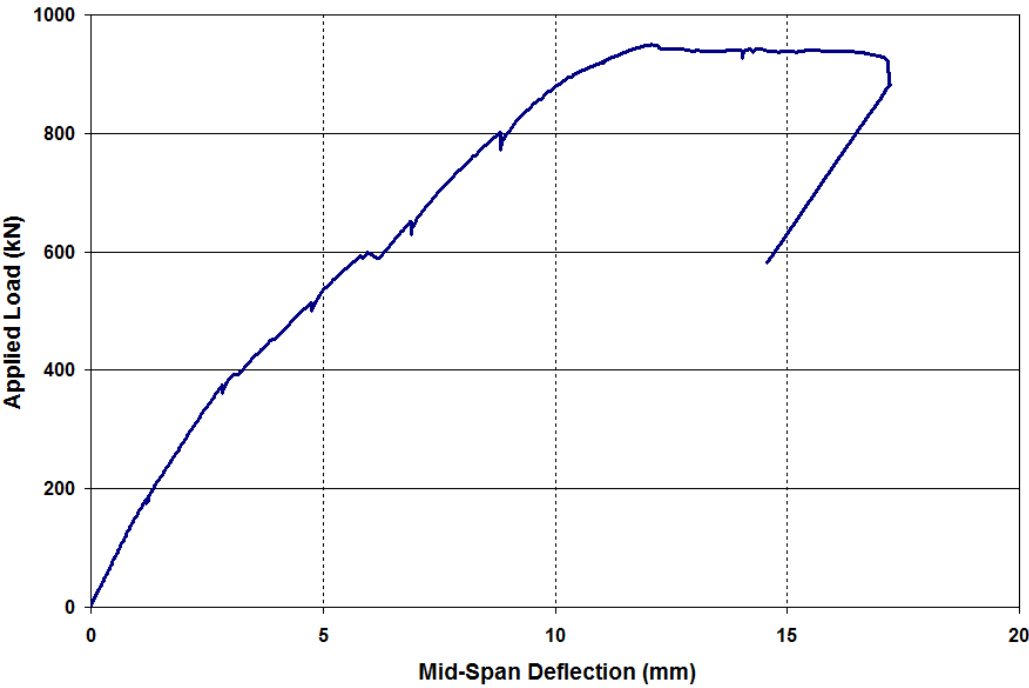
Specimen RM2



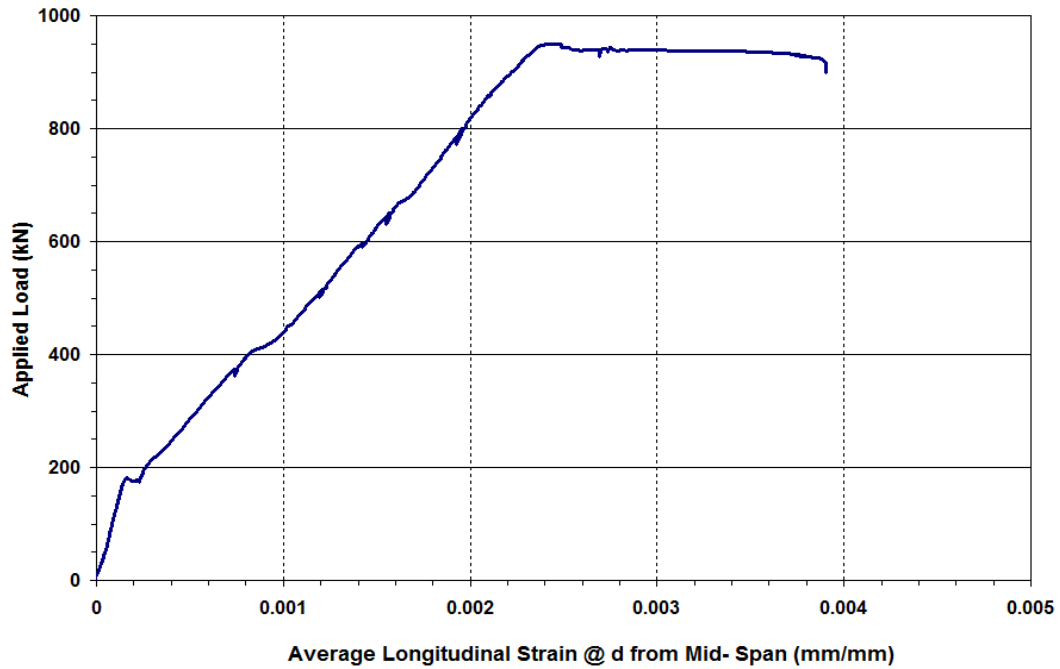
a) Elevation



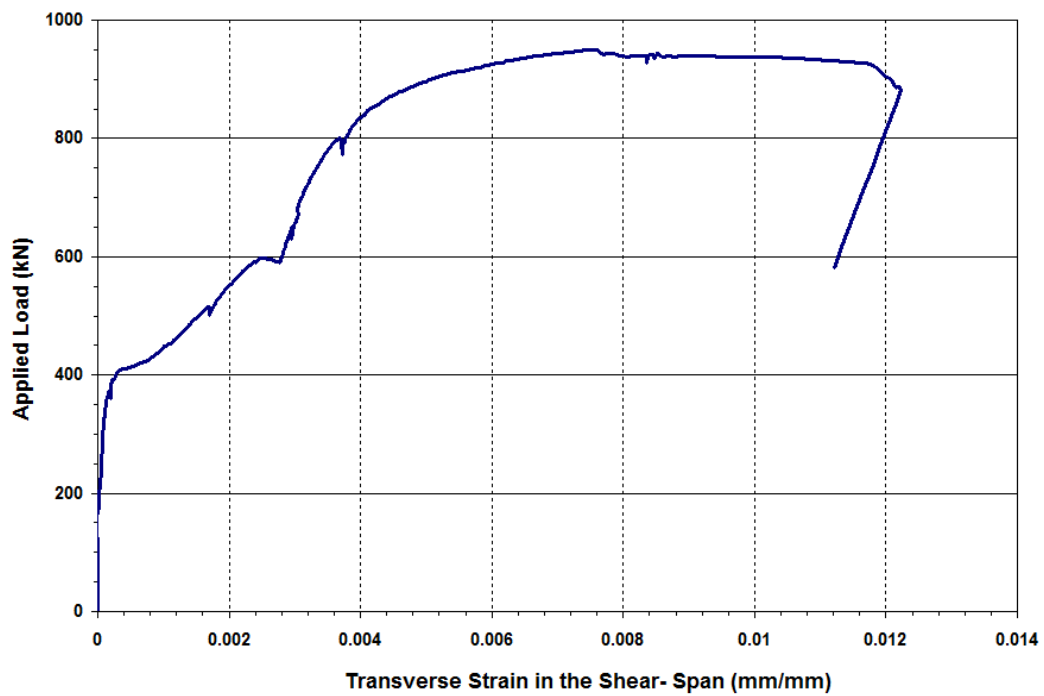
b) Crack Patterns After Failure



c) Load - Mid-Span Deflection Response



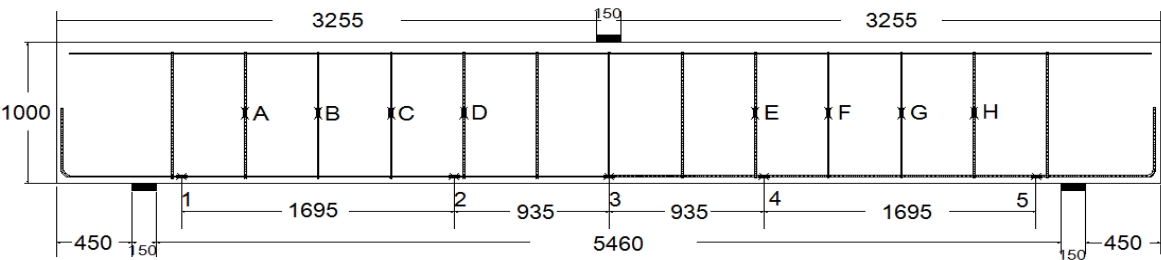
c) Typical Load - Average Longitudinal Steel Strain Response (@ d from mid-span)



d) Maximum Load - Transverse Steel Strain Response

Figure A-14: Test Results of Specimen RM2.

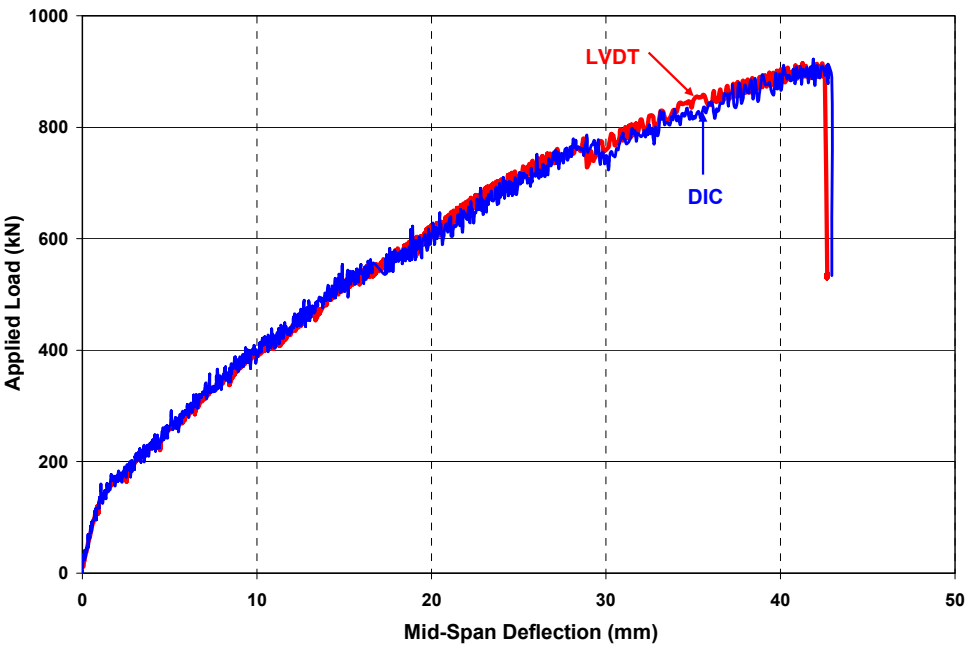
Specimen MR1



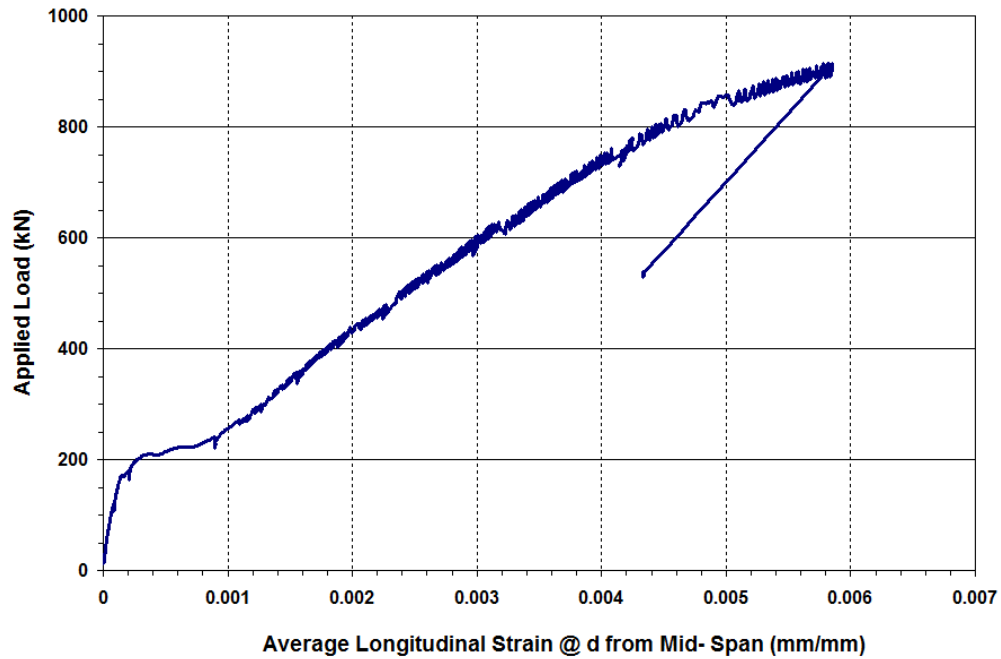
a) Elevation



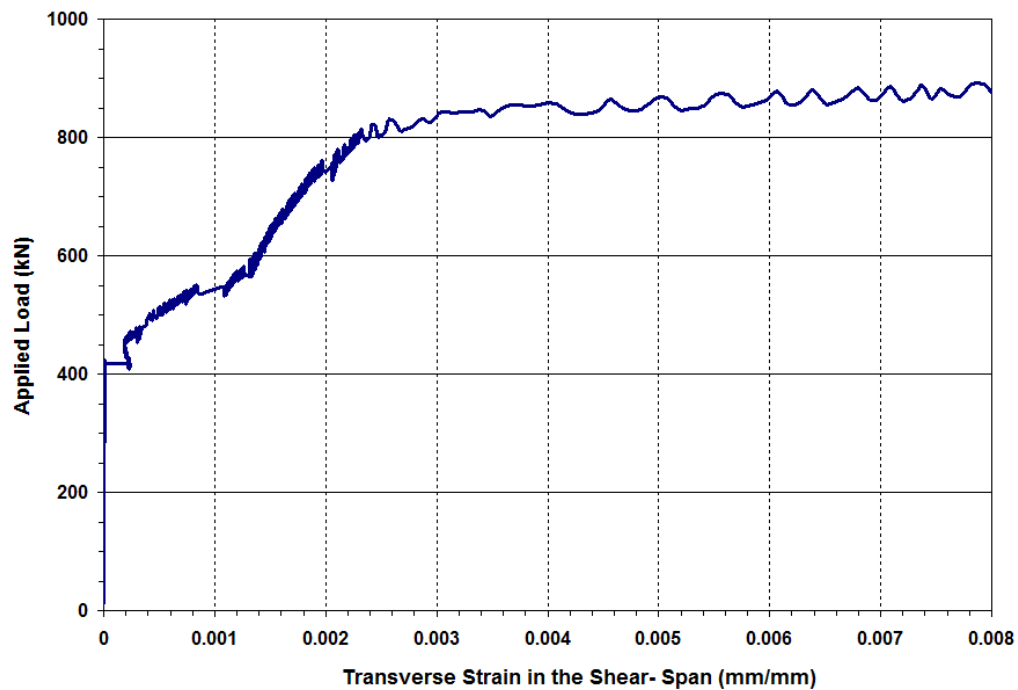
b) Crack Patterns After Failure



c) Load - Mid-Span Deflection Response



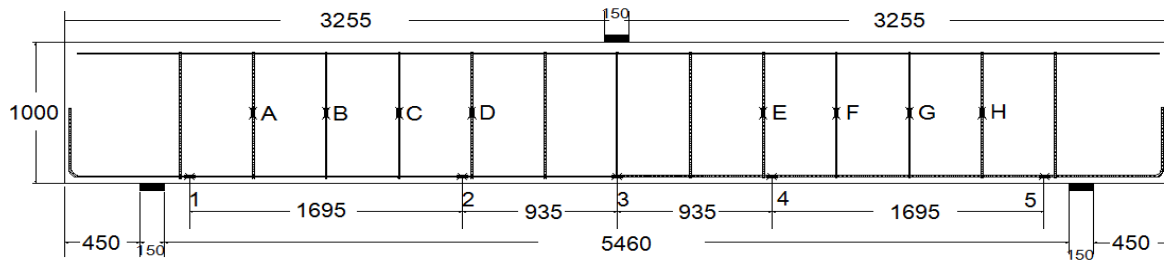
d) Typical Load - Average Steel Strain Response (@ d from mid-span)



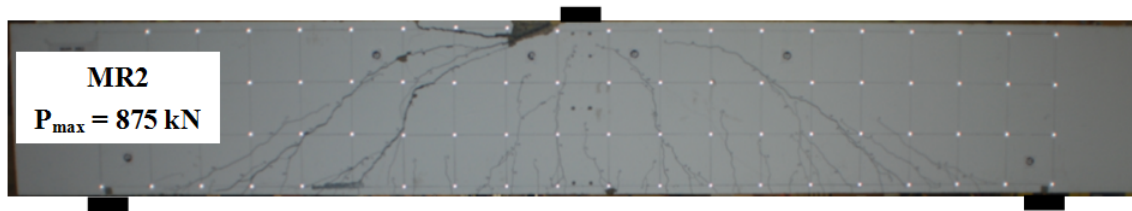
e) Maximum Load - Transverse Steel Strain Response.

Figure A-15: Test Results of Specimen MR1.

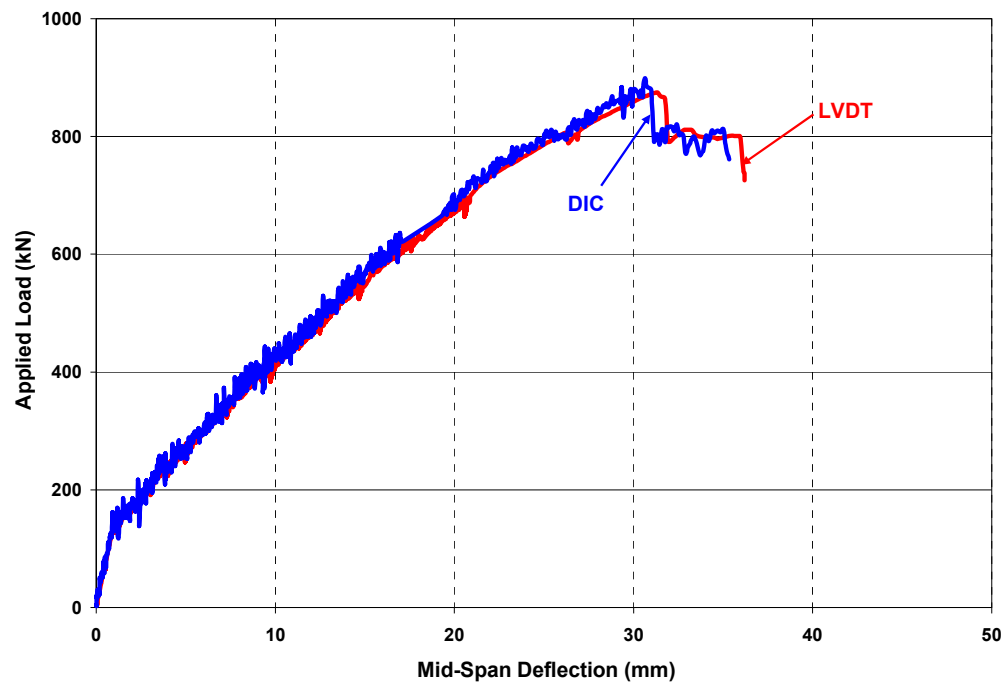
Specimen MR2



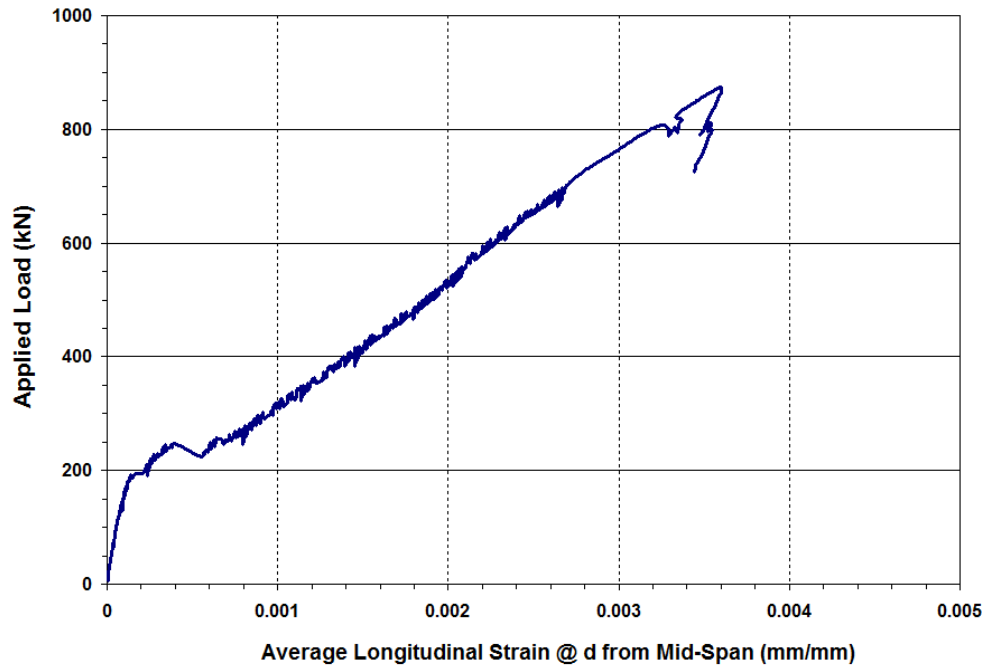
a) Elevation



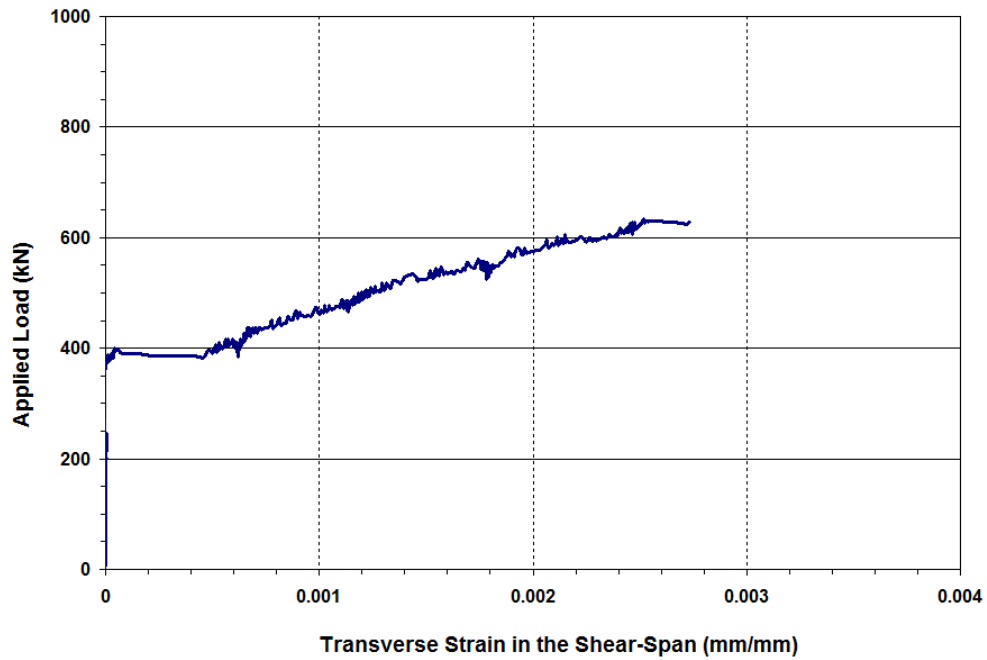
b) Crack Patterns After Failure



c) Load - Mid-Span Deflection Response



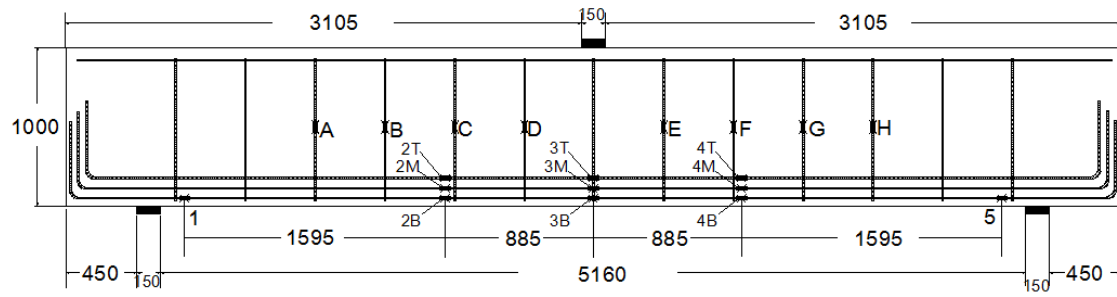
d) Typical Load Versus Average Steel Strain Response (@ d from mid-span)



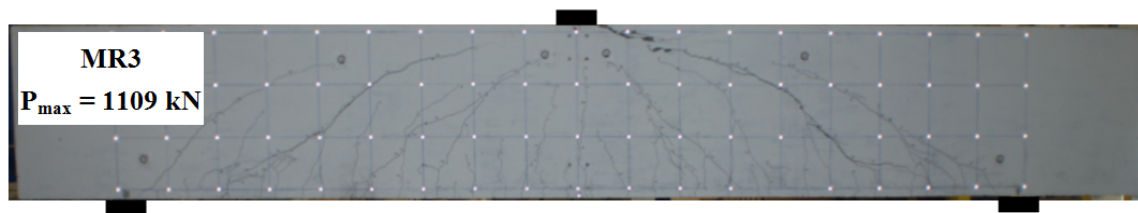
e) Maximum Load - Transverse Steel Strain Response.

Figure A-16: Test Results of Specimen MR2.

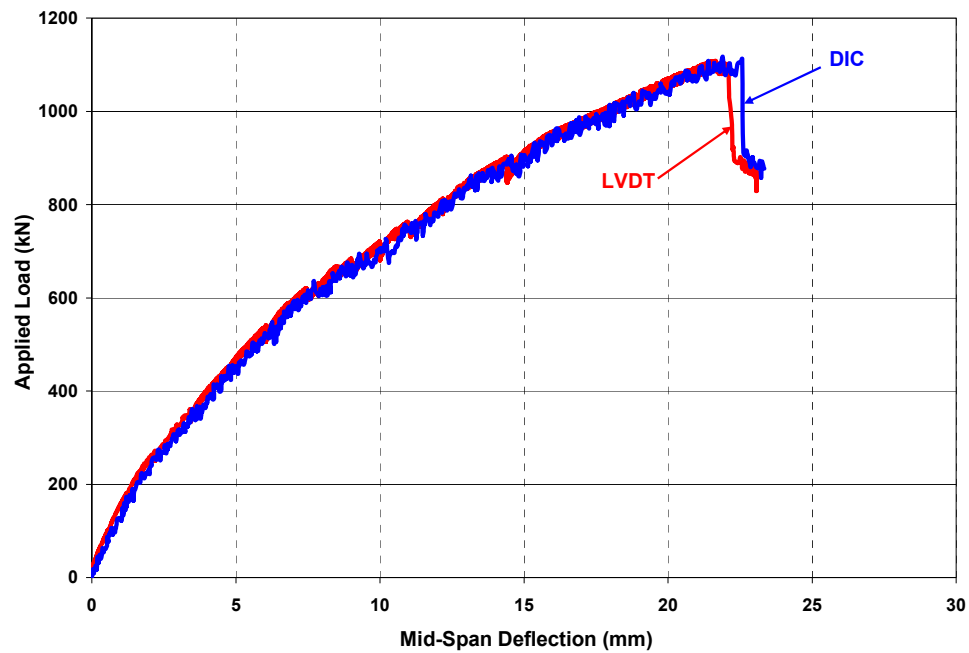
Specimen MR3



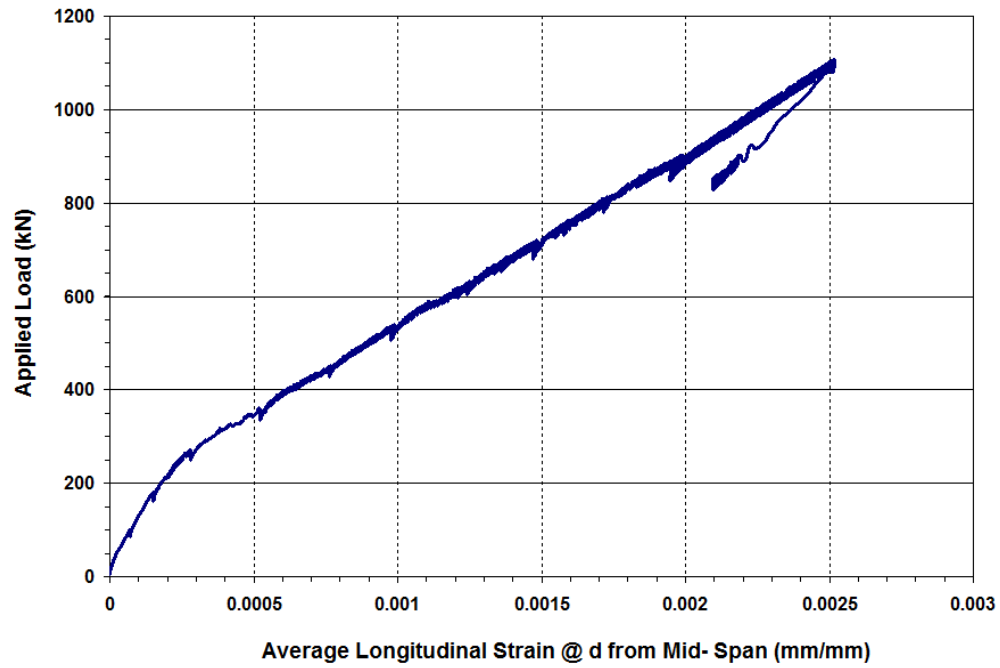
a) Elevation



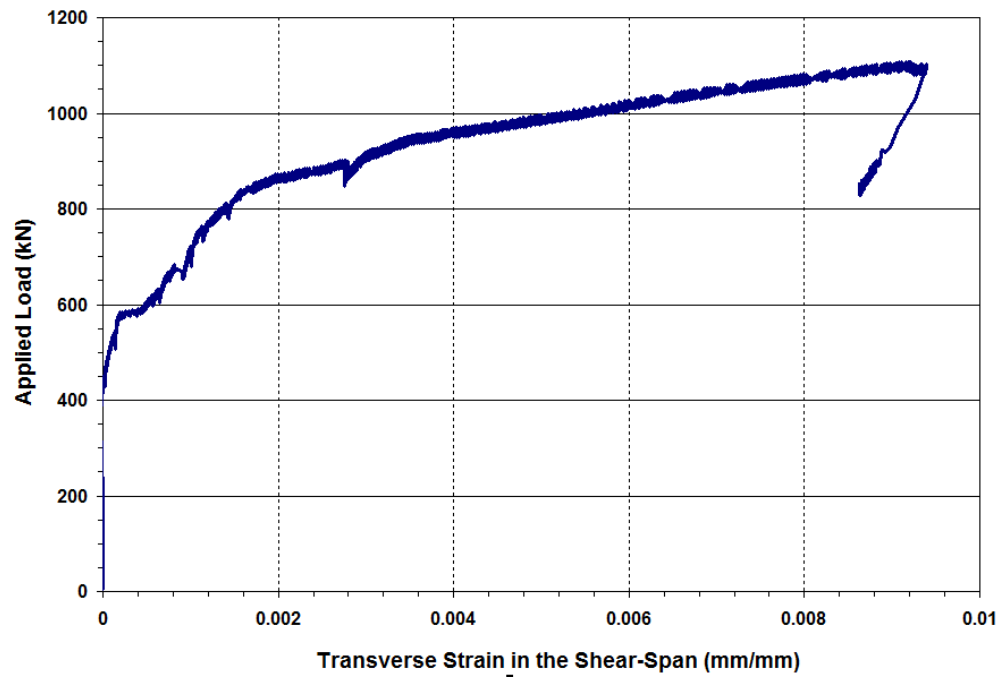
b) Crack Patterns After Failure



c) Load - Mid-Span Deflection Response



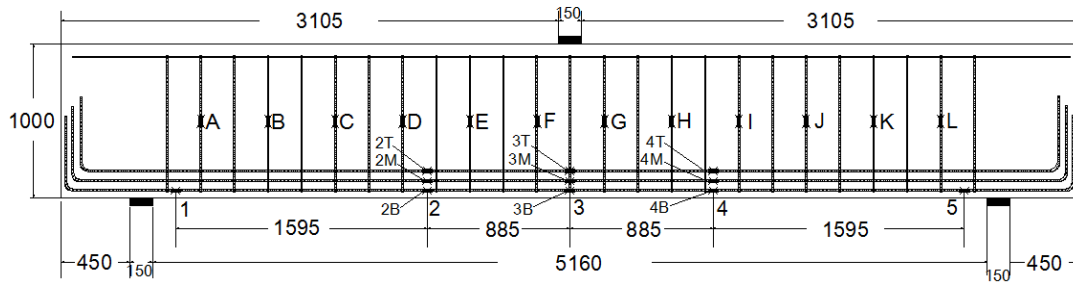
d) Typical Load - Average Steel Strain Response (@ d from mid-span)



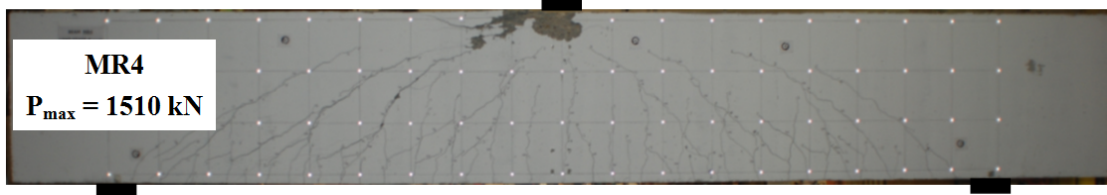
e) Maximum Load - Transverse Steel Strain Response.

Figure A-17: Test Results of Specimen MR3.

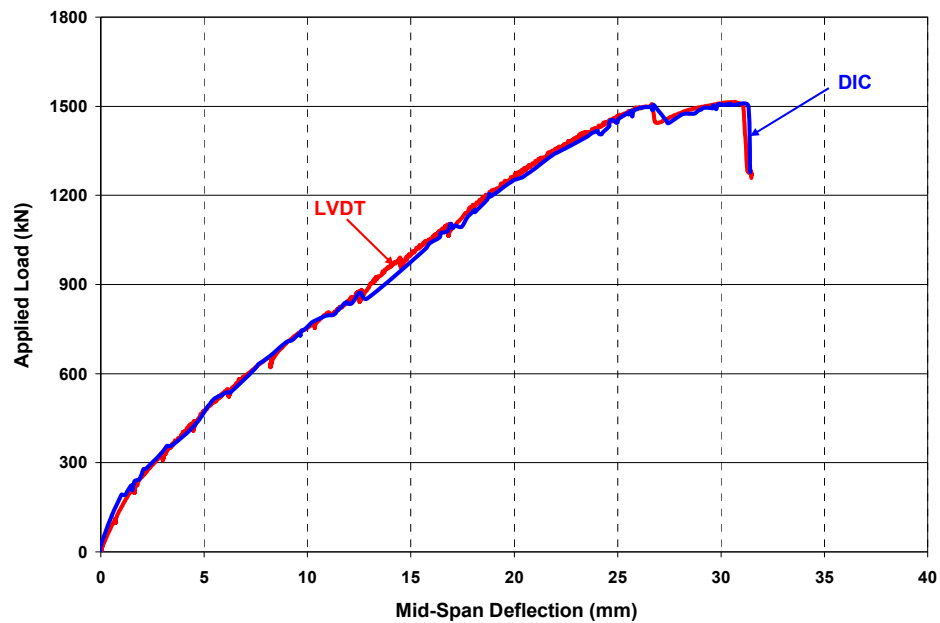
Specimen MR4



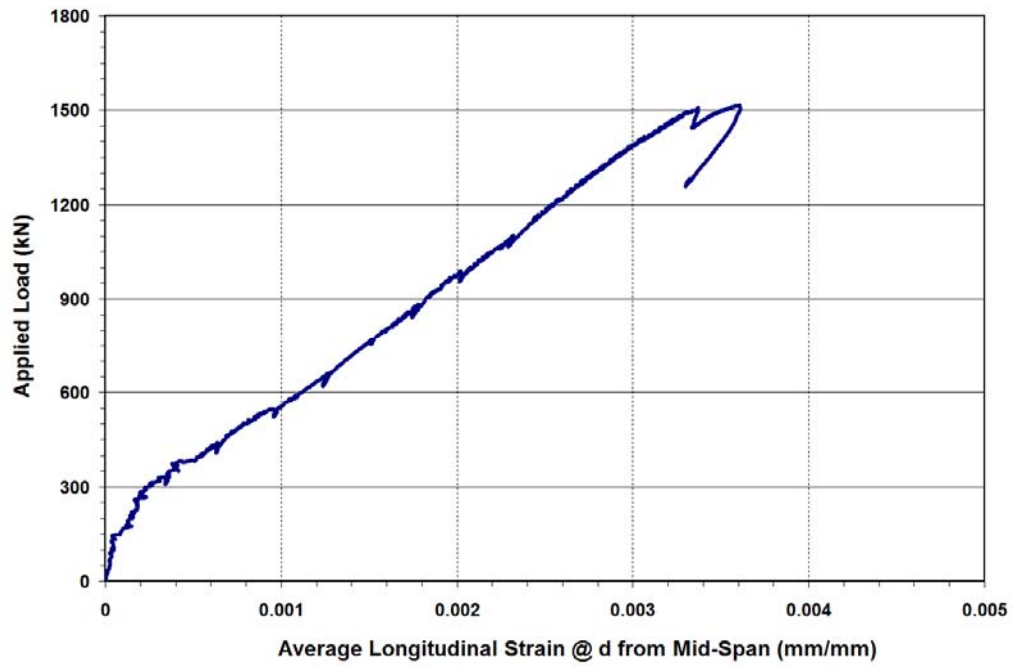
a) Elevation



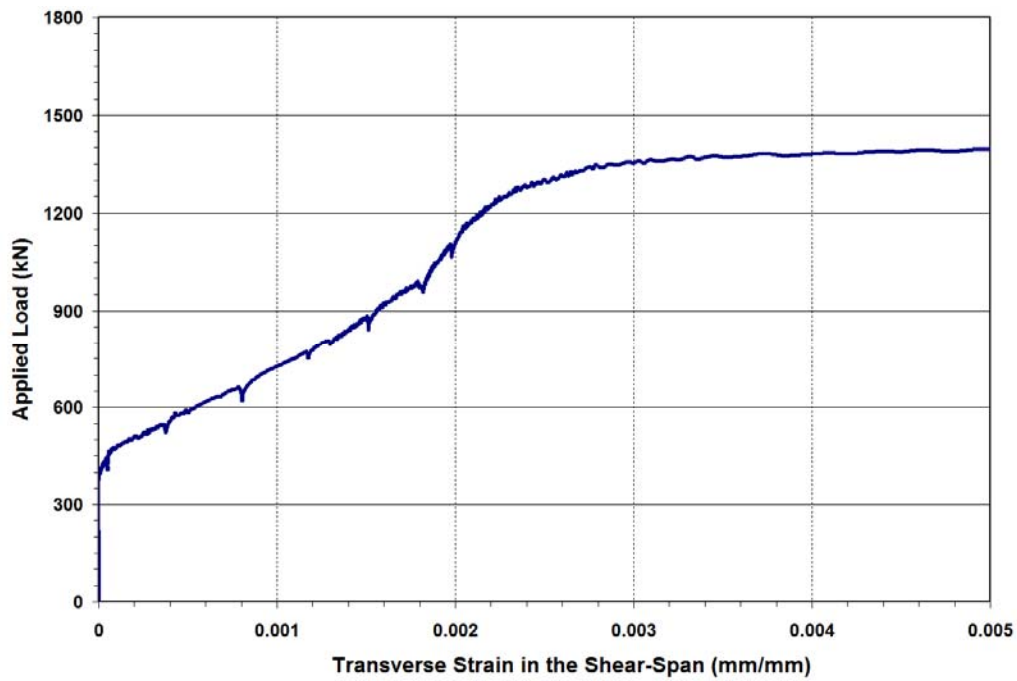
b) Crack Patterns After Failure



c) Load - Mid-Span Deflection Response



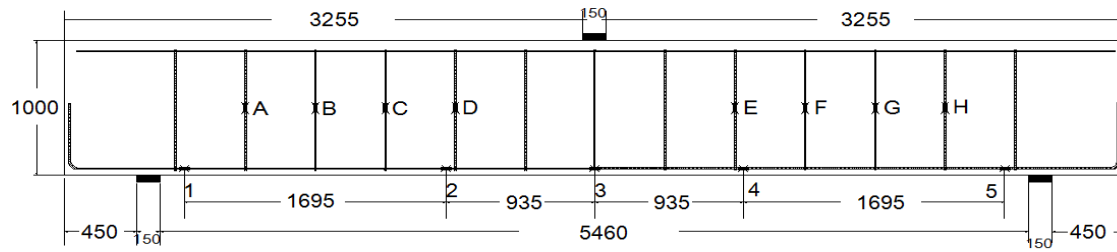
d) Typical Load - Average Steel Strain Response (@ d from mid-span)



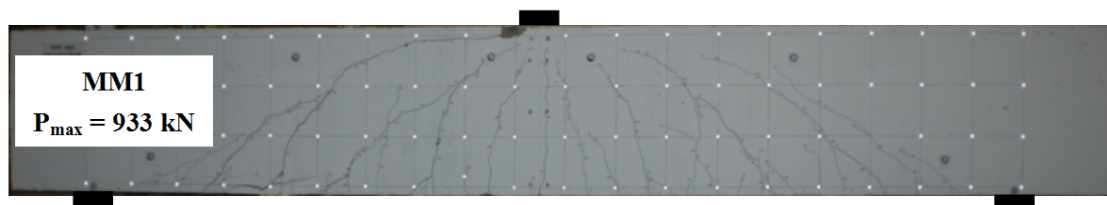
e) Maximum Load - Transverse Steel Strain Response.

Figure A-18: Test Results of Specimen MR4.

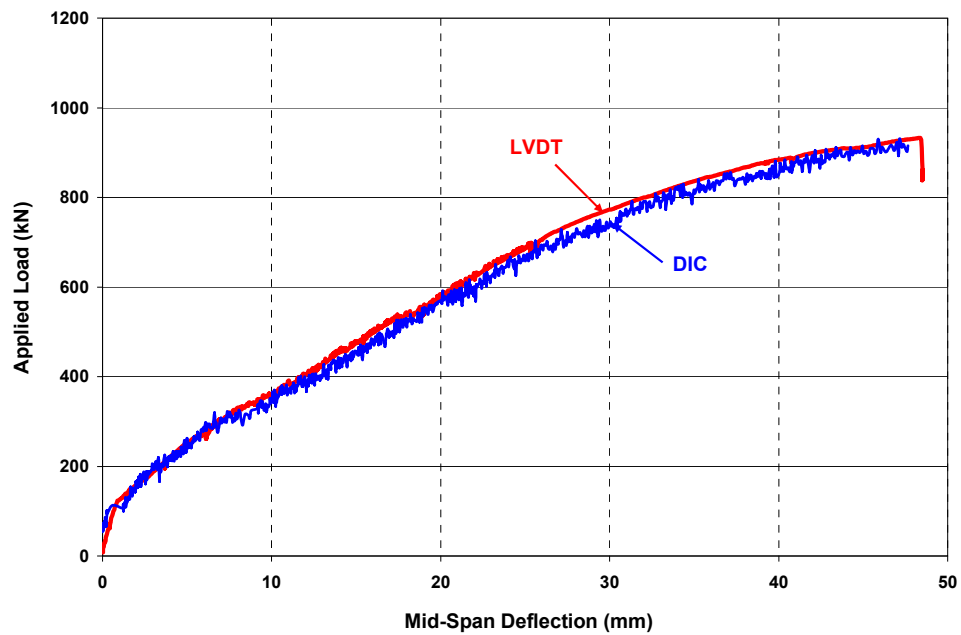
Specimen MM1



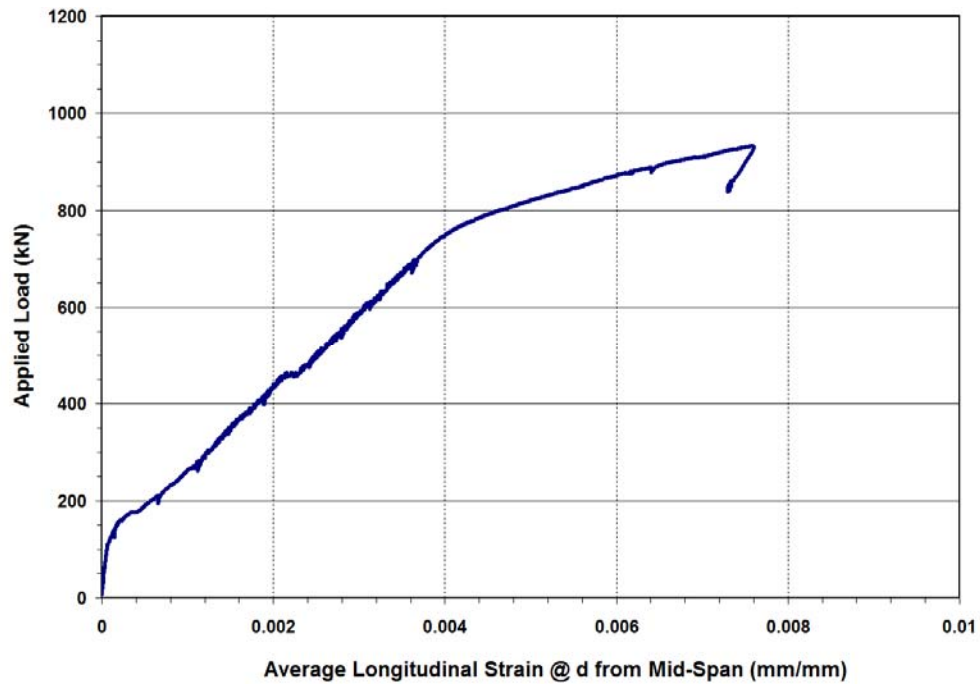
a) Elevation



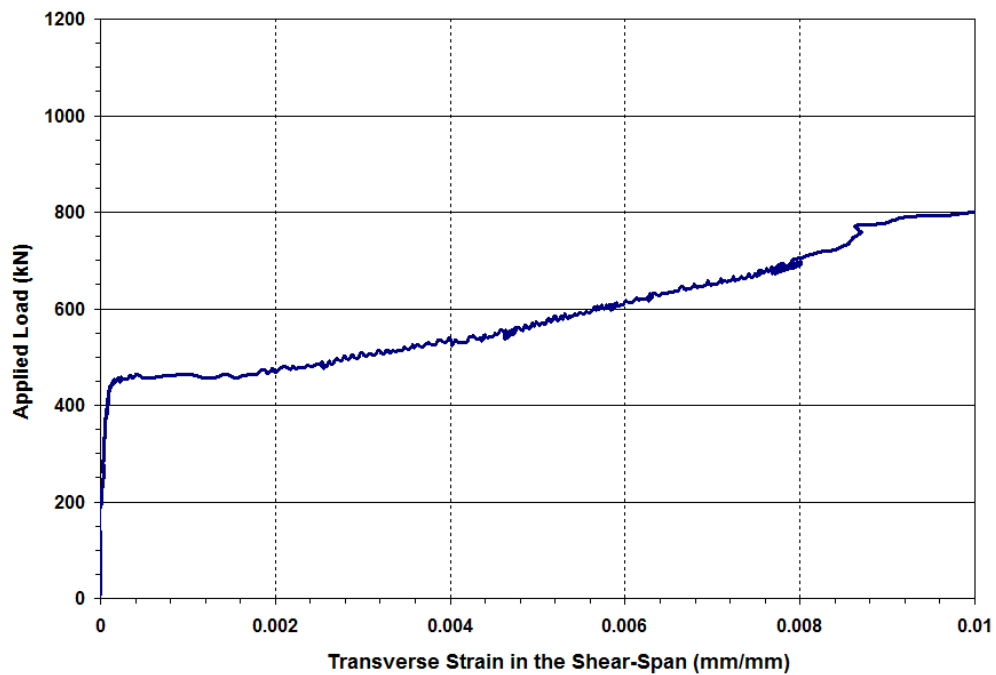
b) Crack Patterns After Failure



c) Load - Mid-Span Deflection Response



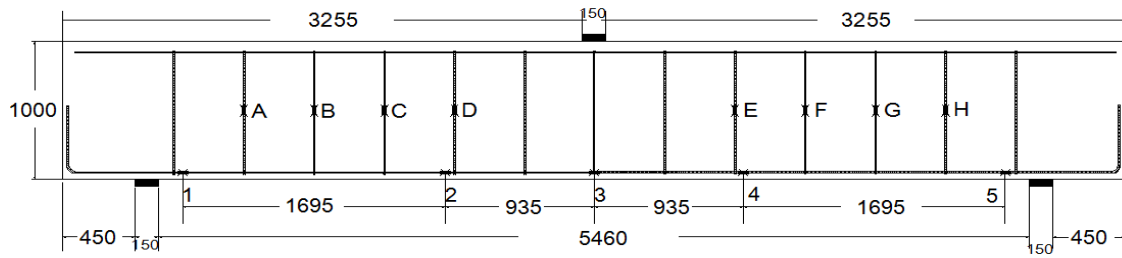
d) Typical Load - Average Steel Strain Response (@ d from mid-span)



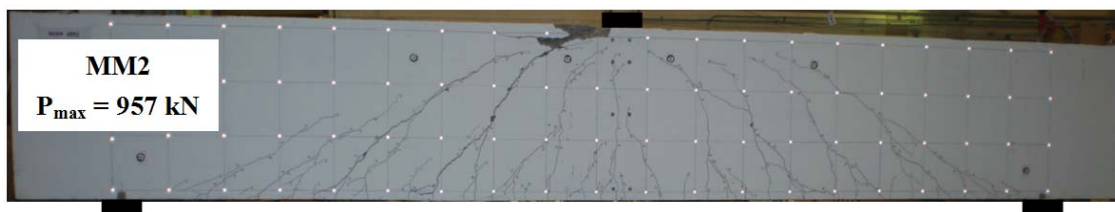
e) Maximum Load - Transverse Steel Strain Response.

Figure A-19: Test Results of Specimen MM1.

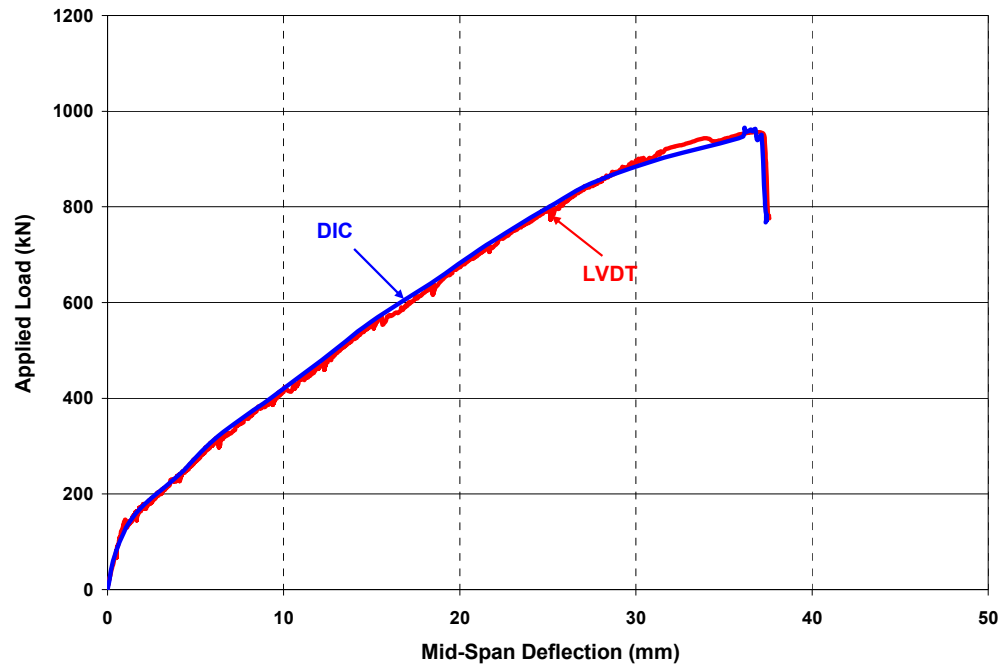
Specimen MM2



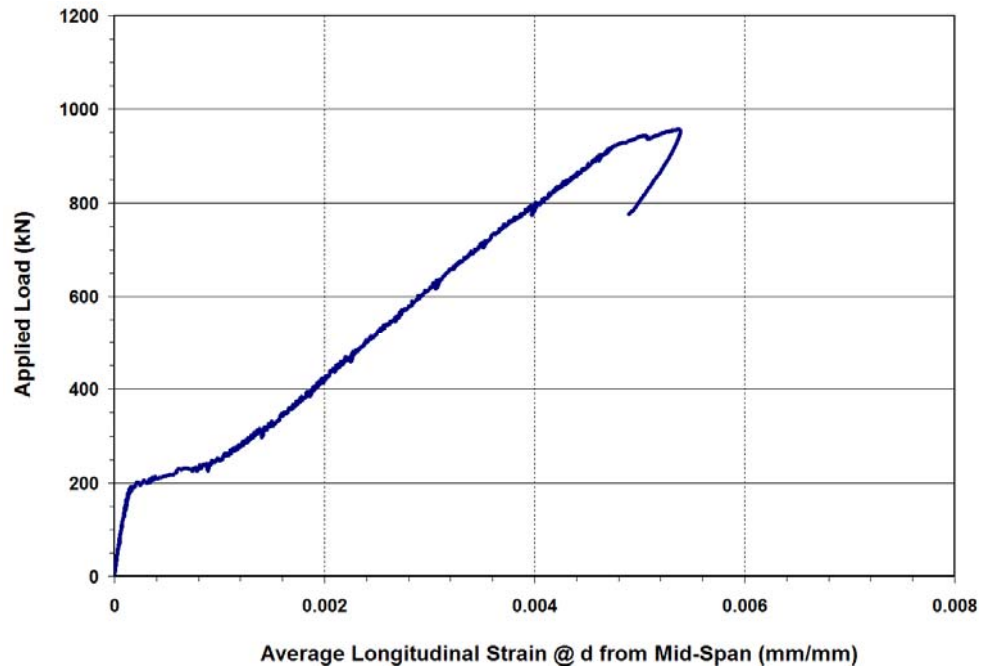
a) Elevation



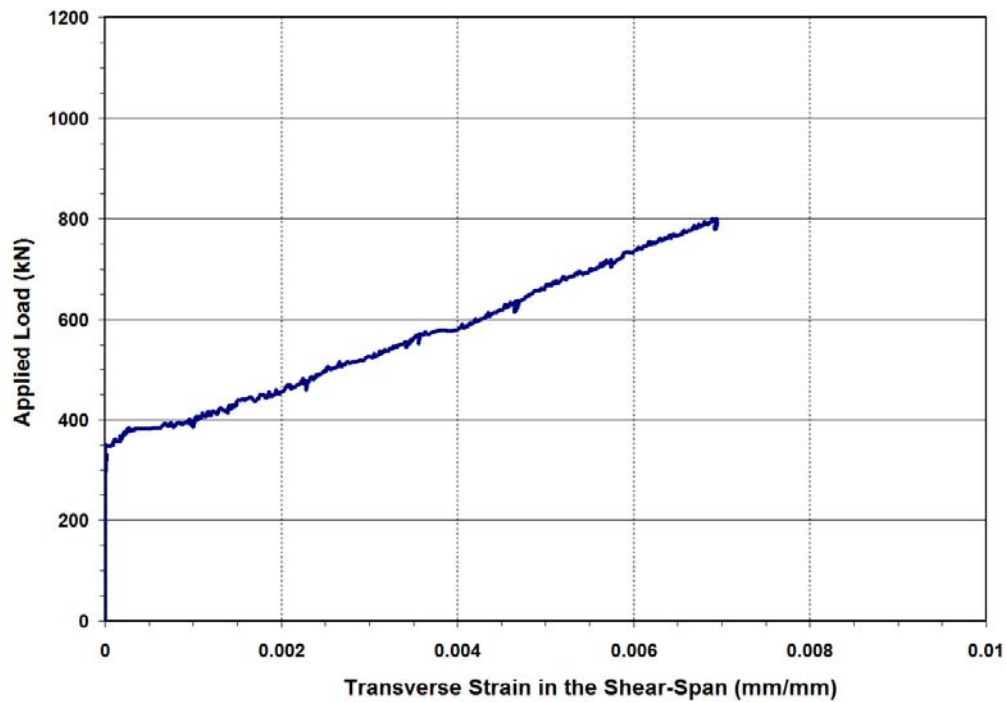
b) Crack Patterns After Failure



c) Load - Mid-Span Deflection Response



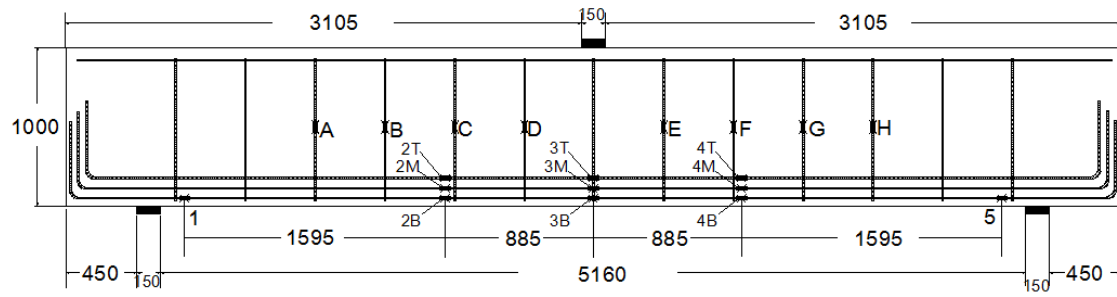
d) Typical Load - Average Steel Strain Response (@ d from mid-span)



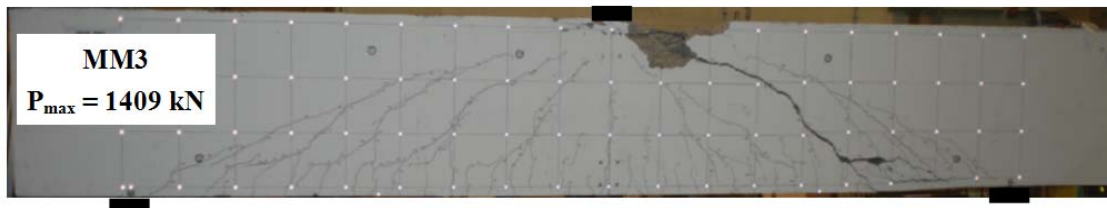
e) Maximum Load - Transverse Steel Strain Response.

Figure A-20: Test Results of Specimen MM2.

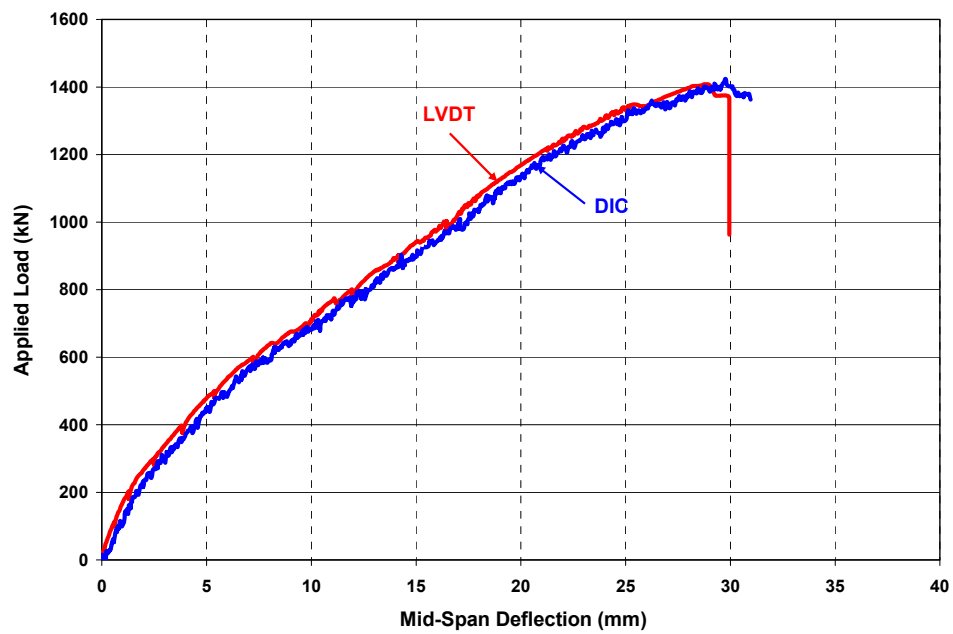
Specimen MM3



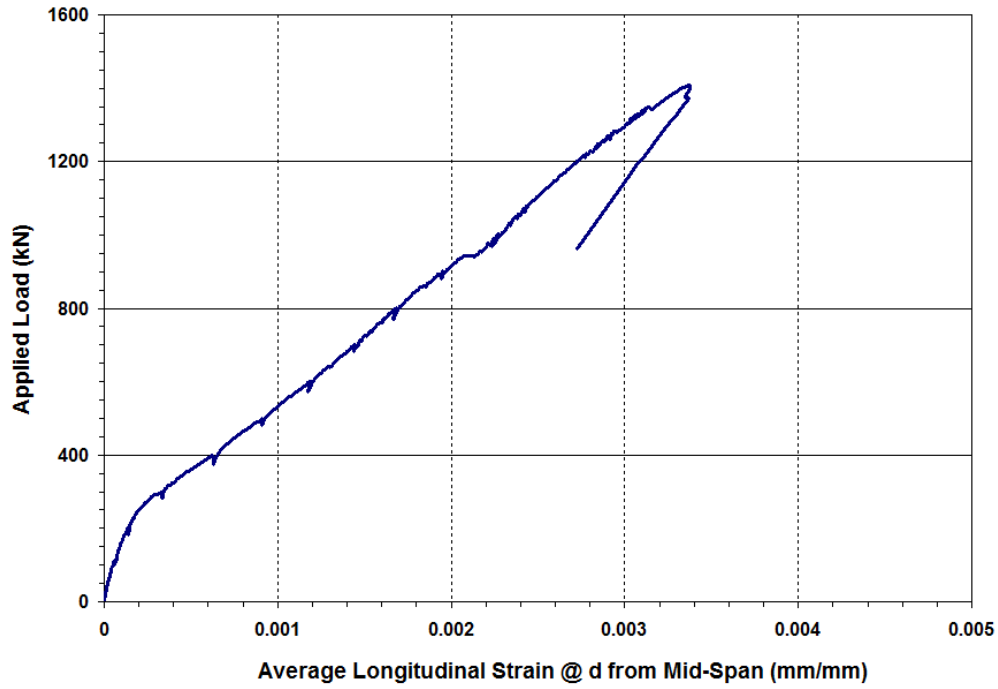
a) Elevation



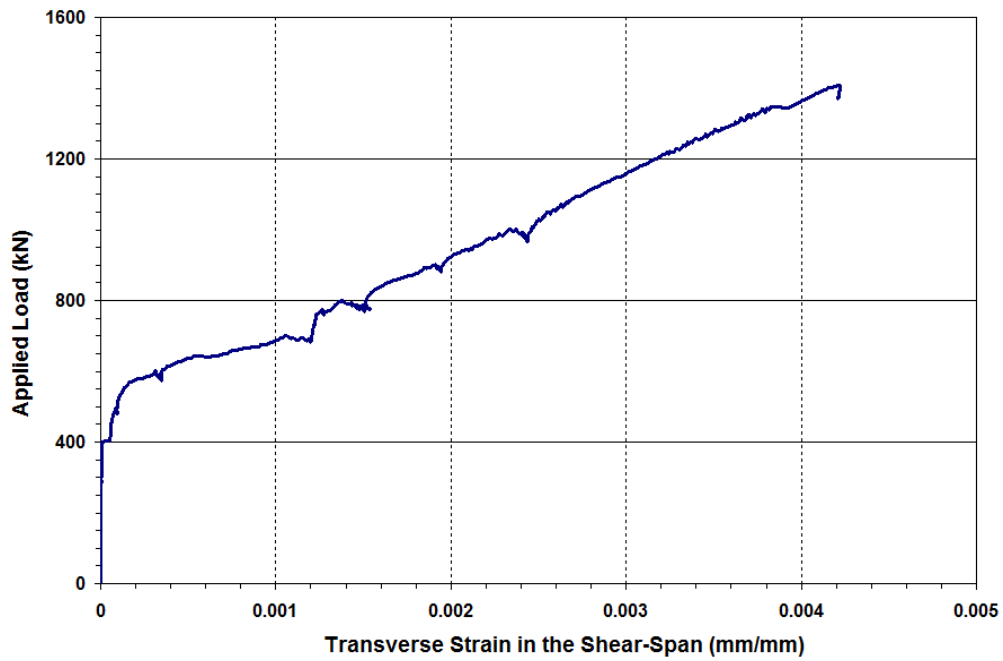
b) Crack Patterns After Failure



c) Load - Mid-Span Deflection Response



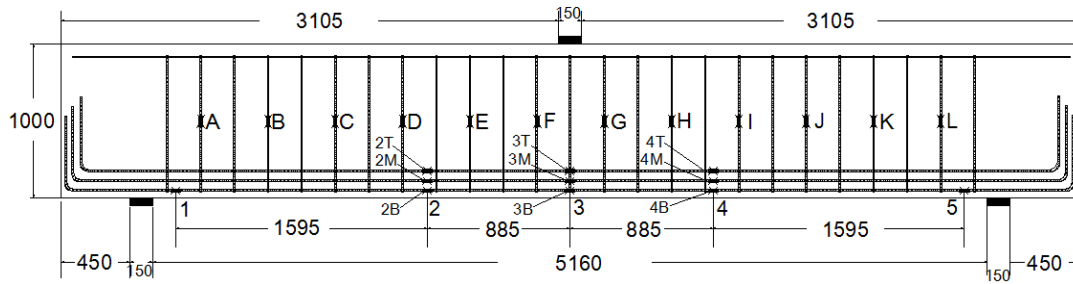
d) Typical Load - Average Steel Strain Response (@ d from mid-span)



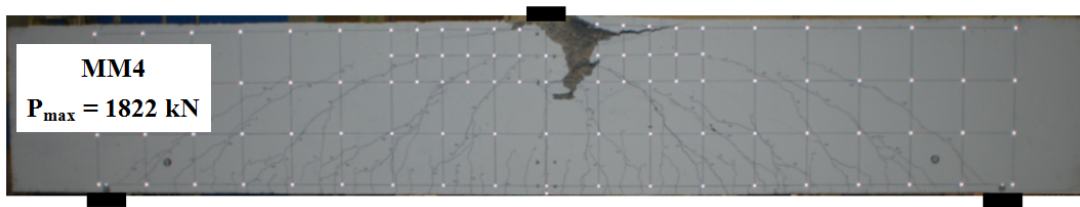
e) Maximum Load - Transverse Steel Strain Response.

Figure A-21: Test Results of Specimen MM3.

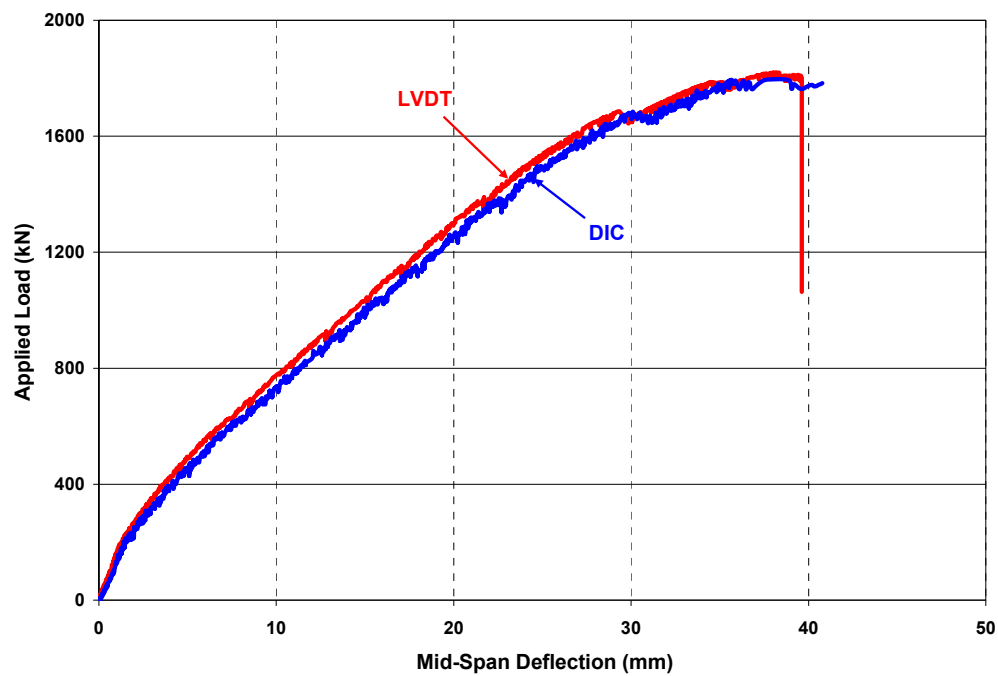
Specimen MM4



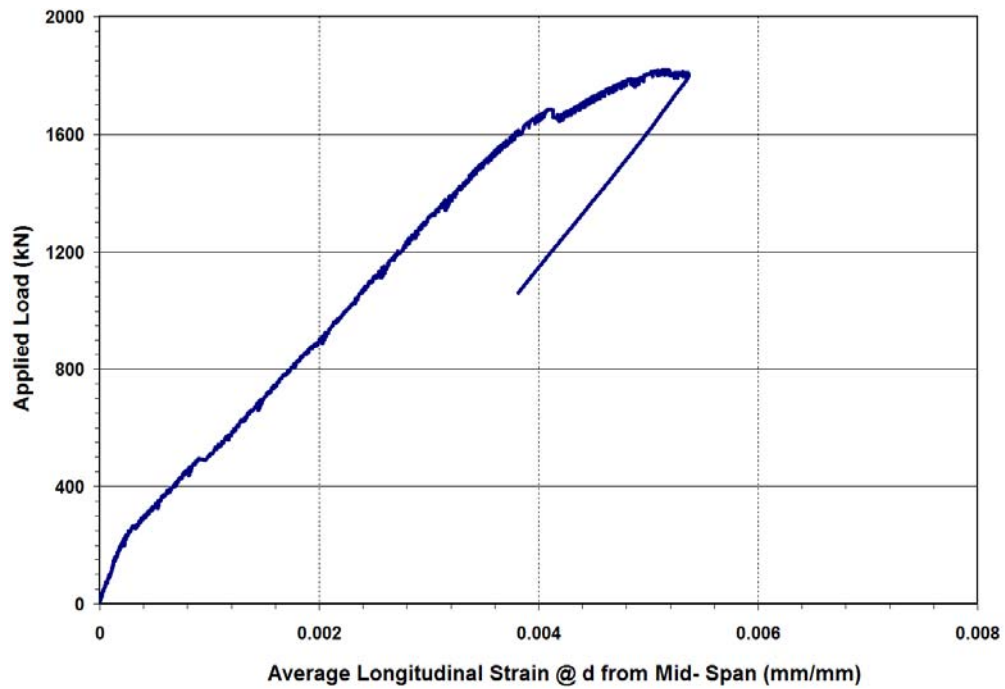
a) Elevation



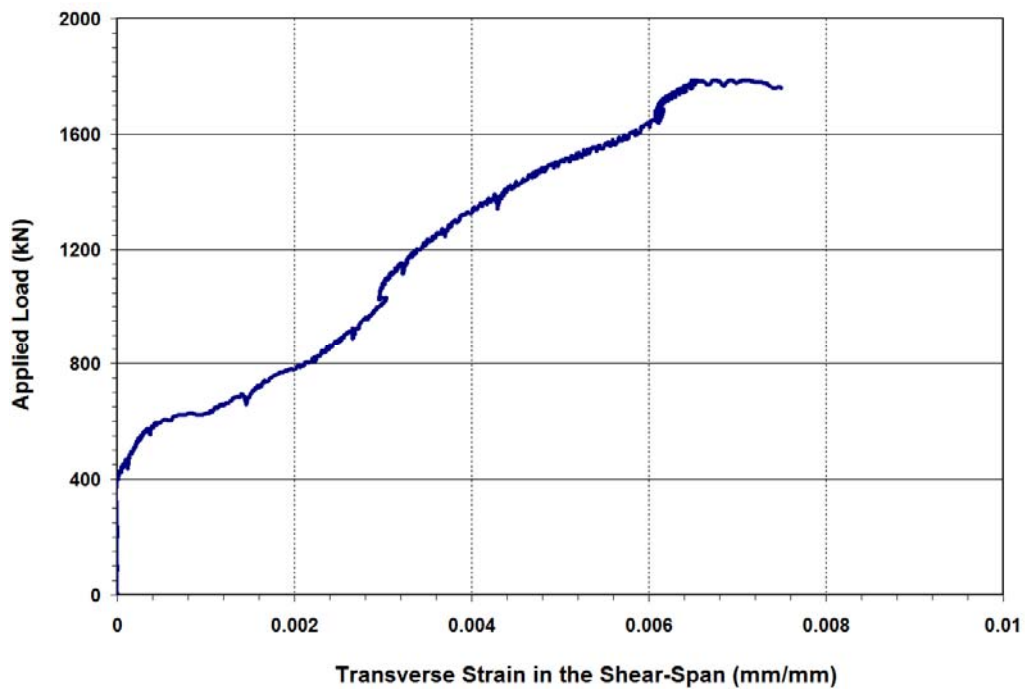
b) Crack Patterns After Failure



c) Load - Mid-Span Deflection Response



d) Typical Load - Average Steel Strain Response (@ d from mid-span)



e) Maximum Load - Transverse Steel Strain Response.

Figure A-22: Test Results of Specimen MM4.

APPENDIX B: SHEAR MODELS

B.1 Analytical and Numerical Shear Models

The shear capacity predictions of concrete slabs and beams reinforced with ASTM A1035 steel were determined using the analytical and numerical models described in Section 2.4. Three design code models (*CSA A23.3-04* with modifications to the non-linear stress-strain response, *ACI ITG-6R* and *Eurocode2-2004*) and the two numerical models (*VecTor 2* and *Response 2000*) were used for comparison. For the *CSA A23.3-04* model the shear capacity prediction of reinforced concrete members with ASTM A1035 steel longitudinal reinforcement involves an iterative calculation procedure. The calculation procedure is summarized in the flow chart shown in Figure B-1 for beams containing stirrups. For the *ACI ITG-6R* and *Eurocode2-2004* code model predictions the equations described in Section 2.4.1 were used.

The analysis for *VecTor2* (*VT2*) model is based on using an idealized bi-linear elastic-plastic stress-strain relationship with a yield strength of 690 MPa for the ASTM A1035 steel longitudinal reinforcement (*ACI ITG-6R-10*). For *Response 2000* (*R2K*) the non-linear stress-strain response of the ASTM A1035 longitudinal steel was simulated as unstressed prestressing steel using a modified Ramberg-Osgoode (R-O) relationship (*Collins and Mitchell, 1997*). The R-O approximation for the stress-strain response of ASTM A1035 longitudinal steel (adapted from *Collins and Mitchell, 1997*) is given by the following equation.

$$f_s = \begin{cases} 200,000 \varepsilon_s \left\{ A + \frac{1-A}{[1 + (B\varepsilon_s)^C]^{\frac{1}{C}}} \right\} \\ 1040 \end{cases} \quad (B-1)$$

The R-O parameters in equation B-1 were solved as $A = 0.006$, $B = 200$ & $C = 2.2$ from the actual stress-strain response of ASTM A1035 steel (equation 3-1) using a technique described in *Collins and Mitchell, 1997*).

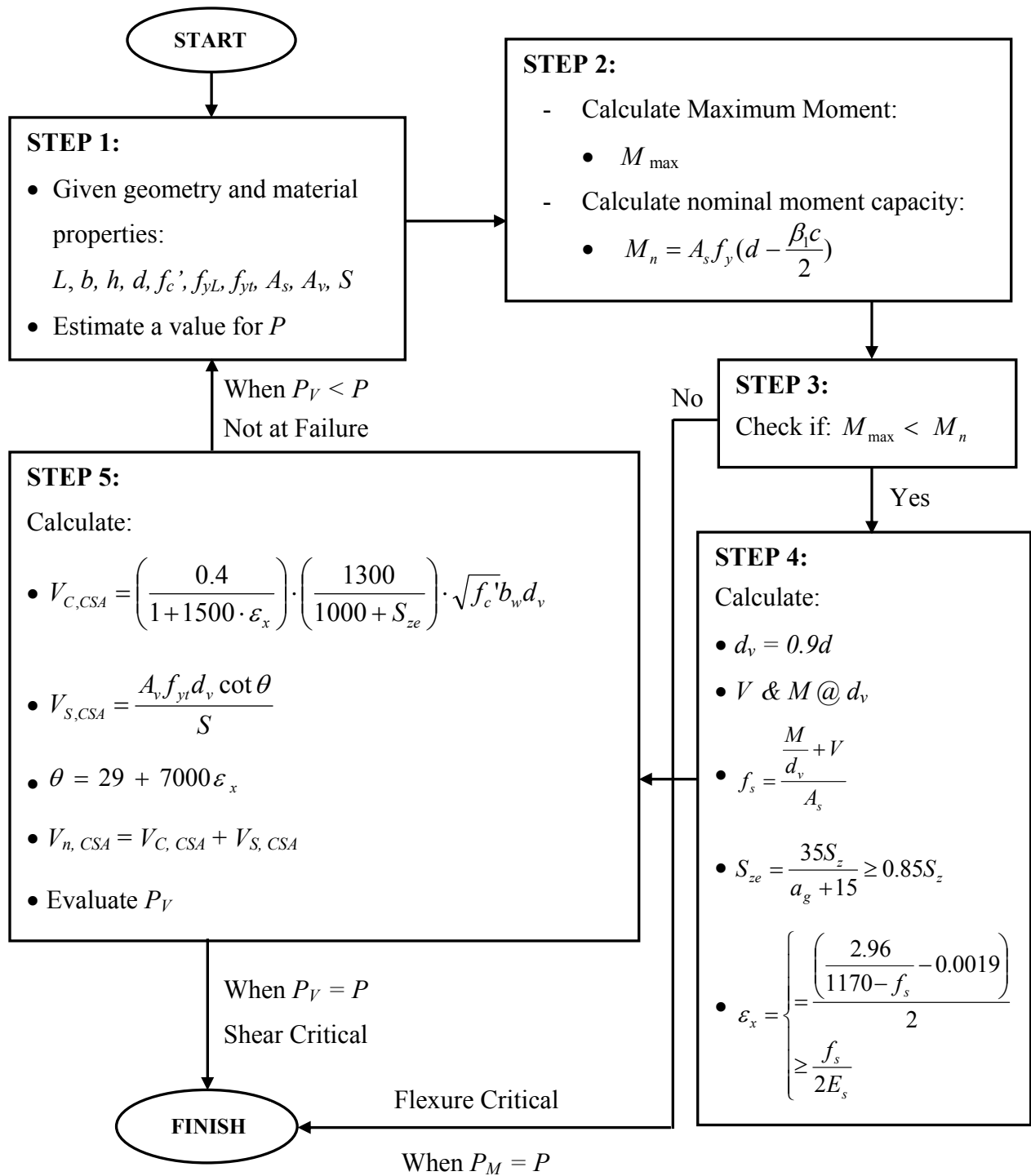


Figure B-1: Flowchart Showing the Prediction of Relationship Between Shear Strain and Member Strain.

B.2 Slab Specimens

B.2.1 Modeling Details and Shear Predictions

Table B-1: Modeling Details of Slab Specimens

<i>Specimen</i>	<i>b_w (mm)</i>	<i>d (mm)</i>	<i>h (mm)</i>	<i>a /d</i>	<i>ρ_L (%)</i>	<i>f_{yL} * (MPa)</i>	<i>f_c ' (MPa)</i>
<i>S-1</i>	305	278	305	3.55	0.46	690	53
<i>S-2</i>	305	278	305	3.55	0.46	690	59
<i>S-3</i>	305	569	600	3.60	0.45	690	49
<i>S-4</i>	305	569	600	3.60	0.45	690	57
<i>S-5</i>	305	573	600	3.57	0.23	690	53
<i>S-6</i>	305	573	600	3.57	0.23	690	57
<i>M-2.7-32</i>	460	850	915	2.75	0.44	690	32
<i>G1-M0</i>	610	645	711	3.11	1.02	690	31
<i>G2-M0</i>	610	645	711	3.11	1.02	690	31
<i>G3-M0</i>	406	457	559	3.00	2.71	690	37

* Yield Stress for ASTM A1035 Steel as Recommended by *ACI ITG-6R-10(2010)*.

Table B-2: Model Predictions of Slabs in the Database.

<i>Specimen</i>	<i>P_{CSA} (kN)</i>	<i>P_{ACI} (kN)</i>	<i>P_{EC2} (kN)</i>	<i>P_{VT2} (kN)</i>	<i>P_{R2K} (kN)</i>
<i>S-1</i>	124	206	163	128	128
<i>S-2</i>	127	218	169	129	121
<i>S-3</i>	213	399	275	221	192
<i>S-4</i>	221	430	289	230	223
<i>S-5</i>	147	418	225	137	169
<i>S-6</i>	149	433	230	131	173
<i>M-2.7-32</i>	463	739	503	458	440
<i>G1-M0</i>	434	551	526	527	403*
<i>G2-M0</i>	555	704	672	632	515*
<i>G3-M0</i>	279	267	366	474	379*

B.2.2 Load-Deflection Response for Slab Specimens Using Numerical Models

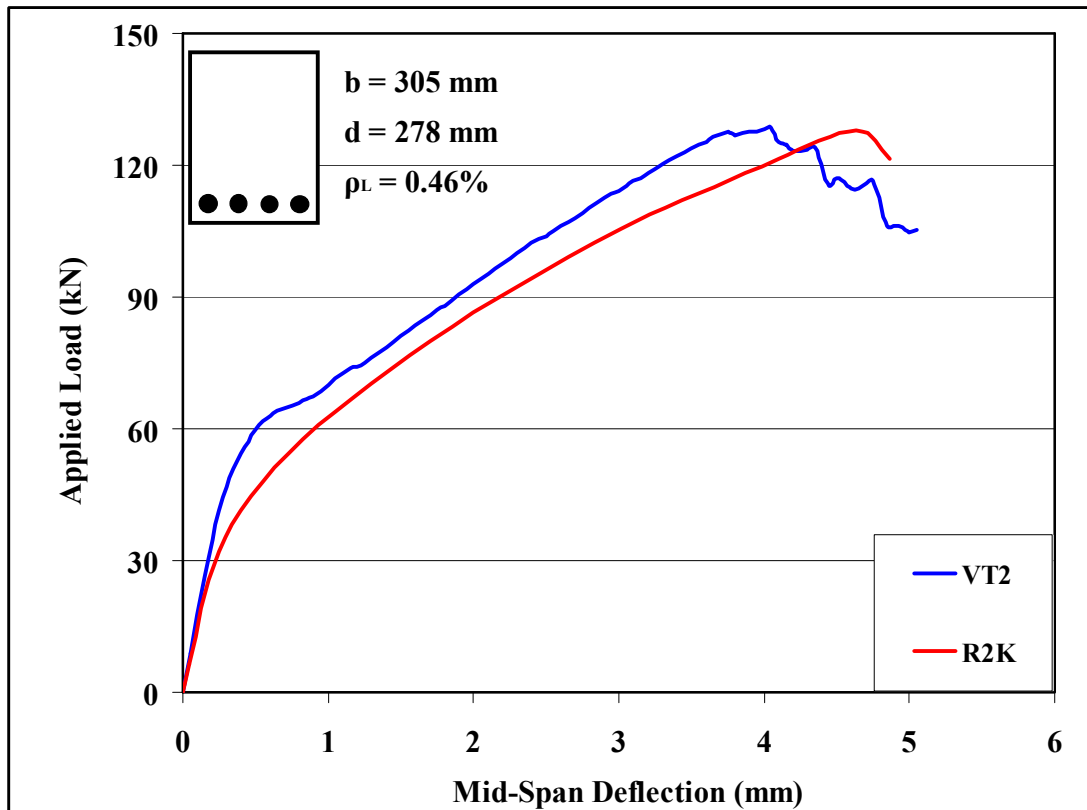


Figure B-2: Load-Deflection Plots of Beam S-1

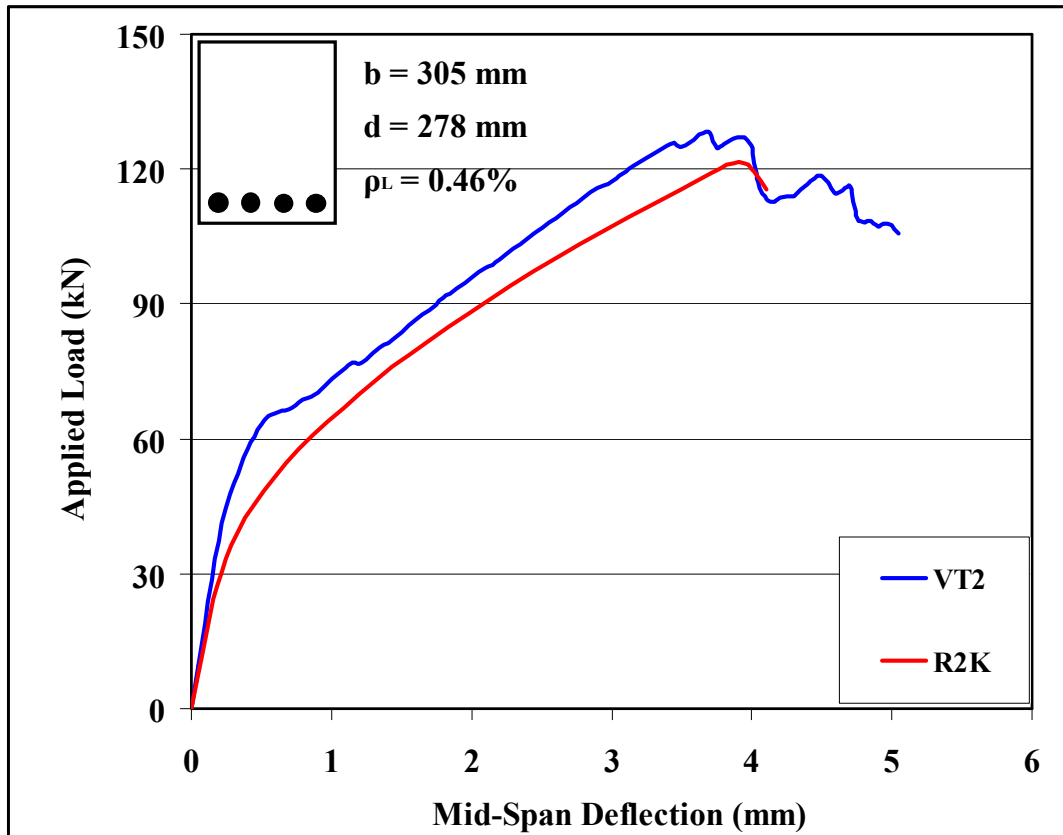


Figure B-3: Load-Deflection Plots of Beam S-2

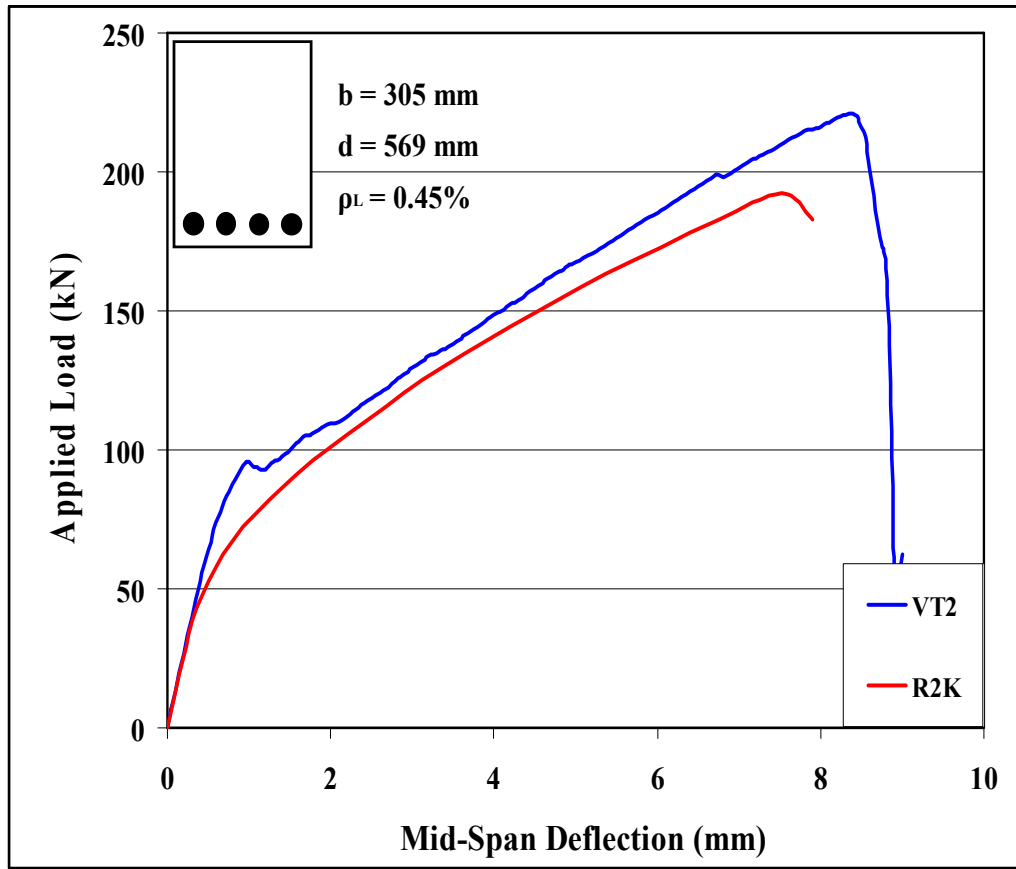


Figure B-4: Load-Deflection Plots of Beam S-3

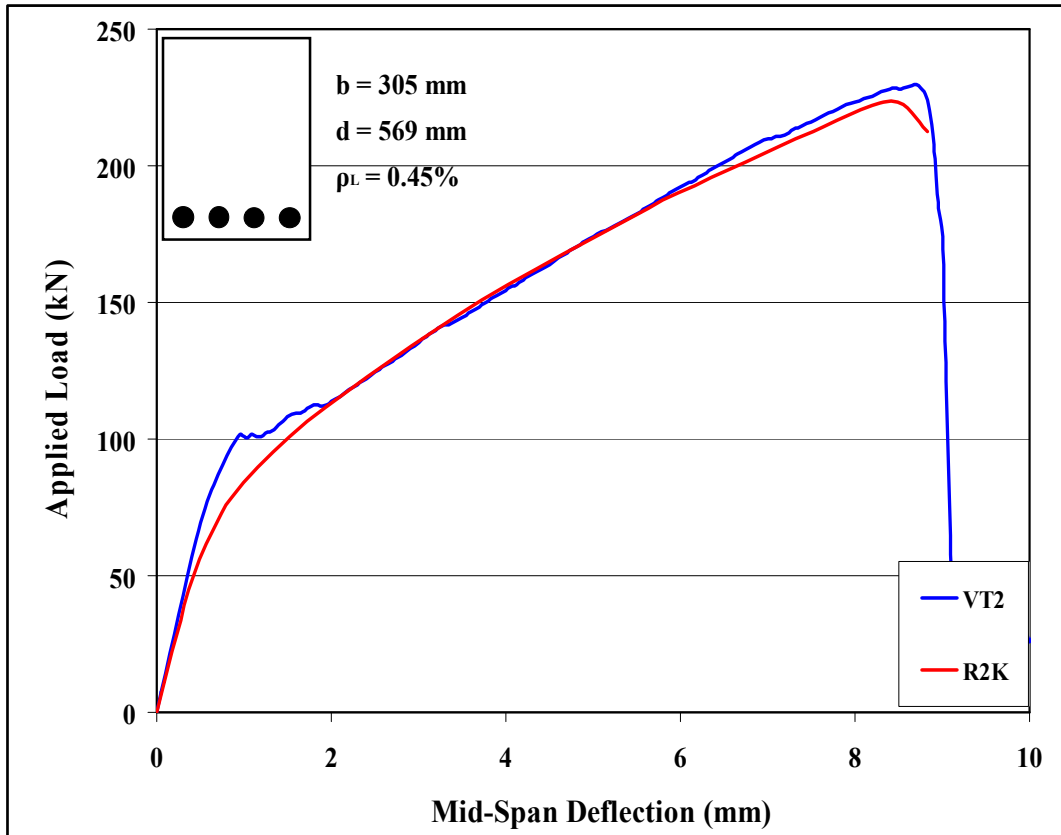


Figure B-5: Load-Deflection Plots of Beam S-4

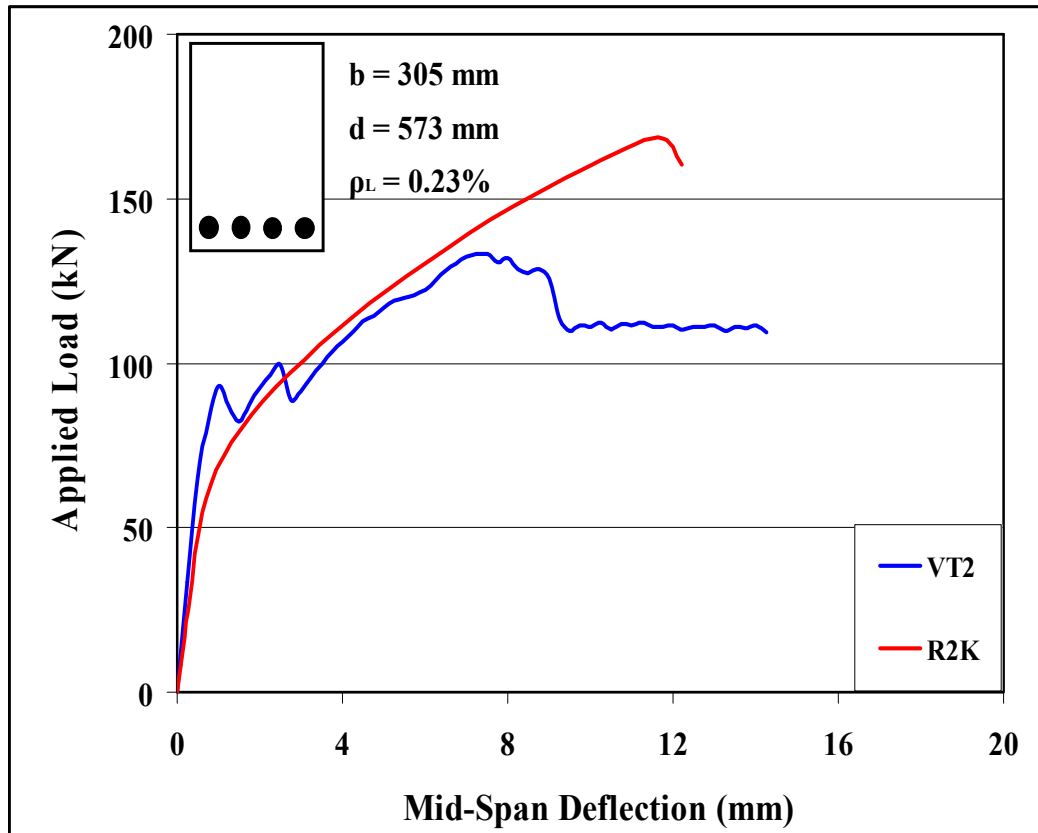


Figure B-6: Load-Deflection Plots of Beam S-5

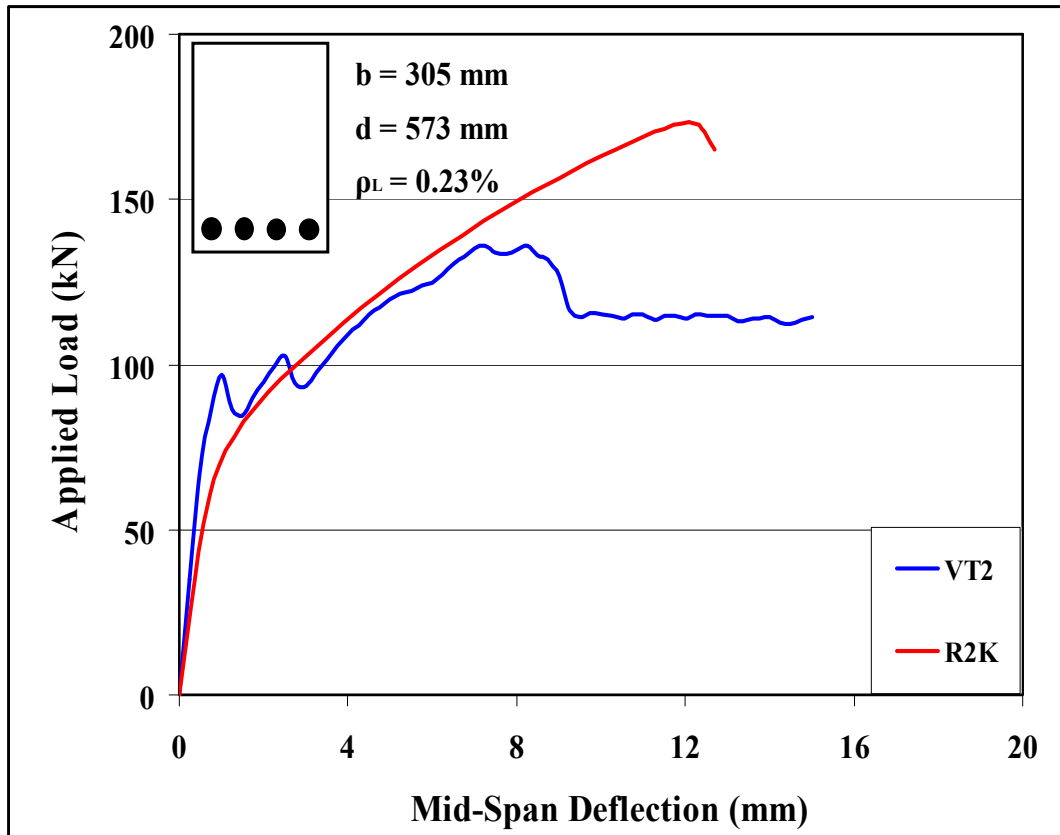


Figure B-7: Load-Deflection Plots of Beam S-6

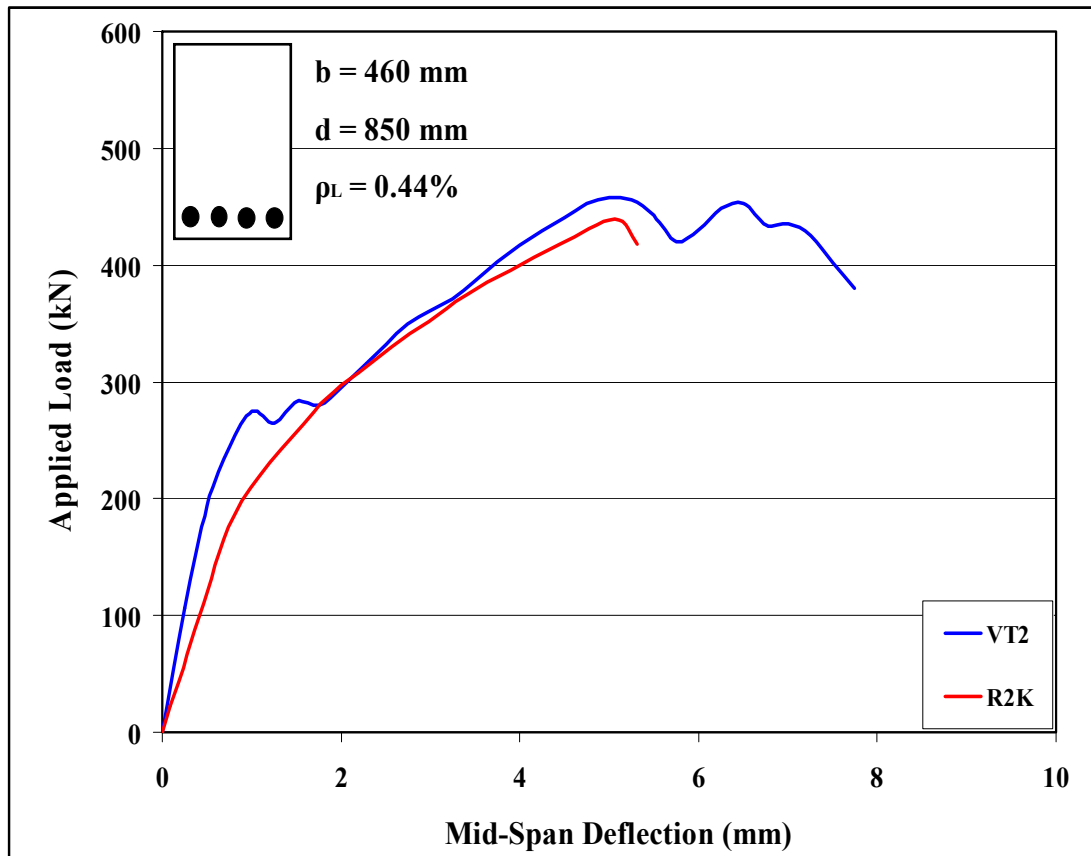


Figure B-8: Load-Deflection Plots of Beam M-2.7-32

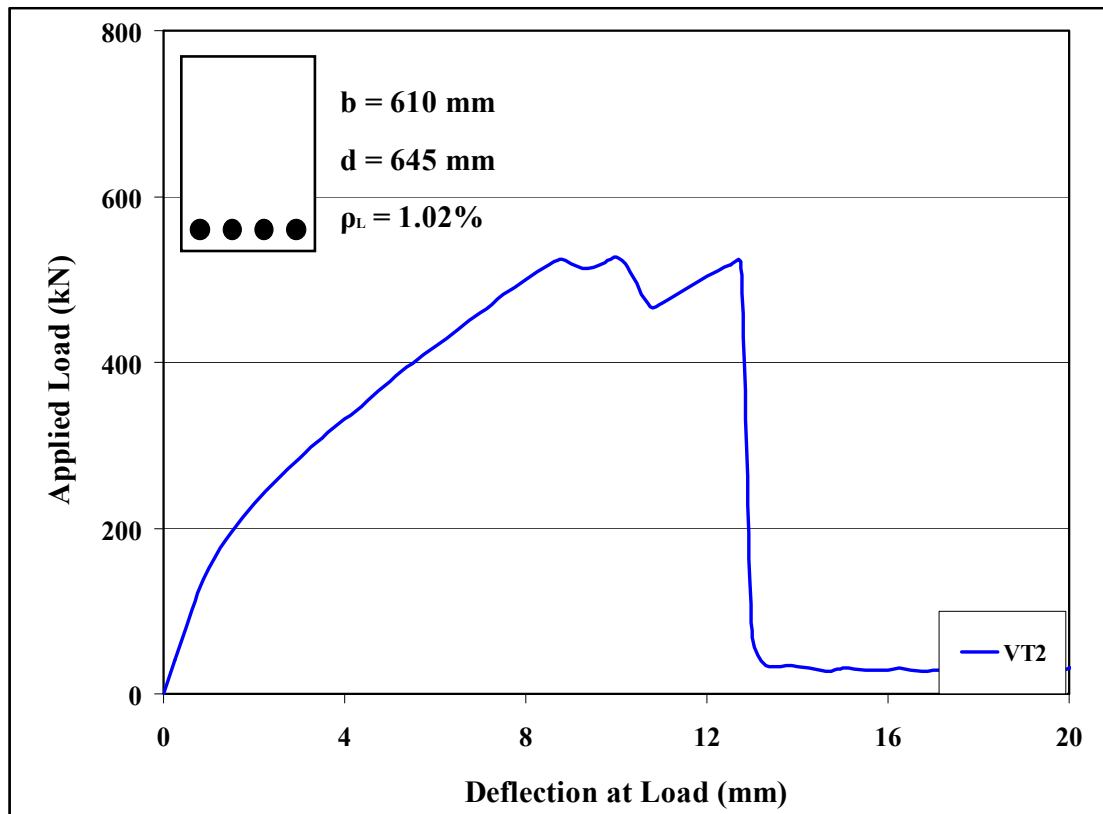


Figure B-9: Load-Deflection Plots of Beam G1-M0

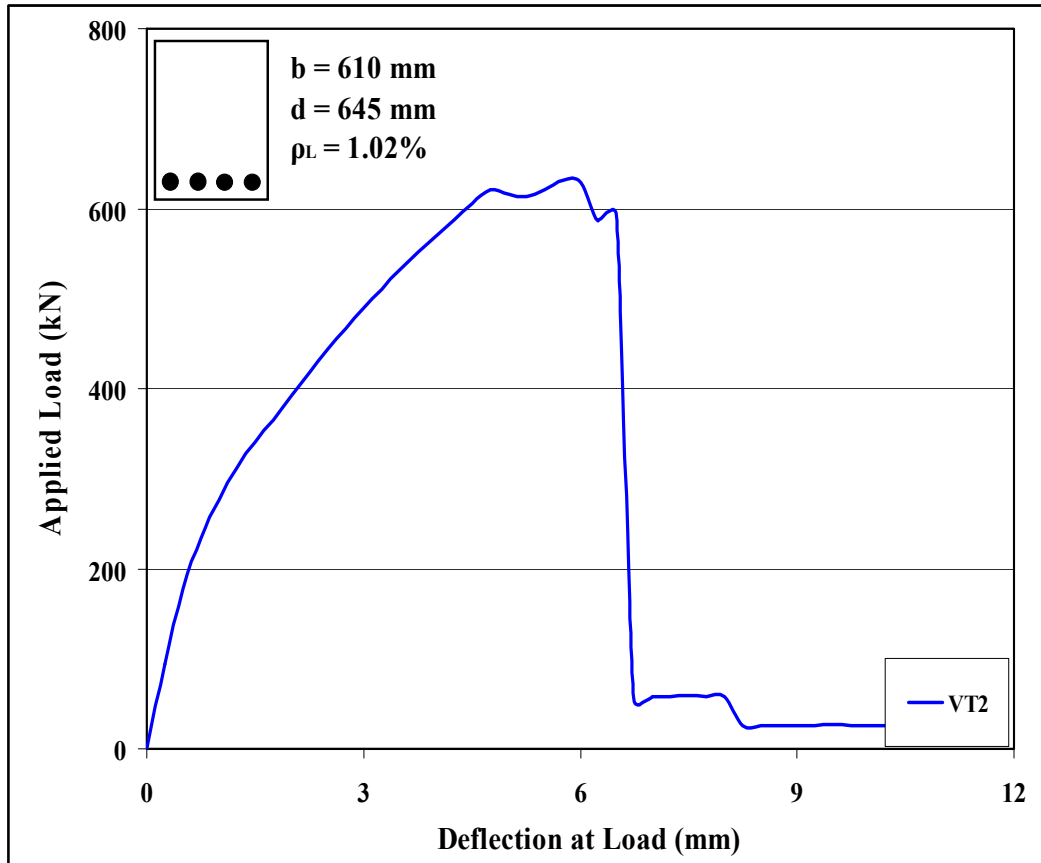


Figure B-10: Load-Deflection Plots of Beam G2-M0

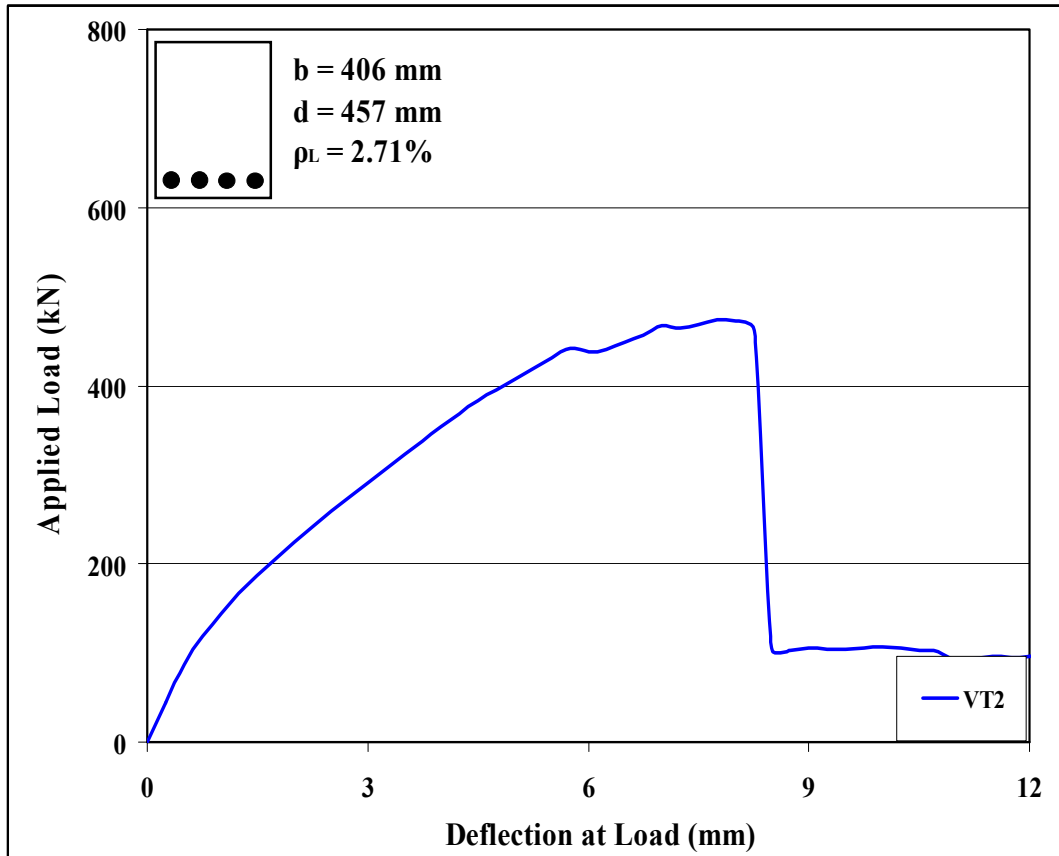


Figure B-11: Load-Deflection Plots of Beam G3-M0

B.3 Beam Specimens

B.3.1 Modeling Details and Shear Predictions

Table B-3: Modeling Details of Beam Specimens

<i>Beam ID</i>	<i>b_w</i> (mm)	<i>d</i> (mm)	<i>a/d</i>	ρ_L (%)	ρ_t (%)	<i>f_{yt}</i> (MPa)	<i>f_{ys}</i> (MPa)	<i>f_c</i> (MPa)
<i>RM1</i>	300	523	3.15	2.55	0.15	408	690	41
<i>RM2</i>	300	523	3.15	2.55	0.18	408	690	45
<i>MR1</i>	300	935	3.00	0.55	0.11	690	426	49
<i>MR2</i>	300	935	3.00	0.69	0.11	690	426	50
<i>MR3</i>	300	885	3.00	1.60	0.11	690	426	48
<i>MR4</i>	300	885	3.00	1.60	0.22	690	426	50
<i>MM1</i>	300	935	3.00	0.55	0.15	690	690	50
<i>MM2</i>	300	935	3.00	0.69	0.15	690	690	52
<i>MM3</i>	300	885	3.00	1.60	0.15	690	690	48
<i>MM4</i>	300	885	3.00	1.60	0.30	690	690	48
<i>C-M-6</i>	305	311	2.62	4.08	0.31	427	690	30
<i>C-M-4</i>	305	311	3.08	4.08	0.46	427	690	31
<i>C-M-3</i>	305	311	3.08	4.08	0.61	427	690	33
<i>M-M-6</i>	305	311	2.62	4.08	0.31	690	690	32
<i>M-M-4</i>	305	311	3.08	4.08	0.46	690	690	32
<i>M-M-3</i>	305	311	3.08	4.08	0.61	690	690	33
<i>G1-M80</i>	610	645	3.11	1.02	0.09	690	550	33
<i>G1-M100</i>	610	645	3.11	1.02	0.07	690	690	34
<i>G2-M80</i>	610	645	3.11	1.02	0.09	690	550	33
<i>G2-M100</i>	610	645	3.11	1.02	0.07	690	690	34
<i>G3-M80</i>	406	457	3.00	2.71	0.25	690	550	36
<i>G3-M100</i>	406	457	3.00	2.71	0.20	690	690	40
<i>F40-1</i>	200	252	3.00	2.52	0.59	690	510	37
<i>F40-3</i>	200	252	3.00	2.52	1.02	690	510	37
<i>F40-5</i>	200	252	3.00	3.78	1.43	690	510	37
<i>F60-1</i>	200	252	3.00	2.55	0.51	690	508	63
<i>F60-2</i>	200	252	3.00	2.55	1.06	690	508	63
<i>F60-3</i>	200	252	3.00	3.82	1.41	690	508	63
<i>F60-4</i>	200	252	3.00	5.54	1.95	690	508	63
<i>F80-1</i>	200	252	3.00	2.55	0.98	690	508	85
<i>F80-2</i>	200	252	3.00	3.82	1.49	690	508	85
<i>F80-3</i>	200	252	3.00	5.10	2.01	690	508	85
<i>F80-4</i>	200	252	3.00	5.54	2.53	690	508	85
<i>F80-5</i>	200	252	3.00	6.92	3.02	690	508	85
<i>SR1 (A)</i>	305	525	3.19	1.91	0.35	690	414	84
<i>SR1 (B)</i>	305	525	3.19	1.91	0.22	690	690	84
<i>SR2 (A)</i>	305	530	3.16	1.57	0.26	690	414	89
<i>SR2 (B)</i>	305	530	3.16	1.57	0.14	690	690	89
<i>SR3 (A)</i>	305	495	3.08	1.69	0.26	690	414	90
<i>SR3 (B)</i>	305	495	3.08	1.69	0.14	690	690	90
<i>SR4 (A)</i>	305	501	3.04	1.67	0.39	690	414	90
<i>SR4 (B)</i>	305	501	3.04	1.67	0.19	690	690	90
<i>SR5</i>	305	510	3.29	1.96	0.22	690	690	116

Table B-4: Model Predictions of Beams in the Database ($f_{yt} = 550$ MPa).

<i>Beam ID</i>	P_{CSA} (kN)	P_{ACI} (kN)	P_{EC2} (kN)	P_{VT2} (kN)	P_{R2K} (kN)
<i>RM1</i>	652	586	673	734	640
<i>RM2</i>	763	655	856	776	730
<i>MR1</i>	659	1018	516	696	819
<i>MR2</i>	748	1021	621	851	850
<i>MR3</i>	983	958	783	1060	838
<i>MR4</i>	1286	1319	1335	1461	1517
<i>MM1</i>	643	978	589	654	740
<i>MM2</i>	731	994	705	688	760
<i>MM3</i>	948	918	694	832	800
<i>MM4</i>	1217	1232	1507	1268	1320
<i>C-M-6</i>	440	327	438	549	321*
<i>C-M-4</i>	601	487	267	637	408*
<i>C-M-3</i>	722	609	260	671	448*
<i>M-M-6</i>	439	332	564	571	343*
<i>M-M-4</i>	603	489	566	646	428*
<i>M-M-3</i>	722	609	565	740	496*
<i>G1-M80</i>	813	855	649	724	589*
<i>G1-M100</i>	765	800	620	680	508*
<i>G2-M80</i>	1039	1093	694	907	589*
<i>G2-M100</i>	977	1023	671	820	508*
<i>G3-M80</i>	999	918	896	1098	776*
<i>G3-M100</i>	882	792	868	986	713*
<i>F40-1</i>	416	405	594	236	244
<i>F40-3</i>	543	512	594	247	304
<i>F40-5</i>	776	512	594	332	350
<i>F60-1</i>	400	393	246	223	282
<i>F60-2</i>	561	667	884	252	348
<i>F60-3</i>	783	667	884	373	381
<i>F60-4</i>	1092	667	884	313	401
<i>F80-1</i>	548	653	1050	265	360
<i>F80-2</i>	809	773	1050	370	403
<i>F80-3</i>	1071	773	1050	500	444
<i>F80-4</i>	1116	711	1000	529	457
<i>F80-5</i>	1507	773	1050	426	487
<i>SR1 (A)</i>	900	952	544	816	986
<i>SR1 (B)</i>	834	867	534	816	858
<i>SR2 (A)</i>	765	847	452	658	778
<i>SR2 (B)</i>	697	755	438	658	616
<i>SR3 (A)</i>	371	397	372	538	478
<i>SR3 (B)</i>	336	354	346	407	378
<i>SR4 (A)</i>	435	489	408	516	688
<i>SR4 (B)</i>	406	403	394	493	477
<i>SR5</i>	823	887	515	779	910

* Results Based on Sectional Response.

Table B-5: Model Predictions of Beams in the Database ($f_{yt} = 690$ MPa).

<i>Beam ID</i>	P_{CSA} (kN)	P_{ACI} (kN)	P_{EC2} (kN)	P_{VT2} (kN)	P_{R2K} (kN)
<i>RM1</i>	722	651	715	810	640
<i>RM2</i>	850	734	748	846	730
<i>MR1</i>	659	1018	516	696	819
<i>MR2</i>	748	1021	621	851	850
<i>MR3</i>	983	958	783	1060	838
<i>MR4</i>	1286	1319	1335	1461	1517
<i>MM1</i>	676	1063	525	694	820
<i>MM2</i>	772	1079	634	728	850
<i>MM3</i>	1018	998	874	1057	915
<i>MM4</i>	1342	1392	1363	1397	1514
<i>C-M-6</i>	501	381	628	578	321*
<i>C-M-4</i>	692	577	755	690	408*
<i>C-M-3</i>	876	673	780	704	448*
<i>M-M-6</i>	503	386	628	599	384*
<i>M-M-4</i>	693	579	776	689	479*
<i>M-M-3</i>	834	673	780	811	558*
<i>G1-M80</i>	813	931	465	724	673*
<i>G1-M100</i>	813	859	463	680	581*
<i>G2-M80</i>	1039	1190	848	907	673*
<i>G2-M100</i>	1039	1098	818	820	581*
<i>G3-M80</i>	999	1085	630	1098	783*
<i>G3-M100</i>	1000	924	629	1093	797*
<i>F40-1</i>	416	405	594	236	244
<i>F40-3</i>	543	512	594	247	304
<i>F40-5</i>	776	512	594	332	350
<i>F60-1</i>	400	393	246	223	282
<i>F60-2</i>	561	667	884	252	348
<i>F60-3</i>	783	667	884	373	381
<i>F60-4</i>	1092	667	884	313	401
<i>F80-1</i>	548	653	1050	265	360
<i>F80-2</i>	809	773	1050	370	403
<i>F80-3</i>	1071	773	1050	500	444
<i>F80-4</i>	1116	711	1000	529	457
<i>F80-5</i>	1507	773	1050	426	487
<i>SR1 (A)</i>	900	952	544	980	986
<i>SR1 (B)</i>	908	964	545	980	970
<i>SR2 (A)</i>	765	847	452	723	778
<i>SR2 (B)</i>	745	819	448	723	724
<i>SR3 (A)</i>	371	397	372	538	478
<i>SR3 (B)</i>	360	384	365	460	436
<i>SR4 (A)</i>	435	489	408	561	688
<i>SR4 (B)</i>	406	444	394	563	556
<i>SR5</i>	885	971	526	1009	1069

* Results Based on Sectional Response.

B.3.2 Load-Deflection Response for Beam Specimens Using Numerical Models

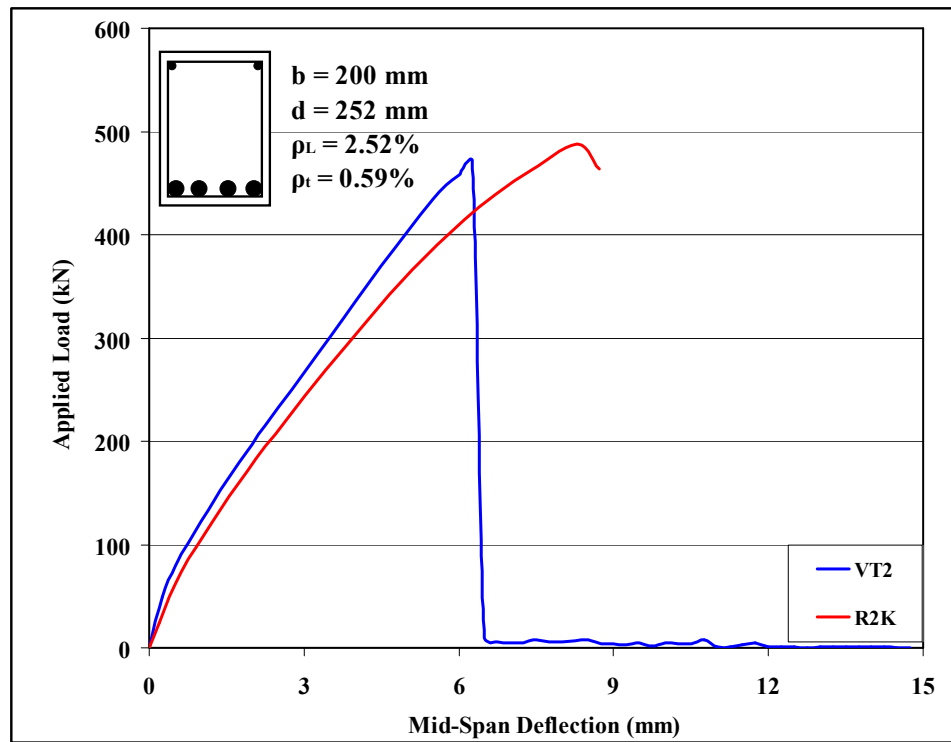


Figure B-2: Load-Deflection Plots of Beam F40-1

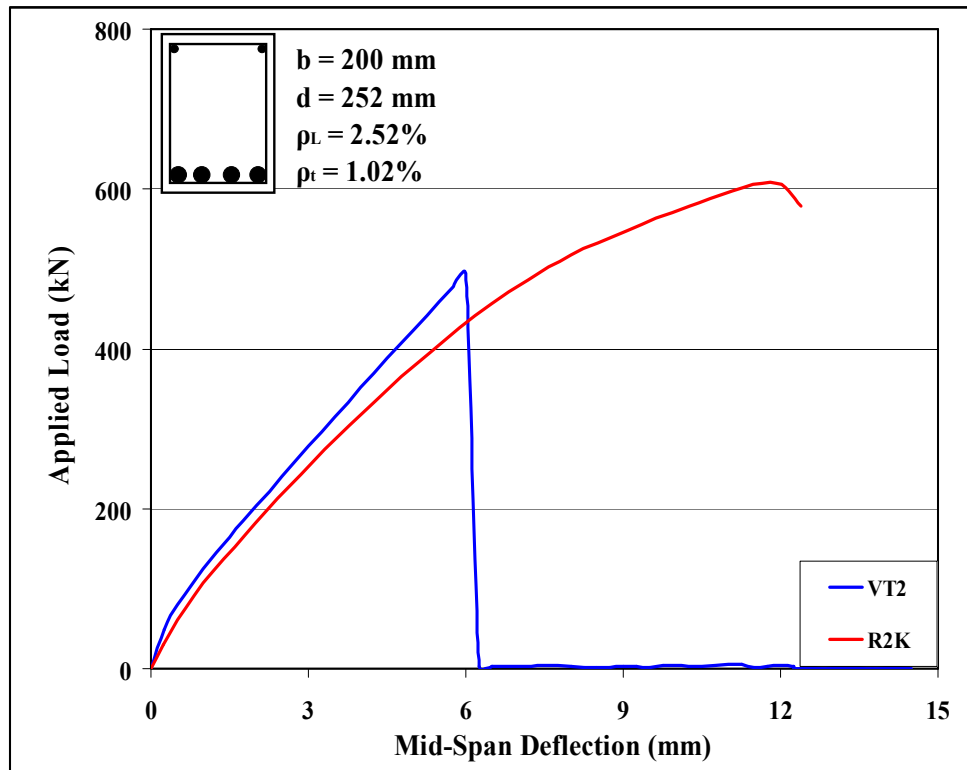


Figure B-2: Load-Deflection Plots of Beam F40-3

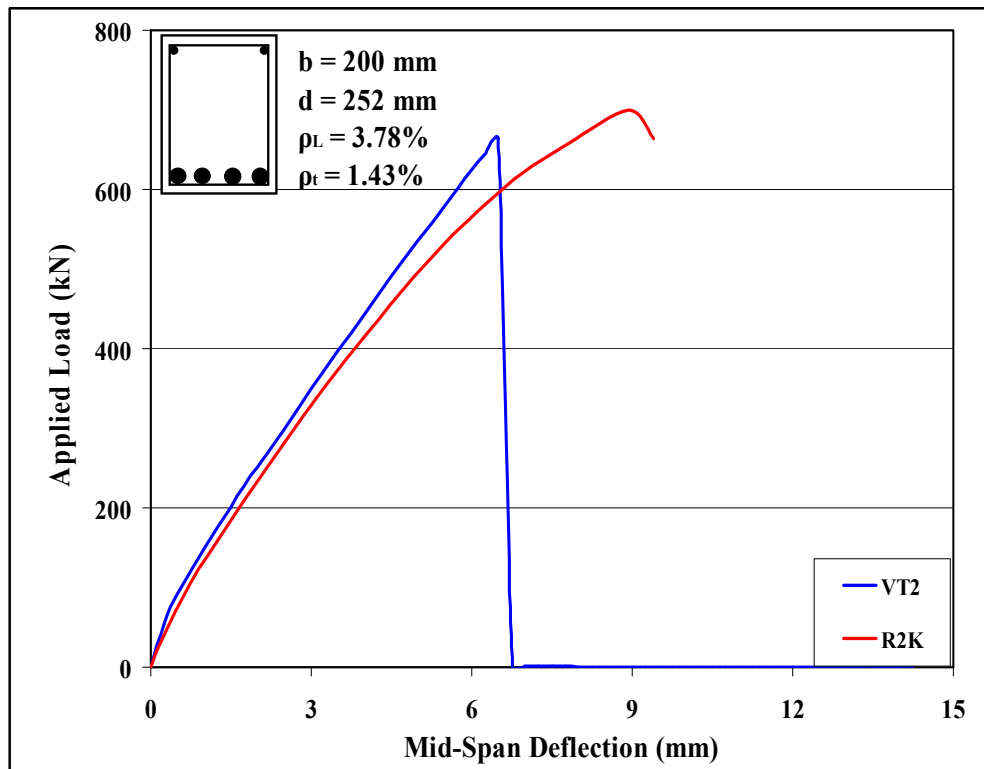


Figure B-2: Load-Deflection Plots of Beam F40-5

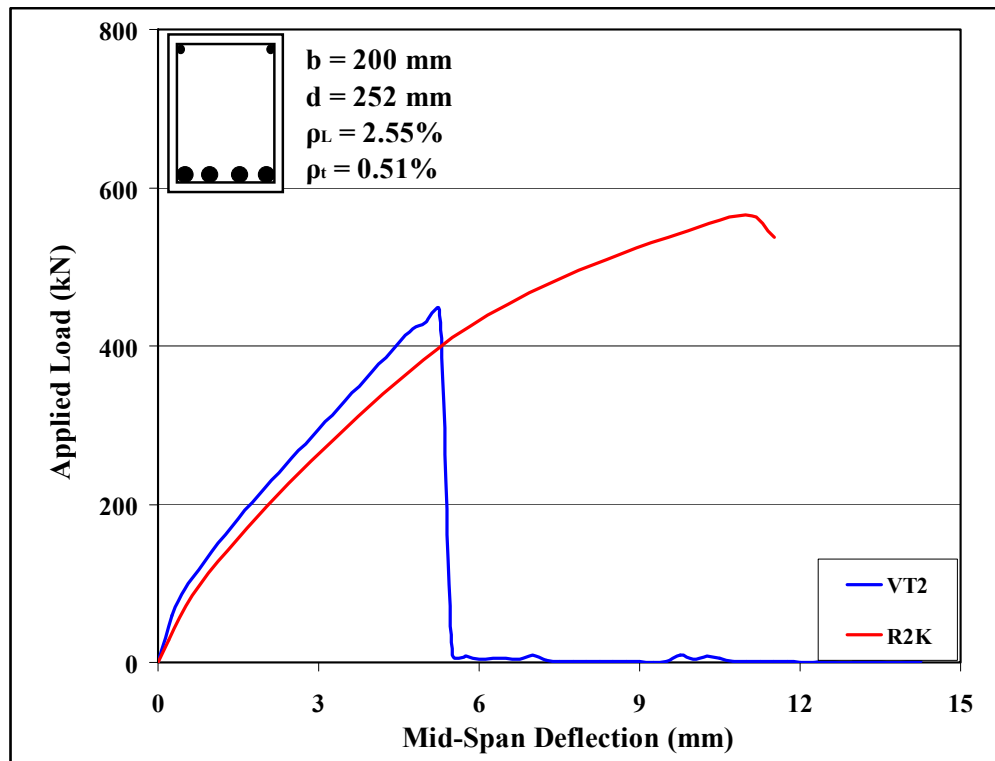


Figure B-2: Load-Deflection Plots of Beam F60-1

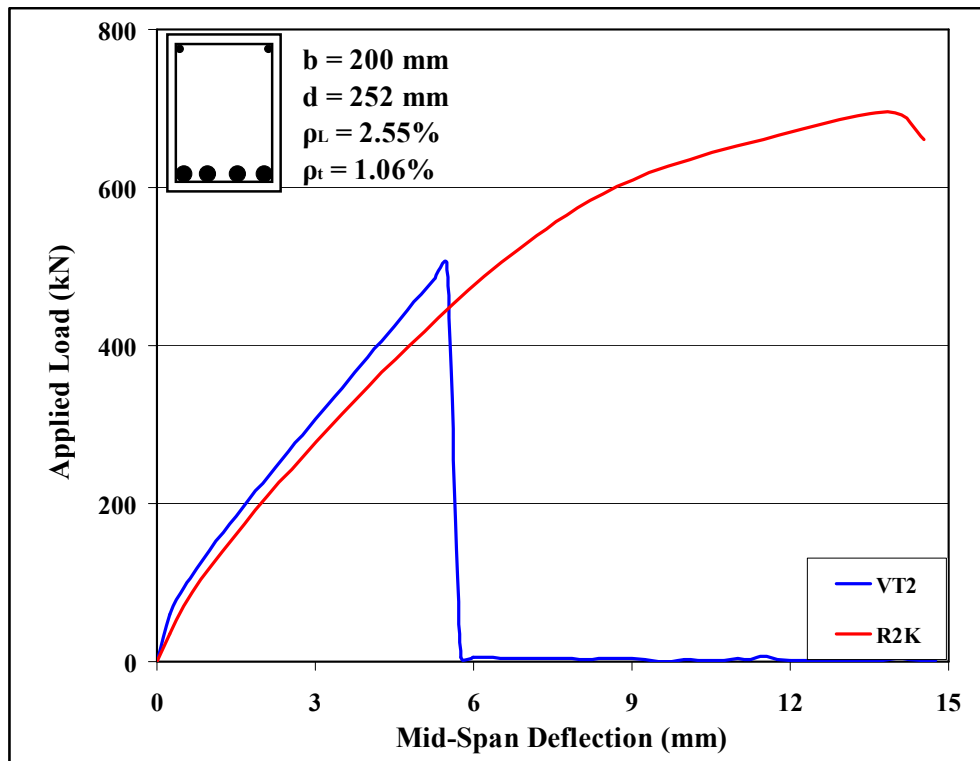


Figure B-2: Load-Deflection Plots of Beam F60-2

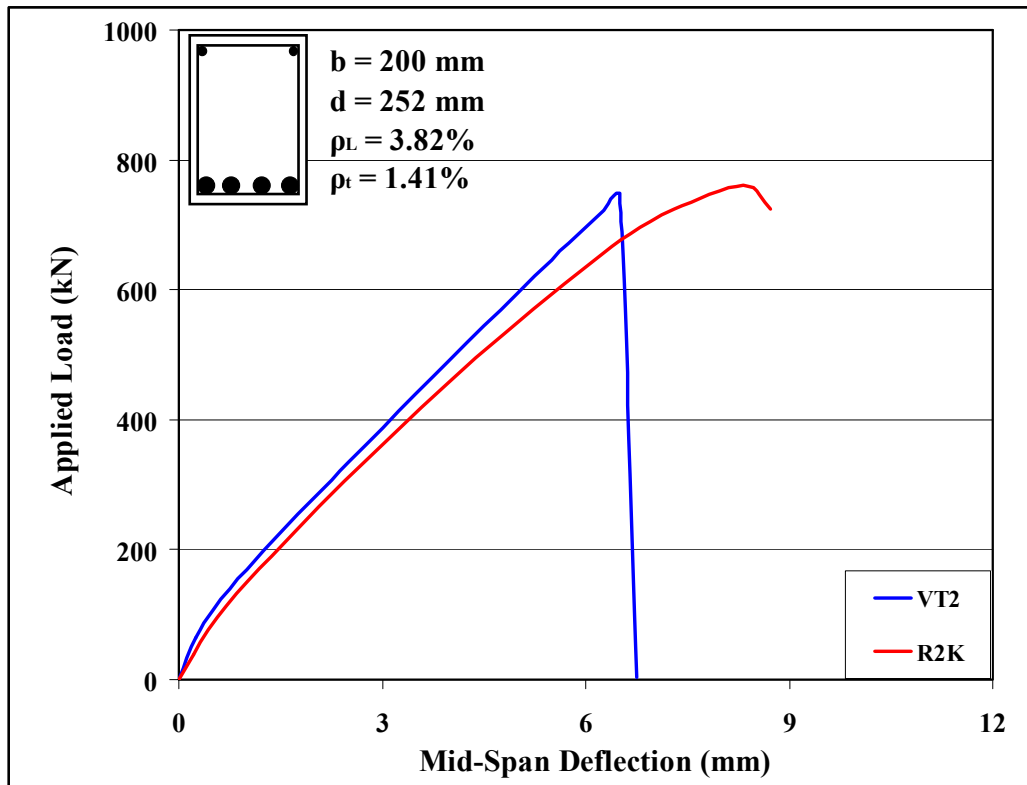


Figure B-2: Load-Deflection Plots of Beam F60-3

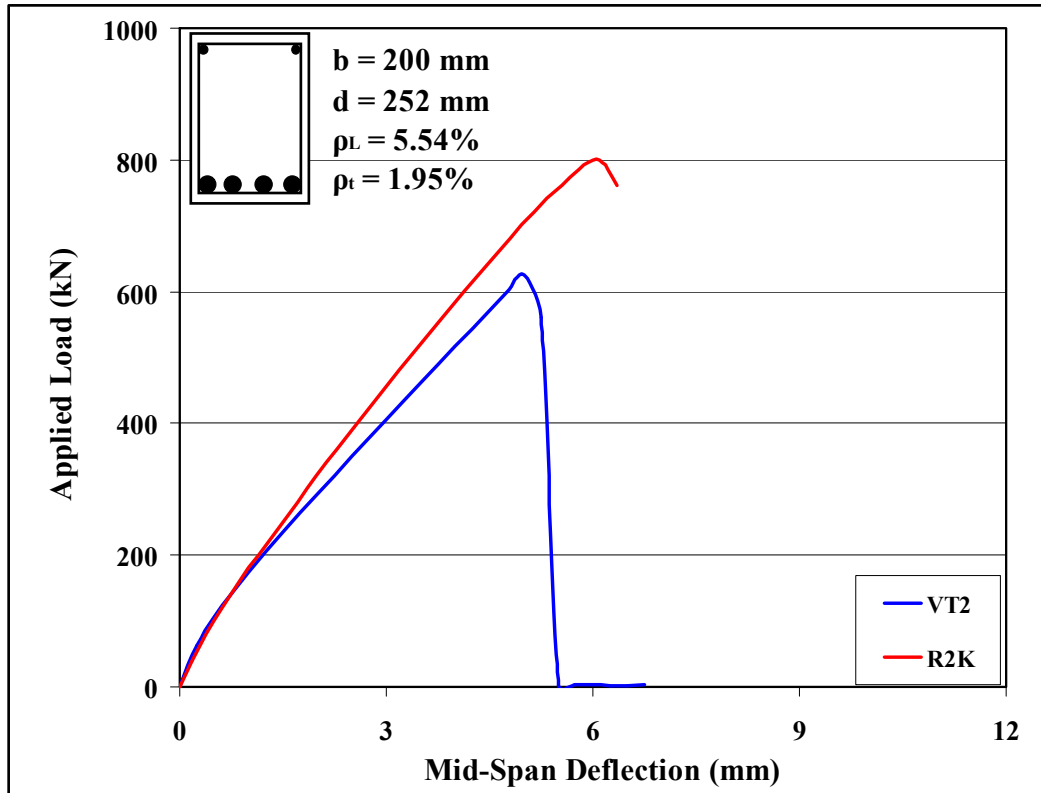


Figure B-2: Load-Deflection Plots of Beam F60-4

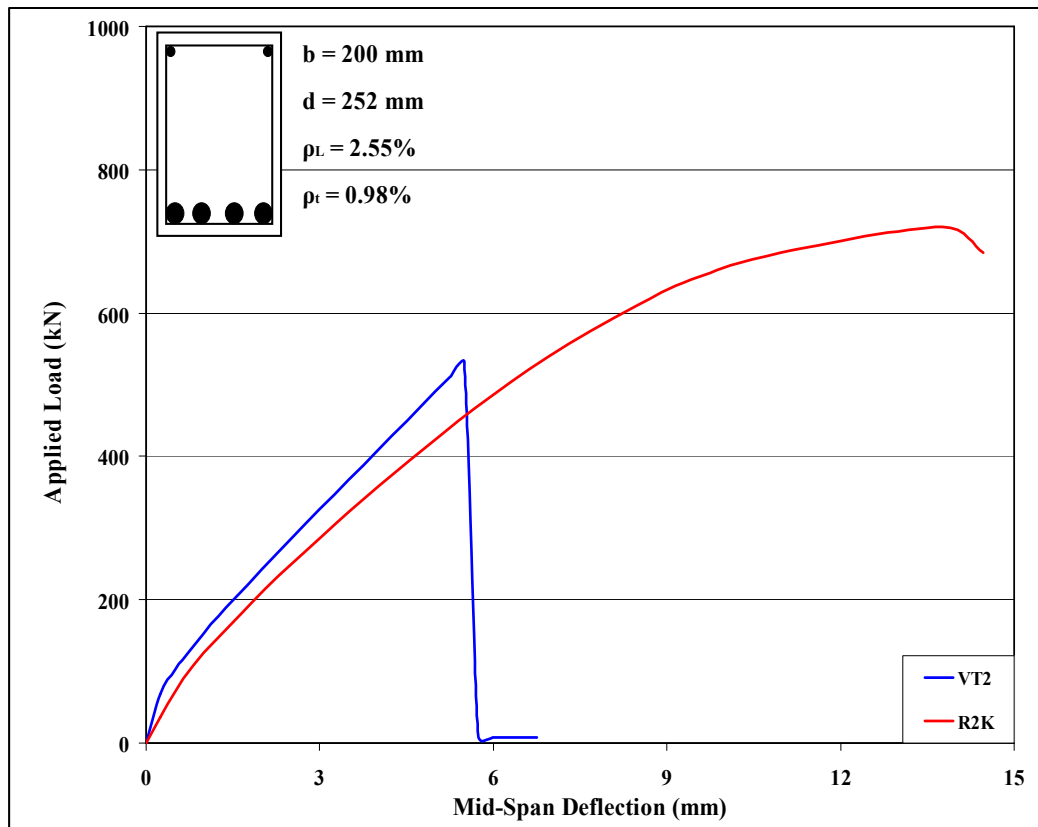


Figure B-2: Load-Deflection Plots of Beam F80-1

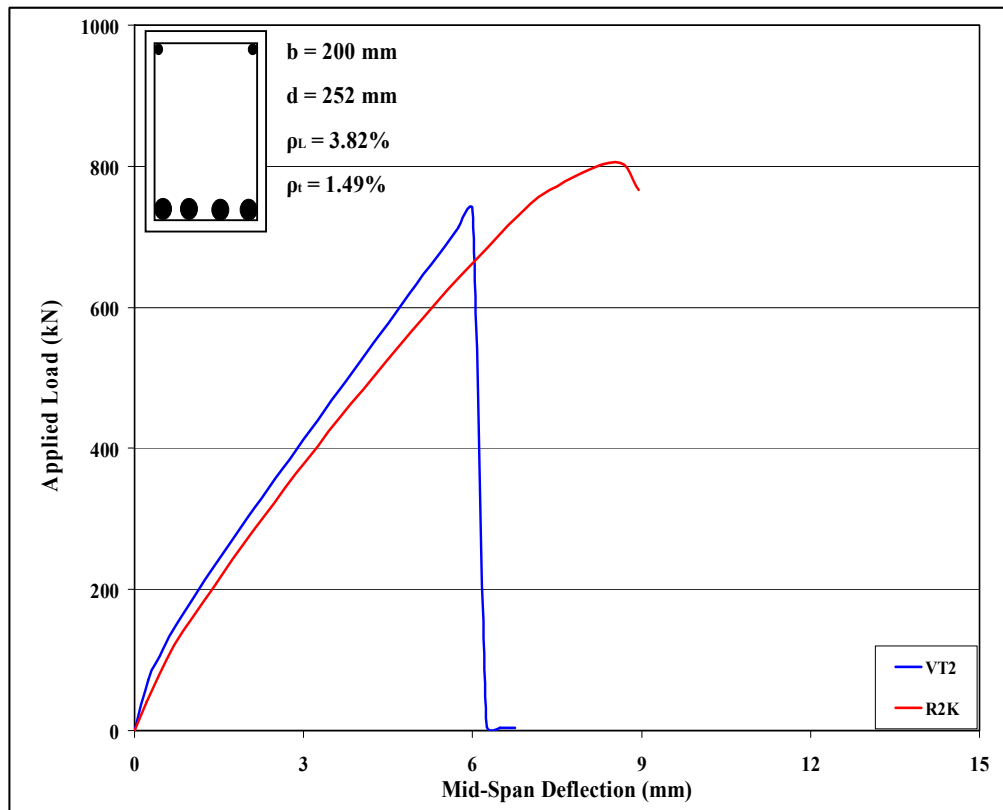


Figure B-2: Load-Deflection Plots of Beam F80-2

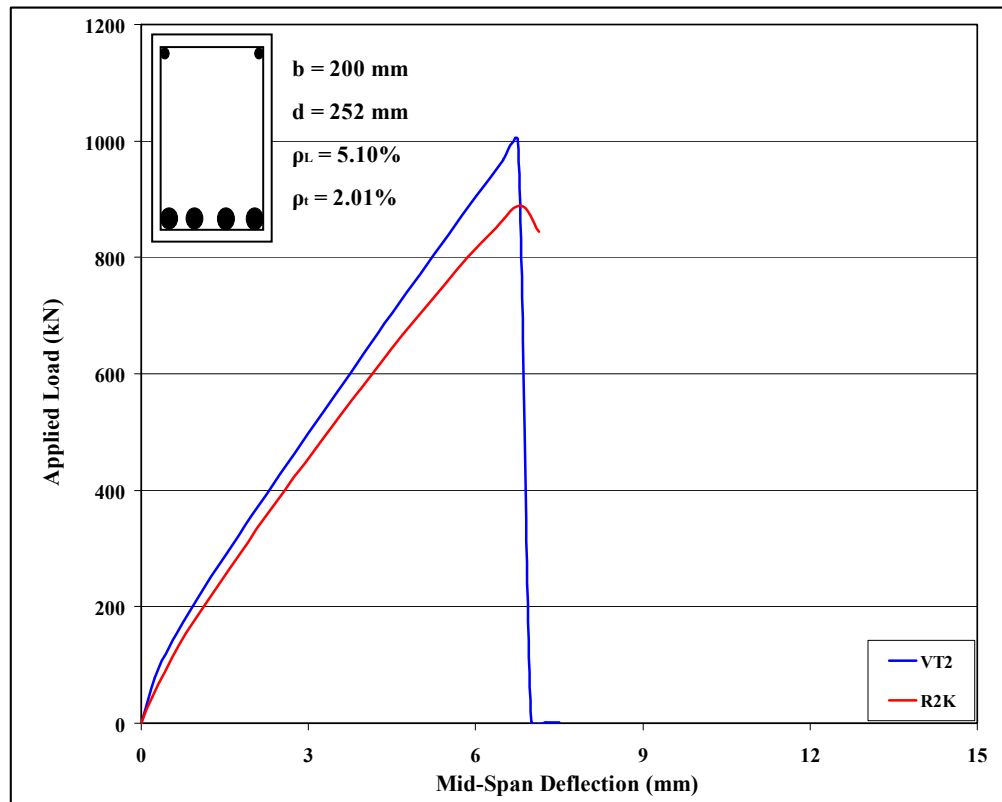


Figure B-2: Load-Deflection Plots of Beam F80-3

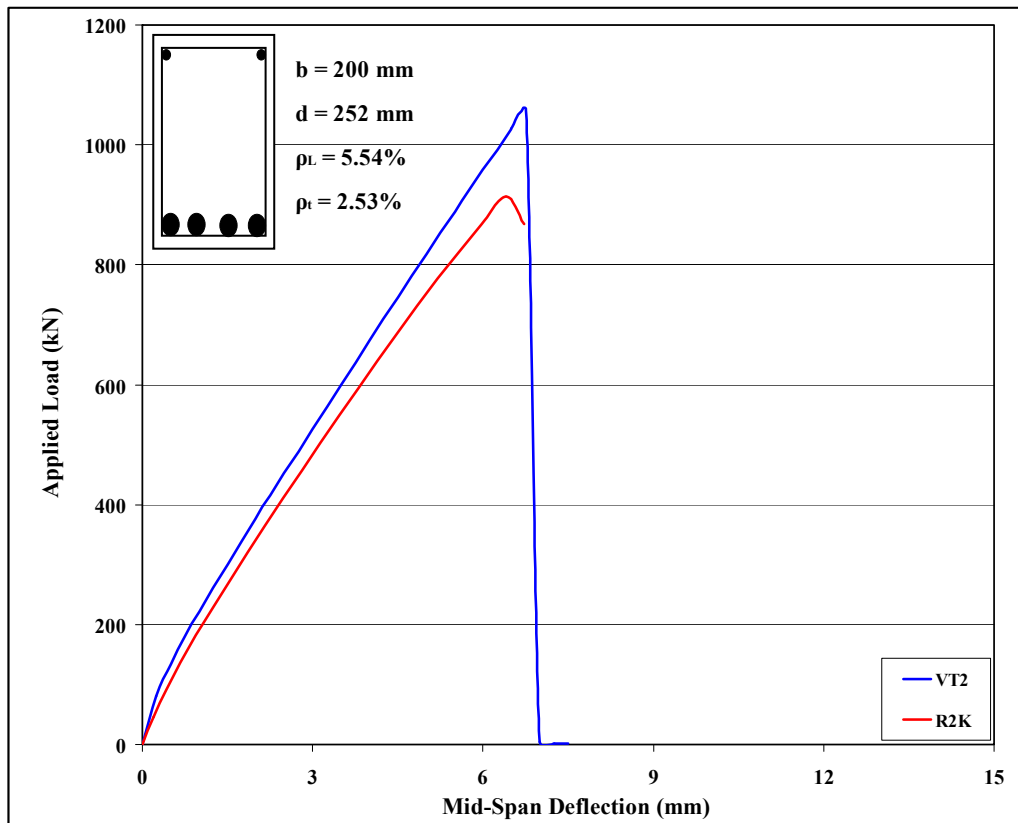


Figure B-2: Load-Deflection Plots of Beam F80-4

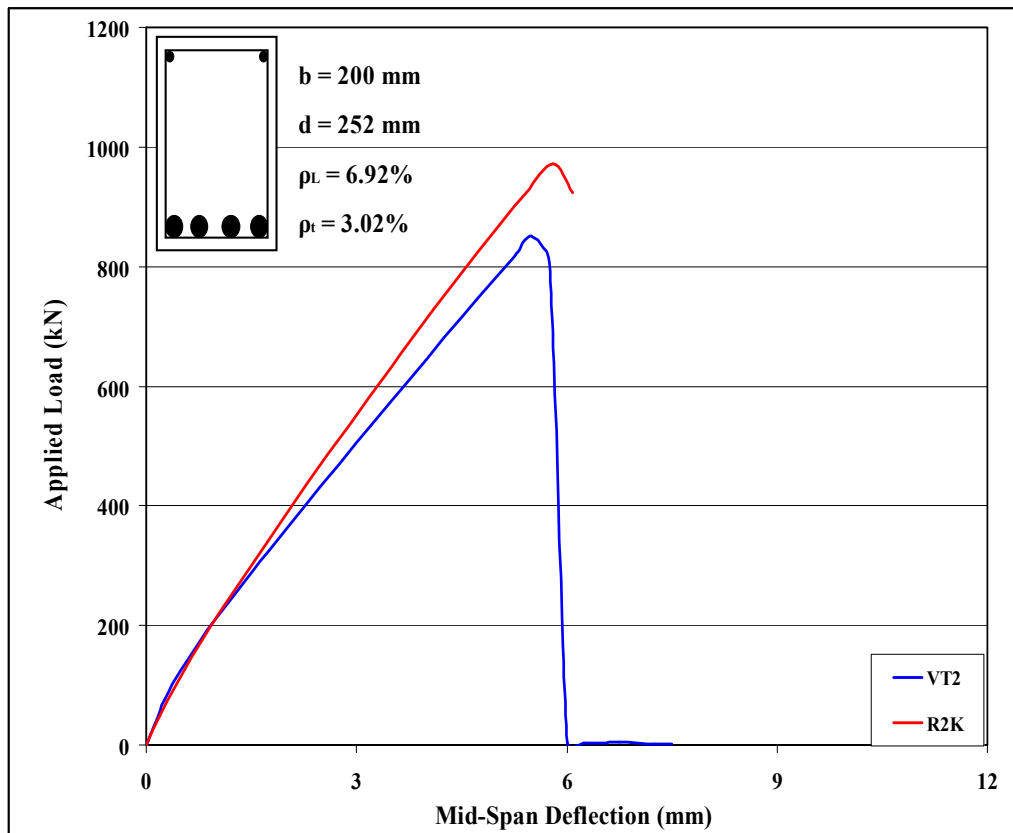


Figure B-2: Load-Deflection Plots of Beam F80-5

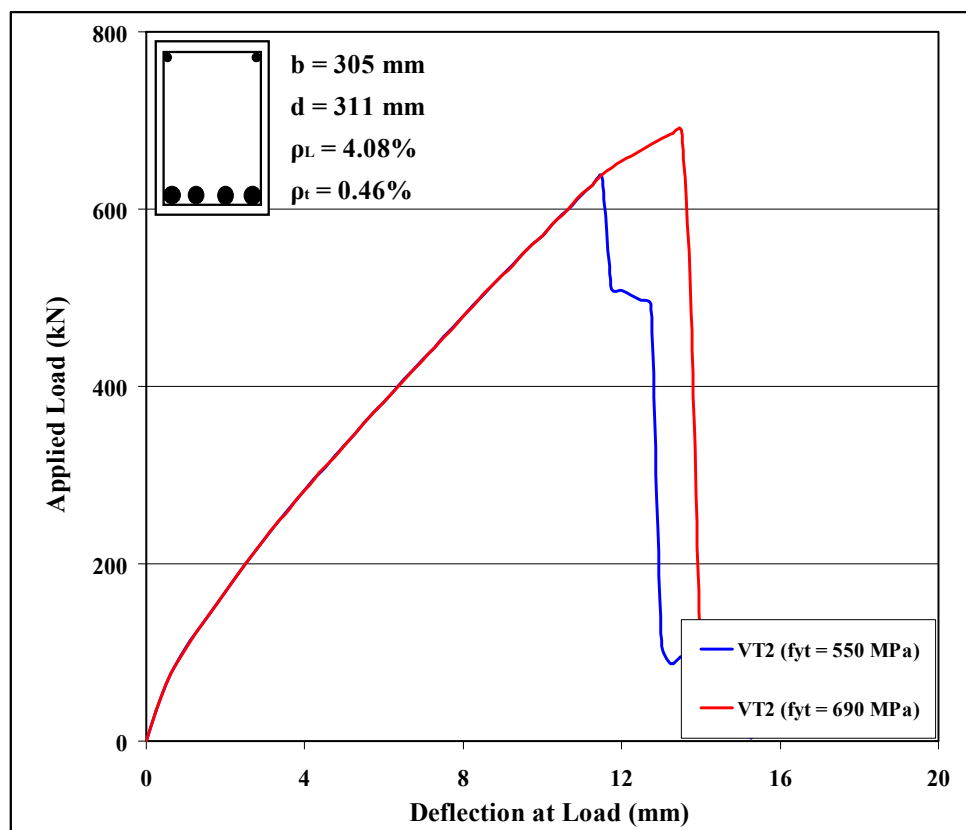


Figure B-2: Load-Deflection Plots of Beam CM4

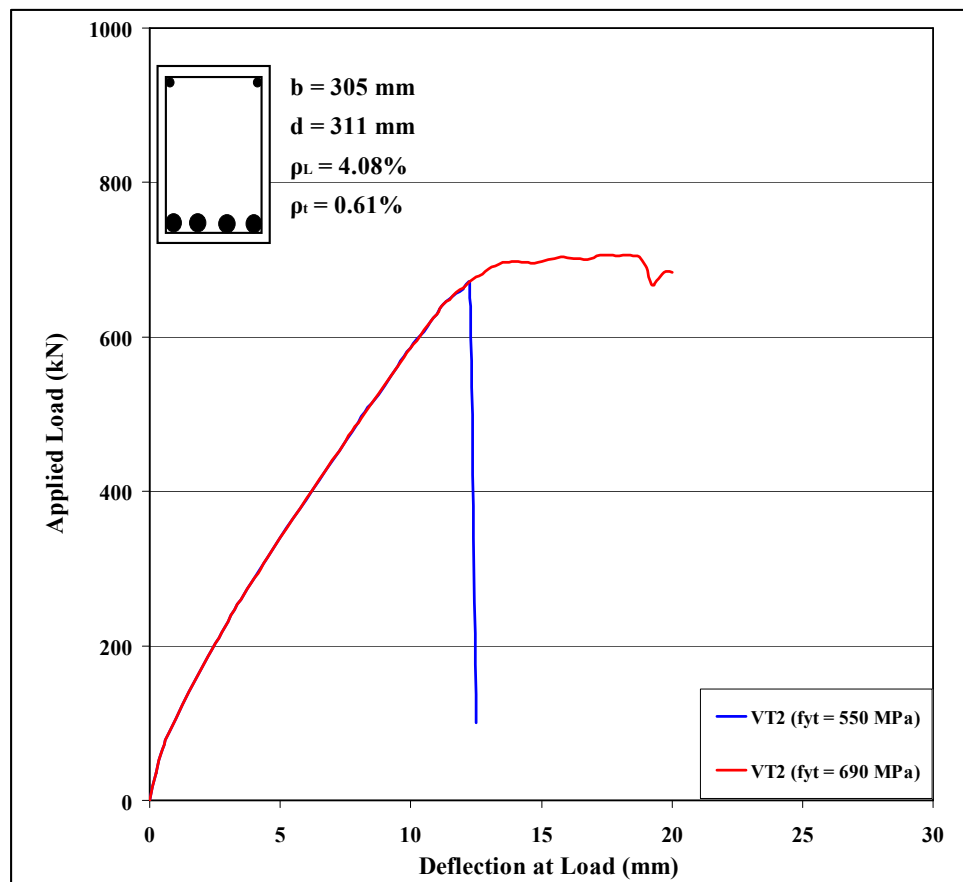


Figure B-2: Load-Deflection Plots of Beam CM3

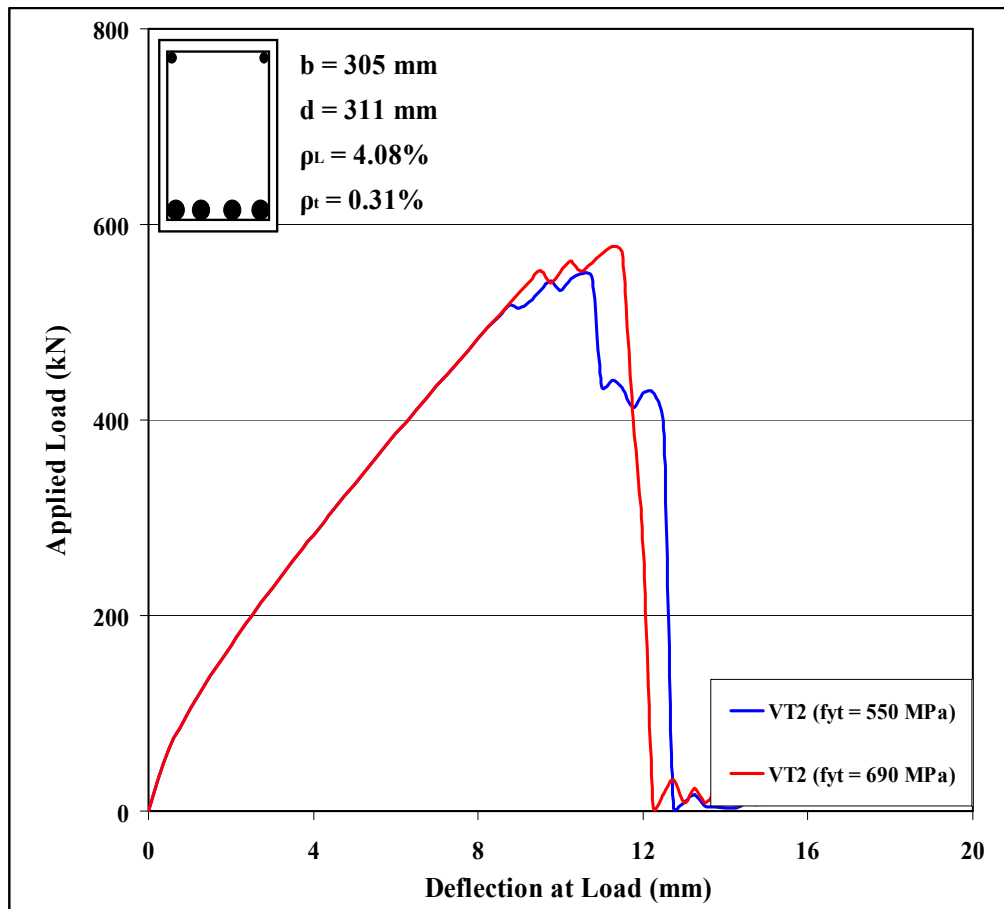


Figure B-2: Load-Deflection Plots of Beam CM6

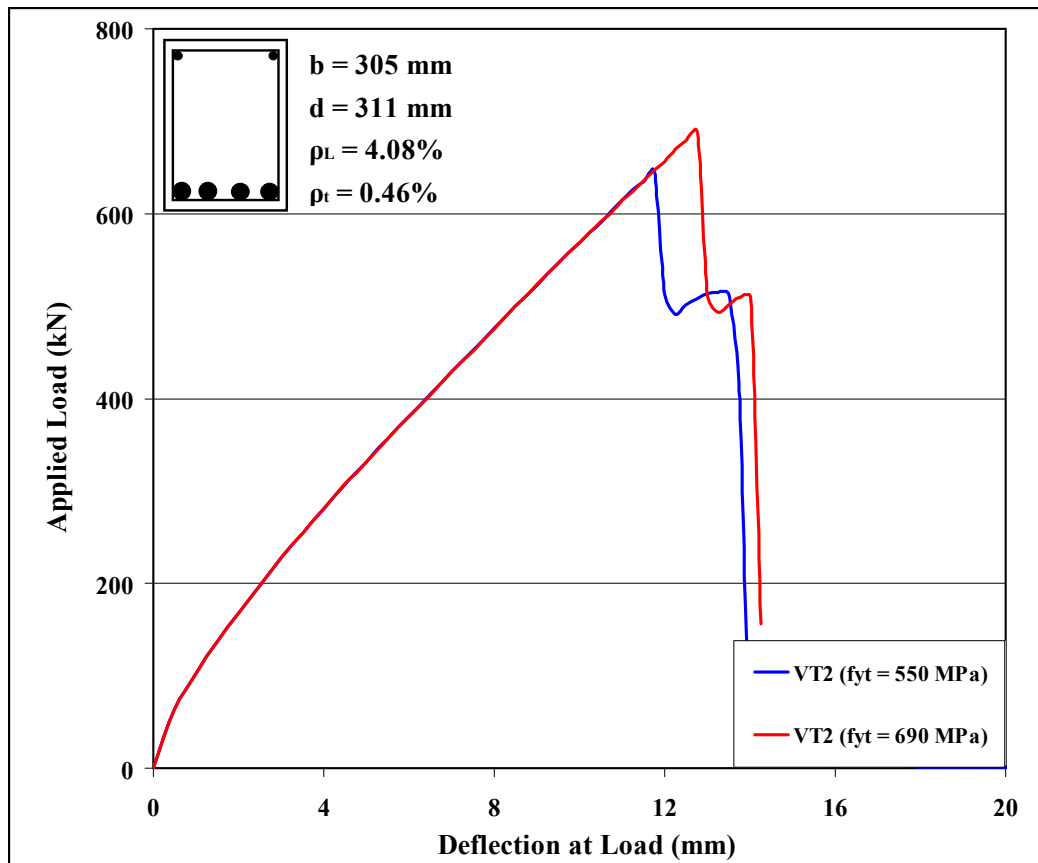


Figure B-2: Load-Deflection Plots of Beam M-M-4

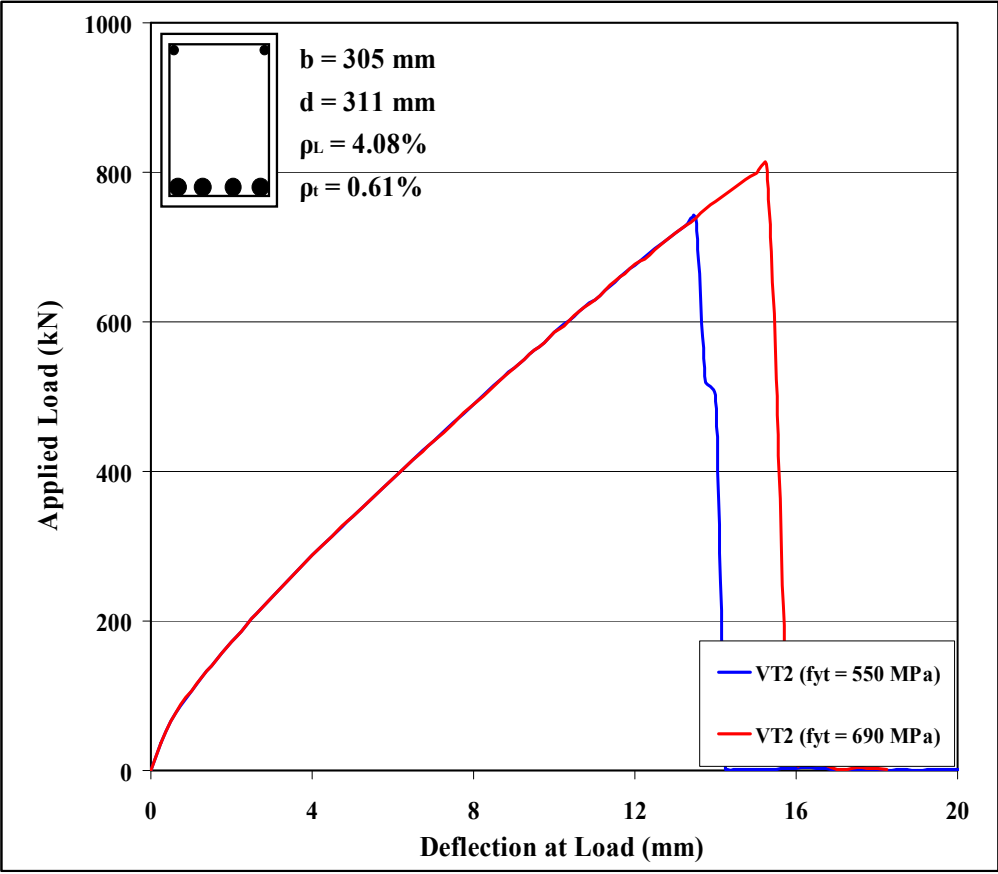


Figure B-2: Load-Deflection Plots of Beam M-M-3

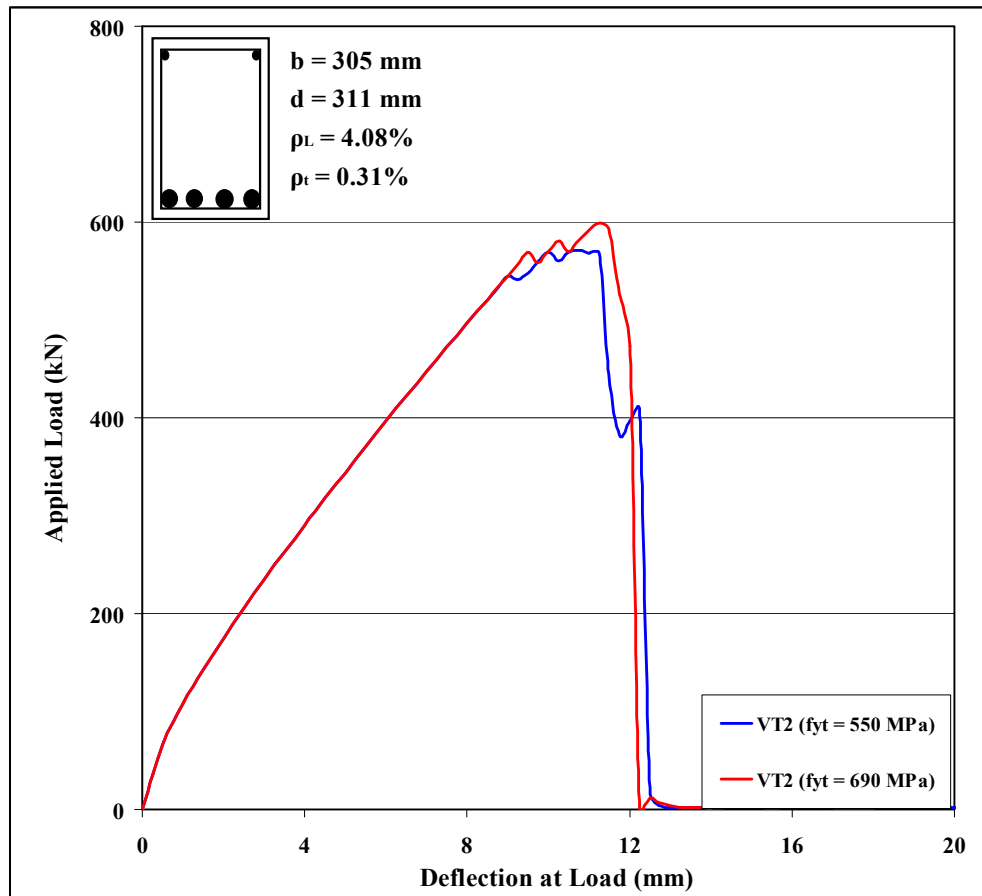


Figure B-2: Load-Deflection Plots of Beam M-M-6

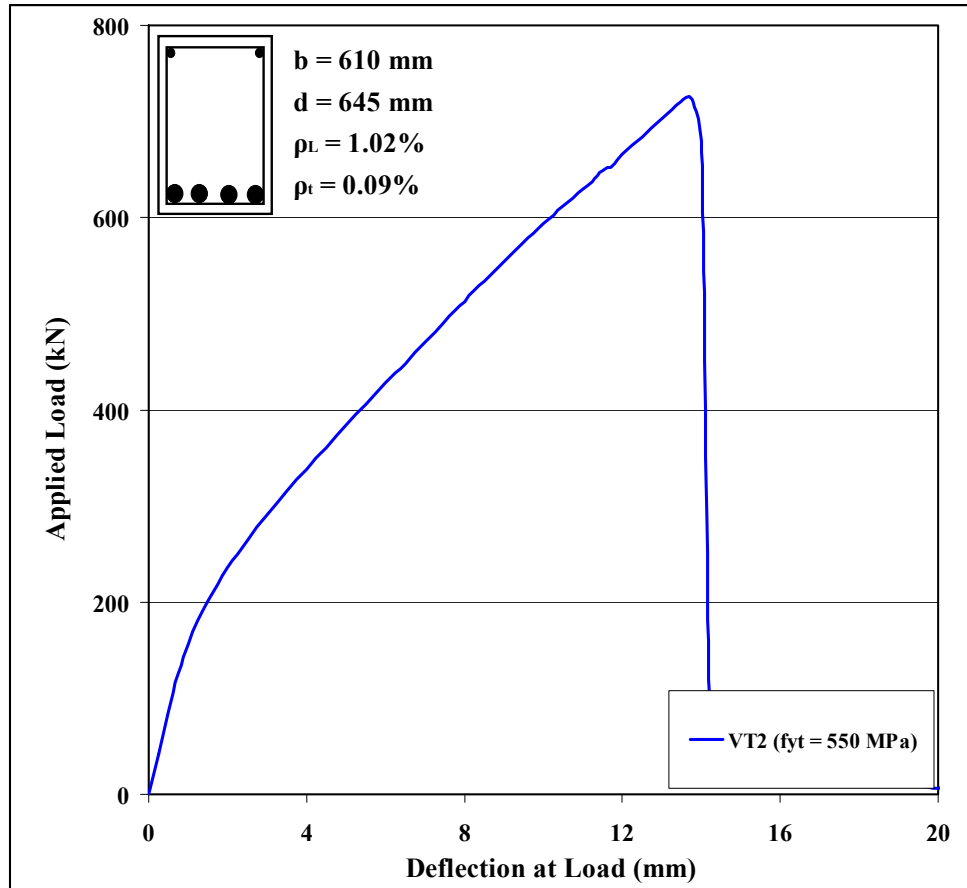


Figure B-2: Load-Deflection Plots of Beam G1-M80

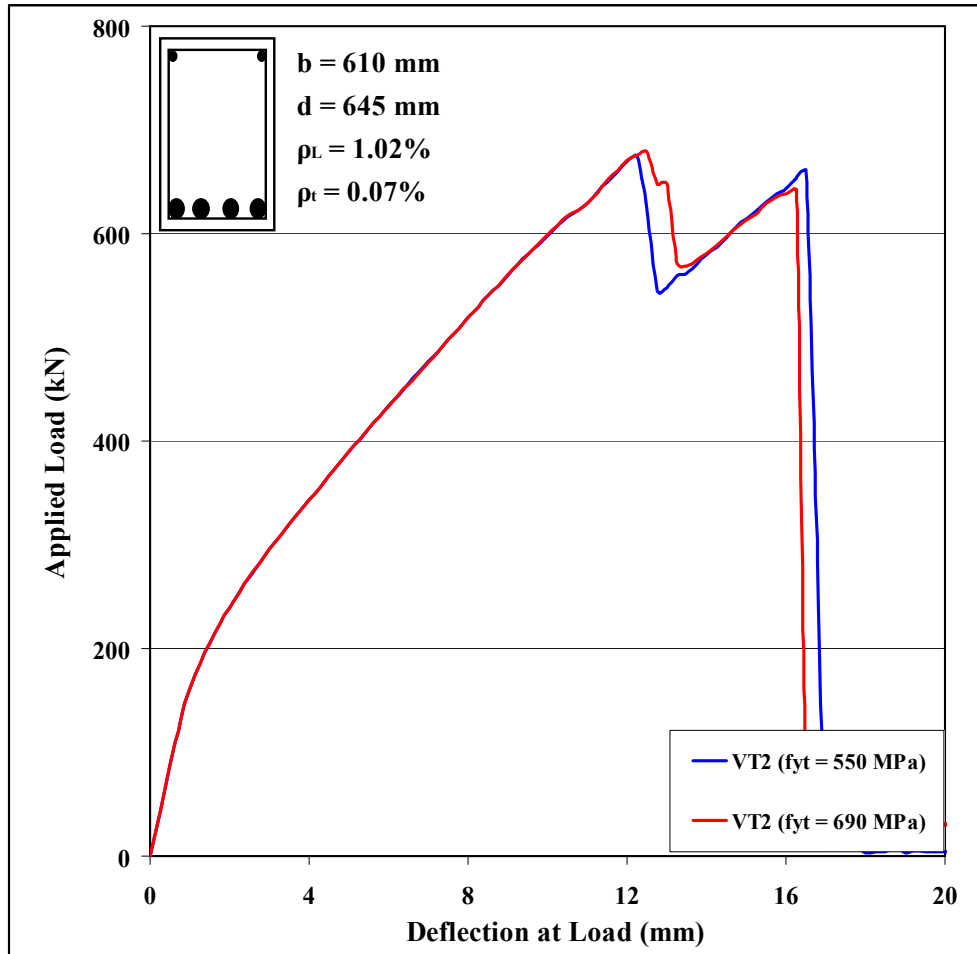


Figure B-2: Load-Deflection Plots of Beam G1-M100

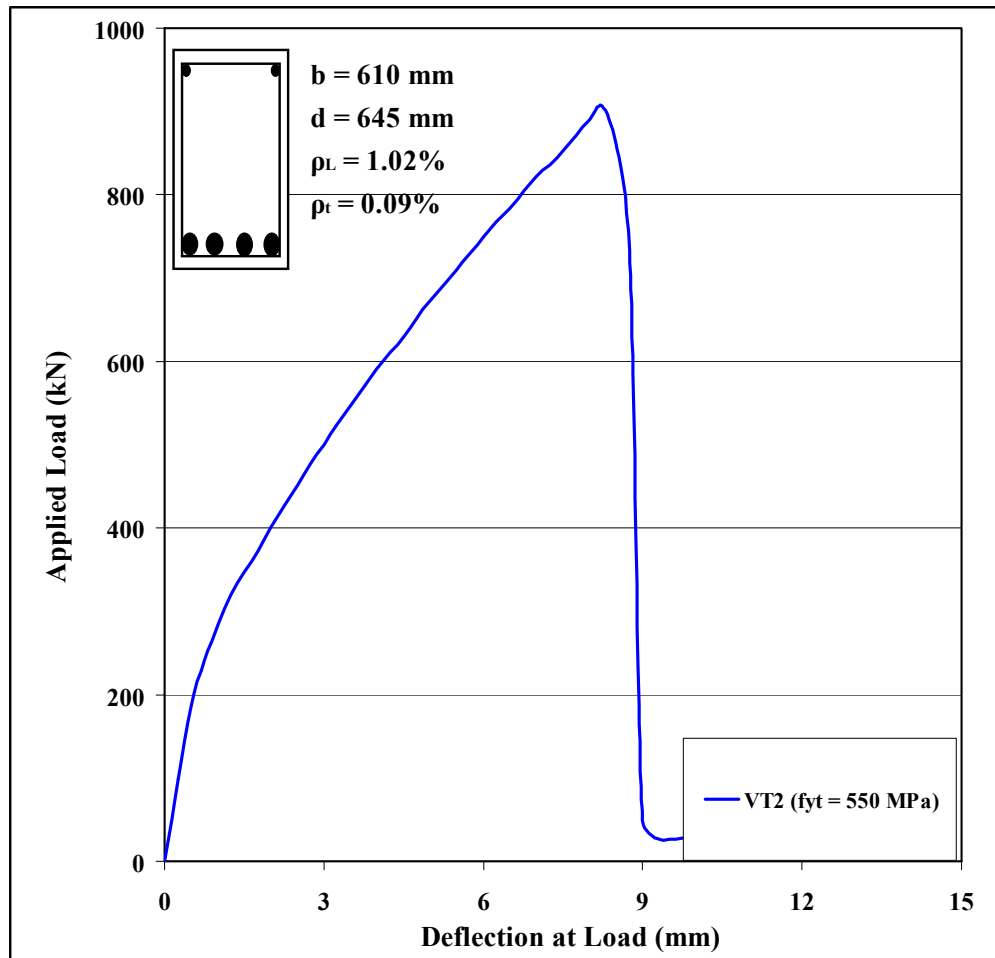


Figure B-2: Load-Deflection Plots of Beam G2-M80

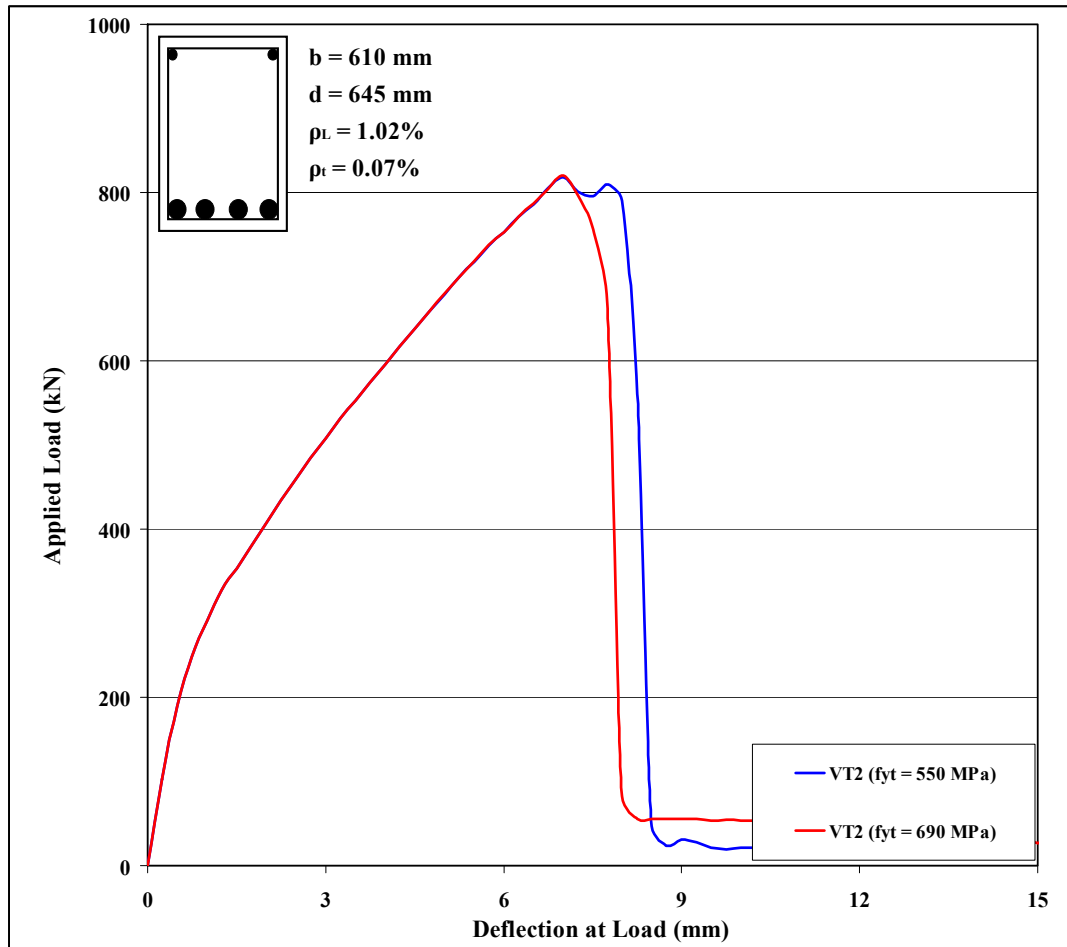


Figure B-2: Load-Deflection Plots of Beam G2-M100

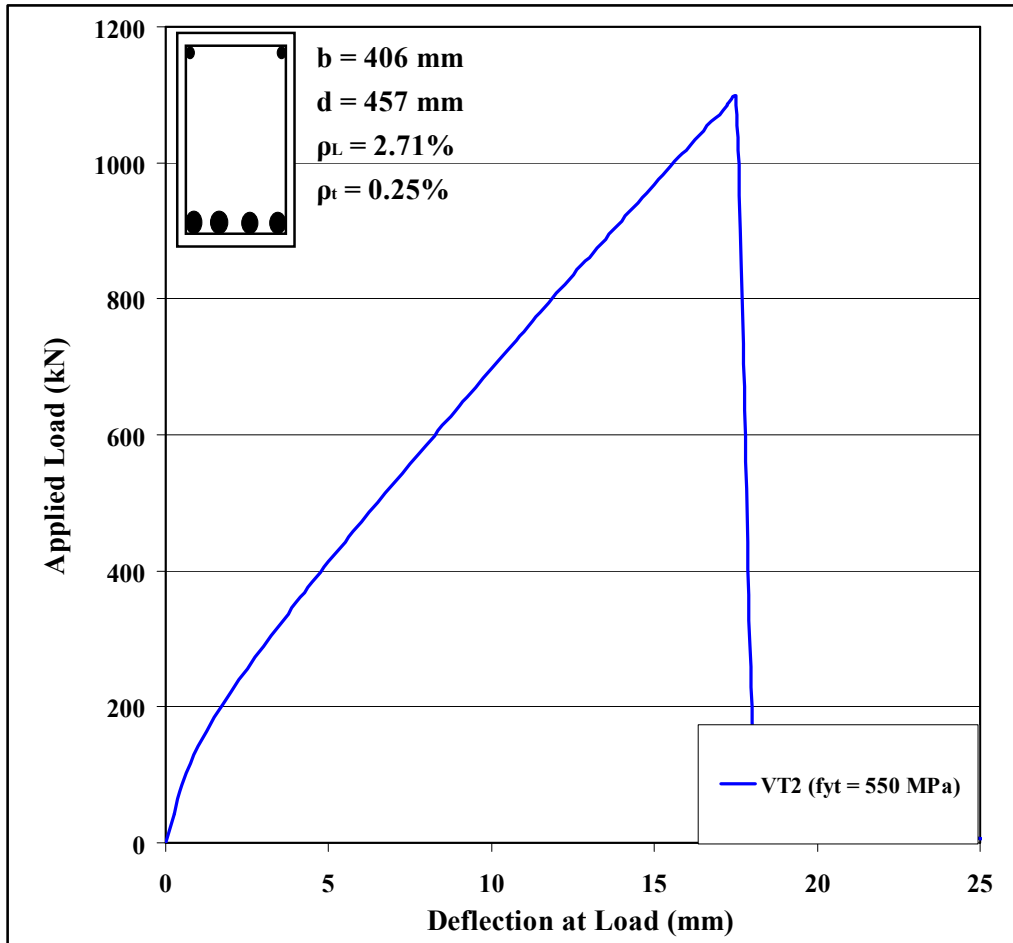


Figure B-2: Load-Deflection Plots of Beam G3-M80

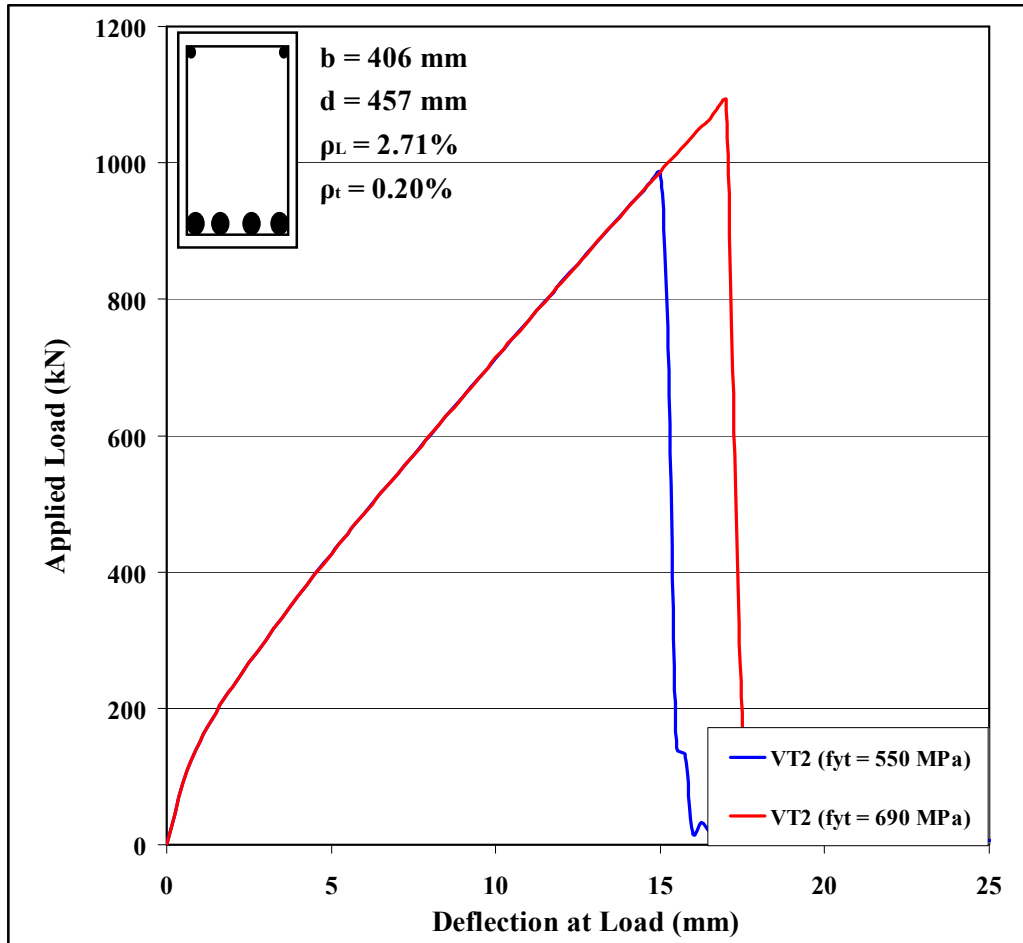


Figure B-2: Load-Deflection Plots of Beam G3-M100

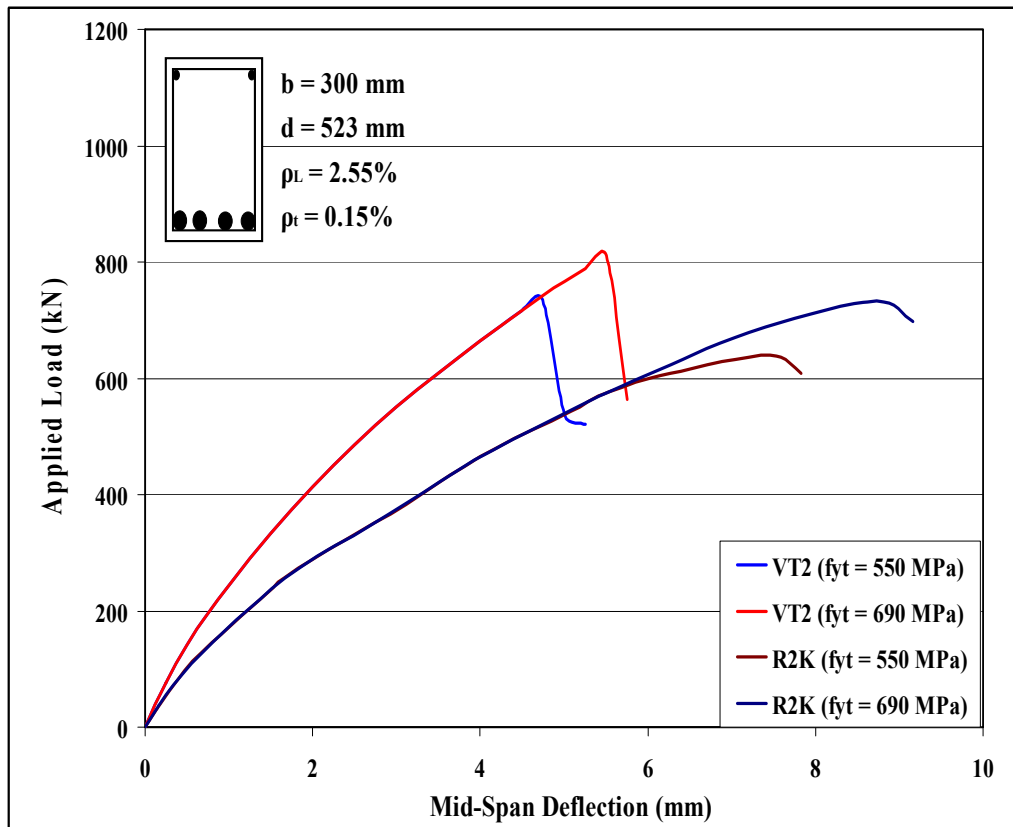


Figure C-2: Load-Deflection Plots of Beam RM1

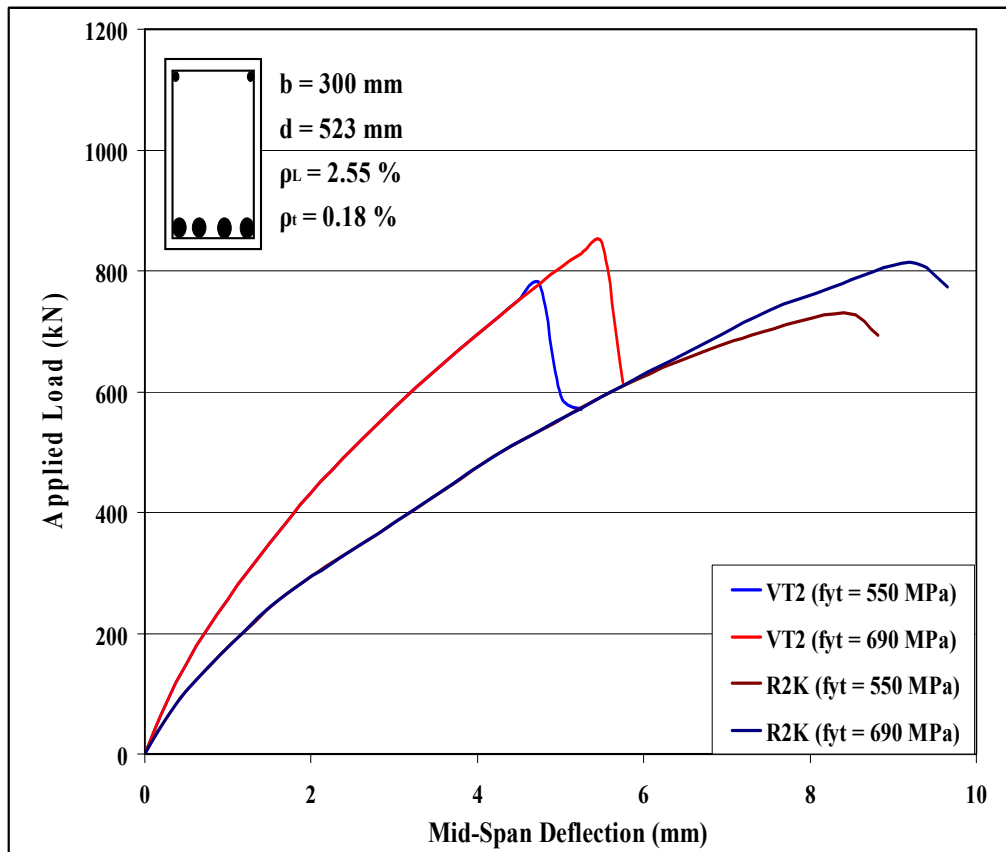


Figure C-3: Load-Deflection Plots of Beam RM2

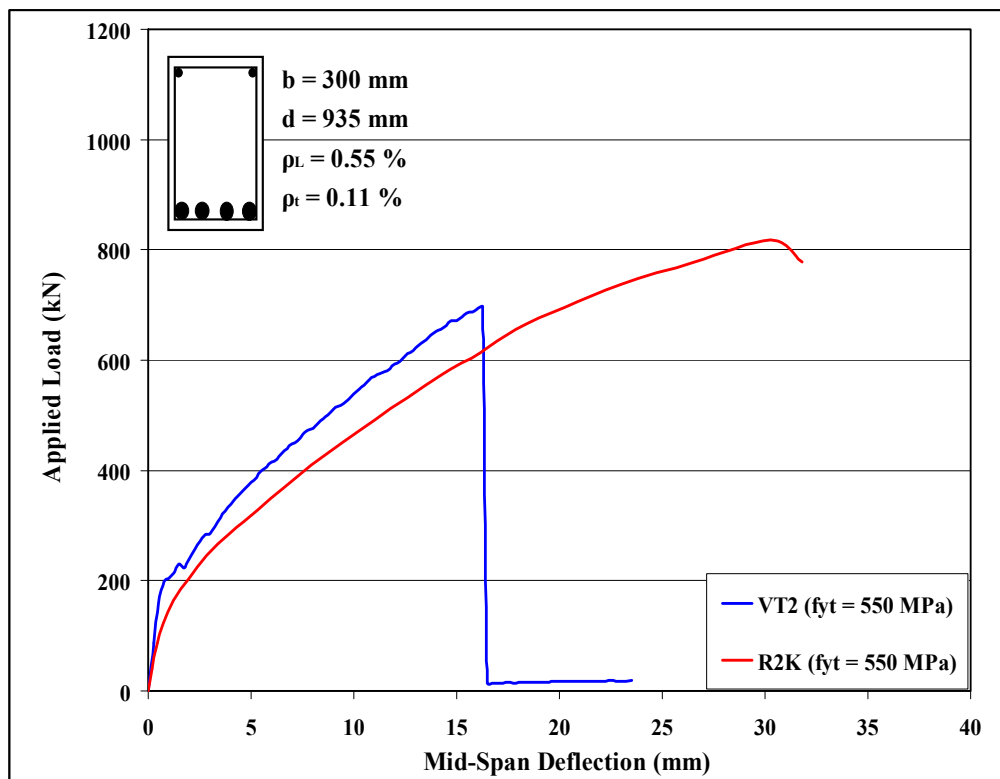


Figure C-3: Load-Deflection Plots of Beam MR1

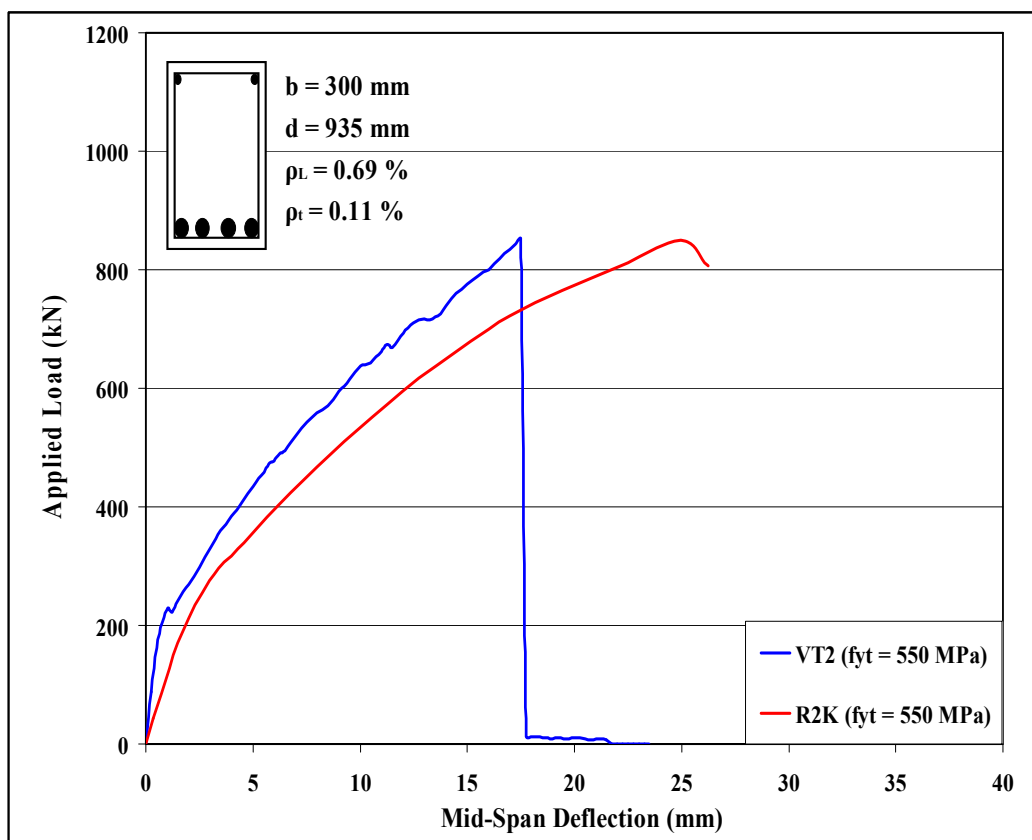


Figure C-4: Load-Deflection Plots of Beam MR2

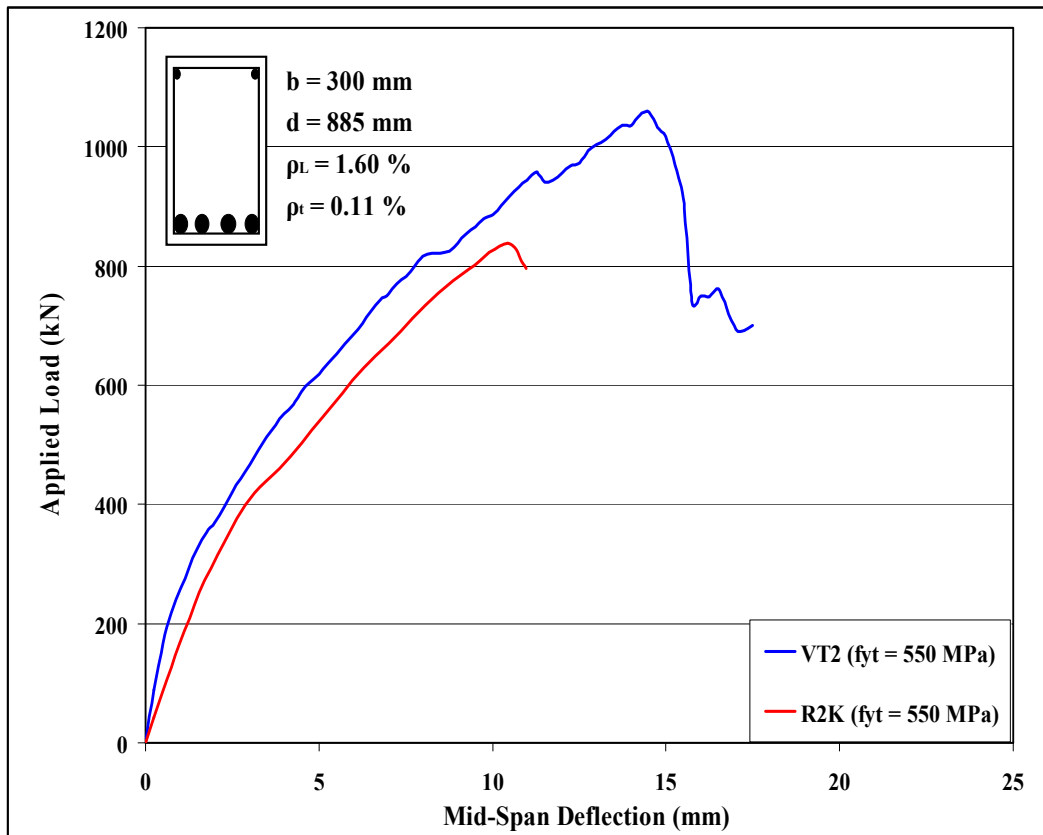


Figure C-5: Load-Deflection Plots of Beam MR3

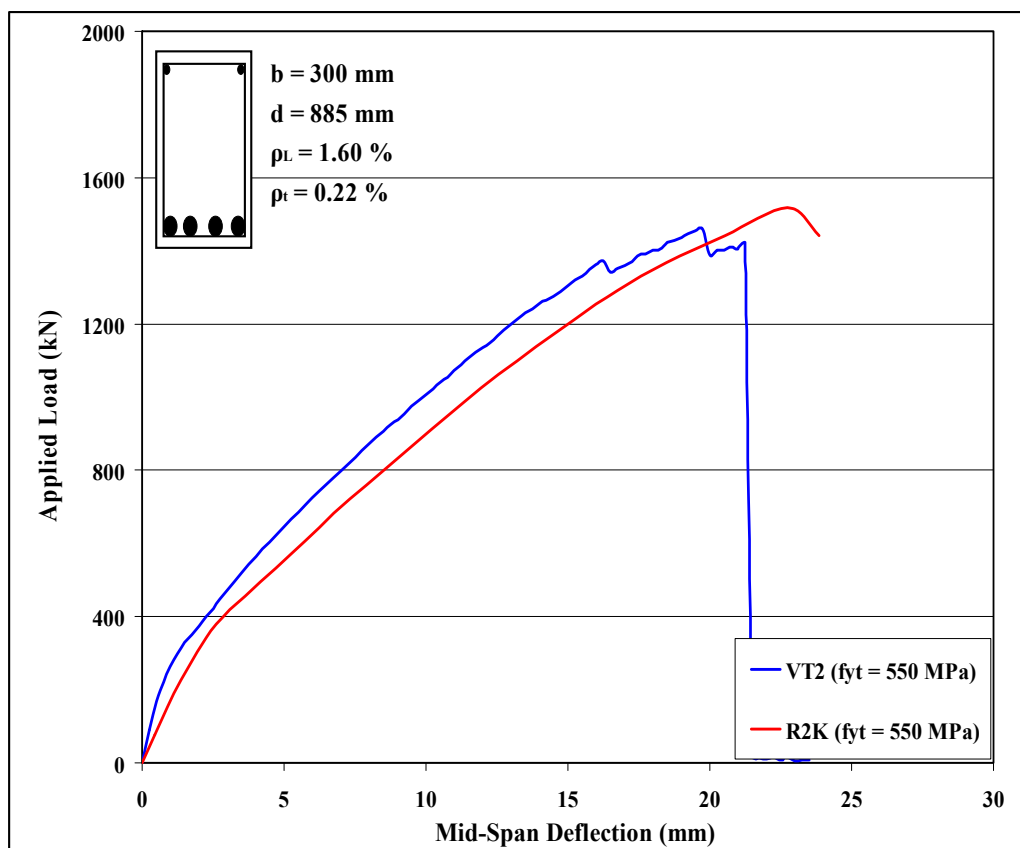


Figure C-6: Load-Deflection Plots of Beam MR4

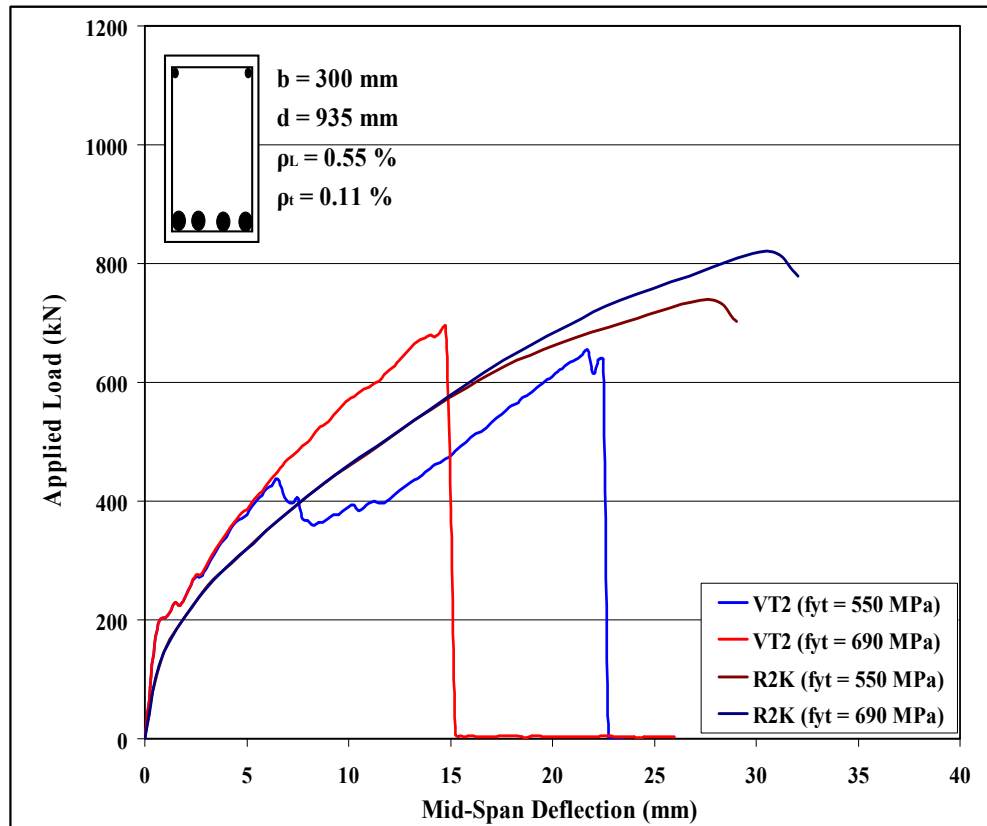


Figure C-7: Load-Deflection Plots of Beam MM1

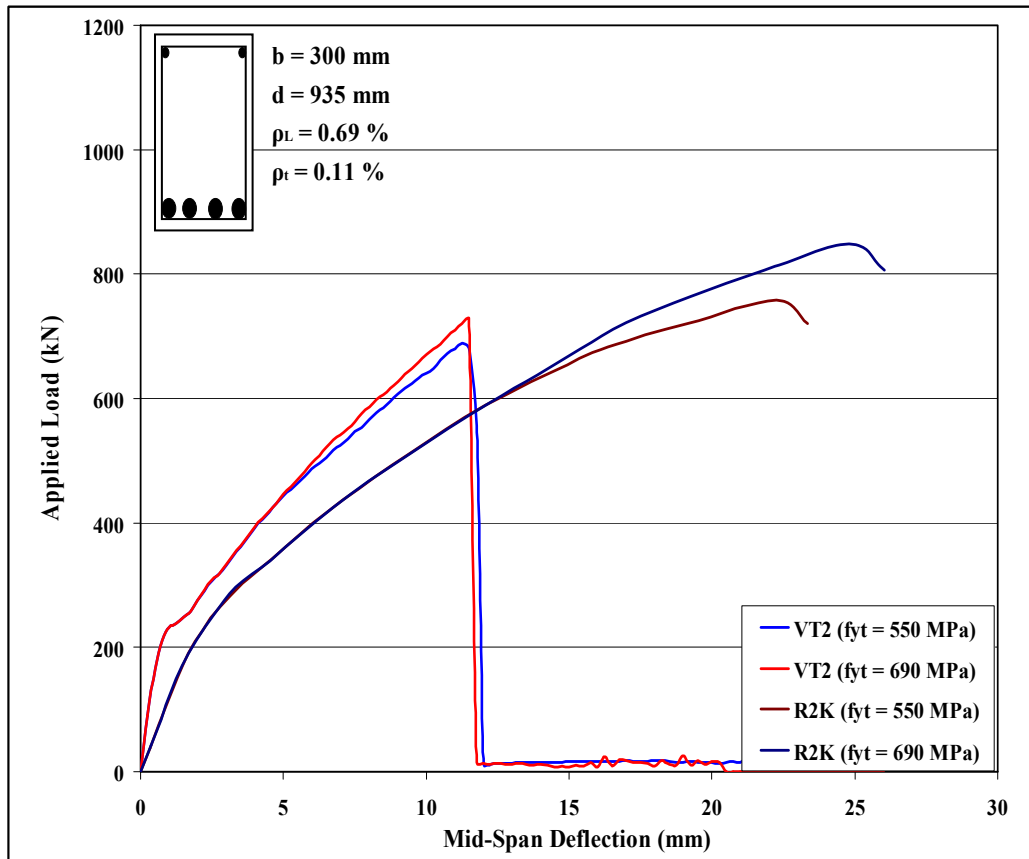


Figure C-8: Load-Deflection Plots of Beam MM2

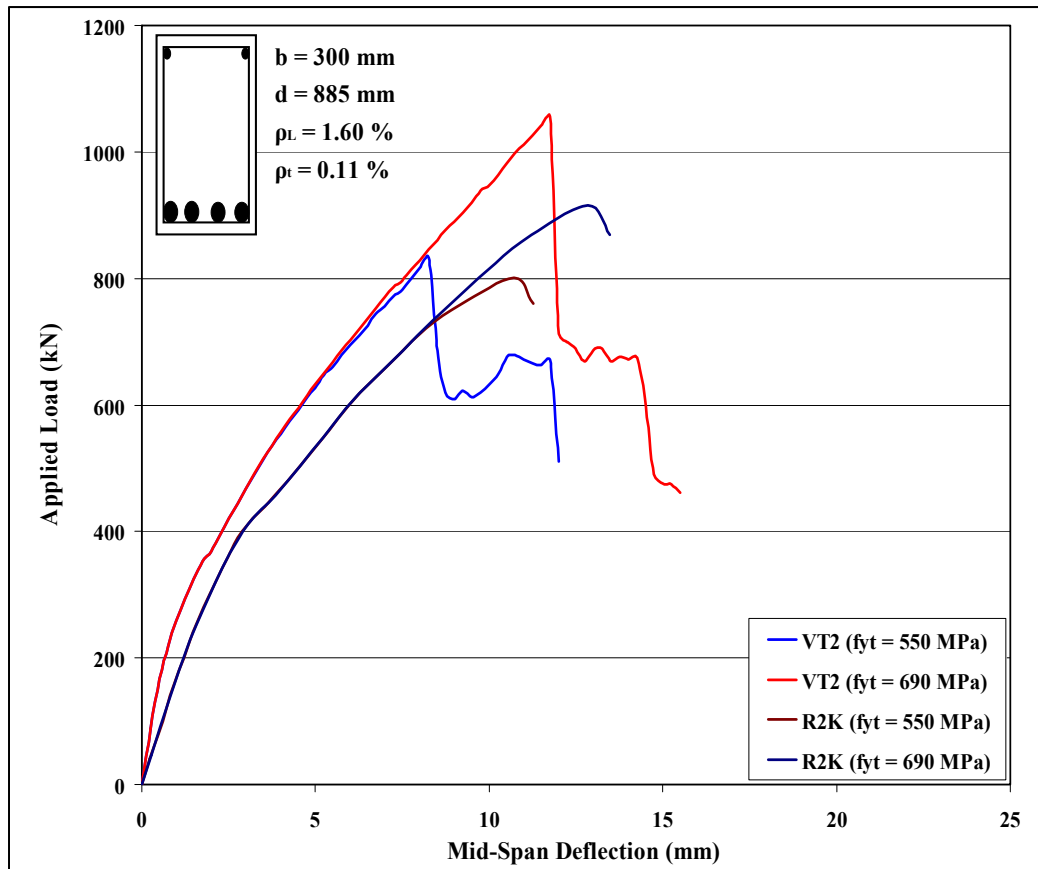


Figure C-9: Load-Deflection Plots of Beam MM3

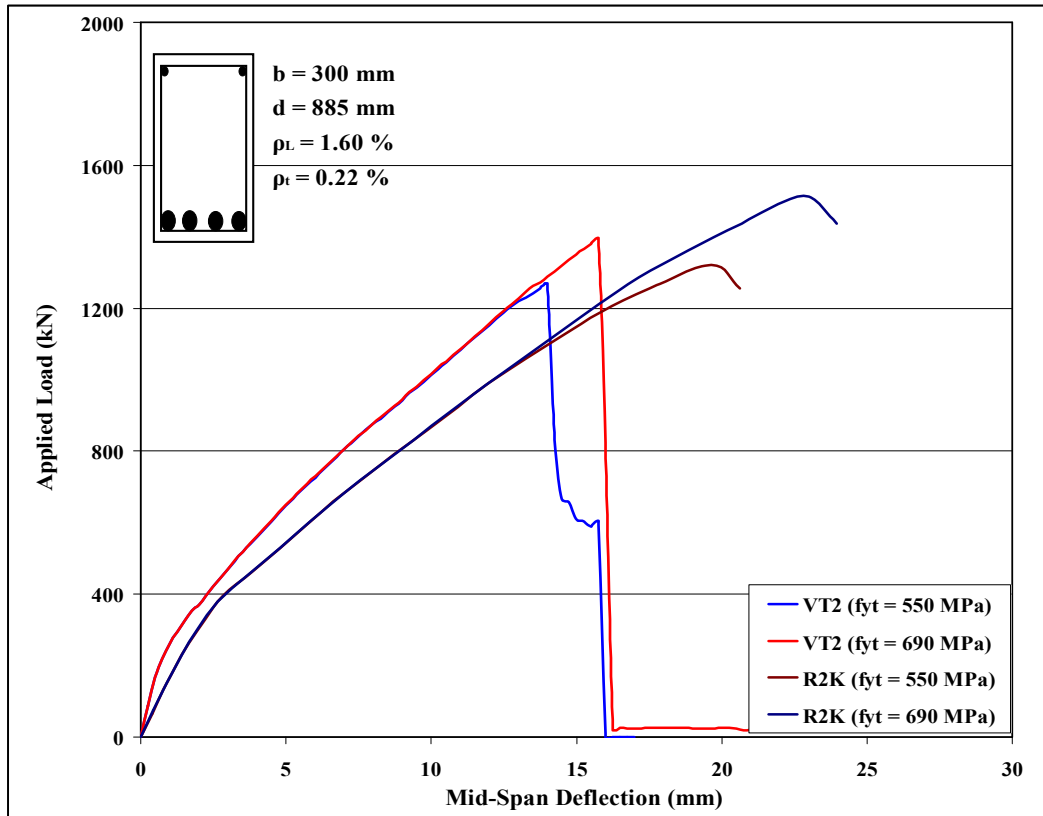


Figure B-10: Load-Deflection Plots of Beam MM4

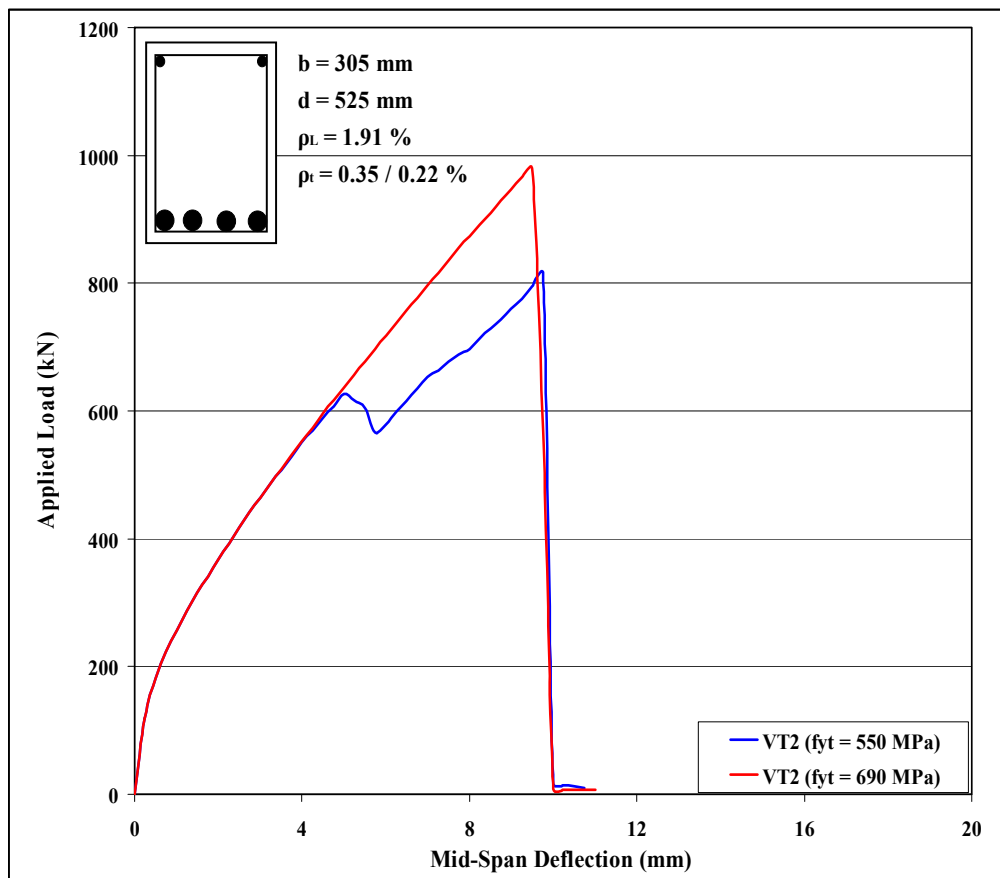


Figure B-10: Load-Deflection Plots of Beams SR1(A) & SR1(B)

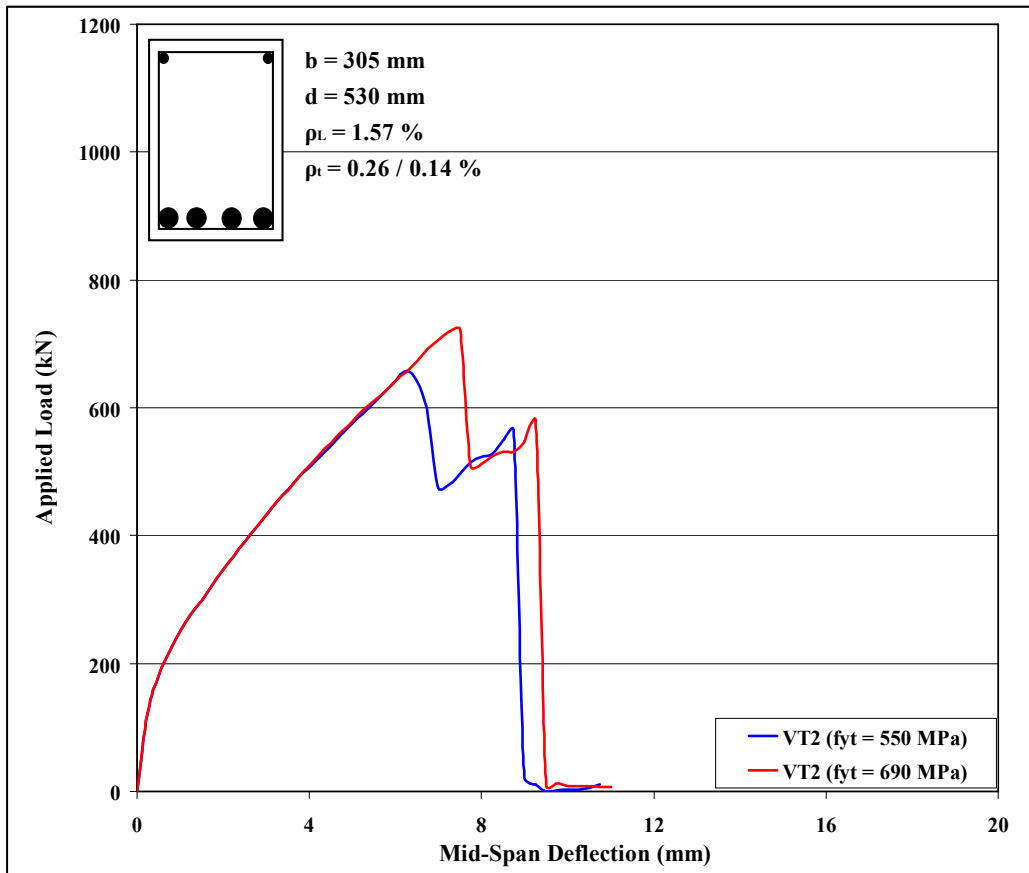


Figure B-10: Load-Deflection Plots of Beams SR2(A) & SR2(B)

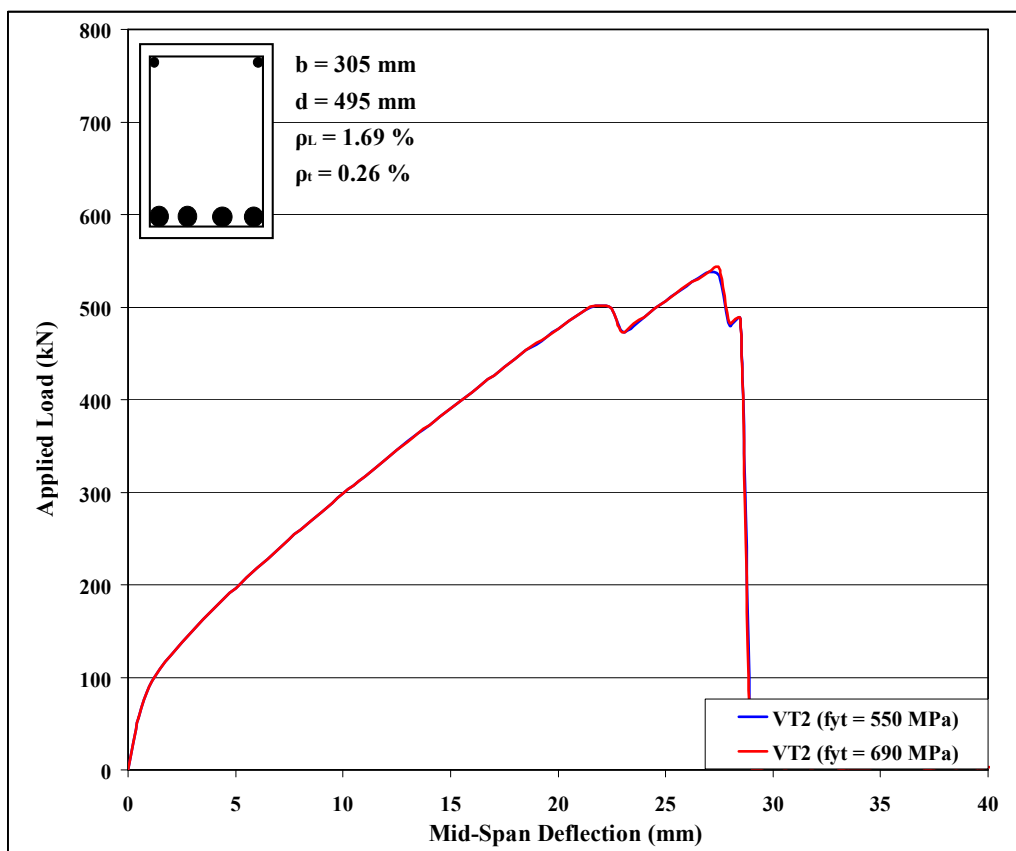


Figure B-10: Load-Deflection Plots of Beams SR3(A)

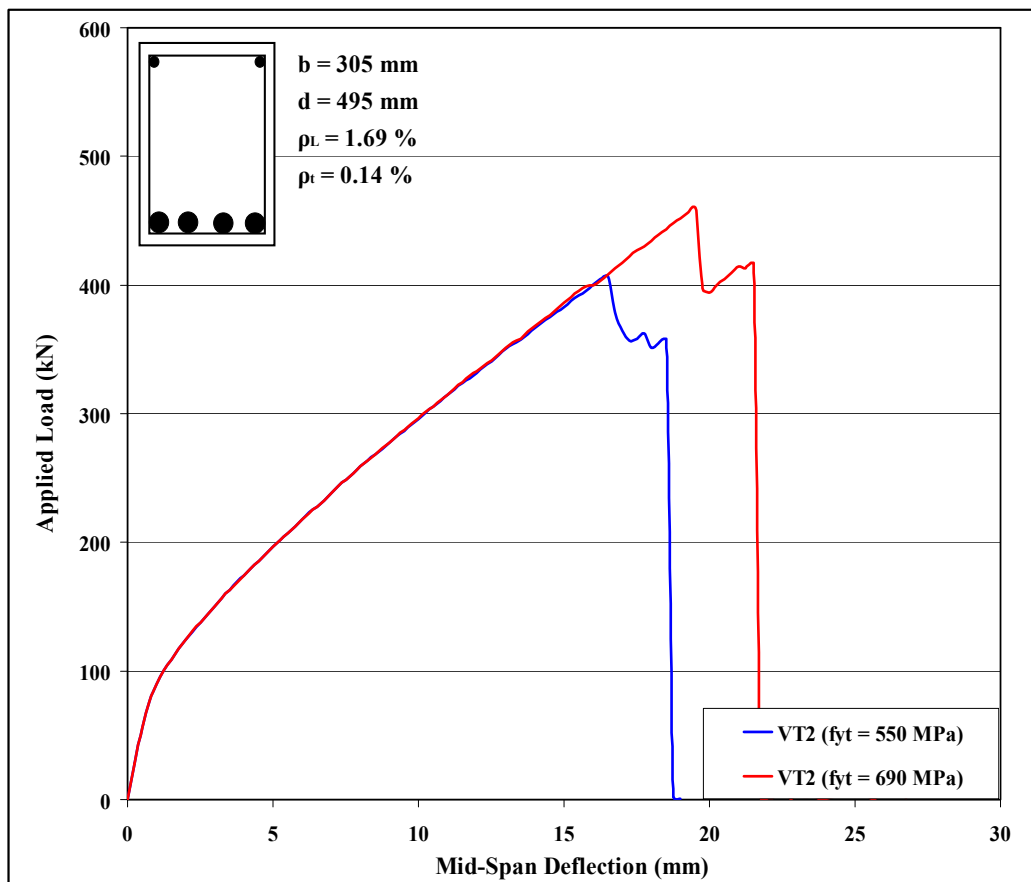


Figure B-10: Load-Deflection Plots of Beams SR3(B)

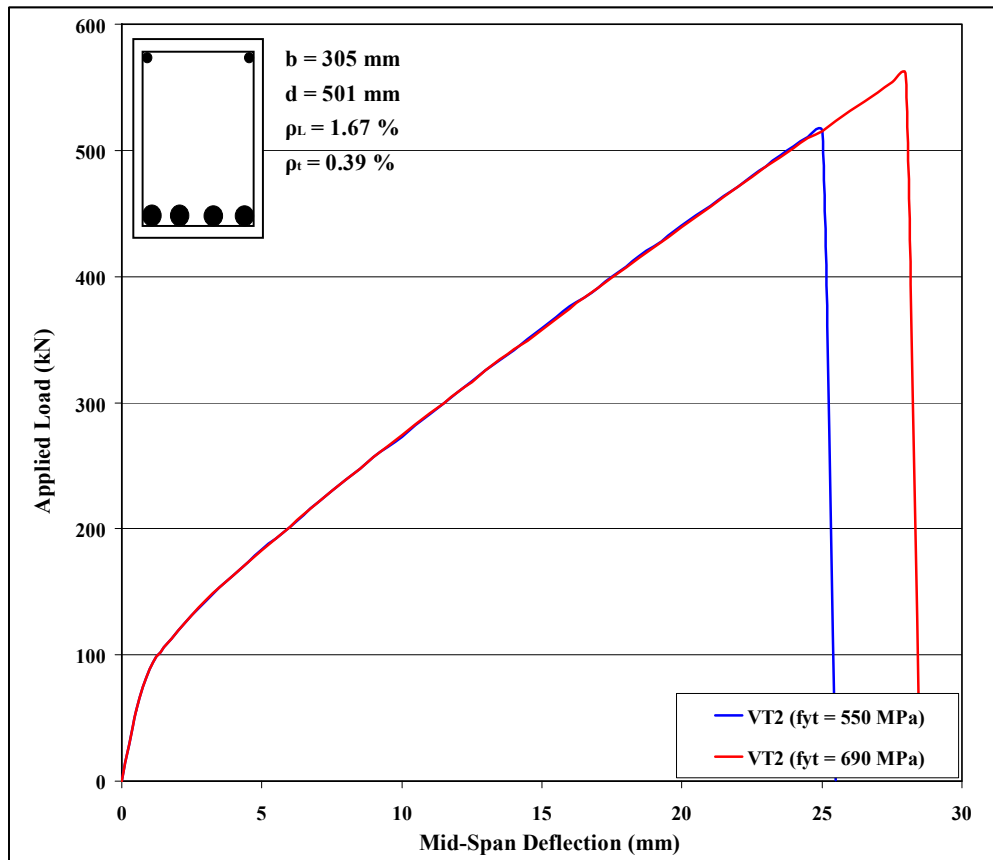


Figure B-10: Load-Deflection Plots of Beams SR4(A)

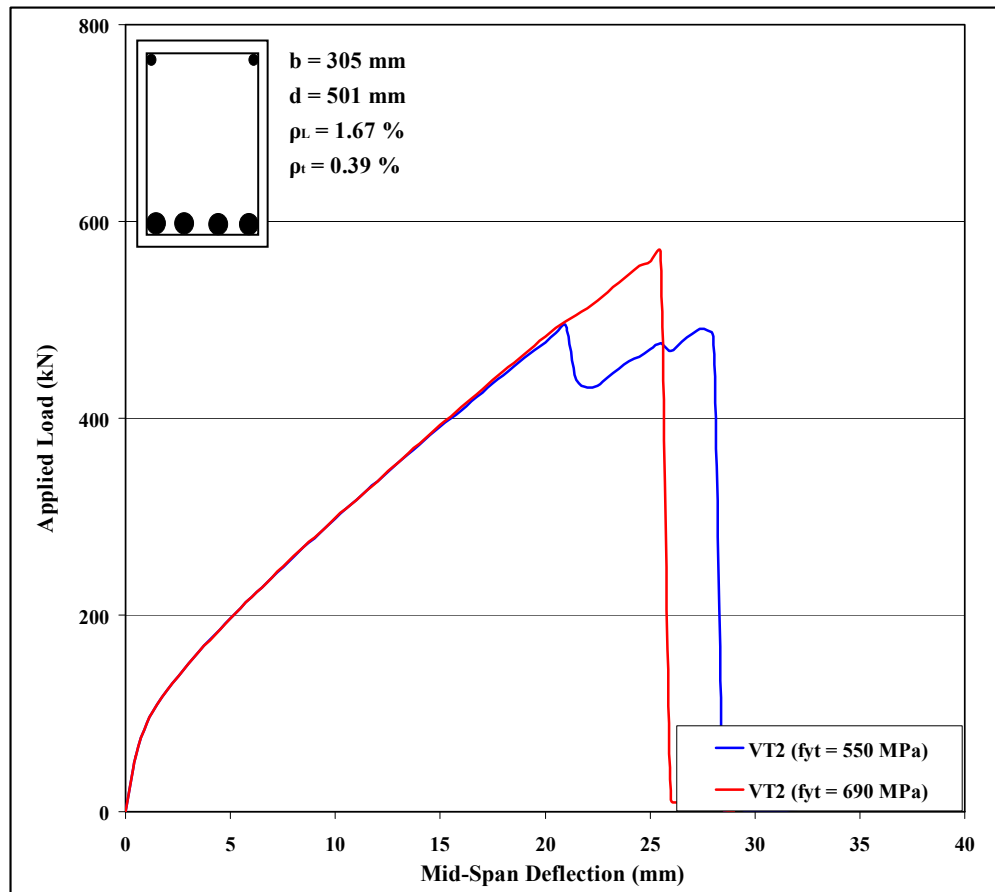


Figure B-10: Load-Deflection Plots of Beams SR4(B)

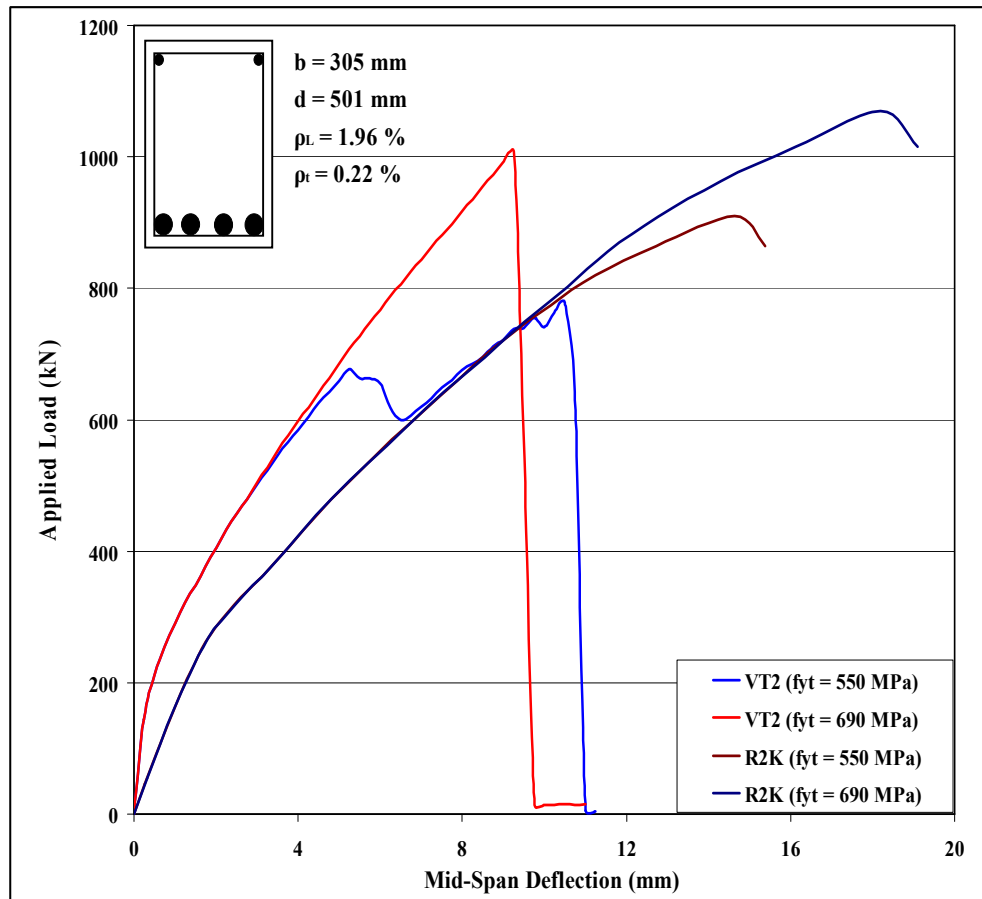


Figure B-10: Load-Deflection Plots of Beams SR5

APPENDIX C: BEAM DEFLECTION MODEL

C.1 General Deflection Model

The relationship between the average longitudinal strain ε_x and the shear strain γ can be solved using an iterative approach based on the Modified Compression Field Theory (*Vecchio and Collins*, 1986) relationships. The required calculations follow the methods described in *Collins and Mitchell* (1997) and are demonstrated using the flow chart shown in Figure C-1.

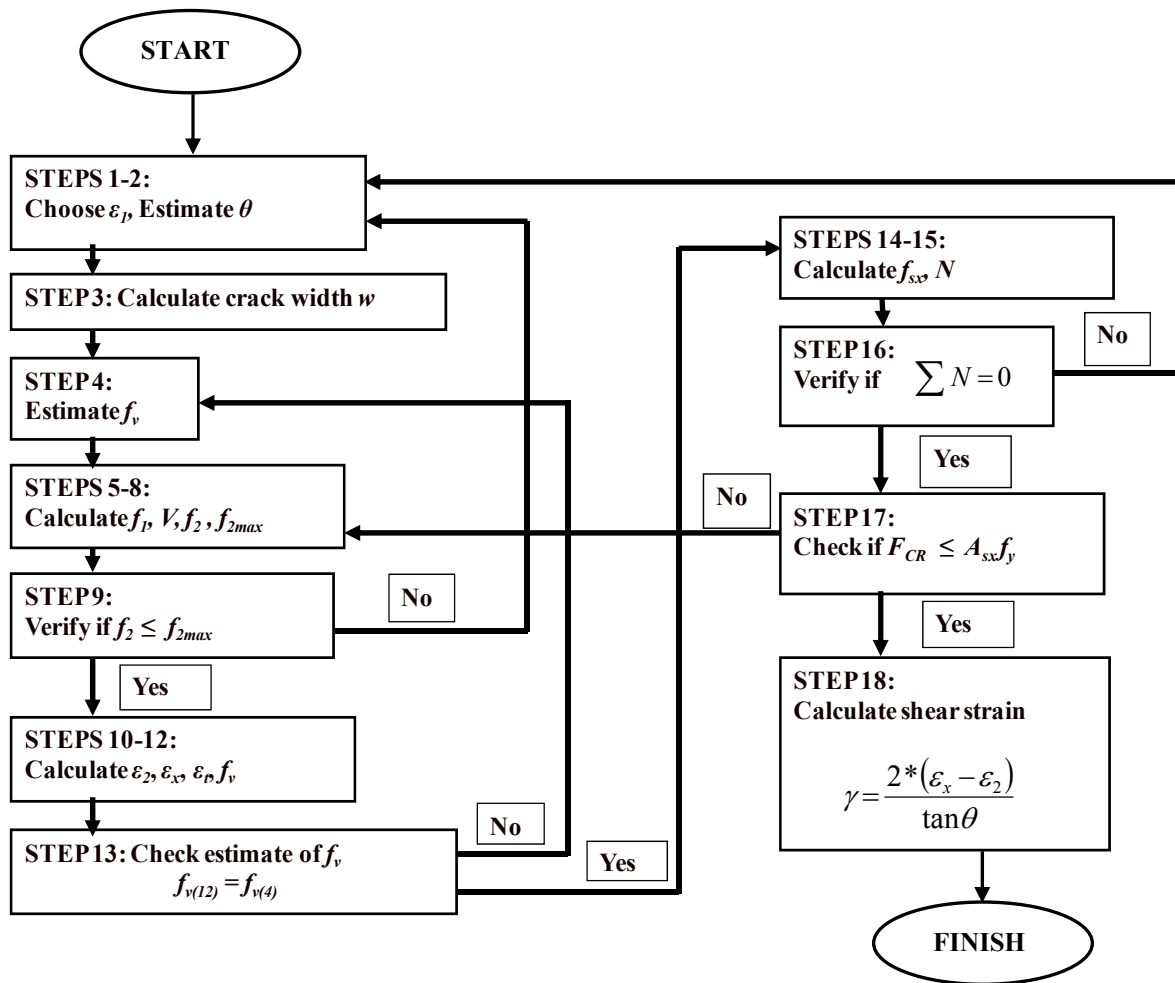


Figure C-1: Flowchart Showing the Prediction of Relationship Between Shear Strain and Member Strain.

An Excel spreadsheet is used to solve each assumed value of the principal concrete tensile strain ε_1 according to the following sequence, adapted from *Collins and Mitchell* (1997):

Step 1: Select a value of principal tensile strain in the concrete ε_1 at which to perform the calculations.

Step 2: Estimate θ .

Step 3: The crack width, ω , can be calculated from the following equations based on crack spacing and the reinforcement configuration:

$$\omega = \varepsilon_1 s_{m\theta} \quad (C-1)$$

$$s_{m\theta} = \frac{1}{\left(\frac{\sin \theta}{s_{mx}} + \frac{\cos \theta}{s_{mv}} \right)} \quad (C-2)$$

$$s_{mx} = 2 \left(c_x + \frac{s_x}{10} \right) + 0.25 k_1 \frac{d_{bx}}{\rho_x} \quad (C-3)$$

$$s_{mv} = 2 \left(c_v + \frac{s}{10} \right) + 0.25 k_1 \frac{d_{bv}}{\rho_v} \quad (C-4)$$

$$\rho_v = \frac{A_v}{(b_w s)} \quad (C-5)$$

$$\rho_x = \frac{A_{sx}}{A_c} \quad (C-6)$$

Step 4: Estimate the stress in the transverse reinforcement, f_v .

Step 5: Calculate the principal tension stress f_1 .

$$f_1 \leq \begin{cases} \frac{\alpha_1 \alpha_2 f_{cr}}{1 + \sqrt{500 \varepsilon_1}} \\ \nu_{ci} \tan \theta + \frac{A_v}{s b_w} (f_{vy} - f_v) \end{cases} \quad (C-7)$$

$$\text{where } f_{cr} = 0.33\sqrt{f'_c} \quad (C-8)$$

Step 6: Calculate the shear resistance of the cross-section from

$$V = f_1 b_w j d \cot \theta + \frac{A_v f_v}{s} j d \cot \theta \quad (C-9)$$

Step 7: Calculate the principal compression stress f_2 from:

$$f_2 = (\tan \theta + \cot \theta) \nu - f_1 \quad (C-10)$$

$$\text{where } \nu = \frac{V}{b_w j d} \quad (C-11)$$

Step 8: Calculate the maximum principal compression stress, which is affected by coincident tensile strains:

$$f_{2\max} = \frac{f'_c}{0.8 + 170 \varepsilon_1} \leq f'_c \quad (C-12)$$

Step 9: Verify if $f_2 \leq f_{2\max}$. If $f_2 > f_{2\max}$, the solution is not possible and the value of ε_1 must be reduced at Step 1.

Step 10: Calculate the principal compression strain:

$$\varepsilon_2 = \varepsilon'_c \left(1 - \sqrt{1 - \frac{f_2}{f_{2\max}}} \right) \quad (C-13)$$

Step 11: Calculate the longitudinal and transverse strains ε_x and ε_t .

$$\varepsilon_x = \frac{\varepsilon_1 \tan^2 \theta + \varepsilon_2}{1 + \tan^2 \theta} \quad (C-14)$$

$$\varepsilon_t = \frac{\varepsilon_2 \tan^2 \theta + \varepsilon_1}{1 + \tan^2 \theta} \quad (C-15)$$

Step 12: Calculate the stress in the shear reinforcement:

For ASTM A1035 and conventional steel:

$$f_v = \begin{cases} E_s \varepsilon_t & \text{for } \varepsilon_t \leq 0.0024 \\ 1170 - \frac{2.96}{\varepsilon_t + 0.0019} & \text{for } 0.0024 < \varepsilon_t \leq 0.02 \\ 1040 & \text{for } 0.02 < \varepsilon_t \leq 0.06 \end{cases} \quad (C-16a)$$

For conventional steel:

$$f_v = E_s \varepsilon_t \leq f_{yt} \quad (C-16b)$$

Step 13: Check estimate of f_v at Step 4. If necessary, revise the estimate and return to Step 5.

Step 14: Calculate the stress in the longitudinal reinforcement:

For ASTM A1035 and conventional steel:

$$f_{sx} = \begin{cases} E_s \varepsilon_x & \text{for } \varepsilon_x \leq 0.0024 \\ 1170 - \frac{2.96}{\varepsilon_x + 0.0019} & \text{for } 0.0024 < \varepsilon_x \leq 0.02 \\ 1040 & \text{for } 0.02 < \varepsilon_x \leq 0.06 \end{cases} \quad (C-17a)$$

For conventional steel:

$$f_{sx} = E_s \varepsilon_x \leq f_{yL} \quad (C-17b)$$

Step 15: Calculate the axial force N on the member based on:

$$N = A_{s_x} f_{sx} - \frac{V}{\tan \theta} + f_1 b_w j d - f_c \quad (C-18)$$

where

$$f_1 = \begin{cases} 0 & \text{if } \varepsilon_x \text{ is tensile} \\ f'_c \left[2 \left(\frac{\varepsilon_x}{\varepsilon'_c} \right) - \left(\frac{\varepsilon_x}{\varepsilon'_c} \right)^2 \right] & \text{if } \varepsilon_x \text{ is compressive} \end{cases} \quad (C-19)$$

Step 16: Verify if the result for N in Step 15 is equal to the actual applied axial load on the member (usually zero). If not, make a new estimate of θ at Step 2. A larger value of θ will increase N at Step 15.

Step 17: Determine if the longitudinal reinforcement can carry the incrementally higher stress at the crack locations. If this requirement is not satisfied, the value of f_l must be decreased at Step 5.

$$A_{sx}f_y \geq A_{sx}f_{sx} + f_l b_w j d + \left[f_1 - \frac{A_v}{b_w s} (f_{vy} - f_v) \right] b_w j d \cot^2 \theta \quad (C-20)$$

Step 18: Calculate the shear strain γ at the cross-section corresponding to the longitudinal strain ε_x .

$$\gamma = \frac{2 * (\varepsilon_x - \varepsilon_2)}{\tan \theta} \quad (C-21)$$

The calculation was repeated for incremental values of ε_l until f_2 is close to f_{2max} and a relationship between average longitudinal member stain ε_x and shear strain γ was solved. This relationship was used to calculate the shear strain corresponding to longitudinal steel stress f_s at any section due to applied loads. The shear deflection and the total deflection (General Deflection) was computed as described in Section 7.4. The most common input and output parameters including important steps in the deflection calculations for beams with ASTM A1035 steel tested in the current study are summarized in the Tables and Figures below.

C.1.1 Deflection of Beam RM1

Table C-1: Details of Beam RM1

$b_w (mm)$	$h (mm)$	$d (mm)$	$f_c' (MPa)$	$f_{yt} (MPa)$	$f_{yL} (MPa)$	$L (mm)$
300	600	523	41	830	430	3300
$A_s (mm^2)$	$A_s' (mm^2)$	$A_v (mm^2)$	$S (mm)$	$E_c (MPa)$	$M_{cr} (kN-m)$	$I_{cr} (mm^4)$
4000	258	142	320	30287	48	3476138840
$a_g (mm)$	$f_{cr} (MPa)$	$\varepsilon_{cr} (mm/mm)$	$E_s (MPa)$	$a (mm)$	$\Delta L (mm)$	$d_v (mm)$
10	2.11	0.070	200000	1650	235	470

Table C-2: ITG-6 Deflection of Beam RM1

$P (kN)$	$M_a (kN-m)$	$I_{eff} (mm^4)$	$\Delta_{ITG-6} (mm)$
0	0	5439027955	0.00
90	74	4126530501	0.54
180	149	3650196521	1.22
270	223	3573912255	1.87
360	297	3547968593	2.51
450	371	3536088872	3.15
540	446	3529669344	3.78
630	520	3525809948	4.42
720	594	3523309616	5.05
810	668	3521597467	5.69
900	743	3520373809	6.32

Table C-3: General Deflection of Beam RM1

$\varepsilon_l * 10^3$	θ (deg)	ω (mm)	v_{ci} (MPa)	f_v (MPa)	f_1 (MPa)	f_2 (MPa)	f_{2max} (MPa)	ε_2 (mm/mm)	ε_x (mm/mm)	ε_t (mm/mm)	f_v (MPa)	f_{sx} (MPa)	γ (mm/mm)
0.000	10.31	0.000	3.84	0	0.000	0.00	41.00	0.0000	0.0000	0.0000	0	0	0.00
0.008	44.99	0.004	3.79	0	0.242	0.24	41.00	0.0000	0.0000	0.0000	0	0	0.02
0.010	44.99	0.005	3.78	0	0.303	0.30	41.00	0.0000	0.0000	0.0000	0	0	0.02
0.500	39.04	0.266	2.11	54	1.409	2.34	41.00	-0.0001	0.0002	0.0003	54	30	0.57
0.750	37.06	0.404	1.71	89	1.311	2.66	41.00	-0.0001	0.0002	0.0004	89	43	0.81
1.500	33.60	0.828	1.08	200	1.132	3.53	38.86	-0.0001	0.0004	0.0010	200	74	1.50
3.000	30.84	1.694	0.62	430	0.950	5.08	31.30	-0.0002	0.0006	0.0022	430	124	2.84
4.500	28.51	2.596	0.43	612	0.555	5.85	26.20	-0.0003	0.0008	0.0034	612	156	4.05
6.000	26.94	3.516	0.33	720	0.328	6.46	22.53	-0.0004	0.0009	0.0047	720	180	5.19
7.500	25.81	4.447	0.26	794	0.179	6.96	19.76	-0.0005	0.0010	0.0060	794	199	6.30
9.000	24.94	5.388	0.22	830	0.102	7.37	17.60	-0.0006	0.0011	0.0073	830	214	7.38
11.000	24.03	6.653	0.18	830	0.080	7.80	15.36	-0.0008	0.0012	0.0090	830	230	8.79
13.000	23.38	7.922	0.15	830	0.065	8.14	13.62	-0.0010	0.0012	0.0108	830	243	10.19
15.000	22.91	9.192	0.13	830	0.055	8.41	12.24	-0.0012	0.0013	0.0125	830	253	11.62
17.000	22.58	10.459	0.12	830	0.048	8.60	11.11	-0.0014	0.0013	0.0143	830	260	13.07
19.000	22.38	11.718	0.10	830	0.043	8.71	10.17	-0.0017	0.0013	0.0160	830	264	14.57
22.000	22.36	13.572	0.09	830	0.037	8.69	9.03	-0.0022	0.0013	0.0185	830	264	17.02

Table C-4: General Deflection of Beam RM1

P (kN)	$\epsilon_x * 10^3$	γ (mm/mm)	Δ_{st} (mm)	Δ_{ITG-6} (mm)	Δ_{GEN} (mm)
0	0.00	0.00	0.00	0.00	0.00
90	0.13	0.62	0.56	0.54	1.10
180	0.25	1.13	1.10	1.22	2.32
270	0.38	1.60	1.57	1.87	3.44
360	0.51	2.10	2.02	2.51	4.53
450	0.63	2.76	2.49	3.15	5.63
540	0.76	3.66	3.01	3.78	6.79
630	0.89	4.91	3.64	4.42	8.05
720	1.01	6.62	4.41	5.05	9.46
810	1.14	8.87	5.37	5.69	11.05
900	1.26	11.52	6.55	6.32	12.87

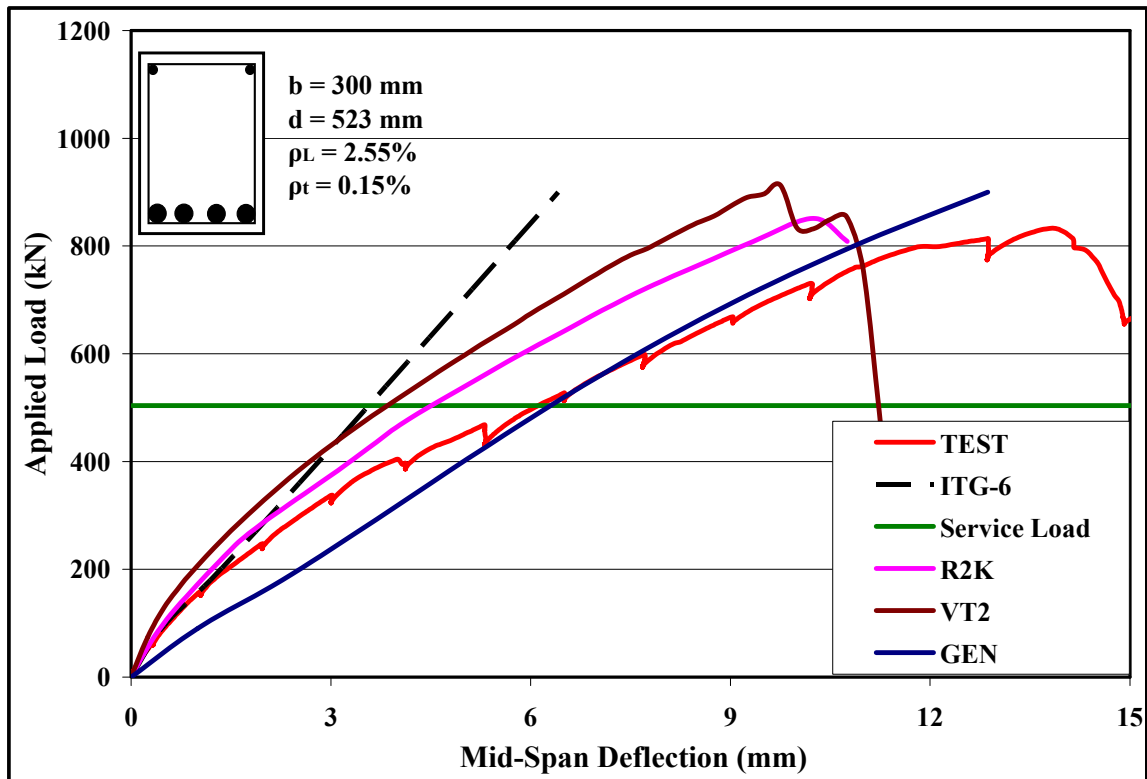


Figure C-2: Load-Deflection Plots of Beam RM1

C.1.2 Deflection of Beam RM2

Table C-5: Modeling Details of Beam RM2

$b_w (mm)$	$h (mm)$	$d (mm)$	$f_c' (MPa)$	$f_{yt} (MPa)$	$f_{yL} (MPa)$	$L (mm)$
300	600	523	45	830	430	3300
$A_s (mm^2)$	$A_s' (mm^2)$	$A_v (mm^2)$	$S (mm)$	$E_c (MPa)$	$M_{cr} (kN-m)$	$I_{cr} (mm^4)$
4000	258	142	265	29171	50	3562940344
$a_g (mm)$	$f_{cr} (MPa)$	$\epsilon_{cr} (mm/mm)$	$E_s (MPa)$	$a (mm)$	$\Delta L (mm)$	$d_v (mm)$
10	2.21	0.076	200000	1650	235	470

Table C-6: ITG-6 Deflection of Beam RM2

$P (kN)$	$M_a (kN-m)$	$I_{eff} (mm^4)$	$\Delta_{ITG-6} (mm)$
0	0	5442337040	0.00
95	78	4188608819	0.58
190	157	3735161576	1.31
285	235	3661857805	2.00
380	314	3636884279	2.68
475	392	3625441401	3.36
570	470	3619256001	4.04
665	549	3615536710	4.72
760	627	3613126883	5.40
855	705	3611476591	6.08
950	784	3610297082	6.75

Table C-7: General Deflection of Beam RM2

$\varepsilon_l * 10^{03}$	θ (deg)	ω (mm)	v_{ci} (MPa)	f_v (MPa)	f_1 (MPa)	f_2 (MPa)	f_{2max} (MPa)	ε_2 (mm/mm)	ε_x (mm/mm)	ε_t (mm/mm)	f_v (MPa)	f_{sx} (MPa)	γ (mm/mm)
0.000	10.31	0.000	4.02	0	0.000	0.00	45.00	0.0000	0.0000	0.0000	0	0	0.00
0.008	44.98	0.004	3.98	0	0.233	0.23	45.00	0.0000	0.0000	0.0000	0	0	0.02
0.010	44.99	0.005	3.97	0	0.292	0.29	45.00	0.0000	0.0000	0.0000	0	0	0.02
0.500	39.38	0.249	2.28	53	1.476	2.42	45.00	-0.0001	0.0002	0.0003	53	30	0.57
0.750	37.47	0.377	1.86	87	1.373	2.75	45.00	-0.0001	0.0002	0.0004	87	43	0.82
1.500	34.18	0.769	1.20	197	1.186	3.68	42.65	-0.0001	0.0004	0.0010	197	76	1.52
3.000	31.60	1.565	0.69	421	0.995	5.37	34.35	-0.0003	0.0006	0.0021	421	128	2.90
4.500	29.76	2.379	0.48	601	0.686	6.45	28.75	-0.0004	0.0008	0.0033	601	166	4.20
6.000	28.18	3.212	0.37	711	0.410	7.12	24.73	-0.0005	0.0010	0.0046	711	193	5.40
7.500	27.04	4.055	0.30	787	0.230	7.67	21.69	-0.0006	0.0011	0.0058	787	214	6.57
9.000	26.16	4.904	0.25	830	0.123	8.13	19.31	-0.0007	0.0012	0.0071	830	231	7.71
11.000	25.23	6.046	0.21	830	0.097	8.59	16.85	-0.0009	0.0012	0.0088	830	249	9.20
13.000	24.56	7.191	0.17	830	0.080	8.96	14.95	-0.0011	0.0013	0.0106	830	262	10.69
15.000	24.08	8.337	0.15	830	0.068	9.24	13.43	-0.0014	0.0014	0.0123	830	273	12.19
17.000	23.74	9.480	0.13	830	0.059	9.44	12.20	-0.0016	0.0014	0.0140	830	280	13.73
19.000	23.54	10.617	0.12	830	0.052	9.56	11.17	-0.0019	0.0014	0.0157	830	285	15.32
21.500	23.50	12.019	0.11	830	0.046	9.56	10.10	-0.0024	0.0014	0.0177	830	285	17.46

Table C-8: General Deflection of Beam RM2

P (kN)	$\epsilon_x * 10^3$	γ (mm/mm)	Δ_{st} (mm)	Δ_{ITG-6} (mm)	Δ_{GEN} (mm)
0	0.00	0.00	0.00	0.00	0.00
95	0.13	0.67	0.60	0.58	1.18
190	0.27	1.22	1.19	1.31	2.49
285	0.40	1.70	1.69	2.00	3.69
380	0.54	2.21	2.16	2.68	4.84
475	0.67	2.84	2.64	3.36	6.00
570	0.80	3.71	3.16	4.04	7.20
665	0.94	4.92	3.78	4.72	8.50
760	1.07	6.57	4.53	5.40	9.93
855	1.20	8.77	5.46	6.08	11.54
950	1.34	11.62	6.62	6.75	13.37

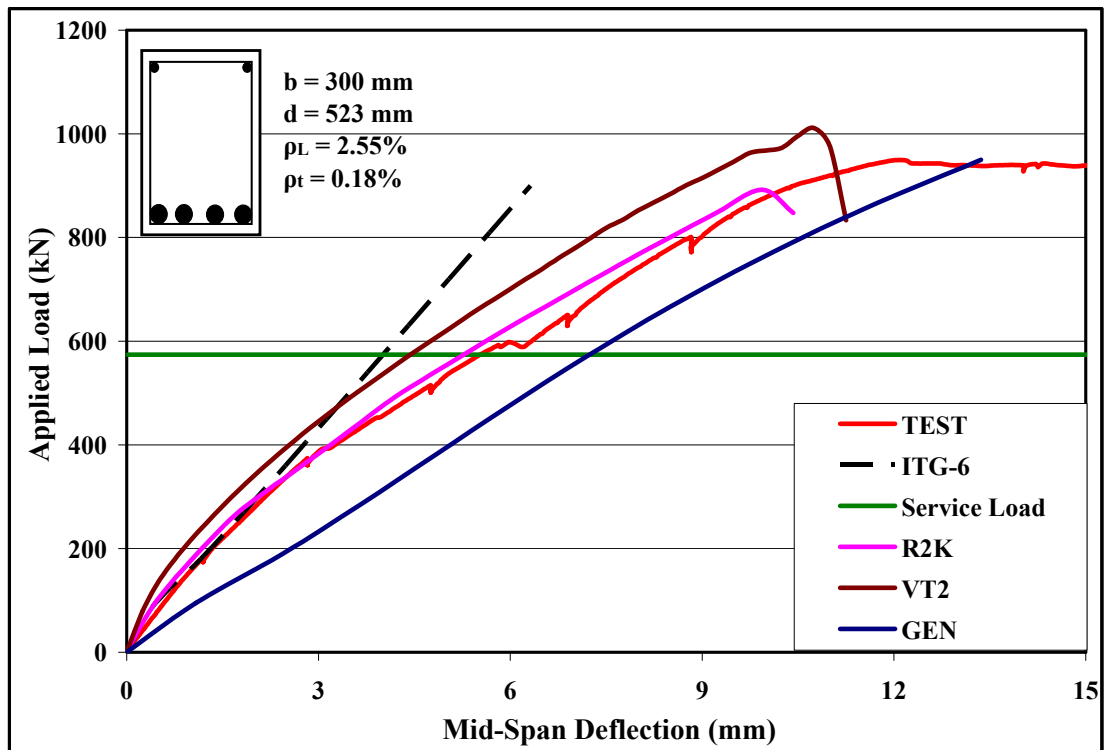


Figure C-3: Load-Deflection Plots of Beam RM2

C.1.3 Deflection of Beam MR1

Table C-9: Modeling Details of Beam MR1

$b_w (mm)$	$h (mm)$	$d (mm)$	$f_c' (MPa)$	$f_{yt} (MPa)$	$f_{yL} (MPa)$	$L (mm)$
300	1000	935	49	430	830	5610
$A_s (mm^2)$	$A_s' (mm^2)$	$A_v (mm^2)$	$S (mm)$	$E_c (MPa)$	$M_{cr} (kN-m)$	$I_{cr} (mm^4)$
1548	258	200	440	30140	146	6316042230
$a_g (mm)$	$f_{cr} (MPa)$	$\epsilon_{cr} (mm/mm)$	$E_s (MPa)$	$a (mm)$	$\Delta L (mm)$	$d_v (mm)$
10	2.31	0.077	200000	2805	401	842

Table C-10: ITG-6 Deflection of Beam MR1

$P (kN)$	$M_a (kN-m)$	$I_{eff} (mm^4)$	$\Delta_{ITG-6} (mm)$
0	0	25036117028	0.00
90	126	25036117028	0.44
180	252	8460740932	2.60
270	379	7142687632	4.61
360	505	6773746063	6.49
450	631	6615643424	8.30
540	757	6532831390	10.09
630	884	6483898180	11.86
720	1010	6452531196	13.62
810	1136	6431201852	15.37
900	1262	6416031885	17.12

Table C-11: General Deflection of Beam MR1

$\varepsilon_I * 10^3$	θ (deg)	ω (mm)	ν_{ci} (MPa)	f_v (MPa)	f_1 (MPa)	f_2 (MPa)	f_{2max} (MPa)	ε_2 (mm/mm)	ε_x (mm/mm)	ε_t (mm/mm)	f_v (MPa)	f_{sx} (MPa)	γ (mm/mm)
0.000	10.31	0.000	4.20	0	0.000	0.00	49.00	0.0000	0.0000	0.0000	0	0	0.00
0.008	44.98	0.006	4.12	0	0.241	0.24	49.00	0.0000	0.0000	0.0000	0	0	0.02
0.010	44.98	0.008	4.10	0	0.301	0.30	49.00	0.0000	0.0000	0.0000	0	0	0.02
0.500	43.53	0.389	1.91	47	1.540	1.85	49.00	-0.0001	0.0002	0.0002	47	41	0.56
0.750	42.80	0.583	1.50	75	1.433	1.91	49.00	-0.0001	0.0003	0.0004	75	62	0.81
1.500	41.02	1.161	0.92	164	1.202	2.16	46.45	-0.0001	0.0006	0.0008	164	121	1.56
3.000	37.76	2.313	0.52	367	0.496	2.31	37.40	-0.0001	0.0011	0.0018	367	212	3.00
6.000	32.24	4.629	0.28	430	0.174	2.72	26.92	-0.0002	0.0016	0.0042	430	321	5.57
9.000	29.02	6.977	0.19	430	0.104	3.10	21.03	-0.0002	0.0019	0.0068	430	397	7.85
12.000	27.14	9.343	0.14	430	0.072	3.40	17.25	-0.0003	0.0022	0.0094	430	453	10.02
15.000	25.84	11.720	0.11	430	0.055	3.66	14.63	-0.0004	0.0025	0.0121	430	500	12.11
20.000	24.22	15.709	0.09	430	0.038	4.06	11.67	-0.0006	0.0028	0.0165	430	570	15.44
27.000	22.74	21.323	0.06	430	0.026	4.51	9.09	-0.0009	0.0032	0.0228	430	648	19.93
34.000	21.78	26.958	0.05	430	0.020	4.85	7.45	-0.0013	0.0035	0.0291	430	707	24.36
40.000	21.23	31.791	0.04	430	0.017	5.07	6.45	-0.0018	0.0037	0.0345	430	746	28.19
46.000	20.91	36.613	0.04	430	0.014	5.21	5.68	-0.0023	0.0038	0.0398	430	769	32.22
50.000	20.90	39.798	0.03	430	0.013	5.21	5.27	-0.0029	0.0038	0.0433	430	768	35.27

Table C-12: General Deflection of Beam MR1

P (kN)	$\varepsilon_x * 10^3$	γ (mm/mm)	Δ_{st} (mm)	Δ_{ITG-6} (mm)	Δ_{GEN} (mm)
0	0.00	0.00	0.00	0.00	0.00
90	0.31	0.96	1.39	0.44	1.83
180	0.63	1.96	3.01	2.60	5.61
270	0.94	2.99	4.60	4.61	9.21
360	1.26	4.14	6.23	6.49	12.71
450	1.57	5.52	7.97	8.30	16.27
540	1.89	7.23	9.89	10.09	19.98
630	2.20	9.35	12.07	11.86	23.93
720	2.52	11.99	14.57	13.62	28.19
810	2.83	15.25	17.47	15.37	32.84
900	3.15	19.22	20.84	17.12	37.96

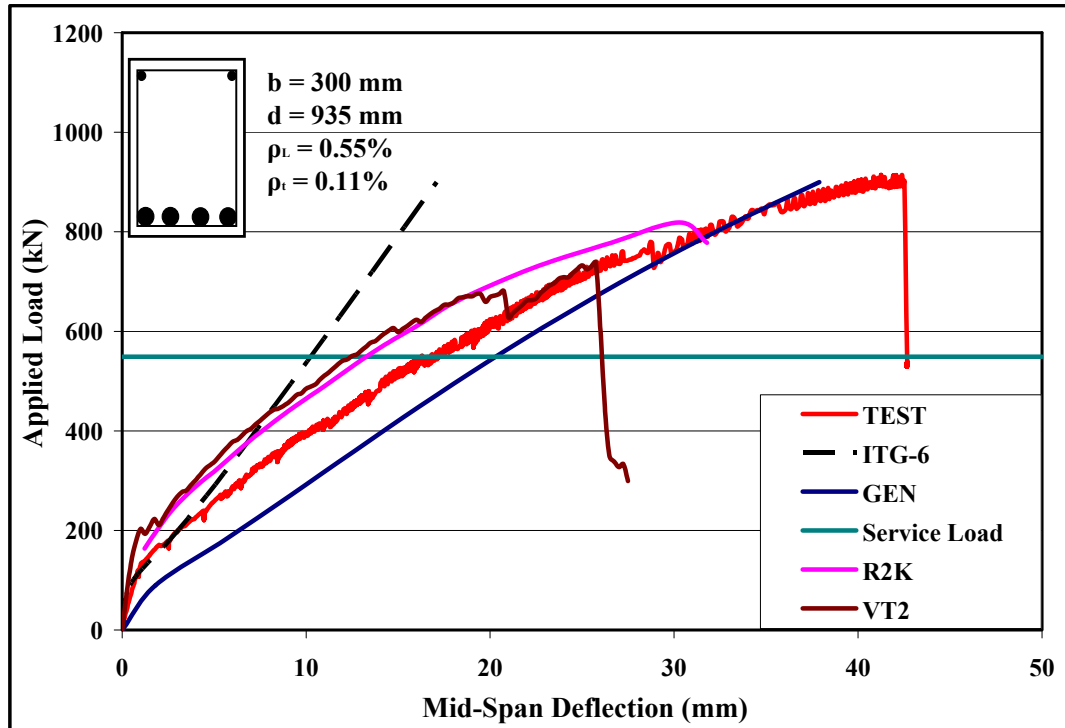


Figure C-3: Load-Deflection Plots of Beam MR1

C.1.4 Deflection of Beam MR2

Table C-13: Modeling Details of Beam MR2

$b_w (mm)$	$h (mm)$	$d (mm)$	$f_c' (MPa)$	$f_{yt} (MPa)$	$f_{yL} (MPa)$	$L (mm)$
300	1000	935	50	430	830	5610
$A_s (mm^2)$	$A_s' (mm^2)$	$A_v (mm^2)$	$S (mm)$	$E_c (MPa)$	$M_{cr} (kN-m)$	$I_{cr} (mm^4)$
1935	258	200	440	30376	148	7535763271
$a_g (mm)$	$f_{cr} (MPa)$	$\epsilon_{cr} (mm/mm)$	$E_s (MPa)$	$a (mm)$	$\Delta L (mm)$	$d_v (mm)$
10	2.33	0.077	200000	2805	401	842

Table C-14: ITG-6 Deflection of Beam MR2

$P (kN)$	$M_a (kN-m)$	$I_{eff} (mm^4)$	$\Delta_{ITG-6} (mm)$
0	0	25046172436	0.00
90	126	25046172436	0.44
180	252	9945019897	2.19
270	379	8476373122	3.86
360	505	8060220431	5.41
450	631	7881200123	6.91
540	757	7787266652	8.40
630	884	7731708398	9.87
720	1010	7696073747	11.33
810	1136	7671833082	12.79
900	1262	7654587908	14.24

Table C-15: General Deflection of Beam MR2

$\varepsilon_1 * 10^3$	θ (deg)	ω (mm)	ν_{ci} (MPa)	f_v (MPa)	f_1 (MPa)	f_2 (MPa)	f_{2max} (MPa)	ε_2 (mm/mm)	ε_x (mm/mm)	ε_t (mm/mm)	f_v (MPa)	f_{sx} (MPa)	γ (mm/mm)
0.000	10.31	0.000	4.24	0	0.000	0.00	50.00	0.0000	0.0000	0.0000	0	0	0.00
0.008	44.98	0.006	4.16	0	0.243	0.24	50.00	0.0000	0.0000	0.0000	0	0	0.02
0.010	44.98	0.008	4.15	0	0.304	0.30	50.00	0.0000	0.0000	0.0000	0	0	0.02
0.500	43.14	0.378	1.96	47	1.556	1.92	50.00	-0.0001	0.0002	0.0002	47	40	0.56
0.750	42.23	0.567	1.55	76	1.447	2.01	50.00	-0.0001	0.0003	0.0004	76	60	0.81
1.500	40.09	1.130	0.95	169	1.194	2.30	47.39	-0.0001	0.0006	0.0008	169	115	1.56
3.000	36.38	2.258	0.53	381	0.468	2.50	38.17	-0.0001	0.0010	0.0019	381	197	2.97
6.000	30.83	4.544	0.28	430	0.169	2.95	27.47	-0.0002	0.0014	0.0044	430	289	5.44
9.000	27.70	6.869	0.19	430	0.101	3.38	21.46	-0.0003	0.0017	0.0070	430	355	7.63
12.000	25.83	9.214	0.14	430	0.070	3.73	17.61	-0.0004	0.0020	0.0097	430	407	9.70
15.000	24.58	11.572	0.12	430	0.053	4.02	14.93	-0.0005	0.0022	0.0123	430	448	11.71
20.000	23.16	15.521	0.09	430	0.037	4.41	11.90	-0.0007	0.0025	0.0168	430	504	14.96
27.000	21.80	21.084	0.06	430	0.026	4.88	9.28	-0.0010	0.0028	0.0231	430	569	19.34
34.000	20.95	26.664	0.05	430	0.020	5.23	7.60	-0.0015	0.0031	0.0295	430	617	23.68
40.000	20.49	31.444	0.04	430	0.016	5.43	6.58	-0.0019	0.0032	0.0349	430	645	27.50
44.000	20.32	34.620	0.04	430	0.015	5.51	6.04	-0.0023	0.0033	0.0384	430	655	30.17
46.000	20.29	36.199	0.04	430	0.014	5.52	5.80	-0.0026	0.0033	0.0402	430	656	31.60

Table C-16: General Deflection of Beam MR2

P (kN)	$\varepsilon_x * 10^3$	γ (mm/mm)	Δ_{st} (mm)	Δ_{ITG-6} (mm)	Δ_{GEN} (mm)
0	0.00	0.00	0.00	0.00	0.00
90	0.25	0.73	1.09	0.44	1.53
180	0.50	1.51	2.31	2.19	4.50
270	0.76	2.35	3.55	3.86	7.40
360	1.01	3.31	4.86	5.41	10.27
450	1.26	4.46	6.28	6.91	13.20
540	1.51	5.86	7.87	8.40	16.27
630	1.76	7.57	9.67	9.87	19.53
720	2.02	9.66	11.71	11.33	23.04
810	2.27	12.18	14.05	12.79	26.84
900	2.52	15.20	16.73	14.24	30.97

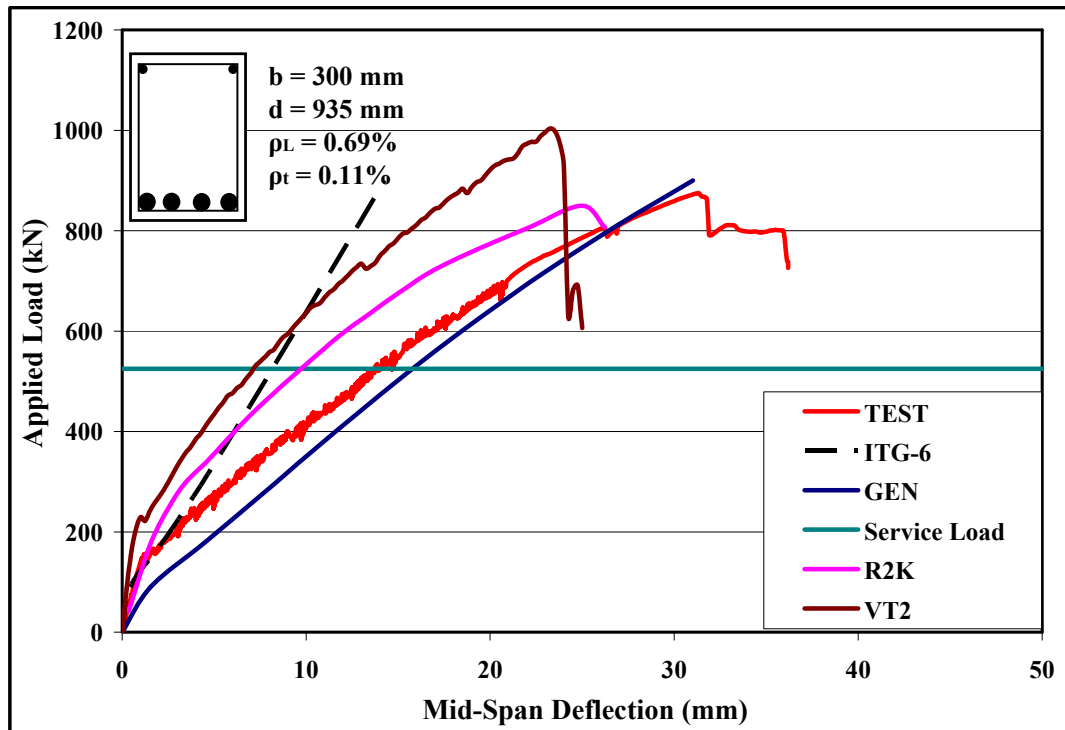


Figure C-4: Load-Deflection Plots of Beam MR2

C.1.5 Deflection of Beam MR3

Table C-17: Modeling Details of Beam MR3

$b_w (mm)$	$h (mm)$	$d (mm)$	$f_c' (MPa)$	$f_{yt} (MPa)$	$f_{yL} (MPa)$	$L (mm)$
300	1000	885	48	430	830	5310
$A_s (mm^2)$	$A_s' (mm^2)$	$A_v (mm^2)$	$S (mm)$	$E_c (MPa)$	$M_{cr} (kN-m)$	$I_{cr} (mm^4)$
4257	258	200	440	29902	145	12361976632
$a_g (mm)$	$f_{cr} (MPa)$	$\varepsilon_{cr} (mm/mm)$	$E_s (MPa)$	$a (mm)$	$\Delta L (mm)$	$d_v (mm)$
10	2.29	0.076	200000	2655	379	797

Table C-18: ITG-6 Deflection of Beam MR3

$P (kN)$	$M_a (kN-m)$	$I_{eff} (mm^4)$	$\Delta_{ITG-6} (mm)$
0	0	25100979561	0.00
140	186	17913617556	0.82
280	372	13486984467	2.17
420	558	12898056335	3.40
560	743	12703988479	4.60
700	929	12616141612	5.79
840	1115	12568933689	6.97
980	1301	12540640523	8.15
1120	1487	12522345787	9.33
1260	1673	12509834037	10.51
1400	1859	12500899909	11.68

Table C-19: General Deflection of Beam MR3

$\varepsilon_l * 10^3$	θ (deg)	ω (mm)	ν_{ci} (MPa)	f_v (MPa)	f_1 (MPa)	f_2 (MPa)	f_{2max} (MPa)	ε_2 (mm/mm)	ε_x (mm/mm)	ε_t (mm/mm)	f_v (MPa)	f_{sx} (MPa)	γ (mm/mm)
0.000	10.31	0.000	4.16	0	0.000	0.00	48.00	0.0000	0.0000	0.0000	0	0	0.00
0.008	44.98	0.006	4.09	0	0.239	0.24	48.00	0.0000	0.0000	0.0000	0	0	0.02
0.010	44.98	0.007	4.07	0	0.299	0.30	48.00	0.0000	0.0000	0.0000	0	0	0.02
0.100	44.62	0.071	3.42	4	1.868	1.93	48.00	-0.0001	0.0000	0.0000	4	3	0.17
0.500	41.15	0.352	1.99	50	1.524	2.17	48.00	-0.0001	0.0002	0.0003	50	35	0.57
1.000	38.36	0.706	1.31	116	1.339	2.59	48.00	-0.0001	0.0003	0.0006	116	66	1.06
2.000	34.11	1.422	0.77	267	0.771	2.96	42.11	-0.0001	0.0006	0.0013	267	110	1.96
4.000	29.07	2.890	0.42	430	0.234	3.51	32.43	-0.0002	0.0008	0.0030	430	162	3.55
6.000	26.16	4.391	0.29	430	0.141	3.93	26.37	-0.0002	0.0010	0.0048	430	193	4.95
8.000	24.38	5.909	0.22	430	0.098	4.30	22.22	-0.0003	0.0011	0.0066	430	218	6.26
10.000	23.15	7.439	0.17	430	0.074	4.62	19.20	-0.0004	0.0012	0.0084	430	240	7.53
14.000	21.54	10.518	0.12	430	0.049	5.14	15.09	-0.0006	0.0014	0.0120	430	273	9.98
18.000	20.53	13.614	0.10	430	0.036	5.55	12.44	-0.0008	0.0015	0.0157	430	299	12.37
22.000	19.82	16.722	0.08	430	0.029	5.88	10.57	-0.0011	0.0016	0.0193	430	320	14.72
28.000	19.17	21.383	0.06	430	0.022	6.22	8.63	-0.0015	0.0017	0.0248	430	341	18.31
34.000	18.88	26.020	0.05	430	0.018	6.37	7.29	-0.0021	0.0017	0.0302	430	351	22.09
40.000	19.03	30.577	0.04	430	0.015	6.25	6.32	-0.0029	0.0017	0.0354	430	343	26.45

Table C-20: General Deflection of Beam MR3

P (kN)	$\epsilon_x * 10^3$	γ (mm/mm)	Δ_{st} (mm)	Δ_{ITG-6} (mm)	Δ_{GEN} (mm)
0	0.00	0.00	0.00	0.00	0.00
140	0.18	0.75	1.15	0.82	1.96
280	0.36	1.38	2.17	2.17	4.34
420	0.53	2.02	3.12	3.40	6.52
560	0.71	2.84	4.10	4.60	8.70
700	0.89	4.02	5.24	5.79	11.02
840	1.07	5.73	6.64	6.97	13.61
980	1.25	8.13	8.43	8.15	16.58
1120	1.43	11.38	10.71	9.33	20.04
1260	1.60	15.67	13.61	10.51	24.12
1400	1.78	21.16	17.24	11.68	28.92

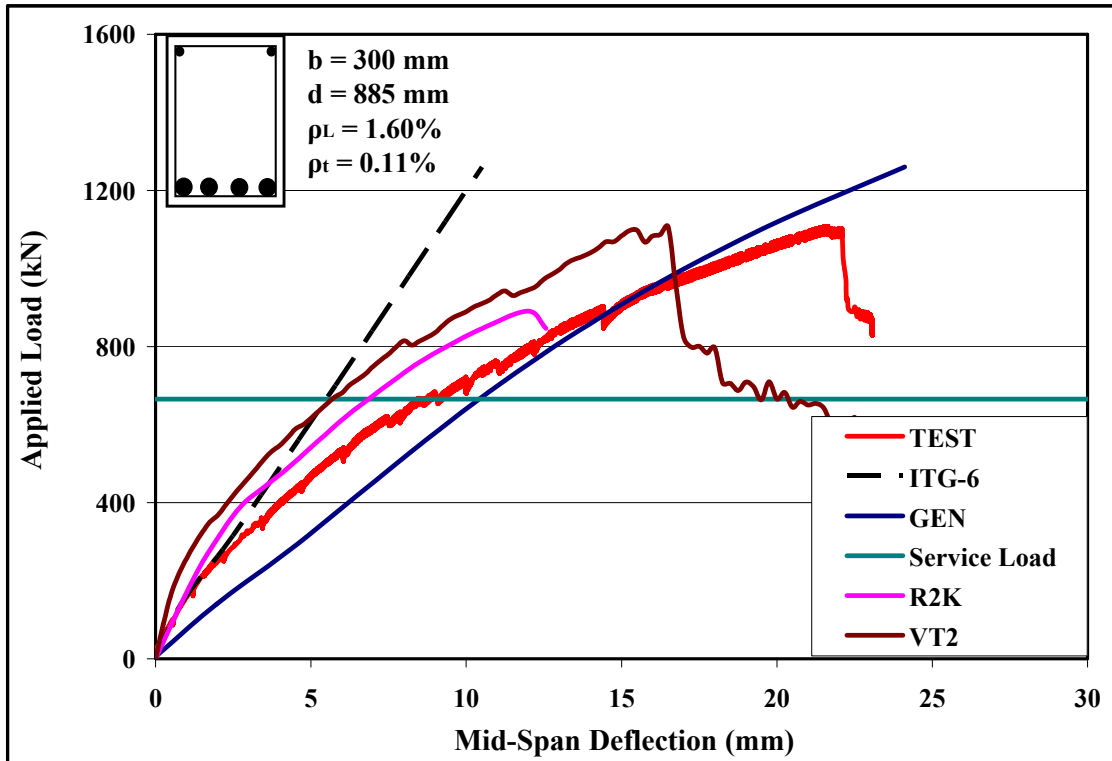


Figure C-5: Load-Deflection Plots of Beam MR3

C.1.6 Deflection of Beam MR4

Table C-21: Modeling Details of Beam MR4

$b_w (mm)$	$h (mm)$	$d (mm)$	$f_c' (MPa)$	$f_{yt} (MPa)$	$f_{yL} (MPa)$	$L (mm)$
300	1000	885	50	430	830	5310
$A_s (mm^2)$	$A_s' (mm^2)$	$A_v (mm^2)$	$S (mm)$	$E_c (MPa)$	$M_{cr} (kN-m)$	$I_{cr} (mm^4)$
4257	258	200	220	30265	148	12222457029
$a_g (mm)$	$f_{cr} (MPa)$	$\varepsilon_{cr} (mm/mm)$	$E_s (MPa)$	$a (mm)$	$\Delta L (mm)$	$d_v (mm)$
10	2.33	0.077	200000	2655	379	797

Table C-22: ITG-6 Deflection of Beam MR4

$P (kN)$	$M_a (kN-m)$	$I_{eff} (mm^4)$	$\Delta_{ITG-6} (mm)$
0	0	25097633666	0.00
160	212	16323645975	1.01
320	425	13123586351	2.50
480	637	12664617140	3.89
640	850	12511525993	5.25
800	1062	12441922334	6.60
960	1274	12404439097	7.95
1120	1487	12381947695	9.29
1280	1699	12367393852	10.63
1440	1912	12357435695	11.97
1600	2124	12350322594	13.30

Table C-23: General Deflection of Beam MR4

$\varepsilon_I * 10^3$	θ (deg)	ω (mm)	ν_{ci} (MPa)	f_v (MPa)	f_I (MPa)	f_2 (MPa)	f_{2max} (MPa)	ε_2 (mm/mm)	ε_x (mm/mm)	ε_t (mm/mm)	f_v (MPa)	f_{sx} (MPa)	γ (mm/mm)
0.000	10.31	0.000	4.24	0	0.000	0.00	50.00	0.0000	0.0000	0.0000	0	0	0.00
0.008	44.98	0.004	4.19	0	0.243	0.24	50.00	0.0000	0.0000	0.0000	0	0	0.02
0.010	44.98	0.005	4.17	0	0.304	0.30	50.00	0.0000	0.0000	0.0000	0	0	0.02
0.100	44.67	0.053	3.64	4	1.907	1.97	50.00	-0.0001	0.0000	0.0000	4	3	0.17
0.500	41.73	0.263	2.34	49	1.556	2.29	50.00	-0.0001	0.0002	0.0002	49	36	0.57
1.000	39.52	0.523	1.63	111	1.367	2.84	50.00	-0.0001	0.0003	0.0006	111	70	1.07
2.000	37.37	1.039	1.01	241	1.167	3.98	43.86	-0.0002	0.0006	0.0012	241	128	2.08
4.000	33.67	2.063	0.58	430	0.385	5.10	33.78	-0.0003	0.0011	0.0027	430	210	3.93
6.000	30.57	3.085	0.40	430	0.239	5.72	27.47	-0.0004	0.0013	0.0044	430	257	5.57
8.000	28.62	4.113	0.31	430	0.170	6.24	23.15	-0.0005	0.0015	0.0061	430	294	7.13
10.000	27.19	5.144	0.25	430	0.130	6.73	20.00	-0.0006	0.0016	0.0078	430	326	8.63
12.000	26.14	6.177	0.21	430	0.104	7.14	17.61	-0.0008	0.0017	0.0095	430	353	10.09
16.000	24.74	8.249	0.16	430	0.074	7.78	14.20	-0.0011	0.0019	0.0130	430	394	12.99
20.000	23.89	10.324	0.13	430	0.057	8.23	11.90	-0.0015	0.0021	0.0165	430	423	15.90
23.000	23.49	11.881	0.11	430	0.049	8.45	10.62	-0.0018	0.0021	0.0191	430	437	18.14
26.000	23.27	13.436	0.10	430	0.043	8.58	9.58	-0.0022	0.0022	0.0216	430	445	20.49
28.000	23.24	14.470	0.09	430	0.040	8.58	8.99	-0.0026	0.0022	0.0232	430	445	22.19

Table C-24: General Deflection of Beam MR4

P (kN)	$\varepsilon_x * 10^3$	γ (mm/mm)	Δ_{st} (mm)	Δ_{ITG-6} (mm)	Δ_{GEN} (mm)
0	0.00	0.00	0.00	0.00	0.00
160	0.20	0.76	1.17	1.01	2.18
320	0.41	1.39	2.20	2.50	4.70
480	0.61	2.01	3.15	3.89	7.04
640	0.81	2.73	4.10	5.25	9.35
800	1.02	3.66	5.12	6.60	11.73
960	1.22	4.93	6.31	7.95	14.26
1120	1.43	6.64	7.73	9.29	17.02
1280	1.63	8.91	9.46	10.63	20.09
1440	1.83	11.85	11.59	11.97	23.56
1600	2.04	15.59	14.19	13.30	27.50

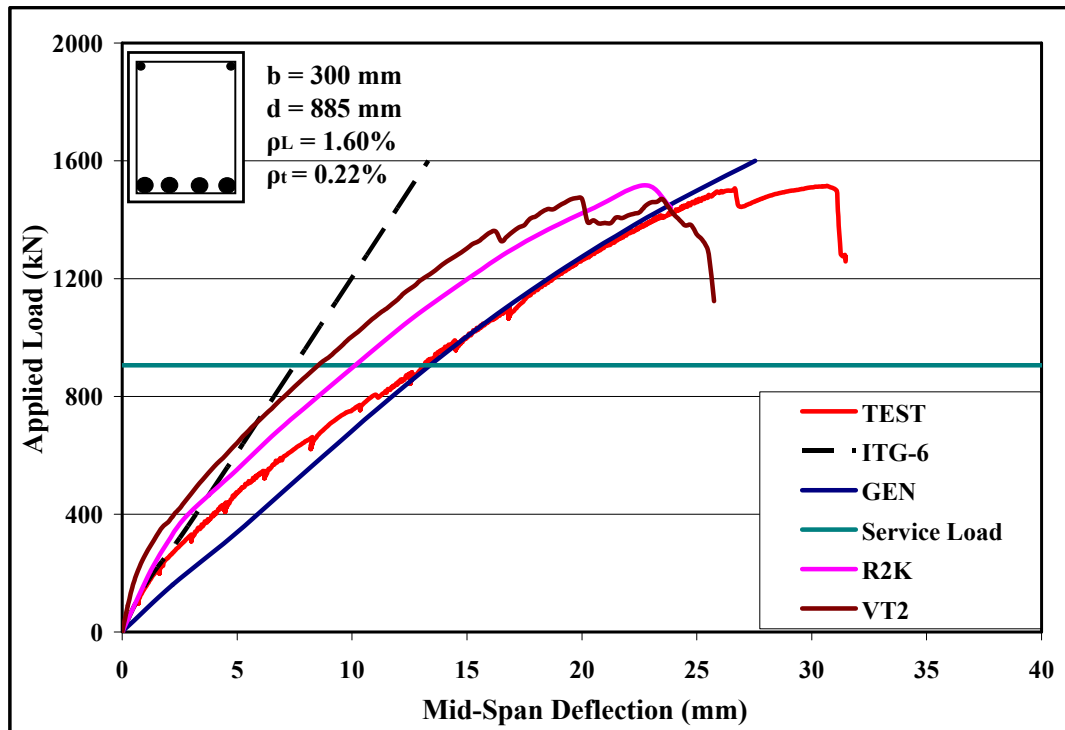


Figure C-6: Load-Deflection Plots of Beam MR4

C.1.7 Deflection of Beam MM1

Table C-25: Modeling Details of Beam MM1

$b_w (mm)$	$h (mm)$	$d (mm)$	$f_c' (MPa)$	$f_{yt} (MPa)$	$f_{yL} (MPa)$	$L (mm)$
300	1000	935	50	830	830	5610
$A_s (mm^2)$	$A_s' (mm^2)$	$A_v (mm^2)$	$S (mm)$	$E_c (MPa)$	$M_{cr} (kN-m)$	$I_{cr} (mm^4)$
1548	258	142	440	30376	148	6275336115
$a_g (mm)$	$f_{cr} (MPa)$	$\epsilon_{cr} (mm/mm)$	$E_s (MPa)$	$a (mm)$	$\Delta L (mm)$	$d_v (mm)$
10	2.33	0.077	200000	2805	401	842

Table C-26: ITG-6 Deflection of Beam MM1

$P (kN)$	$M_a (kN-m)$	$I_{eff} (mm^4)$	$\Delta_{ITG-6} (mm)$
0	0	25035448986	0.00
90	126	25035448986	0.44
180	252	8469499454	2.57
270	379	7116275607	4.59
360	505	6739782441	6.47
450	631	6578748686	8.28
540	757	6494474231	10.07
630	884	6444700403	11.84
720	1010	6412803753	13.60
810	1136	6391118335	15.35
900	1262	6375697137	17.09

Table C-27: General Deflection of Beam MM1

$\varepsilon_l * 10^3$	θ (deg)	ω (mm)	ν_{ci} (MPa)	f_v (MPa)	f_1 (MPa)	f_2 (MPa)	f_{2max} (MPa)	ε_2 (mm/mm)	ε_x (mm/mm)	ε_t (mm/mm)	f_v (MPa)	f_{sx} (MPa)	γ (mm/mm)
0.000	10.31	0.000	4.24	0	0.000	0.00	50.00	0.0000	0.0000	0.0000	0	0	0.00
0.008	44.98	0.007	4.15	0	0.243	0.24	50.00	0.0000	0.0000	0.0000	0	0	0.02
0.010	44.98	0.009	4.13	0	0.304	0.30	50.00	0.0000	0.0000	0.0000	0	0	0.02
0.100	44.86	0.089	3.33	4	1.907	1.93	50.00	-0.0001	0.0000	0.0000	4	4	0.16
0.500	43.38	0.446	1.79	47	1.556	1.85	50.00	-0.0001	0.0002	0.0002	47	41	0.56
1.000	41.80	0.891	1.13	105	1.367	1.96	50.00	-0.0001	0.0004	0.0005	105	82	1.06
2.000	39.59	1.784	0.65	230	1.167	2.31	43.86	-0.0001	0.0008	0.0012	230	152	2.05
4.000	36.17	3.583	0.35	506	0.606	2.70	33.78	-0.0001	0.0013	0.0026	506	261	3.94
6.000	33.58	5.406	0.24	677	0.324	3.11	27.47	-0.0002	0.0017	0.0041	677	349	5.71
8.000	31.73	7.248	0.18	781	0.165	3.47	23.15	-0.0003	0.0020	0.0057	781	417	7.39
10.000	30.36	9.102	0.15	830	0.086	3.74	20.00	-0.0003	0.0023	0.0074	830	468	9.01
15.000	27.73	13.800	0.10	830	0.051	4.31	14.93	-0.0005	0.0028	0.0116	830	569	12.78
20.000	26.04	18.549	0.07	830	0.036	4.78	11.90	-0.0007	0.0033	0.0160	830	651	16.37
25.000	24.88	23.327	0.06	830	0.027	5.17	9.90	-0.0010	0.0036	0.0204	830	718	19.86
30.000	24.04	28.124	0.05	830	0.022	5.49	8.47	-0.0013	0.0039	0.0248	830	773	23.32
35.000	23.43	32.928	0.04	830	0.018	5.74	7.41	-0.0017	0.0041	0.0292	830	817	26.81
43.000	23.23	40.502	0.03	830	0.015	5.81	6.17	-0.0025	0.0046	0.0359	830	830	33.00

Table C-28: General Deflection of Beam MM1

P (kN)	$\epsilon_x * 10^3$	γ (mm/mm)	Δ_{st} (mm)	Δ_{ITG-6} (mm)	Δ_{GEN} (mm)
0	0.00	0.00	0.00	0.00	0.00
90	0.31	0.89	1.41	0.44	1.84
180	0.63	1.80	2.82	2.57	5.39
270	0.94	2.77	4.26	4.59	8.85
360	1.26	3.84	5.76	6.47	12.23
450	1.57	5.08	7.37	8.28	15.66
540	1.89	6.53	9.13	10.07	19.19
630	2.20	8.23	11.05	11.84	22.89
720	2.52	10.24	13.19	13.60	26.79
810	2.83	12.62	15.58	15.35	30.92
900	3.15	15.39	18.24	17.09	35.34

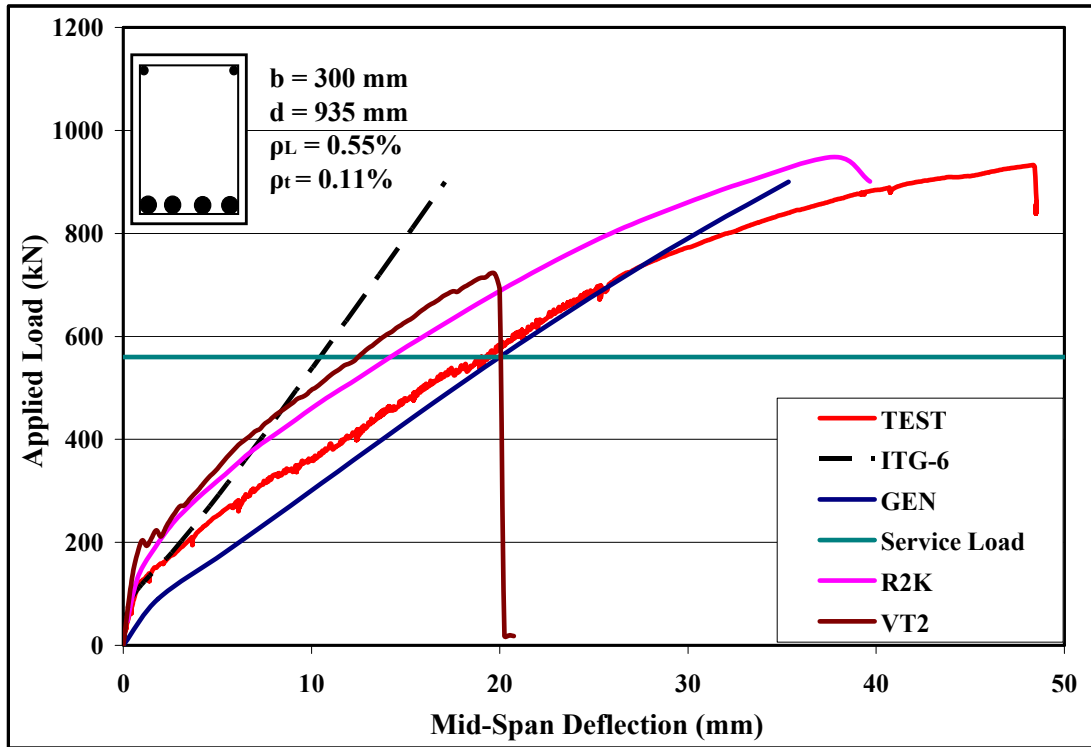


Figure C-7: Load-Deflection Plots of Beam MM1

C.1.8 Deflection of Beam MM2

Table C-29: Modeling Details of Beam MM2

$b_w (mm)$	$h (mm)$	$d (mm)$	$f_c' (MPa)$	$f_{yt} (MPa)$	$f_{yL} (MPa)$	$L (mm)$
300	1000	935	52	830	830	5610
$A_s (mm^2)$	$A_s' (mm^2)$	$A_v (mm^2)$	$S (mm)$	$E_c (MPa)$	$M_{cr} (kN-m)$	$I_{cr} (mm^4)$
1935	258	142	440	30841	151	7443459194
$a_g (mm)$	$f_{cr} (MPa)$	$\epsilon_{cr} (mm/mm)$	$E_s (MPa)$	$a (mm)$	$\Delta L (mm)$	$d_v (mm)$
10	2.38	0.077	200000	2805	401	842

Table C-30: ITG-6 Deflection of Beam MM2

$P (kN)$	$M_a (kN-m)$	$I_{eff} (mm^4)$	$\Delta_{ITG-6} (mm)$
0	0	25044563115	0.00
100	140	25044563115	0.48
200	281	9374115074	2.54
300	421	8222843624	4.35
400	561	7884246313	6.05
500	701	7736837570	7.71
600	842	7659063682	9.34
700	982	7612923908	10.97
800	1122	7583275482	12.58
900	1262	7563082481	14.19
1000	1403	7548704782	15.80

Table C-31: General Deflection of Beam MM2

$\varepsilon_I * 10^3$	θ (deg)	ω (mm)	ν_{ci} (MPa)	f_v (MPa)	f_1 (MPa)	f_2 (MPa)	f_{2max} (MPa)	ε_2 (mm/mm)	ε_x (mm/mm)	ε_t (mm/mm)	f_v (MPa)	f_{sx} (MPa)	γ (mm/mm)
0.000	10.31	0.000	4.33	0	0.000	0.00	52.00	0.0000	0.0000	0.0000	0	0	0.00
0.008	44.98	0.007	4.24	0	0.247	0.25	52.00	0.0000	0.0000	0.0000	0	0	0.02
0.010	44.98	0.009	4.21	0	0.308	0.31	52.00	0.0000	0.0000	0.0000	0	0	0.02
0.100	44.82	0.086	3.42	4	1.945	1.97	52.00	-0.0001	0.0000	0.0000	4	3	0.16
0.500	43.00	0.432	1.86	48	1.586	1.93	52.00	-0.0001	0.0002	0.0002	48	40	0.56
1.000	41.14	0.865	1.18	107	1.394	2.09	52.00	-0.0001	0.0004	0.0005	107	79	1.06
2.000	38.62	1.735	0.68	237	1.184	2.51	45.61	-0.0001	0.0007	0.0012	237	144	2.04
4.000	34.85	3.500	0.37	529	0.580	2.94	35.14	-0.0001	0.0012	0.0026	529	242	3.89
6.000	32.68	5.287	0.25	830	0.161	3.45	28.57	-0.0002	0.0016	0.0042	830	325	5.65
8.000	30.40	7.111	0.19	830	0.111	3.81	24.07	-0.0003	0.0018	0.0059	830	379	7.23
10.000	28.87	8.950	0.15	830	0.084	4.10	20.80	-0.0004	0.0021	0.0076	830	423	8.75
15.000	26.47	13.592	0.10	830	0.050	4.69	15.52	-0.0006	0.0025	0.0119	830	508	12.42
20.000	24.90	18.288	0.08	830	0.035	5.20	12.38	-0.0008	0.0029	0.0163	830	578	15.89
25.000	23.83	23.013	0.06	830	0.027	5.60	10.30	-0.0011	0.0032	0.0207	830	634	19.30
30.000	23.07	27.753	0.05	830	0.021	5.93	8.81	-0.0014	0.0034	0.0252	830	678	22.68
35.000	22.55	32.494	0.04	830	0.018	6.17	7.70	-0.0019	0.0036	0.0296	830	712	26.12
39.000	22.29	36.273	0.04	830	0.016	6.29	7.00	-0.0023	0.0036	0.0331	830	729	29.00

Table C-32: General Deflection of Beam MM2

P (kN)	$\varepsilon_x * 10^{03}$	γ (mm/mm)	Δ_{st} (mm)	Δ_{ITG-6} (mm)	Δ_{GEN} (mm)
0	0.00	0.00	0.00	0.00	0.00
100	0.28	0.86	1.34	0.48	1.82
200	0.56	1.70	2.68	2.54	5.23
300	0.84	2.59	4.03	4.35	8.38
400	1.12	3.58	5.42	6.05	11.47
500	1.40	4.73	6.91	7.71	14.62
600	1.68	6.10	8.53	9.34	17.88
700	1.96	7.76	10.34	10.97	21.30
800	2.24	9.76	12.37	12.58	24.95
900	2.52	12.17	14.66	14.19	28.85
1000	2.80	15.04	17.27	15.80	33.07

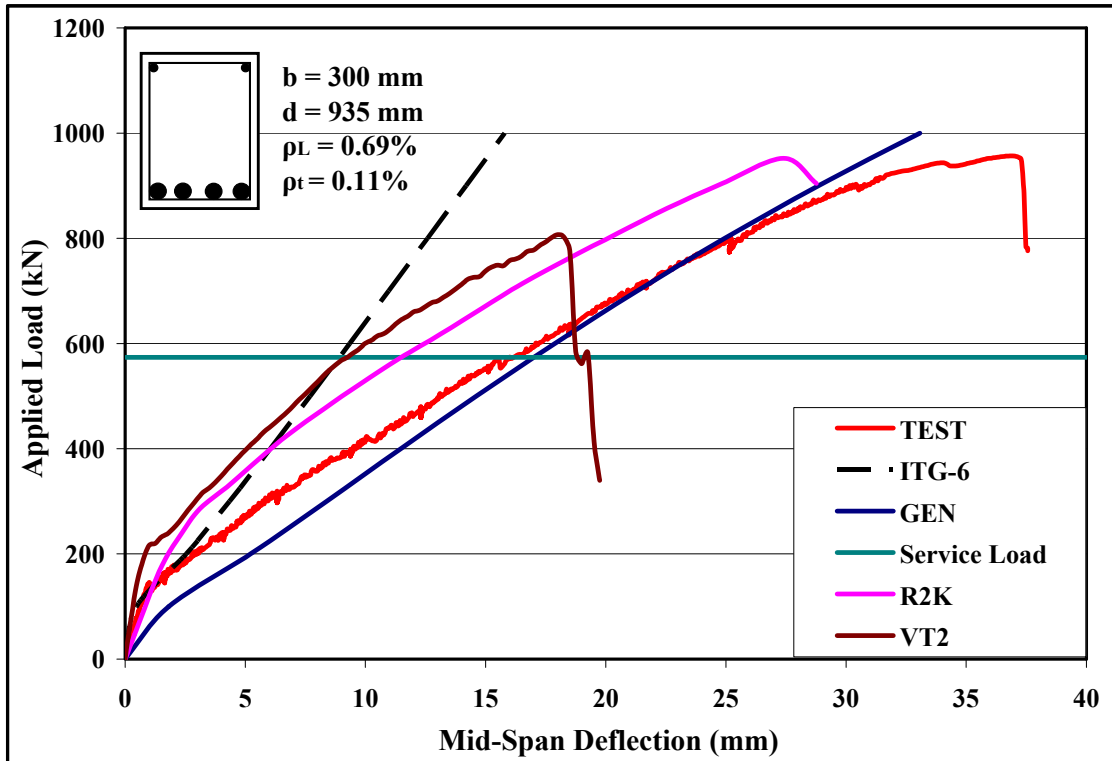


Figure C-8: Load-Deflection Plots of Beam MM2

C.1.9 Deflection of Beam MM3

Table C-33: Modeling Details of Beam MM3

$b_w (mm)$	$h (mm)$	$d (mm)$	$f_c' (MPa)$	$f_{yt} (MPa)$	$f_{yL} (MPa)$	$L (mm)$
300	1000	885	48	430	830	5310
$A_s (mm^2)$	$A_s' (mm^2)$	$A_v (mm^2)$	$S (mm)$	$E_c (MPa)$	$M_{cr} (kN-m)$	$I_{cr} (mm^4)$
4257	258	142	440	29902	145	12361976632
$a_g (mm)$	$f_{cr} (MPa)$	$\varepsilon_{cr} (mm/mm)$	$E_s (MPa)$	$a (mm)$	$\Delta L (mm)$	$d_v (mm)$
10	2.29	0.076	200000	2655	379	797

Table C-34: ITG-6 Deflection of Beam MM3

$P (kN)$	$M_a (kN-m)$	$I_{eff} (mm^4)$	$\Delta_{ITG-6} (mm)$
0	0	25100979561	0.00
140	186	17913617556	0.82
280	372	13486984467	2.17
420	558	12898056335	3.40
560	743	12703988479	4.60
700	929	12616141612	5.79
840	1115	12568933689	6.97
980	1301	12540640523	8.15
1120	1487	12522345787	9.33
1260	1673	12509834037	10.51
1400	1859	12500899909	11.68

Table C-35: General Deflection of Beam MM3

$\varepsilon_I * 10^3$	θ (deg)	ω (mm)	ν_{ci} (MPa)	f_v (MPa)	f_I (MPa)	f_2 (MPa)	f_{2max} (MPa)	ε_2 (mm/mm)	ε_x (mm/mm)	ε_t (mm/mm)	f_v (MPa)	f_{sx} (MPa)	γ (mm/mm)
0.000	10.31	0.000	4.16	0	0.000	0.00	48.00	0.0000	0.0000	0.0000	0	0	0.00
0.008	44.98	0.006	4.08	0	0.239	0.24	48.00	0.0000	0.0000	0.0000	0	0	0.02
0.010	44.98	0.008	4.06	0	0.299	0.30	48.00	0.0000	0.0000	0.0000	0	0	0.02
0.100	44.61	0.080	3.34	4	1.868	1.93	48.00	-0.0001	0.0000	0.0000	4	3	0.17
0.500	40.98	0.400	1.86	51	1.524	2.14	48.00	-0.0001	0.0002	0.0003	51	35	0.57
1.000	38.00	0.807	1.19	118	1.339	2.53	48.00	-0.0001	0.0003	0.0006	118	65	1.05
2.000	34.48	1.637	0.69	264	1.082	3.18	42.11	-0.0001	0.0006	0.0013	264	111	1.98
4.000	30.16	3.347	0.37	588	0.474	3.91	32.43	-0.0002	0.0009	0.0029	588	172	3.65
6.000	27.87	5.093	0.25	830	0.132	4.55	26.37	-0.0003	0.0011	0.0046	830	217	5.20
8.000	26.07	6.876	0.19	830	0.092	5.00	22.22	-0.0004	0.0012	0.0064	830	247	6.62
10.000	24.82	8.676	0.15	830	0.069	5.39	19.20	-0.0005	0.0014	0.0082	830	272	7.99
12.000	23.89	10.488	0.12	830	0.055	5.72	16.90	-0.0006	0.0015	0.0099	830	294	9.33
16.000	22.54	14.141	0.09	830	0.039	6.30	13.64	-0.0009	0.0016	0.0135	830	330	11.94
20.000	21.69	17.809	0.07	830	0.030	6.72	11.43	-0.0012	0.0017	0.0171	830	357	14.53
25.000	21.04	22.391	0.06	830	0.023	7.08	9.50	-0.0016	0.0018	0.0216	830	379	17.82
30.000	20.75	26.942	0.05	830	0.019	7.24	8.14	-0.0021	0.0019	0.0260	830	389	21.31
32.000	20.74	28.741	0.05	830	0.018	7.24	7.69	-0.0024	0.0019	0.0277	830	389	22.81

Table C-36: General Deflection of Beam MM3

P (kN)	$\varepsilon_x * 10^3$	γ (mm/mm)	Δ_{st} (mm)	Δ_{ITG-6} (mm)	Δ_{GEN} (mm)
0	0.00	0.00	0.00	0.00	0.00
140	0.18	0.76	1.16	0.82	1.97
280	0.36	1.40	2.21	2.17	4.37
420	0.53	1.99	3.15	3.40	6.55
560	0.71	2.68	4.08	4.60	8.68
700	0.89	3.59	5.07	5.79	10.86
840	1.07	4.84	6.22	6.97	13.20
980	1.25	6.56	7.61	8.15	15.77
1120	1.43	8.87	9.33	9.33	18.66
1260	1.60	11.91	11.46	10.51	21.97
1400	1.78	15.80	14.09	11.68	25.78

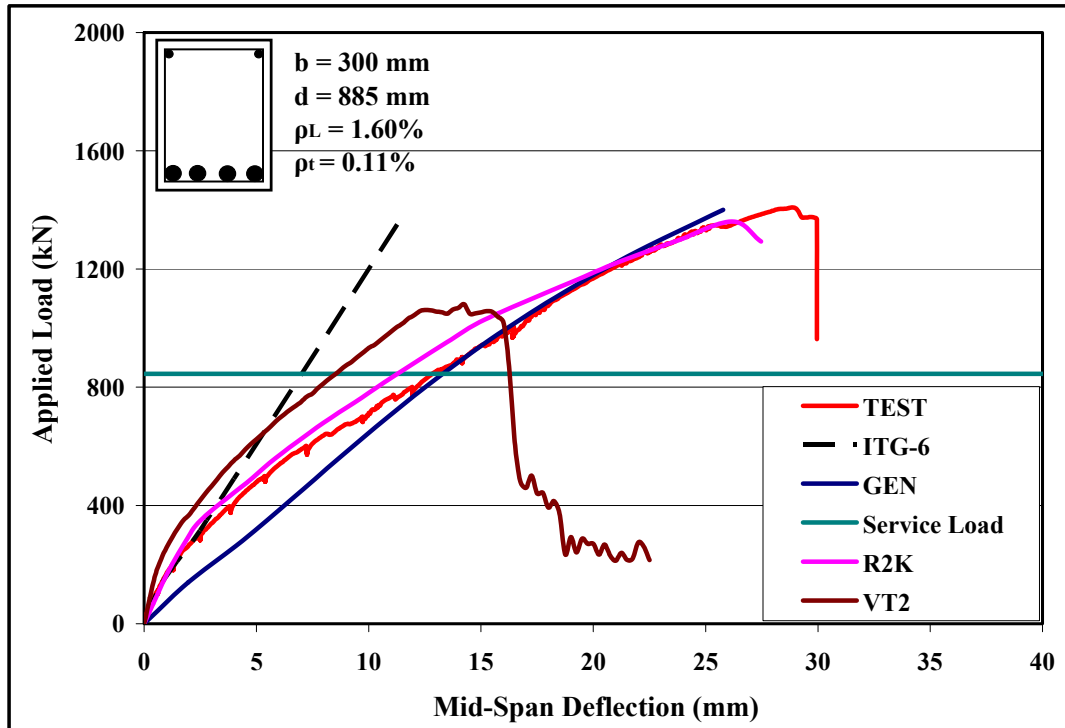


Figure C-9: Load-Deflection Plots of Beam MM3

C.1.10 Deflection of Beam MM4

Table C-37: Modeling Details of Beam MM4

$b_w (mm)$	$h (mm)$	$d (mm)$	$f_c' (MPa)$	$f_{yt} (MPa)$	$f_{yL} (MPa)$	$L (mm)$
300	1000	885	48	830	830	5310
$A_s (mm^2)$	$A_s' (mm^2)$	$A_v (mm^2)$	$S (mm)$	$E_c (MPa)$	$M_{cr} (kN-m)$	$I_{cr} (mm^4)$
4257	258	142	220	29902	145	12361976632
$a_g (mm)$	$f_{cr} (MPa)$	$\varepsilon_{cr} (mm/mm)$	$E_s (MPa)$	$a (mm)$	$\Delta L (mm)$	$d_v (mm)$
10	2.29	0.076	200000	2655	379	797

Table C-38: ITG-6 Deflection of Beam MM4

$P (kN)$	$M_a (kN-m)$	$I_{eff} (mm^4)$	$\Delta_{ITG-6} (mm)$
0	0	25099827947	0.00
182	242	15187693012	1.25
364	484	13046568739	2.91
547	726	12715044689	4.48
729	967	12602986814	6.03
911	1209	12551791234	7.57
1093	1451	12524156626	9.11
1275	1693	12507553028	10.64
1458	1935	12496800381	12.17
1640	2177	12489439164	13.70
1822	2419	12484179090	15.22

Table C-39: General Deflection of Beam MM4

$\varepsilon_I * 10^3$	θ (deg)	ω (mm)	ν_{ci} (MPa)	f_v (MPa)	f_I (MPa)	f_2 (MPa)	f_{2max} (MPa)	ε_2 (mm/mm)	ε_x (mm/mm)	ε_t (mm/mm)	f_v (MPa)	f_{sx} (MPa)	γ (mm/mm)
0.000	10.31	0.000	4.24	0	0.000	0.00	50.00	0.0000	0.0000	0.0000	0	0	0.00
0.008	44.98	0.005	4.18	0	0.311	0.31	50.00	0.0000	0.0000	0.0000	0	0	0.02
0.010	44.98	0.006	4.17	0	0.389	0.39	50.00	0.0000	0.0000	0.0000	0	0	0.02
0.100	44.52	0.060	3.58	5	1.907	1.99	50.00	-0.0001	0.0000	0.0000	5	5	0.15
0.500	41.30	0.299	2.21	51	1.556	2.27	50.00	-0.0001	0.0002	0.0003	51	37	0.55
1.000	38.78	0.595	1.50	116	1.367	2.75	50.00	-0.0001	0.0003	0.0006	116	70	1.05
2.000	36.17	1.187	0.91	253	1.167	3.74	43.86	-0.0001	0.0006	0.0013	253	125	2.01
4.000	34.20	2.372	0.51	533	0.967	5.72	33.78	-0.0002	0.0011	0.0027	533	222	3.93
6.000	32.33	3.559	0.35	830	0.225	6.80	27.47	-0.0003	0.0015	0.0042	830	295	5.73
8.000	30.18	4.755	0.27	830	0.158	7.53	23.15	-0.0005	0.0017	0.0059	830	343	7.35
10.000	28.73	5.956	0.22	830	0.120	8.12	20.00	-0.0006	0.0019	0.0076	830	383	8.93
12.000	27.69	7.161	0.18	830	0.097	8.62	17.61	-0.0007	0.0020	0.0092	830	414	10.48
14.000	26.90	8.368	0.16	830	0.081	9.03	15.72	-0.0009	0.0022	0.0109	830	441	12.02
16.000	26.30	9.577	0.14	830	0.069	9.37	14.20	-0.0011	0.0023	0.0126	830	462	13.57
18.000	25.84	10.786	0.12	830	0.060	9.65	12.95	-0.0013	0.0024	0.0143	830	480	15.12
21.000	25.34	12.600	0.11	830	0.051	9.97	11.44	-0.0016	0.0025	0.0168	830	500	17.52
24.000	25.18	14.406	0.09	830	0.044	10.06	10.25	-0.0022	0.0025	0.0192	830	506	20.20

Table C-40: General Deflection of Beam MM4

P (kN)	$\epsilon_x * 10^{03}$	γ (mm/mm)	Δ_{st} (mm)	Δ_{ITG-6} (mm)	Δ_{GEN} (mm)
0	0.00	0.00	0.01	0.00	0.01
182	0.23	0.85	1.14	1.25	2.39
364	0.46	1.58	2.16	2.91	5.07
547	0.70	2.32	3.12	4.48	7.60
729	0.93	3.16	4.09	6.03	10.13
911	1.16	4.22	5.14	7.57	12.71
1093	1.39	5.60	6.33	9.11	15.44
1275	1.62	7.40	7.73	10.64	18.37
1458	1.85	9.74	9.40	12.17	21.57
1640	2.09	12.72	11.40	13.70	25.10
1822	2.32	16.44	13.81	15.22	29.03

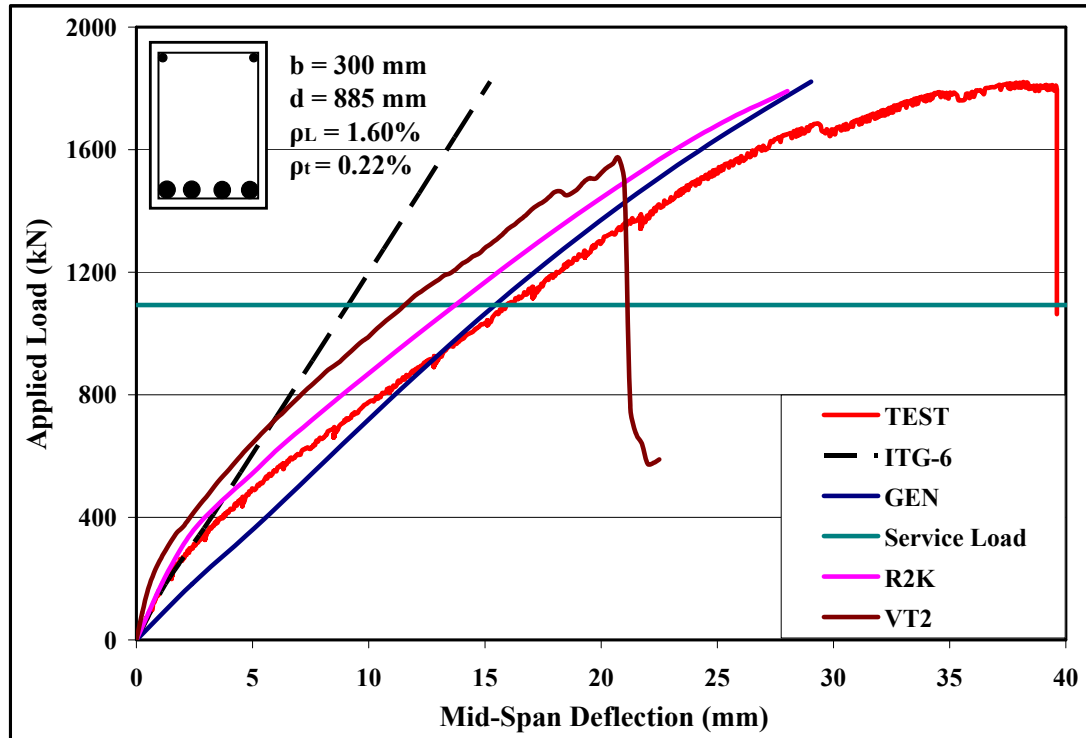


Figure C-10: Load-Deflection Plots of Beam MM4

C.2 Load-Deflection Response for Prior Tested Beams

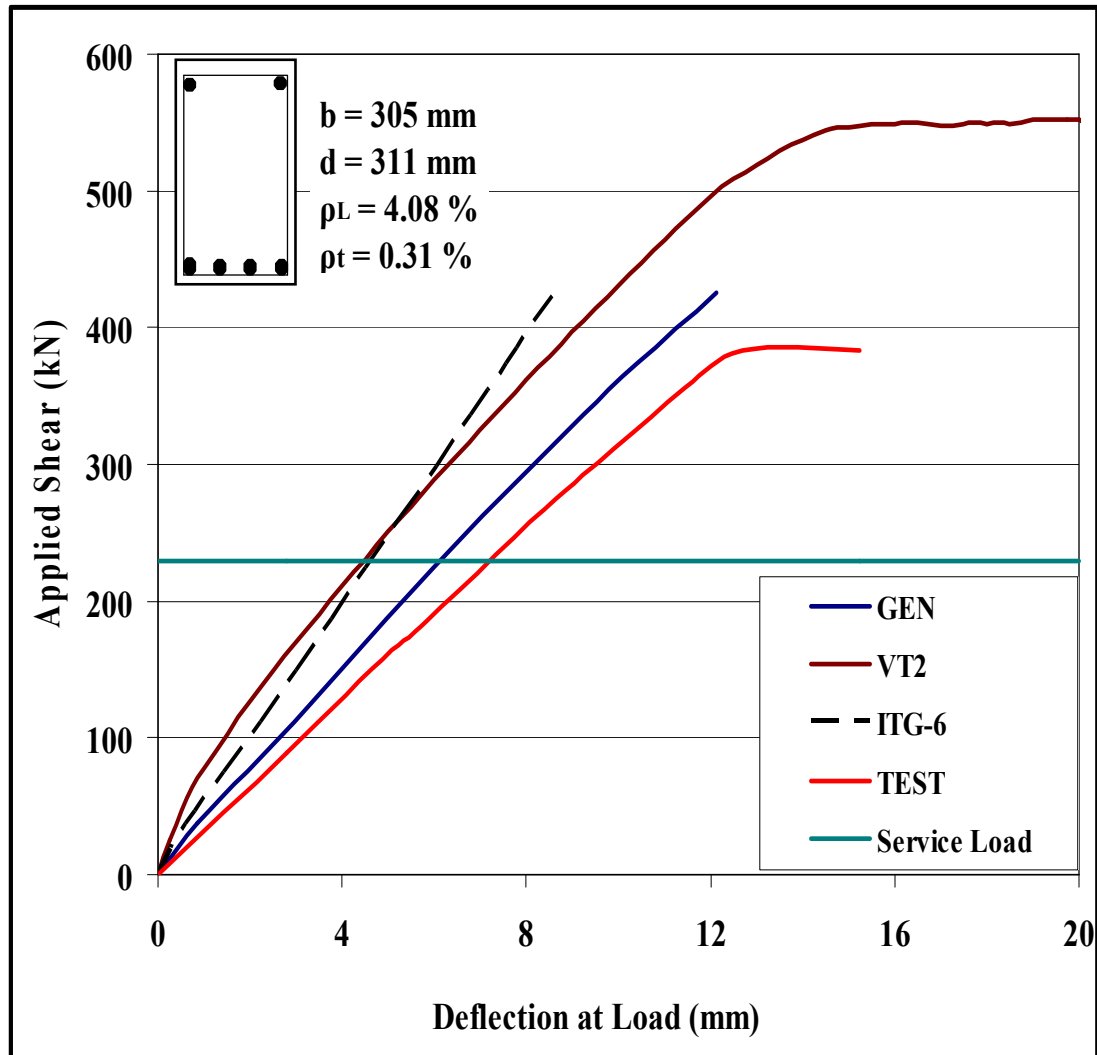


Figure C-11: Load-Deflection Plots of Beam CM6

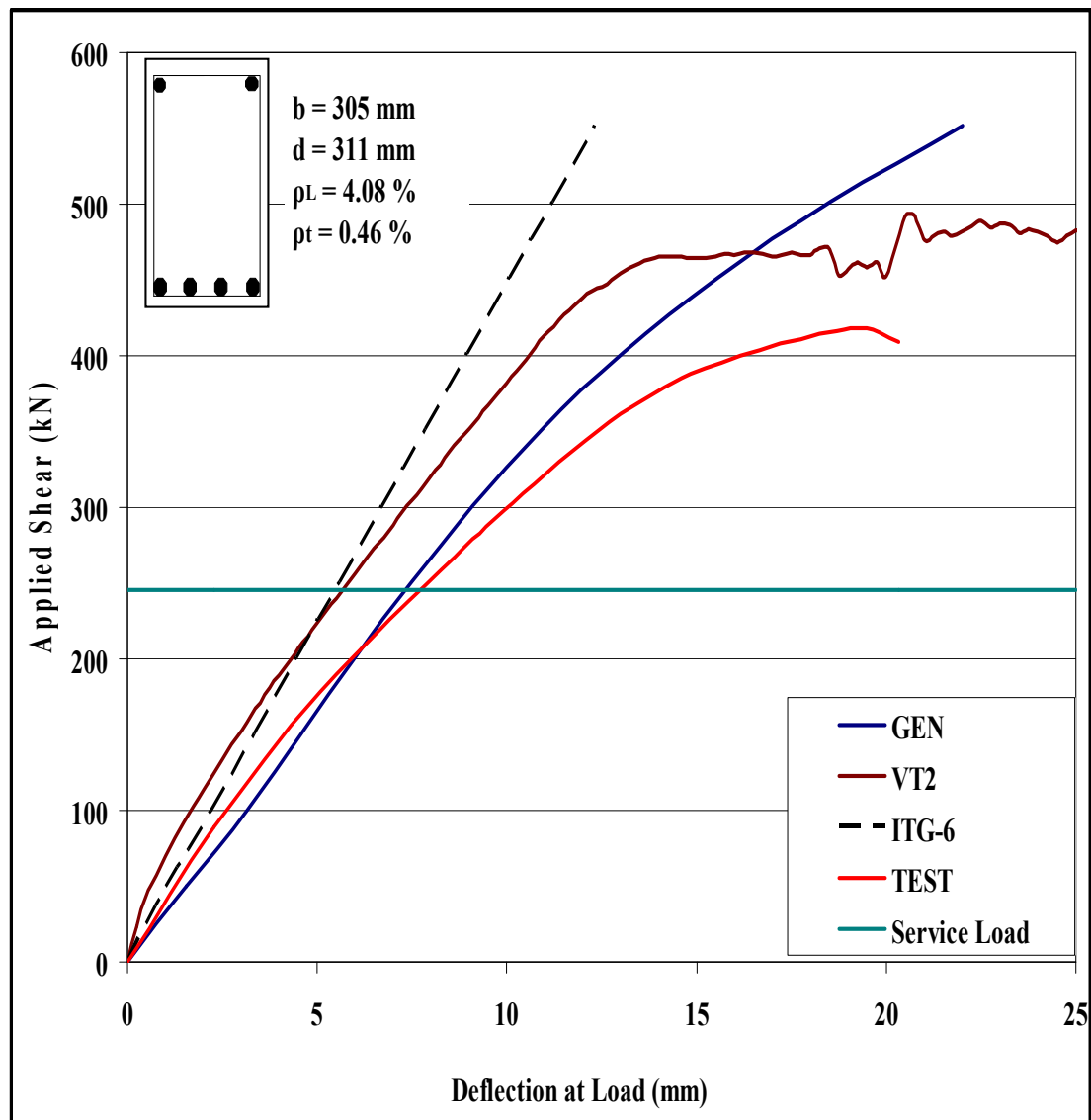


Figure C-12: Load-Deflection Plots of Beam CM4

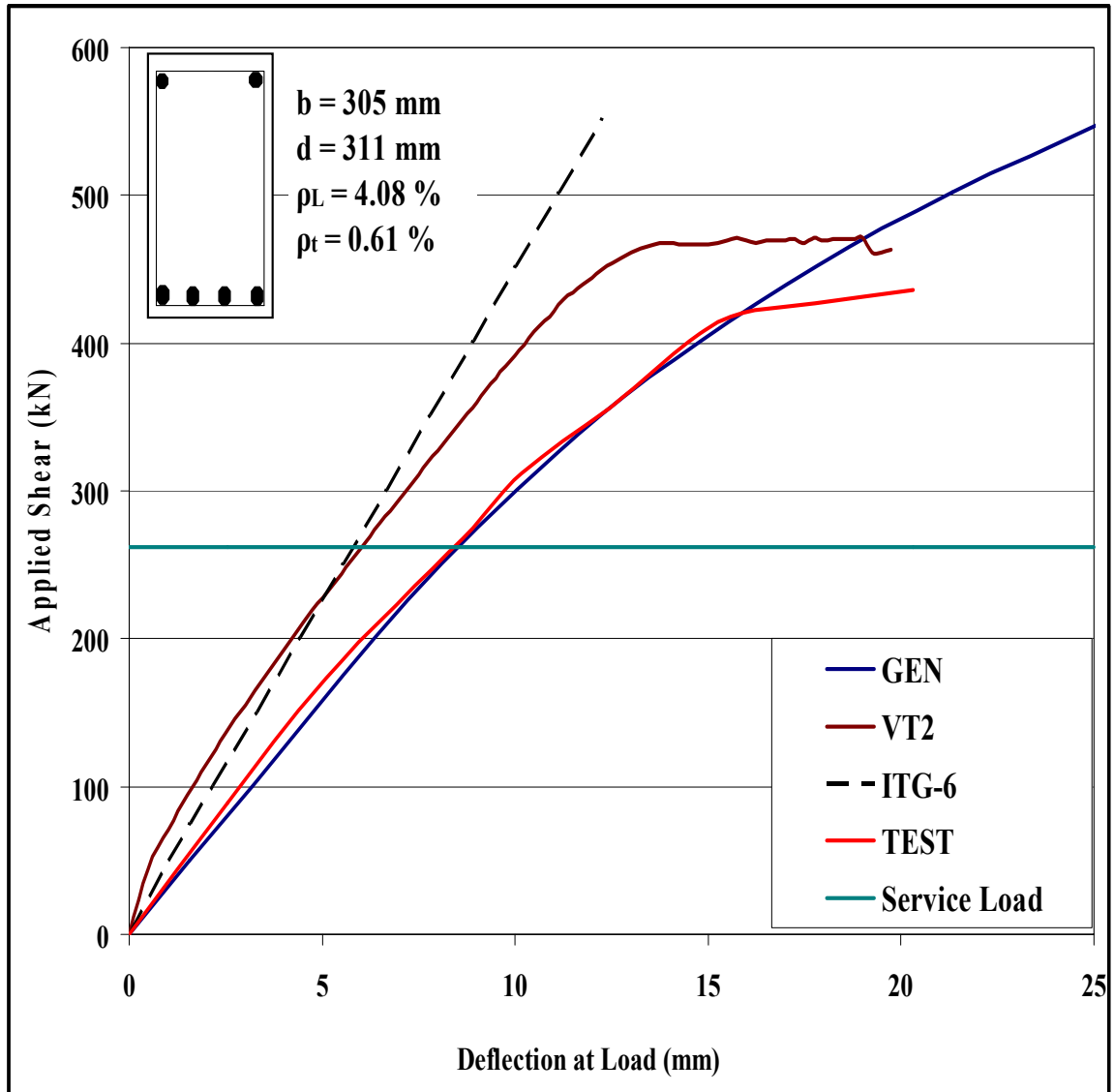


Figure C-13: Load-Deflection Plots of Beam CM3

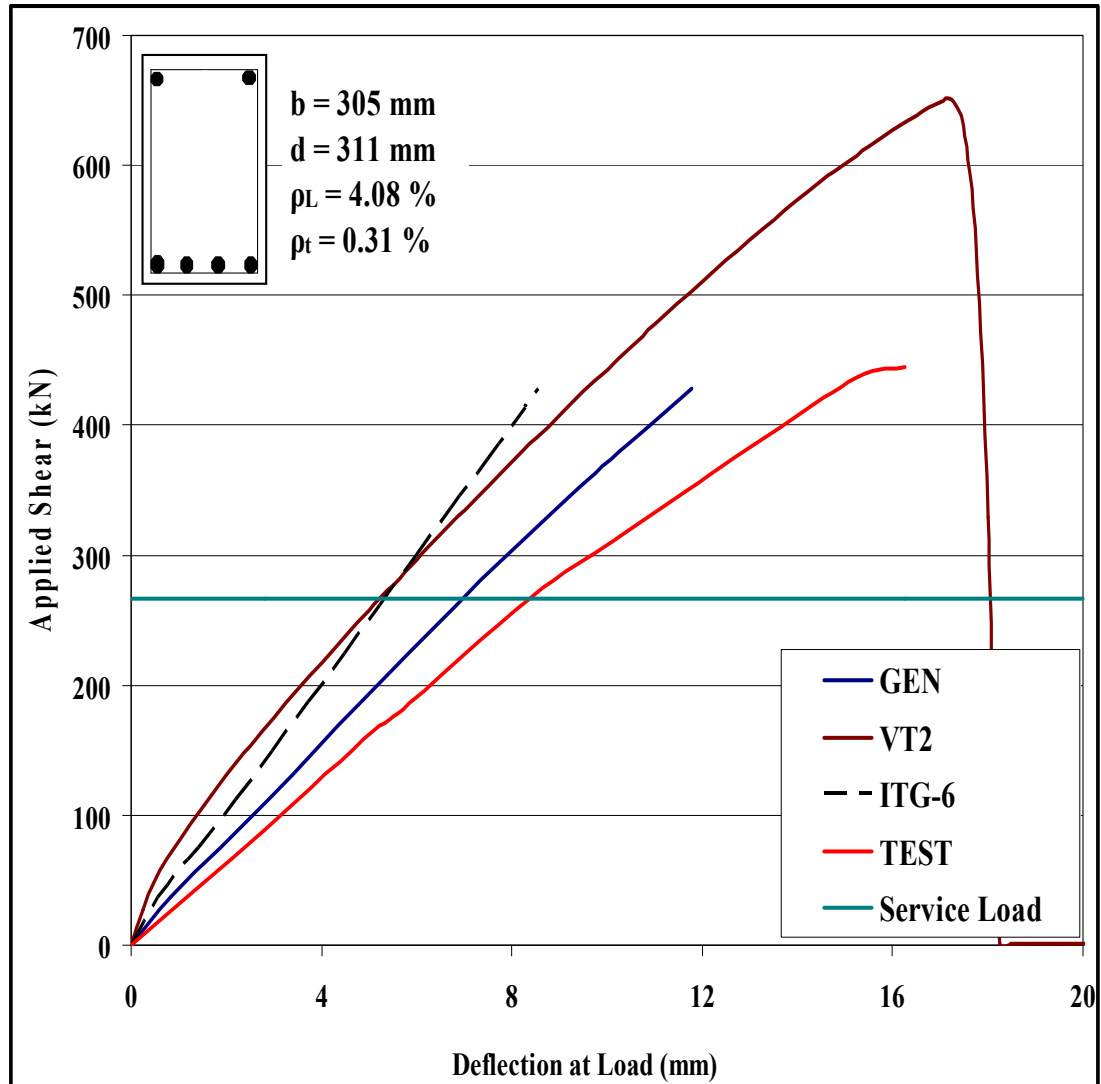


Figure C-14: Load-Deflection Plots of Beam MM6

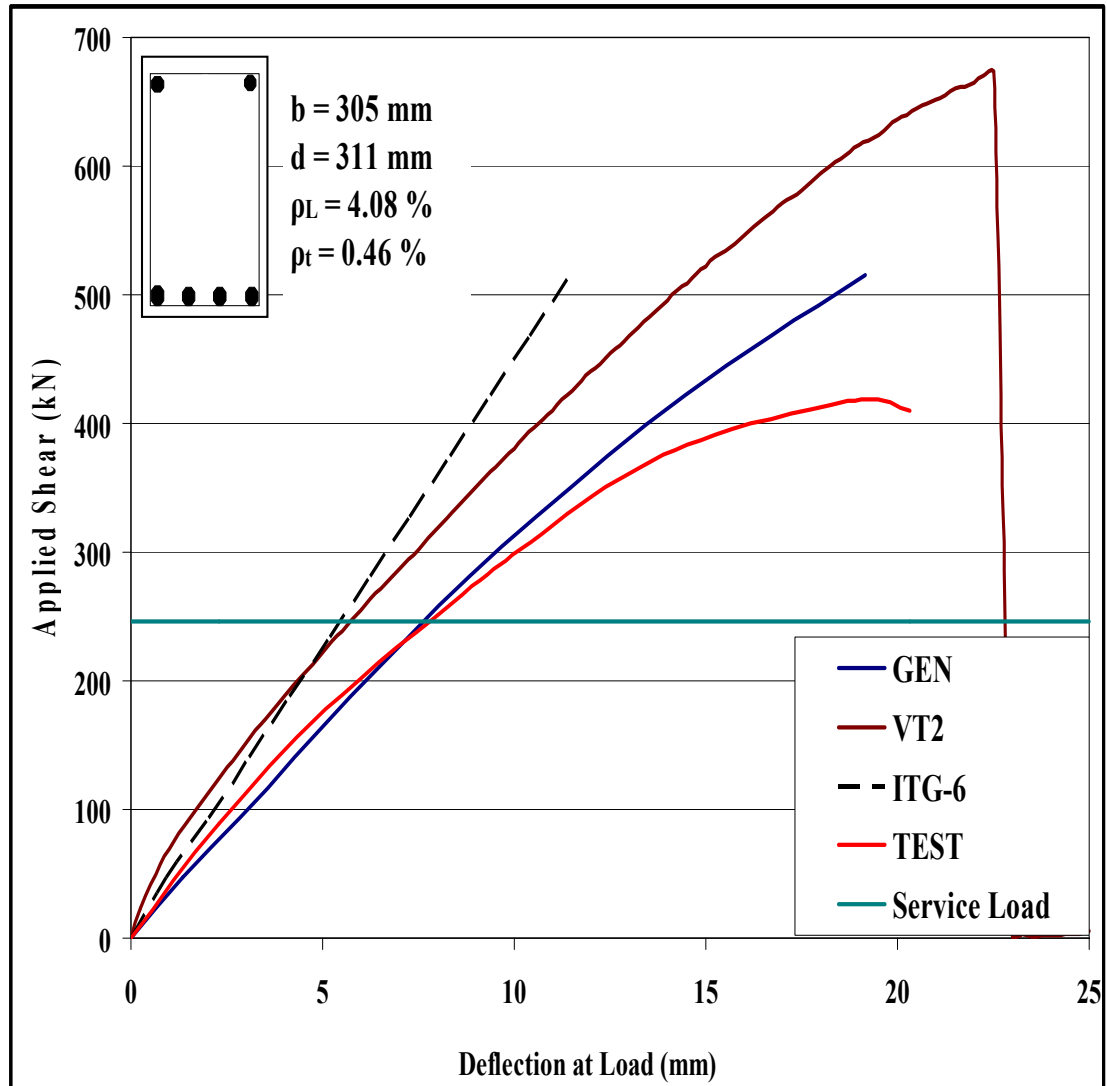


Figure C-15: Load-Deflection Plots of Beam MM4

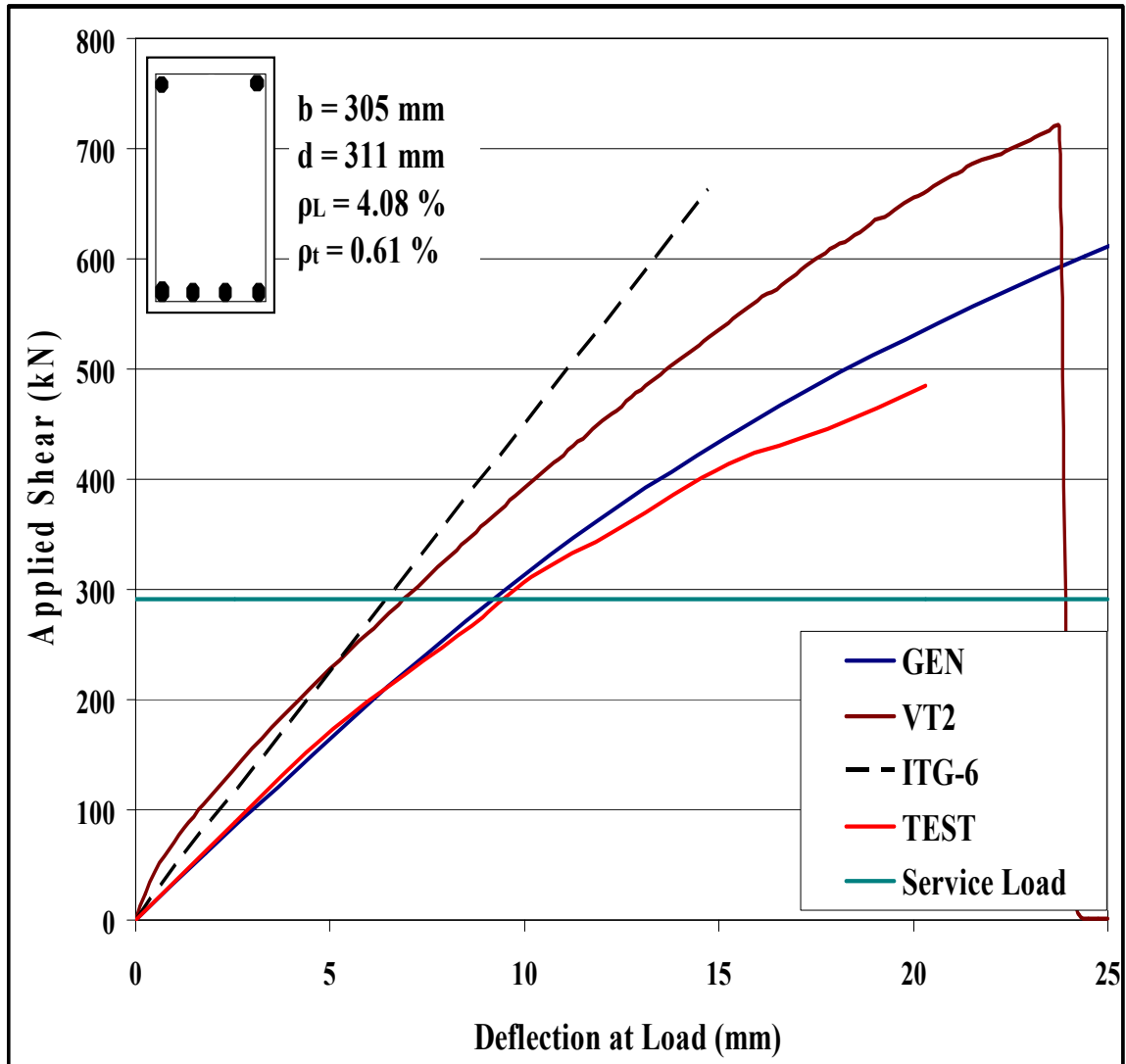


Figure C-16: Load-Deflection Plots of Beam MM3

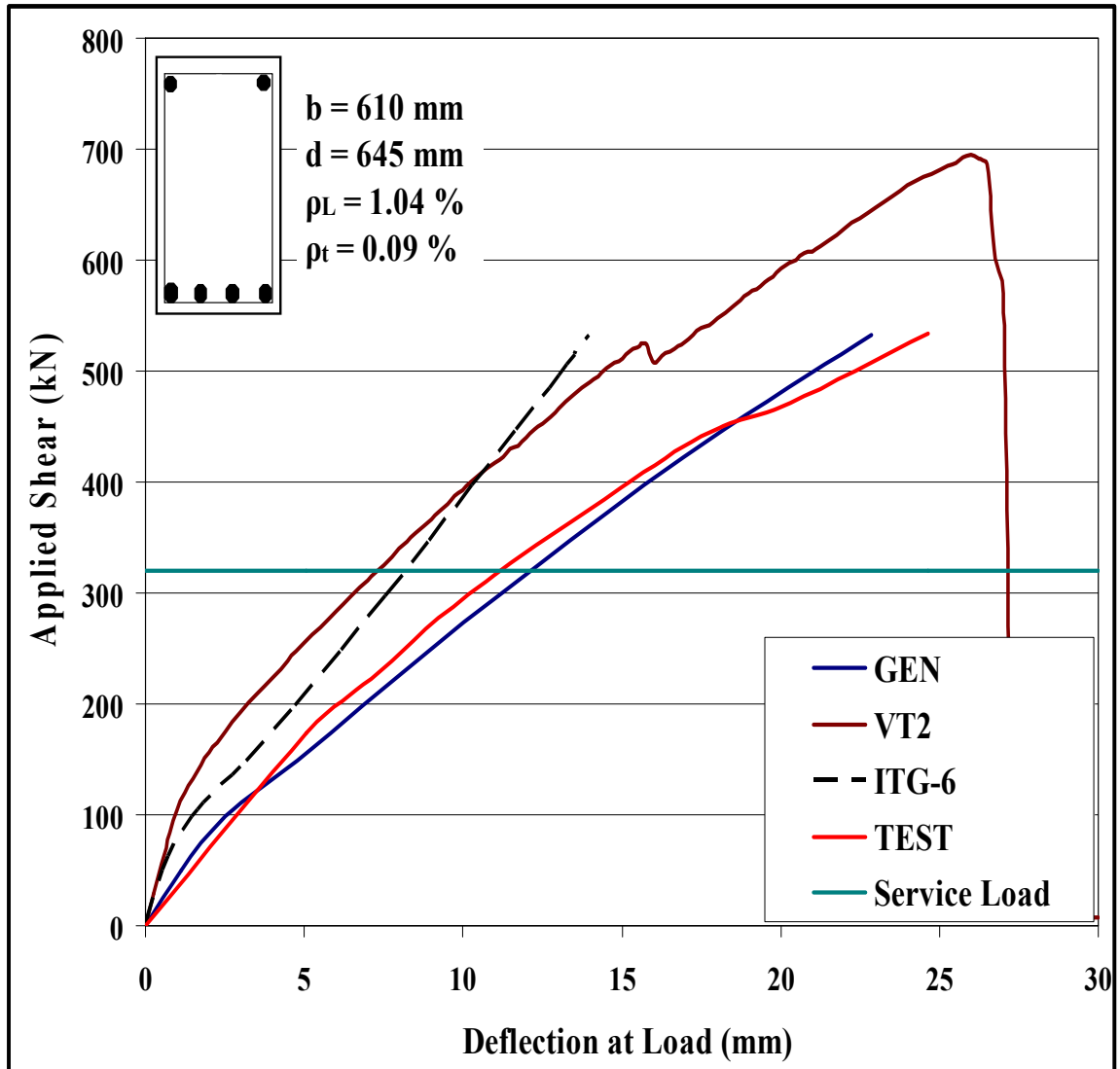


Figure C-17: Load-Deflection Plots of Beam G1-M80

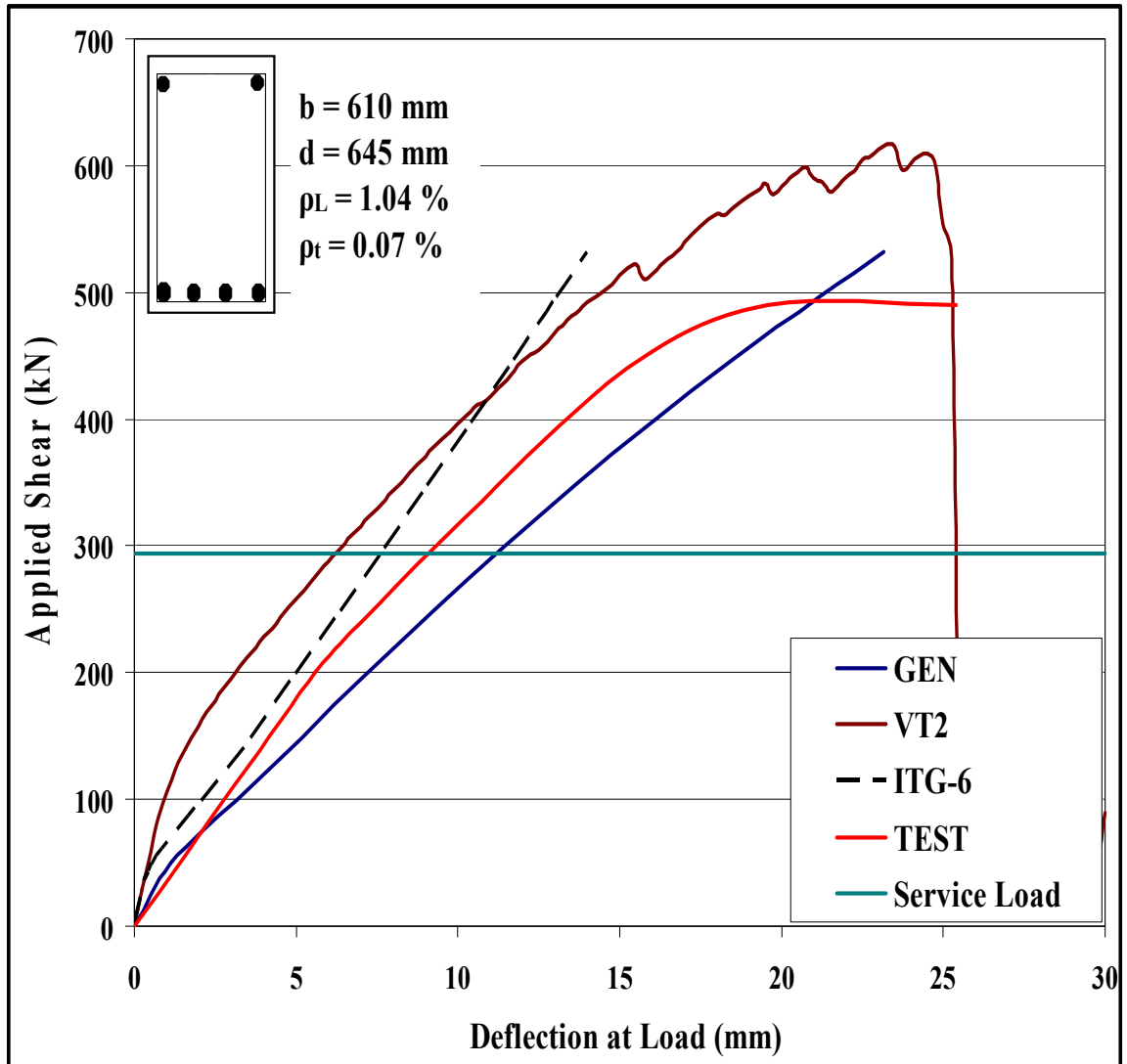


Figure C-18: Load-Deflection Plots of Beam G1-M100

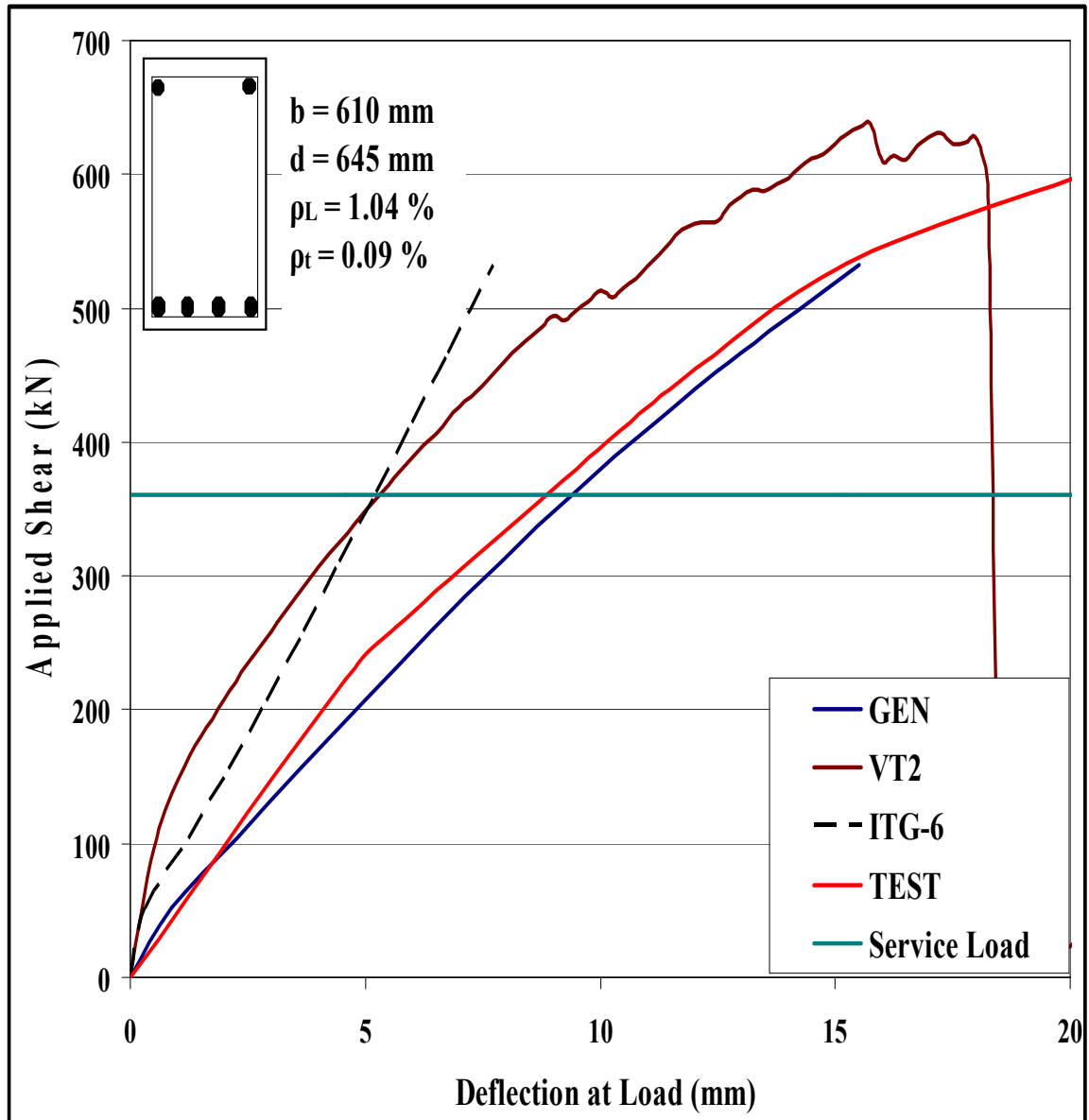


Figure C-19: Load-Deflection Plots of Beam G2-M80

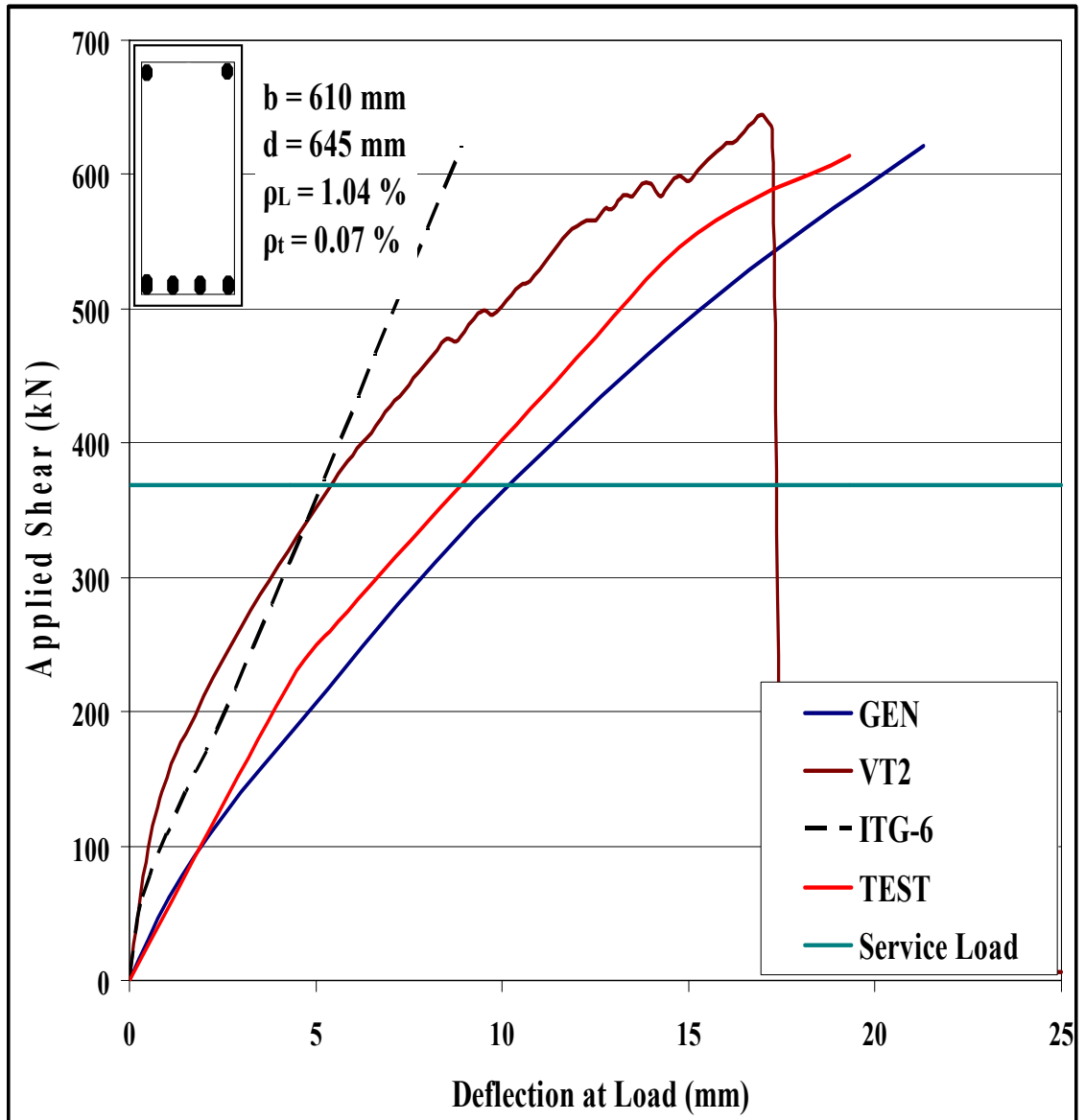


Figure C-20: Load-Deflection Plots of Beam G2-M100

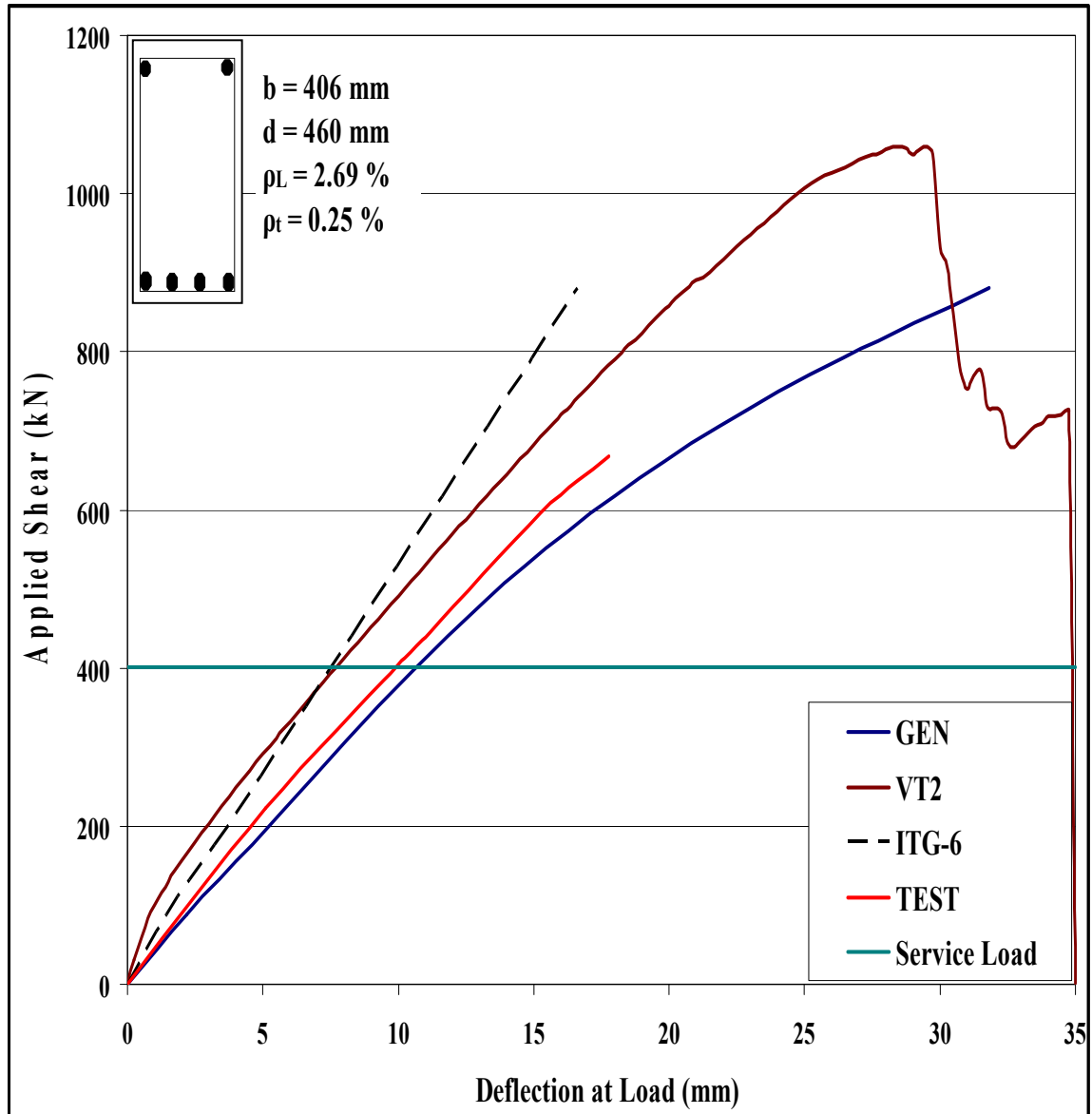


Figure C-21: Load-Deflection Plots of Beam G3-M80

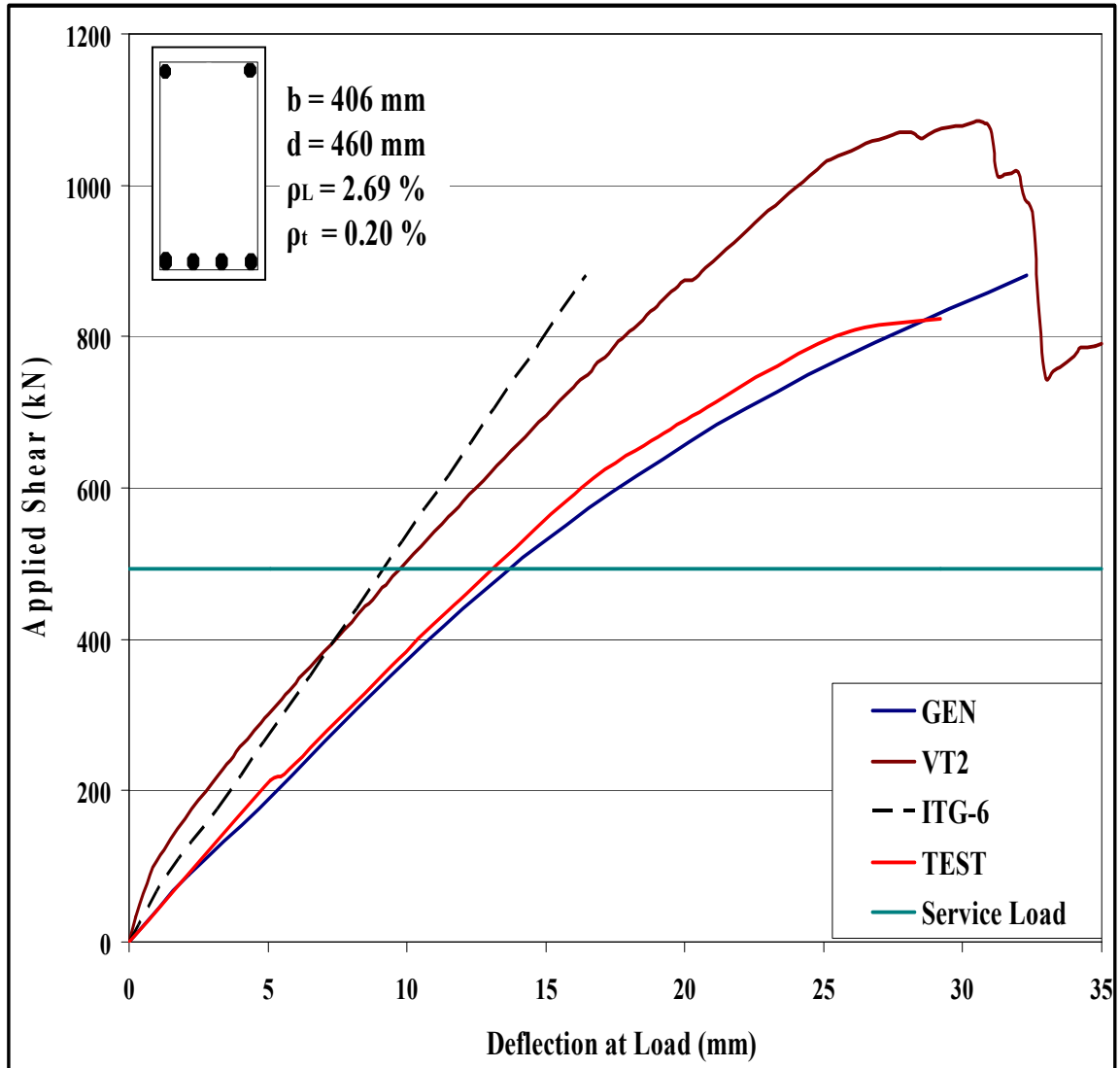


Figure C-22: Load-Deflection Plots of Beam G3-M100

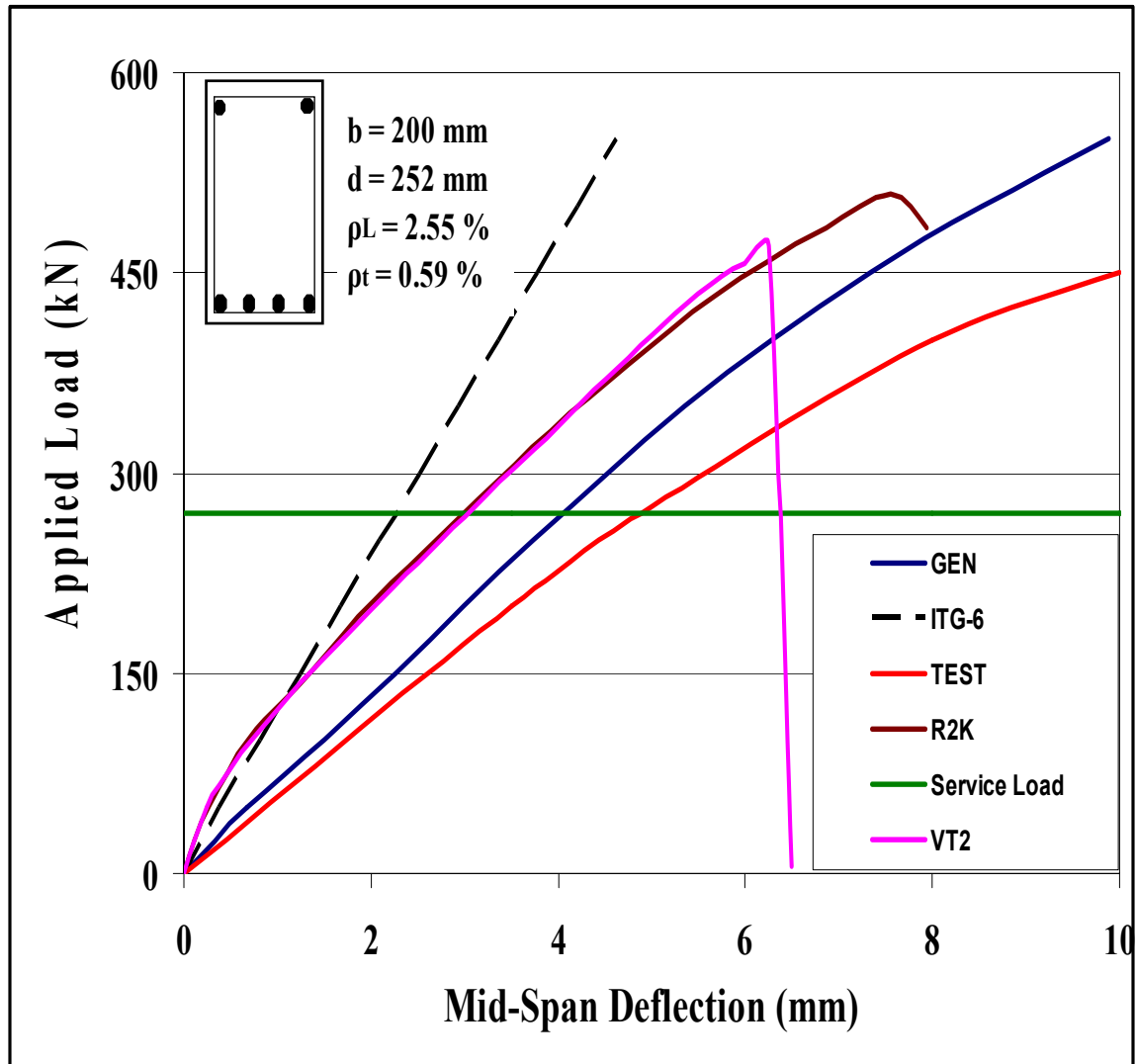


Figure C-23: Load-Deflection Plots of Beam F40-1

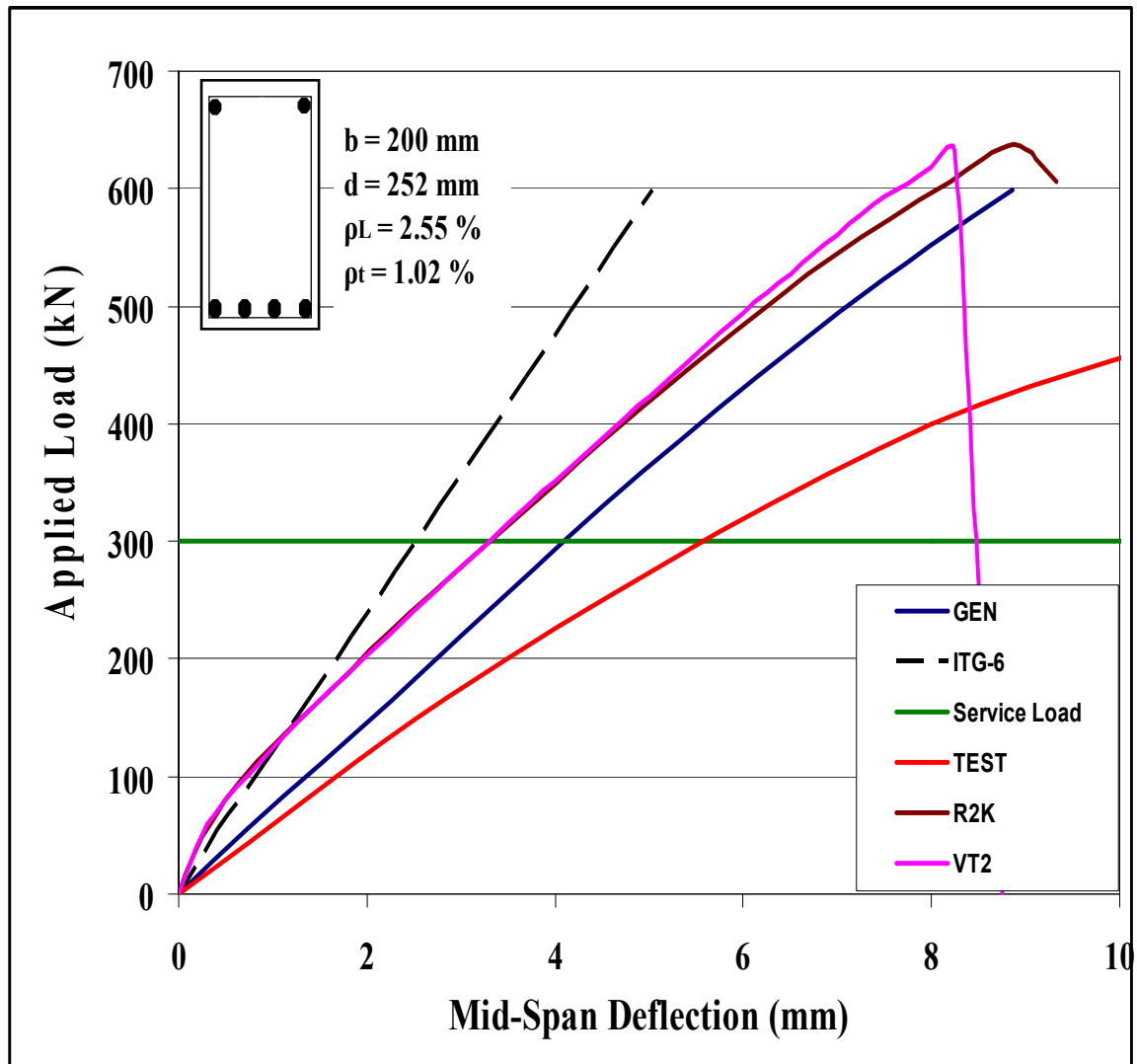


Figure C-24: Load-Deflection Plots of Beam F40-3

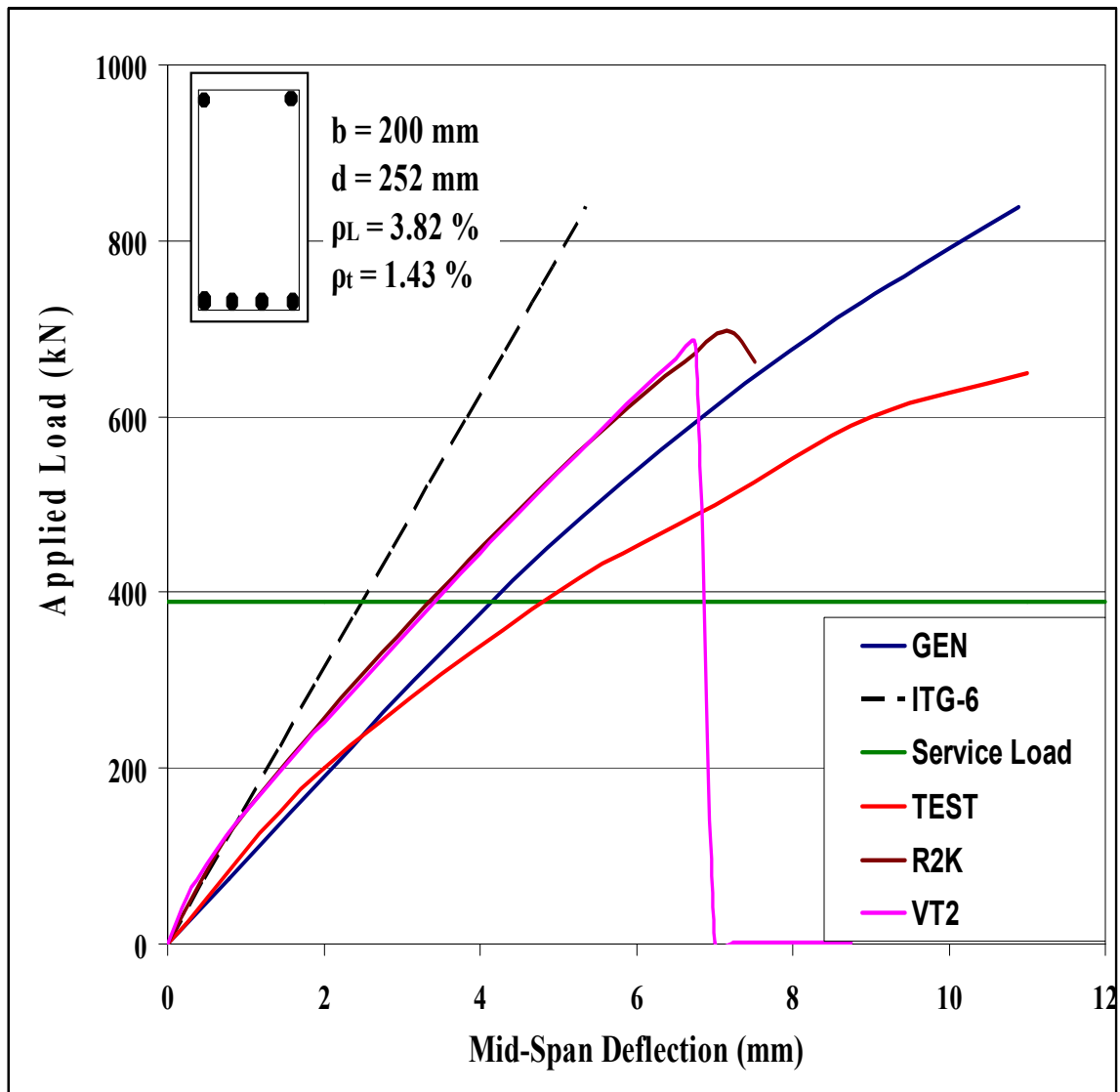


Figure C-25: Load-Deflection Plots of Beam F40-5

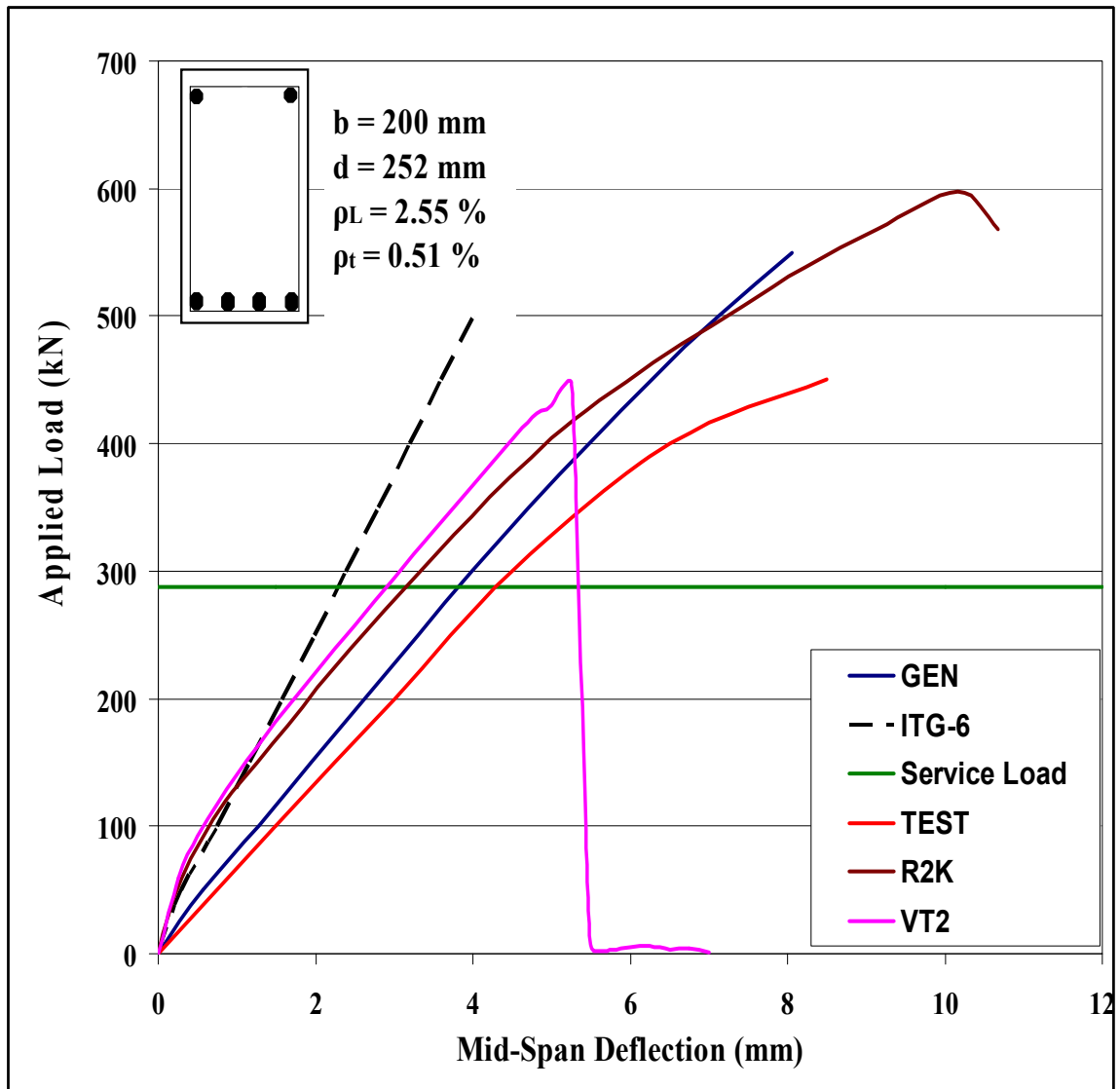


Figure C-26: Load-Deflection Plots of Beam F60-1

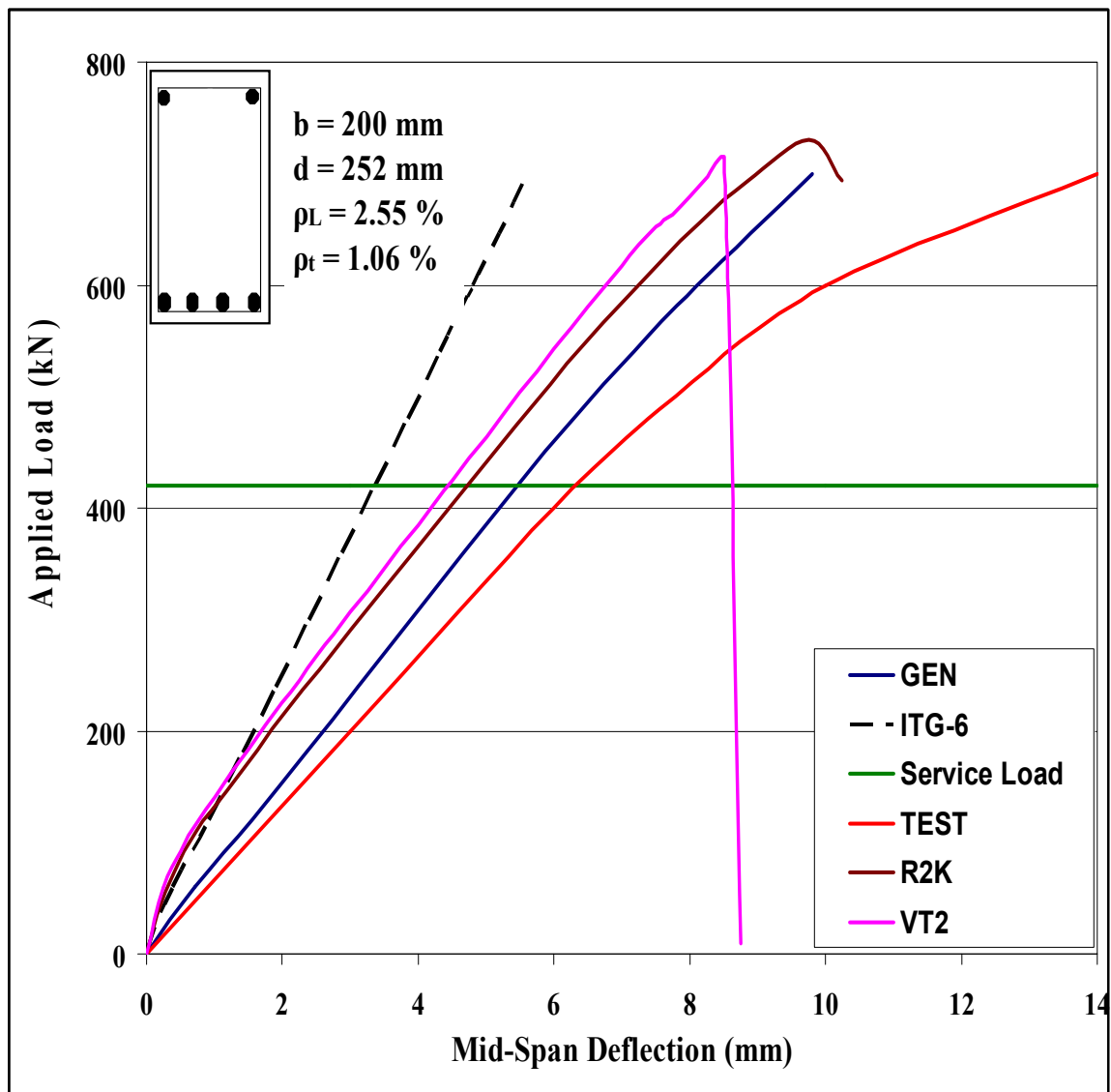


Figure C-27: Load-Deflection Plots of Beam F60-2

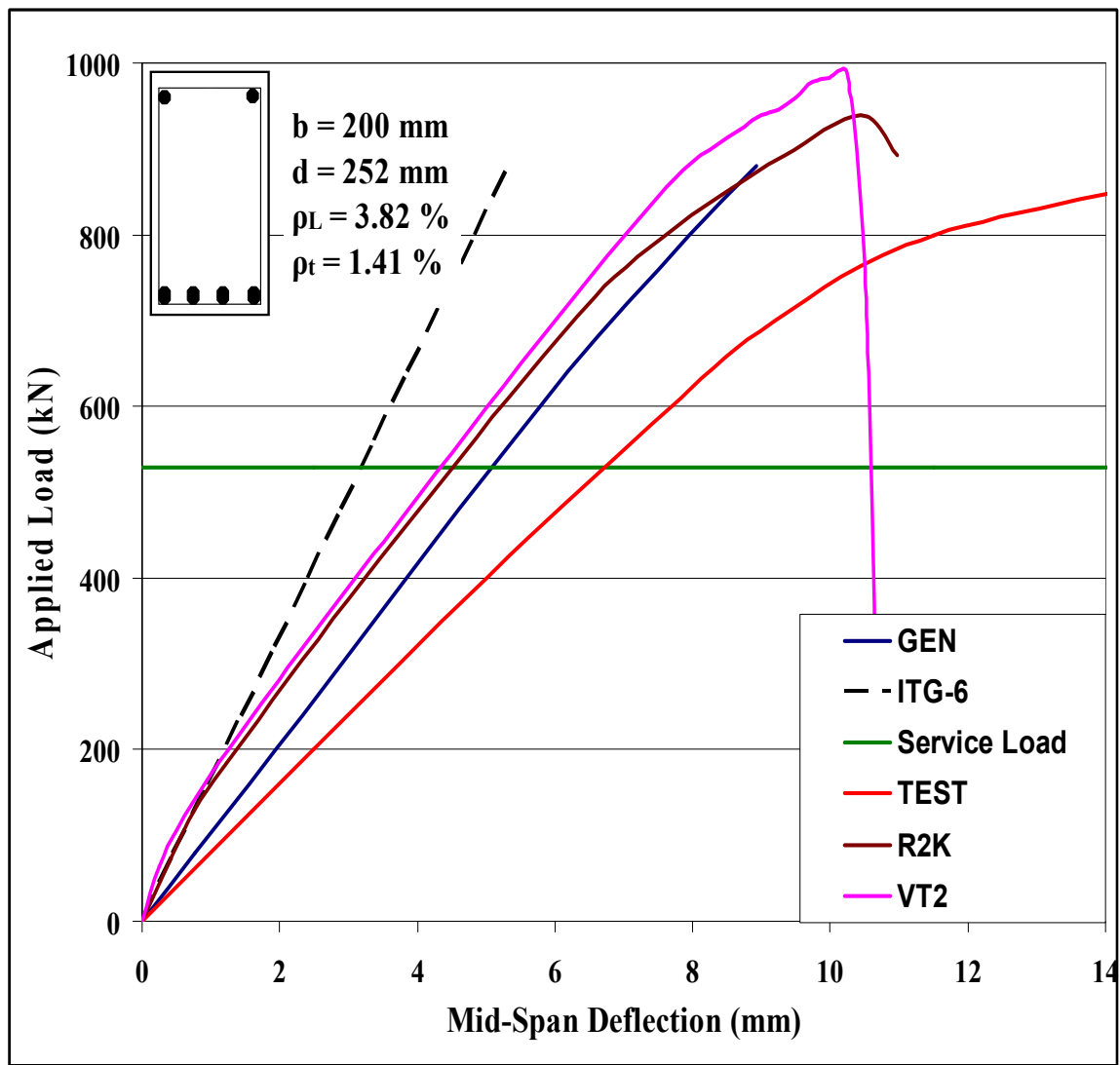


Figure C-28: Load-Deflection Plots of Beam F60-3

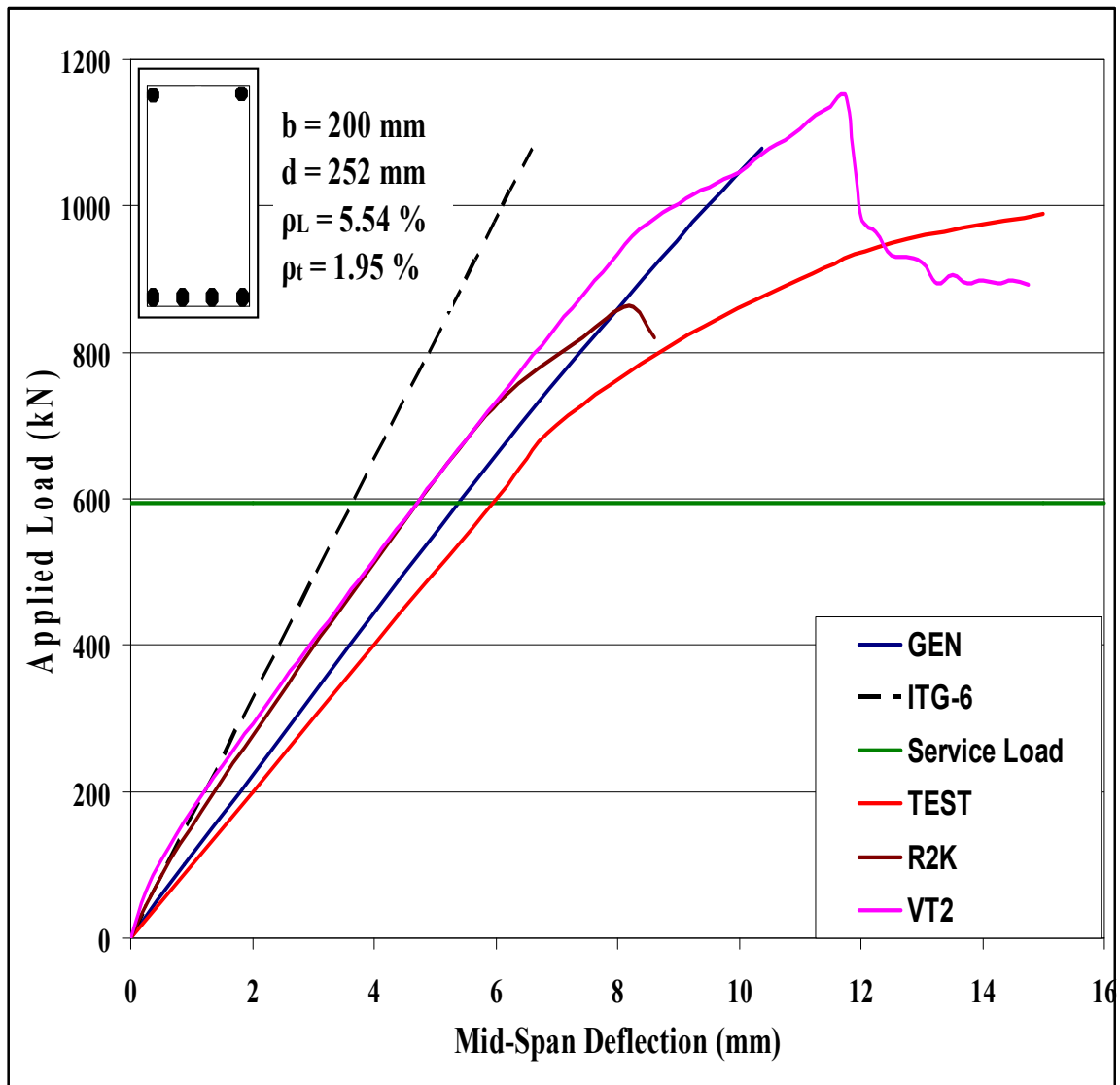


Figure C-29: Load-Deflection Plots of Beam F60-4

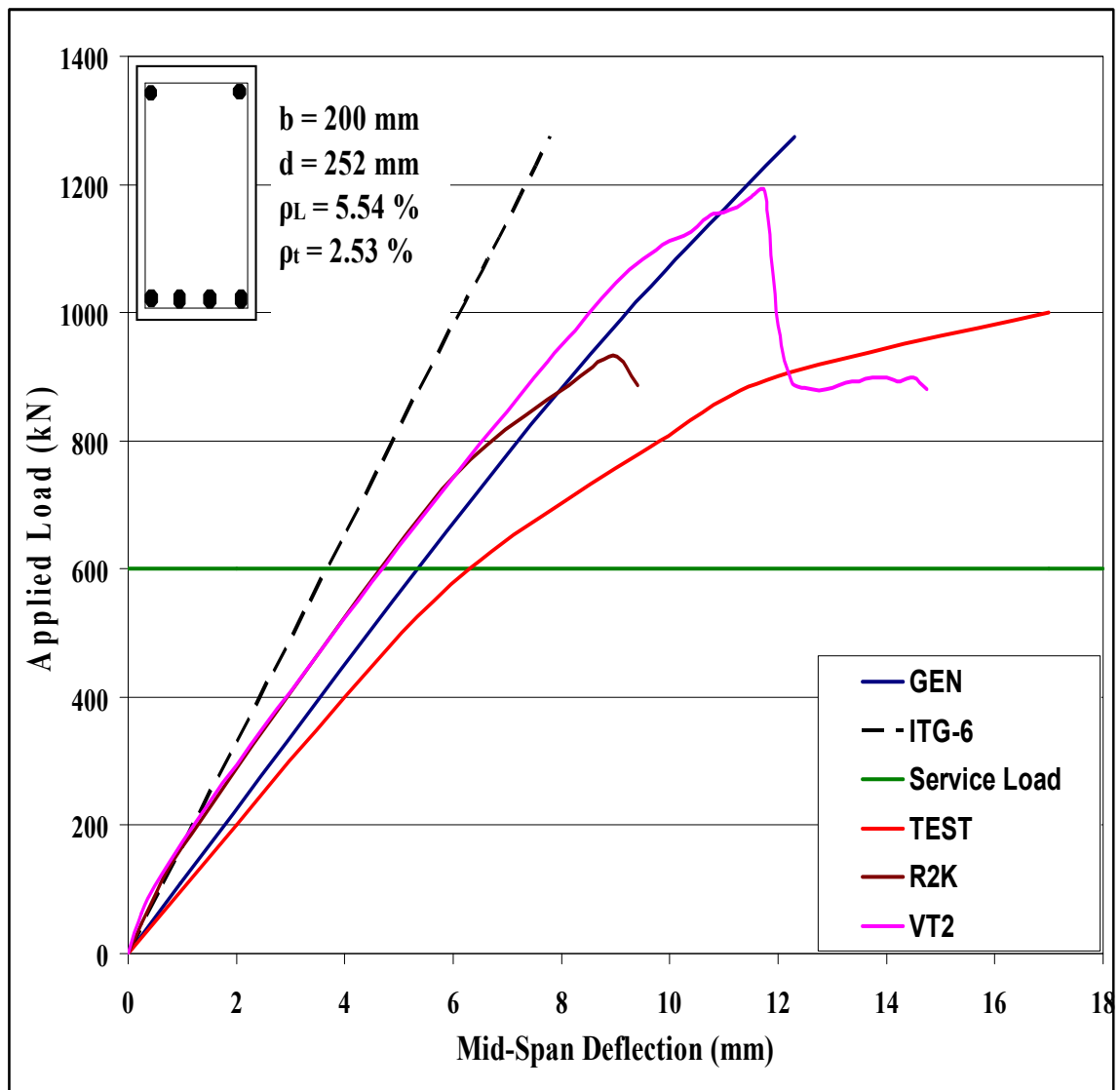


Figure C-30: Load-Deflection Plots of Beam F60-5

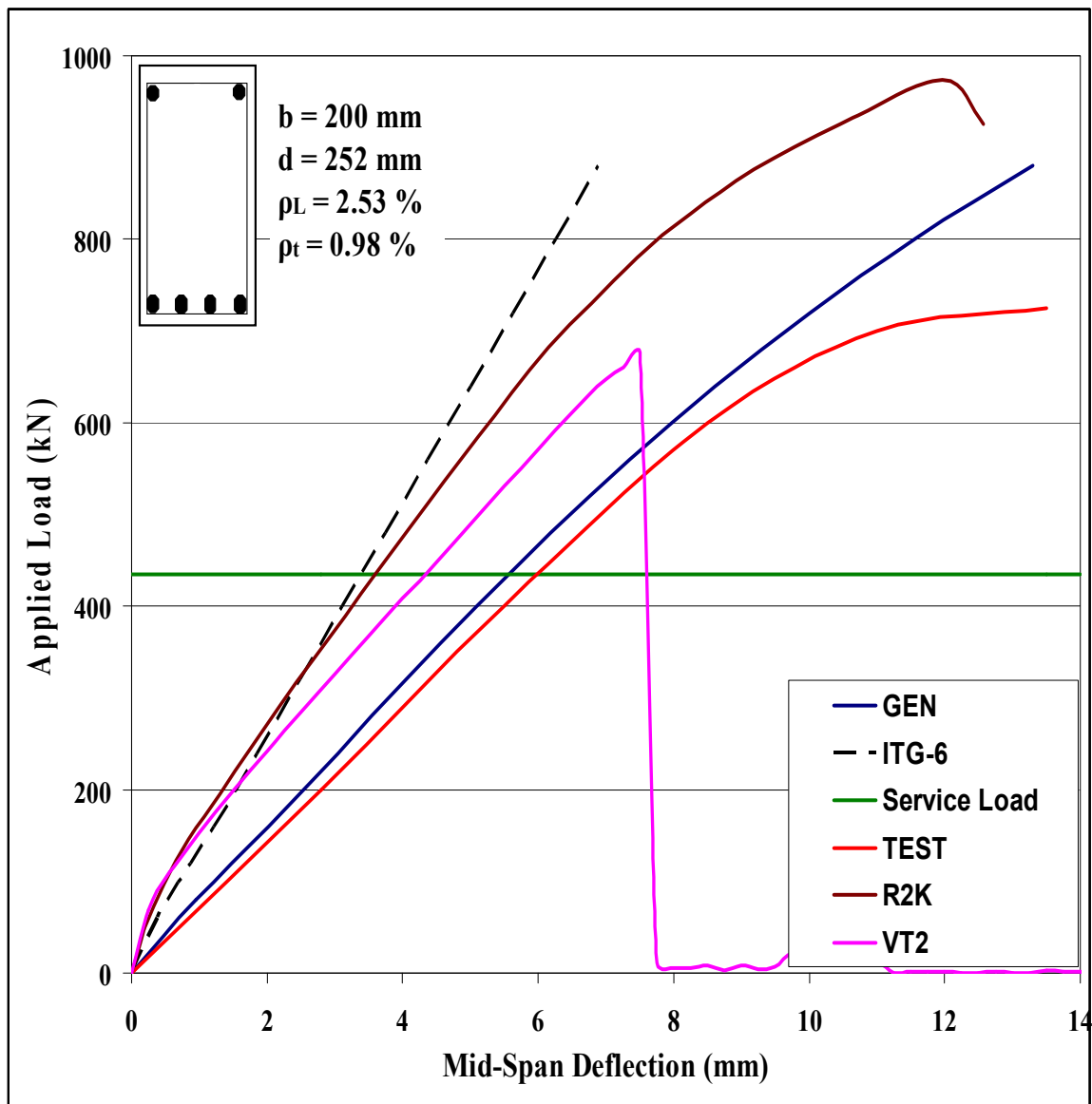


Figure C-31: Load-Deflection Plots of Beam F80-1

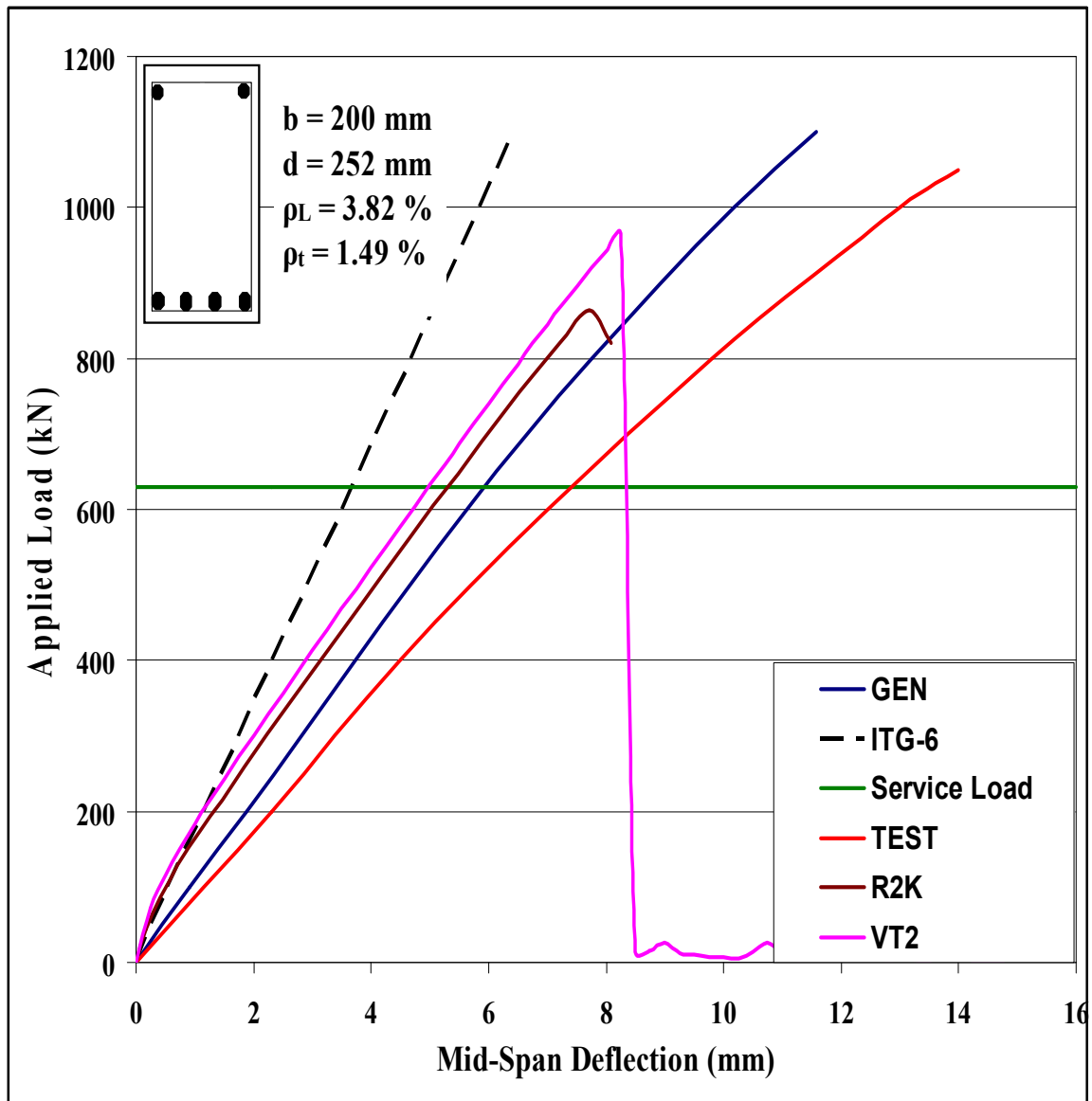


Figure C-32: Load-Deflection Plots of Beam F80-2

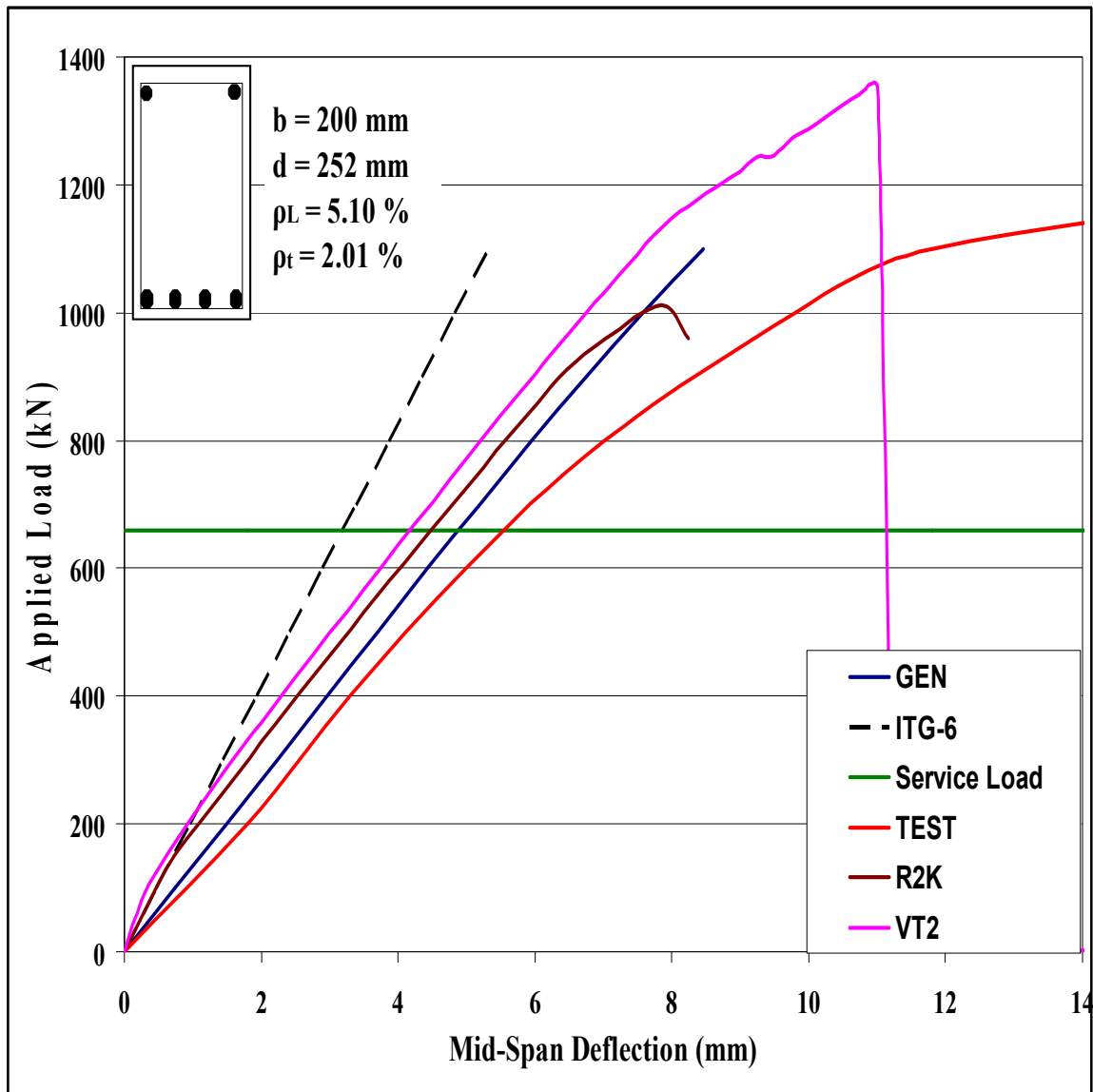


Figure C-33: Load-Deflection Plots of Beam F80-3

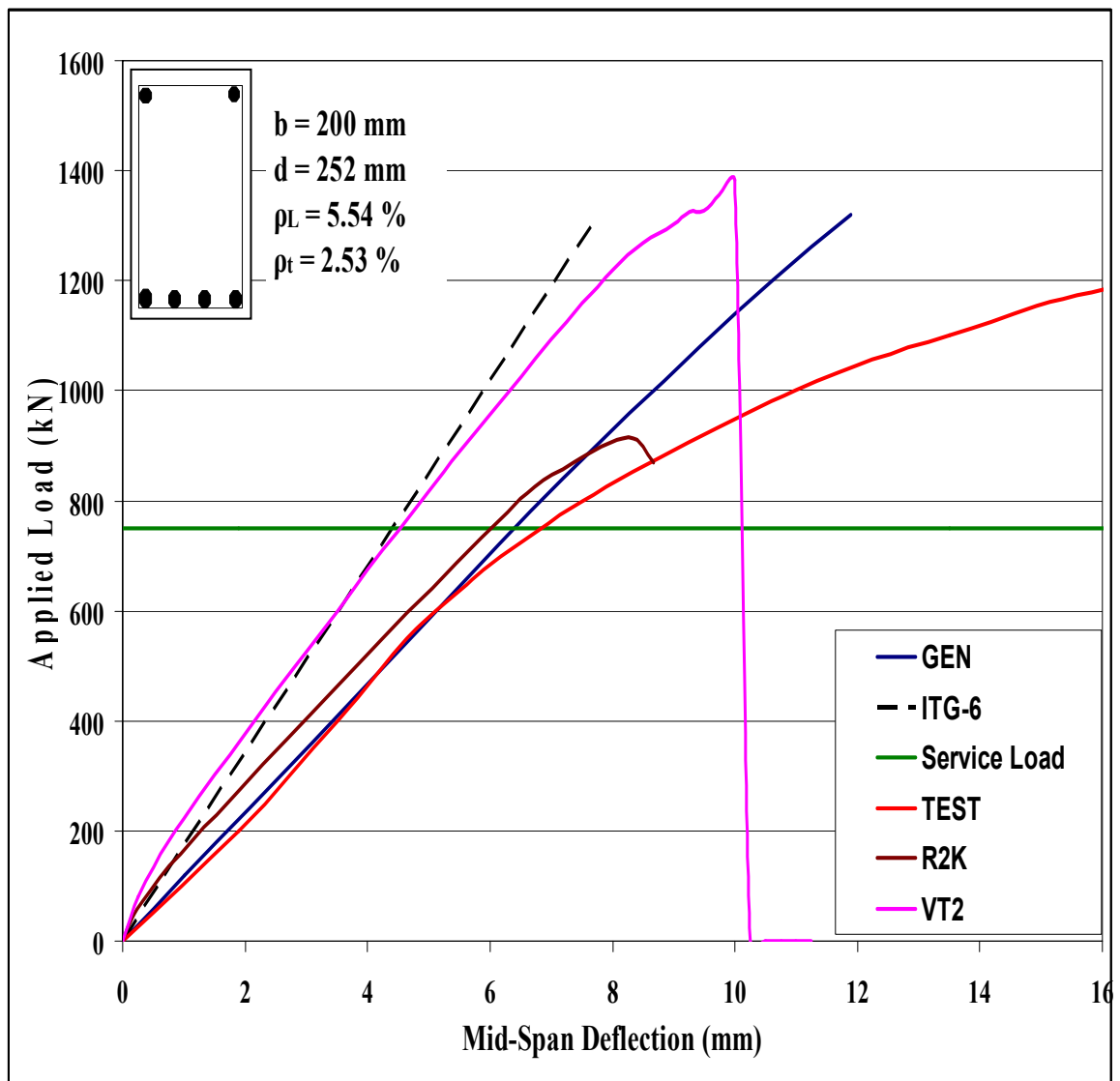


Figure C-34: Load-Deflection Plots of Beam F80-4

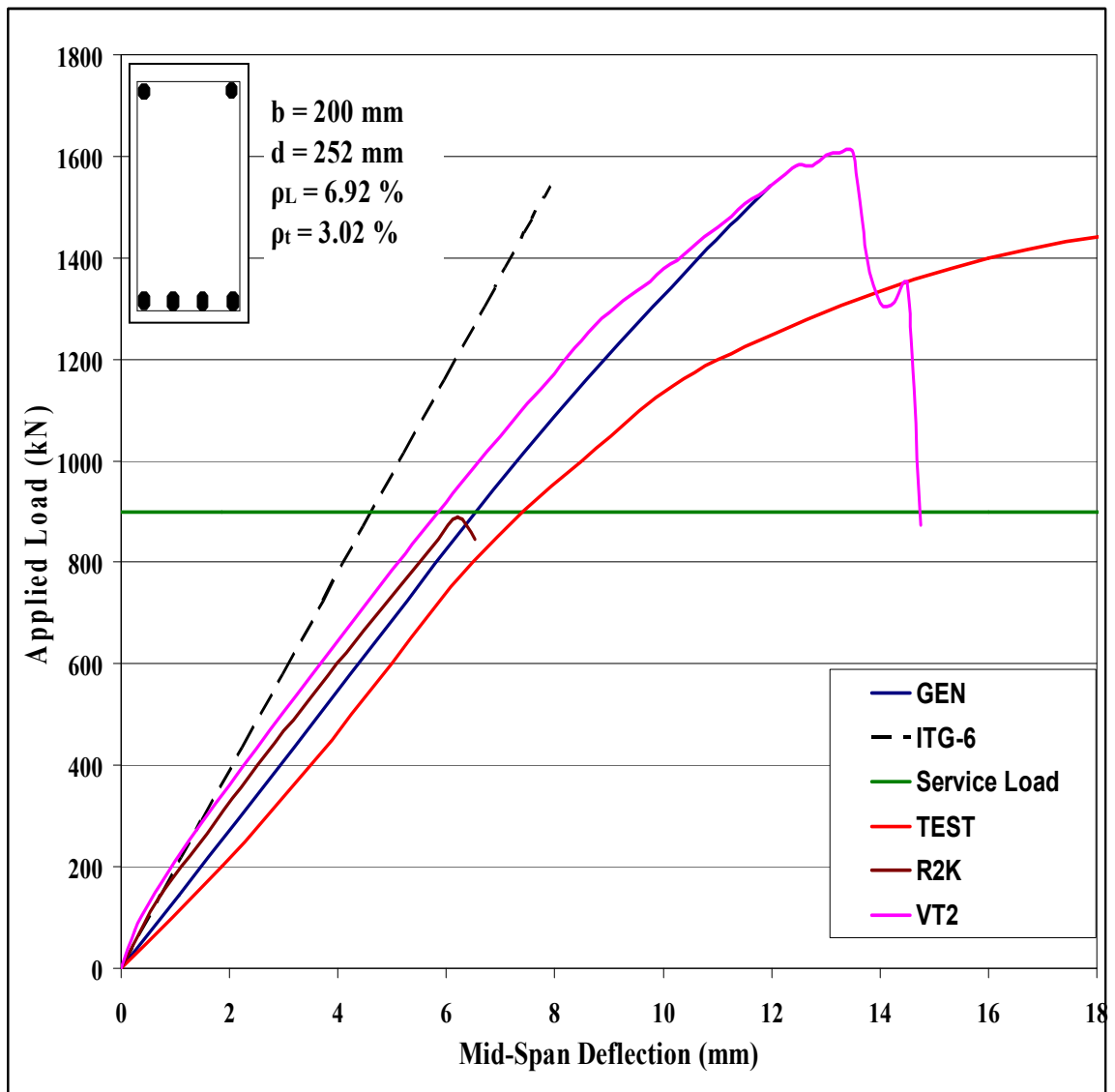


Figure C-35: Load-Deflection Plots of Beam F80-5